

Development of Small Molecule Splice-Switchers as Inducers of Apoptosis

Emma Campbell

Thesis submitted for the degree of

Doctor of Philosophy

25 October 2021

Academic Supervisor: Prof. Glenn A. Burley

Declaration of Authenticity

This thesis is the result of the author's original research. It has been composed by the author and has not been previously submitted for examination which has led to the award of a degree.

The copyright of this thesis belongs to the author under the terms of the United Kingdom Copyright Acts as qualified by University of Strathclyde Regulation 3.50. Due acknowledgement must always be made of the use of any material contained in, or derived from, this thesis.

Signed:  (Emma Campbell)

Date: 25 October 2021

Contents

Acknowledgements 7
Abstract 8
Abbreviations 10
Chapter 1 Introduction 14
1.1 Overview of the Hallmarks of Cancer 15
1.2 Central Dogma of Biology 15
1.3 Nucleic Acid Structure 16
1.3.1 Secondary Structures in Nucleic Acids 17
1.4 Small Molecule DNA G-Quadruplex Binders 20
1.4.1 Modulating the Telomerase Pathway 20
1.4.2 Small Molecules Influence G-quadruplex Regulation in Proto-oncogene Promoters 23
1.5 Small Molecules that Bind RNA G-quadruplexes 27
1.5.1 Small Molecules which Bind to KRAS G-quadruplex mRNA 27
1.5.2 Small Molecules which Bind to NRAS G-quadruplex mRNA 30
1.5.3 Current Challenges of Targeting RNA G-quadruplexes 34
1.6 RNA Synthesis 34
1.6.1 Transcription 34
1.7 RNA Splicing 36
1.7.1 The Spliceosome 38
1.7.2 Splice-Site Selection and Role in RNA Splicing 39
1.7.3 Exonic Splicing Enhancers (ESEs) 40
1.7.4 Exonic Splicing Silencers (ESSs) 40
1.8 Alternative Splicing 41
1.9 Aberrant Splicing Processes and Disease 43
1.9.1 Antisense Oligonucleotide Therapy (ASOs) 43
1.9.2 Splice-Switching Oligonucleotide Therapy (SSOs) - Spinal Muscular Atrophy 45
1.9.3 Splice-Switching Small Molecules 46
1.10 Bcl-2 and Regulation of Apoptosis 49
1.11 Bcl-x and its Role in Apoptosis 50
1.12 Evidence for G-quadruplex Formation in Gene Promotor Regions *in vivo* 51
1.13 Investigating the Structure of Bcl-x-681 51
1.14 Ellipticine Analogues as Small Molecule G4 Stabilisers 54
1.15 Challenges of Ellipticine Synthesis 58
Hypothesis to be Tested 58

Thesis Aims 60
Chapter 2 Establishing a Sequential Palladium-Catalysed Synthesis of 7*H*-Pydridocarbazoles 61
2.1 Palladium-Catalysed Cross Coupling Chemistry 62
2.1.1 General Proposed Mechanism for Pd-catalysed Cross-couplings 62
2.1.2 C-N Bond Formation – Buchwald-Hartwig Amination 63
2.1.2 Direct-arylation as a Route to Access Fused Aromatic Tricycles 66
2.2 Current State-of-the-art in a Sequential Pd-catalysed Process to form Carbazoles 70
2.2.1 One-pot Carbazole Synthesis: Bedford Method 70
2.2.2 One-pot Carbazole Synthesis: Ackermann Method 71
2.3 Chapter Aims 73
2.4 Results and Discussion 74
2.4.1 Optimisation of the Buchwald Amination 74
2.4.2 Establishing the Scope of the Buchwald-Hartwig Amination to Produce **2.41** 76
2.4.3 Establishing the Scope of 5*H*-benzo[*b*]carbazole-6,11-diones and 7*H*-pyrido[3,4-*c*]carbazoles 79
2.4.4 Re-optimisation of the Synthesis of the Pyrdiocarbazole Core 81
2.4.5 Establishing the Scope of Pyridocarbazole Synthesis 82
2.5 Targeted synthesis of natural products and their analogues through the newly developed one pot approach 85
2.5.1 Total Synthesis of Glycozoline, Harmane and Murrayafoline A 85
2.5.2 Synthesis of Ditercalinium and Biologically Active Alkylated Pyridocarbazoles 87
2.5.3 Towards the Synthesis of Deaza-ellipticine 88
2.6 Conclusions and Future Work 92
Chapter 3 Mechanistic Insights into the Palladium-Catalysed Formation of Carbazoles by Direct C-Arylation 94
3.1 Direct-arylation: An Alternative to Traditional C-C Cross Couplings 95
3.1.1 Introduction 95
3.1.2 Scope of the Intramolecular Direct Arylation reaction 95
3.1.3 Carbazole and Pyridocarbazole Synthesis *via* C-C Direct Arylation 100
3.2 Chapter Aims 102
3.3 Results and Discussion 102
3.3.1 Buchwald-Hartwig Amination 102
3.3.2 Direct *C*-arylation Studies to form the Tetracyclic Carbazole Core 102
3.3.3 Density Functional Theory Analysis of Direct Arylation 107
3.4 Conclusions and Future Work 112
Chapter 4 Towards the Total Synthesis of Natural Products Ellipticine and Calothrixin B 114
4.1 Application and Total Synthesis of Ellipticine 115
4.1.1 Structural Studies of Ellipticine Showing DNA Intercalation 116

4.1.2 Topoisomerase II Inhibition by Ellipticine Analogues 116
4.1.3 Splice-switching of Bcl-x using Ellipticine and Quindoline Analogues 118
4.1.4 Late-stage Formation of the Ellipticine C-ring (Gribble method) 120
4.1.5 Late-stage Formation of the Ellipticine D-ring (Cranwell-Saxton method) 121
4.2 Existing Studies Towards the Synthesis of Calothrixin A and B 122
4.2.1 Anticancer Activity of Calothrixins 122
4.3 Chapter Aims 123
4.4 Results and Discussion 123
4.4.1 Towards the Development of a Modular Synthesis of Calothrixin B 123
4.4.2 Towards the Synthesis of 6-Bromo-5,8-dimethylisoquinoline 127
4.4.3 Synthesis of Ellipticine Analogues for *in vitro* Bcl-x Splicing Assays 131
4.4.4 UV-mediated Synthesis of Deaza-GQC-05 134
4.4.5 Biological Evaluation of Deaza-GQC-05 and Analogues in Bcl-x *in vitro* Splicing Assays 136
4.4.6 *In vitro* Bcl-x-681 Splicing Assays of GQC-05 (**1.31**) and its Derivatives 137
4.5 Conclusions and Future Work 139
Chapter 5 Conclusions and Future Work 140
Chapter 6 Experimental 145
6.1.1 General 146
6.1.2 Purification of Solvents 146
6.1.3 Experimental Details 146
6.1.4 Purification of Products 146
6.1.5 Spectroscopic Analysis of Products 146
6.2 General Experimental Procedures 147
6.2.1 General Experimental Procedure A: Microwave Assisted Buchwald-Hartwig Amination Optimisation 147
6.2.2 General Experimental Procedure B: Microwave Assisted One-Pot Buchwald-Hartwig Amination and Direct Arylation Optimisation 147
6.2.3 General Experimental Procedure C: Microwave Assisted Buchwald-Hartwig Amination 147
6.2.4 General Experimental Procedure D: Microwave Assisted One-Pot Buchwald-Hartwig Amination and Direct Arylation 148
6.2.5 General Experimental Procedure E: Microwave Assisted One-Pot Buchwald-Hartwig Amination and Direct Arylation 148
6.3 Microwave Assisted Buchwald-Hartwig Amination Optimisation 149
6.4 Microwave Assisted One-Pot Buchwald-Hartwig Amination/Direct Arylation Optimisation 150
6.5 Experimental Details 151
6.5.1 Chapter 2: Compound Characterisation 151
6.5.2 Chapter 3: Compound Characterisation 179
6.5.3 Chapter 4: Compound Characterisation 183

6.6 DFT Experimental 196
6.6.1 Compound 7a 196
6.6.2 Compound 16 197
6.7 Crystallographic Data 199
6.7.1 Compound 11 199
References 204
Appendix 226

Acknowledgements

First and foremost, I would like to thank Glenn Burley for not only giving me the opportunity to undertake a PhD, but for the continued support, guidance and instruction he provided throughout my four years in his group. I would also like to thank Olivia Rutherford for taking me under her wing in my first few months and for her initial guidance on the project.

I would like to thank all the previous and current members of the Burley group in the University of Strathclyde for their day-to-day support. To Fergus and Imma for putting up with me in the laboratory every day, to Iain, Jack, Jamie and Charlotte for their friendship and always keeping me laughing. And to Andrea, the best friend and colleague I could have asked for, who supported me through every high and low; I would not be where I am without you.

Through our collaboration with the University of Leicester, I would like to thank the Ian Eperon, and Cyril Dominguez groups for their input and continual insight into the project.

For funding, I would like to extend my gratitude to the University of Strathclyde and GSK.

I would like to thank all the post-docs past and present for all proofreading, answered questions and teaching they have supplied throughout the years.

To my family Kenneth, Agnes and Diane Campbell for their unwavering love, support and belief in me. To Shaun, for his support and for always telling me I could do this. I could not have done this without you.

Finally, I would like to dedicate this thesis to two formidable women, Christina Macarthur and Christina Campbell. Both of whom inspired and encouraged me from an early age to achieve my potential in academia. Their unlimited love and support is the reason I am a researcher today and I will forever strive to make them proud.

Abstract

Alternative splicing is the primary source of protein diversity in eukaryotes. Alternative splicing allows the production of multiple isoforms from the same genetic blueprint (DNA). Over 95% of all eukaryotic genes undergo alternative splicing, and although this facilitates great protein diversity, it can instigate disease when the process goes wrong for example in cancer.

The Bcl-2 protein family are essential gatekeeper regulators of apoptosis.[1] One such protein, Bcl-x is of particular interest as a therapeutic target. It has two splicing isoforms; pro-apoptotic Bcl-xS and the anti-apoptotic Bcl-xL; the latter of which is upregulated in a variety of cancers. Thus, exogenous regulation of Bcl-x splicing, which biases the pathway towards the pro-apoptotic Bcl-xS isoform could provide a new a novel mechanism for cancer therapy (Figure 1).[2]

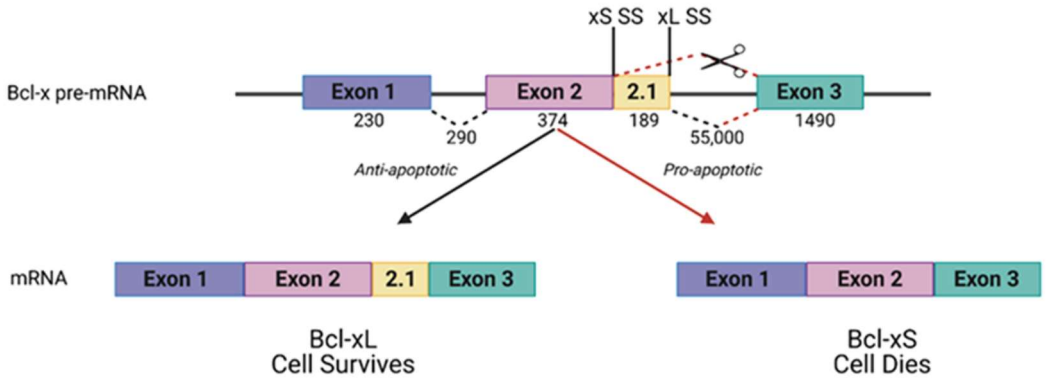


Figure 1. Two antagonistic splicing isoforms of Bcl-x, the anti-apoptotic Bcl-xL and the pro-apoptotic Bcl-xS. Created with BioRender.com

In 2018, Eperon and co-workers found that the ellipticine analogue GQC-05 induces a splice-switch in Bcl-x towards the pro-apoptotic isoform Bcl-xS.[3] This thesis will report the steps taken towards developing a structure activity relationship (SAR) of the interaction between GQC-05 and Bcl-x in an effort to elucidate the splice-switch mode of action.

Chapter 1 discusses the biological importance of splicing and its effect on disease progression. In particular, the recent developments highlighting Bcl-x as a desirable target for novel cancer therapies.

Chapter 2 describes a modular one-pot synthesis of 7*H*-pyridocarbazoles through sequential palladium catalysed Buchwald-Hartwig amination and direct arylation. This method was transferrable to the synthesis of carbazole natural products as well as providing a convergent step-efficient route to the known DNA intercalator, Ditercalinium.

Chapter 3 explores the mechanism of the direct arylation step through designed control reactions and modelling reactivity through DFT calculations.

Finally, Chapter 4 details the application of the methods developed in Chapter 2 to the synthesis of natural products Calothrixin B and Ellipticine. This chapter discusses the limitations of the one-pot synthesis on substrates that are more complex and presents a UV-light mediated synthesis as a solution. Finally, the ellipticine analogues synthesised in this thesis were tested in Bcl-x *in vitro* splicing assays to expand the SAR of the interaction to inform the design of a structural-biological probe (Figure 2).

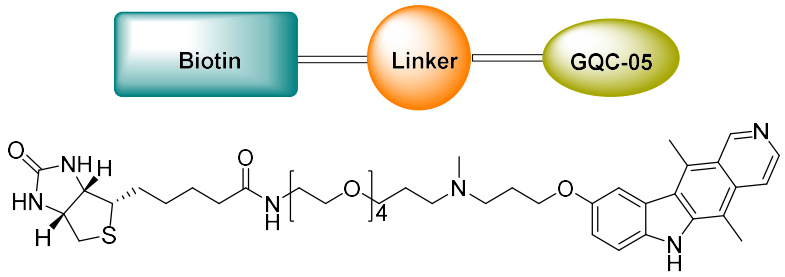


Figure 2. Proposed structural probe for determining mode of action of GQC-05.

Abbreviations

%	Percentage
(ds)DNA	(double stranded) Deoxyribonucleic acid
(ss)RNA	(single stranded) Ribonucleic acid
°C	Degrees celsius
2D	Two-dimensional
A	Adenine/Adenosine
Å	Angstroms
Ac	Acetyl
ASO	Antisense oligonucleotide
ATP	Adenosine triphosphate
au	Atomic unit
b	Broad
Bcl-2	B-cell lymphoma 2
Bcl-xL	B-cell lymphoma-extra large
Bcl-xS	B-cell lymphoma-extra small
BH	Bcl-2 homology
Bn	Benzyl
BPS	Branch point sequence
Bu	Butyl
C	Cytosine/Cytidine
c-Kit	Mast/stem cell growth factor receptor
CMD	Concerted metalation deprotonation
c-Myc	V-Myc avian myelocytomatosis viral oncogene homolog
Cy	Cyclohexyl
CYP	Cytochrome P450
d	Doublet
DCM	Dichloromethane
dd	Doublet of doublets
ddd	Doublet of doublet of doublets
DDQ	2,3-Dichloro-5,6-dicyano-1,4-benzoquinone
DFT	Density functional theory
DMAc	Dimethylacetamide
DMAP	4-Dimethylaminopyridine
DMF	Dimethylformamide
DMSO	Dimethylsulfoxide
dppe	1,2-Bis(diphenylphosphino)ethane
e.g.	Exempli gratia
EDG	Electron donating group
EMSA	Electrophoretic mobility shift assay
equiv	Equivalent
ESE	Exonic splicing enhancer
ESI	Electrospray ionisation
ESS	Exonic splicing silencer
EtOH	Ethanol
EWG	Electron withdrawing group

FDA	Food and drug administration (US)
FTIR	Fourier transform infrared
G	Guanine/Guanosine
g	gram
G4	G-quadruplex
GDP	Guanosine diphosphate
GFP	Green fluorescent protein
GQC-05	G-quadruplex compound 05
GTP	Guanosine triphosphate
h	Hour
H-bonding	Hydrogen bonding
hnRNPs	Heterogeneous nuclear ribonucleoproteins
HOMO	Highest occupied molecular orbital
HRMS	High resolution mass spectroscopy
HTP	High throughput
Hz	Hertz
IC_{50}	Half maximal inhibitory concentration
IR	Infrared radiation
ISE	Intronic splicing enhancer
ISS	Intronic splicing silencer
Kd	Equilibrium dissociation constant
KIE	Kinetic isotope effect
k-ras	Kirsten Rat Sarcoma Viral Oncogene Homologue
λ	Wavelength
LC-MS	Liquid chromatography mass spectroscopy
LR-MS	Low resolution mass spectroscopy
m	Multiplet
M	Molar
m/z	Mass to charge ratio
Me	Methyl
MeCN	Acetonitrile
MeOH	Methanol
mg	Milligram
mins	Minutes
miRNA	Micro ribonucleic acid
mL	Millilitre
mmol	Millimole
mRNA	Messenger ribonucleic acid
MW	Microwave
ncRNA	Non-coding ribonucleic acid
NHC	*N*-heterocyclic carbenes
NHE	Nuclease hypersensitive element
nm	nanometer
NMP	*N*-Methyl-2-pyrrolidone
NMR	Nuclear magnetic resonance
NRAS	Neuroblastoma RAS viral oncogene homologue

Ns	Nosyl
nt	Nucleotide
PAGE	Polyacrylamide gel electrophoresis
$Pd_2(dba)_3$	Tris(dibenzylideneacetone)dipalladium(0)
PDB	Protein data bank
Ph	Phenyl
PivOH	Pivalic acid
PMB	Para-methoxybenzyl
Pol	Polymerase
POT1	Protection from telomeres 1
ppm	Parts per million
PPT	Polypyrimidine tract
QGRS	Quadruplex forming G-rich sequences
r.t.	Room temperature
RDS	Rate determining step
RNA	Ribonucleic acid
ROS	Reactive oxygen species
RP-HPLC	Reverse phase high pressure liquid chromatography
rRNA	Ribosomal ribonucleic acid
RT-PCR	Reverse transcription polymerase chain reaction
s	Singlet
SAR	Structure activity relationship
S_E3	Substitution electrophilic trimolecular
S_EAr	Electrophilic aromatic substitution
SMA	Spinal muscular atrophy
SMN	Survival of moto neutron
snRNA	Small nuclear ribonucleic acid
snRNP	Small nuclear ribonucleic protein
SR proteins	Serine arginine proteins
SS	Splice site
SSO	Splice-switching oligonucleotide
t	Triplet
T	Thymine/Thymidine
TBAB	Tetra-*n*-butylammonium bromide
TFA	Trifluoroacetic acid
THF	Tetrahydrofuran
TLC	Thin layer chromatography
T_m	Melting temperature
U	Uracil/Uridine
U2AF	U2 small nuclear RNA auxiliary factor
U2AF35	U2 small nuclear RNA auxiliary factor 35
U2AF64	U2 small nuclear RNA auxiliary factor 64
UTR	Untranslated region
UV	Ultraviolet
W	Watt

WHO	World health organisation
Δ	Change
δ	Chemical shift
θ	Cone angle
μM	Micromolar
π	Pi
ω	Bite angle

Chapter 1 Introduction

1.1 Overview of the Hallmarks of Cancer

Cancer research is an ever-evolving field, ranging from developing early detection methods to new modes of therapy.[4] This research area is expanding just as the number of new cancer cases reported are each year. The World Health Organisation (WHO) reported that 1 in 6 deaths that occurred globally in 2018 were a result of cancer.[5] The number of new cases reported each year is only set to increase in the next decade, requiring more diverse and effective treatments. Traditional chemotherapies available exploit that cancer cells are fast replicating, and do so at a much higher rate than healthy cells.
However, many small molecule cancer treatments are not fully selective for cancer cells, which results in an array of side effects ranging from damage to cells associated with the immune system to vital organ toxicity.[6,7] It has become apparent that developing therapies that can target cancerous cells would be greatly advantageous in the ongoing fight against cancer.[8]

Another major hallmark of cancer cells is their effective evasion of cell death. Cell death mechanisms, such as those under the control of the p53 pathway, are either absent or malfunctioning resulting in uncontrolled cell growth and eventual metastasis of abnormal cells throughout the body.[9] A particular regulatory protein family of the cell death pathway, Bcl-2, has been shown to be instrumental in the control of cancer cell death.[10] The motivation of the work described in this thesis is to develop strategies, which manipulate this pathway through alternative RNA splicing, to target cancer cells to programme their own cell death.

1.2 Central Dogma of Biology

In 1958, Francis Crick first introduced a concept what would later become the cornerstone of nucleic acid research.[11] The central dogma of biology, as it was termed, detailed that the flow of genetic information was reversible until a protein was synthesised.[11] Once a protein formed, the genetic information was 'locked in' and could not be transferred back to RNA, DNA or to even another protein. This flow of information refers to the sequential transfer of information from nucleic acid to nucleic acid, and eventually to protein. Lack of the abundant genetic research available today inevitably led to this initial discovery being an oversimplification. A point that was raised by Crick himself in a later article published in Nature in 1970,[12] revealed that the model only accounts for the flow of information but does not encompass the machinery required for that transfer, the control mechanisms, or the errors associated with the transfer as it was assumed the accuracy was high. The initial model (Figure 3a) proposed tentatively by Crick in 1970 separated the transfers into three main classes: general (solid lines), special (dotted lines) and unknown transfers (not shown in Figure 3).

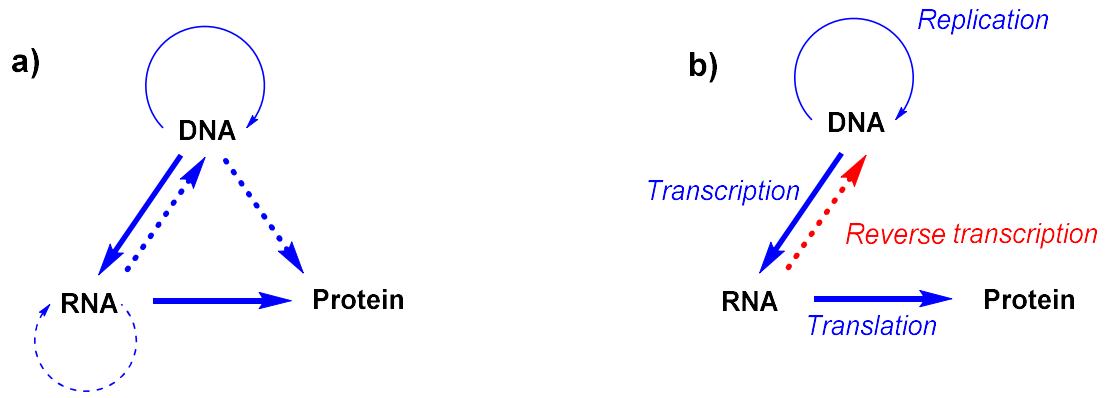
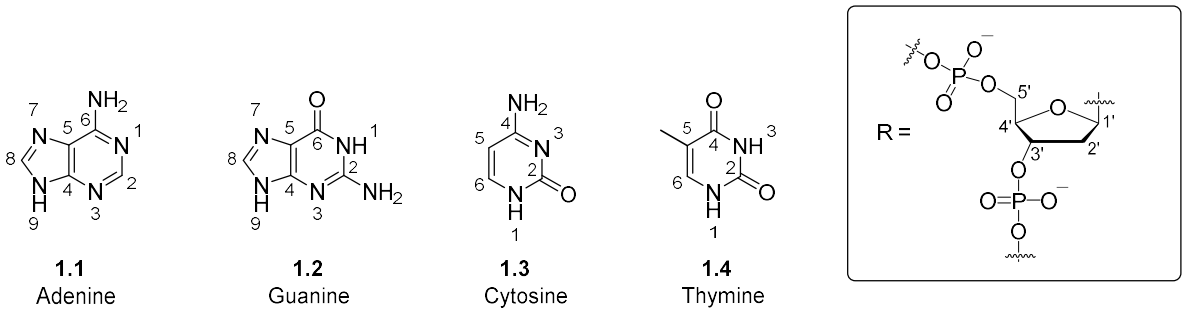


Figure 3. (a) Crick's early interpretation of information flow from DNA to protein, general transfers (solid lines); special transfers (dotted lines). (b) Current 'state of the art' depiction of information flow.[11,12]

General genetic transfer was those that were supported by some experimental evidence at the time and occurred in all cells. The working hypothesis was that the special transfers were largely due to viral studies showing evidence of RNA to RNA and RNA to DNA transfer.[12] Finally, the unknown transfers (not shown in Figure 3a), relate to transformations that the central dogma deemed impossible; the transfer of information from protein in reverse to DNA, RNA or to another protein. Incredibly, the model has not changed significantly in the past 50 years. The discovery of reverse transcription confirmed the special transfer from RNA to DNA,[13] and it was further confirmed that once a protein was synthesised, the flow of information was terminated (Figure 3b).

1.3 Nucleic Acid Structure

Deoxyribonucleic acid (DNA) is a molecule made up of two strands of nucleotide chains, which contain the genetic blueprint for the synthesis of proteins. DNA comprises four nitrogenous bases; Adenine (A), Guanine (G), Cytosine (C) and Thymine (T) attached to a deoxyribose sugar. These nucleoside subunits are linked together through phosphodiester bonds which form the backbone of the primary sequence of DNA and RNA (Figure 4).[14]



1.1 Adenine **1.2** Guanine **1.3** Cytosine **1.4** Thymine

Figure 4. Structure of DNA bases; Adenine (**1.1**), Guanine (**1.2**), Cytosine (**1.3**) and Thymine (**1.4**). The bases are attached to the ribose sugar at the 1′-position (shown in box).

Ribonucleic acid (RNA) is a polymer of nucleotides that is essential in coding and regulation of gene expression. RNA comprises four nitrogenous bases like DNA, however Thymine (**1.4**) is replaced by

the Uracil (**1.5**) base which are attached to a ribose sugar. These nucleoside subunits are linked together through phosphodiester bonds which form the backbone of the primary sequence of the RNA (Figure 5).[14]

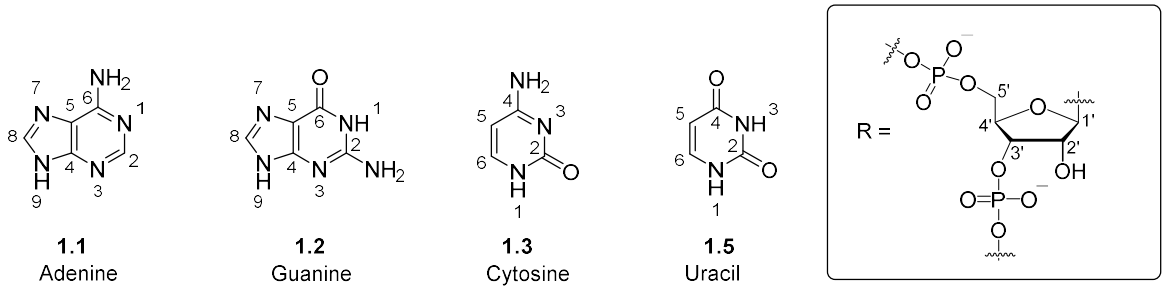


Figure 5. Structure of RNA bases; Adenine (**1.1**), Guanine (**1.2**), Cytosine (**1.3**), Uracil (**1.5**). The bases are attached to the ribose sugar at the 1′-position (shown in box).

1.3.1 Secondary Structures in Nucleic Acids

RNA is predominantly found as a single stranded species; therefore, its conformation is more flexible than the more rigid double stranded structures typically formed by DNA. This flexibility allows the formation of a variety of higher-order structures through folding and H-bond formation. Secondary structures of nucleic acids consist of stem loops and helices. The formation of these structures is a consequence of a combination of Watson-Crick base pairing, whereby the bases can be paired through Hydrogen bonding in A – U, and G – C patterns (Figure 6a) and Hoogsteen base-pairing (Figure 6b).[15]

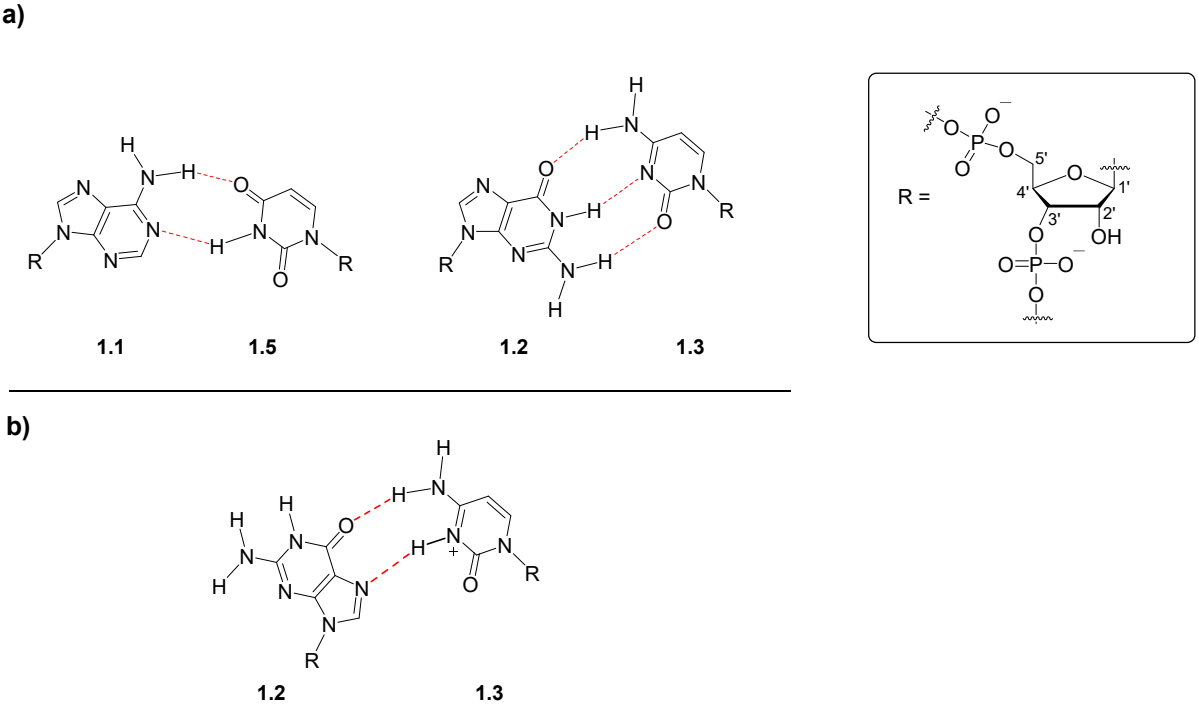


Figure 6. (a) Watson-Crick H-bond interactions of Adenine (**1.1**) with Uracil (**1.5**) and Guanine (**1.2**) with Cytosine (**1.3**). The bases are attached to the ribose sugar at the 1′-position (shown in box). (b) Hoogsteen-base pairing of Guanine (**1.2**) with Cytosine (**1.3**).[15]

1.3.1.1 G-Quadruplexes

Beyond the secondary double helical structures and stem-loops, DNA and RNA have been found to form four-stranded non-canonical tertiary structures, evidence of which has been noted over 100 years ago when the Bang laboratory observed that guanylic acid formed gels at high concentrations.[16] This unusual physical property was explained 50 years later when X-ray diffraction showed assembly of tetrameric units into helical structures that could account for the gel formation.[17] These structures, now known as G-quadruplexes (G4s), are higher-order tetrads of RNA or DNA.[18] Their structure arises from a pairing of one Watson-crick face of G to the Hoogsteen face of another (Figure 7) in sequences that are rich in repeated guanine residues (G-tracts).

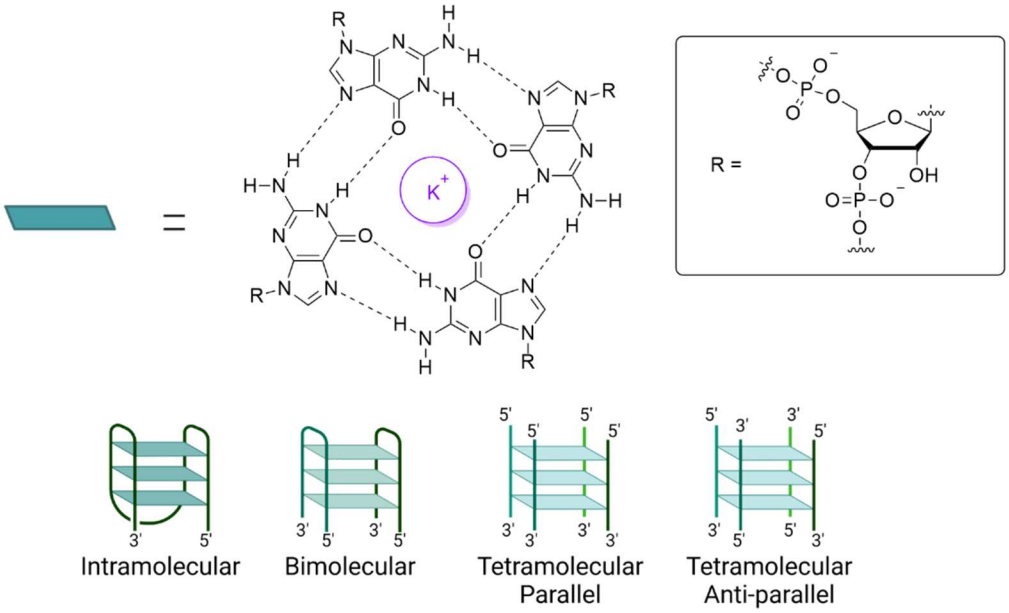


Figure 7. G-quadruplex structure: Four Guanine bases arrange in a tetrad to form the structural basis of G4s. The N7 of one Guanine H-bonding to the exocyclic amino group of another. Created with BioRender.com

Metal cations coordinate to the O6 of the Guanine residues and assemble within the centre of the complex, improving stability. Different metal ions have different stabilizing effects, running in order of greatest stability with $K^+ > NH_4^+ > Na^+ > Li^+$.[19] The nucleotide loops in G4s are able to form external cavities that may facilitate ligand binding.[20] The length of these loops are highly variable between different sequences and this variety results in different conformations. Studies carried out by the Balasubramanian laboratory observed that shorter loops of two nucleotides were restricted to parallel folded conformations whereas longer loops (five nucleotides) showed a mixture of parallel and antiparallel structures.[21] There are three main classifications of G4 loops; diagonal, edgewise and propeller loops (Figure 8).[22, 23] G4s are also able to form from on unimolecular, bimolecular, and tetramolecular structures. Further diversity in construction leads to varied topologies being observed, including altering directions of RNA strands to produce parallel, antiparallel and hybrid G4s (Figure 7).

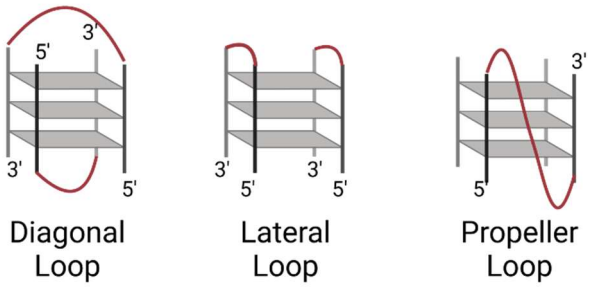


Figure 8. Schematic of different loop formations in G4s. Loops shown in red. Created with BioRender.com

The prevalence of DNA G4 forming sequences in promoter regions of genes that correspond directly to disease make them an attractive target for controlling the expression of disease.[24] G4 sequences have been found in the promoter regions of vascular endothelial growth factor, and in the oncogenes bcl-2,[25] c-myc,[26] k-ras[27] and c-kit[28] which are associated with many cancers, including, but not limited to; B-cell lymphoma, Burkitt lymphoma and prostate cancer.[29]

Whilst there have been extensive studies on the presence and significance of G4s in RNA and DNA. There is some doubt as to the longevity and functional significance of their structure *in vivo*. In particular, a study conducted in 2016 by Guo and Bartel highlighted global unfolding of RNA-G4s *in vivo* by helicases.[30] Dimethyl sulfate (DMS) footprinting showed methylated residues of unwound G4s, however the experiments did not account for the dynamic nature of G4 formation and were not replicated as they were only carried out once. These initial findings further the debate on whether biological function alterations were due to the G4 itself being the target or due to other interactions such as protein binding (co-factors) being displaced. Unfortunately, finding evidence G4 motif *in vitro* is not confirmation of their formation *in vivo*. Although conclusive proof for their continued presence *in vivo* is in continual progress, there is accumulating evidence, through deep sequencing and *in silico* methods to suggest that G4 forming sequences are ubiquitous throughout the genome (700,000 potential G4 forming regions are present in the human genome).[31, 32] These sequences are found extensively within regions of regulation i.e. telomeric regions and gene-promoters, given that 40% of promoter regions in the human genome contain a putative G4 forming sequence.[33] Additionally that stabilization of G4s has an effect on gene expression and that they have shown to have specific interactions with certain proteins e.g. helicases.[34]

Due to their specific location in regions of regulation, G4s have been associated with the regulation of multiple processes including; chromosomal extension and degradation, apoptosis, modifications post translation and in cancer protein expression.[35,36] This role in regulation has made them a target of research, with particular aims at developing small molecule drugs to treat cancer.

1.4 Small Molecule DNA G-Quadruplex Binders

1.4.1 Modulating the Telomerase Pathway

The telomere is a region of repetitive DNA nucleotides and associated proteins which is located at the ends of all chromosomes.[37] It serves as a 'cap', protecting the end of the chromosome that acts as a buffer for truncation through DNA replication and prevents improper activation of DNA repair mechanisms. Enzymes, called telomerases, replenish this cap by elongating the sequence by adding the repetitive sequences to the ends of the DNA. This region consists of repeated nucleotide sequences (TTAGGG), rich in guanine residues, which make the likelihood of G4 forming sequences vastly increased. Protection from telomere shortening by elongation can be decreased by the presence of G4s through preventing exposure of the G-overhang to the telomerase, thus preventing replenishment of the cap.[36]

Numerous areas of regulation contain G-rich sequences. If small molecule ligands could interact with these sequences, could they modify their effect on disease expression as well? Studies have indicated that since telomerase is over-expressed in over 80% of cancer cells,[38] the unchecked proliferation seen in cancer cells could be a result of protecting the ends of the chromosomes with telomeric repeat sequences, facilitated by the enzyme. The hypothesis being, a G4-ligand could interact with and sequester the telomeric ends, making them unavailable for extension, thus stopping un-regulated cell division. This was shown to be the case in 1991 when Cech *et al* demonstrated that when sequestered into a G4, the telomeric overhang was protected from telomerase extension.[39] More recently, studies have shown that this also inhibits the association of vital proteins with their telomeric targets.[40, 41, 34]

In 2003, the first crystal structure of a parallel DNA quadruplex-drug complex was obtained of Daunomycin and telomeric DNA. The unit consists of four parallel d(TGGGGT) strands, that together with three Daunomycin molecules creates a intermolecular parallel G4 (Figure 9).[42] Interestingly, no Daunomycin was shown to intercalate in between the guanine residues and was only seen to be stacking on top or at the bottom of the G4 (Figure 9a). Since this initial discovery, many more G4-ligands have been designed and as such, has led to certain characteristics being highlighted as advantageous to binding. Like Daunomycin, G4-ligands generally have a flat, electron rich aromatic core that can facilitate π-π stacking to the coordinated guanine residues. Additionally, G4-ligands have a basic or protonated moiety that can add additional stability through binding with the negatively charged phosphodiester backbone of the DNA. Finally, ligands that have additional bulk have been shown to be more effective due to preventing interaction with double stranded DNA. G4 ligands are sometimes categorised by their source of cationic nature i.e. protonation of a basic residue *in situ*, a quaternary methylated aromatic nitrogen functional group, the inclusion of a metal centre or non-cationic ligands.

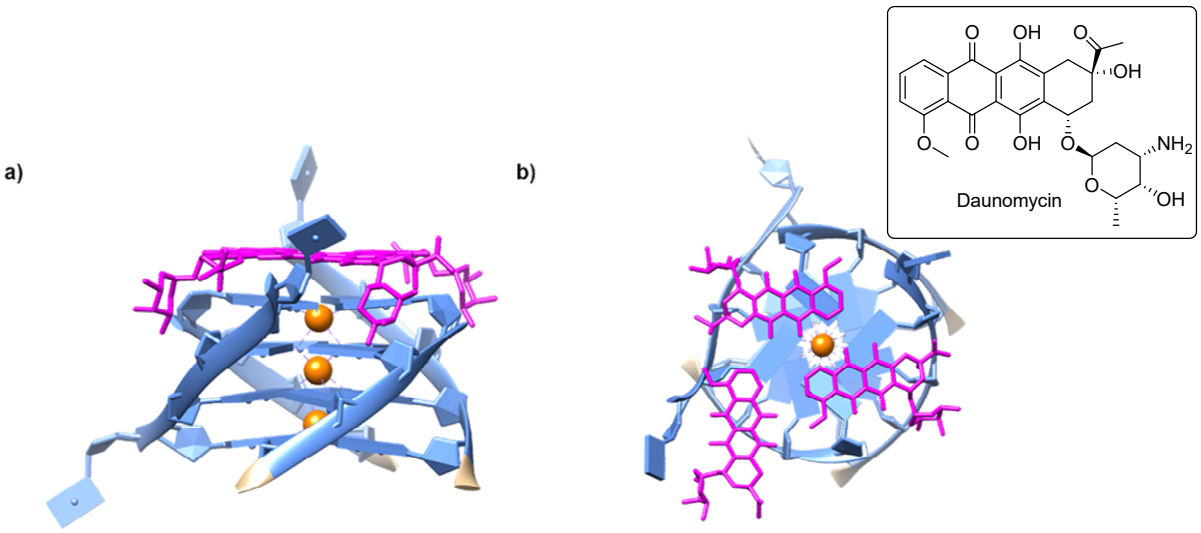


Figure 9. The first X-ray crystal structure of a parallel G4 with daunomycin trimer. (a) Side-on view, (b) Top-down view of Daunomycin (magenta) and K^+ (orange). (PDB: 1O0K).[42]

In 2008, Balasubramanian *et al*. developed a novel small compound, later called pyridostatin (**1.6**), which showed a stabilising effect on G4 sequences (Figure 10).[43] Pyridostatin (**1.6**) is an example of a G4 ligand that utilises amine sidechains that are protonated *in situ*. This also increases the solubility of an otherwise poorly soluble aromatic core.

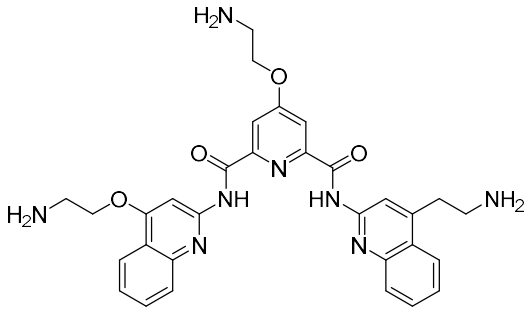


Figure 10. Structure of Pyridostatin (**1.6**).

FRET-melting experiments showed that pyridostatin (**1.6**) stabilised the telomeric G4 with a maximum ΔT_m = 35 K in 60 mM K^+ and 44 K in 100 mM Na^+ at 0.18 and 0.35 μM of pyridostatin (**1.6**) respectively, in addition to showing high selectivity over duplex DNA.[43] Furthermore, pyridostatin (**1.6**) uncapped the protein coding gene POT1 (protection from telomeres 1), which regulates the length of telomeres through cis-inhibition of telomerase, in a dose dependent manner (IC_{50} 200 nM) *in vitro*.

To confirm these results *in vivo*, the human cancer cell line HT1080 was modified with GFP-POT1 fusion protein so that on uncapping of the POT1 the fluorescence would be lost. On incubation of 1 μM pyridostatin (**1.6**) for 72 h, the GFP signal was almost completely lost (Figure 11). These results were

in-line with the *in vitro* findings, and it was postulated that the compound was inducing folding of the G-overhang into the G4 resulting in the uncapping.

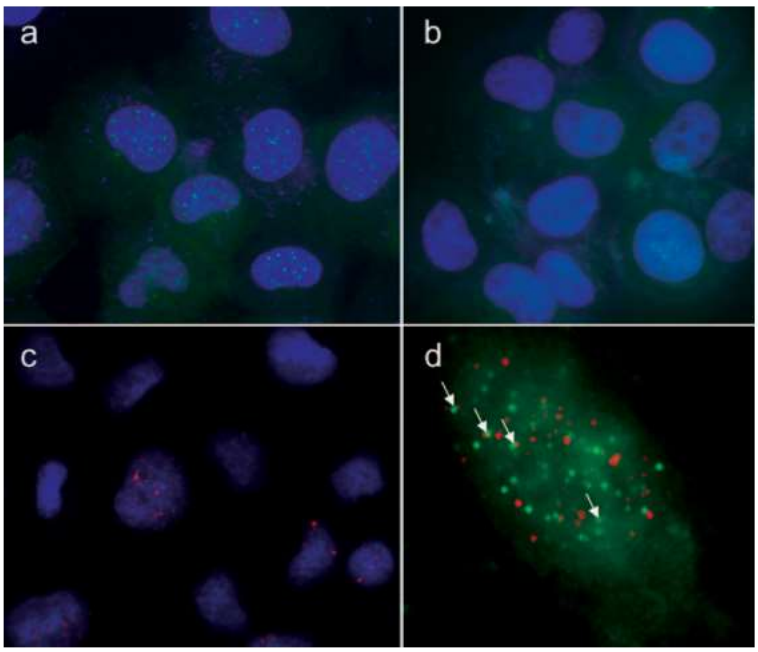


Figure 11. HT1080GFP-POT1 cells treated with Pyridostatin (**1.6**), DAPI used as DNA stain. (a) GFP-POT1 (green), control (no ligand added). (b) Treatment with **1.6** (1 μM) for 72 h. (c) γH2AX foci (red) incubated with **1.6** (3 μM) for 24 h. (d) Arrows point to co-localisation of foci and GFP-POT1 in the telomeres. Reprinted with permission. Copyright 2021, American Chemical Society.[43]

MMQ_3 (**1.7**), that utilises amino side chains to affect protonation *in situ,* was developed by Mergny *et al.* (Figure 12). MMQ_3 (**1.7**) was of note due to its extended π-system that would increase the π-π stacking interaction with the G-tetrad.

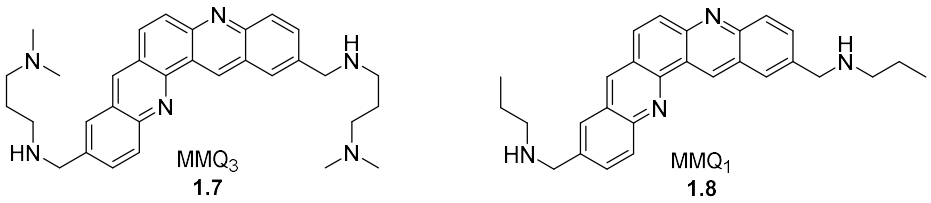


Figure 12. Structure of MMQ_3 (**1.7**) and MMQ_1 (**1.8**).

MMQ_3 (**1.7**) showed great promise with a stabilization of $\Delta T_m = 20$ °C and $IC_{50} = 28$ nM for telomerase inhibition.[44] An NMR structure of MMQ_1 (**1.8**) (side chains replaced by dipropylamino) elucidated the expected overlap of the aromatic core with the G-tetrad, but more interestingly showed the interaction of the protonated amino side chains with the negatively charged backbone (Figure 13).[45]

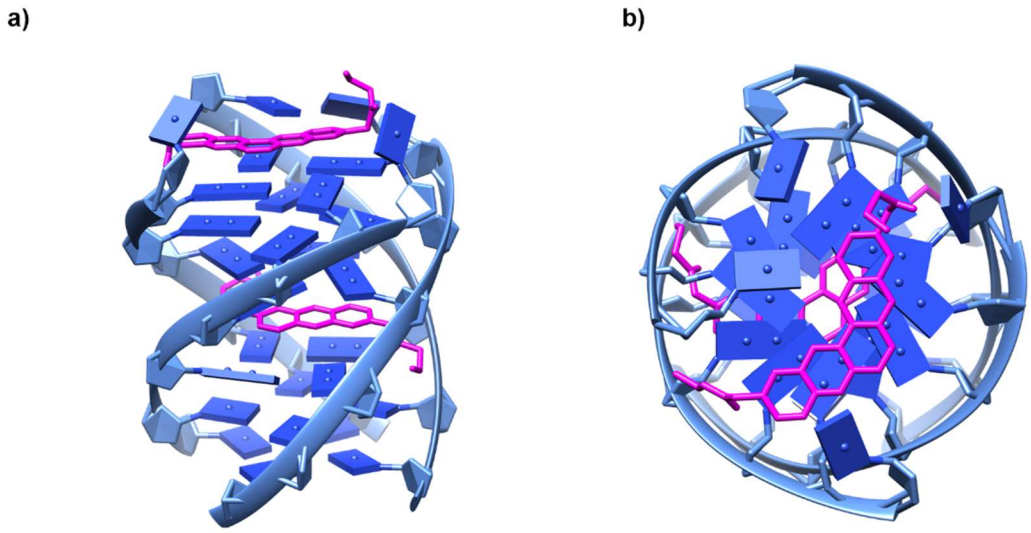


Figure 13. NMR structure of MMQ_1 (magenta) complexed with G4 DNA $(d[T_2AG_3T])_4$. (a) Side-on view, (b) Top-down view, PDB = 2JWQ.

1.4.2 Small Molecules Influence G-quadruplex Regulation in Proto-oncogene Promoters

A combination of deep sequencing and *in silico* predictions has shown that potential G4 forming sequences are over-represented in the promoter regions of many proto-oncogenes.[33,46] There have been extensive studies into designing G4-ligands to exploit this ability to downregulate oncogene transcription e.g. *MYC*.[47] *MYC* is of particular interest for targeting at the transcriptional level as its protein is considered undruggable. *MYC* is over-expressed in many cancers including breast, ovarian and non-Hodgkin's Lymphoma, making it an attractive target for cancer therapy.[48] A prominent example of such ligands are the N-methylated porphyrin structures.

N-methylated ligands are another core structure that fit the characteristics of G4 ligands. Of particular interest is the porphyrins family which was highlighted by Hurley *et al.*[49,26] In particular, the porphyrin structure TMPyP4 (**1.9**) (Figure 14) was highlighted of interest when it was shown to stabilise G4 formation resulting in telomerase inhibition.[50] TMPyP4 (**1.9**) has all the characteristics of an effective G4-ligand. TMPyP4 (**1.9**) is aromatic and planar, allowing for effective π-π stacking with the G-tetrad. Furthermore, it has positively charged methylated amine residues to interact with the negatively charged phosphodiester backbone and finally, it is bulky, allowing stacking with G4 structures but limits binding to other DNA secondary structures.

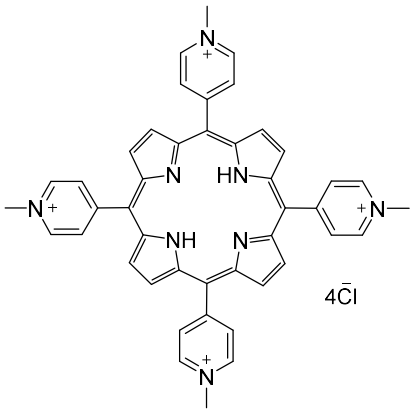


Figure 14. Structure of TMPyP4 (**1.9**).

To further scope its use as a potential therapeutic, a cDNA microarray carried out which showed downregulation of c-*MYC* as well as further downstream-regulated genes. The assay was incubated with 100 μM TMPyP4 (**1.9**) over 12, 24, 36 and 48 h before analysis (Table 1).[49]

Table 1. TMPyP4 (**1.9**) effects on gene expression.[49]

Induced Genes	**Down-regulated Genes**
Apoptosis genes	**c-MYC- associated genes**
Caspase 1	*c-MYC*
Cell signalling genes	Ornithine decarboxylase
TGF-β	CDC25A
CD47	**Cell cycle genes**
CD9	*CDK-4*
CO-29	*CDK-6*
RAB-1A	*Cyclin B1*
RAB-9	**Cell signalling oncogenes**
Proliferation association gene A	c-FOS
DNA repair genes	c-MYC
MLH1	JUN-B
ERCC5	c-MYB
	STAT1

Of particular interest in this experiment are *c-FOS* and *c-MYB*. Both genes were downregulated in the presence of TMPyP4 (**1.9**). However, they are also proto-oncogenes that possess G-rich sequences that have the potential to form G4s.[46]

TMPyP4 (**1.9**) is a particularly effective telomerase inhibitor (IC_{50} = 6 μM) and showed high stabilisation for G4s (ΔT_m = 17 °C). Further studies highlighted that its structural isomer TMPyP2 (**1.10**) (Figure 15) does not have the same effect and has limited to no effect on stabilisation, making it a useful control.[49,51,52] It was thought that the restricted rotation induced by the altered structure was the cause of inactivity. TMPyP2 (**1.10**) was ineffective at preventing G4 unwinding due to yeast Sgs1p helicase when compared with its structural analogues.[53] In this study, TMPyP3 (**1.11**) (Figure 15) induced the formation of a parallel G4 structures. Furthermore, when subjected to helicase unwinding assays TMPyP3 (**1.11**) showed the strongest inhibitory effect for parallel G4s over TMPyP4 (**1.9**). However the inverse was the case for antiparallel structures.[53] Initially studies carried out by Hurley *et al*., demonstrated TMPyP4 (**1.9**) had a 20 fold selectivity for G4s over dsDNA,[51,54] This degree of selectivity was particularly unusual given that duplex DNA is much more abundant that G4 DNA. The selectivity was biased due to the unobserved equilibria of the structure shifting between other structures, and the high K^+ concentrations in addition to the drug being analysed bias the system towards the G4. The authors' hypothesis was that once the strong binding of TMPyP4 (**1.9**) formed the G4, it would form a stable complex. Once the TMPyP4 (**1.9**) was released it would be kept in close proximity by surrounding unwound dsDNA residues thus allowing it to bind again. Supporting this mode of action is the 'trapping' of the sequence as a G4 by the tightly bound TMPyP4 (**1.9**), resulting in a biological response. However studies conducted by the Telaude-Fichou and Mergny laboratories indicated that in the presence of a dsDNA competitor, TMPyP4 (**1.9**) was poorly selective for G4s.[55,56] This contradiction may suggest that the balance between selectivity of the ligand and target sequence is very complex and is sequence and assay dependent.

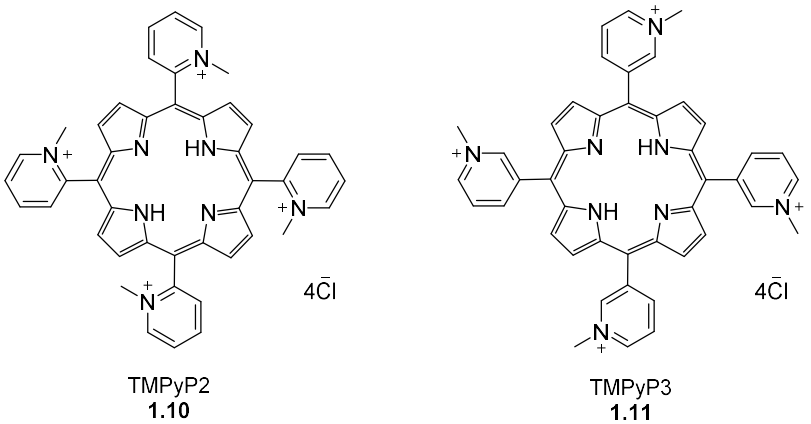


Figure 15. Structures of TMPyP2 (**1.10**) and TMPyP3 (**1.11**).

In recent years, the use of metals such as Manganese, Copper and Ruthenium has become more prevalent in the design of G4 binding ligands. The premise of having the metal centre is that it will align over the ion channel through the centre of the G4 further aiding increasing π-π interactions between the ligand and the DNA as well as their cationic centre interacting with the negatively charged backbone. The first examples included modifying the already established TMPyP4 (**1.9**) with a metal centre (**1.9a**).

Mn-TMPyP4 (**1.9**) gave approximately 10-fold selectivity to G4 over dsDNA with a decreased IC_{50} = 26 μM for telomerase inhibition (in comparison to IC_{50} = 6 μM for native TMPyP4 (**1.9**)). Pt (**1.12a**)[57] and Cu (**1.12b**) have shown promise also, however Mn(III) porphyrin showed a staggering 10,000 fold selectivity for G4 DNA over dsDNA (Figure 16).[58]

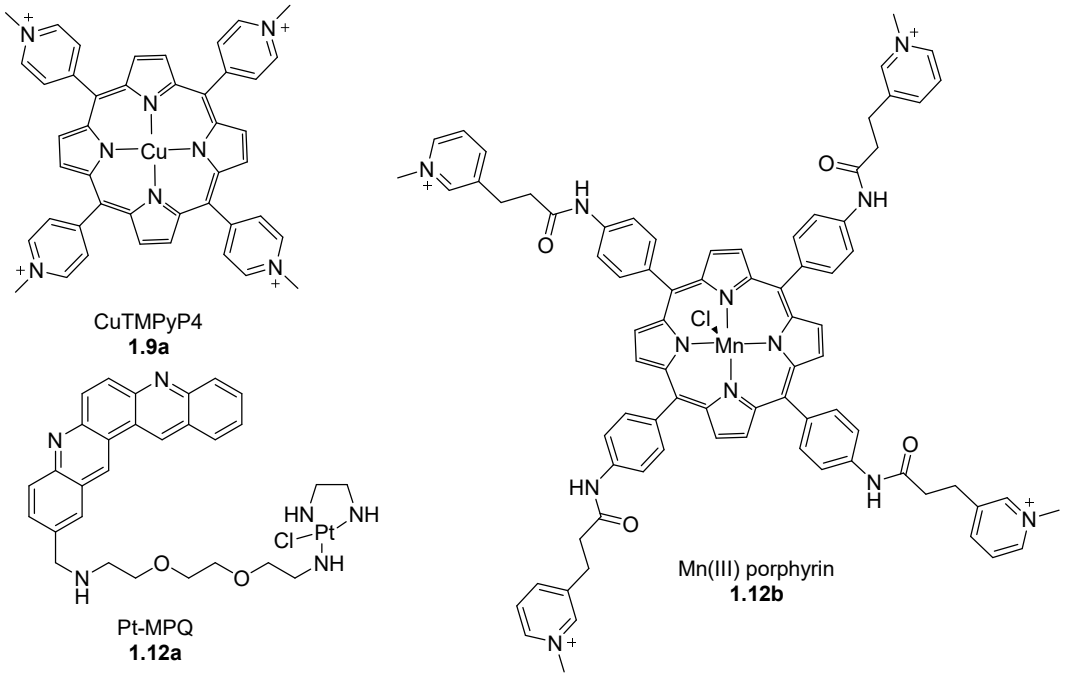
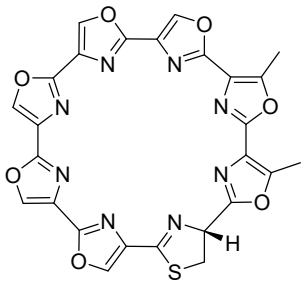


Figure 16. Structures of CuTMPyP4 (**1.9a**), Pt-MPQ (**1.12a**), and Mn (III) porphyrin (**1.12b**).

The last group consist of non-cationic ligands, which do not have any specific mode of protonation pre- or post- *in situ*. The prime example of this type is a natural product called telomestatin that has been extracted from *Streptomyces annulatus*.[55] Telomestatin (**1.13**) has been widely studied and has shown very good stabilisation of G4s (ΔT_m = 24 °C, 1 μM) and has shown a greater than 70-fold selectivity for G4 over dsDNA (Figure 17).[59,60] This high selectivity has been attributed to its neutrality, which destroys its affinity for dsDNA in addition to its circular shape which is more suited to align with a G4-tetrad. In addition to this extensive selectivity it has also shown increased activity for telomerase inhibition (IC_{50} = 5 nM) even working well in salt deficient environments. Although extremely promising, the ligand is insoluble and difficult to obtain. Although a total synthesis has been published, at present the complexity of synthesising it does not lend to widespread use.[61]



Telomestatin
1.13

Figure 17. Structure of Telomestatin (**1.13**).

1.5 Small Molecules that Bind RNA G-quadruplexes

In theory, RNA is the perfect template for a G4; its predominantly single stranded, so has no competing complimentary strand and its secondary structures have been shown to be more thermodynamically stable than their DNA counterparts particularly in a parallel G4 conformation.[62,63,64] The stability of these secondary structures is dependent on the cation used. In the case of K^+, the majority of RNA G4s studied by Hartig *et al.,* were more stable than their equivalent DNA G4s.[64] However, in comparison with DNA G4s the studies for RNA G4s are greatly outnumbered. There has been extensive work showing small molecule fluorophores interacting with RNA G4s as visualizers.[65] Although it is estimated that there are around 3000 RNA G4 motifs in the human genome, particularly in the 5′ UTR, very few published small molecules have been shown to be effective for RNA G4s.

1.5.1 Small Molecules which Bind to KRAS G-quadruplex mRNA

KRAS has been shown to be mutated in over 90% of cases of patients with pancreatic ductal adenocarcinoma.[66] *KRAS* is primarily responsible as the genetic blueprint of GTPases that regulate processed by alternating between being GTP-bound (active) or GDP-bound (inactive). When active the complex facilitates multiple biological processes e.g., differentiation, proliferation, and apoptosis. KRAS mRNA has a very G-rich 5′ UTR (77% GC) and as a result has the potential to form RNA G4s. In the first 80 nucleotides, there are three distinct domains that have the potential to form a G4 (*utr-1, utr-z and utr-c*) (Figure 18). It was thought that increasing the secondary structure abundance, especially in the 5′ UTR could regulate translation.[67]

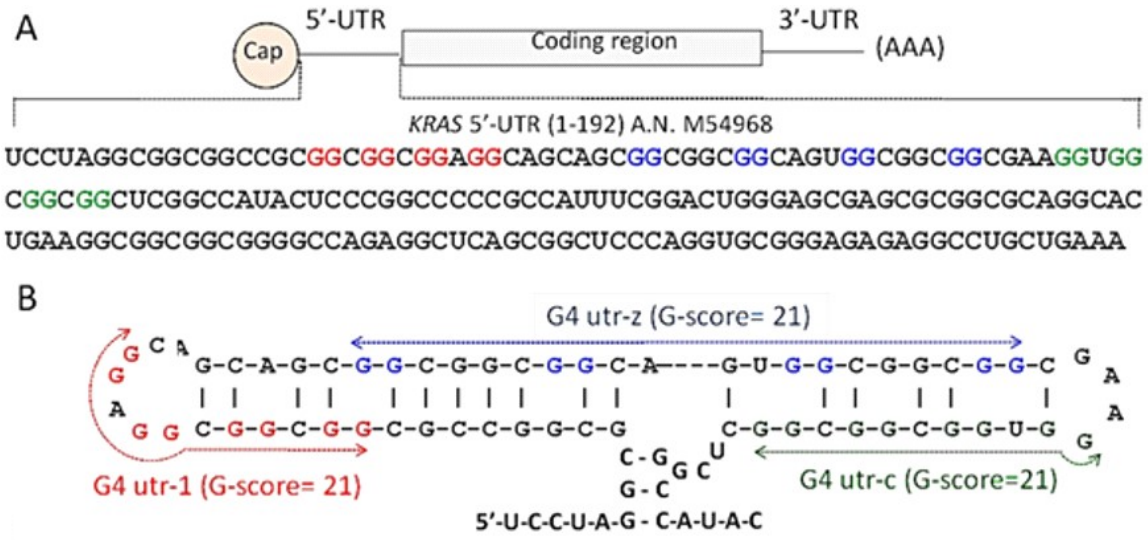
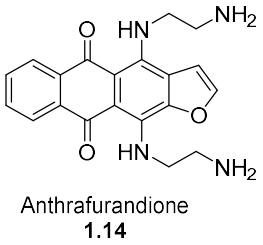


Figure 18. (a) 5′ UTR of human *KRAS*. (b) Mfold predicted structure of s-80[68] (c) Three distinct G4 forming domains in s-80: utr-1 (red), utr-z (blue) and utr-c (green). Adapted with permission.[67] Copyright 2021 American Chemical Society.

First, a streptavidin-pull down assay determined the small molecule anthrafurandione (**1.14**) could effectively target *KRAS* mRNA (Figure 19).



Anthrafurandione
1.14

Figure 19. Structure of Anthrafurandione (**1.14**).

Luciferase assays showed that not only was **1.14** an inhibitor of translation but it was suppressed in a dose-dependent manner (Figure 20).

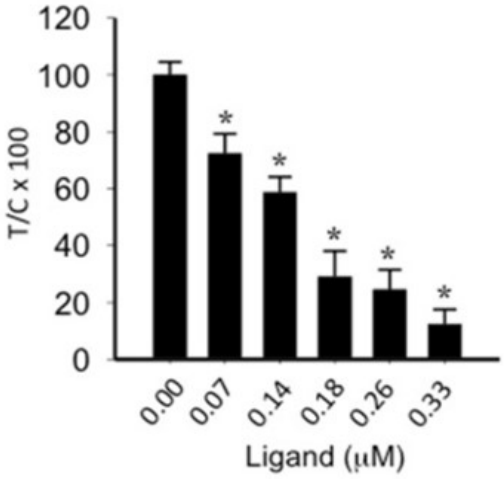


Figure 20. Anthrafurandione (**1.14**) treated PANC1 cells show a dose dependent suppression of luciferase signal up to 0.33 μM. Adapted with permission.[67] Copyright 2021 American Chemical Society.

Following this, a BG4 antibody EMSA was carried out. BG4 antibody has been determined to be specific for G4s and has since been used widely in the field as indication of G4 formation.[69, 70] Figure 21 shows binding of the antibody to the beginning 80 nt of the 5′ UTR (s-80). Whereas no complex was formed with the double stranded control, suggesting the presence of a G4 in the first section of the 5′ UTR.

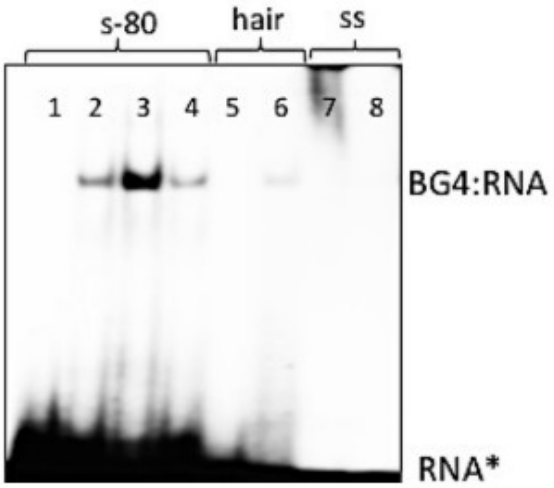


Figure 21. 5% polyacrylamide Electron Mobility Shift Assay (EMSA): s-80 (Lane 1-4) RNA hairpin (hair) 5′-GGCCGCCGCAGUGGCGGCGG (lane 5 and 6) and ssRNA 5′-UGUAAACAUCCUACACUCAGCU (lane 7 and 8). BG4 Dosage per lane: control (lane 1), 1 μg (lane 2), 2 μg, (lane 3), 1 μg in Li+-buffer (lane 4); hairpin control (lane 5), 1 μg (lane 6), ssRNA control (lane 7), 1 μg (lane 8). All mixtures ran in K^+ buffer except 4. Adapted with permission.[67] Copyright 2021 American Chemical Society.

Quantitative RT-PCR highlighted that only **1.14** had an effect on mRNA percentage, decreasing it by around 50% in comparison to the control. However, all the compounds tested **1.14**, **1.15**, **1.16** and **1.17** (Figure 22) were effective at decreasing the KRAS protein levels, with **1.14** (2a in Figure 23) and **1.15** (2b in Figure 23) being standout suppressors reducing the protein level to just 10%.

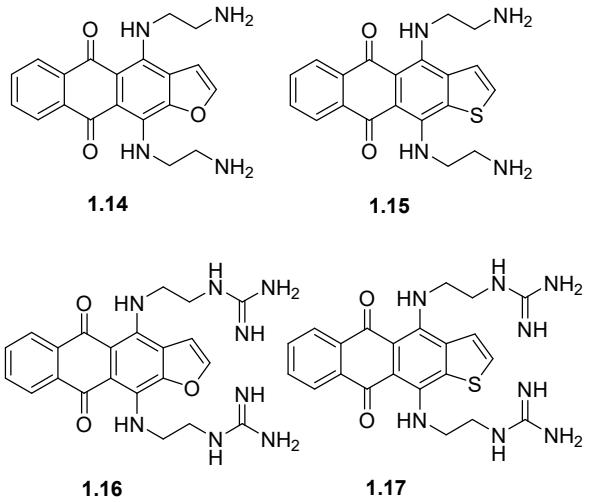


Figure 22. Structures of Anthrafurandione (**1.14**), Anthrafurandione sulphur analogue (**1.15**) and guanidine analogues (**1.16**) and (**1.17**).

It was concluded from these results that it was likely **1.14** and **1.15** are active to inhibit the translation of KRAS. Finally the activity of compounds **1.14** and **1.15** were analysed in Panc-1 cells by a reazurin assay showing IC_{50} = 0.26 μM and IC_{50} = 0.9 μM respectively, aligning with previous data showing **1.14** to be a more effective inhibitor (Figure 23).[67]

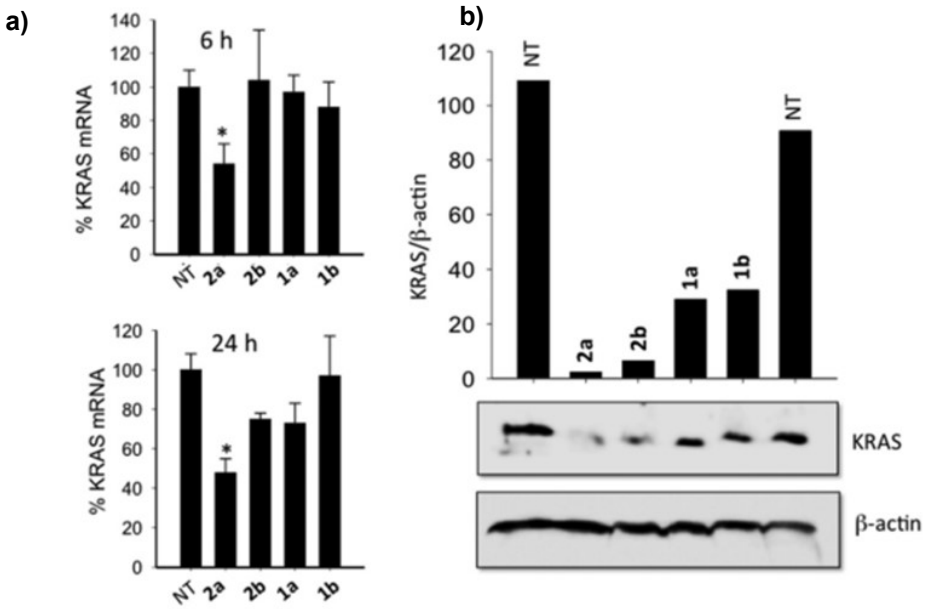


Figure 23. (a) Quantitative RT-PCR of *KRAS* mRNA. Compounds **1.14** (2a in graph), **1.15** (2b in graph), **1.16** (1a in graph) and **1.17** (1b in graph) (1.6 μM) were incubated with Panc-1 cells for 6 and 24 h (b) Western blot analysis for Panc-1 cells treated with **1.14** (2a in graph), **1.15** (2b in graph), **1.16** (1a in graph) and **1.17** (1b in graph) (1.6 μM) over 48 h. Adapted with permission.[67] Copyright 2021 American Chemical Society.

1.5.2 Small Molecules which Bind to NRAS G-quadruplex mRNA

In 2007, Balasubramanian *et al*. published the discovery of an mRNA G4 in the 5′ UTR of the *NRAS* proto-oncogene modulating translation.[71] On the basis of this work, they published the first example of a small molecule interacting with the sequence to regulate translation, three years later.[72] The 5′ UTR

of *NRAS* is now one of the more established endogenous RNA G4s which upon deletion results in an increase in translation, suggesting it has a vital role in its regulation.[73]

To begin the investigation, a set of luciferase reporter assays was developed to determine the role of the G4 sequence that they had previously determined. The first construct (NRAS UTR(+)Q) included the G4 sequence, upstream of the luciferase coding sequence beginning +14 nt from the 5′ cap. The second construct has the G4 sequence removed to be used as a control to ensure any effects observed were due the G4 sequence (NRAS UTR(-)Q) (Figure 24).[72]

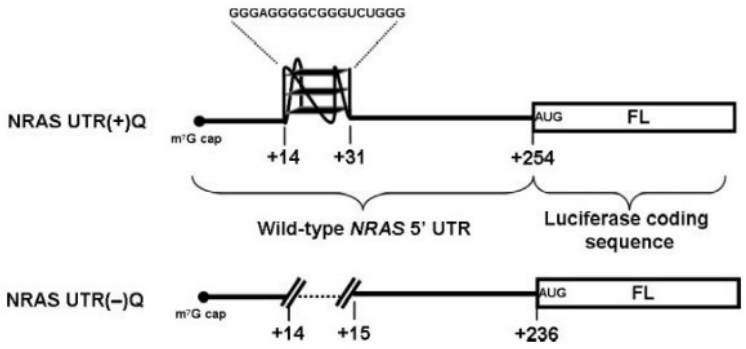


Figure 24. Luciferase reporter assays (NRAS UTR(+)Q) and (NRAS UTR(-)Q). Reprinted with permission. [72] Copyright 2021 Royal Society of Chemistry.

The group carried out a screen of their in-house library of DNA G4 ligands and found pyridostatin (**1.6**) showed a level selective inhibition of NRAS translation through the luciferase assay. Interestingly the commonly used G4 stabiliser TMPyP4 (**1.9**) showed no activity for this assay. This phenomena could be down to the ligand unfolding the mRNA as has been previously observed by the Basu laboratory in MT3-MMP G4 mRNA.[74] At low concentrations (1.25 μM), RR82 showed a decrease of just under 50% of translation in comparison to a retained 80% efficiency in the control. Incrementally increasing the dose to 10 μM showed a decrease in % translation in both (NRAS UTR(+)Q) and (NRAS UTR(-)Q) in a dose dependent manner. Even though the control was also effected as the concentration increased, this was still considered a promising result as at each concentration, (NRAS UTR(+)Q) was more effective at inhibiting translation, maintaining a level of selectivity over the control.

Following on from this result, RR110 (**1.18**), an analogue of pyridostatin (**1.6**) was tested in the translation assay. Ligand **1.18** is structurally different from pyridostatin (**1.6**) due to the replacement of one alkyl-amine side chain with a Fluorine atom. This modification proved greatly beneficial for RNA G4 selectivity up to 10 μM, where translation was inhibited by 40% but had no effect on the control (Figure 25).

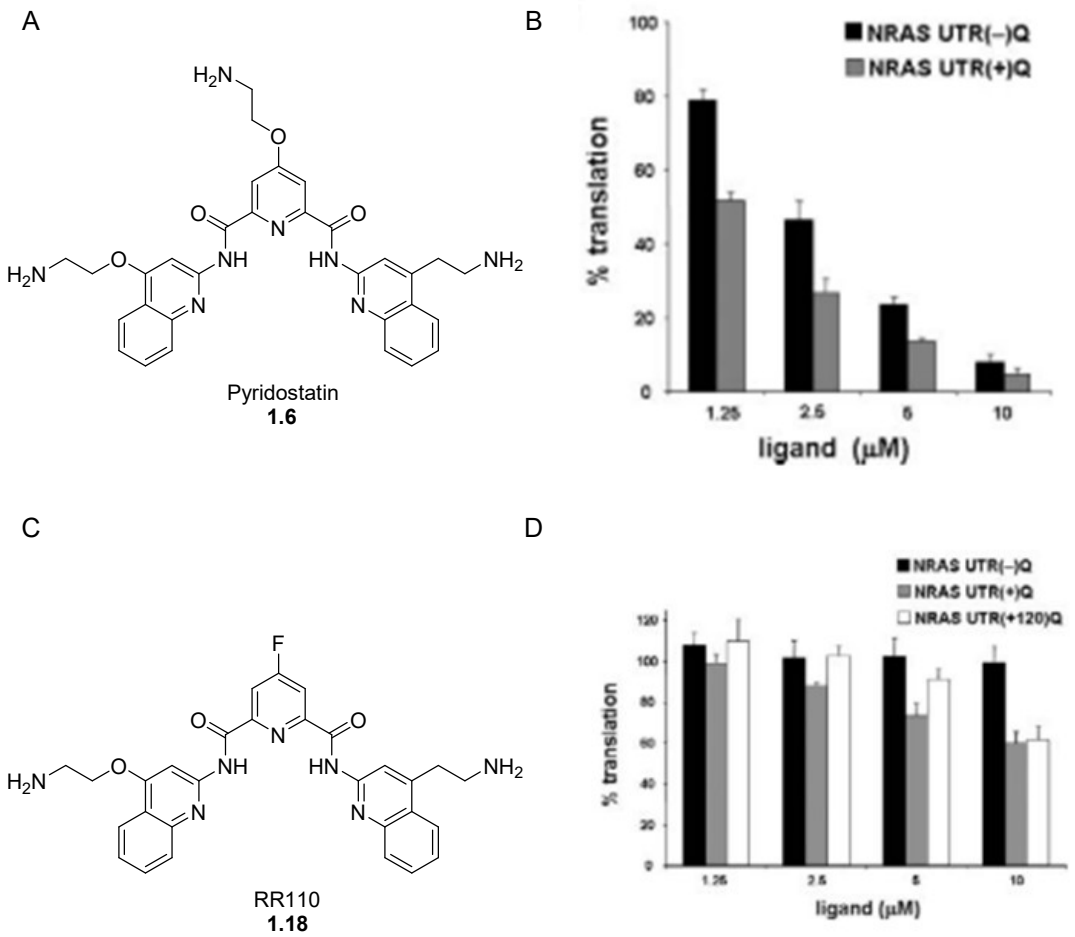


Figure 25. (a) Structure of Pyridostatin (**1.6**), (b) Effect of **1.6** on (NRAS UTR(+)Q) and (NRAS UTR(-)Q) n=3. Presented values are an average shown with standard error bars. (c) Structure of RR10 (analogue of **1.6**). (d) Effect of **1.18** on (NRAS UTR(+)Q) and (NRAS UTR(-)Q) n=3. Presented values are an average shown with standard error bars. Adapted with permission. [72] Copyright 2021 Royal Society of Chemistry.

To further confirm the selectivity seen in Figure 25 , an excess of DNA duplex or RNA hairpin was added as a competitor and showed neither were efficient at inhibiting the suppression effect of RR110 (**1.18**). In contrast, when NRQ RNA G4 was used as a competitor, the % translation was comparable to the previous controls when no RR110 (**1.18**) was added at all, suggesting the addition of a G4 competitor was effective at suppressing the RR110 (**1.18**) activity, adding further evidence that the molecule is G4 selective (Figure 26).

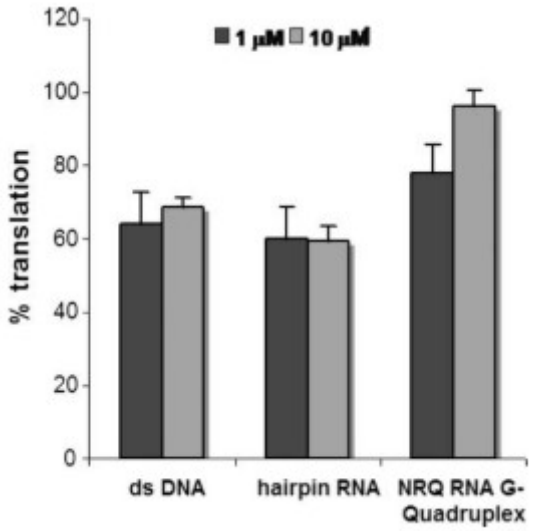


Figure 26. Translation efficiency: RR110 (1.18) added in the presence of dsDNA, hairpin RNA and NRQ RNA G4 competitors. n=3. The values shown are an average with standard error bars. Adapted with permission. [72] Copyright 2021 Royal Society of Chemistry.

^{1}H NMR titrations confirmed binding of the NRQ to RR110 as line broadening of was observed in the NRQ signals as RR110 was added (Figure 27).[72] Furthermore, chemical shifts in the imino region for NRQ suggest a close proximity effect potentially due to π-π stacking of the NRQ and the ligand. As RR110 was added, a decrease in hydrogen-deuterium exchange kinetics was observed. This was either due to the ligand having increased interactions with the H-bond network, or due to induced sequestering of the imino protons on structural change on ligand addition, slowing the proton exchange (Figure 27).

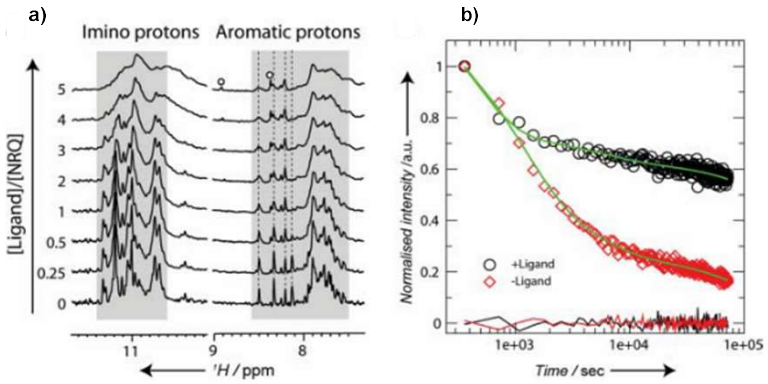
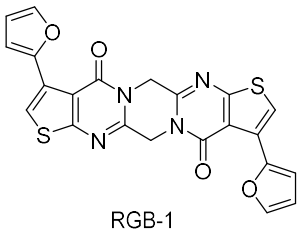


Figure 27. Interaction of RR10 (**1.18**) with RNA G4 NRQ. (a) Titration experiment: Peaks corresponding to RR10 (**1.18**) are indicated by circles. (b)Hydrogen-deuterium exchange kinetics experiment In the presence of ligand (black) in absence (red). Reprinted with permission. [72] Copyright 2021 Royal Society of Chemistry.

Following on from this work, Uesugi *et al.* reported in 2016 a G4 ligand that showed selectivity for RNA G4s over DNA. Uesugi *et al.* carried out a chemical library screen of 8000 compounds, against the model G4 sequence TERRA to attempt to highlight alternative scaffolds to the already established porphyrins and pyridostatin analogues. This screen highlighted RGB-1 as the most promising ligand with a K_d = 8.8 μM and a ΔT_m = ≥5°C.[73]



RGB-1
1.19

Figure 28. Structure of RGB-1 (**1.19**).

However when it was subjected to stem loop RNA, dsRNA and DNA G4s it showed no discernible effect on melting temperature, suggesting RGB-1 is selective for RNA G4s. When incubated with the 5′ UTR of *NRAS* in MCF-7 cells, RGB-1 caused a dose-dependent decrease of *NRAS* protein which could indicate stabilisation of a RNA G4.[73]

1.5.3 Current Challenges of Targeting RNA G-quadruplexes

Although work carried out by Balasubramanian has highlighted selectivity of RGB-1 for G4 RNA over dsDNA and DNA G4s, this is unfortunately a result currently in the minority.[72] A major limitation of the field currently is the selectivity of the current ligands for not only RNA G4s over DNA G4s, but also between competing RNA G4s themselves. This is primarily due to the structural similarities seen between G4s throughout eukaryotes.[75] Therefore, structural studies into pinpointing sites of interest for the desired biological response could pose a solution for advancing the field further towards therapeutic applications.

1.6 RNA Synthesis

As suggested by the central dogma of biology, RNA is synthesized from its parent structure DNA. DNA is comprised of repeating nucleotide sequences of Adenosine, Thymine, Cytosine, and Guanosine (Figure 3). Each of these nucleotides is comprised of a purine (A or G) or pyrimidine (C or U) base connected to a sugar at the 1′ position and one or more phosphate groups. With the assistance of a protein machine called RNA polymerase II (RNA Pol II), the RNA is synthesized in a process called transcription.

1.6.1 Transcription

Expression of a gene requires that the ‘blueprint’ DNA be converted into the functional protein that goes on to regulate processes in the body. The first step in this conversion is known as transcription and is the transfer of information from DNA to a messenger RNA (mRNA) molecule (Figure 29). Three polymerase enzymes facilitate the conversion to RNA. RNA polymerase I (Pol I) and Pol II transcribe precursor RNA to ribosomal RNA (rRNA) and non-coding RNA (ncRNAs) respectively. However, it is RNA Pol II that is responsible for the transfer of information from protein-coding genes to their corresponding mRNA sequences and subsequently to synthesize the required protein. Pol II is made up of 12 sub units and is a vital enzyme that is responsible for multiple biological processes including, but

not limited to; cell differentiation control, protein production and the cells response to environmental stress.[76,77]

Only one strand of the DNA double helix is required as a template for transcription. The strand contains three distinct regions. The coding sequence, which contains the information to be transferred. A regulatory sequence upstream of the coding region called the 5′-untranslated region (UTR) and another regulatory sequence downstream called the 3′-untranslated region (UTR).[78]

Transcription begins with the binding of promoter DNA by RNA Pol II and transcription factors. The action of binding causes a 'bubble like' shape to form as the DNA unwinds due to the breakage of the H-bonds holding the two strands together.[76] Within this bubble, the RNA Pol II sequentially adds in RNA nucleotides that are corresponding pairs to the template DNA antisense-strand.[76] This machinery moves from the 5′ to the 3′ end of the antisense strand. The enzyme adds nucleotides in sequentially, while the phosphodiester bonds that constitute the backbone of the mRNA form to complete the synthesis. The H-bonds holding the RNA and DNA in close proximity are broken and the free mRNA begins to be processed.

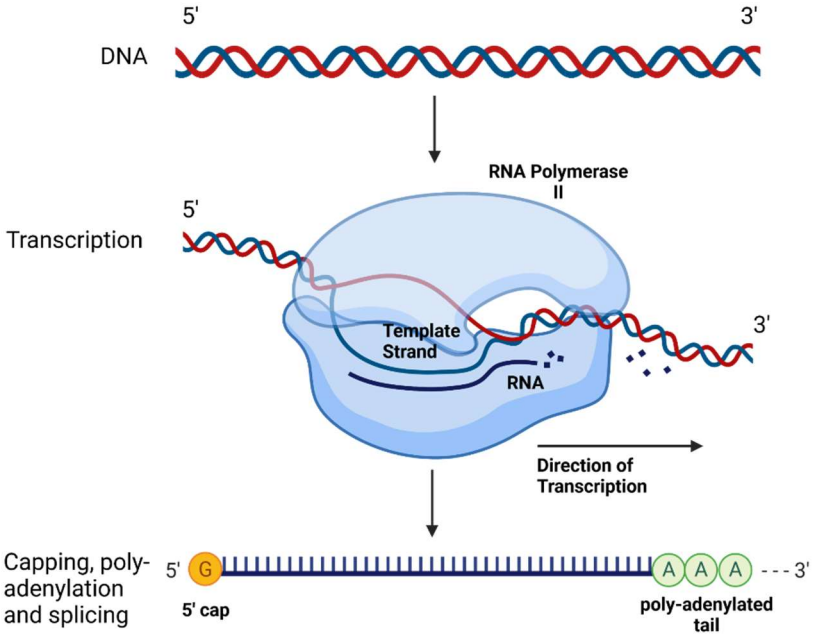


Figure 29. Schematic of Transcription. RNA polymerase II transcribes the RNA from the DNA template strand in the 5′ to 3′ direction by sequential addition of complementary nucleotides. The process is completed through 5′-capping, polyadenylation and splicing (not shown in diagram). Created with BioRender.com.

To finalize processing, the RNA goes through polyadenylation, capping and splicing. Once the transcribing is complete, the sequence downstream of the 3′ UTR is cleaved and replaced by an extended sequence of repeated adenine subunits called the poly-A tail.[79] This extended tail serves as a protection mechanism against RNA degradation as well as nuclear export. Stability of the 5′ end is facilitated by the 5′ cap which consists of a guanine nucleotide with a 5′ to 5′ triphosphate bond in place of the standard

5′ to 3′ making it more stable to 5′ degradation.[80] Unlike polyadenylation and capping, splicing serves to increase protein diversity instead of modulating stability or transport through the cell. Splicing is the process that determines the coding sequences that are joined together and which are removed from the final RNA transcript. This ‘mix and matching’ of coding regions of the mRNA is the main source of protein diversity in the human body.[81]

1.7 RNA Splicing

RNA splicing is a rich source of genetic diversity within higher eukaryotes.[82] Genes with sequences of coding and non-coding DNA are known as split genes. Split genes are transcribed into long pre-mRNA transcripts containing coding and non-coding regions called exons and introns, respectively.

The pre-mRNA construct goes through the process of splicing, which excises the non-coding introns and joins the coding exons together (ligation). Splicing is a carried out by two sequential transesterification steps of S_N2-like reactions (Figure 30). The first transesterification is nucleophilic attack of the 5' splice site (SS) phosphodiester bond by the 3' hydroxyl of the branch point Adenosine. This leaves the hydroxyl of the 5' exon free to attack the phosphodiester bond at the 3'SS. These two reactions effectively cleave out the intron, *via* the ‘Lariat structure’ formation, and ligate the 5'SS and 3'SS to form the mature mRNA.

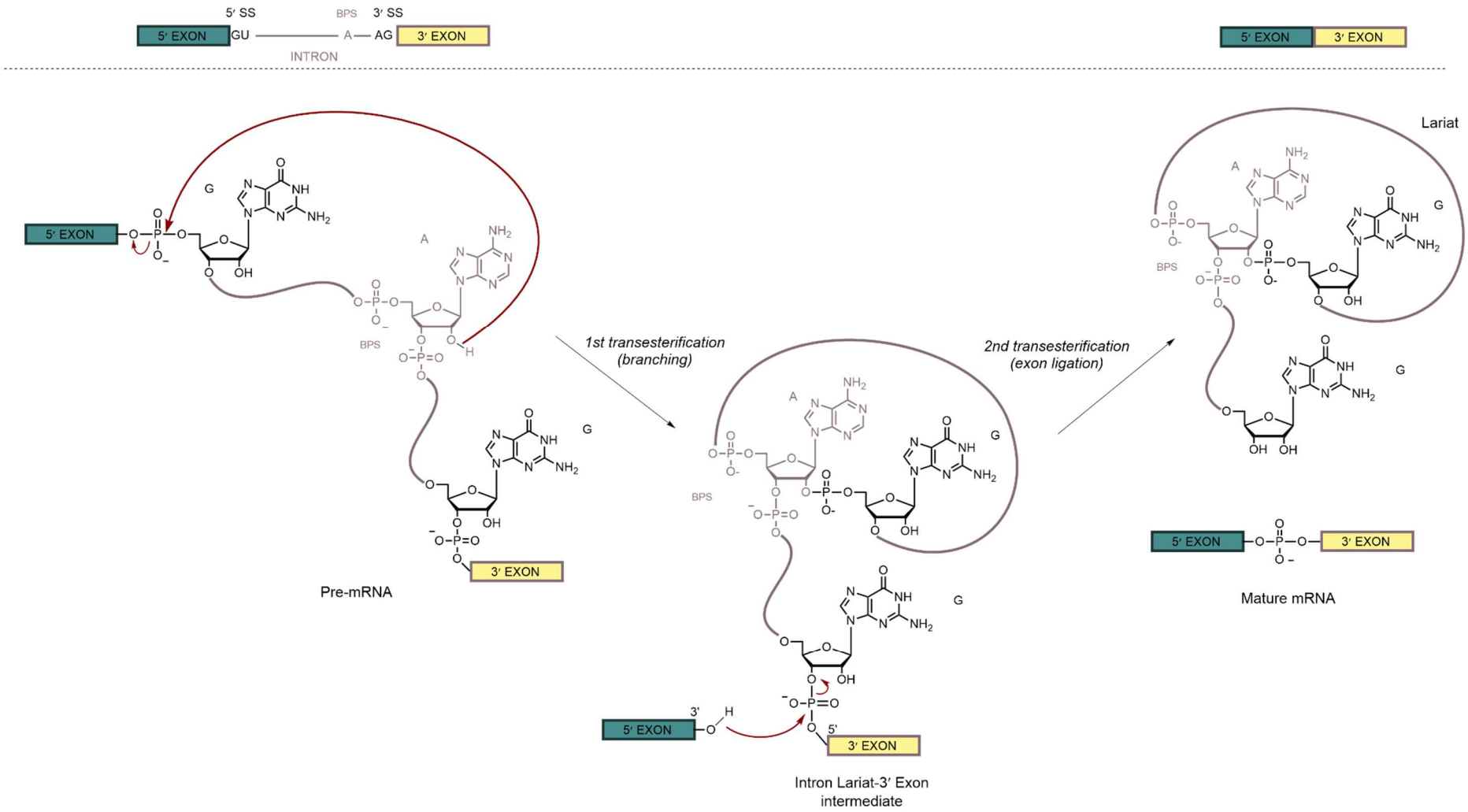


Figure 30. Transesterification splicing reactions: Branching: 2′-hydroxylgroup a conserved adenine residue in the branch point sequence (BPS) attacks a phosphate of the guanine at the 5′end of the intron. Exon ligation: The produced 3′-hydroxyl group at the 3′end of the 5′-exon attacks a phosphate at the 3′splice site (3′-SS) to ligate the exons and release the lariat intron.[83]

1.7.1 The Spliceosome

The spliceosome is a molecular machine which facilitates the excising of introns from pre-mRNA transcripts.[84] It is constructed of small nuclear RNAs (snRNAs) and ~ 80 proteins, in particular the small nuclear ribonucleoproteins (snRNPs) U1, U2 and U4-6 (denoted as U due to high uridine content). The spliceosome is constructed over a number of steps in sequence (Figure 31).[84] Formation is initiated by recruitment of snRNP U1 to the 5' GU sequence in the intron. This binding acts as a marker for the point of excision. Following this, snRNP U2 is recruited to bind to the branch point A completing the prespliceosome complex A and marking the boundaries of the sequence that is to be excised.[85] Additional snRNPs U4/6 and U5 bind to complex A to form a catalytically inactive form of the spliceosome, complex B. Although complex B contains all the necessary components required to initiate the first transesterification, the complex undergoes conformational rearrangements to become the active complex B*. This rearrangement includes the dissociation of U4 and U1, which are recycled to form complex B in the next cycle. The first transesterification can then occur, instigating formation of the Lariat structure, to form complex C. The second transesterification reaction commences after further rearrangements, which excises the non-coding intron and produces the ligated exons as mRNP (mRNA bound by proteins).[84] The remaining snRNPs U1, U5 and U6 are released back into the splicing cycle to aid in the next set

of transesterifications. Each of these steps has relatively weak binding interactions, and are stabilized by supporting proteins e.g. SR proteins, and are powered by ATP interactions.

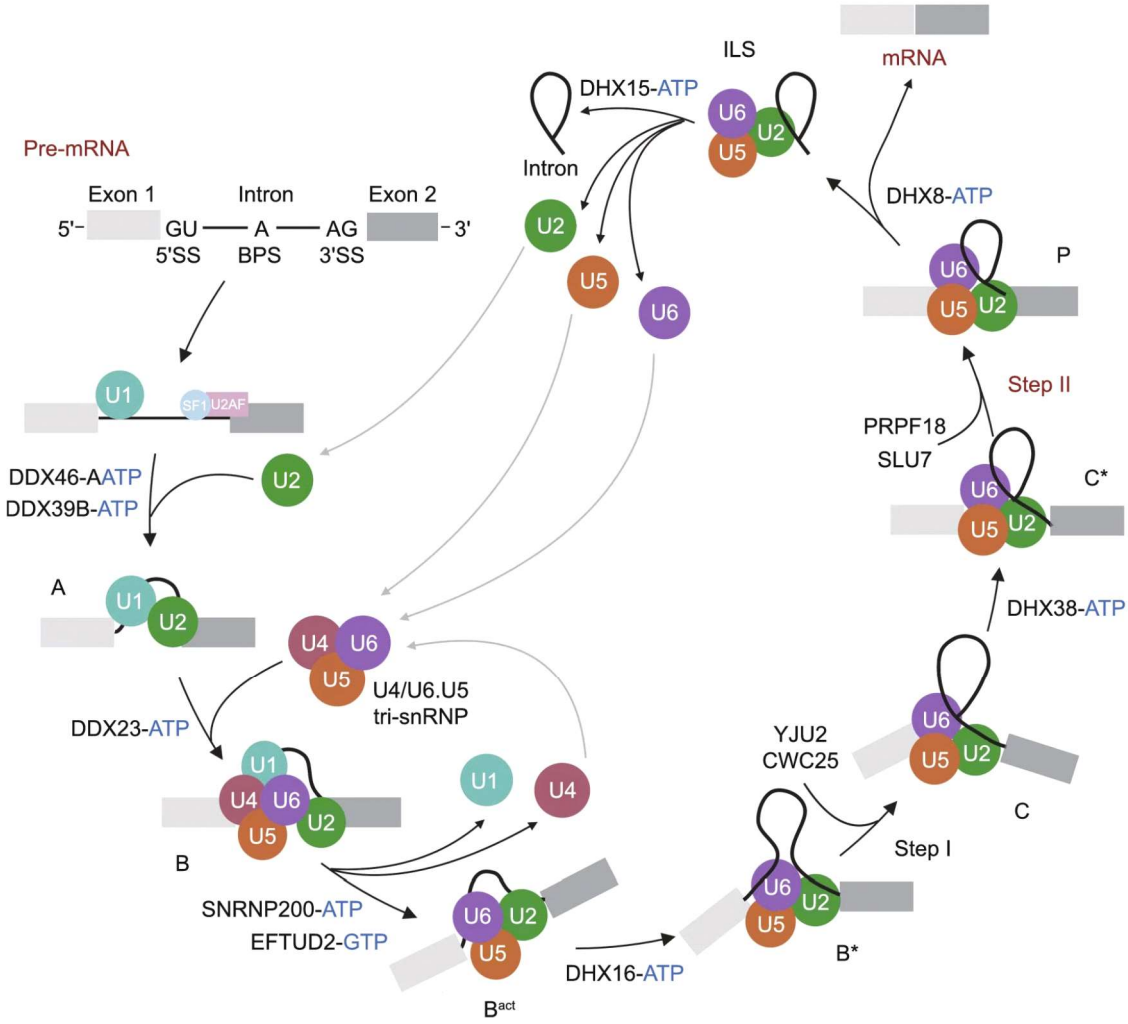


Figure 31. Formation and function of the spliceosome through the splicing cycle. Licensed under CC BY 4.0.[86]

1.7.2 Splice-Site Selection and Role in RNA Splicing

Splice-site (SS) selection primarily mediated by spliceosome recognition. Points of recognition along the pre-mRNA include the 5' SS and 3' SS positioned at the intron-exon boundaries, the branch site, and the polypyrimidine tract (PPT), which is upstream of the 3' SS.[87]

SS selection is mediated by the control of snRNP binding at the 5' SS and 3' SS. Binding of snRNP U1 to the 5' SS and of U2 binding to the 3' SS can be either disturbed or promoted to augment selection of the splice site by the spliceosome. Regulation is further obtained by short sequences within the exons and introns that bind additional splicing facilitator proteins. These binding sites

are arranged into four categories, governed by their impact on splicing and the region on which they act: intronic splicing enhancers and silencers (ISEs and ISSs) and exonic splicing enhancers and silencers (ESEs and ESSs).[88]

1.7.3 Exonic Splicing Enhancers (ESEs)

ESEs are vital to the successful progression of pre-mRNA splicing. ESEs are RNA sequences contained within an exon that facilitate recognition of the correct splice site *via* interaction with specific proteins that are arginine and serine rich (SR proteins).[89] Once SR proteins bind to ESEs; they initiate formation of the spliceosome by recruiting the snRNPs U1 and U2AF to the pre-mRNA (Figure 32). Once bound, snRNPs U1 and U2 determine the sites due to be spliced - the 3' SS and 5' SS respectively. In particular, ESEs are involved in the formation of the lariat structure by increasing the availability of U2 snRNPs. Additionally, SR proteins promote the binding of snRNPs U4-U6, to further spliceosome formation.

1.7.4 Exonic Splicing Silencers (ESSs)

Conversely, ESSs are sequences that silence regions for splicing and facilitate alternative splicing sites (Figure 32). They are typically 4 – 18 nucleotides long and recruit proteins that inhibit the progression of splicing.[87] Unlike ESEs interacting with SR proteins, ESSs interact with heterogeneous ribonucleoprotein particles (hnRNPs) that are involved with the blocking or skipping of the correct splice sites.[90] Protein recruitment by ESSs can interrupt the machinery of splicing by inhibiting snRNP (U1 and U2) binding and promoting the use of alternative splice sites.[90] This is particularly important as atypical splicing, or alternative splicing, has the potential to instigate a number of genetic diseases.[91]

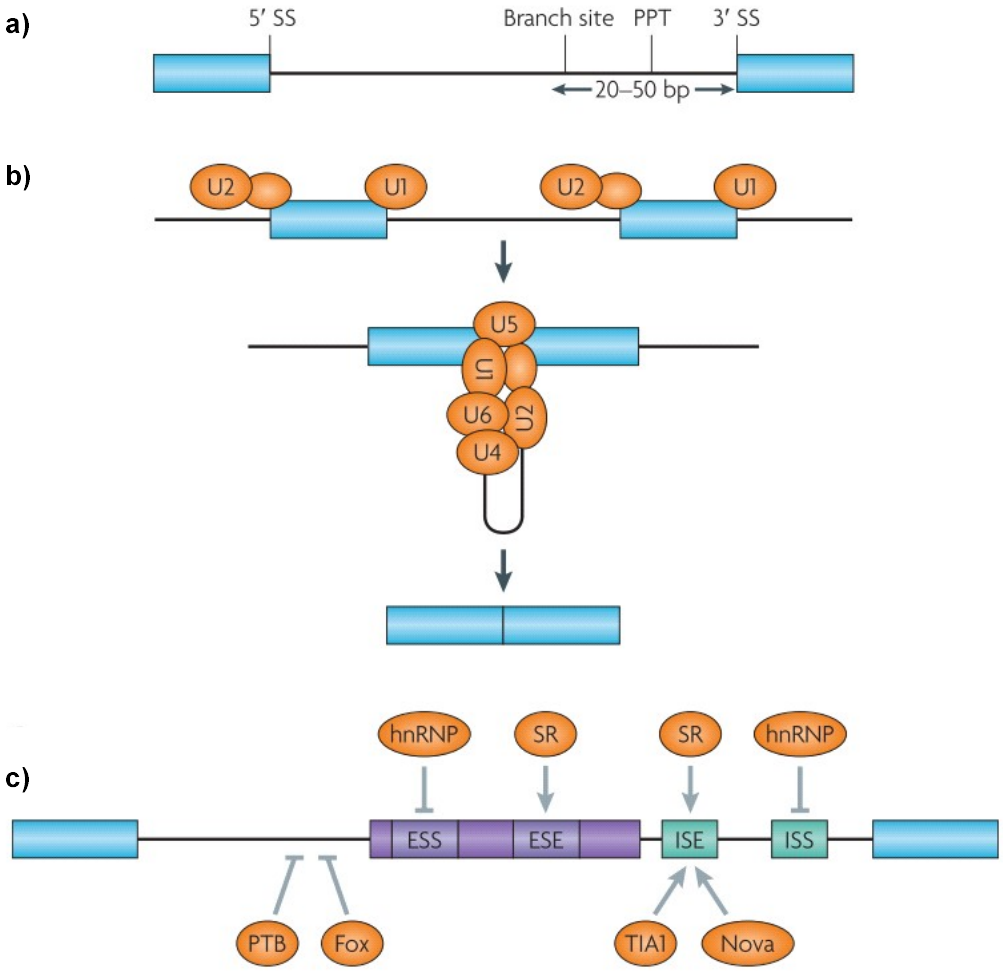


Figure 32. (a) pre-mRNA splicing transcript (b) binding of Uridine rich snRNPs at SSs, recruitment of U5 and U4/6 to form spliceosome complex, and subsequent ligation of exons (c) Depiction and location of splicing facilitator structures including associated enhancer proteins and intron/exon sequences that enhance or silence splicing. Reprinted with permission.[87] Copyright 2021 Springer Nature.

1.8 Alternative Splicing

Splicing is most commonly seen as *cis*-splicing, where the exons are spliced together in order of their sequence and all exons originate from the same pre-mRNA transcript (Figure 33-Protein A).[92] However, within this splicing mechanism there can be great diversity from alternative splicing.

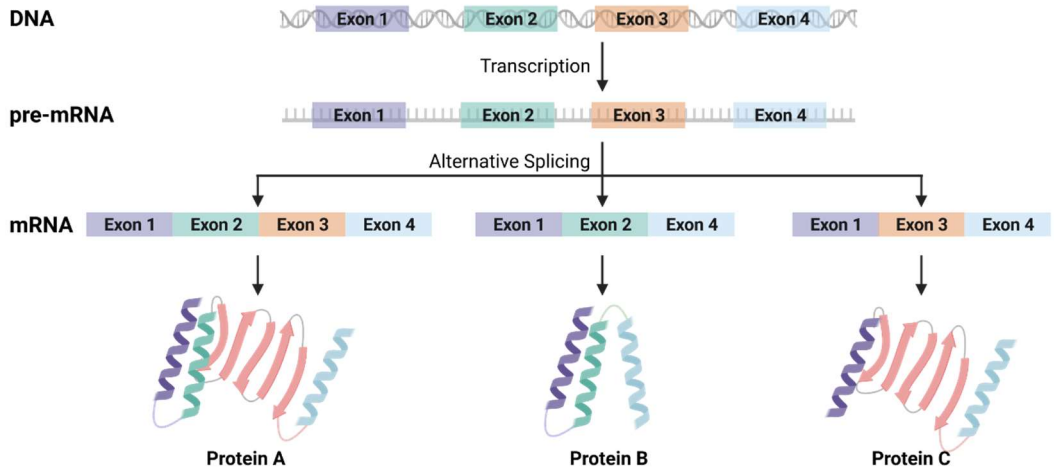


Figure 33. Potential splicing mechanisms of the same pre-mRNA transcript. Protein A has been transcribed by cis splicing, Proteins B and C have been alternatively spliced through exon skipping of exon 3 and exon 4 respectively.[93] Created with BioRender.com.

Alternative splicing events are common with studies showing 90-95 % of multi exon human genes producing transcripts that have been synthesized via an alternative splice site.[94] There are five main categories of alternative splicing processes (Figure 34). Exon skipping is the most common and results exon excision from the pre-mRNA transcript where it should be retained (Figure 34a).[87] Mutually exclusive exons are a variation of exon skipping where only one of two exons excised, but never both (Figure 34b). Furthermore, there are alternative 5' and 3' acceptor sites (also known as alternative 5' SS and 3' SS) (Figure 34c and d). These are both upstream of the native 5' SS and 3' SS of the pre-mRNA transcript and can be promoted by supplementary protein or ligand binding. The least common type of alternative splicing seen in mammals is intron retention and results in an intron, which typically is excised by the spliceosome, being retained in the final transcript (Figure 34e).

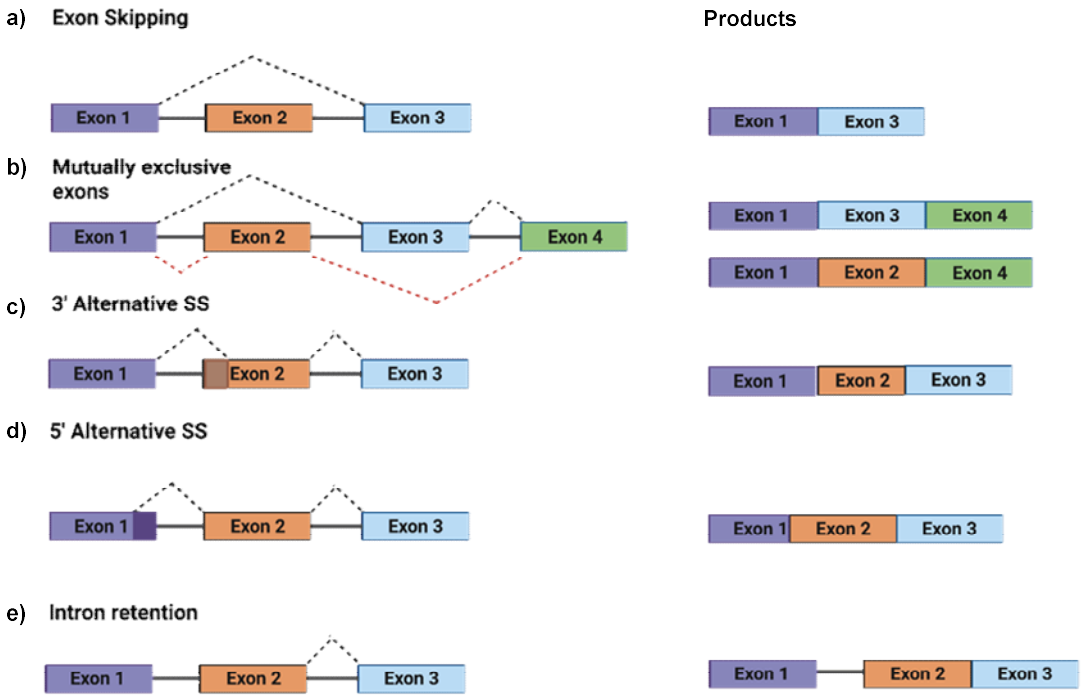


Figure 34. Five primary mechanisms for pre-mRNA alternative splicing. Created with BioRender.com[87]

1.9 Aberrant Splicing Processes and Disease

Alternative splicing is a great source of diversity within organisms. It is no surprise that there are many diseases that can arise from aberrant splicing e.g. cancer and genetic disease.[81] As alternative splicing is so prevalent in disease formation, extensive studies have been carried out to attempt to understand the process and develop treatments.[78,81] As a result, three main strategies have developed as therapies for these diseases: Antisense therapy, splice-switching oligonucleotide (SSO) therapy and small molecule therapy.

1.9.1 Antisense Oligonucleotide Therapy (ASOs)

Antisense oligonucleotide (ASO) therapy targets diseases where the gene responsible is known. When the mRNA from a gene is transcribed it is a single stranded construct; for the active protein to be translated it must remain single stranded.[95] Antisense therapy uses antisense oligonucleotides, usually 8-50 base pairs in length, to bind the mRNA to inhibit its translation into the disease causing protein. This effectively inactivates the gene. Additionally, the ASO may be designed to bind to a specific splice site, which will then interfere with the abnormal splicing that results in disease by changing which exons are retained. There are three categories of ASO

therapy: affecting recruitment of RNaseH, splicing modification and targeting of microRNAs (miRNA) (Figure 35).

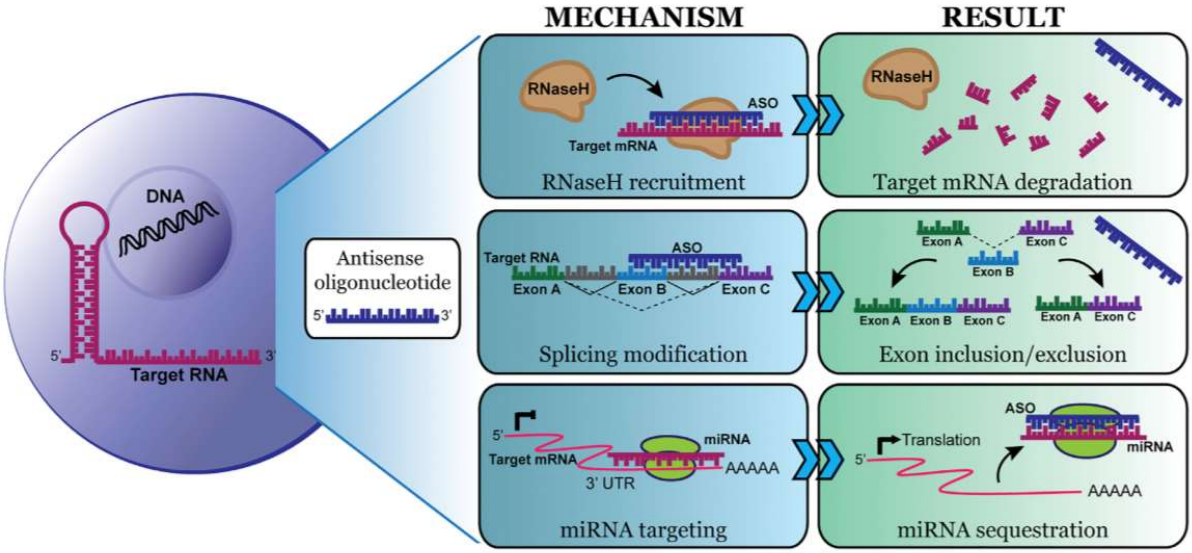


Figure 35. ASO mechanism of action. Reprinted with permission. [95] Copyright 2021 Cell Press.

Target mRNA degradation works by destroying the mRNA sequence that promotes disease formation. It is facilitated by the binding of the target mRNA sequence by a complementary ASO. The act of binding recruits an RNaseH enzyme which then cleaves the target mRNA, thereby treating the cause of potential disease.[96] Another mechanism is *via* ASO binding of a sequence of miRNA that is required for successful translation. The final mechanism involves the complementary ASO binding to the pre-mRNA construct to promote/sequester alternative splice sites to promote exon inclusion or excision.[97]

The specific mode of action governs the design of the ASO. Although this appears to be, an advantage with respect to specificity of binding as there is a level of control within design, ASO therapy has been plagued by toxicity and off-site effects regardless. Each ASO is designed for a specific disease/sequence and complications arise, as each system must then be considered separately as toxicity will be unique to each system. In particular, ASO systems that lower protein levels present unknown challenges and dangers that could arise from over suppression, resulting in on-target toxicity. Although ASOs are designed to be target specific, there will no doubt be some 'overlap' elsewhere in the genome, opening up the door to off-target toxicity. Finally, each ASO is regarded as a foreign body, which can lead to an inappropriate immune response. Despite

these challenges, development of these types of therapies is proving promising, particularly in the development of splicing modification.

1.9.2 Splice-Switching Oligonucleotide Therapy (SSOs) - Spinal Muscular Atrophy

Spinal muscular atrophy is a fatal muscle wasting disease that arises from a faulty gene, *SMN1*, which encodes the SMN protein that is responsible for the viability of motor neurons.[98] It is the greatest cause of genetic infant mortality (1 in every 10,000 live births have the disease).[99] SMA stems from a deficiency of a widespread protein, SMN, leading to body-wide muscle atrophy. *SMN2* is another gene responsible for SMN protein production. Most people affected by SMA have a faulty *SMN1* gene, leaving *SMN2* as the sole provider of the protein. SMN2 is almost identical to *SMN1* except for a common mutation is present in exon 7 of the *SMN2* gene (C6U) that changes an ESE into a silencer (Figure 36).[98] This substitution results in exon 7 skipping when *SMN2* is spliced resulting in the most predominant protein formed being the non-functioning SMNΔ7, which leads to SMA.

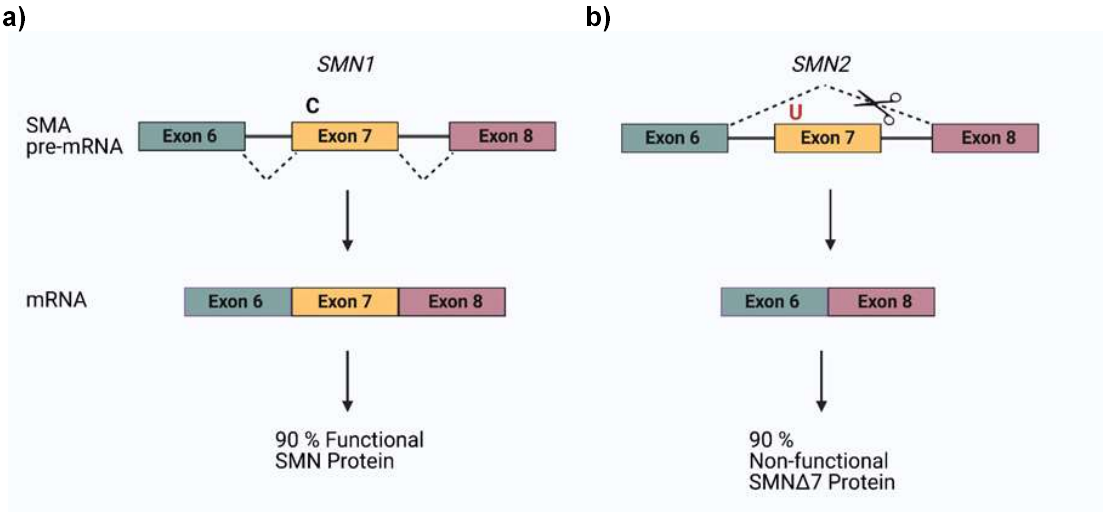


Figure 36. Expression of Spinal Muscular Atrophy: (a) *SMN1* produces 90% functional protein but is damaged or missing in SMA patients, (b) Poorly functioning *SMN2* (only 10% functional protein produced), Created with BioRender.com.

Ultimately, the exon 7 skipping observed in SMA causes disruption to essential protein production. The disease varies from patient to patient and can be subcategorized into 5 main types (Type 0 – 4). Type 4 is this least severe and mild symptoms present themselves in early childhood, the life expectancy of a patient with type 4 is thought to be relatively unaffected by the disease. Type 3, is more severe and presents itself, before the patient is 18 months. Although the disease appears earlier, and the symptoms are more severe than type 3, patients can continue to walk and survive into adulthood. Type 2 also appears before 18 months, however is distinguished from type

3 by the patients inability to walk. Type 1 is the most severe case in living patients where respiratory support is needed and the life expectancy is only 2 years. Type 0, the most severe of all results in the patient's death before birth.[100]

A mechanism to combat this exon skipping could have promising therapeutic applications, as *SMN 2* is present in all SMA patients. This hypothesis was confirmed with the discovery of the ISS-N1, a 15 nt sequence which was shown to modulate the exon skipping.[101] Splice-switching oligonucleotides (SSOs) were developed to regulated this inhibition in SMA patients. This was eventually developed to create the SSO Nusinersen (marketed as Spinraza) which acts by modulating alternative splicing, blocking the binding of hnRNP proteins to an ISS site (ISS-N1 targeting SSO) (Figure 37).[102] ISS site binding by hnRNP proteins promotes exon 7 skipping in SMA, and so blocking this action promotes inclusion of exon 7 and thus production of full length SMN RNA and subsequent protein production. In trials, injections of Nusinersen stopped the progression of SMA in 60 % of affected infants with SMN type 1. As of December 2016, the drug became the first FDA approved drug for the treatment of SMA.[103]

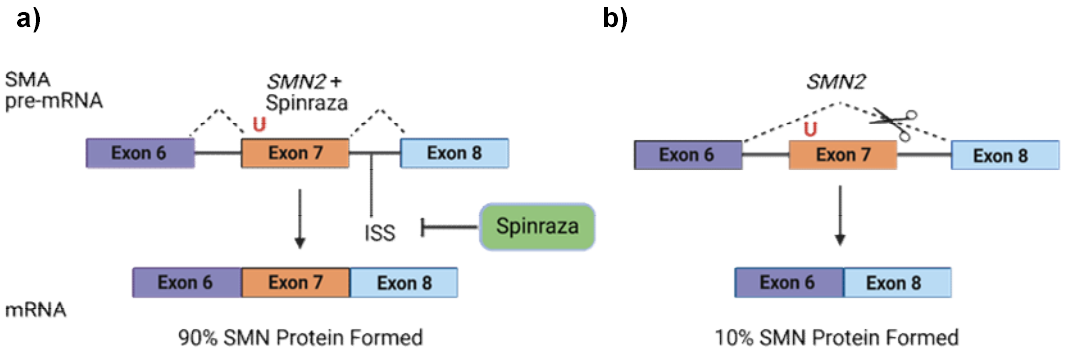


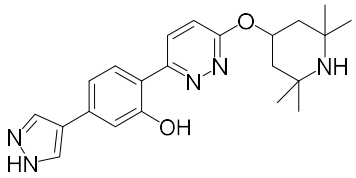
Figure 37. Schematic of the process of SMA development from gene regulation. SSO Spinraza is a treatment that targets splicing mechanisms to enhance SMN protein production. Created with BioRender.com

Although Spinraza was undoubtedly a significant breakthrough for not only SMA but for the wider splicing research community, it was not without its drawbacks. The large molecular weight of ASOs leads to poor distribution throughout the body meaning administration is an invasive injection through the spinal cord. Development of small molecule drugs became the next focus of investigation, to improve bioavailability and thus use less invasive administrative techniques.

1.9.3 Splice-Switching Small Molecules

There is currently an intense push to develop small molecules, which induce a splice-switch in SMA to enhance SMN protein production. The most prominent examples to date have been published by Novartis and PTC therapeutics, partnered with Hoffmann-La Roche.[2,104]

Novartis designed a small molecule called NVS-SM1 Branaplam, a pyridazine derivative, which is currently in phase II clinical trials for SMA type I (Figure 38). Branaplam was found to not only increase the SMN protein levels in mice but also extended their lifespan, and additionally protecting their neuro-muscular circuit.[104]



Branaplam
1.20

Figure 38. Structure of Novartis compound Branaplam (**1.20**).

Computational studies were carried out to determine the mode of action, and it was observed that the small molecule was able to stabilise the complex between the 5'SS and the U1 snRNP. This stabilisation was able to increase SMN protein levels by increasing the inclusion of the normally excised exon 7.[105] Through computational modelling of this interaction by analysis of 2D NMR in comparison with the published crystal structure of U1 (Figure 39). It was found that stabilisation from the molecule was only effective once the complex was formed.

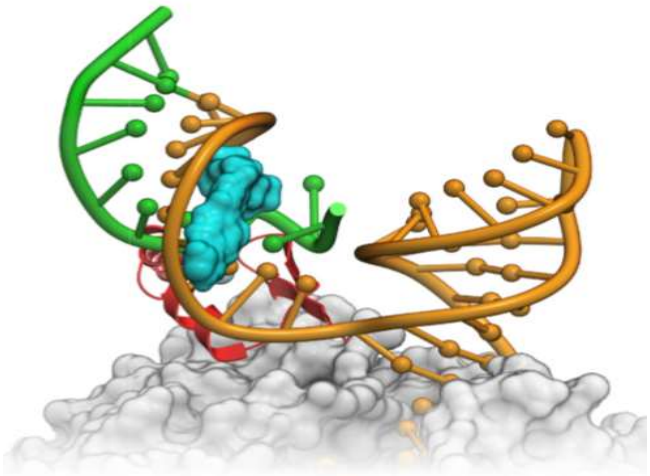


Figure 39. Computational model of Novartis compound interacting with U1 crystal structure. Reprinted with permission.[105] Copyright 2021 Springer Nature.

Hoffman-La Roche and PTC Therapeutics have developed the most successful molecules. A HTP-Luciferase assay screen of small molecules highlighted three small compounds for further investigation for drugging splicing (SMN-C1-3) (Figure 40). SMN-C3 (**1.23**) proved to be the most promising showing increased target specificity on SMA fibroblasts (type 1).[104]

PTC-Roche then began the process of designing analogues of SMN-C3 (**1.23**) to develop a drug suitable for the clinic. The first drug put through clinical trials was RG7800. Unfortunately, the trial was terminated as the drug proved to cause permanent off-target damage to the retina in monkeys.[106]

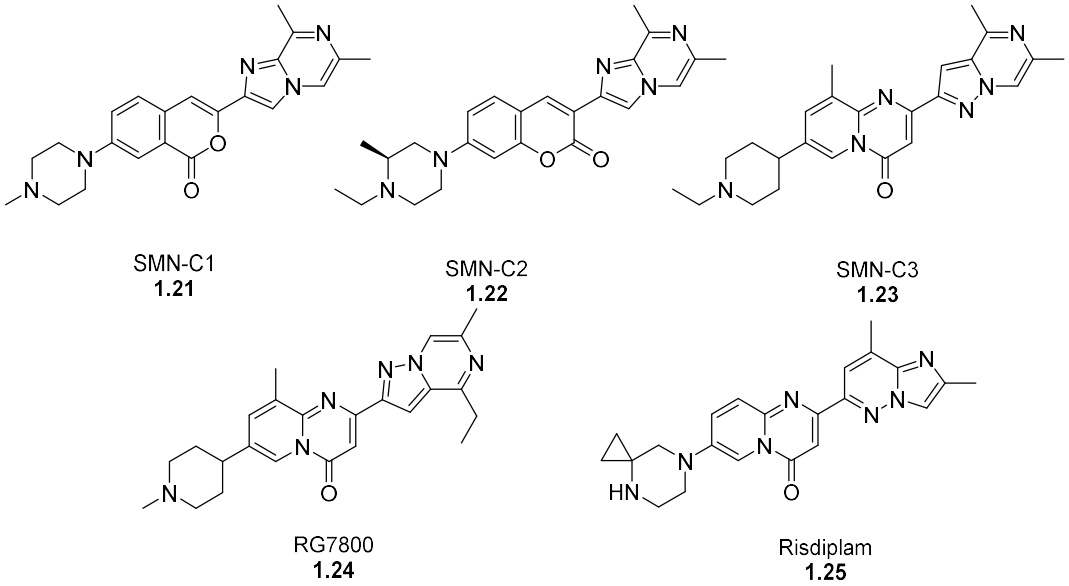


Figure 40. Structures of Roche/PTC therapeutics compounds SMN-C1 (**1.21**), SMN-C2 (**1.22**), SMN-C3 (**1.23**), RG7800 (**1.24**), Risdiplam (**1.25**).

The next generation of drugs developed provided the RG7800 (**1.24**) analogue Risdiplam (**1.25**) which showed improved biological properties and was more selective in SMA fibroblasts than its predecessor RG7800 (**1.24**) (Figure 40).[107] Risdiplam was successful through clinical trials and was approved by the FDA in August 2020.

At present, the precise mode of action of Risdiplam (**1.25**) remains unclear. Studies carried on its predecessor SMN-C3 (**1.23**) suggest interaction with an AGGAAG sequence present in exon 7. Upon binding to this region, recruitment of splicing factors (FUBP1 and KHSRP) was increased, and was proposed to promote exon 7 inclusion.[108] Another study carried out by Hoffman La Roche proposed that binding of this AG rich region inhibits the recruitment of hnRNP G, which has been previously shown to be important in exon 7 inclusion through interaction with ESE2.[2]

In 2018, Schultz and Johnson investigated the splicing activity of SMN-C2 (**1.22**) and SMN-C3 (**1.23**) with SMA RNA.[108] Through the design of a diazirine-SMN-C2 biological probe, pull down experiments discovered a purine-rich binding sequence (AGGAAG) which was remarkably similar to ESE2.

The Allain lab through NMR-analysis investigated a fluorinated analogue (SMN-C5). These studies highlighted a binding interaction between SMN-C5 and 54A (Adenine) in a U1 snRNA: 5′ SS complex. It was proposed that the stabilisation of this complex improved the interaction of a previously hindered U1-C zinc finger with the complex through the minor groove (Figure 41).[109]

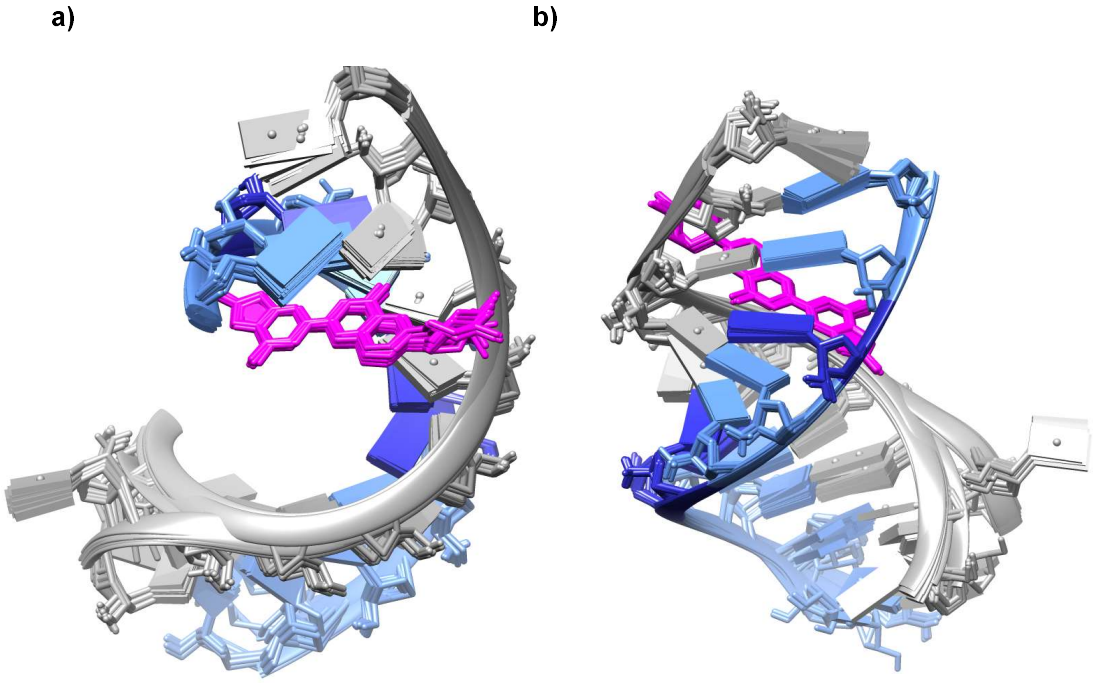


Figure 41. 20 NMR structures overlaid of the interaction of U1 SnRNA (grey), E7 5′SS (cornflower blue) and SMN-C5 (magenta). Adenosines are highlighted in dark blue in E7 5′SS sequence.[109]

Although significant steps have been made in determining the interaction of the SMN-C class drugs with SMN, limited investigation has been carried out with Risdiplam itself, and instead with analogues with a similar core.

The question stands, if small molecules are effective in treating SMA by modulating splicing, can the same be achieved in other splicing-induced disease?

1.10 Bcl-2 and Regulation of Apoptosis

The B-cell lymphoma 2 (Bcl-2) family of proteins is responsible for the regulation of programmed cell death, or apoptosis, as part of a healthy cell cycle and are located on the outer-membrane of the mitochondria.[110] They are produced from the transcription and translation of the Bcl-2 gene located on chromosome 18 in humans. Bcl-2 derives its name from being one of a number of protein families that have a substantial impact on the development of lymphoma.

Bcl-2 proteins are known regulators of apoptosis in the cell cycle by promoting the production of cytochrome c and reactive oxygen species (ROS), both vital signals within the cycle. Apoptosis is the body's safeguard against cancer development as any pre-cancerous cells are signalled to enter the cell-death pathway. However, if the pathway is damaged and abnormal cells are allowed to propagate unchecked cancer can quickly develop. In particular, different isoforms of a Bcl-2 protein, Bcl-x, have been seen to be upregulated in certain cancers, e.g. prostate cancer.

1.11 Bcl-x and its Role in Apoptosis

Bcl-x, a member of the Bcl-2 protein family, has been shown to be upregulated in some cancers, and it is present in two isoforms Bcl-x_L and Bcl-x_S. These isoforms arise from alternative splicing between two splice sites; 5' x_S and 5' x_L.[111] Splicing at the 5' x_L splice site provides the pathway to Bcl-x_L, the longer isoform containing all four BH domains. Bcl-x_L codes for an anti-apoptotic response, promoting cell growth and proliferation. Conversely, splicing at the 5' x_S splice site results in the shorter Bcl-x_S which lacks the BH1 and BH2 domains seen in Bcl-x_L. Bcl-x_S codes for the pro-apoptotic response, which initiates a cascade to cell death (Figure 42).

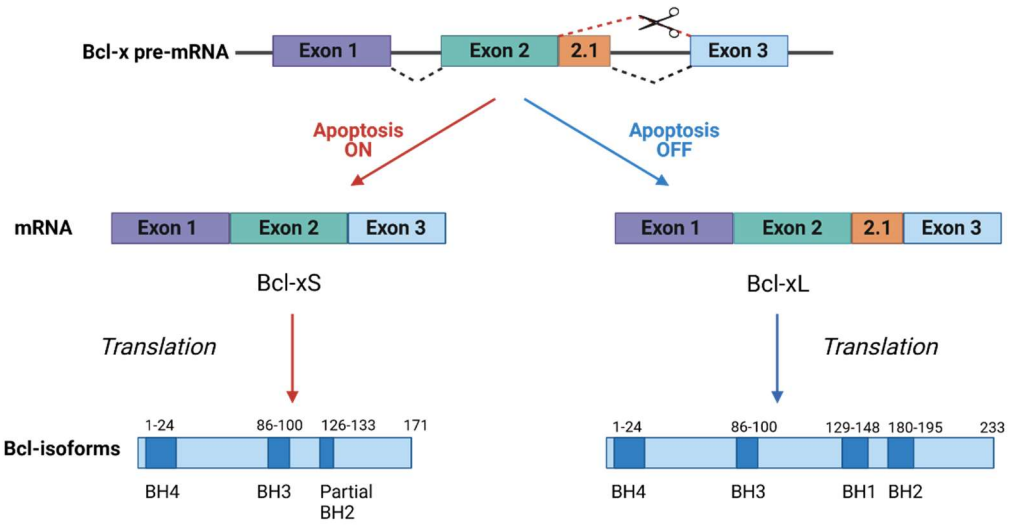
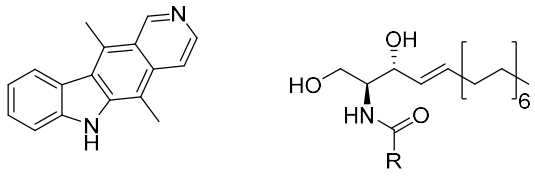


Figure 42. Possible splicing pathways of Bcl-x, towards two splicing isoforms: the pro-apoptotic Bcl-x_S and the anti-apoptic Bcl-x_L. Created with BioRender.com.

The Bcl-x pre-mRNA pathway is of interest because if it is possible to bias the ratio of Bcl-x_S: Bcl-x_L in favour of the pro-apoptotic pathway in cancer cells then this pathway can be utilised effectively as a novel cancer therapy. Certain families of drugs have already been discovered to influence this ratio. Ceramides, a family of lipid molecules, have been shown to bias the system towards Bcl-x_S alternative splicing in adenocarcinoma cell lines.[112] Alkaloids have also proven to

increase production of the Bcl-x_S pre-mRNA; in particular, the analogues of a known DNA intercalator, Ellipticine (**1.26**) (Figure 43).



Ellipticine
1.26

Ceramide
1.27

Figure 43. Structure of Ellipticine and Ceramide (R = alkyl chain of fatty acid).

1.12 Evidence for G-quadruplex Formation in Gene Promotor Regions *in vivo*

Research into the formation of G4s is predominantly carried out *in vitro. In vivo* identification of G4s are more challenging as their formation is in competition with binding proteins in addition to an equilibrium bias towards less strained secondary structures. [30] Many Guanine-rich sequences also have the potential to form multiple G4 structures of different sizes and different nucleotide loop lengths. This ambiguity makes analysis of the G4 structures difficult, meaning certain constraints are required to identify them through a combination of techniques. NMR analysis has been used to identify the more stable DNA G4s, using circular dichroism and DNA footprinting to confirm their presence *in vitro*.[20] However, these techniques prove more challenging *in vivo* as a result of conformational heterogeneity. Therefore, evidence for G4 presence *in vivo* must be deduced from less direct methods. If analysing the DNA sequence itself is not possible, investigating the presence of enzymes and proteins that have important interactions with the G4 is used to provide evidence to their formation. Currently, there are a paucity of techniques available to confirm their formation *in vivo*, particularly in reference to RNA G4s. A working hypothesis is that the abundance of Guanine rich sequences, and thus potential G4 formation, found close to regulatory regions in the cell, e.g. RNA SS, suggests that G4 formation is important in cell signalling and regulation.

1.13 Investigating the Structure of Bcl-x-681

Difficulties in analysing pre-mRNA structures arises in part due to the extensive length of the construct and its propensity to form multiple structures *in vivo.* To circumvent this, Eperon *et al.* developed a novel technique: footprinting of long 7-deazaguanine-substitutued RNAs (FOLDeR). This method demonstrated that a modified sequence of Bcl-x, denoted as Bcl-x-681 (Figure 44), forms G4s under biological conditions.

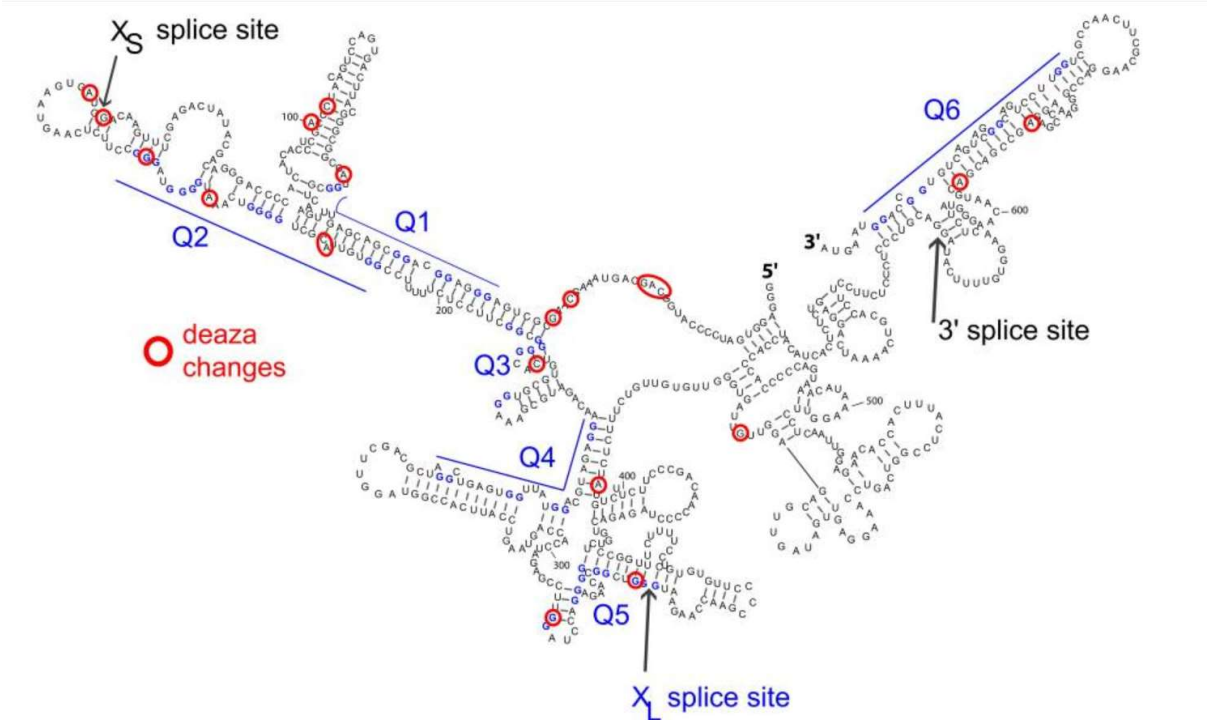


Figure 44. RNA footprinting proposed construct of Bcl-x-681.

Previous studies on the formation of G4s have focused their analysis on short sequences of RNA that have been picked from a longer pre-mRNA construct, or use ligands that target G4s. However, these methods fall short of biological conditions as G4 formation in the full pre-mRNA faces competition from other stable secondary structures. The binding of proteins or small molecule ligands may also bias the structure towards or away from the G4.

The FOLDeR technique analyses an entire pre-mRNA construct by comparison of the native pre-mRNA with its 7-deazaguanine counterpart. As seen in Figure 45, guanine N7 is required for the formation of the tetrad in G4s. As a result, the 7-deazaguanine structure can no longer form G4s; however, its ability to form other secondary structures remains unchanged (Figure 45).

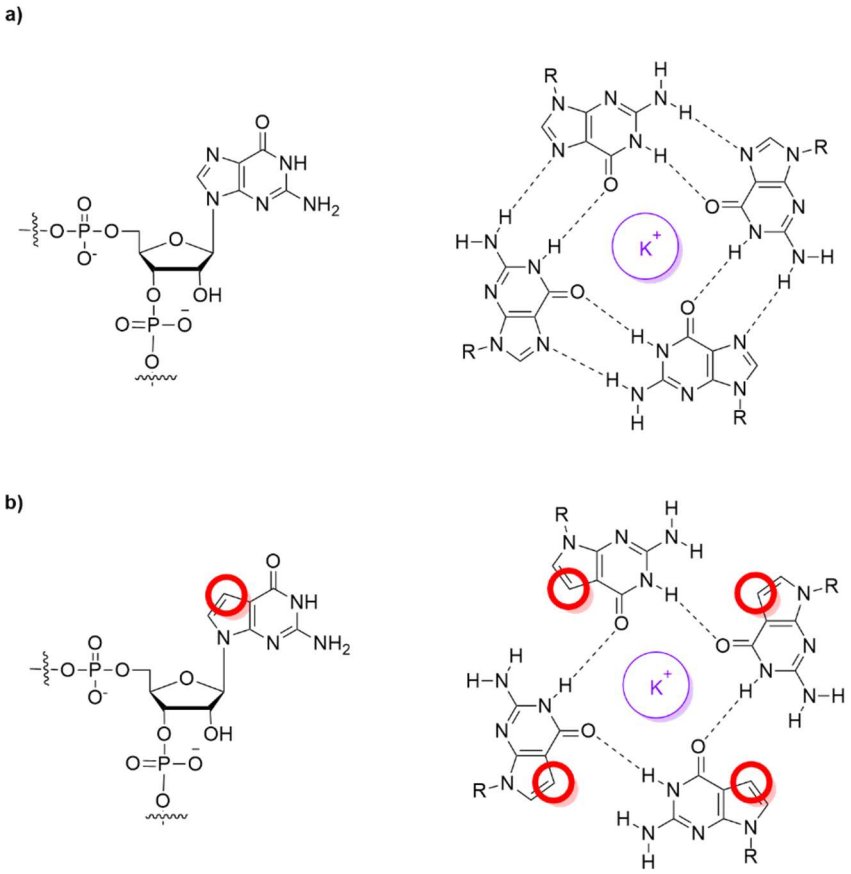


Figure 45. (a) Guanosine phosphodiester backbone and the formation of a G4 tetrad through Hoogsteen base pairing, facilitated by N7 H-Bonding. (b) 7-Deazaguanosine cannot form a stable G4 tetrad as the removal of N7 disrupts the Hoogsteen base pairing.

By comparing footprinting analyses, it is possible to determine areas where G4s may form. Bcl-x was chosen as it contains a number of G-rich sequences close to its alternative splice sites and it is anti-apoptotic isoform Bcl-x_L is upregulated in a number of cancers, e.g., prostate cancer.

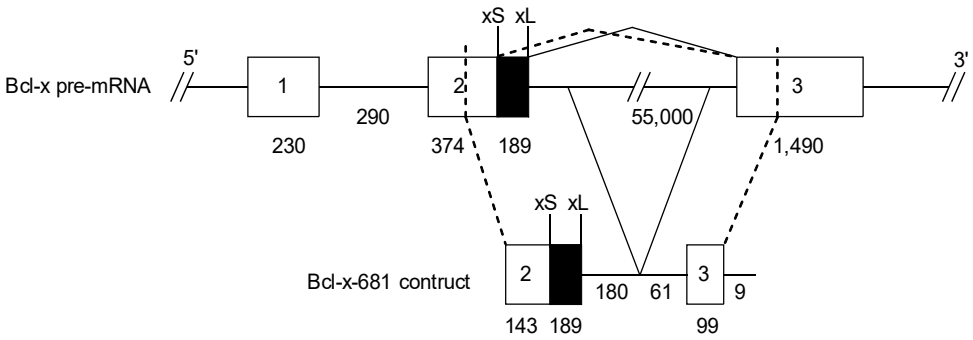


Figure 46. Schematic of alterations carried out to downsize pre-mRNA Bcl-x to Bcl-x-681.

Bcl-x-681 was made as a functional version of the native Bcl-x. The intron between exon 2 and 3 is 55,000 nt, which makes the entire sequence too long to be studied effectively *in vitro*. To

circumvent this without losing integrity of the construct, the intron was shortened from 55,000 nt to 241 nt and exon 3 shortened to 99 nt (Figure 46). However, the sequence between the x_L and x_S SSs was conserved as these regions were seen as the point of interest. The entire sequence was shortened from 57,573 nt to 681 nt, and this new sequence showed a bias towards Bcl-x_L when subjected to splicing assays, confirming that the functionality of the sequence remained the same after alteration.

Initially, circular dichroism was carried to determine the presence of G4s. All of the potential G4 forming sequences (Q1-Q6) showed a positive signal at 265 nm and a negative signal at 240 nm, consistent with what is seen in parallel G4s.[3] However, this analysis does not give an accurate representation of their formation in the presence of competing interactions.

Therefore, the structure of Bcl-x-681 was structurally mapped by RNA footprinting (Figure 44) which depicted four structurally different domains (x_L, x_S, the intron and 3' SS) all of which were transcribed independently and showed similar footprint patterns to the native RNA. The footprint patterns of the 7-deazaguanine transcripts were compared to the native Bcl-x-681 footprinting patterns by calculating an index factor for each nucleotide. Changes due to 7-deazaguanine substitution greater than two standard deviations from the mean were deemed to be significant. It was found that the Q2 and Q5 regions contained many nucleotides fitting this change in standard deviation, suggesting that G4s form in regions, which are in close proximity to the 3' SS and 5' SS. The advantage of FOLDeR over other techniques is it can be successfully carried out in nuclear extracts, as it does not require the addition of K^+ or Na^+ buffers. RNase H cleavage was carried out on both constructs, revealing sequestered regions in the both x_S and x_L compared to the 7-deazaguanine construct.

1.14 Ellipticine Analogues as Small Molecule G4 Stabilisers

Known stabilisers of G4s are typically planar in structure and it has been found that the inclusion of basic extended alkyl side chains increases activity.[20] Alkaloids in particular, such as derivatives of quindoline, have been shown to have substantial anti-proliferative activity in the down-regulation of MYC in cancer cell lines.[113,114] If G4 formation at splice sites promotes apoptosis, stabilising that pathway could lead to an effective anti-proliferative response for cancer cells.

In 2011, Hurley *et al.* demonstrated that quindoline and ellipticine analogues could down regulate *MYC* in non-Hodgkin's lymphoma through interaction with a DNA G4 (Figure 47). The majority of initiation of *MYC* transcription (80 – 90 %) occurs in the upstream promoter region, which contains the nuclease hypersensitive element (NHE),[2] III_1, which is an upstream GC-rich promoter

region that binds transcriptional factors. As the region is GC rich it has been shown to fold into a G-quadraplex (G4) structure.[113] This sequence of DNA is highly dynamic, which if stabilized by a small molecule could be used to address *MYC* overexpression in cancer cells through G4 formation.[48]

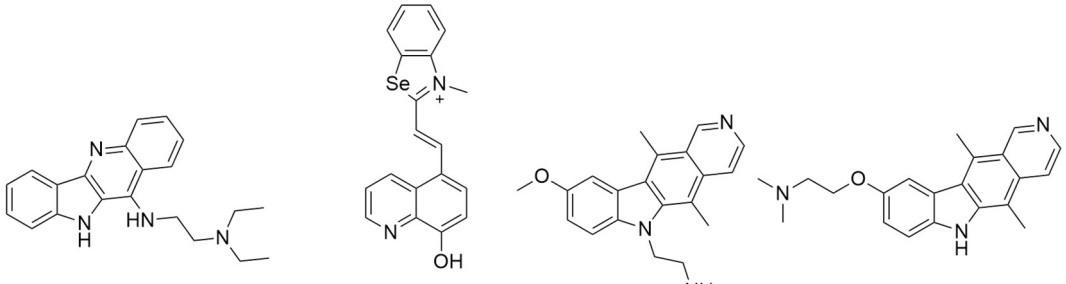


Figure 47. Structures of Quindoline i (**1.28**), NSC86374 (**1.29**), NSC176327 (**1.30**) and GQC-05 (**1.31**).

Following on from this discovery, in 2017 Eperon *et al.* investigated a range of G4 ligands for their effect on alternative splicing in the pre-mRNA of Bcl-x, including the known MYC down regulator, GQC-05 (**1.31**).[115] Splicing assays carried out showed that the known G4s stabilising scaffolds Pyridostatin (**1.6**),Quarfloxin (**1.32**), and TMPyP4 (**1.9**) (Figure 48), had no discernible effect on the selection of the splice site in Bcl-x (Figure 49).[20,115]

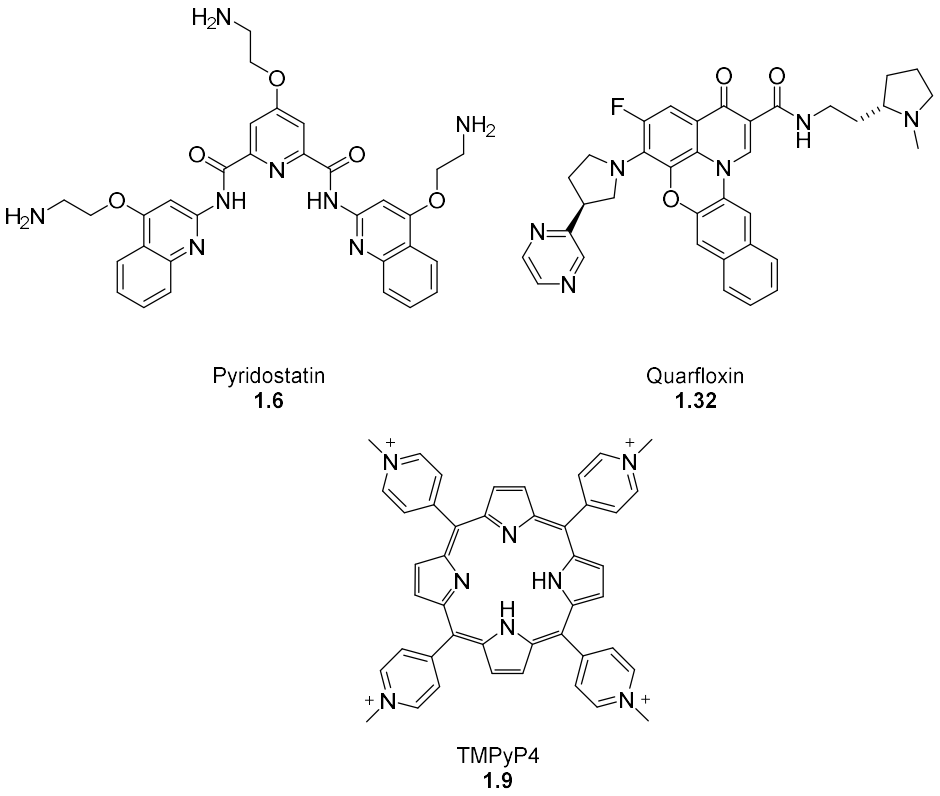


Figure 48. Structure of G4 binding ligands Pyridostatin (**1.6**), Quarfloxin (**1.32**) and TmPyP4 (**1.9**).

However, a distinct splice-switch towards the Bcl-x_S isoform was observed with GQC-05 (**1.31**) (Figure 49). Interestingly, at a 10 μM concentration, GQC-05 (**1.31**) showed increased splicing for Bcl-x_S with no change to Bcl-x_L, but when increased to 40 μM, not only did splicing for Bcl-x_S increase but splicing for Bcl-x_L also decreased resulting in a 65 % increase of selection for the pro-apoptotic Bcl-x_S 5' SS. This study highlighted ellipticine analogues as potential probes for anti-cancer candidates by manipulating the alternative splicing in Bcl-x.

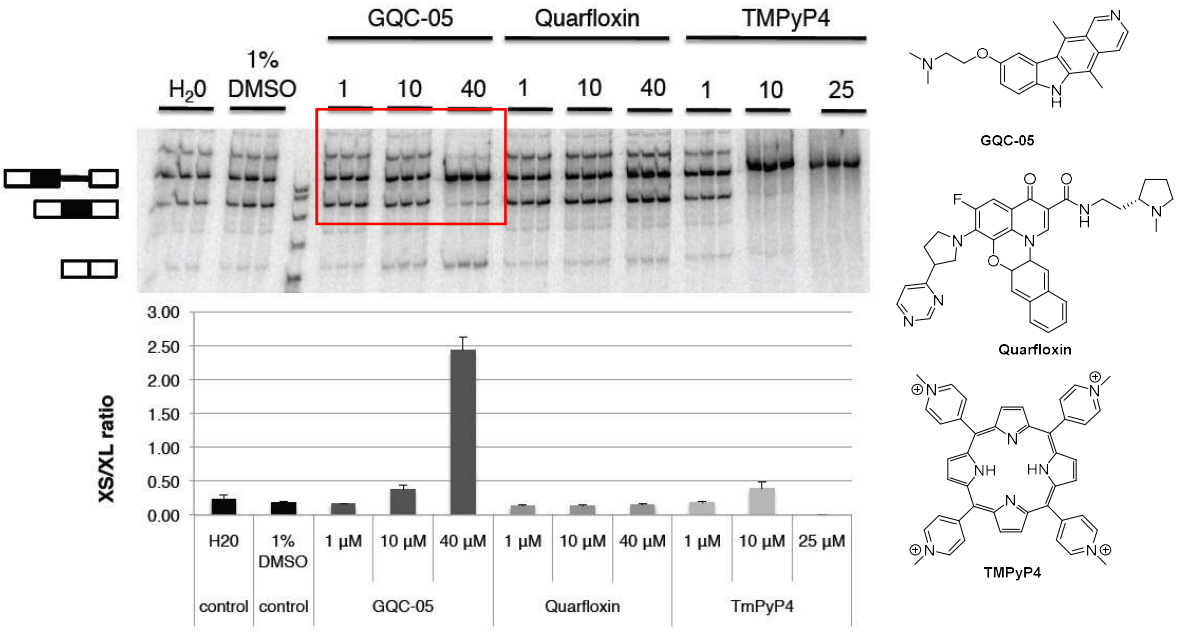


Figure 49. (a) In vitro splicing of Bcl-x-681 in the presence of G4 ligands. All concentrations shown are in µM. (b) The proportion of mRNA spliced to the x_S splice site. Licensed under CC BY 4.0.[115]

The experiment was translated into HeLa cells which were incubated with GQC-05 (**1.31**) (10 µM) for 4 h. The results shown in Figure 50 confirm those seen *in vitro*; on application of GQC-05 (**1.31**) a decrease of Bcl-x_L, the anti-apoptotic isoform, was observed with an increase in Bcl-x_S (the pro-apoptotic isoform).

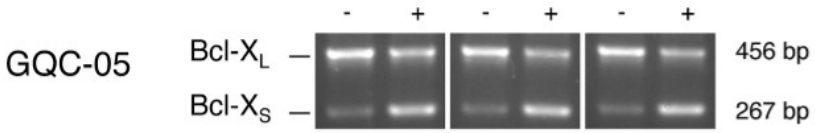
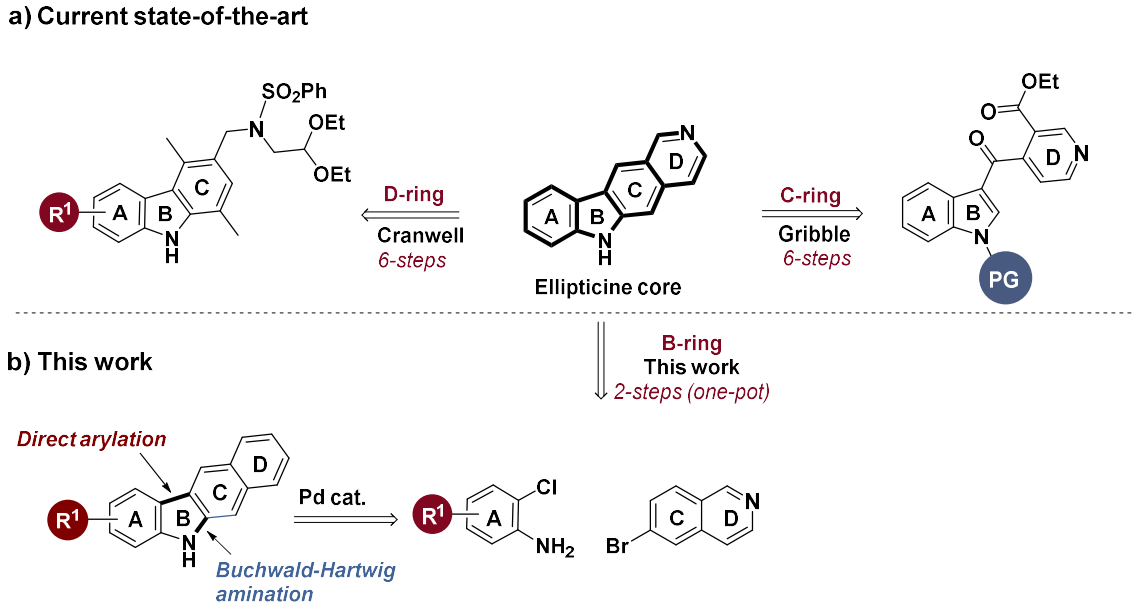


Figure 50. GQC-05 (**1.31**) affects Bcl-x splicing in HeLa cells: Cells were incubated with GQC-05 (**1.31**) (10 µM) for 4 h. Licensed under CC BY 4.0. [115]

Although the mode of action was unclear, the result proved very promising for further development. The natural product Ellipticine was deemed highly toxic, however, given that, it produces two antagonistic outcomes (both increased x_L and decreased x_S), it is a powerful ligand for further investigation. Development of a library of structural analogues and biotinylated or crosslinking probes utilizing GQC-05 (**1.31**), could further clarify the mode of action and thereafter can be designed and analogue to be more in-line with drug-like properties.

1.15 Challenges of Ellipticine Synthesis

To access a library of ellipticine analogues, a convergent, step-efficient synthesis is desirable. The current 'state of the art' for ellipticine synthesis are covered by the Cranwell-Saxton method and the Gribble method in 4 and 5 steps respectively. Both synthetic pathways are linear and achieve the tetracyclic core through building up of the C and D-rings sequentially (Scheme 1).



Scheme 1. Ellipticine synthesis: a) Current state of the art, Cranwell (D-ring synthesis) and Gribble methods (C-ring synthesis). b) Proposed synthesis through B-ring formation in one-pot.

However, previous attempts in the group to replicate these two methods were unsuccessful.[116] Furthermore, due to the linearity, derivatisation for developing a large library of analogues was inaccessible. Therefore a more convergent route towards to the tetracyclic core would be advantageous.

To access a broad palette of ellipticine analogues a convergent route through formation of the B-ring was proposed. This could be achieved by a two-step sequential Buchwald-Hartwig amination and a Direct Arylation. This method would lead to easy derivatisation due to the broad-range of cheap and commercially available bromoisoquinolines. Additionally pre-functionalisation of the A-ring chloroaniline could be achieved prior to the final cross-coupling step.

Hypothesis to be Tested

Previous work carried out by Hurley *et al.* has shown the ellipticine analogue GQC-05 (**1.31**) (**1.31**) can modulate regulation of biological processes (down-regulation of c-*MYC*) through interaction with G-rich G4 forming sequences.[48] Following on from this work Eperon *et al.*

showed the same compound (**1.31**) could be used to modulate splicing in Bcl-x, a regulator of apoptosis with G-rich sequences close the alternative splice sites in exon 2.[115] These secondary structure of these regions were shown to rely on the presence of guanine (N7) which is also a requirement for Hoogsteen base pairing in G-quadruplexes (G4s).[3]

The hypothesis for this research is that GQC-05 (**1.31**) can stabilise G4 formation close to regions of splicing regulation in Bcl-x. This stabilisation either exposes or sequesters the alternative splice-site resulting in bias of the splicing-isoforms back to the pro-apoptotic Bcl-x_s.

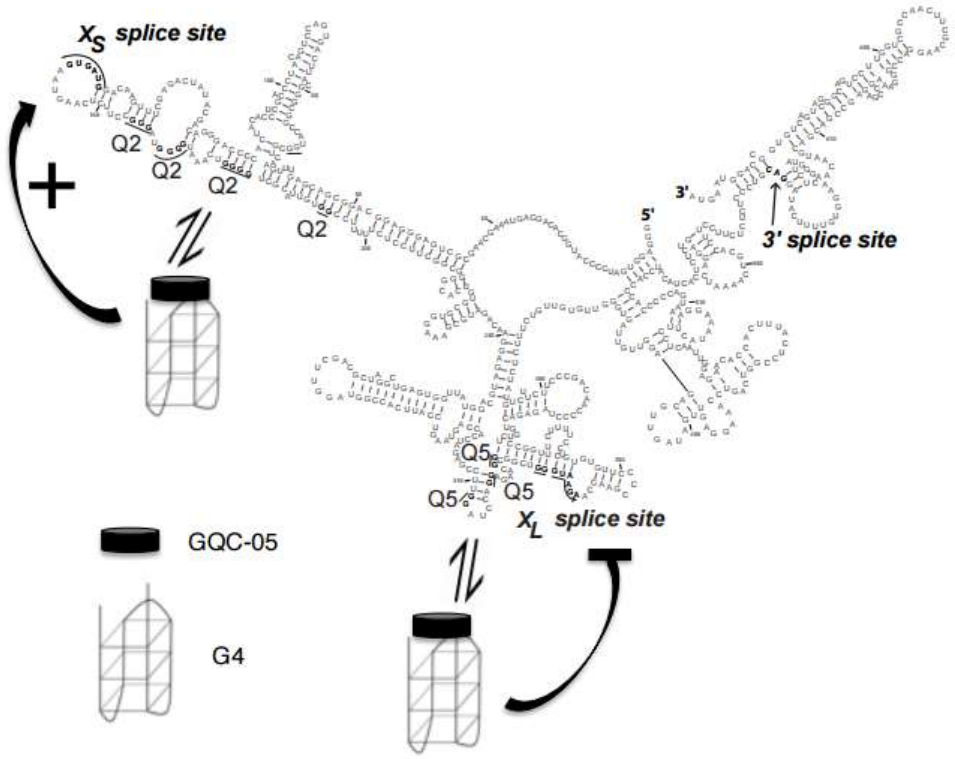
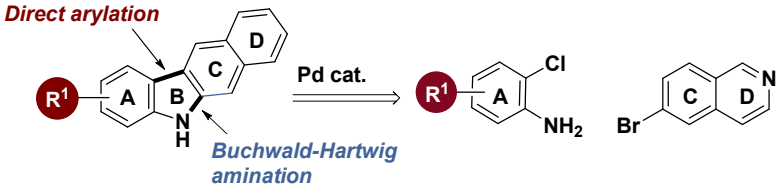


Figure 51. Proposed mode of action: GQC-05 (**1.31**) interacts with G-tracts upstream of the X_L and X_S splice sites through stabilisation of RNA G4s.

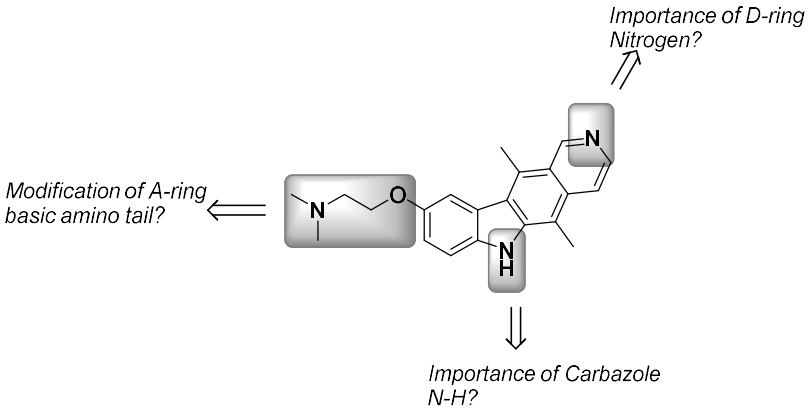
Thesis Aims

The aims of this project are to expand the understanding of GQC-05 (**1.31**) acting as a Bcl-x splice-switching ligand, through the design and subsequent testing of a library of GQC-05 analogues to establish a structure-activity relationship (SAR) profile. This will be achieved through:

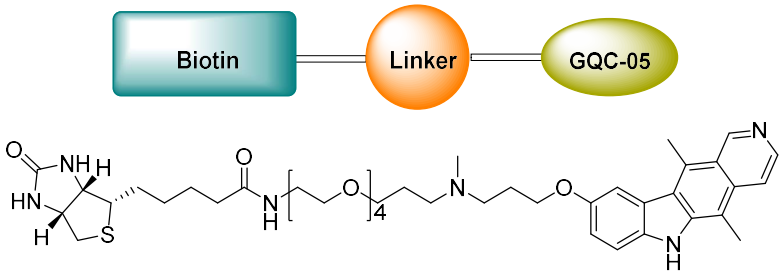
1) Development of a modular, convergent synthesis of the pyridocarbazole ellipticine core.



2) Synthesis and splicing assay biological testing of ellipticine analogies to establish an SAR profile.



3) And finally, with the optimised SAR profile results, development of a biological probe for biotin pull down assays to determine site of action.

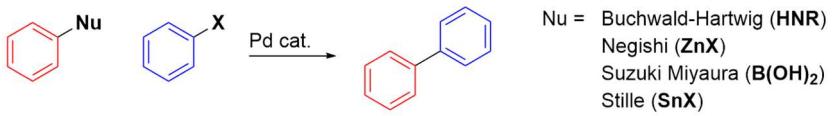


Chapter 2 Establishing a Sequential Palladium-Catalysed Synthesis of 7*H*-Pydridocarbazoles

2.1 Palladium-Catalysed Cross Coupling Chemistry

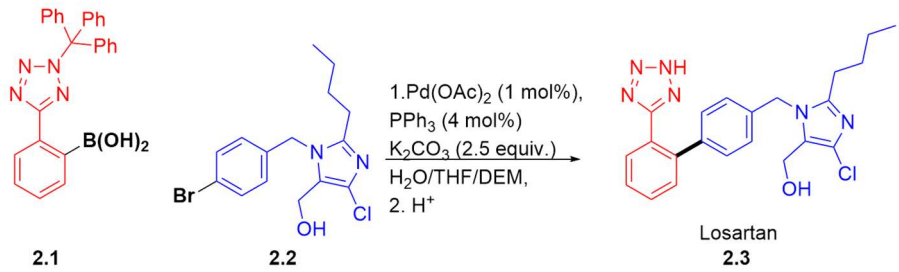
Metal-mediated cross-coupling reactions have been a staple of synthetic chemistry for the past 50 years.[117] Since their discovery in the 1970s, cross-coupling reactions have expanded the synthetic field through C-C and C-X (*e.g.,* X=N,O,S) bond-forming reactions that, without metals, would previously have been challenging to prepare in a step efficient manner.[118] Arguably, the most impactful area has been the discovery and expansion of cross-couplings using a catalytic Pd source.

Pd-catalysed cross-coupling reactions classically consist of an organometallic nucleophile and a sp^2-hybridised aryl halide electrophile (Scheme 2).



Scheme 2. General schematic of Pd-catalysed cross-couplings.

The hallmark of these reactions are categorised according to the nucleophile chosen to react with the corresponding aryl halide. The Suzuki-Miyaura reaction, for example, uses an organoborane nucleophile and since it's discovery has become one of the most commonly used transformations in drug discovery.[119] Along with Negishi[120] and Heck couplings,[121] these reactions have expanded the landscape of drug design allowing for a more convergent approach to synthesis that is achievable through late stage functionalisation (Scheme 3).[122]



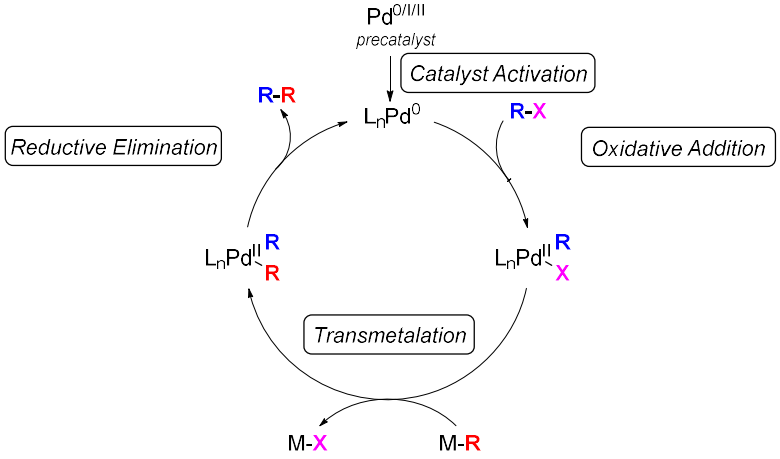
Scheme 3. A representative Suzuki-Miyaura cross-coupling used in Losartan total synthesis.[122]

Their namesakes were recognised for their contributions to synthetic chemistry when they were awarded the Nobel Prize for Chemistry in 2010.[123]

2.1.1 General Proposed Mechanism for Pd-catalysed Cross-couplings

Although there are subtle mechanistic differences between Pd-catalysed cross-couplings depending on the reagents used, the general mechanism (Scheme 4) has been proposed for the Buchwald-Hartwig amination.[124,125] The catalytic cycle commences by the formation of a Pd^0

source typically formed via reduction of a Pd^{II} pre-catalyst. The catalyst then oxidatively adds into an aryl-halide bond of the electrophile resulting in the formation of an aryl Pd^{II} species. The R group from the nucleophile is transferred to the active complex while a ligand is transferred out. The completion of the cycle is achieved through reductive elimination to form the desired chemical bond and reforming the Pd^0 catalyst (Scheme 4).



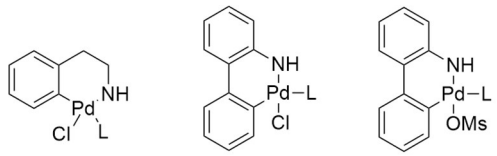
Scheme 4. General proposed mechanism of Pd-catalysed cross-coupling reactions.

2.1.2 C-N Bond Formation – Buchwald-Hartwig Amination

The Buchwald-Hartwig amination was established in the 1990s by both Stephen Buchwald and John Hartwig simultaneuously.[126,127] It is a coupling of an aryl halide electrophile with an amine nucleophile to synthesise C-N bonds. Arylated amines are ubiquitous across synthetic chemistry and are a strong presence in natural products, drugs and materials.[124] This universal presence has led to the continued development of the reaction, resulting in great strides in catalyst, ligand and scope development. Consequently, the Buchwald-Hartwig reaction has become a fundamental to the advancement of drug discovery.

2.1.2.1 Development of Buchwald-Hartwig Pd catalysts

A large area of development has been the design of air stable Pd^{II} pre-catalysts that are converted to the catalytically active Pd^0 species *in-situ*. This allows for ease of synthesis and better atom economy as a separate phosphine ligand is not required. In 2008, Buchwald *et al.* published the first general scope of base-mediated cyclometalated pre-catalysts (Scheme 5).[128]



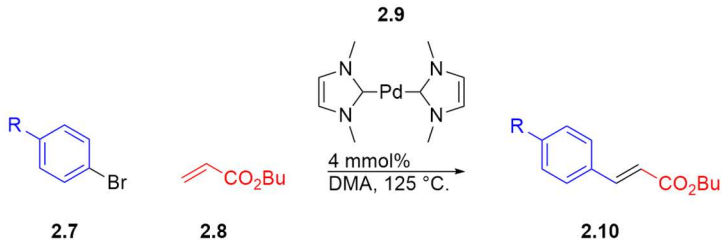
2.4 **2.5** **2.6**

Scheme 5. Structure Pd palladacycle pre-catalysts.

These pre-catalysts decrease the percentage of catalyst required as well as being equally efficient in milder reaction conditions i.e. lower temperatures, particularly when comparing to traditional Cu-catalysed cross couplings that require elevated temperatures circa 160 °C (Ullmann coupling).

2.1.2.2 Development of Buchwald-Hartwig Ligands

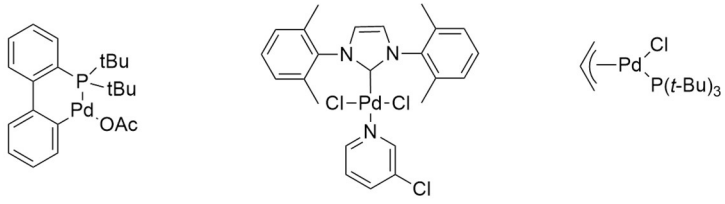
Palladium cross-coupling ligands generally fall into two categories: N-heterocyclic carbenes (NHCs) and phosphine ligands and both have been shown to have great advantages over classical catalysis methods.[129,130,131] Since Herrmann and co-workers published that NHC ligands can effectively catalyse carbon-carbon cross coupling reactions (Scheme 6), they have become the main alternative to the extremely well established phosphine ligands.[132]



2.7 **2.8** **2.10**

Scheme 6. Heck cross-coupling using a Pd-NHC catalyst.

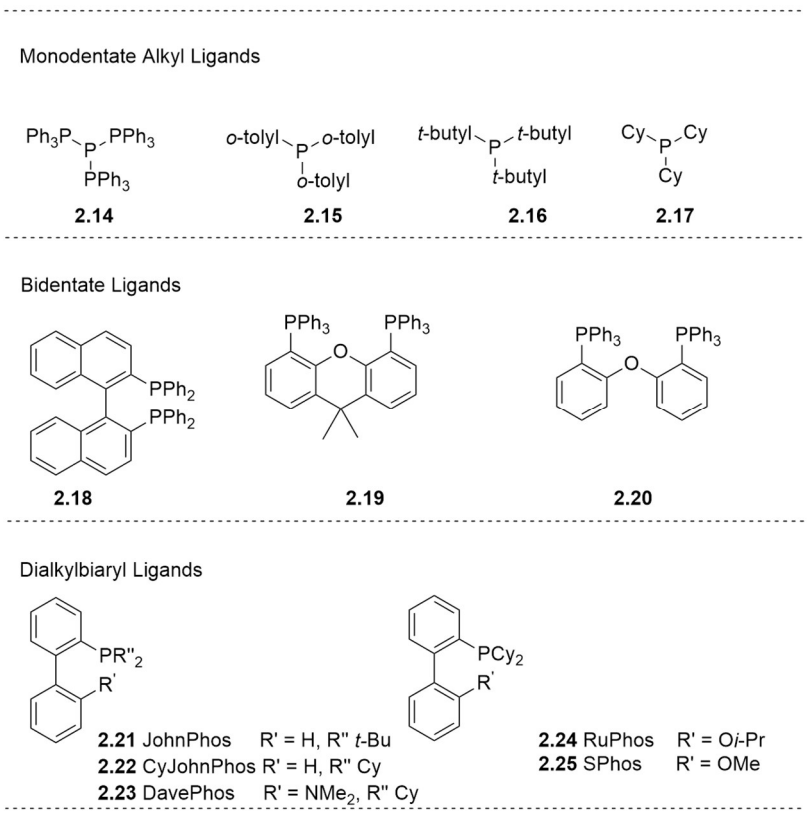
NHC ligands have been greatly expanded from the simple traditional bicyclic systems and have now been developed to include palladocycles,[133] π-allyl palladium complexes and pyridine containing NHCs (Scheme 7).[134]



2.11 **2.12** **2.13**

Scheme 7. Structures of Pd NHC ligands: Pd-palladacycle (**2.11**), pyridine NHC (**2.12**) and π-allyl Pd complex (**2.13**).

Phosphine ligands have undoubtedly dominated the field due to their efficiency and robustness.[135] Phosphine ligands are a trivalent compound that are used as σ-donors to aid stability and solubility to the complexes they form with metals through their available lone pair. Phosphine ligands have been extensively studied for their effect on reactivity and as a result, rules and trends have been illuminated on designing the best ligand for a specific system.



Scheme 8. Various phosphine ligands arranged by structural characteristics.

To maximise oxidative addition electron-rich phosphines, such as cyclohexyl functionalised ligands (**2.22**, **2.23**, **2.24** and **2.25**), can donate electron density to the metal centre increasing reactivity. Additionally, increasing the bulk surrounding the phosphorous increases the rate of reductive elimination. Bulky, electron dense ligands such as tri-*tert*-butyl phosphine (**2.16**) can greatly improve the efficiency of a reaction by enhancing the rates of both oxidative addition and reductive elimination (Scheme 8).

The bulk of phosphine ligands can be measured by the angle created, in-space between the metal and the ligand. Monodentate angles are measured by the cone angle (θ) and bidentate by the bite angle (ω) (Figure 52).

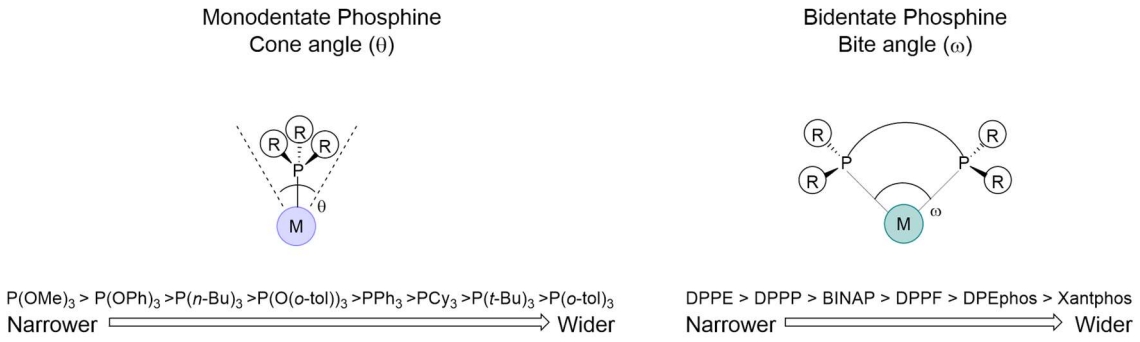


Figure 52. Generalised depictions of the monodentate phosphine cone angle (θ) and bidentate phosphine bite angle (ω). Examples of ligands, in order of increasing angle are listed below each image.

Wider cone/bite angles indicates increased bulk of the ligand, resulting in greater reductive elimination efficiency.[136]

Dialkylbiarylphosphine ligands have also risen to the challenge of becoming some of the most universally used phosphine ligands in palladium cross couplings. Their increased diversity in structure allows for greater expansion of the current phosphine ligand scope (Figure 53).

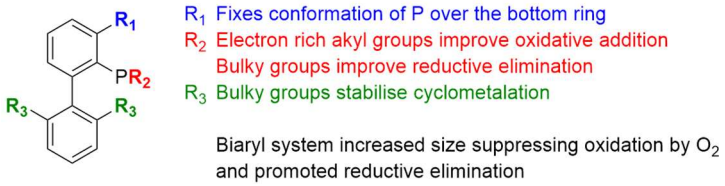


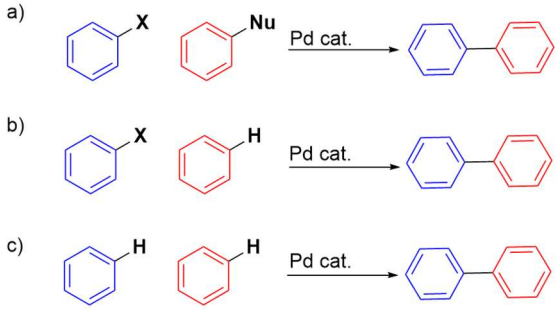
Figure 53. Summary of substituent effects on dialkylbiaryl phosphine ligands.

The lower aryl ring adds stability by reducing oxidation by oxygen as well as promoting reductive elimination. In addition, varying R groups on the aryl rings can increase Pd^0 formation and modulate stability of the active complex (Figure 53).

2.1.2 Direct-arylation as a Route to Access Fused Aromatic Tricycles

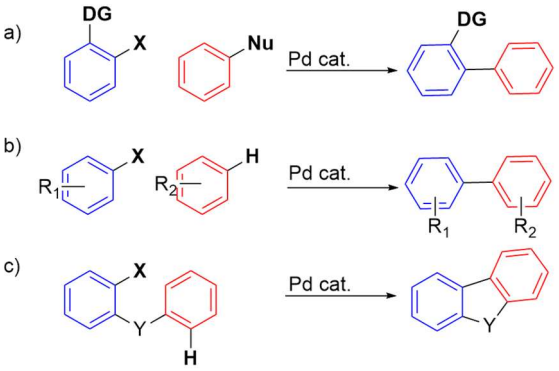
There are many established routes to synthesise an aryl-aryl bond. Suzuki-Miyaura, Negishi and Heck reactions have all established themselves as cornerstones of current synthetic methodology. These couplings are the result of bond formation between and aryl halide and, specifically activated aryl derivatives e.g. organoboranes. However, they are not without their drawbacks, at times requiring multi-step synthesis to make suitable starting materials due to the required functionality. These synthesises require stoichiometric transformations and often result in regioselectivity issues and the formation of harmful waste and side products. This problem scales poorly when transferred to an industry setting particularly when considering the extra cost to not only the company, but importantly the environment.[137] Direct C-C bond formation between an

aryl halide and a C-H sp^2 bond of a heteroaryl substrate would be far more attractive, further expanding the capabilities of metal mediated cross couplings, with a better, cleaner atom economy.[138]



Scheme 9. General scheme of metal cross-couplings: (a) Aryl halide and Aryl Nucleophile – Suzuki-Miyaura reaction, (b) Aryl halide and C-H activation – Assisted Direct Arylation, (c) Double C-H activation – Oxidative Coupling.

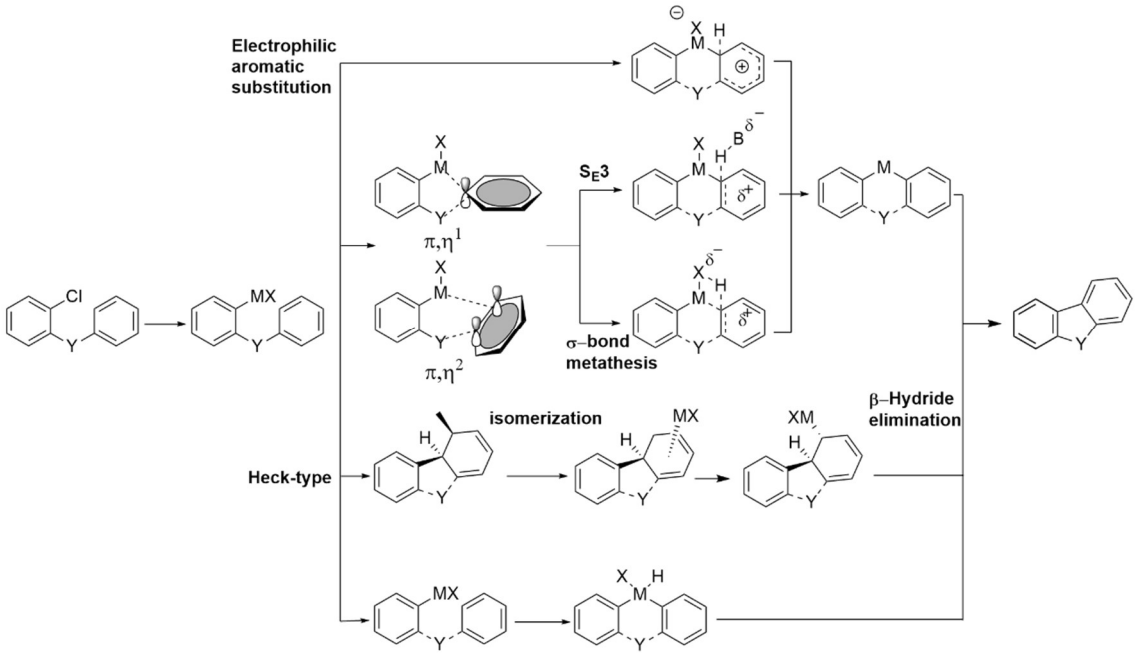
Taking all these considerations into account, the transformation that would be the most desirable would be the coupling of two C-H bonds together (Scheme 9c). This has been achieved through oxidative coupling. However, activating C-H bonds is challenging, leading to synthetic difficulties such as poor conversions due to the high-energy barrier. Furthermore, even when the reaction overcomes the significant energy barrier, there are multiple potential C-H bonds for activation in any aryl compound, compromising chemoselectivity. Therefore, the method most commonly exploited method is exchanging only one of the functionalities with the C-H substrate (Scheme 9b). However, the reaction still has one substrate with multiple aryl C-H bonds available for reaction. This was resolved by the application of directing groups (Scheme 10a), designed electronics (Scheme 10b), or by sterics (Scheme 10c).



Scheme 10. Examples of modified direct Arylations. (a) Directing group functionality. (b) R-groups that direct electronics, and (c) Intramolecular substrate assists through restricted sterics.

2.1.2.1 Current Mechanistic Understanding of Direct Arylation

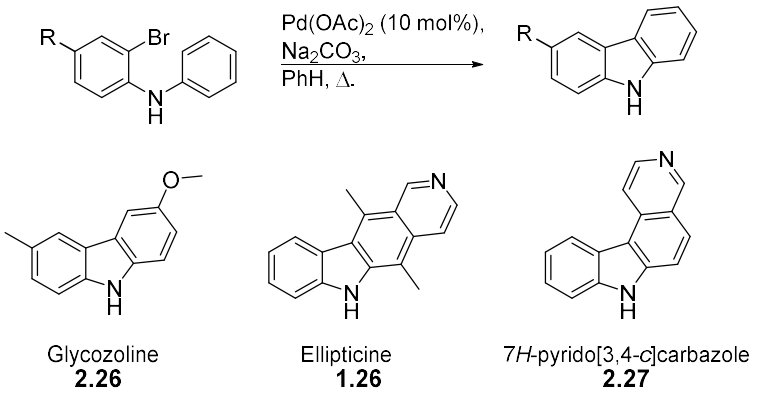
Direct arylations that occur through C-H insertion have varied methods depending on the reaction conditions e.g. potential use of directing groups. However, there are currently four general proposed mechanisms of direct arylation (Scheme 11).



Scheme 11. Four proposed mechanisms for C-H activation, direct arylation.

All reaction pathways, with exception of oxidative addition of the C-H bond (Scheme 9), begin with the oxidative insertion of the metal into the aryl halide bond followed by a distinct C-C bond formation that takes *via* one of four routes. They are achieved through electrophilic aromatic substitution, an S_E3 mechanism, a σ-bond metathesis transformation, or through insertion and β-hydride elimination through a Heck-type reaction.

Combining these direct arylations with the previous Pd-catalysed Buchwald-Hartwig amination could give access to extended fused ring structures such as carbazoles and ellipticines.

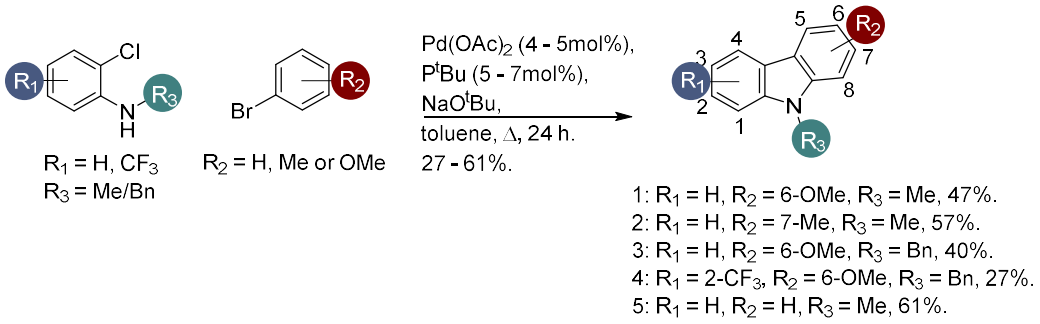


Scheme 12. Structure of Glycozoline (**2.26**), Ellipticine (**1.26**) and 7*H*-pyrido[3,4-*c*]carbazole (**2.27**).[139]

2.2 Current State-of-the-art in a Sequential Pd-catalysed Process to form Carbazoles

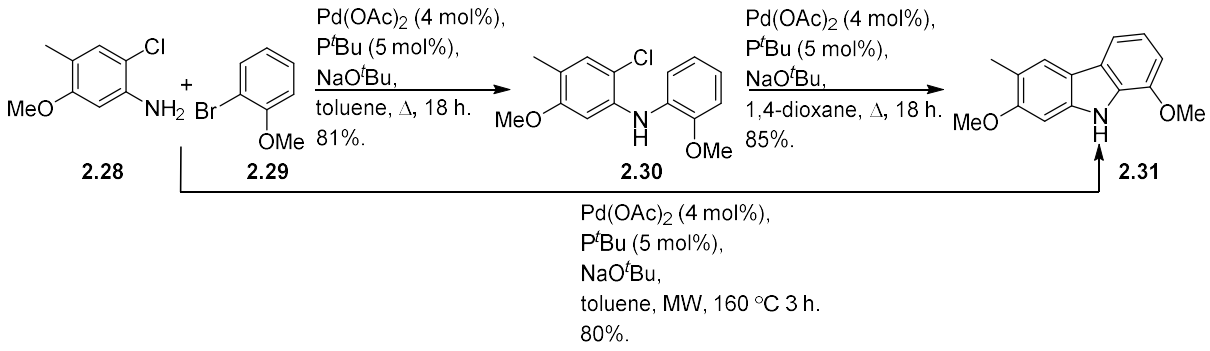
2.2.1 One-pot Carbazole Synthesis: Bedford Method

Tricyclic carbazoles have had strong presence in medicinal chemistry as drugs and pharmacophores for decades.[140] As a result, there have been many synthetic routes developed for their production. An improved method reported by the Bedford group involved a two-step, one-pot synthesis encompassing sequential Buchwald-Hartwig amination followed by direct arylation to thermally access a wide range of carbazole scaffolds in 2002 (Scheme 13).[141]



Scheme 13. Bedford Method: 9*H*-protected carbazole synthesis.[141]

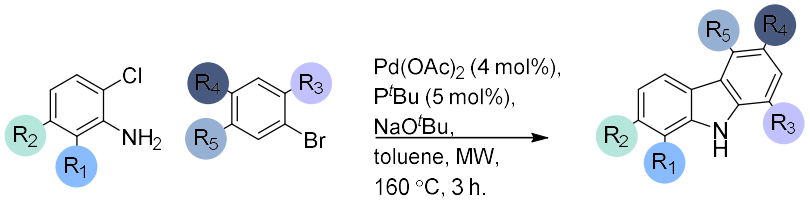
This method improved on the previous literature in step-efficiency, diversity of products and laid the ground work for its utility to be expanded to carbazole multicycles.[142,143] Bedford *et al.* discovered that when a secondary aniline was employed, the desired carbazole was obtained from a thermally activated one-pot system across a range of analogues. Unfortunately, when these conditions were applied to the synthesis of 9*H*-carbazoles, it proved initially problematic. Under thermal conditions, it was found that the reaction stalled at the Buchwald-Hartwig intermediate (**2.30**). However, upon optimization of the direct arylation, it was found that a change of solvent to 1,4-dioxane to facilitate elevated temperatures expedited the second step (**2.31**).[144]



Scheme 14. Total synthesis of Clausine P (**2.31**).[144]

The same reaction was subjected to microwave irradiation, which resulted in both transformations occurring in one-step over 3 h (Scheme 14).

This one-pot method was applied to the synthesis of various carbazoles and was found to be generally applicable across the board in good to excellent yield (Scheme 15). However, this synthesis required R^3 substitution (Scheme 15) or the reaction would stall at the Buchwald-Hartwig intermediate.



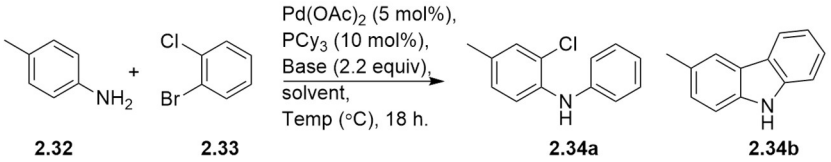
R_1	R_2	R_3	R_4	R_5	Yield (%)
H	H	Me	H	H	88%
H	H	OMe	H	H	83%
H	H	Me	H	Me	79%
Me	H	Me	H	H	92%

Scheme 15. Bedford method: Generalised one pot synthesis of carbazoles (substitution required at R^3)[144].

2.2.2 One-pot Carbazole Synthesis: Ackermann Method

Further building on this work, Ackermann *et al.* developed a parallel method of carbazole synthesis via cross coupling anilines with commercially available 1,2-dihaloarenes.[145] The optimization revealed that weak inorganic bases, such as K_3PO_4, in conjunction with polar-aprotic solvents i.e. NMP or DMAc, gave excellent yields. Non-polar aprotic solvents like toluene stalled at the aminated intermediate (**2.34a**), in line with results observed by Bedford in thermal

conditions (Table 2, entry 1). This method overcame the problems observed by Bedford of the *ortho*-aniline deactivating the chloride by moving the *ortho*-chloride moiety to the aryl-halide starting material. Ackermann *et al.* used this method to gain access to a wide range of carbazole compounds through a one-pot thermal process in excellent yield. Although this is an improvement on the two-step thermal method, Ackermann's group unfortunately did not translate this method to microwave conditions, which Bedford *et al.* had previously shown to significantly reduce reaction time (18 h to 3 h) in a one-pot system.



2.32 **2.33** **2.34a** **2.34b**

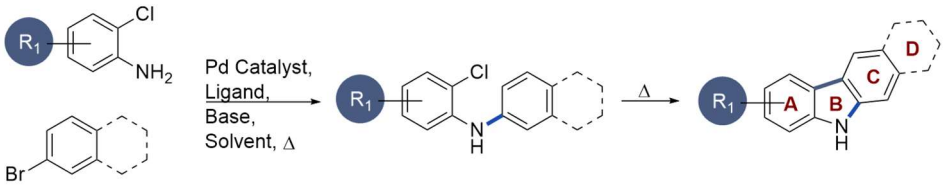
Entry[a]	Solvent	Base	Temp. (°C)	Yield (%)[b]
1	Toluene (0.1 M)	NaO^{t}Bu	105	-[c]
2	DMAc (0.1 M)	K_2CO_3	130	60
3	DMAc (0.1 M)	Cs_2CO_3	130	51
4	DMAc (0.1 M)	K_3PO_4	130	79
5	NMP (0.1 M)	K_3PO_4	130	81
6	NMP (0.5 M)	K_3PO_4	130	69

Table 2. Optimisation of one-pot, two step cross coupling: [a]Conditions: aniline (1.2 equiv), bromide (1.0 equiv), $Pd(OAc_2)$ (5 mol%), PCy_3 (10 mol%), base (2.2 equiv), solvent, 18 h. [b]Yields of isolated products. [c]The aminated product (**2.34a**) was isolated in 94% yield.[145]

With these publications in mind, it was postulated that the one-pot method demonstrated by Bedford *et al.* could be translated to tetracyclic scaffolds to access ellipticine analogues for testing in Bcl-x splicing assays.

2.3 Chapter Aims

The overall objective of this chapter is to develop a novel, modular synthesis for tetracyclic carbazoles for expanding the library of available splice-switching scaffolds for testing. Although there are many established methods for their synthesis, these methods to not allow for easy derivatization due to their multistep nature.[146–148] This chapter will outline the development of a two-step, one-pot synthesis via consecutive Buchwald-Hartwig amination and direct arylation from inexpensive, commercially available starting materials (Scheme 16).



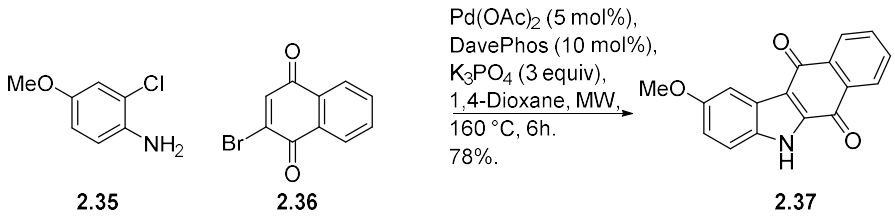
Scheme 16. Proposed two-step, one-pot synthesis of tetracyclic-carbazoles.

This method will then be used to generate a comprehensive library of GQC-05 (**1.31**) analogues to be tested for activity in Bcl-x splicing assays.

2.4 Results and Discussion

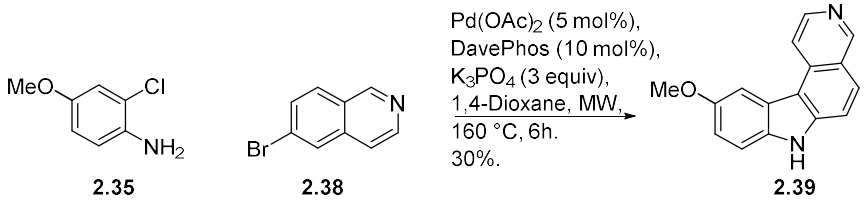
2.4.1 Optimisation of the Buchwald Amination

Previous work in the group carried out by Dr. Olivia Rutherford, included a model synthesis that gave a 78% isolated yield when synthesising **2.37** using a one-pot synthesis similar to Ackermann's synthesis (Scheme 17).[116]



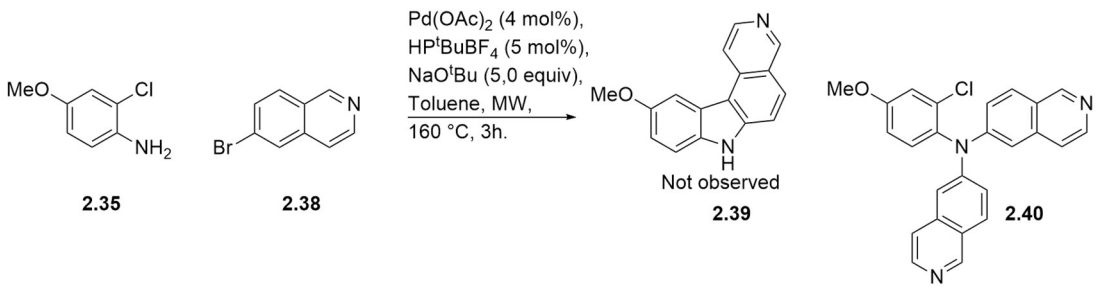
Scheme 17. Modified Ackermann method[145]: Pilot synthesis of **2.37**.

NMP was exchanged for 1,4-dioxane as the preferred solvent as it provides a similar heating range but is easier to remove on purification. Although these conditions worked well for this system, when transferred to the synthesis of a corresponding 7*H*-pyrido[3,4-*c*]carbazole (**2.39**), the yield was significantly lower (30%). The mass balance was lost to the Buchwald-Hartwig intermediate and to the dehalogenated degradation product that were not isolated, but observed by LC-MS (m/z 250.11).



Scheme 18. Modified Ackermann method[145]: Synthesis of pyridocarbazole **2.39.**

The synthesis previously reported by Bedford was then attempted.[144] Upon analysis of the crude by LC-MS **2.39** was not observed however the major product observed had an m/z = 411.11 which aligns with the formation of **2.40**.

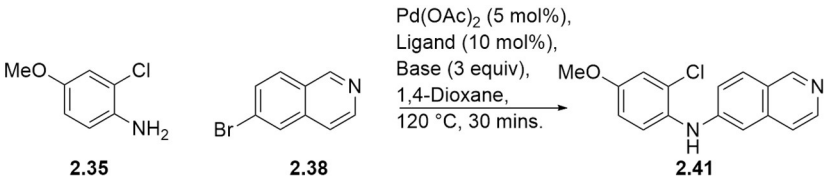


2.35 **2.38** **2.39** **2.40**

Scheme 19. Bedford Method: Attempted synthesis of pyridocarbazole **2.39**.

In an attempt to both improve these yields, and minimise degradation of the Buchwald-Hartwig intermediate from the elevated reaction temperatures, it was decided to heat the reaction in two steps. The first step heated at a milder 120 °C to allow completion of the Buchwald-Hartwig amination before increasing the temperature to 160 °C for the direct arylation.

To begin, conditions similar to Ackermann's synthesis were used as a benchmark.[145] The first reaction was heated to 120 °C for 30 mins with $HPCy_3BF_4$ as the ligand (Table 3, entry1). It was found that the reaction mixture only showed a 10% conversion to **2.41** after 30 mins. Although increasing the temperature to 160 °C had been shown previously in the group to give access to the final pyridocarbazole product (**2.39**). In an effort to improve the final conversion, the aim moving forward was to optimise the Buchwald-Hartwig first step in milder conditions to minimise degradation due to elevated temperatures. Therefore it was determined a more comprehensive optimisation was required where the ligand and base are varied (Table 3).



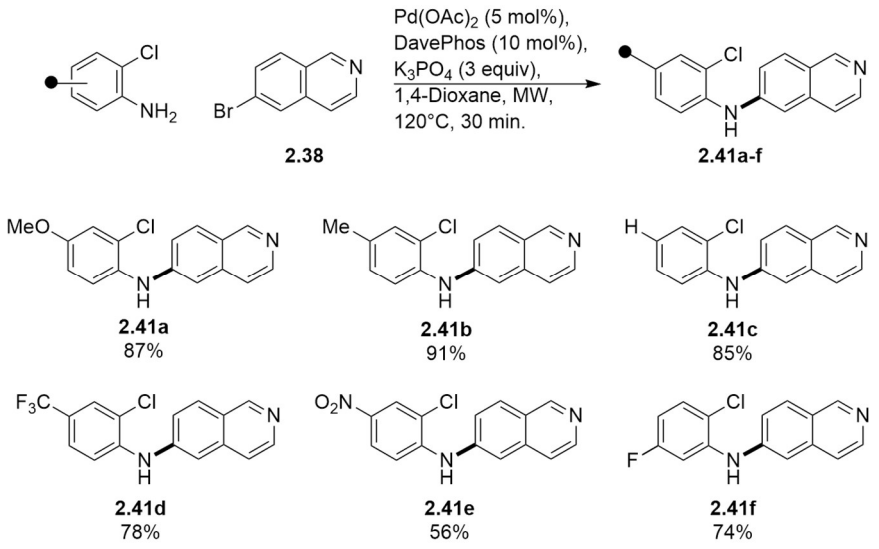
Entry	Ligand	Base	Conversion (%)
1	$HPCy_3BF_4$	K_3PO_4	10
2	$HPCy_3BF_4$	Cs_2CO_3	10
3	$HPCy_3BF_4$	NaO^tBu	75
4	**DavePhos**	**K_3PO_4**	**85 (87)[a]**
5	DavePhos	Cs_2CO_3	74
6	DavePhos	NaO^tBu	12
7	$HP^tBu_3BF_4$	K_3PO_4	65
8	$HP^tBu_3BF_4$	Cs_2CO_3	70
9	$HP^tBu_3BF_4$	NaO^tBu	7
10	XPhos	K_3PO_4	77
11	XPhos	Cs_2CO_3	76
12	XPhos	NaO^tBu	47

Table 3. Optimisation of Buchwald-Hartwig Amination. All reactions carried out according to general procedure A.[a] Isolated yield shown in brackets.

K_3PO_4 proved to be the most consistent base, in line with the carbazole scope carried out by Ackermann (Table 2).[145] Interestingly it was the dialkylbiaryl ligands, DavePhos and Xphos that proved to be the most successful with conversions of 85% and 77%, respectively. The reaction conditions from Entry 4 (Table 2) were repeated, producing 87% of **2.41**. With these optimised conditions in hand, a scope of the reaction was carried out to determine the limitations of the transformation.

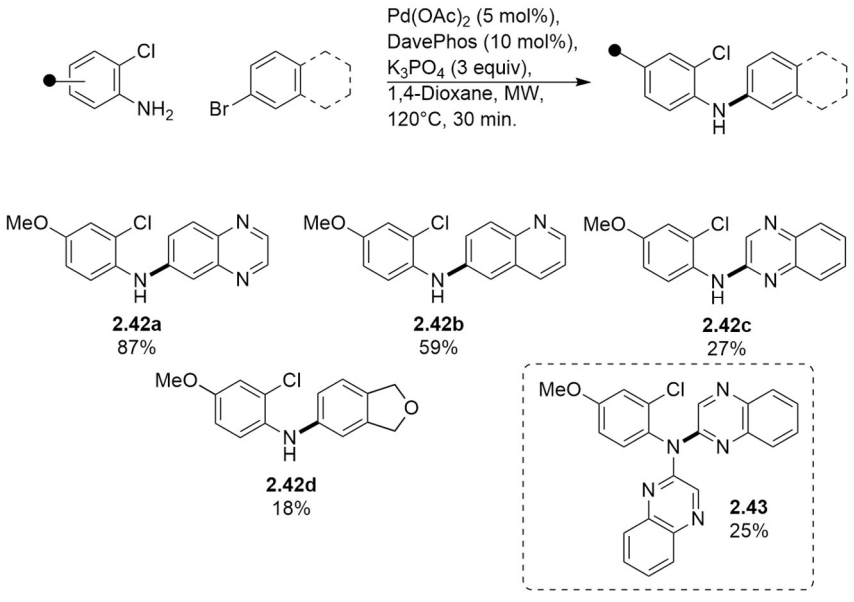
2.4.2 Establishing the Scope of the Buchwald-Hartwig Amination to Produce **2.41**

To begin the investigation, the functional group on the A-ring was varied: increasing in electron withdrawing character from a methoxy group (**2.41a**) to a nitro (**2.41f**) to determine the effect on the nucleophilic character of the aniline. This variation was well tolerated in the 4-position giving yields between 56% - 91%. However, strongly electron-withdrawing groups; nitro (**2.41e**) resulted in a reduction in the yield (56%) As aligned with literature precedent.[124] However, slightly more moderate electron withdrawing groups such as CF_3 (**2.41d**) are fairly well tolerated at 78%.



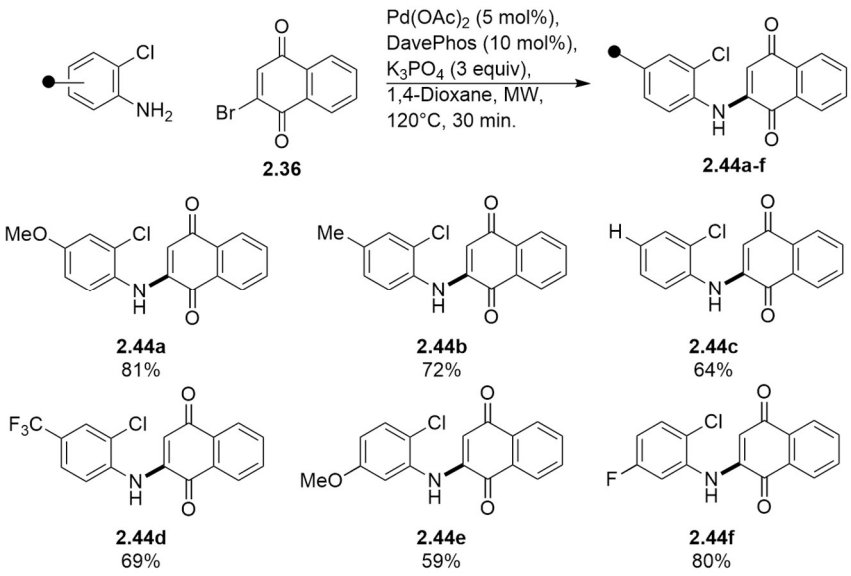
Scheme 20. Scope of A-ring variations in Buchwald-Hartwig Amination. Ligand = DavePhos.

Next, the 6-bromoisoquinoline was substituted for different heterocycles. Reactions where the nitrogen positions in the D-ring were varied were well tolerated (**2.42a** and **2.42b**). However, on reaction with 2-bromoquinoxaline, there was a significant loss in yield to only 27% (**2.42c**). The mass balance was being lost to the double aminated product (**2.43**) presumably due to the over-activation of the aryl-bromide from the added electron deficiency created from the endocyclic nitrogen atoms in the C-ring. Whilst adding sp^3 character was tolerated in the D-ring (**2.42d**), yield was low (18%).



Scheme 21. Scope of C/D ring variations on Buchwald-Hartwig Amination. Ligand = DavePhos.

To further investigate the scope of this approach, 2-bromo-1,4-napthoquinone (**2.36**) was used as a coupling partner, replacing 6-bromoisoquinoline (**2.38**). The 2-bromo-1,4-napthoquinone provides potential access to the tetracyclic deaza core of ellipticine (Scheme 22).[149,150]

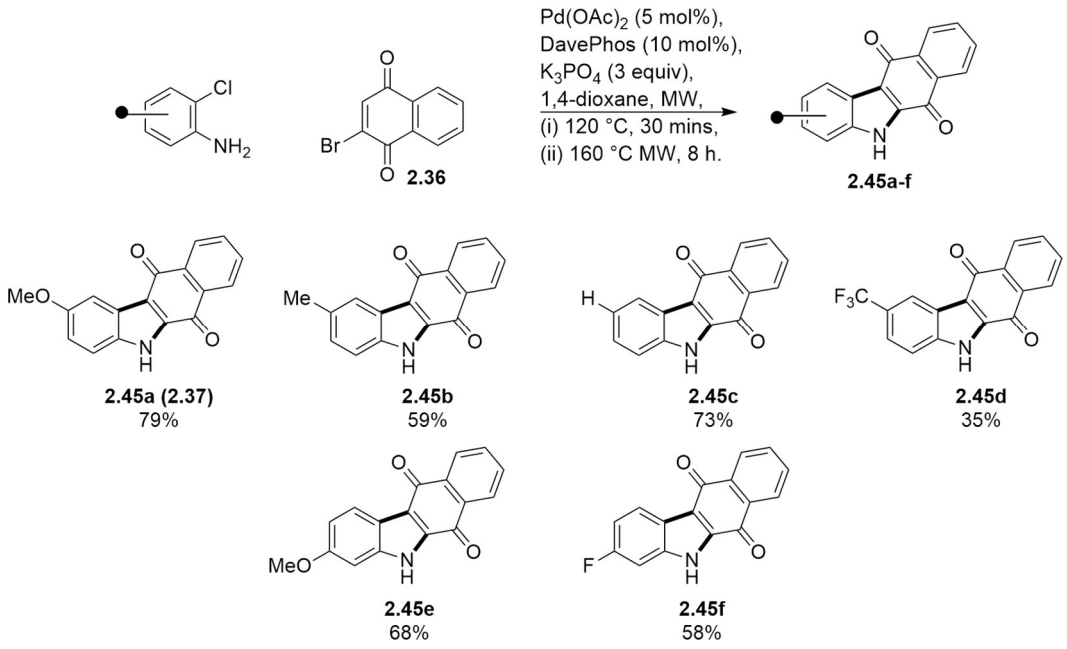


Scheme 22. Scope of A-ring variations in Buchwald-Hartwig amination. Ligand = DavePhos.

Increasing electron deficiency in the A-ring and moving functionality to the 5-position was also well tolerated, as observed with the isoquinoline scope in Scheme 20.

2.4.3 Establishing the Scope of 5*H*-benzo[*b*]carbazole-6,11-diones and 7*H*-pyrido[3,4-*c*]carbazoles.

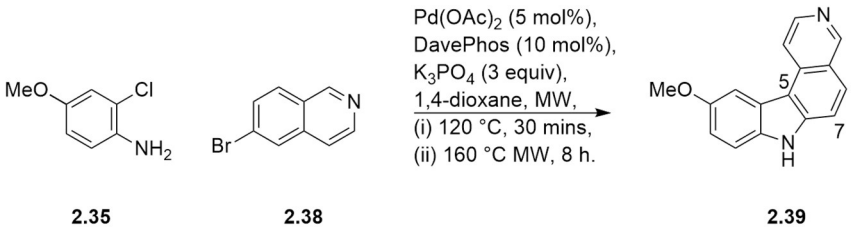
With these optimised conditions in hand, a range of tetracyclic analogues was synthesised, beginning first with 5*H*-benzo[*b*]carbazole-6,11-diones synthesis.



Scheme 23. Scope of two-step, one-pot synthesis of 5*H*-benzo[*b*]carbazole-6,11-diones analogues. Ligand = DavePhos

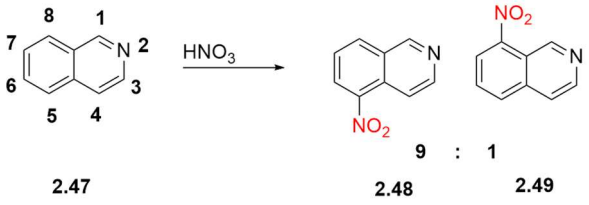
Electron-rich and neutral functional groups were well tolerated in the A-ring with yields of 59 – 79% (**2.45a – c**) with a predicted fall in isolated yield to 35% with the electron withdrawing -CF_3 (**2.45d**). It should be noted that reaction of chloroaniline substrates with 2-bromo-1,4-napthoquinone gave good yields of 58 – 79% (**2.45a – 2.45f**) on a 0.5 mmol scale upon heating under microwave conditions (Scheme 23). Scaling up the reaction to 1.0 mmol resulted in superheating and subsequent vial explosion due to excessive precipitation. This also provided very challenging purifications as the final products were poorly soluble in most solutions, with some solubility achieved with chlorinated solvents.

Next, a scope of 7H-pyrido[3,4-c]carbazole was developed using the starting materials that showed promising results in the previous amination step. The reaction mixture was heated to 120 °C by microwave irradiation followed by 8 h at 160 °C to complete the direct arylation (Scheme 24). Even though the Buchwald-Hartwig intermediate formation had been optimised to give 87%, the initial one-pot, two step reaction carried out showed poor conversion to **2.39** (36%).



Scheme 24. Two-step, one-pot synthesis of 7*H*-pyrido[3,4-*c*]carbazole (**2.39**). Ligand = DavePhos

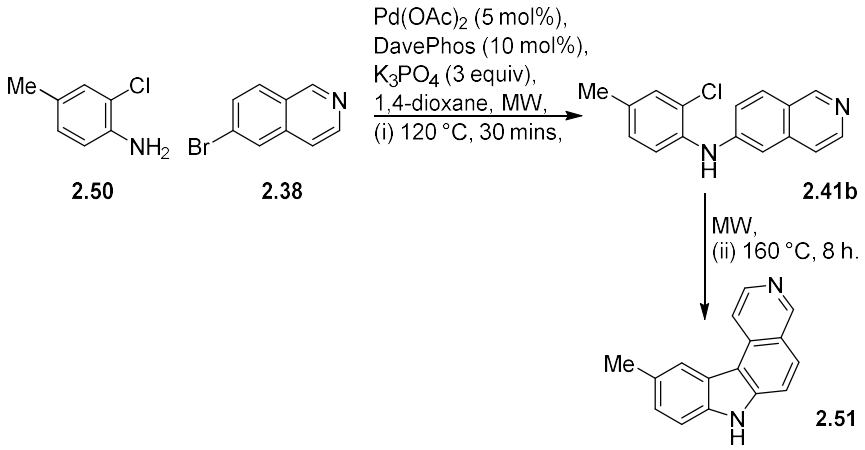
Upon isolation of **2.39** it was realised that the reactivity of isoquinoline was directing selectivity of the C-H arylation closure to occur at the 5-position instead of the desired 7-position (Scheme 25). Of particular interest was that the rest of the mass balance could be attributed to the Buchwald-Hartwig intermediate (**2.41a**), meaning the reaction is entirely regioselective for direct arylation at the 5-position. As a result, the regioisomer of direct arylation at the 7-position was not obtained. A result that has precedent in literature covering the reactivity of isoquinolines in electrophilic substitution reactions (Scheme 25).[151]



Scheme 25. Electrophilic reactions with isoquinolines are regioselective.

Menendez *et al*. reported that when $Cu(OAc)_2$ (2 equiv) was added as an oxidant the reaction gave yields of 85 – 91 % for direct arylations in a similar system.[152] Compound **2.41b** showed the highest conversion in Scheme 20 so was used as a model substrate for the improvement of the direct arylation, The various conditions attempted are outlaid in Table 4**.**

Table 4. Conditions attempted for yield improvement by addition of oxidant



$Pd(OAc)_2$	Stage $Cu^{II}(OAc)_2$ added	Quantity $Cu^{II}(OAc)_2$	Yield
5 mol%	None added	0 mmol	43%
5 mol%	Stage 1	2 equiv	0% (By LC-MS)
5 mol%	Stage 2	2 equiv	0% (By LC-MS)
5 mol%	Stage 2	5 mol%	26%

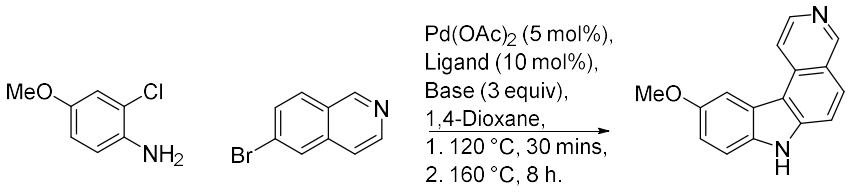
The reaction was conducted without any additive as a baseline experiment to obtain **2.51** in 43% yield and the remaining mass balance as the Buchwald-Hartwig intermediate **2.41b** in 55%.

$Cu^{II}(OAc)_2$ was added (2 equiv) to both the one pot system and to a reaction with the isolated Buchwald product **2.41b**. Neither reaction showed conversion to **2.51**. $Cu^{II}(OAc)_2$ was then added (5 mol %) to the one pot reaction after 30 mins at 120 °C. From this reaction, **2.51** was isolated in 26 % yield. Instead of an expected increase in yield with the addition of an oxidant, a decrease of 17 % was observed. This suggests the low yield cannot be overcome by methods observed in Menendez's research.[152]

Initially, it was thought that the low yields from these reactions could be circumvented with the addition of an oxidant. However, experiments carried out with the addition of $Cu^{II}(OAc)_2$ actually reduced the yield of **2.51**.

2.4.4 Re-optimisation of the Synthesis of the Pyrdiocarbazole Core

Optimisation of pyridocarbazole formation was explored using the same substrates as that reported earlier in Table 2 (Table 5).



2.35 **2.38** **2.39**

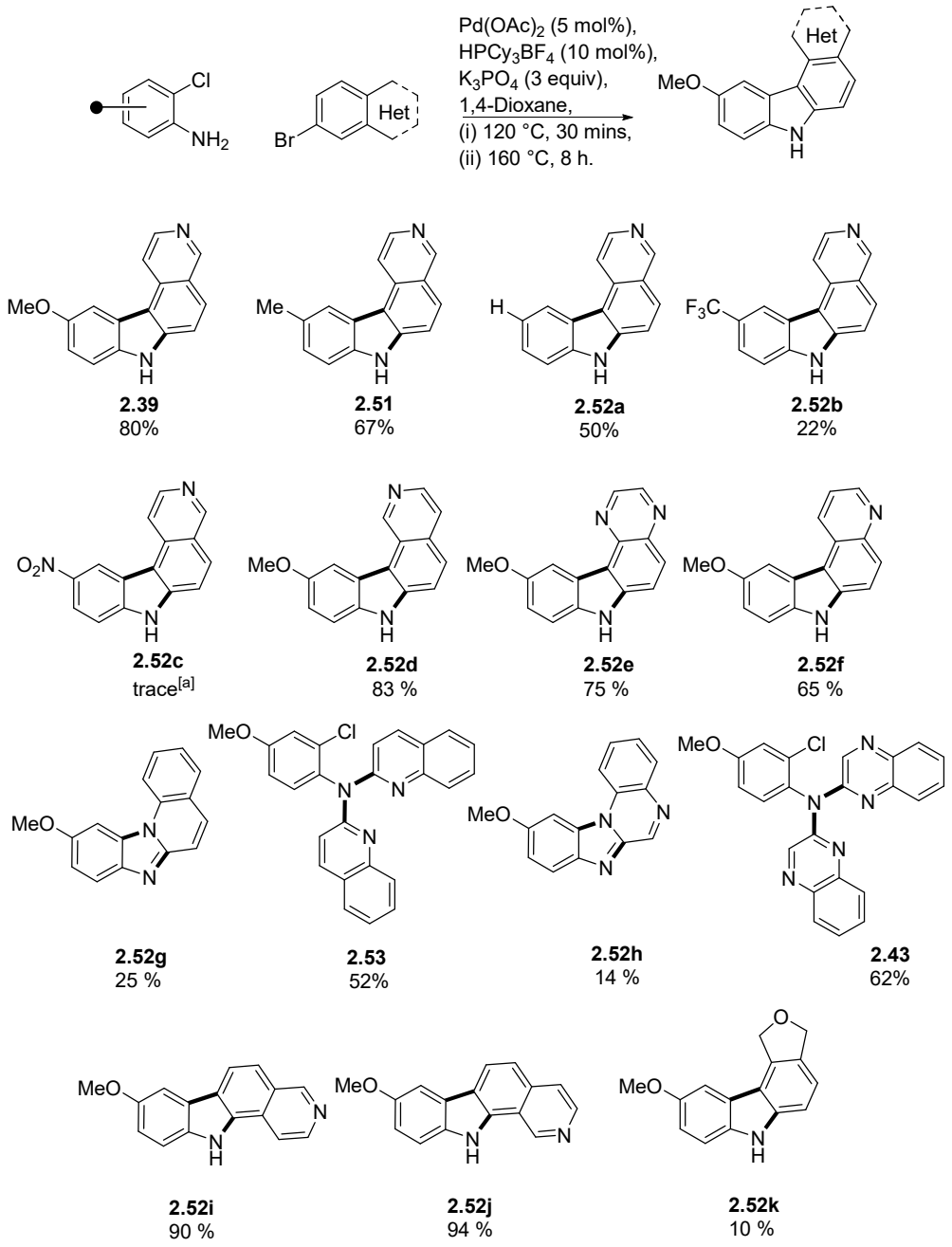
Entry	Ligand	Base	Conversion (%)
1	DavePhos	NaO^tBu	10
2	DavePhos	Cs_2CO_3	28
3	DavePhos	K_3PO_4	36
4	$HPCy_3BF_4$	NaO^tBu	45
5	$HPCy_3BF_4$	Cs_2CO_3	50
6	**$HPCy_3BF_4$**	**K_3PO_4**	**78 (80)**
7	$HP^tBu_3BF_4$	NaO^tBu	3
8	$HP^tBu_3BF_4$	Cs_2CO_3	25
9	$HP^tBu_3BF_4$	K_3PO_4	31
10	XPhos	NaO^tBu	19
11	XPhos	Cs_2CO_3	18
12	XPhos	K_3PO_4	22

Table 5. Optimisation of Buchwald-Hartwig Amination/Direct Arylation. All reactions carried out according to general procedure B. [a] Isolated yield shown in brackets.

Using DavePhos as a ligand was first investigated and showed that the conditions used for the synthesis of **2.39** with K_3PO_4 as base gave the highest conversion of 36% (Table 5, entry 3). In-line with observed results in the Buchwald-Hartwig optimisation, K_3PO_4 gave the highest conversions across all the ligands used (Table 5, entries 3, 6, 9 and 10), in comparison with NaO^tBu and Cs_2CO_3. However, it was the $HPCy_3BF_4$ ligand that was overwhelmingly the most effective at 78% conversion (Table 5, entry 6). This was over twice the efficiency of the corresponding DavePhos set of conditions (Table 5, entry 3). A scope of the reaction was carried out using the conditions from Table 5, entry 6.

2.4.5 Establishing the Scope of Pyridocarbazole Synthesis

As seen in both the Buchwald-Hartwig amination and 5*H*-benzo[*b*]carbazole-6,11-dione substrate scopes, increasing the electron withdrawing effect in the A-ring decreased the efficiency of the reaction (**2.39**, **2.51**, **2.52a-c**).

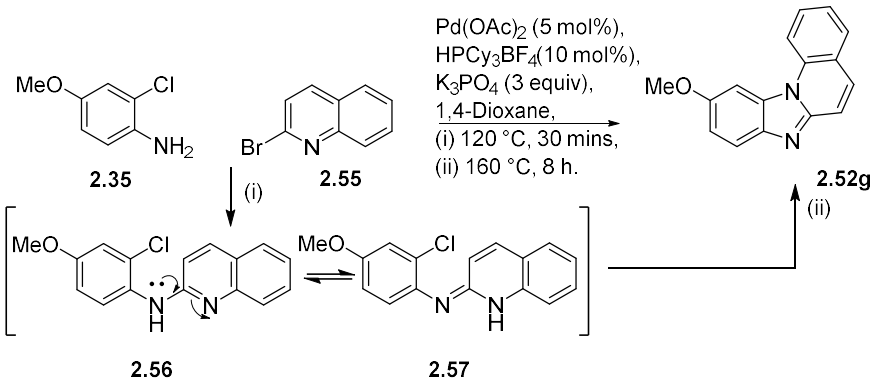


Scheme 26. Substrate scope of consecutive Buchwald-Hartwig amination and direct arylation reactions to form **2.39**, **2.51** and **2.52a-k**. [a]Buchwald-Hartwig intermediate (**2.41e**) isolated in 79% yield.

In-line with this trend, when 4-nitro-2-chloroaniline was subjected to these conditions, the reaction stalled at the Buchwald-Hartwig intermediate (**2.41e**) with only a trace of **2.52c** observed by LC-MS analysis. Changes to the D-ring showed very little effect on reaction efficiency with yields ranging from the lower 65% (**2.52f**) observed with the quinolone analogue up to 94% (**2.52j**) with the 8-bromoisoquinoline substrate.

An unexpected result was observed when reacting aryl-bromides with a nitrogen ortho to the bromide. Instead of the direct arylation occurring as the second step, a second Buchwald-Hartwig amination occurred between the aryl-chloride of the A-ring and the activated N-H in the C-ring. 2-bromoquinoline gave the product (**2.52g**) in 25% yield and 2-bromoquinoxaline gave **2.52h** in 14% yield. A similar transformation through a copper catalysed Chan-Lam reaction was reported by the Saini laboratory in 2020.[153]

The majority of the mass balance was lost to the double aminated Buchwald-Hartwig intermediates **2.53** and **2.43** (52% and 62% respectively). Compound **2.43** had been previously shown to form even at the lower temperature of 120 °C (Scheme 21). No further direct arylation occurred on compound **2.53**. Therefore it can be determined that once **2.53** or **2.54** have been formed they are not synthetically productive for further transformation. In particular, the nitrogen lone pair is now tied up and cannot activate the *ortho*-nitrogen in the C-ring for further reaction (Scheme 27**Error! Reference source not found.**).



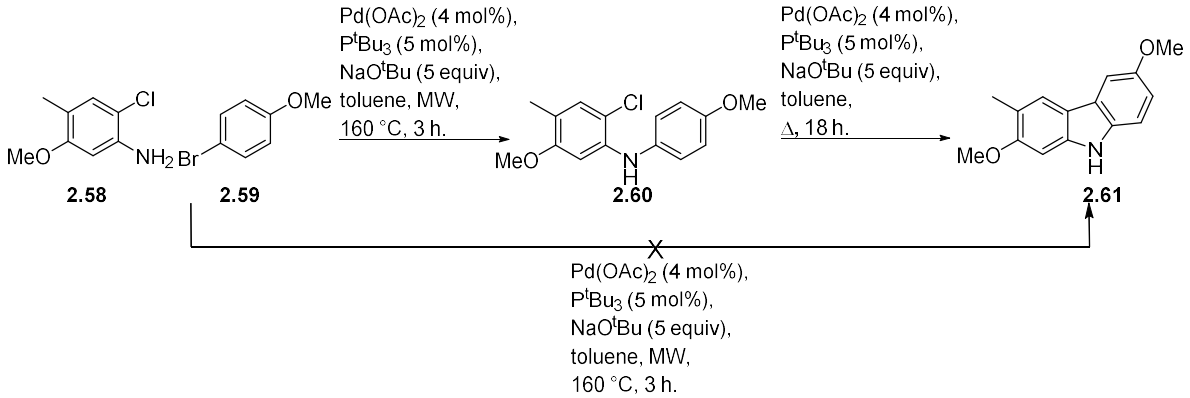
Scheme 27. Proposed mechanism for two consecutive Buchwald-Hartwig aminations to form **2.52g**.

Increasing the number of equivalents of the 4-methoxy-2-chloroaniline from 1.2 to 2.4 equiv was explored to see if stoichiometry had control over the formation of the product **2.52g**. Just by increasing the aniline equivalents, an increase from 25% to 42% was observed. Further optimisation of this reaction could be achieved by carrying out temperature studies. Maximising the formation of the mono Buchwald-Hartwig intermediate over **2.53** with milder reaction conditions, before increasing the temperature for the second reaction.

2.5 Targeted synthesis of natural products and their analogues through the newly developed one pot approach

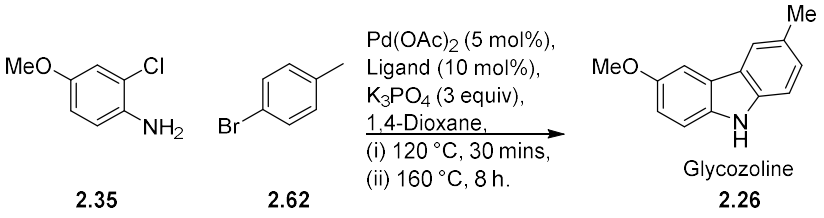
2.5.1 Total Synthesis of Glycozoline, Harmane and Murrayafoline A

Although this general type of cross coupling had been previously established on a focused set of substrates problems were encountered when translating the conditions to more complex natural products (Scheme 28).[144]



Scheme 28. Bedford method: Total synthesis of Glycozolidine.[144]

Glycozoline (**2.26**) was chosen as a model natural product target. Using the conditions established for the pyridocarbazoles (Scheme 26), the natural product was synthesised in 22% yield. A change in ligand to DavePhos resulted in an increase in the yield of **2.26** (36%). It was postulated, that the poor conversion was likely due to the deactivation of the catalyst.

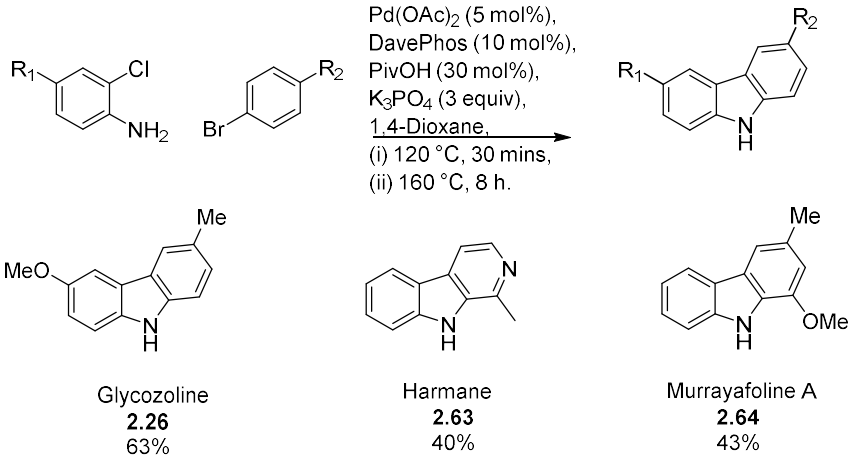


Scheme 29. Total synthesis of Glycozoline (**2.26**).

To investigate, a second charge of $Pd(OAc)_2$ and DavePhos was added to the reaction before increasing the temperature to 160 °C for 8 h. Surprisingly this modification actually decreased the yield to 25%.

Previous work carried out by the Fagnou lab discovered pivalic acid can act as a 'proton shuttle' in direct arylations which could potentially increase the efficiency of the second step.[154] Pivalic acid after the Buchwald-Hartwig step, resulted in an increase in yield to 56%. However, when added at the start of the one-pot process the isolated yield increased to 63%.

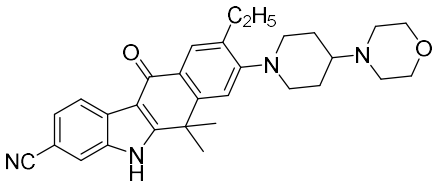
With these conditions in hand the natural products Harmane (**2.63**) and Murrayafoline A (**2.64**) were synthesised in moderate yields (40% and 43% respectively) in one-pot. Although the yields were modest, previous syntheses of the three carbazoles involve multi-step processes, that either have a comparable or lower overall yield to those shown in Scheme 30.



Scheme 30. Total synthesis of Glycozoline (**2.26**), Harmane (**2.63**) and Murrayafoline A (**2.64**). Ligand = DavePhos, Additive = PivOH.

In 2018, glycozoline (**2.26**) was synthesised in an overall 56% yield over a six step synthesis.[155] However this synthesis required harsh reaction conditions such as DDQ oxidation and Pd/C hydrogenation. Additionally the starting materials were substituted indoles that are not easy to diversify nor acquire commercially. The total synthesis of harmane (**2.63**) was reported in 65% over two steps from the starting material tryptamine. Although an improvement on the 40% in Scheme 30 it does require one additional step. Finally, Murrayafoline A has been synthesised recently through an Ullmann cross coupling reaction in an overall 49% yield over two steps.[156] This synthesis uses a similar direct-arylation strategy in the second step as shown in Scheme 30, however the reaction times are greater than 12 h and a comparable yield can be obtained in one-step using the one-pot process.

Further expansion of this synthesis could allow access to carbazole containing drug molecules e.g. alectinim (**2.65**) (Figure 54).



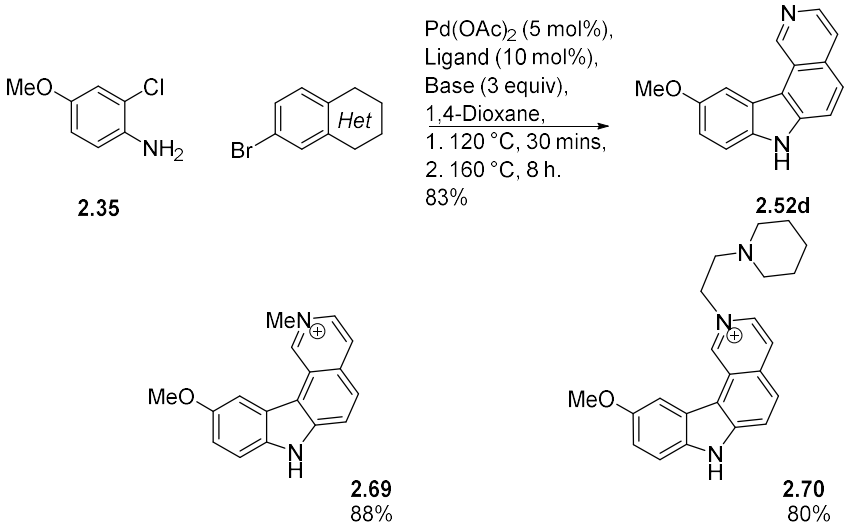
Alectinib
2.65

Figure 54. Structure of alectinim, an ALK inhibitor

2.5.2 Synthesis of Ditercalinium and Biologically Active Alkylated Pyridocarbazoles

Pyridocarbazole **2.52d** is a precursor to the anticancer drug Ditercalinium. Previous literature published by Roques *et al*. in 1980, synthesised **2.52d** in 32% yield over 6 steps. Methylation of **2.52d** yielded **2.69** in 73%, translating to an overall yield of 24%. Compound **2.70** was synthesised in 50% for an overall yield of 16%.[157]

2.52d was synthesised in one-pot from commercially available starting materials in 83% yield (Scheme 26). Further functionalisation obtained **2.69** in 88% yield and **2.70** in 80% yield (73% and 67% overall yields respectively) (Scheme 31).



2.35

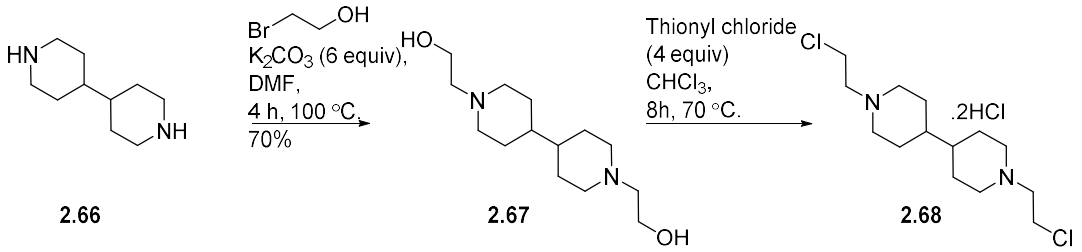
2.52d

2.69
88%

2.70
80%

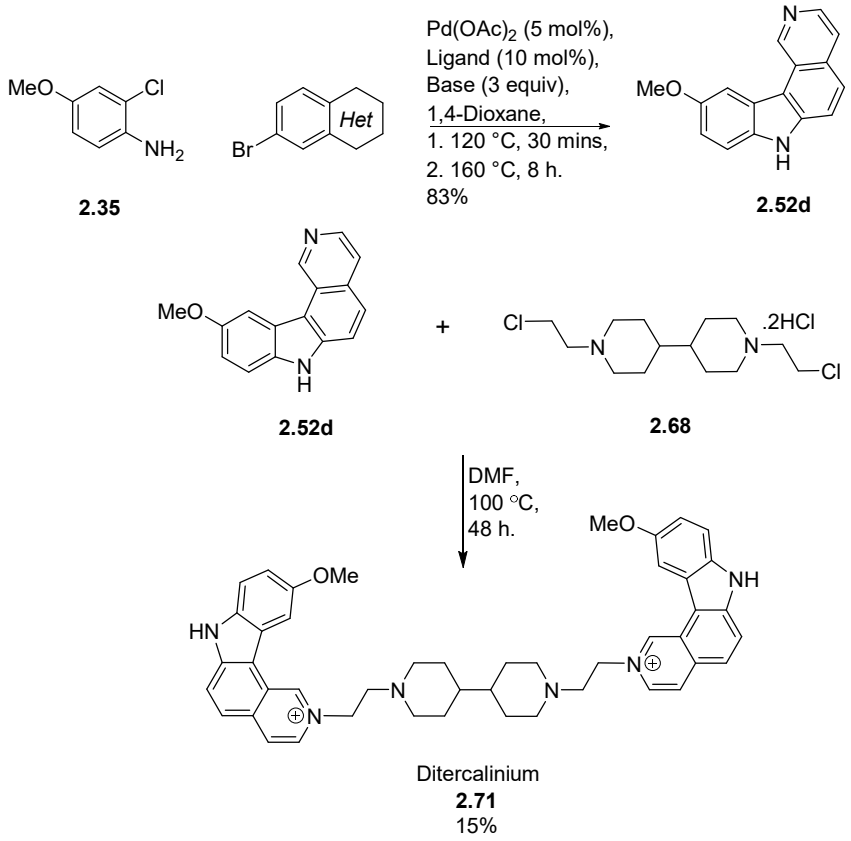
Scheme 31. Synthesis of **2.52d** and alkylated products **2.69** and **2.70**.

The bipiperidyl nitrogen mustard linker (**2.68**) was synthesised by alkylation of compound **2.66** with bromoethanol to give **2.67** in 70% yield, followed by halogen exchange with thionyl chloride and used in the synthesis of Ditercalinium (**2.71**) without further purification (Scheme 32).



Scheme 32. Synthesis of 1,1′-bis(2-chloroethyl)-4,4′-bipiperidine (**2.68**).

Ditercalinium (**2.71**) was isolated in 15% yield (Scheme 33). Whilst the conversion of this reaction was higher according to RP-HPLC, purification was challenging and required multiple re-crystallisations resulting in a much lower isolated yield than expected. Even with the difficulties in purification the resulting yield from the bis-alkylation was in-line with literature precedent.[158]

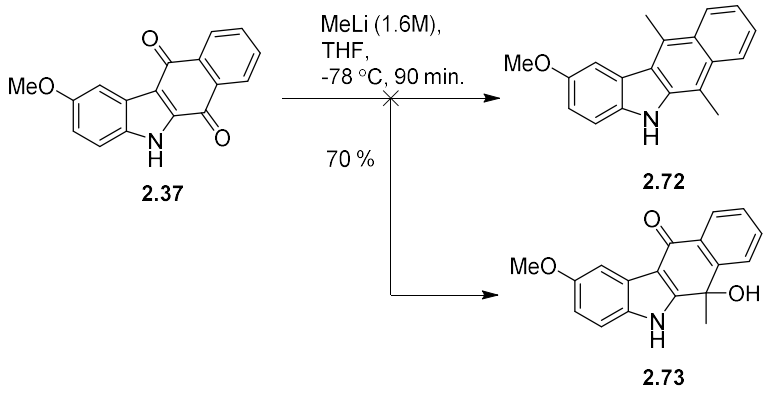


Scheme 33. Total synthesis of Ditercalinium (**2.71**).

2.5.3 Towards the Synthesis of Deaza-ellipticine

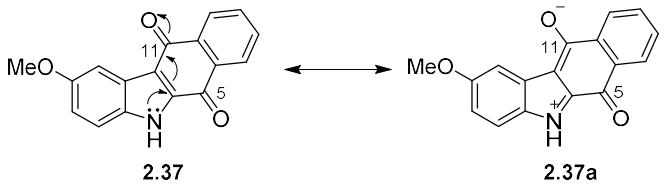
Given the optimization and scope of this synthesis established in Scheme 23, the tetracyclic diones (**2.45a-f**) could be utilised to access an analogue of GQC-05 (**1.31**), which had been previously shown to induce a splice-switch in Bcl-x, to upregulate the pro-apoptotic Bcl-x_S.[115] It was

proposed that methylation followed by reduction of the dione moiety in (**2.45a**) would give rise to 9-methoxydeazaellipticine.[149] However, previous work by group member Dr Olivia Rutherford showed the monomethylated side product **2.73** was isolated in 70% yield in place of the dimethylated **2.72** (Scheme 34).



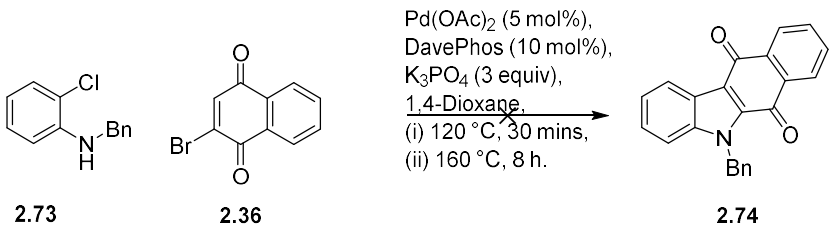
Scheme 34. Attempted synthesis of **2.72** carried out by Dr Olivia Rutherford.[116]

Characterisation determined the methylation was occurring only at the 5-position as a consequence of the vinylic amide nature of position 11. This is due to conjugation with the lone-pair of the N-carbazole (Scheme 35).



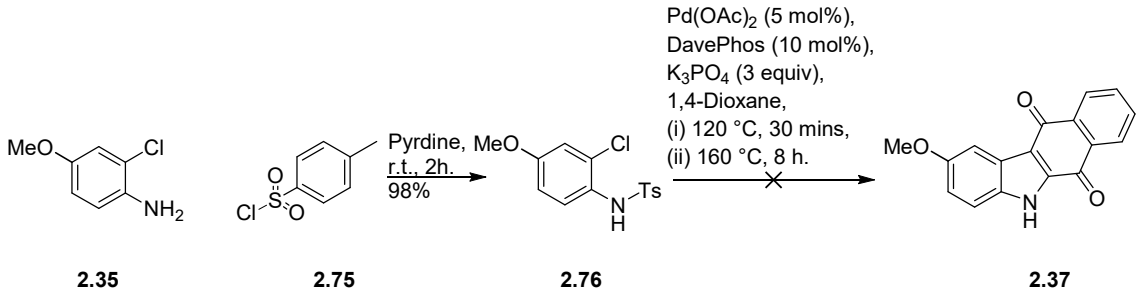
Scheme 35. Conjugation of N lone pair with ketone (**2.37**) stabilises the 11 position carbonyl to nucleophilic attack, increasing electron density at the point of attack.

Initially, coupling with the benzyl protected aniline **2.73** was attempted to break the conjugation of the N-lone pair, thereby facilitating di-methylation. However, coupling of 2-bromonaphthalene-1,4-dione with **2.73** afforded only a mixture of aniline **2.73** and the degraded de-chlorinated starting material. (Scheme 36).



Scheme 36. Attempted synthesis of benzylated **2.74**.

From this result, it was deduced that the reactivity of aniline **2.73** is diminished by the benzyl protecting group. To avoid this, the tosyl-protected aniline **2.76** was prepared. Tosyl-protected aniline **2.76** was isolated in 98% and used in the one-pot cross coupling (Scheme 37).

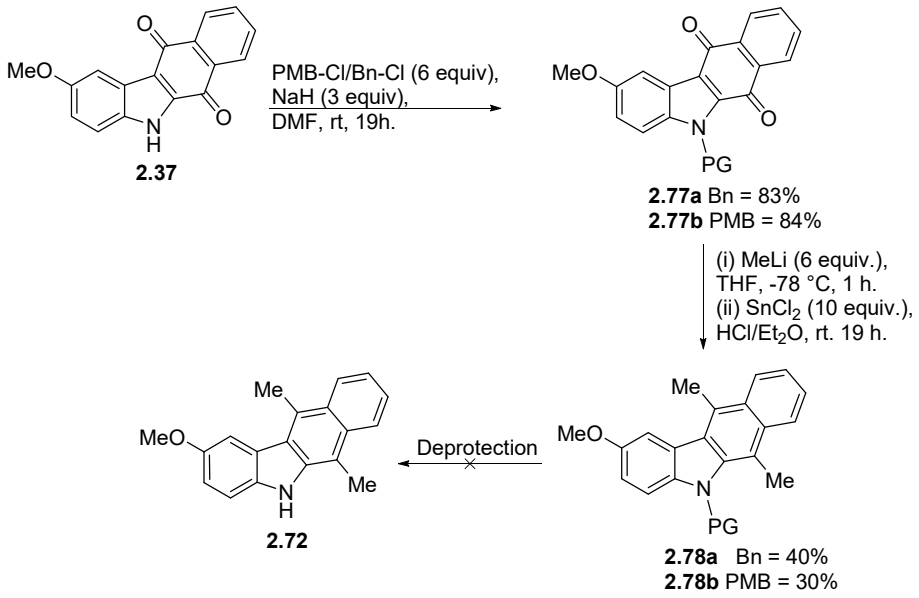


2.35 **2.75** **2.76** **2.37**

Scheme 37. Attempted synthesis of tosyl-protected **2.37**.

This reaction was unsuccessful with analysis by LC-MS showing a mixture of starting material **2.76** and the de-tosylated coupled product **2.37**, suggesting that the protected aniline **2.76** was not capable of the Buchwald amination step. It was decided at this point to abandon protection prior to the one-pot coupling and to attempt protection of **2.37**.

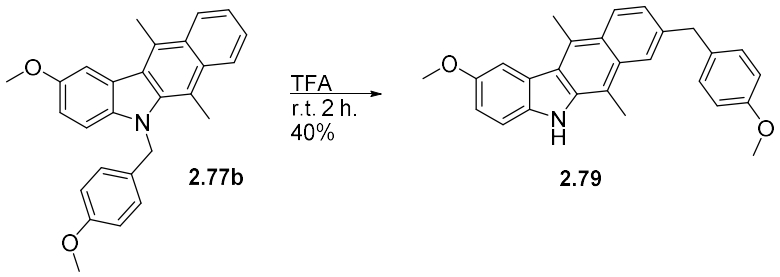
Compound **2.37** was unsuccessfully subjected to various protection conditions using inorganic bases. It was proposed that bases such as K_2CO_3 and Na_2CO_3 were not strong enough to deprotonate the indole nitrogen and facilitate the protection. Therefore, **2.37** was reacted with benzyl bromide in the presence of NaH for 2 h to afford the desired compound **2.77a** in 83% yield.



Scheme 38. Towards the synthesis of 2-deaza-9-methoxyellipticine (**2.72**). PG = Protecting group (Bn/PMB).

Compound **2.77a** was dissolved in THF and cooled to −78 °C. MeLi was added dropwise over 10 mins, allowed to warm to room temperature and then stirred for 3 h. The reaction was cooled and analysed by TLC showed full consumption of starting material. $SnCl_2$/HCl in ether was added and the reaction stirred vigorously for 3 h, resulting in the formation of **2.78a** in 40% yield.[149] Compound **2.78a** was then subjected to hydrogenation at room temperature overnight, which resulted in recovery of starting material. The hydrogenation was repeated but this time at 50 °C overnight. Unfortunately, no conversion to **2.72** was observed. Aluminium chloride in acidic conditions has been shown to deprotect N-Bn functional groups,[159] however this resulted in degradation of **2.78a**.[160]

Exchange of the benzyl group (**2.77a**) for PMB-group was carried out, in the hope that the additional stability from the para-methoxy moiety would facilitate an easier deprotection. The PMB analogue (**2.77b**) was synthesised in the same route as the benzyl **2.77a** in comparable yields, and subjected to various deprotection methods. Reaction with $AlCl_3$ showed no conversion to **2.72**. However, reaction with TFA/H_2SO_4 did show some conversion to the deprotected **2.72** although multiple side-products were observed by TLC. The major product was migration of the PMB group to the D-ring (**2.79**) as previously observed for the deprotection of tricyclic PMB-protected carbazoles.[161]



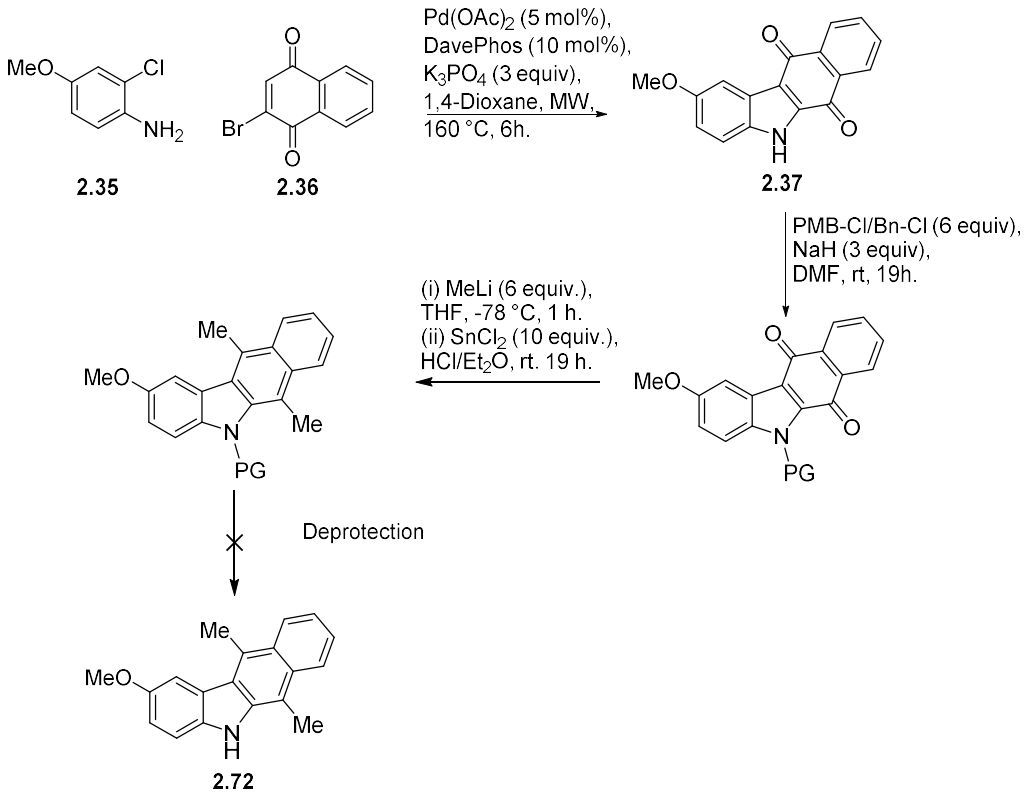
Scheme 39. Proposed structure of PMB migration (**2.79**) in TFA.

2.6 Conclusions and Future Work

A convergent route to access 5*H*-benzo[*b*]carbazole-6,11-diones and 7*H*-pyridocarbazoles was achieved through a one-pot consecutive Buchwald-Hartwig amination and direct arylation reaction. It was found that choice of base and ligand was crucial for direct arylation efficiency particularly to access 7H-pyridocarbazoles analogues. Quaternization of pyridocarbazole **2.52d**, gave access to known anti-tumour agents **2.69**, **2.70**, and Ditercalinium (**2.71**) in overall yields 73%, 66% and 13% respectively.[157]

With the addition of a proton-shuttle, pivalic acid, this one-pot method was translated to the total synthesis of three carbazole natural products; Glycozoline (**2.26**), Harmane (**2.63**) and Murrayafoline A (**2.64**) in one step.

The synthesis of 2-deaza-9-methoxyellipticine (**2.72**) was attempted upon the isolation of **2.37** (Scheme 40). It was thought that the methylation of the dione moiety would grant access to a convergent route to **2.72**. However, the 'amide-like' electronics observed resulted in only mono-methylation from occurring (Scheme 34). Protection of the carbazole nitrogen overcame this issue, however deprotection to obtain **2.72** has provided a significant synthetic challenge. Deprotection was successful in TFA (Scheme 39), however the PMB protecting group migrated to the D ring to produce **2.79**. Next steps to be undertaken are the use of oxidising agents e.g. DDQ, in attempt to complete the synthesis.



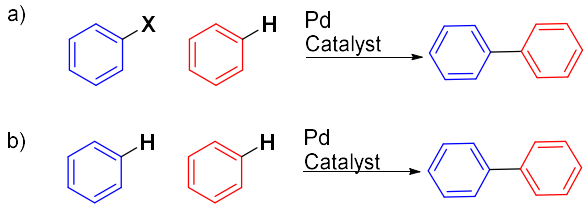
Scheme 40. Overview of the attempted synthesis of 2-deaza-9-methoxyellipticine (**2.72**). PG = protecting group.

Chapter 3 Mechanistic Insights into the Palladium-Catalysed Formation of Carbazoles by Direct C-Arylation

3.1 Direct-arylation: An Alternative to Traditional C-C Cross Couplings

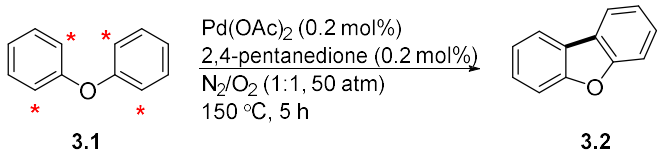
3.1.1 Introduction

Direct-arylation reactions have become a cornerstone of developmental chemistry and can be divided into two distinct categories: 1) coupling to aryl halides and 2) oxidative coupling (Scheme 41).[139]



Scheme 41. Schematic of palladium cataylysed direct arylations. (a) coupling to aryl halides, (b) oxidative coupling.

Oxidative coupling between two aryl C-H bonds is advantageous as it requires little pre-functionalisation using readily available starting materials. A pertinent example of this approach has been the preparation of bibenzofurans (e.g., **3.2**) from a biaryl ether precursor, such as **3.1** (Scheme 2).[162]



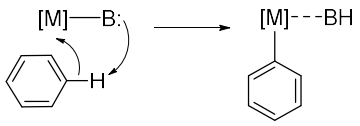
Scheme 42. Palladium catalysed intramolecular oxidative direct arylation. Sites of potential arylation highlighted by red astericks.

Although a highly economical route, oxidative *C*-arylation is not without its drawbacks. The lack of functionality makes selectivity of the transformation difficult with activation of two C-H bonds possible when substituted aromatics are used (Scheme 42).[163]

An effective strategy to circumvent this chemoselectivity issue is to replace one of the C-H bonds with an aryl halide (Scheme 41a). Palladium cross coupling reactions with aryl-halides primarily proceed through an oxidative addition into the aryl-halide bond. This controls the site of *C*-arylation of the nucleophile as the oxidative addition directs regioselectivity on the electrophile.

3.1.2 Scope of the Intramolecular Direct Arylation reaction

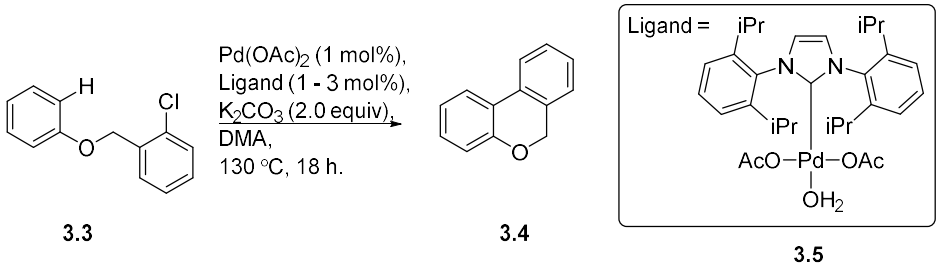
Metal-base mediated deprotonation is another method which is an effective strategy to control the site of the nucleophile (Scheme 43).[164,165,166]



Scheme 43. Early metal/base mediated deprotonation mechanism.

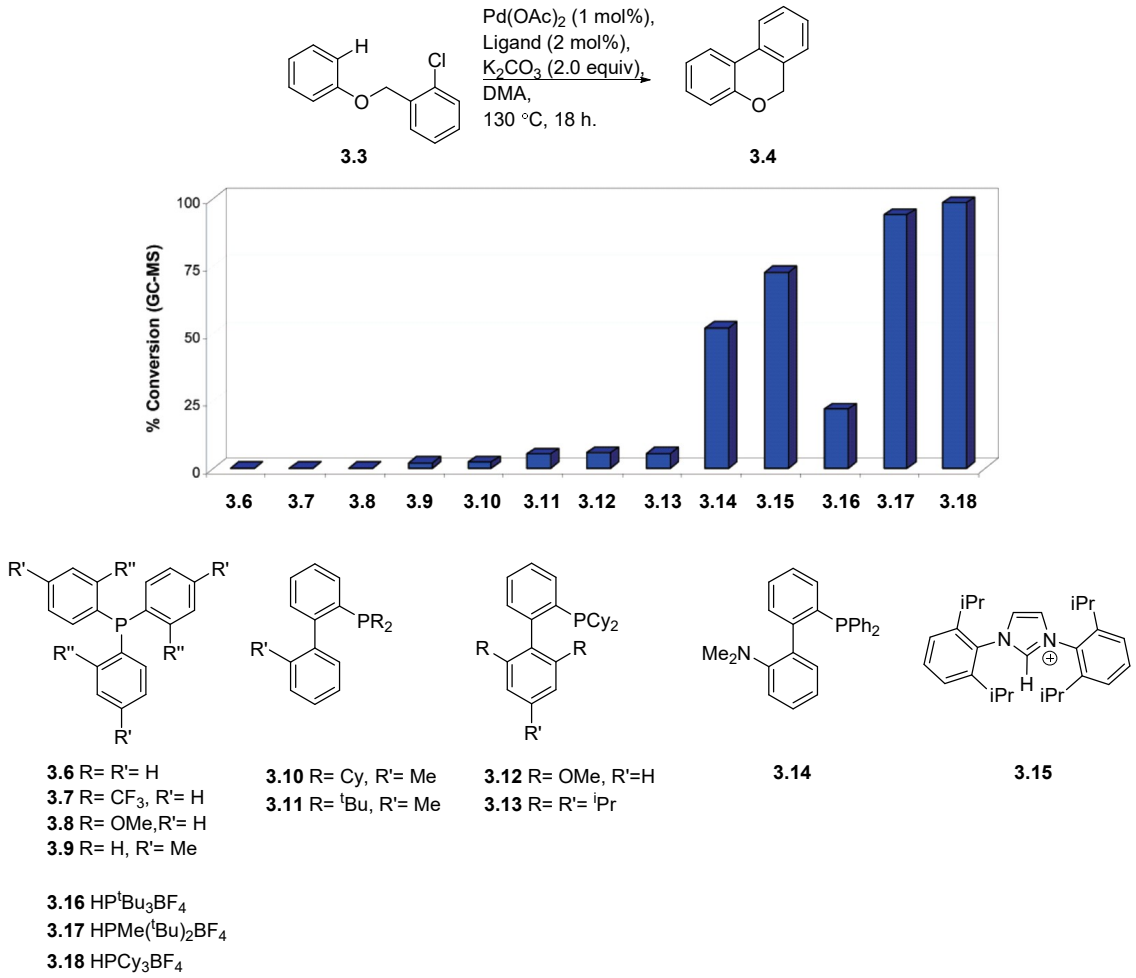
The first studies directed at using this mechanism for the metalation of arenes were conducted by Davidson and coworkers in 1968.[167] These studies highlighted that the choice of metal was essential for successful C-H activation. $Pd(OAc)_2$ was found to be the most successful as the aceto-ligand carries out multiple roles through the reaction e.g. increased solvation (in comparison to $PdCl_2$) and increased electrophilicity of the metal centre.

In 2005, Fagnou and coworkers developed a palladium mediated C-H activation to form six membered biaryl rings (Scheme 44).[168,123]



Scheme 44. Fagnou synthesis: palladium-catalysed direct arylation to form six-membered biaryl ethers.[123]

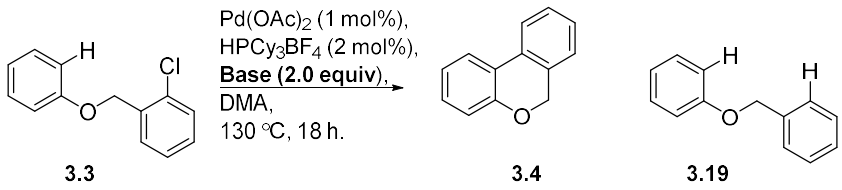
Fagnou *et al*. demonstrated that the use of NHC ligands for direct *C*-arylation was sufficient for simple direct arylations. However efficiency was lost when more sterically bulky substrates were used.[123,169] A re-optimisation through a more extensive scope of catalysts was carried out to find a more generally applicable system. A catalyst and ligand screen in dimethylacetamide (DMA) was explored and heated thermally to 130 °C.[170]



Scheme 45. Pd-Catalysed *C*-arylation to form benzofurans as reported by Fagnou *et al.* Re-optimisation of ligand scope. Reactions heated until catalyst deactivation was complete.[171]

The bi-aryl and tri-aryl phosphines gave poor conversion of benzofurans (**3.6 – 3.13**) overall, with the exception of **3.14** which gave over 50% conversion. The stand-out ligands were the trialkylphosphine ligands (**3.16 – 3.18**). In particular, $HPCy_3BF_4$ (**3.18**) gave close to quantitative conversion even with low catalytic loading of Pd (0.1 mol%) (Scheme 45).

Varying the base, also showed to be influential on the reaction (Scheme 46), specifically on the rate of de-halogenation (**3.19**). K_2CO_3 showed the best results (Table 6, entry 2), however changing just the counter-ion had devastating effects on conversion: Na_2CO_3 (Table 6, entry 1) and Cs_2CO_3 (Table 6, entry 3). Hydroxide bases like KO^{t}Bu (Table 6, entry 4) showed extensive degradation of the starting material with a ratio of 2.3: 1.0 (**3.4**: **3.19**).



3.3 3.4 3.19

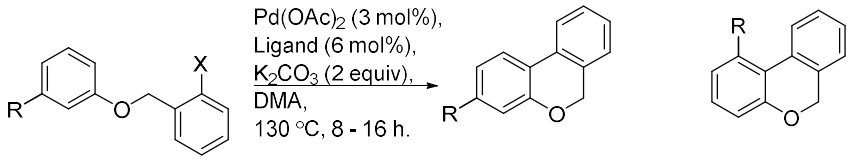
Scheme 46. Pd-Catalysed *C*-arylation to form benzofurans as reported by Fagnou *et al*. Scope of base used in direct arylation.[171]

Table 6. Fagnou synthesis: Conversions and ratios of compounds **3.4** and **3.19** when varying the type of base used.

Entry	Base	Conversion (%)	Ratio 3.4: 3.19
1	Na_2CO_3	11	20:1
2	K_2CO_3	100	>99:1
3	Cs_2CO_3	25	15:1
4	KO^{t}Bu	84	2.3:1
5	K_3PO_4	13	5:1
6	KOAc	81	>99:1
7	NaOAc	41	28:1
8	Et_3N	3	2:1
9	DIPEA	2	1.8:1
10	Cy_2MeN	4	3:1

The effect of the halide employed for the reaction was also studied and found that although aryl iodides are the most effective coupling partners in many *C*-arylations,[172,173,168] they performed relatively poorly in the previously optimised conditions (64% conversion). It was postulated that an accumulation of iodide ions in solution was poisoning the catalyst. It was subsequently found that adding a AgOTf or Ag_2CO_3 overcame this issue effectively by sequestering the excess iodide.

The regioselectivity of the transformation was then investigated through a scope of R-group substituents on the arene ring.



3.3 3.4 3.20

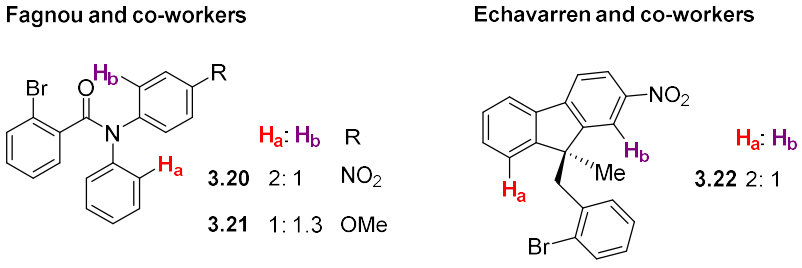
Scheme 47. Pd-Catalysed *C*-arylation to form benzofurans as reported by Fagnou *et al*. Substituent effects on regioselectivity of direct arylation.[171]

Table 7. Substituent effects on regioselectivity of direct arylation (**3.4**: **3.20**).

Entry	Substituent	Halide	Ligand	Ratio 3.4: 3.20
1	OMe	Br	$HPCy_3BF_4$	10:1
2	Me	Br	$HPCy_3BF_4$	15:1
3	*i*-Pr	Br	$HPCy_3BF_4$	>30:1
4	*t*-Bu	Br	$HPCy_3BF_4$	>30:1
5	CF_3	Br	$HPCy_3BF_4$	>30:1
6	NO_2	Br	$HPCy_3BF_4$	>30:1
7	CO_2Me	Br	$HPCy_3BF_4$	>30:1
8	Cl	Br	$HPCy_3BF_4$	3.2:1
9	F	Br	$HPCy_3BF_4$	1:4.3
10	F	Cl	$HPCy_3BF_4$	1:8.3
11	F	Br	$HP^tBu_3BF_4$	1:1.3
12	F	Br	HP*t*Bu2MeBF4	1:6.9

It was found that in general, the reaction proceeded via activation of the least sterically hindered C-H bond (Table 7, entries 1-7). Interestingly when replaced with halide substituents the selectivity was drastically decreased (Table 7, entries 8-12) to as low as 1:1.3 in favour of **3.20** (Table 7, entry 11).

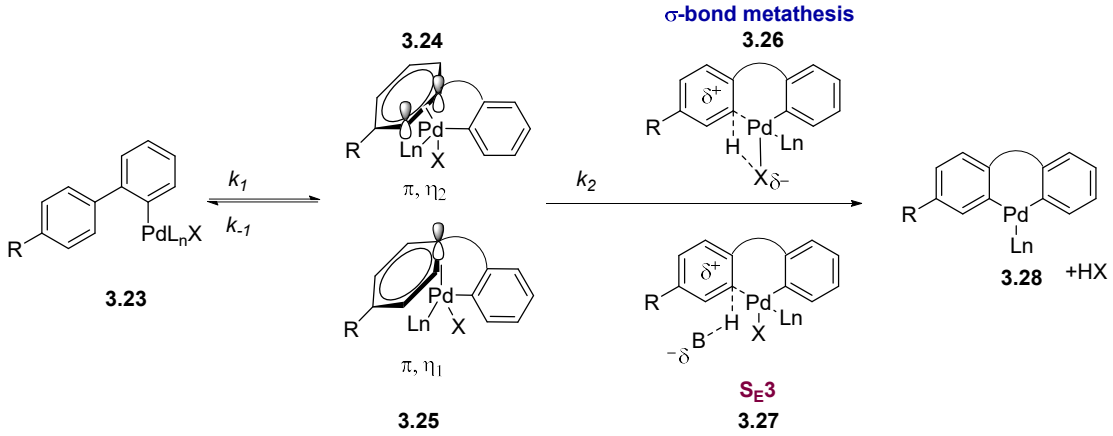
Work carried out by the Echavarren and Fagnou groups concurrently identified that the nature of the reaction was governed by the choice of base, ligand and aryl halide.[174,175,176] Furthermore, their work highlighted that for the substrates analysed that the selectivity of the C-H activation was not solely directed by electronically biased arene substrates (Scheme 48).



Scheme 48. Fagnou and Echavarren work on selectivity of direct arylation. H_a (red) = least hindered direct arylation site.

Isotopic studies obtained revealed a large KIE (3.5 – 6.7) value suggesting cleavage of the C-H bond and the Pd-C bond formation are happening simultaneously. These observations were in-line with a CMD type transformation.[174,175,]

Although a C-H oxidation mechanism is not contradictory to the results observed by Fagnou and Echavarren, computational studies have shown that it is less favourable than a σ-bond metathesis or S_E3 mechanism.[177]

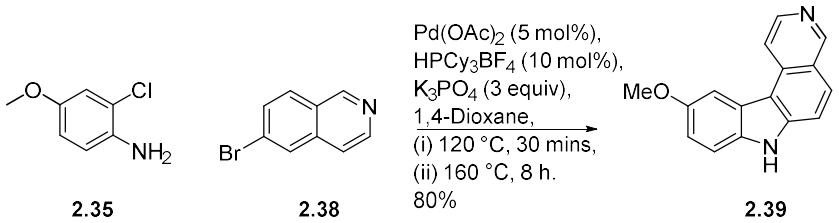


Scheme 49. Two possible direct arylation mechanisms: σ-bond metathesis (blue) and S_E3 (red).[170]

Classically, electrophilic aromatic substitution reactions cannot be analysed by KIEs because the deprotonation step is too fast to observe in comparison to the formation of the σ –aryl complex. However, a primary KIE was measured for this transformation suggesting a route other than electrophilic aromatic substitution. Two potential routes can account for the high KIE observed (Scheme 49). A primary KIE indicates that the second step is kinetically significant. For this to be the case, the first step would have to be very fast and reversible in comparison to k_2. This can be rationalised by either the σ-bond metathesis (deprotonation is facilitated by a palladium ligand) or by the S_E3 mechanism (deprotonation is facilitated by an external base).

3.1.3 Carbazole and Pyridocarbazole Synthesis *via* C-C Direct Arylation

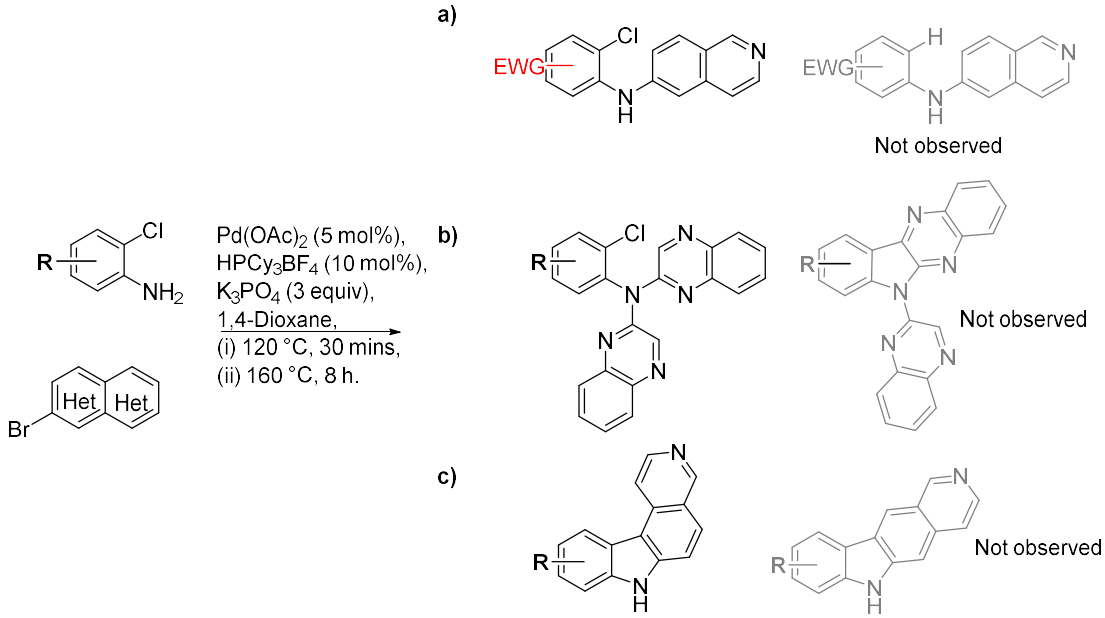
Building on the direct arylation work carried out by Fagnou[168], Bedford[144] and Ackermann[145], a novel convergent route to access pyridocarbazoles was established in Chapter 2 (Scheme 50).



Scheme 50. Consecutive Buchwald-Hartwig amination and direct arylation reactions to form **2.39.**

Development of the synthesis required optimisation of the literature precedent as the conditions proposed by Bedford for carbazole synthesis resulted in no conversion to **2.39**. Interesting

observations through scope expansion, warranted further investigation. Firstly, reactions with electron withdrawing groups in the A-ring e.g. attempted synthesis of **2.52c**, showed poor conversion for the direct arylation step. Interestingly, no de-halogenation was observed suggesting the barrier to the reaction being oxidative addition (Scheme 51a). Secondly, direct arylation was also prevented in reactions where the double-Buchwald-Hartwig aminated bi-product was formed (Scheme 51b). And finally, the regiochemistry observed for pyridocarbazoles was entirely selective for the ring closure at the 5-position of the isoquinoline (Scheme 51c).



Scheme 51. Direct arylation limitations from scope in Chapter 2.

3.2 Chapter Aims

The overall objective of this chapter is to investigate the mechanism of the two-step, one-pot palladium catalysed synthesis developed in Chapter 2.

This will be investigated through:

1. Ligand and base investigation,
2. Designed control reactions to determine essential functionality for the transformation,
3. And through density functional theory (DFT) molecular orbital calculations.

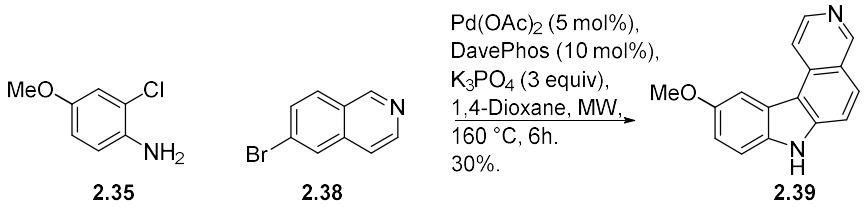
3.3 Results and Discussion

3.3.1 Buchwald-Hartwig Amination

The Buchwald-Hartwig amination is a well-established transformation and the optimisation and scope outlaid in (Scheme 20-Scheme 22) followed trends seen throughout literature.[124] Electron-rich anilines improves transmetallation over electron-poor substrates. Interestingly it was the dialkylbiaryl ligands in conjunction with K_3PO_4 that yielded the highest conversions over the alkyl cyclohexlphosphine or tri-*tert*-butylphosphine ligands. The biaryl systems are electron rich, improving oxidative addition, but the additional added bulk from the biaryl system will concomitantly improve reductive elimination.

3.3.2 Direct *C*-arylation Studies to form the Tetracyclic Carbazole Core

The mechanism of the second-step is of particular interest. As reported previously by Fagnou and co-workers, there is great evidence to suggest similar transformations occur through the concerted metalation pathway (Scheme 49).[178] Investigation into the reaction mechanism began with the observation of poor yields when using DavePhos as a ligand for the formation of **2.39** (Scheme 52).

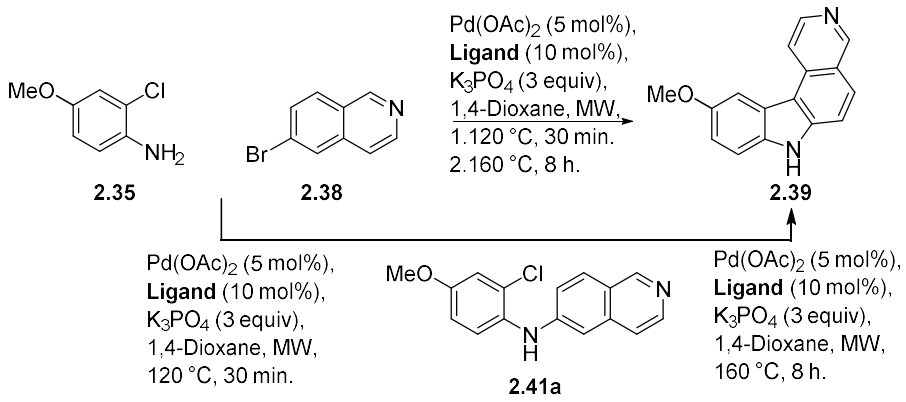


Scheme 52. Consecutive Buchwald-Hartwig amination and direct arylation to form 10-methoxy-7H-pyrido[3,4-c]carbazole (**2.39**).

Initially it was thought that the lower conversion could be due to poor catalyst turnover, potentially from interaction with chelation of the Pd species with either the anilinic or pyridinic nitrogens presentin the substrates. However, addition of $Cu^{II}OAc_2$ as an oxidant proved

detrimental to yield (43% to 26% conversion). Re-optimisation highlighted that $HPCy_3BF_4$ resulted in a doubling of conversion to 78% when compared to DavePhos (36%). This could potentially be due to steric hindrance having more of a factor in the second step due to the limited space once the Buchwald-Hartwig intermediate has been formed.

This is particularly interesting, as $HPCy_3BF_4$ showed only 10% conversion for the first Buchwald-Hartwig step when reacted with K_3PO_4 at 120 °C for 30 mins. This suggested, that in these conditions, the first step required higher temperatures to react. This brought into question the reaction mechanism, particularly whether the Buchwald-Hartwig reaction was required to facilitate the direct arylation in a sequential manner when heated to 160 °C.

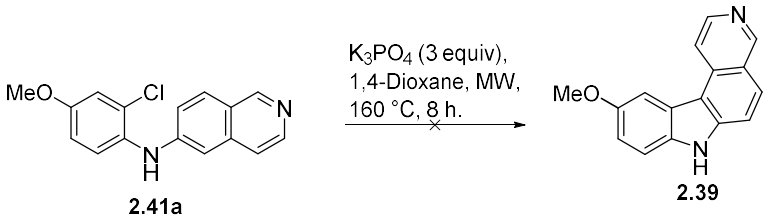


Scheme 53. Consecutive Buchwald-Hartwig amination (**2.41a**) and direct arylation to form 10-methoxy-7H-pyrido[3,4-c]carbazole (**2.39**). Ligand (see Table 8)

Table 8. Ligand effects on conversion to **2.39**.

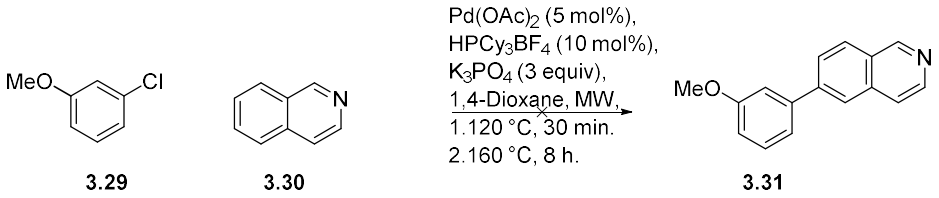
Entry	Ligand	2.41a Conversion (%)	2.39 Conversion (%)
1	DavePhos	85	36
2	$HPCy_3BF_4$	10	78

The importance of the palladium catalyst was then investigated to determine whether *C*-arylation was proceeding through a metal-catalysed pathway. To investigate this, **2.41a** was heated with base at 160 °C for 8 h (Scheme 54). No conversion to **2.39** was observed by LC-MS, with only starting material present in the reaction mixture. This confirmed that the second step is indeed mediated through a palladium-catalysed pathway.



Scheme 54. Control experiment highlighting that direct *C*-arylation required a palladium catalyst (0 mol%).

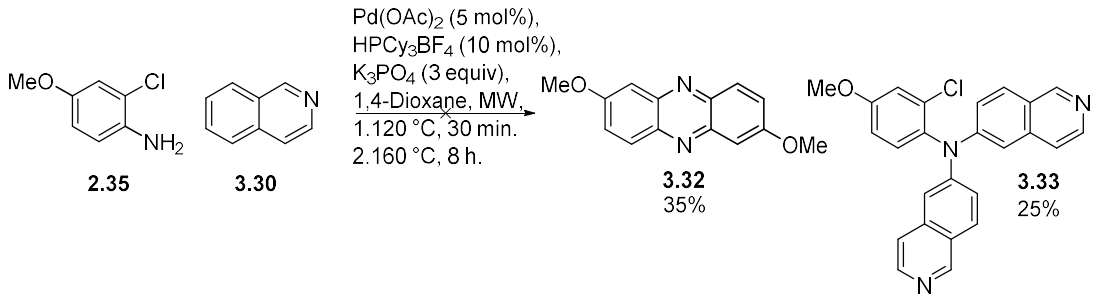
To determine whether the transformation requires a sequential two-step process, the functionality required for the Buchwald-Hartwig amination was removed.



Scheme 55. Control experiment: consecutive Buchwald-Hartwig amination and direct arylation to form **3.31**.

Compound **3.29** was reacted with isoquinoline (**3.30**) (Scheme 55). The hypothesis was that if the process was sequential, then the formation of the secondary amine **2.41a** would be essential to enable the second *C*-arylation step. Upon reaction at 160 °C for 8 h, isoquinoline **3.30** was recovered in 96% yield with no conversion to **3.31**. This suggests a pathway whereby the formation of the secondary aniline is essential for Pd-catalysed *C*-arylation.

Next, the influence of the heteroaryl bromide was investigated. 2-Chloro-4-methoxyaniline (**2.35**) was reacted with isoquinoline (**3.30**) under the standard one-pot conditions (Scheme 56).



Scheme 56. Consecutive Buchwald-Hartwig amination and direct arylation to form **3.32** and **3.33**.

Surprisingly, this resulted in the formation of the double aminated product **3.33** in 25% isolated yield. Given the lack of a bromide on the isoquinoline, a Buchwald-Hartwig amination is not feasible. Therefore, a potential Pd-catalyzed C-H activation at the 6-position could occur due to the elevated temperatures achieved in 1,4-dioxane. It is probable that this activation occurred in

the reaction highlighted in Scheme 55**,** however in this instance, a nucleophilic aniline is now present to complete transmetallation. Remarkably the C-H activation is regioselective for the 6-position of the isoquinoline with no formation of **2.41a** or **3.34**. Previous reactions where the double aminated product was formed also showed this to be synthetically non-productive, preventing any direct arylation from occurring (**Error! Reference source not found.**). This further strengthens the hypothesis that the free lone pair on the secondary aniline is vital for the direct arylation to proceed.

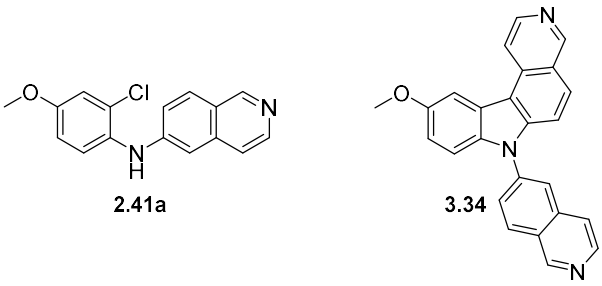
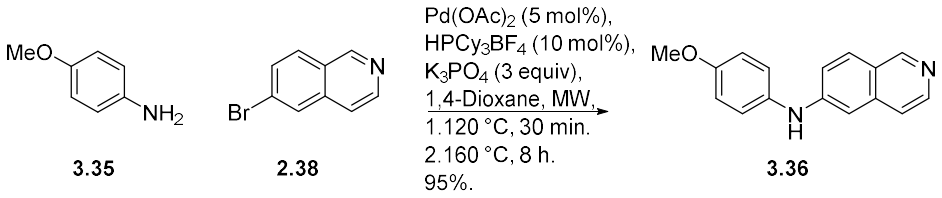


Figure 55. Structures of N-(2-chloro-4-methoxyphenyl)isoquinolin-6-amine (**2.41a**) and 7-(isoquinolin-6-yl)-10-methoxy-7H-pyrido[3,4-c]carbazole (**3.34**).

Although **3.33** was isolated, this was not the major product of the reaction. Phenazine (**3.32**) was isolated in 35% yield. This product is a result of two sequential Buchwald-Hartwig aminations between two molecules of 2-chloro-4-methoxyaniline (**2.35**). Compound **3.32** had not previously been isolated throughout the scope (**Error! Reference source not found.**) and appears to only have been formed as a result of poor reaction with the isoquinoline.

Direct *C*-arylations are known to proceed through an oxidative mechanism where two aryl C-H bonds are activated to couple together (Scheme 42). The importance of the aryl chloride in this system was investigated by reacting 4-methoxyaniline (**3.35**) in the standard one-pot conditions.



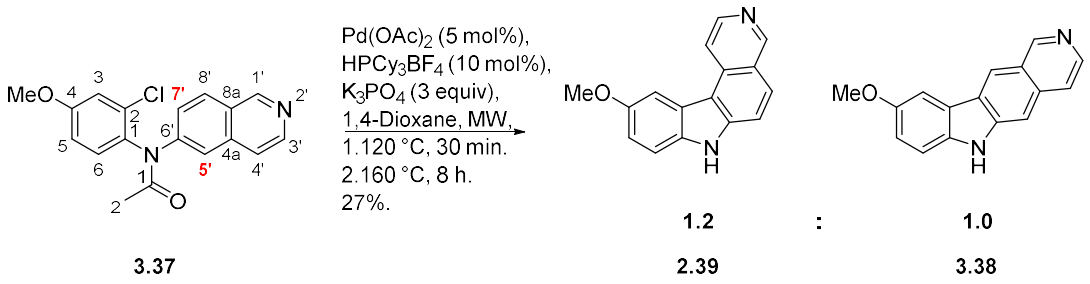
Scheme 57. Consecutive Buchwald-Hartwig amination and direct arylation to form **3.36**.

As expected from an oxidative addition reliant mechanism, **2.39** was not isolated and only the Buchwald Hartwig intermediate **3.36** was formed in 95% yield, suggesting the aryl chloride is essential for *C*-arylation.

The selectivity of the direct *C*-arylation was then investigated. As shown in previous literature, selectivity of direct *C*-arylation reactions is poor unless there is a directing groups or the is sufficient difference in the electronics of the competing C-H bonds.[139,124,178] In this case, it was hypothesised the electronics of the isoquinoline rings were directing the selectivity of the direct arylation. In classic electrophilic substitution with isoquinoline substrates, the 5′ and 8′ positions are activated as the electron density is most stable at these positions, with 5′ being the most nucleophilic.

In this system, the working hypothesis is the C-ring in the isoquinoline is acting as the nucleophile through transmetallation. Given that the classical electrophilic substitution has very little electron density on the 7′ position, this provides strong evidence for the observed regiochemistry.

To investigate the importance of the nitrogen lone-pair in the direct arylation, the secondary nitrogen was protected as an acetamide (**3.37**). It was thought that the unavailability of the lone pair would deactivate the C-ring and hinder the direct arylation efficiency.



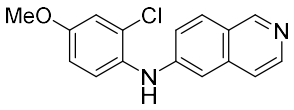
Scheme 58. Consecutive Buchwald-Hartwig amination and direct arylation to form **2.39** and **3.38**. Sites of direct arylation are highlighted in red on **3.37**.

Acetylated **3.37** was subjected to the standard-one pot conditions optimised in Chapter 2 and an unexpected mixture of isomers was isolated. De-acetylated compounds **2.39** and **3.38** were isolated in a 1.2: 1.0 ratio, respectively in a total yield of 27%. Indeed, the efficiency of the direct arylation was compromised as a drop in yield from 80% to 27% was observed. However, acetylation of **3.37** gave access for the first time to the linear analogue of the ellipticine core **3.38**. In all previous reactions, the regioselectivity was solely for **2.39**. Interestingly, no acetylated products were isolated and it was surmised the acetyl group was deprotected due to the elevated temperatures in the presence of base. However, isolation of **3.38** suggests it is favoured when the acetyl group is present prior to C-C arylation. Presumably **2.39** is formed as a result of **3.37** being deprotected prior to C-C arylation, however further investigation is required to confirm.

To investigate this result further molecular orbital calculations were carried out to determine whether the change in regio-selectivity can be attributed to the change in electronics or through a directing-group effect of the carbonyl.

3.3.3 Density Functional Theory Analysis of Direct Arylation

The regioselectivity of the direct *C*-arylation was investigated by calculating the molecular orbital calculations on compound **2.41a**. Compound **2.41a** was first minimised then frequency calculations carried out using the B3LYP correlation functional (6-31+G(d,p)).



2.41a

Figure 56. Structure of N-(2-chloro-4-methoxyphenyl)isoquinolin-6-amine (**2.41a**).

The Mulliken charges displayed through the electron distribution not only showed that the electron density was focused on the carbon atoms at the 5′ (-0.658 au) and 8′ (-1.620 au) position of the isoquinoline, it also highlighted that the 7′ position was very electropositive in comparison (+0.914 au). This corroborates the reqioselectivity observed at the 5′ over the 7′ position as the 7′ position is not nucleophilic enough to affect transmetalation.

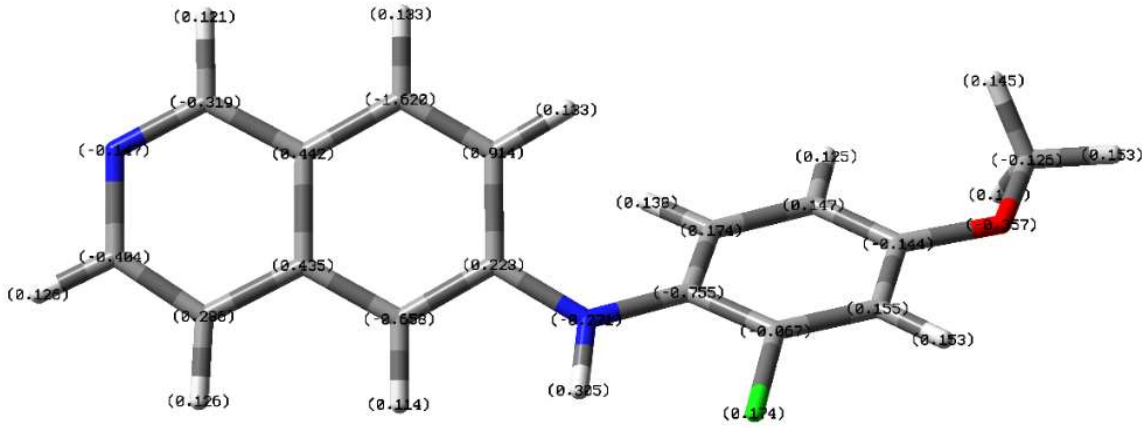


Figure 57. DFT analysis: Mulliken charge distribution of **2.41a**. Values shown are in a.u. Nitrogen atoms (blue), carbon atoms (grey), hydrogen atoms (white), oxygen atoms (red) and chlorine atoms (green).

The HOMO orbital was then visualised in Gaussview. This again showed the concentration of electron density on the 5′ over the 7′ position.

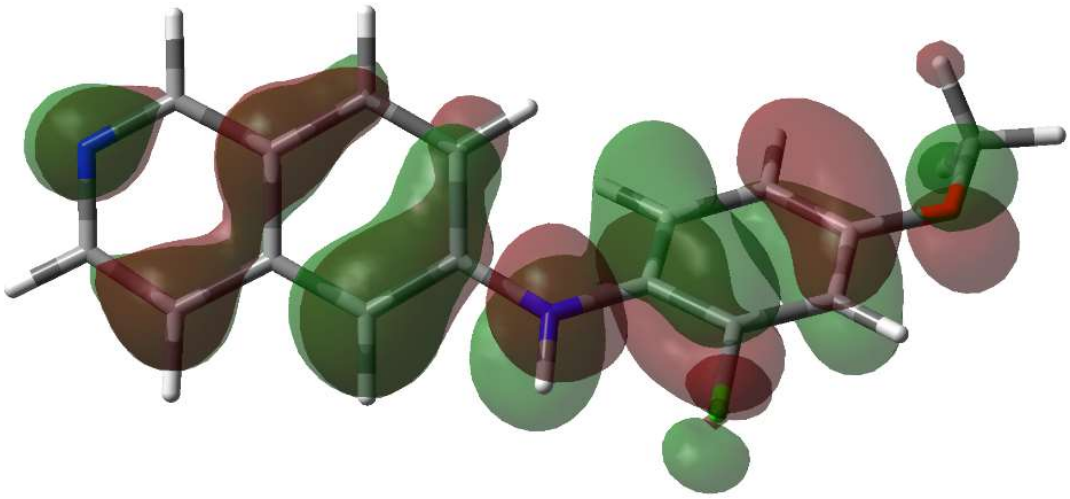


Figure 58. Calculated HOMO molecular orbitals of **2.41a** calculated by DFT (B3LYP correlation functional (6-31+G(d,p)).

Molecular orbital calculations were also carried out on amide (**3.37**).

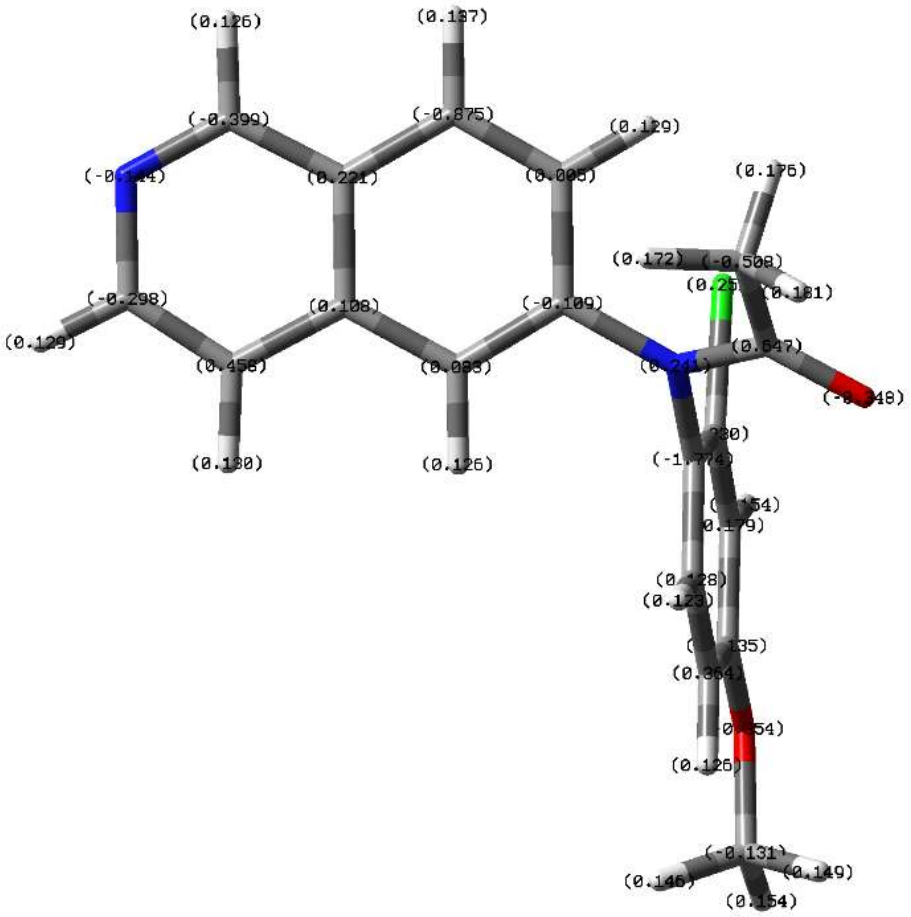


Figure 59. DFT analysis: Mulliken charge distribution of **3.37**. Values shown are in a.u. Nitrogen atoms (blue), carbon atoms (grey), hydrogen atoms (white), oxygen atoms (red) and chlorine atoms (green). Calculated by DFT B3LYP correlation functional (6-31+G(d,p)).

The Mulliken charges calculated for the acetylated amide (Figure 59) were of great interest in comparison to Figure 57**.** The 5′ position had increased in electropositivity from – 0.658 au in **2.41a** to +0.083 au in **3.37**. In contrast, the 7′ position had increased in electronegativity from +0.914 au **2.41a** to +0.005 au in **3.37**. The two sites for direct arylation appear to have the electron density more equally distributed between the two carbons, with the 5′ position still slightly more electronegative. This re-distribution of electron density aligns with the mixture of regiosomers observed in Scheme 58 . In particular it could account for the slight bias towards **2.39** due to the bias in electronegativity of the 5′ carbon.

Next, the HOMO of **3.37** was visualised and provided a surprising molecular orbital picture. Although the charge density distribution showed an increase in electronegativity at the 7′ position, this was not reflected in the HOMO calculations. Once visualised, the HOMO showed electron density to be almost entirely focused on the 5′-position (Figure 60).

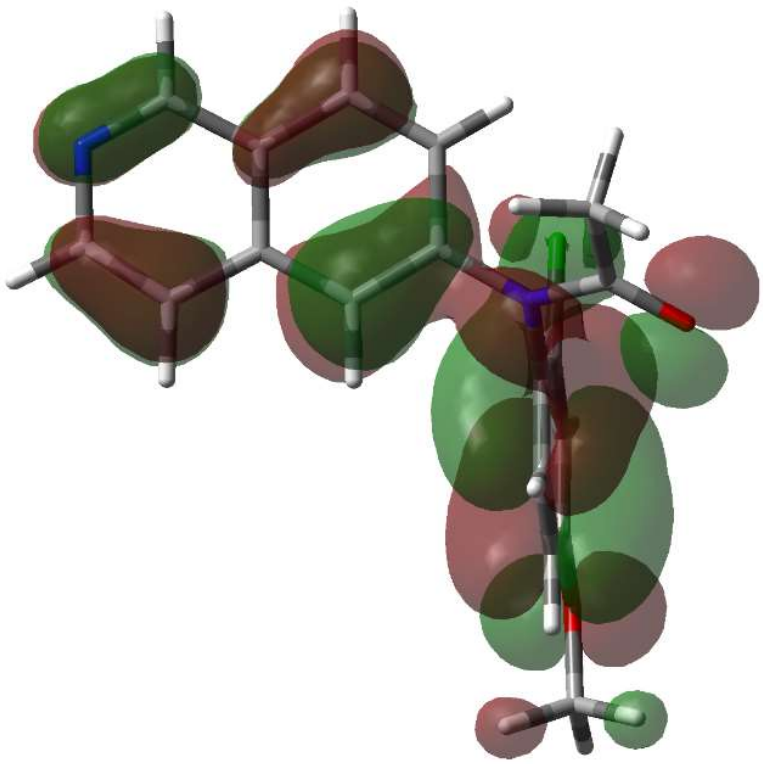
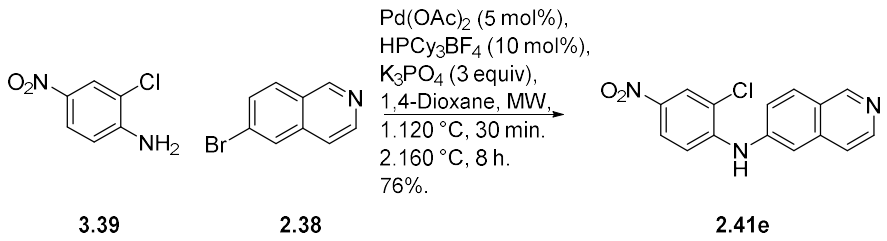


Figure 60. Calculated HOMO molecular orbitals of **2.41a** calculated by DFT B3LYP correlation functional (6-31+G(d,p)).

This could suggest the change in regioselectivity for **3.38** may not be the result of electron re-distribution but from steric control *in space* through coordination of the palladium catalyst complex to the carbonyl of amide **3.37**. Extensive work carried out by the Yu laboratory has developed 'internal ligands' by installation of a directing group on the substrate to coordinate the metal catalyst to one specific C-H bond to achieve selectivity.[179] In particular, installation of amides has been shown to direct cross-coupling selectivity *via* co-ordination of the palladium, 'locking' the direct-arylation to occur at the para position.[180]

Finally, the poor yields observed with electron withdrawing functional groups in the A-ring was investigated. Upon optimisation of reaction conditions using $HPCy_3BF_4$ and K_3PO_4 no de-halogenated degradation product was observed, even for the low yielding 7*H*-pyridocarbazoles. Of particular note is the sole isolation of **2.41e** upon microwave irradiation for 8 h with no isolatable degraded by-products (Scheme 59).



3.39 2.38 2.41e

Scheme 59. Failed consecutive Buchwald-Hartwig amination and direct arylation. Reaction stalled at Bichwald-Hartwig intermediate (**2.41e**).

This indicates that oxidative addition is likely the barrier causing poor efficiency for electron-deficient aniline substrates. Molecular orbital calculations were carried out on compound **2.41a**, **2.41d** and **2.41e** and the aryl chloride bond investigated (Table 9).

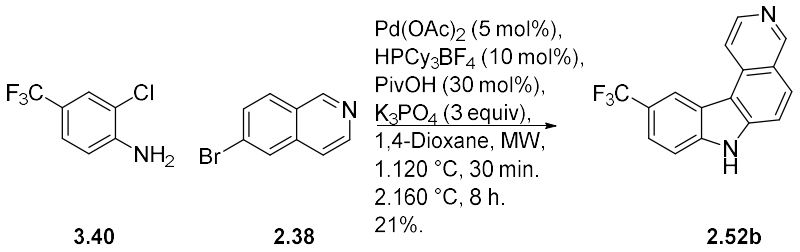
Table 9. DFT anaylsis: Substituent effects on Ar-halide bond length. Calculated by DFT B3LYP correlation functional (6-31+G(d,p)).

Entry	R-group	Ar-Cl bond length (Å)
2.41a	-OMe	1.76244
2.41d	$-CF_3$	1.74992
2.41e	$-NO_2$	1.74789

Interestingly, with increasing electron deficiency the aryl-chloride bond shortened in length. This indicates that the Buchwald-Hartwig amination intermediates with strong electron withdrawing groups e.g. $-NO_2$, result in the shortening of the C-Cl bond increasing its stability. This extra stabilisation makes oxidative addition by the palladium more difficult resulting in poor reaction efficiency.

To further confirm oxidative addition as the barrier to full conversion, 2-chloro-4-(trifluoromethyl)aniline (**3.40**) and 6-bromoisoquinoline (**2.38**) were subjected to microwave irradiation at 160 °C for 8 h (Scheme 60). Compound **2.41d** was chosen as it showed poor conversion, but showed the reaction could proceed, unlike its –nitro counterpart **2.41e**. Pivalic acid was added to this reaction in an attempt to give optimal conditions for the direct *C*-arylation. Pivalic acid has been shown by Fagnou and co-workers to facilitate direct arylation in similar systems by acting as a proton shuttle aiding in the efficiency of transmetalation.[154]

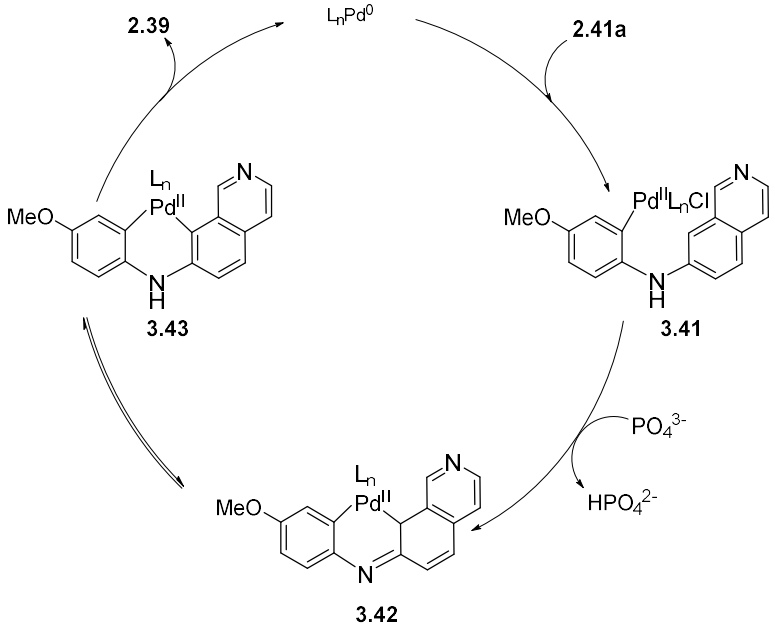
However, upon isolation, there was no increase in **2.52b** yield (21%). This suggests the oxidative addition into the aryl chloride bond is the limiting factor when electron deficient functional groups were employed in the A-ring.



3.40 2.38 2.52b

Scheme 60. Consecutive Buchwald-Hartwig amination and direct arylation with PivOH (30 mol%) additive.

Based on these studies, a proposed mechanism for *C*-arylation proceeds is presented in Scheme 19. Oxidative addition of the Pd^0 catalyst into the aryl-chloride bond of **2.41a** forms **3.41**. De-protonation of **3.41** by K_3PO_4 gives **3.42** followed by tautomerisation to form palladacycle **3.43**. Finally, reductive elimination to form the desired product **2.39** (Scheme 61).



Scheme 61. Proposed mechanism of *C*-arylation to form 7*H*-pyridocarbazoles.

3.4 Conclusions and Future Work

Key conclusions arising from this study are: *(i)* the reaction requires a palladium catalyst; *(ii)*the lone pair of the secondary aniline in the Buchwald-Hartwig intermediate is essential in order to effect the *C*-arylation step; *(iii)* the use of an aryl bromide prevents dimerization of the primary aniline to phenazine (**3.32**); and *(iv)* no *C*-arylation occurs without the aryl-chloride substituent present.

Furthermore, reqgioselectivity of the direct arylation can be modulated by the inclusion of a acetyl-protecting group on the secondary amine, to access the previously unavailable **3.38**. This

should be further investigated with a pivolyl group in an attempt to prevent de-protection *in situ*. This study would confirm if the acetyl-protecting group is selective for **3.38** production by preventing access to **2.41a** to proceed to the traditional **2.39**.

Chapter 4 Towards the Total Synthesis of Natural Products Ellipticine and Calothrixin B

4.1 Application and Total Synthesis of Ellipticine

Ellipticine (**1.26**) is an alkaloid that was first extracted from the trees *Ochrosia elliptica* and shown great anti-tumour activity (Figure 61).[181, 182] Due to its highly planar structure, ellipticine molecules are able to insert between the base pairs of DNA and perturb replication.

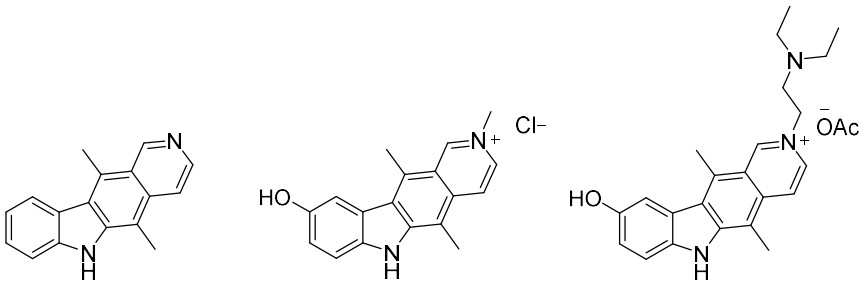


Figure 61. Structures of Ellipticine (**1.26**), Celiptium (**4.1**) and Datelliptium (**4.2**).

Other mechanisms of anti-tumour activity of ellipticines include topoisomerase II inhibition, an enzyme essential for DNA replication.[183] Although ellipticine is known to cause reduction in tumour growth it has disadvantages due to its lack of specificity and high toxicity resulting in a range of side effects including, but not limited to, nausea, vomiting and hypertension. Development of analogues of ellipticine have been explored increase specificity and decrease toxicity could become of interest in the clinic.[183]

Initially, a study carried out by Dalton and coworkers in 1967 showed ellipticine (**1.26**) cytotoxicity in humans and mice.[147] Drug development efforts were initially focused on treatment for acute myeloid leukeamia. Although originally promising, problems with solubility led to the abandonment of ellipticine and the development of its methylated analogue, celiptium (**4.1**) (Figure 61). Trials of celiptium showed promising results with 25 % of patients showing remission for 18 months; however, development of nephrotoxicity resulted in further trials of celiptium (**4.1**) being abandoned.[184] Another derivative, datelliptium (**4.2**), was submitted to clinical trials for toxicity against breast cancer given in escalating doses over 24 h from 40 to 500 mg/m^2. However, the majority of the phase I trial patients showed no response. One cervical cancer patient showed a minor response and a metastatic resistant rhabdomyosarcoma patient showed some stabilisation. However the patients experienced increased levels of hepatic toxicity at doses ≥330 mg/m^2.[182]

Although these alkaloids have not been shown to be successful in the clinic, using them as structural probes for elucidating new modes of action to be exploited, is an attractive avenue for

future drug development, particularly in their development as probes for the modulating the outcome of alternative RNA splicing.

4.1.1 Structural Studies of Ellipticine Showing DNA Intercalation

Ellipticine analogues have been studied at length as an anti-cancer treatment due to their anti-tumor activity.[185,186] Intercalation of DNA was presented as a mode of action after being observed in the crystal structure attained by Canals *et al.* in 2005.[187] The structure showed the two ellipticine structures intercalating between two sets of G-C base pairs. Interestingly, the A-T base pairs were not intercalated by ellipticine (**1.26**), suggesting a bias towards associating with G-C base-pairing (Figure 62).

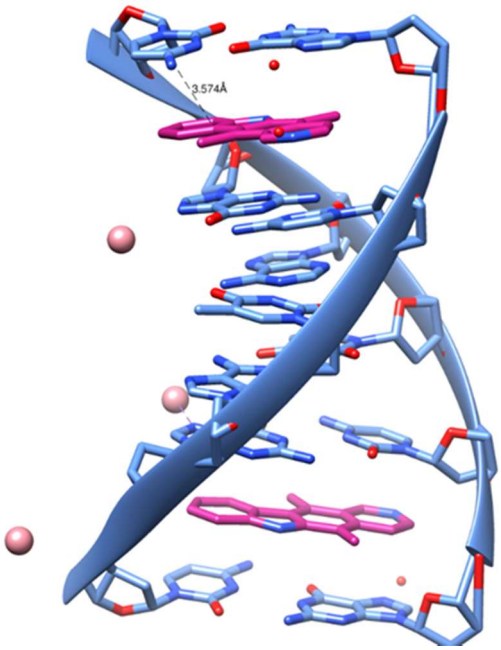
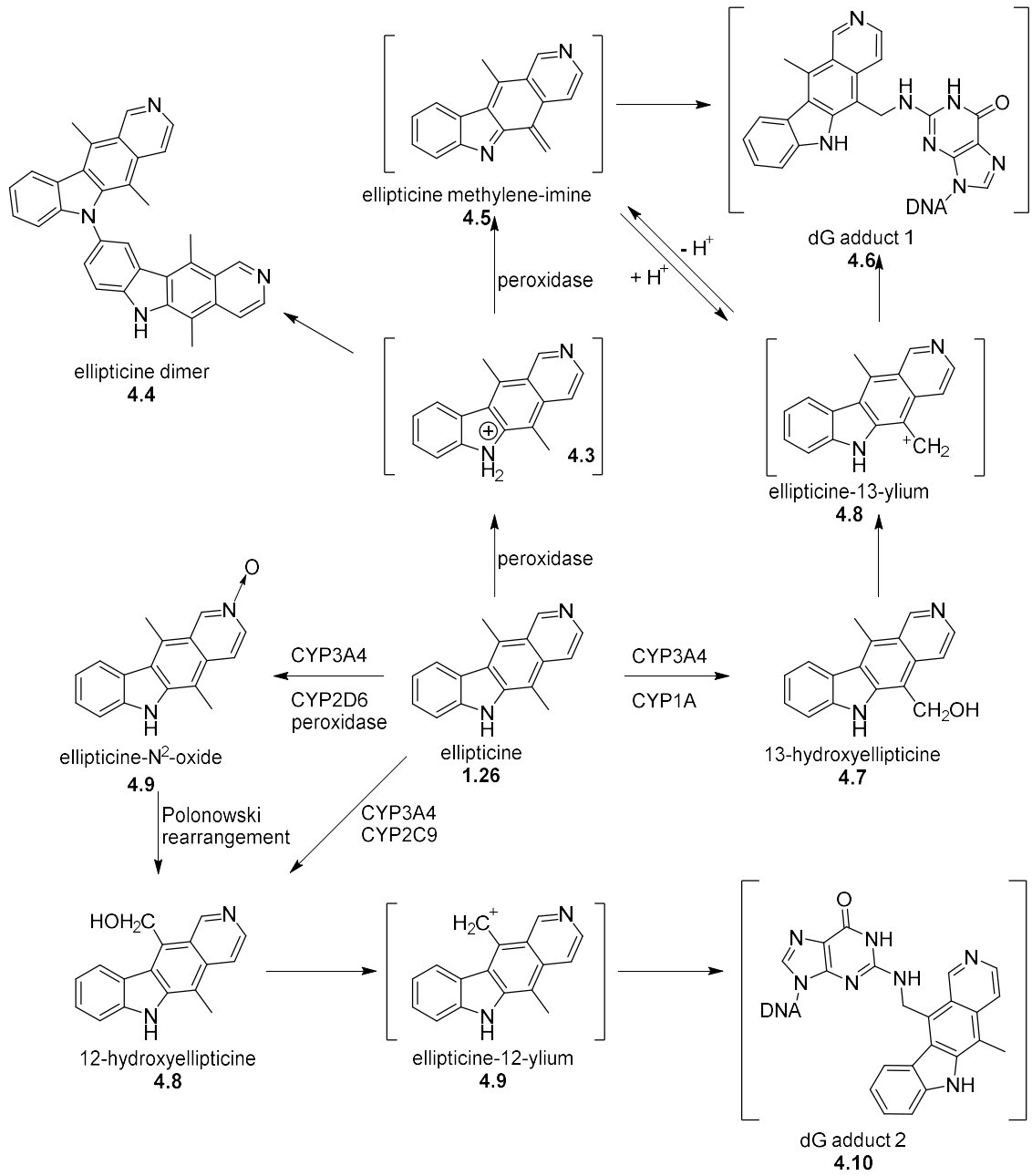


Figure 62. Bis-intercalated asymmetric d(CGATCG)$_2$ hexanucleotide and ellipticine unit. Ellipticine (**1.26**) (shown in magenta). PDB (IZ3F).[187]

4.1.2 Topoisomerase II Inhibition by Ellipticine Analogues

Ellipticine has been shown to act as an inhibitor of topoisomerase II.[185] Topoisomerase II is an enzyme that is involved in regulation of DNA structure by cutting the DNA helices if they become entangled in knots. It has been reported that activation of the ellipticine by various peroxidases and cytochromes P450 (CYPs) promotes binding of topoisomerase II and that this binding occurs *via* crosslinking alkylations of the DNA (Scheme 62).[185] CYPs are a family of enzymes that serve important functions in the synthesis and breakdown of hormones. Additionally they are responsible for the metabolism of toxic compounds, including drugs, primarily in the liver. DNA

adducts formed from 13-hydroxyellipticine (**4.7**) and 12-hydroxyellipticine (**4.8**) have been shown to form *in vitro* and *in vivo* in mice models when dosed with ellipticine (**1.26**).[188,189]



Scheme 62. Ellipticine activation *via* CYPs and peroxidases.

Further studies showed ellipticine (**1.26**) was found to be cytotoxic across multiple human cancer cell lines in micromolar range (Table 10).

Table 10. Ellipticine (**1.26**) cytotoxicity studies in human cells lines.

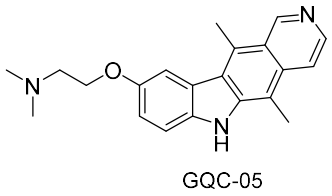
Cell line	IC_{50} (μM)
MCF-7 (breast adenocarcinoma)	1.25±0.13
HL-60 (Leukemia)	0.67±0.06
CCRF-CEM (Leukemia)	4.70±0.48
IMR-32 (Neuroblastoma)	0.27±0.02
UKF-NB-3 (Neuroblastoma)	0.44±0.03
UKF-NB-4 (Neuroblastoma	0.49±0.04
U87MG (Glioblastoma)	1.48±0.62

The cells were dosed with increasing levels of ellipticine (0.1 – 10 μM) for 48 h and the DNA was isolated. Ellipticine:DNA adducts were found in all the cells treated in Table 10.

Crosslinking of DNA is a well-established mode of action for cytotoxicity of many cancer drugs. However, whether this mechanism is related to the cytotoxity of ellipticines in this model is currently unclear.

4.1.3 Splice-switching of Bcl-x using Ellipticine and Quindoline Analogues

Ellipticine analogue, GQC-05 (**1.31**), showed success in biasing the splicing pathway of Bcl-x towards the pro-apoptotic isoform (Figure 63).[115]



GQC-05

Figure 63. Structure of ellitpicine analogue GQC-05 (**1.31**).

Previous collaborative work explored the biological activity of ellipticine analogues in splicing assays *in vitro*. **4.11** and **4.12** showed a decrease in pro-apoptotic Bcl-x_S with no change to the anti-apoptotic Bcl-x_L production (Figure 64).[115]

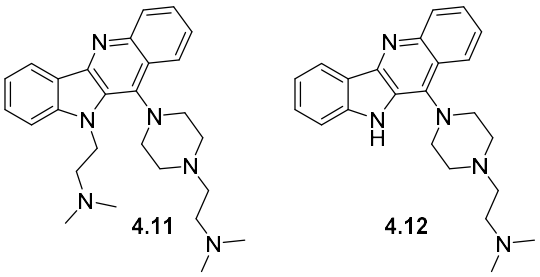


Figure 64. Structures of quindoline analogues (**4.11**) and (**4.12**) that showed a decrease of Bcl-x_S with no change to Bcl-x_L.

Compounds **4.13** and **4.14** showed no observable change to the splicing ratio of Bcl-x, however compounds **4.15 – 4.18** showed a splice-switch towards the production of the pro-apoptotic Bcl-x_S and a decrease in the splicing towards Bcl-x_L (Figure 65).

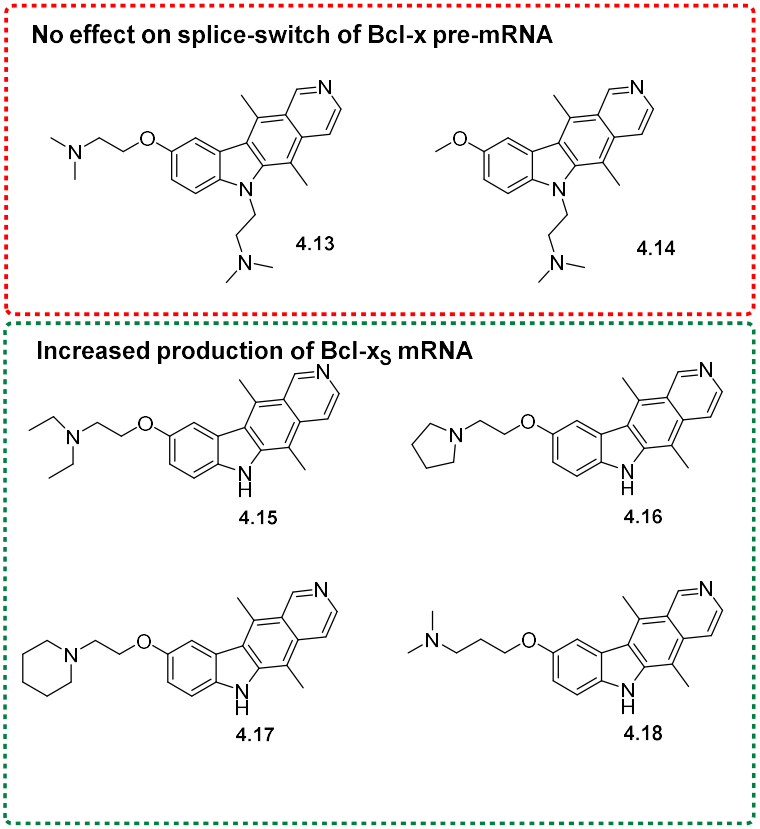


Figure 65 Ellipticine analogues tested for increasing Bcl-x_S production. The ratio of Bcl-x_L to Bcl-x_S was unaffected with compounds **4.13** and **4.14** (in red). Bcl-x_S production was increased with compounds **4.14 – 4.18** (in green).

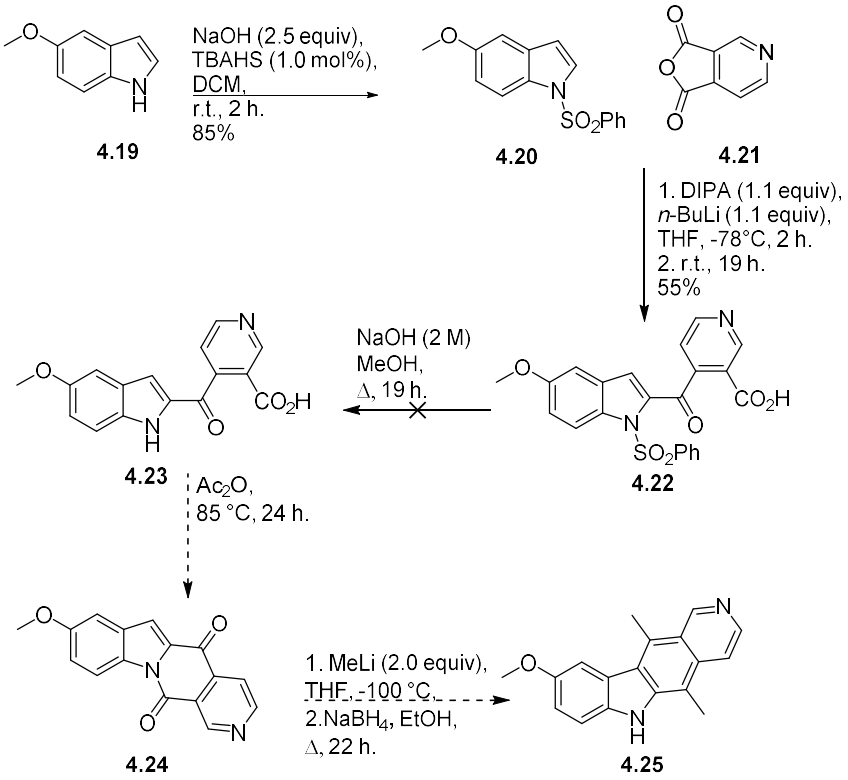
These results were in-line with previous literature reports that the inclusion of a basic amino tail aids in the binding of G4 ligands.[24] From this, it was inferred that modification of the A-ring has the potential for further derivatization without negatively impacting the ligand's splice-switching functionality. However, substitution at the N-5 position would not maintain splice switch activity.

Although structures **4.15 – 4.18** showed splice-switching capability, GQC-05 (**1.31**) remained the most potent ligand for altering the splicing ratio at 40 μM (Figure 63).

Current synthesis of ellipticine analogues does not allow access to a large library of compounds. This is because current 'state of the art' ellipticine synthetic routes are linear, low yielding and/or lack potential for modularity.[148,190,191] Therefore, a modular, convergent route towards ellipticine compounds is required.

4.1.4 Late-stage Formation of the Ellipticine C-ring (Gribble method)

Previous work carried out, by Dr. Olivia Rutherford, in the Burley group explored a variety of syntheses to develop a modular route towards ellipticine analogues.[116] The first method explored was reported in 1992 by Gribble *et al.*[148] This route was initially chosen as substituted indoles are readily available, the synthesis gave a good overall yield of 9-methoxyellipticine (48% over six steps), and it had the potential to tolerate A-ring modification (Scheme 63).



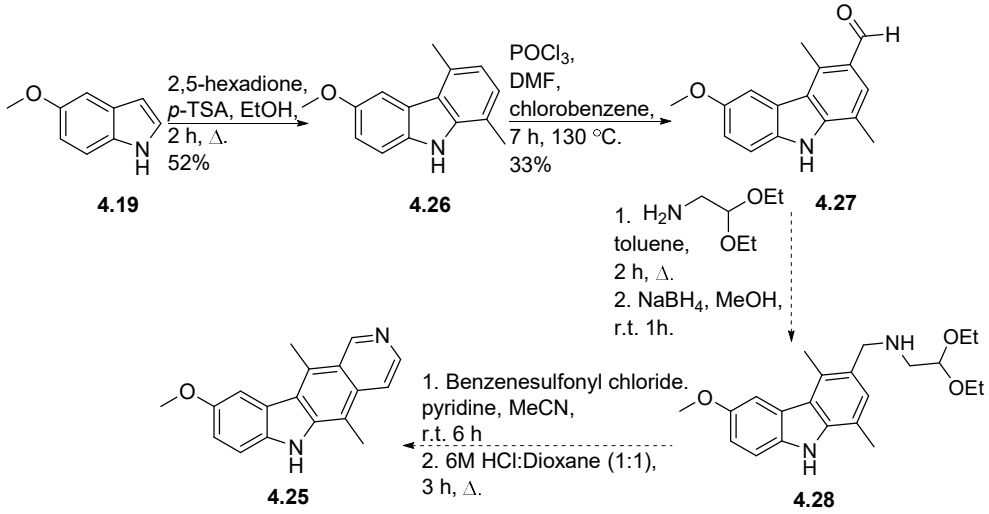
Scheme 63. Modified Gribble method by Dr. Olivia Rutherford; Attempted synthesis of 9-methoxyellipticine (**4.25**).

Sulfonyl protection of the indole **4.19** proceeded in 85% yield, followed by the addition of 3,4-pyridinedicarboxylic anhydride (**4.21**) to produce **4.22** (55% yield). However, difficulties arose when deprotection of the sulfonyl group was attempted, yielding only starting material (**4.22**) when heated with K_2CO_3 at reflux. The deprotection was successful when the base was changed

to NaOH, however this also led to degradation of the compound back to the starting indole (**4.19**) in 50% yield. Following these challenges, a new synthesis based on the Cranwell-Saxton Method was investigated.

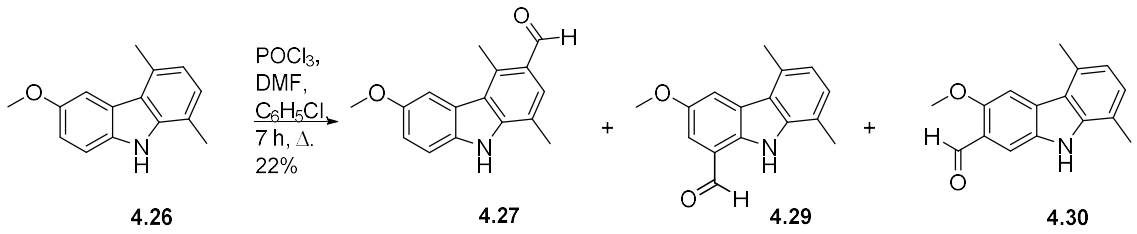
4.1.5 Late-stage Formation of the Ellipticine D-ring (Cranwell-Saxton method)

Although the Cranwell-Saxton method of ellipticine synthesis was well-established,[192] it was hoped this method would allow for facile functionalization of the A-ring just as the Gribble method, starting from the same indole **4.19** (Scheme 64). The condensation reaction of indole **4.19** and 2,5-hexadione produced **4.26** in a moderate 52% yield.



Scheme 64. Modified Cranwell-Saxton method by Dr. Olivia Rutherford; Attempted synthesis of 9-methoxyellipticine (**4.25**).

However, when the Vilsmeier-Hack formylation was attempted, **4.27** was isolated in only 33% yield. Poor conversion in this transformation had also previously been reported by the Mccarthy group.[190] In 2010, Mccarthy and coworkers investigated the selectivity of Vilsmeier-Hack formylation on carbazole for the synthesis of ellipticine and found the reaction was not selective for **4.27**.[190] The desired **4.27** was isolated in only 22% yield in part due to the formation of carbazole biproducts **4.29** and **4.30**.



Scheme 65. Mccarthy synthesis; Selectivity studies on the Vilsmeier-Hack reaction for the synthesis of **4.27**.

Further synthetic difficulties where encountered when the reductive amination to produce **4.28** was attempted. The reaction profile showed multiple bi-products and NMR and LC-MS analysis could not deduce whether product **4.28** had been formed. Due to low yielding primary reactions and synthetic difficulties, this route was unfortunately abandoned.

4.2 Existing Studies Towards the Synthesis of Calothrixin A and B

Calothrixins are another class of alkaloids that have been extensively studied for both anti-parasitic and anti-cancer activity.[193] In 1999, Rickards and coworkers extracted Calothrixin A and B from *Calothrix Cyanobacteria* and have since explored their potential for biological activity in disease (Figure 66).

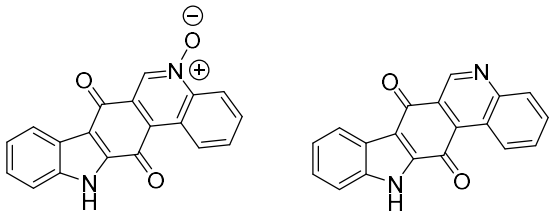


Figure 66. Stuctures of Calothrixin A (**4.31**) and Calothrixin B (**4.32**).

The calothrixin core consists of an indole, quinolone and a quinone, making them distinctive in the scope of natural products as these three moieties are prominent in active drug compounds.

4.2.1 Anticancer Activity of Calothrixins

After their discovery in 1999, Rickards and coworkers found calothrixins had activity in the micromolar range against HeLa cells with an IC_{50} of 40 and 350 nM for Calothrixin A and B respectively. (Table 11).[193]

Table 11. Calothrixin A and B *in vitro* activity in *P. falciparum* and HeLa cells.[193]

Compounds	**IC_{50} (nM)**	
	P. falciparum	**HeLa cells**
Calothrixin A	58 ± 8	40 ± 9
Calothrixin B	180 ± 4	350 ± 82
Chloroquine	83 ± 17	-

Furthermore, Khan and co-workers, determined that calothrixin A and B were biologically active against leukemia cell lines on the micormolar level.[194] Their studies revealed that Calothrixin B

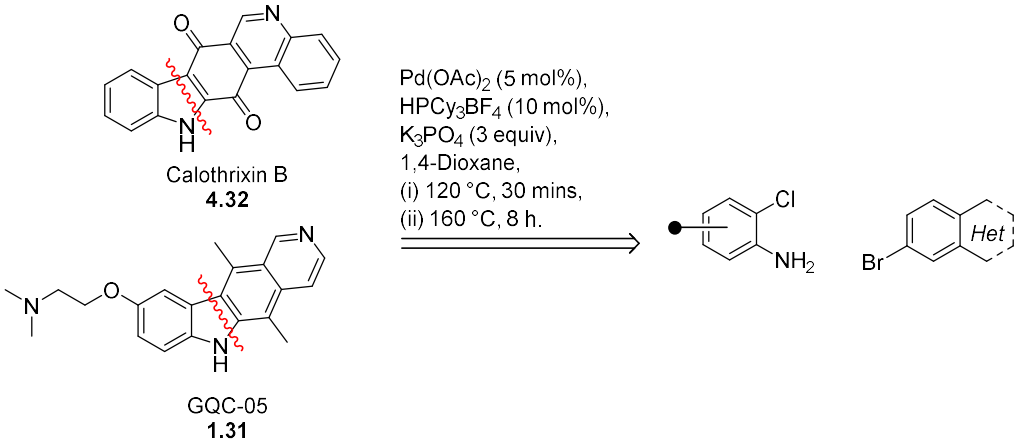
induced G_1 arrest in the cell cycle and at concentrations above 0.1 μM caused cell arrests in the G_2/M phases aswell and indicated it's potential as a topoisomerase I inhibitor.

Table 12. Calothrixin A and B *in vitro* activity in CEM Leukemia cells.[194]

Compounds	IC_{50} (μM)
	CEM Leukemia cells
Calothrixin A	0.20 ± 0.02
Calothrixin B	1.05 ± 0.03
***N*-Methylcalothrixin B**	5.13 ± 0.72

4.3 Chapter Aims

The overall objective of this chapter is the application of the sequential one-pot synthesis developed in Chapter 2 to the synthesis of ellipticine, calothrixin B and their analogues. Once synthesised these analogues will be tested for their splice-switch activity in Bcl-x *in* vitro splicing assays to expand the SAR and thus highlight structurally significant chemical moieties in the interaction with Bcl-x.

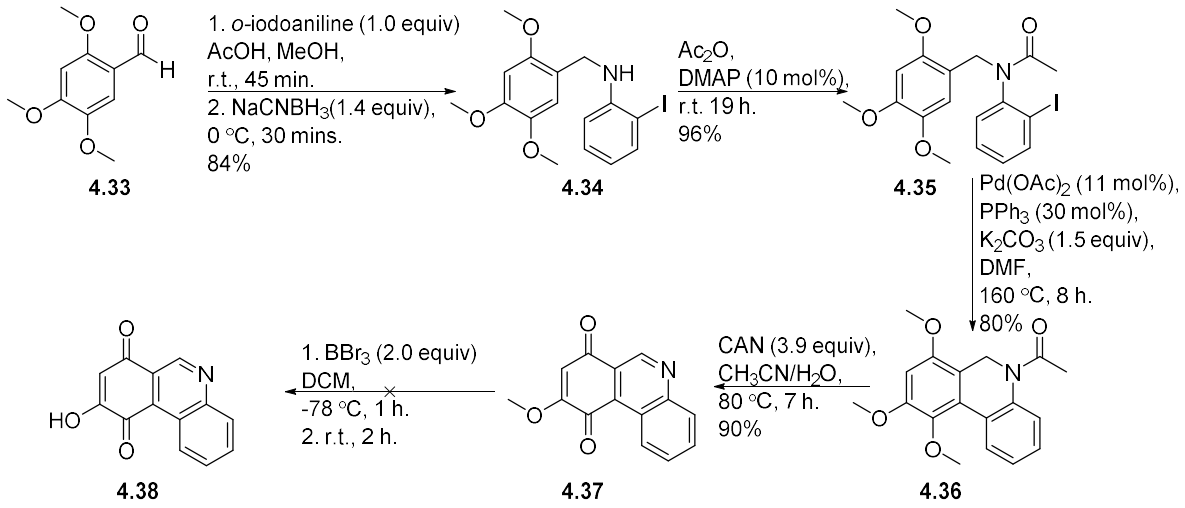


4.4 Results and Discussion

4.4.1 Towards the Development of a Modular Synthesis of Calothrixin B

The synthesis of Calothrixin B was attempted to expand the diversity of compounds accessible through the one-pot method described in Chapter 2. Xu *et al.* published a total synthesis of Calothrixin B *via* the methoxy derivative of **4.37** which was then subjected to 3 further steps to afford Calothrixin B.[195] The palladium-catalysed convergent synthesis developed during this project would require only one further step. Initially Xu's synthesis was replicated as it was thought the methoxy functional group of **4.37** could be replaced by a triflate.

Using Xu's approach, the synthesis progressed in good to excellent yields to afford **4.37** in an overall yield of 58% over 4 steps, in concurrence with the reported results (Scheme 66).[195]



Scheme 66. Modified Xu synthesis of Calothrixin B methoxy fragment (**4.37**) for the synthesis of **4.38**.[195]

However, attempts to demethylate **4.37** to obtain **4.38** were not successful. The only product observed by LC-MS showed an m/z [M-H] = 302 which corresponds to an analogue of **4.38** that is brominated (Figure 67).

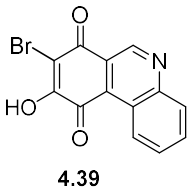
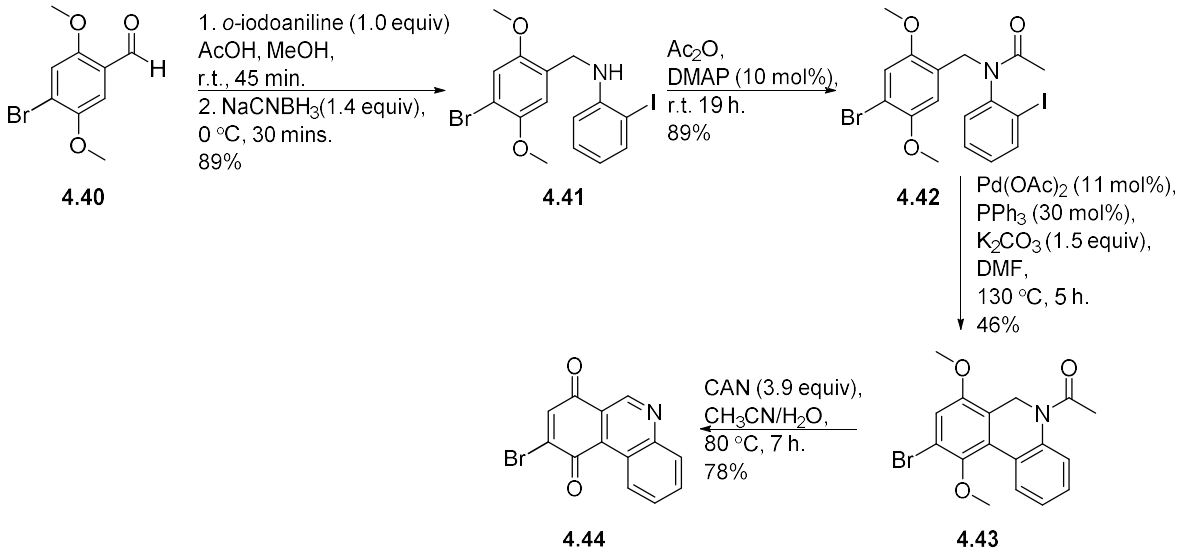


Figure 67. Proposed tentative structure of product from demethylation of **4.37**.

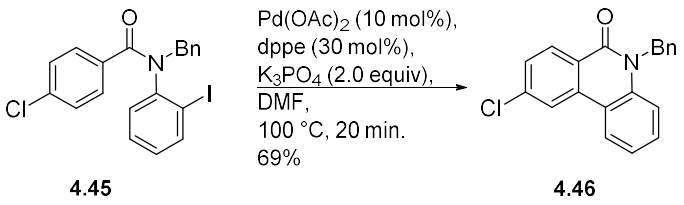
The synthesis shown in Scheme 66 was not continued, as an alternative route was concomitantly explored where installation of a bromide was incorporated into the starting material. A modified Xu *et al.* synthesis was carried out (Scheme 67).



Scheme 67. Synthesis of Calothrixin B bromide precursor **4.44**.[195]

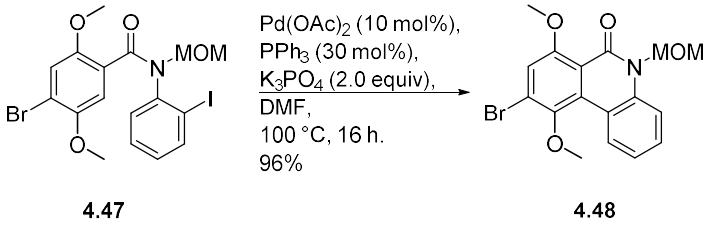
First, a reductive amination to incorporate the iodoaniline moiety was carried out to produce **4.41** in 89% yield. **4.42** was N-protected with acetic anhydride in 89 % yield. The next step was a cyclisation through C-H activation with $Pd(OAc)_2$ and PPh_3. This reaction was heated to reflux (160 °C) in DMF and no formation of product **4.43** was observed after 6 h. Only the degraded de-iodinated **4.42** was successfully isolated. The reaction was repeated at 100 °C and was monitored by LC-MS at 2-hour increments. Again, no conversion to **4.43** was observed with starting material **4.42** recovered. The reaction was then repeated at 130 °C for 5 hours afforded **4.43** in 46% yield. There is precedent in literature that these reactions can be low yielding, however Bernini *et al.* showed the incorporation of a bulky protecting group dramatically increased yields and decreased reaction times.[196] In this particular system, the incorporation of a bromide moiety in place of a methoxy group in Xu's original synthesis will deactivate the ring as a nucleophile for the C-H activation by reducing its electron density.

In literature this reaction is precedented, and has shown great success on a number of analogues with halide functionalities incorporated.[196,197] However these analogues differ from **4.42** in that they possess and amide functionality (Scheme 68). It has been postulated that the Pd catalyst coordinates with this moiety to bring the aryl iodide into proximity with the reacting aryl ring.[196]



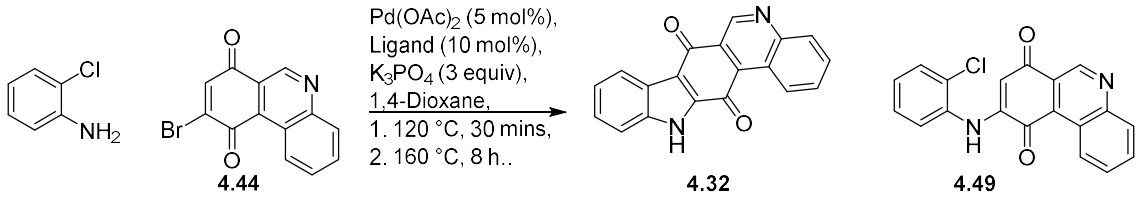
Scheme 68. Bernini's synthesis; Pd catalysed C-H activation synthesis of **4.46**.

Furthermore, work carried out by Chai *et al*., successfully synthesized **4.48** in excellent yield by incorporating this amide functionality in **4.47** (Scheme 69).[198] Chai's synthesis used **4.48** in the total synthesis of Calothrixin B, however their route goes *via* a Suzuki coupling and a subsequent Cadogan reaction.[198] Employing the one-pot synthesis developed in Chapter 2 would decrease this synthesis by two-steps.



Scheme 69. Chai's synthesis: Pd catalysed C-H activation synthesis of **4.48**.[198]

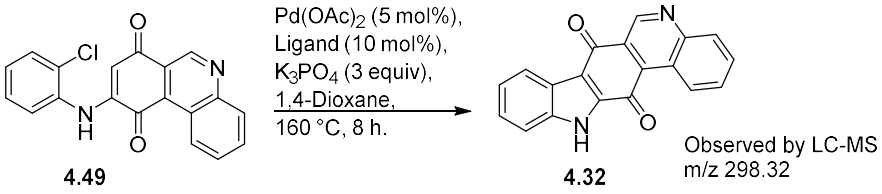
Compound **4.43** was oxidised with ceric ammonium nitrate (CAN) and **4.44** was obtained in 78% yield (overall 28% yield over 4 steps). Compound **4.44** was submitted to the one-pot cross coupling conditions developed in Chapter 2 in an attempt to obtain calothrixin B (Scheme 70).



Scheme 70. Test reaction of **c**onsecutive Buchwald-Hartwig amination (**4.49**) and direct arylation to form Calothroxin B (**4.32**).

Unfortunately, the reaction showed only conversion to the Buchwald-Hartwig intermediate **4.49** after 30 mins at 120 °C. However, on further heating for 8 h at 160 °C only a trace of amount of **4.32** could be observed by LC-MS. It should be noted that monitoring the reaction highlighted that both the Buchwald-Hartwig intermediate **4.49** and Calothrixin B **4.32** were poorly soluble in the reaction mixture. This was further exemplified on purification where the crude mixture was only soluble in chloroform and precipitated out of solution was the column progressed. The

Buchwald-Hartwig intermediate **4.49** was isolated in 22% yield and a small scale reaction ran where it was submitted for microwave irradiation at 160 °C for 8 h (Scheme 71).

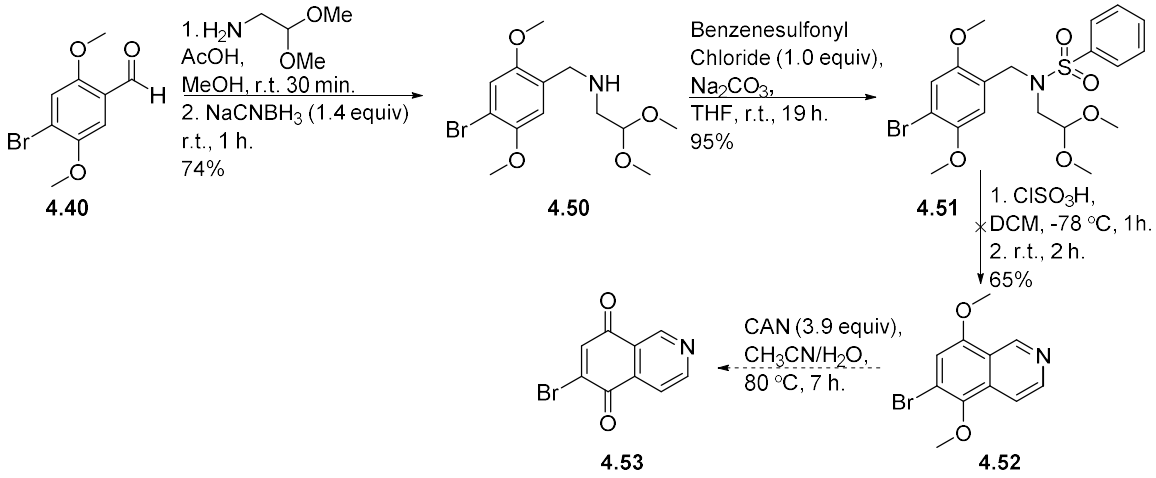


Scheme 71. Direct C-arylation to form Calothroxin B (**4.32**).

Although too small a scale to isolate, this test reaction showed almost complete conversion to the final product Calothrixin B by LC-MS. Unfortunately, due to time constraints of the project and the poor conversion of the first Buchwald-Hartwig step, this synthesis was not completed. However, on optimisation of the poorly soluble Buchwald-Hartwig amination step, the small test reaction in Scheme 71 shows great promise for the total synthesis of Calothrixin B via this method.

4.4.2 Towards the Synthesis of 6-Bromo-5,8-dimethylisoquinoline

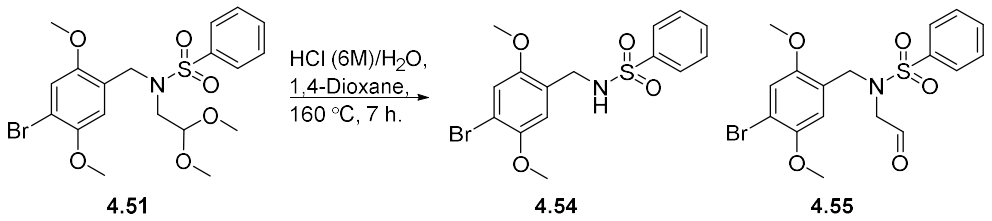
To access GQC-05 (**1.31**) *via* the one pot cross coupling, the synthesis of compound **4.53** was required. Compound **4.53** was previously isolated in the group by bromination of 5-hydroxyisoquinoline which was then oxidised in HNO_3/H_2SO_4.[116] However, this reaction proved difficult to replicate. Therefore, an alternative route was proposed to prepare **4.53**. (Scheme 72).



Scheme 72. Modified Pomeranz-Fritsch isoquinoline synthesis; 6-Bromo-5,8-quinolinedione (**4.53**).[195]

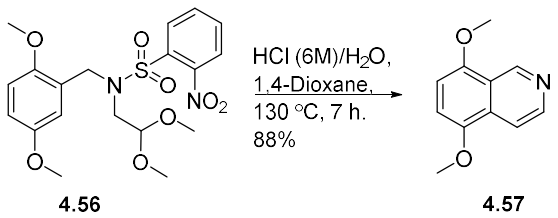
First, a reductive amination produced **4.50** in 74% yield. Protection of the secondary amine **4.50** was achieved through reaction with benzenesulfonyl chloride yield **4.51** in 95% yield. Cyclisation

for isoquinoline (**4.52**) formation was initially attempted by heating **4.51** to reflux in a 4:1 mixture of 1,4-dioxane and 6M HCl. Reaction monitoring by TLC showed multiple intermediates formed after 7 h. Following the reaction by LC-MS showed no conversion to **4.52**, instead two bi-products were obtained. The starting material (**4.51**) had degraded to **4.54** and the Pomeranz-Fritsch precursor **4.55** (Scheme 73).



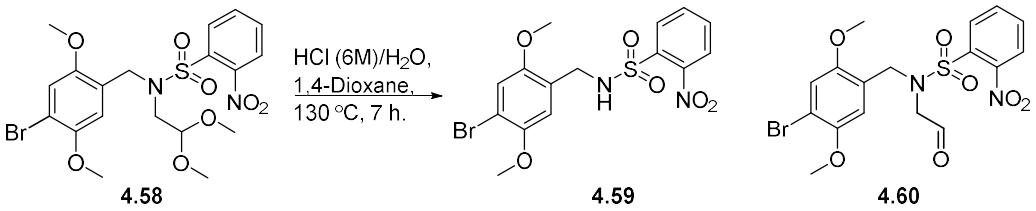
Scheme 73. Modified Pomeranz-Fritsch isoquinoline cyclisation of **4.51**.

The use of a nosyl protecting group has been previously reported to form **4.57** in good yield when carried out on a similar analogue without the bromide moiety **4.56** (Scheme 74).[199]



Scheme 74. Miranda and co-workers modified Pomeranz-Fritsch isoquinoline cyclisation of **4.56**.[199]

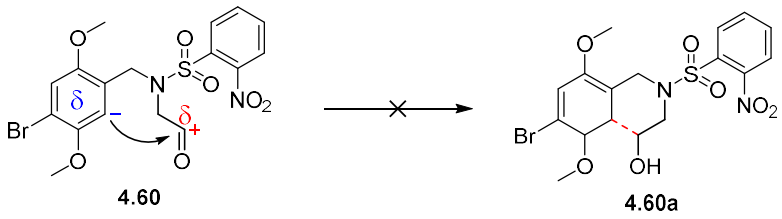
However, when this was attempted with **4.58** only the secondary amine and the Pomeranz-Fritsch intermediate **4.60** were isolated (Scheme 75).



Scheme 75. Modified Pomeranz-Fritsch isoquinoline cyclisation of **4.58**.

From these reactions it can be concluded that the Pomeranz-Fritsch style cyclisation that is seen to be ubiquitous in isoquinoline synthesis is not viable with our tri-substituted aryl-bromide **4.58** in these conditions. Admittedly, this variation of the cyclisation is not prominent in literature where there is not only tri-substitution but also a bromide between methoxy groups. Aldehyde **4.60** is a known intermediate of the Pomeranz-Fritsch reaction, so its formation suggests the limiting step is the final step of the ring closure. As this seems to be non-problematic for the non-

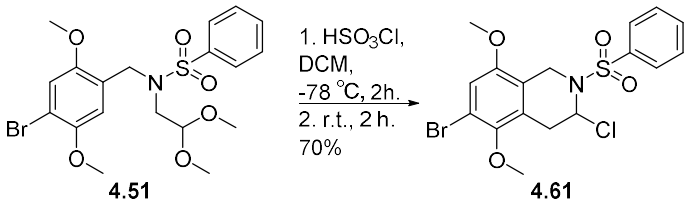
brominated analogue **4.56**, the electron withdrawing nature of the aryl-bromide could be enough to destabilise the formation of the reactive anion to prevent electrophilic substitution (Scheme 76).



Scheme 76. Ring closure is proposed to be prevented through stabilised anion (in blue) of **4.60**.

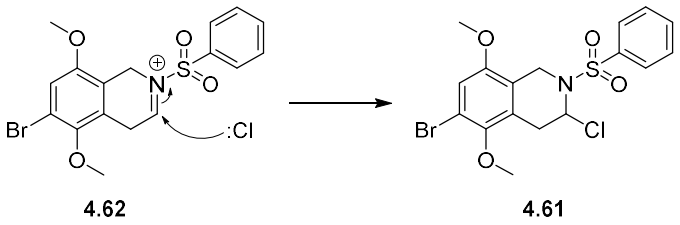
The bromide withdraws electron density into the aryl ring and are additionally ortho/para directing which further deactivates the meta-position that needs to be electron rich under these conditions. The presence of water may also be directing the equilibria of the reaction, particularly if the nucleophilic position on the aryl-ring is less activated.

The reaction was repeated with chlorosulfonic acid, an weaker acid than HCl in the hope that the cyclisation would occur without degradation (Scheme 77) and also minimising water content in the reaction. These conditions are also milder as the reaction occurs at room temperature instead of 160 °C. **4.51** was dissolved in DCM and cooled to < -78 °C with liquid N_2 and Hexane. Chlorosulfonic acid was also cooled to < -78 °C in DCM and added dropwise to the solution of **4.51** in DCM. The reaction was allowed to warm to rt and stirred for 2 h.[200] Upon isolation it was determined that **4.61** was obtained in 70 % yield, resulting from addition of chloride ions from solution.



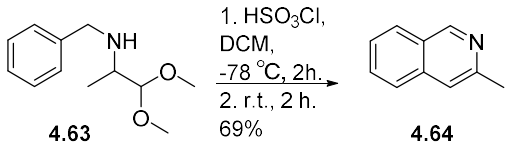
Scheme 77. Attempted isoquinoline synthesis: (i) HSO_3Cl, DCM, - 78 °C, 2 h, (ii) rt, 2 h.

Formation *via* the imine may account for the apparent selectivity of halide addition (Scheme 78). Indeed, this chloride addition has been observed in previous literature.[201]



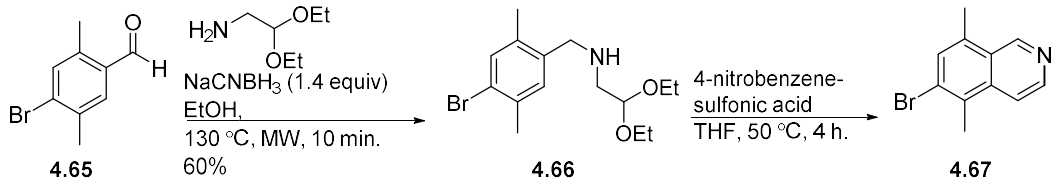
Scheme 78. Proposed mechanism of chloride addition *in situ* to form **4.61**.

Furthermore, an extensive study by Hertel and co-workers has previously shown successful cyclisation through a Pomeranz-Fritsch type cyclisation for the synthesis of isoquinolines (Scheme 79). However, these analogues all had substitution that would block the chloride addition observed in Scheme 77.



Scheme 79. Hertel and co-workers modified Pomeranz-Fritsch cyclisation to produce **4.64**.

Concurrently a synthesis whereby two methyl groups are pre-installed in the starting material was also explored (Scheme 80). This route followed a classic Pomeranz-Fritsch reaction scheme, however when the cyclisation was attempted 4-nitrobenzenesulfonic acid was used in place of chlorosulfonic acid.

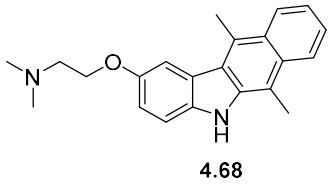


Scheme 80. Modified Pomeranz-Fritsch cyclisation; synthesis of **4.67**

It was thought the bulkier anion from 4-nitrobenzene sulfonic acid would prevent unwanted addition into the desired isoquinoline **4.67**. This reaction was first attempted in DCM at -78 °C, however no conversion was observed, primarily due to the insolubility of 4-nitrobenzenesulfonic acid in DCM. The solvent was exchanged for THF and the reaction heated to 50 °C for 4 h. Due to time constraints in the project compound **4.67** was not isolated, however a mass matching **4.67** (m/z $[M+H]^+$= 236) was observed as the sole product formed with the rest of the mass balance being attributed to the unreacted starting material (**4.66**). These reaction conditions, once optimised, could lead to a step efficient convergent route to ellipticine and subsequently allow quick and easy derivatisation for synthesising GQC-05 (**1.31**) analogues for biological activity.

4.4.3 Synthesis of Ellipticine Analogues for *in vitro* Bcl-x Splicing Assays

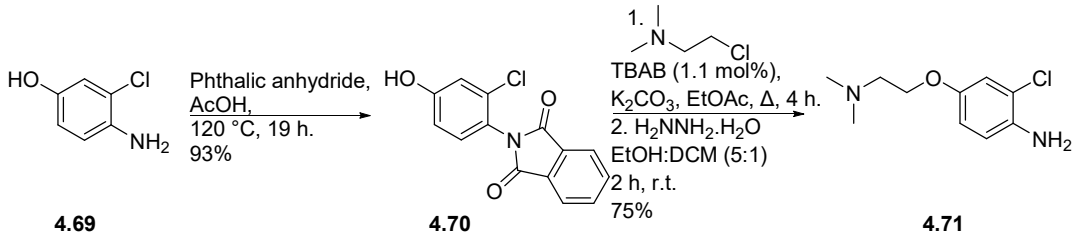
Previous work by collaborators at the University of Leicester, Eperon and coworkers showed that variation of the A-ring tertiary amine tail was tolerated in the splicing assays, however blocking the carbazole N-H resulted in loss of activity.[115] However, no information collected as to the importance of the nitrogen in the D-ring. It was envisaged, that the previous synthesis outlaid in Chapter 2 could be utilized for the synthesis of 2-deaza-GQC-05 (**4.68**) (Figure 68).



4.68

Figure 68. Structure of 2-deaza-GQC-05 (**4.68**).

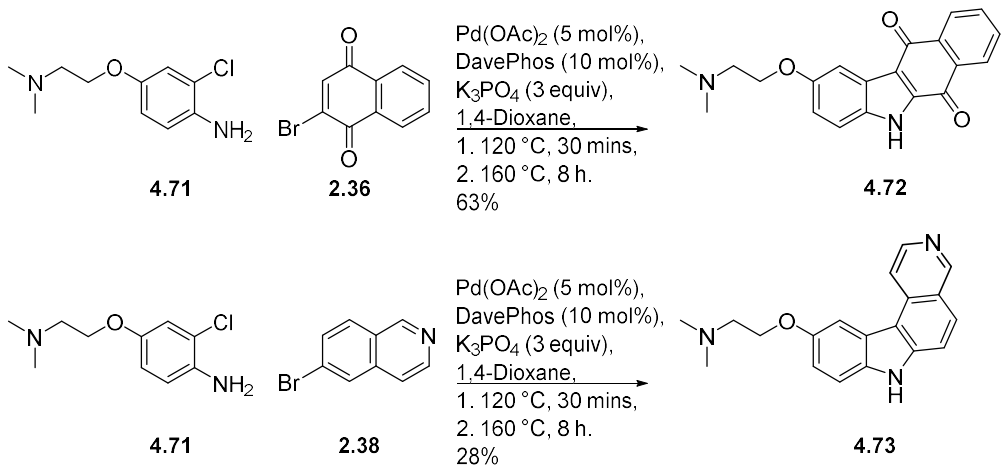
However, this first required synthesis of the functionalized A-ring **4.71** (Scheme 81). First, a standard S_N2 reaction of **4.70** with NaH in DMF was ran with 2-chloro-*N,N*-dimethylethylamine hydrochloride. This was carried out at room temperature overnight and showed no consumption of starting material. There was some literature precedent that desalting the hydrochloride salt before addition into the reaction would facilitate the transformation.[202,203] The 2-chloro-*N,N*-dimethylethylamine hydrochloride was desalted by the addition of NaOH (30 %w/v) and extracted into toluene. The toluene mix was then added directly into a reaction containing **4.70**, K_2CO_3 and TBAB in EtOAc and heated to reflux for 2 h.



4.69 **4.70** **4.71**

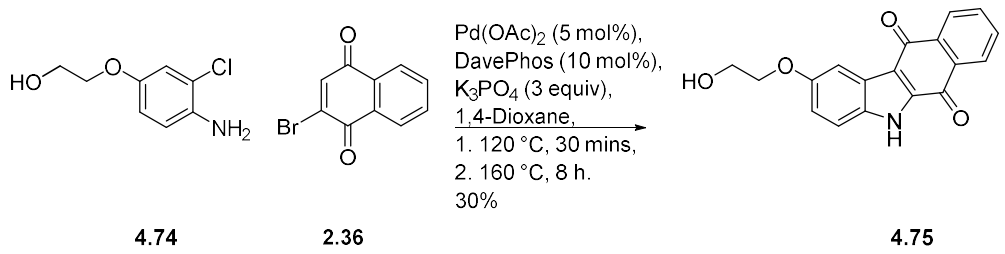
Scheme 81. Synthesis of GQC-05 aniline (**4.71**).

The solution was filtered, upon which deprotection with hydrazine monohydrate afforded aniline **4.71** in 75% yield over two steps. The A-ring synthesis was optimized to a 70% overall yield on a 2 g scale. Firstly, aniline **4.71** was reacted with 2-bromonaphthalene-1,4-dione and 6-bromoisoquinoline under the conditions optimised in Chapter 2 to synthesise **4.72** and **4.73** in 63% and 28% yield, respectively.



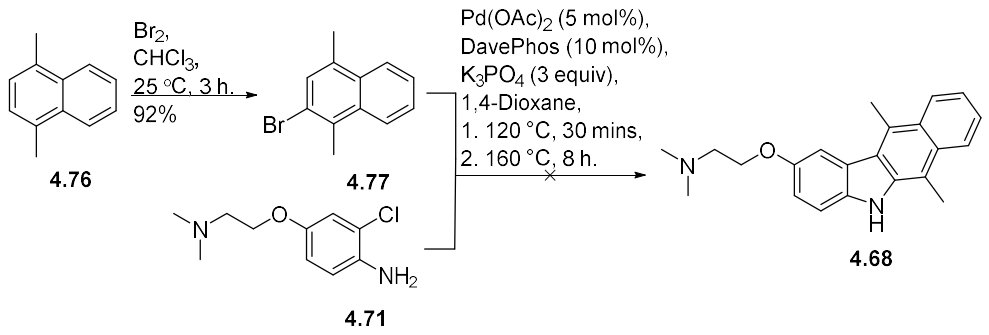
Scheme 82. Consecutive Buchwald-Hartwig amination and direct arylation to form **4.72** and **4.73.**

Following on from the synthesis of **4.72** and **4.73**, **4.75** was synthesised using the same reaction conditions in 30% yield. It was thought that compound **4.75** could be a useful control in splicing-activity assays as it maintains the same shape and core as **4.72** but lacks the dimethylamino basic tail. Both the Buchwald-Hartwig intermediate and **4.75** were only partially insoluble in 1,4-dioxane. This insolubility could account for the poor conversion due to precipitation of active reagents as the reaction proceeds.



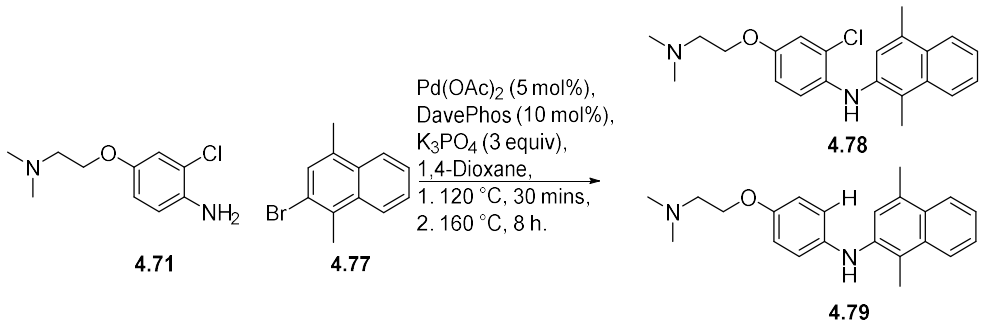
Scheme 83. Consecutive Buchwald-Hartwig amination and direct arylation to form **4.75.**

From the successful isolation of **4.72**, **4.73** and **4.75**, aniline **4.71** was then taken forward into cross coupling reactions with bromide **4.77** (Scheme 84) to synthesise 2-deaza-GQC-05 (**4.68**).



Scheme 84. Attempted synthesis of **4.68**.

Unfortunately, under the previously optimised cross coupling conditions, **4.68** was not observed by LC-MS in the crude reaction mixture. The trace showed a major peak corresponding to the Buchwald intermediate (**4.78**) and a minor peak observed corresponding to de-halogenated Buchwald intermediate (**4.79**) (Scheme 85).



Scheme 85. Attempted consecutive Buchwald-Hartwig amination and direct arylation **4.68**. Only Buchwald-Hartwig intermediate (**4.78**) and degradation product (**4.79**) were observed.

It was thought that either the additional aromatic ring or the added steric bulk could be hindering the C-H activation step. Therefore, ligands of less steric bulk, different solvents and different bases were tested to obtain **4.68**.

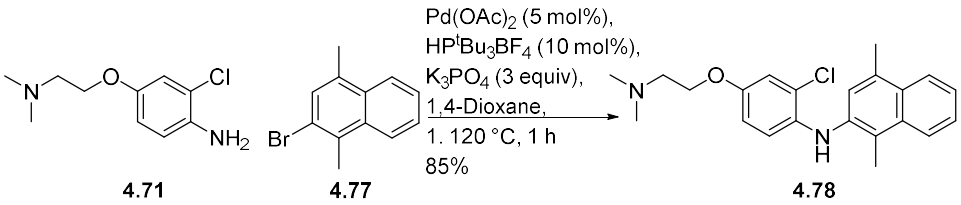
Table 13. Conditions for optimising 2-deazaGQC05 (**4.68**) synthesis, [a]Observed by LC-MS; [b]isolated yield (impure by NMR); [c]Reaction was sampled after first time point, and re-subjected to heating for the second time point.

Entry	Ligand	Base	Solvent	Time	Temperature	%Yield (4.68)
1	$HPCy_3BF_4$	K_3PO_4	1,4-Dioxane	18 h	160 °C	0[a]
2	$HPCy_3BF_4$	K_3PO_4	NMP	18 h	160 °C	0[a]
3	$HPCy_3BF_4$	K_3PO_4	1,4-Dioxane	4 h + 8 h[c]	140 °C	trace[a]
4	$P(t\text{-}Bu)_3$	K_3PO_4	1,4-Dioxane	8 h	160 °C	0[a]
5	$HPCy_3BF_4$	NaO^tBu	1,4-Dioxane	4 h + 4 h[c]	160 °C	8%[b]

It was evident from entries 1-4 (Table 13), that utilising less bulky ligands had no positive effect on yield, suggesting the role of steric hindrance in preventing the transformation is minimal in this case. After reacting for 8 h in 1,4-dioxane, a ring of solid was observed above the solvent line of the microwave vial, which may suggest solubility problems. The solvent was changed to NMP (entry 2, Table 13) to see if increased solubility aided in the production of **4.68**. Unfortunately no product was observed by LC-MS. Lowering the temperature (entry 3, Table 13) to minimise degradation of the Buchwald intermediate, showed very minimal conversion to **4.68** with the Buchwald intermediate **4.78** being the major peak followed by de-halogenated **4.79**. This reaction was subjected to a further 8 h at 160 °C, in the hope that the Buchwald intermediate **4.78** would convert to the desired **4.68**. However, further heating resulted in further degradation to the de-halogenated **4.79**. Changing the base (entry 5, Table 13) to NaO^{t}Bu showed a slightly greater conversion to **4.68** by LC-MS, although the product was isolated in only 8% yield, with the final compound being 10% impure by NMR. Unfortunately, although an improvement on (Table 13, entry 3), the major product from the reaction was seen to be the de-halogenated **4.79**. This suggests that when Na^{t}OBu is used, although the conversion was greater, degradation was more pronounced, meaning no further conversion to **4.68** was obtained. This finding aligned with previous reports from Fagnou and Echavarren.[204,171] It was determined that an alternative route to access GQC-05 analogues with methyl substituents in the C-ring was required.

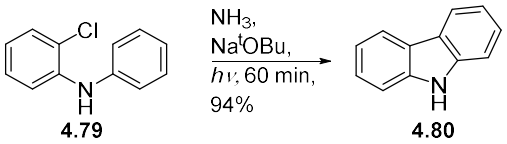
4.4.4 UV-mediated Synthesis of Deaza-GQC-05

The penultimate step in the synthesis of 2-deaza-GQC-05 (**4.78**) proceeded in excellent yield when reacted in modified conditions from Chapter 2 (Scheme 86).



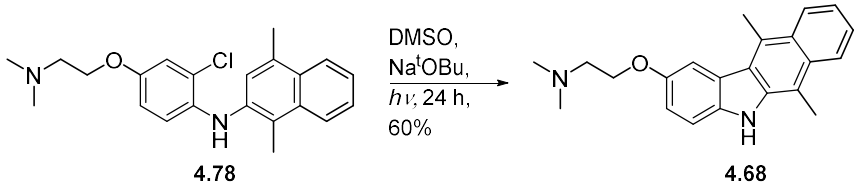
Scheme 86. Buchwald-Hartwig amination to synthesise **4.78**.

Therefore, it was decided to focus synthetic development solely on the direct C-arylation portion of the one-pot reaction. In 2009, Rossi and co-workers published a UV-mediate C-C bond formation for the synthesis of 9*H*-carbazole structures.[205]



Scheme 87. Rossi UV-mediated direct arylation for the synthesis of **4.80**.

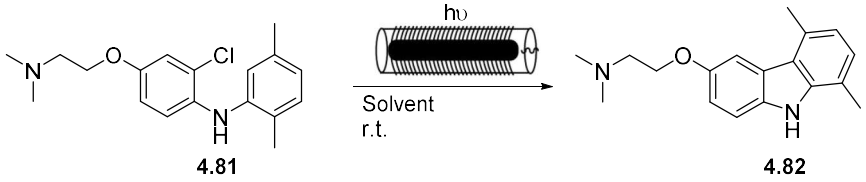
The reaction was irradiated at 350 nm maximum with two 400W lamps. These conditions were translated to the synthesis of **4.68**, however a 9W lamp was initially used for the first test reaction. DMSO was used in place of ammonia as it had also shown comparable results and is less toxic than its amine counterpart. The reaction proceeded to 60% conversion to **4.68** by LC-MS over 24 h. Given the reduced power of the lamp used in comparison to reported literature, this was a promising first result.



Scheme 88. UV mediated C-C direct arylation, 9W lamp, batch conditions. Reaction carried out in quartz glass.

The reaction was translated into a UV flood lamp oven (400W) that irradiates with a wavelength range of 320-400 nm. Full conversion, by analytical RP-HPLC, to **4.68** was observed after only 1 h of irradiation in the more powerful setup. The reaction was scaled up for isolation and although full conversion was obtained previously, only 19% yield of **4.68** was isolated. This loss in yield can be attributed to the set-up of the UV flood lamp. Reactions cannot be stirred when irradiated so the reaction mixture was separated into six glass vials (5 mL) and the vials dispersed equally under the lamp. It was found that UV-light penetration was poorer the further from the centre of the oven the vials were located. As a result only two vials out of six reached full conversion after 30 mins.

However, an advantage of UV-light reactions is that they are easily translated into a flow-reactor system. Flow reactors increase the reaction surface area and thus will greatly increase UV light penetration. Indeed, this proved to be the case. Dr. Andrea Taladriz-Sender ran optimisation trials on the model carbazole system (Scheme 89).



Scheme 89. UV mediated C-C direct arylation, 9W lamp, flow conditions.

Table 14. Reaction optimisation of UV mediated reaction in flow. Conversion by LC-MS. Isolated yield shown in bold.

	Cycle number	Residence time (h)	Solvent	Base	Conversion
1	1	0.75	THF	-	20%
	2	1.5	THF	-	35%
	3	3	THF	-	60%
2	1	1.5	THF	^{t}BuOK	70%
3	2	1.5	DMSO	-	85% (**45%**)

THF was chosen as the solvent for these studies to attempt to move away from the high boiling point DMSO. It was found the base was not actually required when the reaction was passed through a flow system in comparison to batch and that a residence time of 3 h obtained 60% conversion to **4.82** (Table 14, entry 1). Adding the base back into the reaction increased the reaction rate with 70% conversion achieved after only 1.5 h (Table 14, entry 2). However, the best conversion was seen in DMSO, with 85% conversion after 1.5 h. This reaction required no base, however, isolation was particularly difficult, as GQC-05 analogues are difficult to extract from DMSO as a result of the dimethylamino basic tail. Therefore the compromise of addition of base with the lower boiling THF is an attractive alternative route.

4.4.5 Biological Evaluation of Deaza-GQC-05 and Analogues in Bcl-x *in vitro* Splicing Assays

With this small suite of GQC-05 analogues in hand, they were submitted for biological testing in splicing assays with collaborators in the University of Leicester (Figure 69).

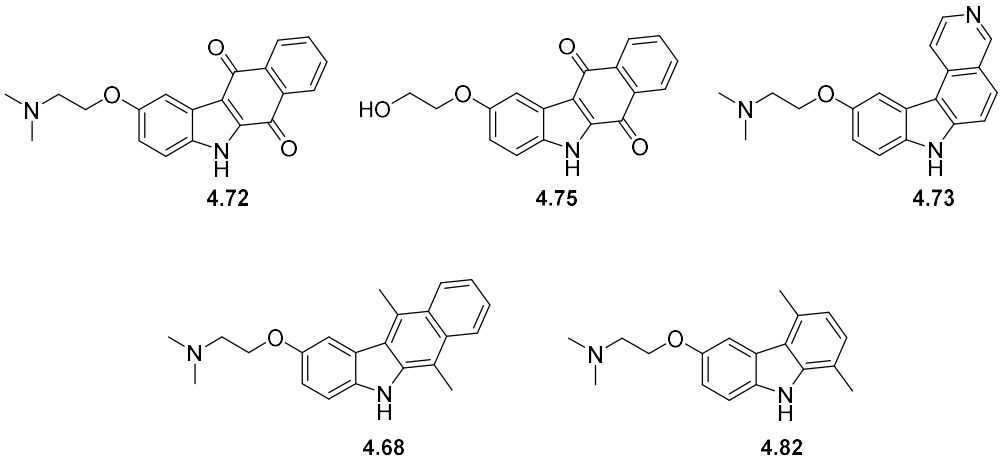


Figure 69. Focussed suite of GQC-05 analogues for biological testing.

4.4.6 *In vitro* Bcl-x-681 Splicing Assays of GQC-05 (**1.31**) and its Derivatives

The analogues synthesised in Figure 69 were submitted for testing for splicing activity and the results laid out in Figure 70 and Figure 71.

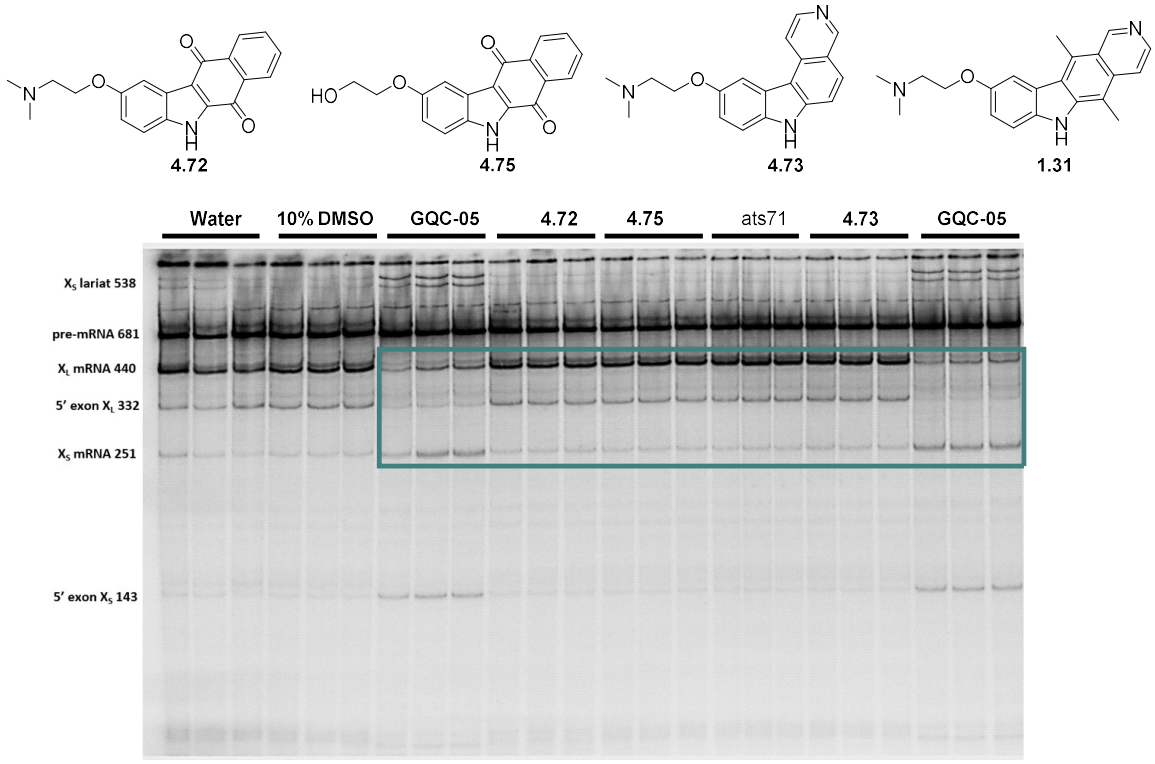


Figure 70. *In vitro* splicing assay on addition of ligands **4.72**, **4.75**, **4.73** and GQC-05 (**1.31**). Experiments ran by Dr. Sudipta Ghosh at the University of Leicester.

Compounds **4.72, 4.73** and **4.75** all showed to have no effect on splicing activity when compared to the 10 % DMSO control. By comparison, GQC-05 (**1.31**) was also tested as a positive control which showed an increase in intensity of the x_S mRNA 251 band and a decrease in intensity of x_L mRNA 440 band indicating an active splice switch towards the pro-apoptotic Bcl-x_S.

These results are notable in that they indicate the shape of the core structure and the methyl groups in the C-ring are desirable for biological activity in this system. In particular, although **4.73** is similar in structure to GQC-05 (**1.31**), it was surprisingly completely inactive.

Next compounds **4.68** and **4.82** were tested and the results laid out in Figure 71.

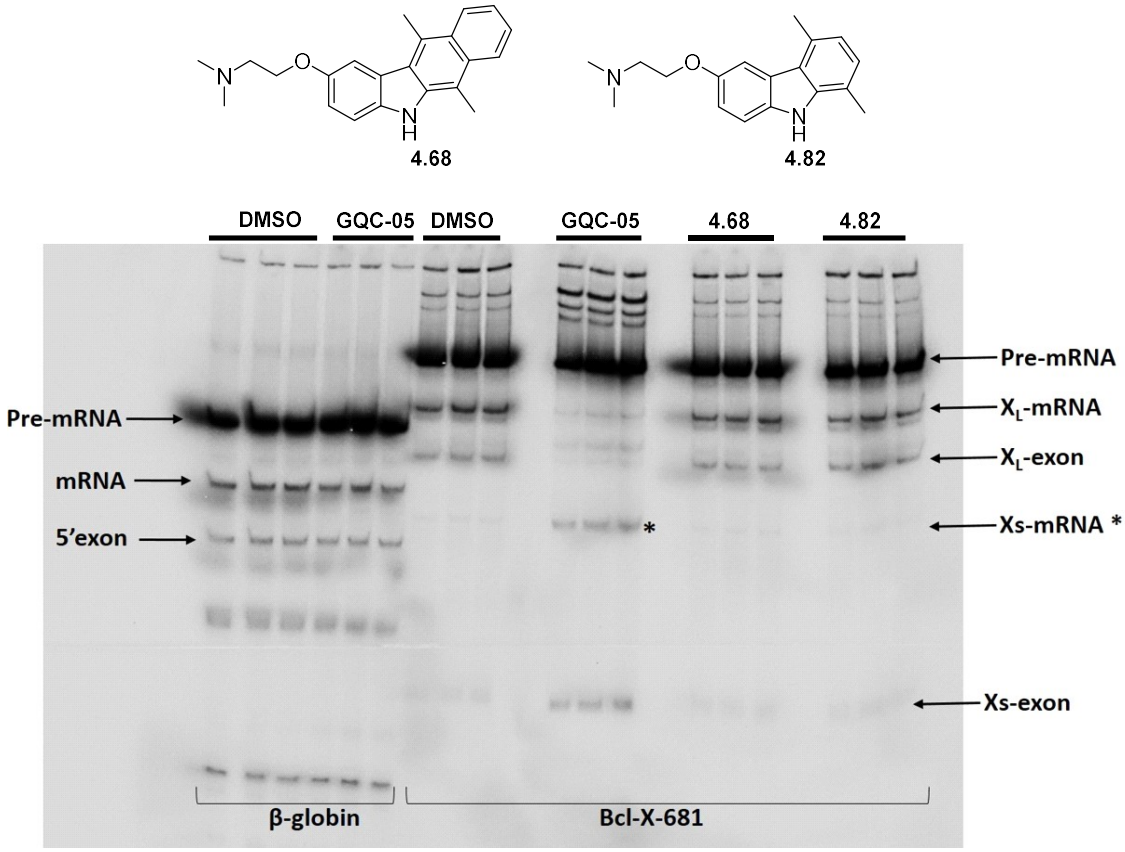


Figure 71. *In vitro* splicing assay on addition of ligands **4.68**, **4.82**, and **GQC-05** (**1.31**). Experiments ran by Dr. Sudipta Ghosh at the University of Leicester.

It was found that again, compounds **4.68** and **4.82** showed no splice-switch activity when compared to the DMSO control. This result was remarkable, as it showed that one single atom change could knock out the splice-switch altogether. GQC-05 without the D-ring (**4.82**) showed no activity but the single change of the D-ring nitrogen to a carbon abolished activity altogether indicating the pyrido-D-ring is essential for activity (Figure 72).

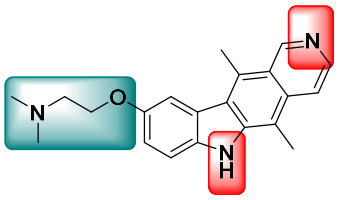
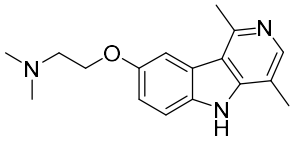


Figure 72. SAR-profile of GQC-05 (**1.31**) from analogue testing in Bcl-x splicing assays.

4.5 Conclusions and Future Work

The sequential Buchwald-Hartwig amination followed by direct arylation method developed in Chapter 2 proved to be unsuccessful in the preparation of GQC-05 analogues with methyl-substitution in the C-ring. A novel UV-mediated arylation method has been developed to access a wide range of GQC-05 analogues. Deaza-GQC-05 was synthesised and showed no splice-switching activity in Bcl-x *in vitro* splicing assays. This result highlights the importance of the pyridyl moiety in the D-ring of GQC-05 (**1.31**) for biological activity in this system suggesting it is essential for splice-switching.

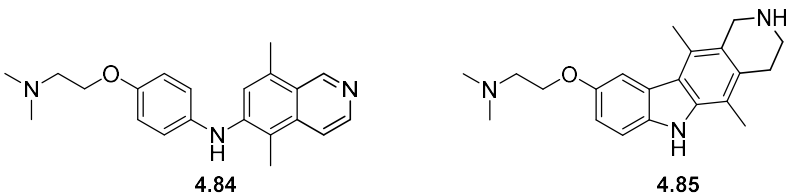
Future aims of this study could be to further expand the library of GQC-05 (**1.31**) analogues to further enrich the SAR study. In particular, synthesis of carbazole **4.83**, could be enlightening to the study as the analogue retains the H-bond acceptor ability, but is a tricycle instead of a tetracycle.



4.83

Figure 73. Future carbazole GQC-05 analogue for *in vitro* Bcl-x splicing assays.

Further development of GQC-05 (**1.31**) could be explored. GQC-05 (**1.31**) is flat in shape due to its fused aromatic rings, this leads to GQC-05 (**1.31**) being a very effective intercalator of DNA. Disruption of this planarity could be explored for splice-switching activity in an attempt to improve selectivity by preventing intercalation through compound **4.84** and **4.85** (Figure 74).



4.84 **4.85**

Figure 74. Expansion of SAR-profile through disruption of planarity with compounds **4.84** and **4.85**.

Chapter 5 Conclusions and Future Work

The aims of this thesis were to develop a convergent synthesis of GQC-05 (**1.31**) and its analogues for assessing the mode of action of splice-switching in Bcl-x *in vitro* assays for the development of novel cancer therapies.

Firstly, a modular one-pot synthesis via microwave irradiation was developed for the synthesis of 5*H*-benzo[*b*]carbazole-6,11-diones and 7*H*-pyridocarbazoles. A range of analogues were synthesised and it was found that increasing electron deficiency in the A-ring suppressed the efficiency of the direct arylation. Interestingly, no de-halogenation was observed in these cases indicating that the barrier was insufficient oxidative addition. This method was then applied to the total synthesis of carbazole natural products Glycozoline (**2.26**), Harmane (**2.63**) and Murrayafoline A (**2.64**) in one step, in addition to the synthesis of known antitumor agents **2.69**, **2.70**, and Ditercalinium (**2.71**) in two steps.

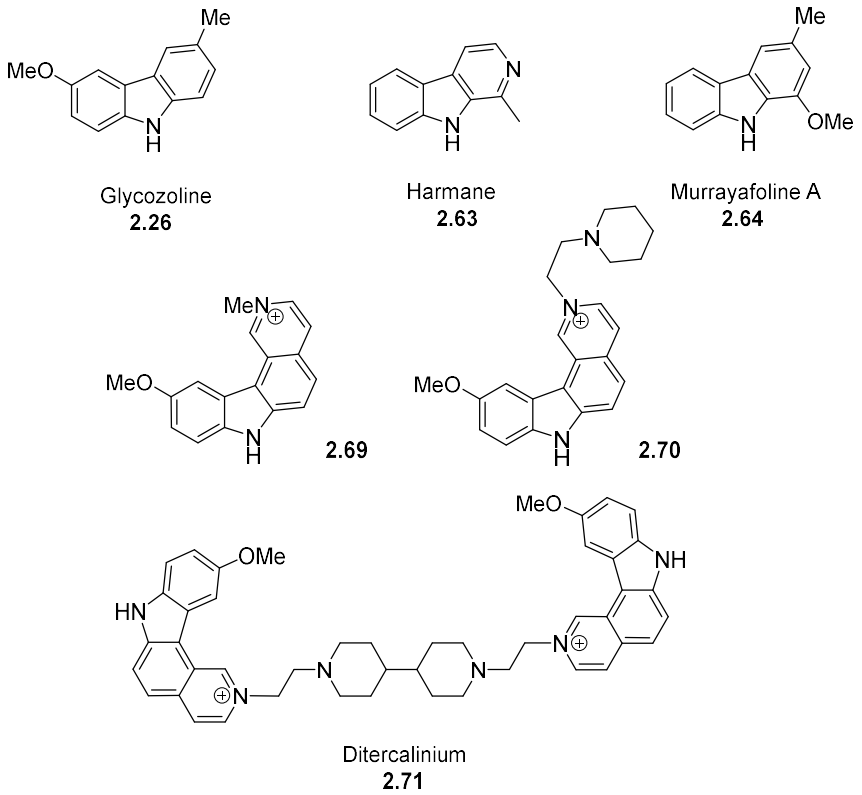


Figure 75. Structures of natural products Glycozoline (**2.26**), Harmane (**2.63**), Murrayafoline A (**2.64**) and alkylated pyridocarbazoles **2.69**, **2.70** and Ditercalinium (**2.71**).

The mechanism of the direct-arylation was investigated and it was found that the palladium catalyst was essential. Futhermore, the lone pair of the secondary aniline must be available to facilitate the C-C bond formation and finally no direct arylation occurs when the aryl-chloride substituent is absent. Acetylation of the secondary aniline, to protect the lone-pair, further

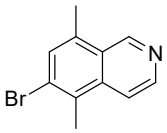
confirmed its requirement for conversion as the yield decreased from 83% to 27%. However, this reaction also surprisingly highlighted that the regioselectivity could be modulated towards the linear isomer **3.38**. DFT calculations confirmed, through molecular orbital calculations, that the electron density was still centred on the 5-position suggesting that incorporation of an acetyl-direct group can overcome the inherent electronic bias of the reaction and result in C-C bond formation to the 7-position instead.

The Pd-catalysed method developed in Chapter 2 was applied to the synthesis of GQC-05 (**1.31**) analogues and was unsuccessful. Consequently, a novel UV-mediated method was established to synthesise deaza-GQC-05 and its carbazole equivalent. The GQC-05 (**1.31**) analogues generated were then tested for splice-switching activity and were found to be inactive in *in vitro* splicing assays. These results highlighted the significance of the nitrogen in the D-ring for biological activity.

To expand on this work, the following future studies are proposed:

(i) *Confirm regioselectivity of acetylated **3.37**.* Initial studies carried out in this thesis have indicated that the change in regioselectivity observed is a result of a directing group effect from the carbonyl of the acetamide. However, the sequence of events remain currently unclear with respect to deacetylation *in situ*. It is proposed that the acetylated **3.37** starting material co-ordinates with the palladium complex to direct the site of arylation, however, it has been observed through developing the scope that the lone pair of the secondary aniline must be available for C-C arylation to proceed. To investigate this a more stable protecting group, e.g. pivolyl, could be used. This would be an interesting study to see if preventing deprotection, suppresses the direct arylation. Furthermore, preventing deprotection should theoretically prevent formation of pyridocarbazole (**2.39**), accessing selectivity for the linear isomer (**3.38**).

(ii) *Synthesis of 6-bromo-5,8-dimethylisoquinoline (**4.67**)*. As the D-ring nitrogen has been shown to be essential for splice-switching activity, synthesis of 6-bromo-5,7-dimethylisoquinoline, will open up a convergent route to GQC-05 (**1.31**) and its analogues through the UV-mediated synthesis. It is proposed that a design of experiments (DoE) is carried out varying temperature, concentration, water content and acid source to obtain **4.67** for further expansion of the SAR.



4.67

Figure 76. Structure of 6-bromo-5,8-dimethylisoquinoline (**4.67**).

(iii) *Development of a High Through-Put (HTP) testing platform*. Bcl-x splicing assays are not an accessible process, as they require radioactive ^{32}P, and must be run individually. Development of a HTP Luciferase assay that is designed to be 'light-up' when a splice-switch has occurred could give access to screening large libraries to find new hits for developing novel cancer therapies (Figure 77 and Figure 78). Luciferase assay screening platforms have been successfully utilised in the discovery of small molecule splice-switchers for the treatment of SMA.[105]

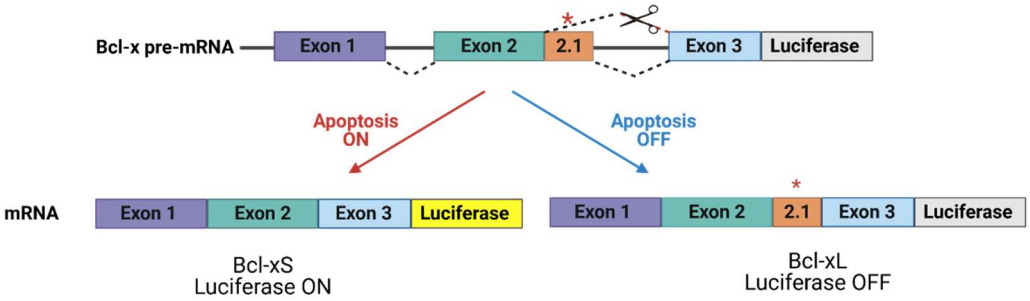


Figure 77. Schematic of proposed Bclx-681-Luc assay. Inserted nucleotide position denoted by red asterix. Nucleotide insertion in exon 2.1 ensures the luciferase is out of frame in the pre-mRNA (Light off). On excision of exon 2.1, the in frame luciferase (light on) to indicate a splice-switch turning on apoptosis.

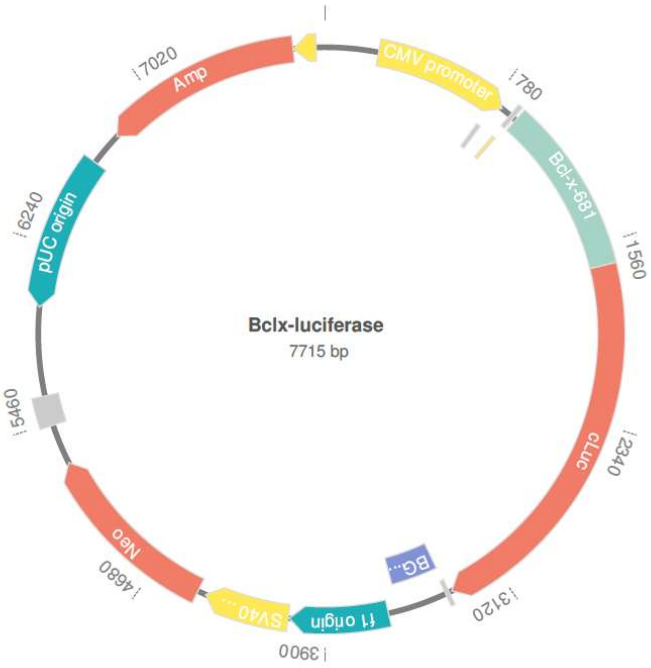


Figure 78. Potential plasmid design for Bcl-x-681-Luc reporter.

Chapter 6 Experimental

6.1.1 General

All reagents and solvents were obtained from commercial suppliers and were used without further purification unless otherwise stated. Purification was carried out according to standard laboratory methods.[206]

6.1.2 Purification of Solvents

Dry solvents for reactions were purchased from Sigma-Aldrich and stored under nitrogen. Dichloromethane, chloroform, methanol, ethyl acetate, and petroleum ether (40 – 60 °C) for purification purposes were used as obtained from suppliers, without further purification.

6.1.3 Experimental Details

Reactions were carried out using conventional glassware for the preparation of starting materials. Microwave reactions were carried out in capped 2 - 5 mL microwave vials purchased from Biotage®. Microwave reactions were carried out at elevated temperatures using a Biotage® Initiator + equipped with a Robot Eight and Sixty microwave system.

6.1.4 Purification of Products

Thin layer chromatography was carried out using Merck silica plates coated with fluorescent indicator UV254 and were analysed under both 254 nm and 375 nm UV light or developed using potassium permanganate solution. Normal phase flash chromatography was carried out using 60A 40-63 μm silica gel from Fluorochem. Semi-preparative reversed-phase HPLC purification was carried out using a DIONEX 3000 series HPLC system equipped with a VWD3400 variable wavelength detector. Purifications were performed method, 30 – 90% gradient B (solvent A: 0.1% TFA in water, solvent B: 0.1% TFA in acetonitrile). Flow rate 12.0 mL/min. The absorbance was detected at 254 nm.

6.1.5 Spectroscopic Analysis of Products

Fourier Transformed Infra-Red (FTIR) spectra were obtained on a Shimadzu IR Affinity-1 machine. ^{1}H NMR, ^{13}C NMR and ^{19}F NMR spectra were obtained on a Bruker AV 400 at 400 MHz, 101 MHz and 376 MHz, respectively. Chemical shifts are reported in ppm and coupling constants are reported in Hz with DMSO-d_6 referenced at 2.50 ppm (^{1}H) and 39.52 ppm (^{13}C) and MeOD-d_4 referenced at 3.31 ppm (^{1}H) and 49.0 ppm (^{13}C) . Assignment of ^{13}C NMR signals is based on HSQC and HMBC experiments. High-resolution mass spectra were obtained through analysis at the SIRCAMs facility at the University of Edinburgh.

6.2 General Experimental Procedures

6.2.1 General Experimental Procedure A: Microwave Assisted Buchwald-Hartwig Amination Optimisation

Aryl bromide (0.50 mmol, 1.00 equiv), chloroaniline (0.60 mmol, 1.20 equiv), $Pd(OAc)_2$ (5 mol%), ligand (10 mol%) and base (1.50 mmol, 3.0 equiv) were added to a microwave vial (2 – 5 mL). 1,4-Dioxane (5 mL, 0.01 M) was added and the vial was capped, evacuated and purged with argon 3 times. The reaction was heated at 120 °C for 30 mins under microwave irradiation in a Biotage® Microwave. The crude reaction mixture was analysed by Shimadzu analytical HPLC using a Hypersil Gold Luna Polar column. The crude reaction was sampled by taking 10 µL into 990 µL of DMSO using a 12 minute method, 5 – 95% gradient B (solvent A: 0.1% TFA in water, solvent B: 0.1% TFA in acetonitrile). Flow rate 2.0 mL/min. Conversions to products were calculated by analytical HPLC against a calibration curve. All reactions were run in duplicate.

6.2.2 General Experimental Procedure B: Microwave Assisted One-Pot Buchwald-Hartwig Amination and Direct Arylation Optimisation

Aryl bromide (0.50 mmol, 1.00 equiv), chloroaniline (0.60 mmol, 1.20 equiv), $Pd(OAc)_2$ (5 mol%), ligand (10 mol%) and base (1.50 mmol, 3.0 equiv) were added to a microwave vial (2 – 5 mL). 1,4-Dioxane (5 mL, 0.01 M) was added and the vial was capped, evacuated and purged with argon 3 times. The reaction was heated at 120 °C for 30 mins, followed by 160 °C for 8 hours under microwave irradiation in a Biotage® Microwave. The crude reaction mixture was analysed by Shimadzu analytical HPLC using a Hypersil Gold Luna Polar column. The crude reaction was sampled by taking 10 µL into 490 µL of DMSO using a 12 minute method, 5 – 95% gradient B (solvent A: 0.1% TFA in water, solvent B: 0.1% TFA in acetonitrile). Flow rate 2.0 mL/min. Conversions to products were calculated by analytical HPLC against a calibration curve. All reactions were run in duplicate.

6.2.3 General Experimental Procedure C: Microwave Assisted Buchwald-Hartwig Amination

Aryl bromide (0.50 mmol, 1.00 equiv), chloroaniline (0.60 mmol, 1.2 equiv), $Pd(OAc)_2$ (5 mol%), DavePhos (10 mol%) and K_3PO_4 (1.50 mmol, 3 equiv) were added to a microwave vial (2 – 5 mL). 1,4-Dioxane (5 mL, 0.1 M) was added and the vial was capped, evacuated and purged with argon 3 times, then heated at 120 °C for 30 minutes under microwave irradiation in a Biotage® Microwave. The reaction was allowed to cool to rt, diluted with ethyl acetate (50 mL) and paper filtered under vacuum. The organic phase was washed with water, brine, dried with Na_2SO_4,

filtered and the solvent was removed *in vacuo*. The crude compound was purified by silica column chromatography.

6.2.4 General Experimental Procedure D: Microwave Assisted One-Pot Buchwald-Hartwig Amination and Direct Arylation

Aryl bromide (0.50 mmol, 1 equiv), chloroaniline (0.60 mmol, 1.2 equiv), $Pd(OAc)_2$ (5 mol%), DavePhos (10 mol%) and K_3PO_4 (1.50 mmol, 3 equiv) were added to a microwave vial (2 – 5 mL). 1,4-Dioxane (5.0 mL, 0.1 M) was added and the vial was capped, evacuated and purged with argon 3 times and heated at 120 °C for 30 min followed by 160 °C for 8 hours under microwave irradiation in a Biotage® Microwave. The reaction was allowed to cool to rt and diluted with DCM (50 mL) and filtered under vacuum. The solvent was removed *in vacuo* and the crude sample dry-loaded onto silica gel without work up. The crude compound was purified by silica column chromatography.

6.2.5 General Experimental Procedure E: Microwave Assisted One-Pot Buchwald-Hartwig Amination and Direct Arylation

Aryl bromide (0.50 mmol, 1 equiv), chloroaniline (0.60 mmol, 1.2 equiv), $Pd(OAc)_2$ (5 mol%), $P(Cy_3).HBF_4$ (10 mol%) and K_3PO_4 (1.50 mmol, 3 equiv) were added to a microwave vial (2 – 5 mL). 1,4-Dioxane (5.0 mL, 0.1 M) was added and the vial was capped, evacuated and purged with argon 3 times and heated at 120 °C for 30 min followed by 160 °C for 8 hours under microwave irradiation in a Biotage® Microwave. The reaction was allowed to cool to rt and diluted with DCM (50 mL). The solvent was removed *in vacuo* and the crude sample dry-loaded onto silica gel without work up. The crude compound was purified by silica column chromatography.

6.3 Microwave Assisted Buchwald-Hartwig Amination Optimisation

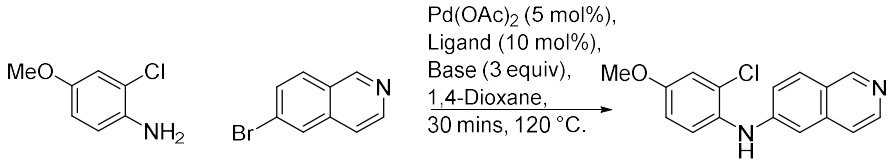


Table 15. Optimisation of Buchwald-Hartwig Amination. All reactions carried out according to general procedure A.[a] Isolated yield shown in brackets.

Ligand	Base	Conversion (%)
DavePhos	NaO^tBu	12
DavePhos	Cs_2CO_3	74
DavePhos	**K_3PO_4**	**85 (87)[a]**
$HPCy_3BF_4$	NaO^tBu	75
$HPCy_3BF_4$	Cs_2CO_3	10
$HPCy_3BF_4$	K_3PO_4	10
$HP^tBu_3BF_4$	NaO^tBu	7
$HP^tBu_3BF_4$	Cs_2CO_3	70
$HP^tBu_3BF_4$	K_3PO_4	65
XPhos	NaO^tBu	47
XPhos	Cs_2CO_3	76
XPhos	K_3PO_4	77

6.4 Microwave Assisted One-Pot Buchwald-Hartwig Amination/Direct Arylation Optimisation

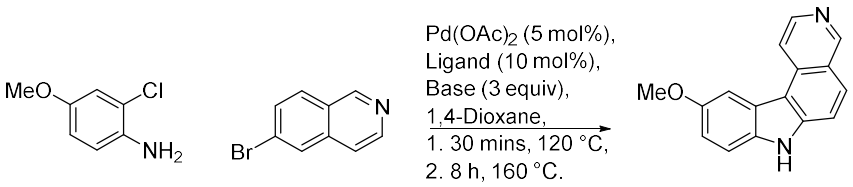


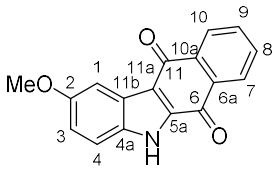
Table 16. Optimisation of Buchwald-Hartwig Amination/Direct Arylation. All reactions carried out according to general procedure B. [a] Isolated yield shown in brackets.

Ligand	Base	Conversion (%)
DavePhos	NaO^tBu	10
DavePhos	Cs_2CO_3	28
DavePhos	K_3PO_4	36
$HPCy_3BF_4$	NaO^tBu	45
$HPCy_3BF_4$	Cs_2CO_3	50
$HPCy_3BF_4$	**K_3PO_4**	**78 (80)**
$HP^tBu_3BF_4$	NaO^tBu	3
$HP^tBu_3BF_4$	Cs_2CO_3	25
$HP^tBu_3BF_4$	K_3PO_4	31
XPhos	NaO^tBu	19
XPhos	Cs_2CO_3	18
XPhos	K_3PO_4	22

6.5 Experimental Details

6.5.1 Chapter 2: Compound Characterisation

2-methoxy-5*H*-benzo[*b*]carbazole-6, 11-dione (**2.37**)



The reaction was carried out according to general procedure D using 2-bromonaphthalene-1,4-dione (119 mg, 0.50 mmol, 1 equiv), 2-chloro-4-methoxyaniline (94 mg, 0.60 mmol, 1.2 equiv) as starting materials. The crude residue was purified by silica-gel column chromatography, petroleum ether (40 – 60 °C): EtOAc: NEt_3 (70: 30: 1) to obtain compound **2.37** in 78% yield (93 mg, orange solid).

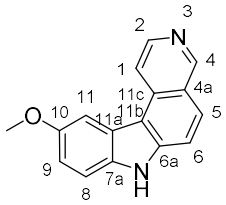
IR $\bar{\nu}_{max}$ (cm^{-1}): 3195 (N-H stretch), 1673 (C=O stretch), 1644 (C=O stretch), 1592 (C=C stretch), 1530 (C=O stretch), 1223 (C-O stretch), 1020 (C-O stretch).

^{1}H NMR (400 MHz, DMSO-d_6) δ 13.02 (s, 1H, -N*H*), 8.15 – 8.08 (m, 2H, $H^{7,10}$), 7.86 (dd, *J* = 7.5, 1.5 Hz, 1H, H^9), 7.81 (dd, *J* = 7.4, 1.7 Hz, 1H, H^8), 7.63 (d, *J* = 2.5 Hz, 1H, H^1), 7.51 (d, *J* = 9.1 Hz, 1H, H^4), 7.10 (dd, *J* = 9.0, 2.6 Hz, 1H, H^3), 3.86 (s, 3H, -OCH_3).

^{13}C NMR (101 MHz, DMSO-d_6) δ 180.2 (C^{11}), 177.2 (C^6), 157.0 (C^2), 137.0 (C^{5a}), 134.2 (2×$C^{9, 10a}$), 133.4 (C^{4a}), 133.1 (C^8), 132.7 (C^{6a}), 126.0 (2×$C^{7, 10}$), 124.8 (C^{11b}), 118.4 (C^3), 117.0 (C^{11a}), 115.0 (C^4), 102.1 (C^1), 55.4 (-O*C*H_3).

HRMS-ESI: m/z: $[M+H]^+$ Calculated for $C_{17}H_{12}O_1N_3$; 278.0811, Found 278.0802.

10-methoxy-7*H*-pyrido[3,4-*c*]carbazole (**2.39**)



The reaction was carried out according general procedure E using 6-bromoisoquinoline (104 mg, 0.50 mmol, 1.0 equiv) and 2-chloro-4-methoxyaniline (95 mg, 0.60 mmol, 1.2 equiv) as starting materials. The crude residue was purified by silica gel column chromatography petroleum ether (40 – 60 °C): EtOAc (1: 1) to obtain compound **2.39** in 82% yield (102 mg, brown solid).

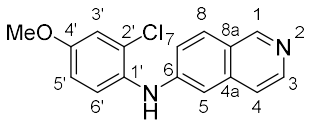
IR $\bar{\nu}_{max}$ (cm^{-1})**:** 2830 (C-H stretch), 1616 (C=N stretch), 1458 (C=C stretch), 1229 (C-O stretch), 1031 (C-O stretch).

^{1}H NMR (400 MHz, DMSO-d_6) δ 11.94 (s, 1H, -N*H*), 9.30 (s, 1H, H^4), 8.63 (d, *J* = 5.8 Hz, 1H, H^2), 8.58 (d, *J* = 5.8 Hz, 1H, H^1), 8.05 – 7.99 (m, 2H, $H^{5,11}$), 7.85 (d, *J* = 8.8 Hz, H^6), 7.60 (d, *J* = 8.8 Hz, H^8), 7.13 (dd, *J* = 8.8, 2.4 Hz, H^9), 3.96 (s, 3H, -OCH_3).

^{13}C NMR (101 MHz, DMSO-d_6) δ 154.1 (C^{10}), 152.0 (C^{4}), 144.1 (C^{2}), 140.0 (C^{6a}), 133.6 (C^{7a}), 132.1 (C^{11c}), 125.9 (C^{5}), 123.6 (C^{11b}), 123.0 (C^{11a}), 116.4 (C^{1}), 115.0 (C^{6}), 114.3 (C^{9}), 112.6 (C^{8}), 112.3 (C^{4a}), 103.9 (C^{11}), 55.8 (-O*C*H$_3$).

HRMS-ESI: m/z: [M+H]$^+$ Calculated for $C_{16}H_{13}O_1N_2$; 249.1022, Found 249.1021.

N-(2-chloro-4-methoxyphenyl)isoquinolin-6-amine (**2.41a**)



The reaction was carried out according to general procedure C using 6-bromoisoquinoline (104 mg, 0.50 mmol, 1.0 equiv) and 4-methoxy-2-chloroaniline (95 mg, 0.60 mmol, 1.2 equiv) as starting materials. The crude residue was purified by silica-gel column chromatography, petroleum ether (40 – 60 °C): EtOAc (7: 3) to obtain compound **2.41a** in 87% yield (123 mg, brown solid).

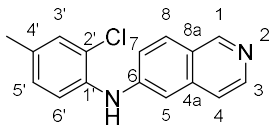
IR $\bar{\nu}_{max}$ (cm^{-1}): 3230 (N-H stretch), 1618 (C=N stretch), 1476 (C=C stretch), 1284 (C-N stretch), 1212 (C-O stretch), 1039 (C-O stretch), 847 (C-Cl stretch).

^{1}H NMR (400 MHz, DMSO-d_6) δ 8.95 (s, 1H, H^{1}), 8.29 (s, 1H, -N*H*), 8.20 (d, J = 4.6 Hz, 1H, H^{3}), 7.87 (d, J = 7.1 Hz, 1H, H^{8}), 7.41 – 7.38 (m, 2H, $H^{6',4}$), 7.24 (dd, J = 7.1, 1.7 Hz, 1H, H^{7}), 7.18 (d, J = 2.3 Hz, 1H, $H^{3'}$), 7.00 (dd, J = 7.0, 2.3 Hz, 1H, $H^{5'}$), 6.67 (d, J = 1.7 Hz, 1H, H^{5}), 3.81 (s, 3H, -OC*H*$_3$).

^{13}C NMR (101 MHz, DMSO-d_6) δ 157.1 ($C^{4'}$), 151.0 (C^{1}), 147.9 (C^{6}), 143.1 (C^{3}), 137.3 (C^{4a}), 130.6 ($C^{2'}$), 130.3 ($C^{1'}$), 128.8 (C^{8}), 127.9 ($C^{6'}$), 122.9 (C^{8a}), 119.2 (C^{7}), 118.6 (C^{4}), 115.2 ($C^{3'}$), 114.3 ($C^{5'}$), 103.0 (C^{5}), 55.7 (-O*C*H$_3$).

HRMS-ESI: m/z: [M+H]$^+$ Calculated for $C_{16}H_{14}O_1N_2Cl_1$; 285.0789, Found 285.0787.

N-(2-chloro-4-methylphenyl)isoquinolin-6-amine (**2.41b**)



The reaction was carried out according to general procedure C using 6-bromoisoquinoline (104 mg, 0.50 mmol, 1.0 equiv) and 4-methyl-2-chloroaniline (85 mg, 0.60 mmol, 1.2 equiv) as starting materials. The crude residue was purified by silica-gel column chromatography, petroleum ether (40 – 60 °C): EtOAc (6: 4) to obtain compound **2.41b** in 91% yield (122 mg, brown solid).

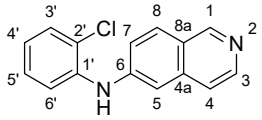
IR $\bar{\nu}_{max}$ (cm^{-1}): 3234 (N-H stretch), 3031 (C-H stretch), 1608 (C=N stretch), 1474 (C=C stretch), 821 (C-Cl stretch).

^{1}H NMR (400 MHz, DMSO-d_6) δ 8.97 (s, 1H, H^1), 8.35 (s, 1H, -N*H*), 8.23 (d, J = 5.8 Hz, 1H, H^3), 7.89 (d, J = 8.9 Hz, 1H, H^8), 7.45 (d, J = 5.8 Hz, 1H, H^4), 7.40 (d, J = 1.4 Hz, 1H, $H^{3'}$), 7.38 (d, J = 8.1 Hz, 1H, $H^{6'}$), 7.32 (dd, J = 8.9, 2.2 Hz, 1H, H^7), 7.19 (dd, J = 8.1, 1.5 Hz, 1H, $H^{5'}$), 6.90 (d, J = 2.1 Hz, 1H, H^5), 2.32 (s, 3H, -CH_3).

^{13}C NMR (101 MHz, DMSO-d_6) δ 151.1 (C^1), 146.8 (C^6), 143.1 (C^3), 137.1 (C^{4a}), 135.3 ($C^{2'}$), 135.1 ($C^{1'}$), 130.5 ($C^{3'}$), 128.8 (C^8), 128.7 ($C^{5'}$), 127.5 ($C^{4'}$), 124.9 ($C^{6'}$), 123.2 (C^{8a}), 119.8 (C^7), 118.8 (C^4), 104.3 (C^5), 20.1 (-CH$_3$).

HRMS-ESI: m/z: [M+H]$^+$ Calculated for $C_{16}H_{14}N_2Cl_1$; 269.0840, Found 269.0859.

N-(2-chlorophenyl)isoquinolin-6-amine (**2.41c**)



The reaction was carried out according to general procedure C using 6-bromoisoquinoline (104 mg, 0.50 mmol, 1.0 equiv) and 2-chloroaniline (77 mg, 0.60 mmol, equiv) as starting materials. The crude residue was purified by silica-gel column chromatography, petroleum ether (40 – 60 °C): EtOAc (1: 1) to obtain compound **2.41c** in 85% yield (108 mg, green solid).

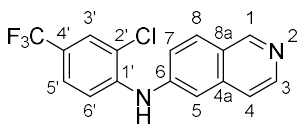
IR $\bar{\nu}_{max}$ (cm^{-1}): 3215 (N-H stretch), 3029 (C-H stretch), 1627 (C=N stretch), 1588 (C=C stretch), 1471 (C=C stretch), 737 (C-Cl stretch).

^{1}H NMR (400 MHz, DMSO-d_6) δ 9.00 (s, 1H, H^1), 8.43 (s, 1H, -N*H*), 8.26 (d, 1H, J = 5.8 Hz, H^3), 7.93 (d, 1H, J = 8.9 Hz, H^8), 7.55 (dd, J = 8.0, 1.4 Hz, 1H, $H^{3'}$), 7.51 (dd, J = 8.0, 1.4 Hz, 1H, H^7), 7.49 – 7.47 (m, 1H, $H^{6'}$), 7.41 – 7.33 (m, 2H, $H^{4,5'}$), 7.18 – 7.12 (m, 1H, $H^{4'}$), 7.06 (d, J = 2.1 Hz, 1H, H^5).

^{13}C NMR (101 MHz, DMSO-d_6) 151.1 (C^1), 146.1 (C^6), 143.1 (C^3), 138.2 ($C^{1'}$), 137.0 (C^{4a}), 130.3 ($C^{3'}$), 128.9 (C^8), 128.1 ($C^{5'}$), 126.7 ($C^{2'}$), 124.8 ($C^{4'}$), 123.7 (C^7), 123.5 (C^{8a}), 120.2 (C^4), 118.9 ($C^{6'}$), 105.5 (C^5).

HRMS-ESI: m/z: [M+H]$^+$ Calculated for $C_{15}H_{12}N_2Cl_1$; 255.0683, Found 255.0688.

N-(2-chloro-4-(trifluoromethyl)phenyl)isoquinolin-6-amine (**2.41d**)



The reaction was carried out according to general procedure C using 6-bromoisoquinoline (104 mg, 0.50 mmol, 1.0 equiv) and 2-chloro-4-(trifluoromethyl)aniline (117 mg, 0.60 mmol, 1.2 equiv) as starting materials. The crude residue was purified by silica-gel column chromatography, petroleum ether

(40 – 60 °C): EtOAc (6: 4) to obtain compound **2.41d** in 78% yield (116 mg, yellow crystalline solid).

IR $\bar{\nu}_{max}$ (cm^{-1}): 3220 (N-H stretch), 1612 (C=N stretch), 1487 (C=C stretch), 823 (C-Cl stretch).

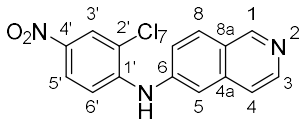
^{1}H NMR (400 MHz, DMSO-d_6) δ 9.12 (s, 1H, H^1), 8.71 (s, 1H, -N*H*), 8.35 (d, *J* = 5.7 Hz, 1H, H^3), 8.03 (d, *J* = 8.9 Hz, 1H, H^8), 7.88 (s, 1H, $H^{5'}$), 7.64 – 7.61 (m, 3H, $H^{4,\,3',\,6'}$), 7.55 (dd, *J* = 8.8, 2.2 Hz, 1H, H^7), 7.49 (d, *J* = 2.0 Hz, 1H, H^5).

^{13}C NMR (101 MHz, DMSO-d_6) δ 151.4 (C^1), 143.6 (C^6), 143.3 (C^3), 142.9 ($C^{1'}$), 136.6 (C^{4a}), 129.0 (C^8), 127.2 (q, *J* = 3.7 Hz, $C^{5'}$), 125.2 (q, J = 3.7 Hz, $C^{3'}$), 124.4 (C^{8a}), 123.7 (q, *J* = 272.9 Hz, -*C*F$_3$), 123.6 ($C^{2'}$), 122.4 (q, *J* = 33.2 Hz, $C^{4'}$), 121.8 (C^7), 119.4 ($C^{4,\,6'}$), 110.3 (C^5).

^{19}F NMR (471 MHz, DMSO-d_6) δ −60.20.

HRMS-ESI: m/z: $[M+H]^+$ Calculated for $C_{16}H_{11}N_2Cl_1F_3$; 323.0557, Found 323.0542.

N-(2-chloro-4-nitrophenyl)isoquinolin-6-amine (**2.41e**)



The reaction was carried out following general procedure C using 6-bromoisoquinoline (104 mg, 0.50 mmol, 1.0 equiv), and 4-nitro-2-chloroaniline (104 mg, 0.60 mmol, 1.2 equiv) as starting materials. The crude residue was purified by silica-gel column chromatography, petroleum ether (40 – 60 °C): EtOAc (1: 1) to obtain compound **2.41e** in 56% yield (83 mg, yellow solid).

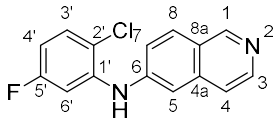
IR $\bar{\nu}_{max}$ (cm^{-1}): 3221 (N-H stretch), 1584 (C=N bend), 1508 (N-O stretch), 1474 (C=C stretch), 1333 (N-O stretch), 821 (C-Cl stretch).

^{1}H NMR (400 MHz, DMSO-d_6) δ 9.20 (s, 1H, H^1), 9.07 (s, 1H, -N*H*), 8.42 (d, *J* = 5.8 Hz, 1H, H^3), 8.34 (d, *J* = 2.7 Hz, 1H, $H^{3'}$), 8.12 (d, *J* = 8.8 Hz, 1H, H^8), 8.10 (dd, *J* = 9.2, 2.7 Hz, 1H, $H^{5'}$), 7.73 (d, *J* = 2.0 Hz, 1H, H^5), 7.71 (d, *J* = 5.8 Hz, 1H, H^4), 7.64 (dd, *J* = 8.8, 2.0 Hz, 1H, H^7), 7.48 (d, *J* = 9.2 Hz, 1H, $H^{6'}$).

^{13}C NMR (101 MHz, DMSO-d_6) δ 151.7 (C^1), 146.3 ($C^{4'}$), 143.4 (C^3), 142.1 (C^6), 139.5 ($C^{1'}$), 136.3 (C^{8a}), 129.2 (C^8), 125.9 ($C^{3'}$), 125.2 (C^{4a}), 124.3 ($C^{5'}$), 123.2 (C^7), 121.0 ($C^{2'}$), 119.7 (C^4), 115.7 ($C^{6'}$), 114.4 (C^5).

HRMS-ESI: m/z: $[M+H]^+$ Calculated for $C_{15}H_{11}O_2N_3Cl_1$; 300.0534, Found 300.0538.

N-(2-chloro-5-fluorophenyl)isoquinolin-6-amine (**2.41f**)



The reaction was carried out according to general procedure C using 6-bromoisoquinoline (104 mg, 0.50 mmol, 1.0 equiv) and 2-chloro-5-fluoroaniline (87 mg, 0.60 mmol, 1.2 equiv) as starting materials. The crude residue was purified by silica-gel column chromatography, petroleum ether (40 – 60 °C): EtOAc (6: 4) to obtain compound **2.41f** in 74% yield (101 mg, yellow solid).

IR $\bar{\nu}_{max}$ (cm^{-1}): 3221 (N-H stretch), 1592 (C=N stretch), 1474 (C=C stretch), 852 (C-Cl stretch).

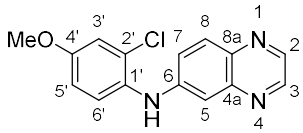
^{1}H NMR (400 MHz, DMSO-d_6) δ 9.06 (s, 1H, H^{1}), 8.51 (s, 1H, -N*H*), 8.31 (d, *J* = 5.8 Hz, 1H, H^{3}), 7.98 (d, *J* = 8.9 Hz, 1H, H^{8}), 7.58 (d, *J* = 5.8, 1H, H^{4}), 7.57 (dd, *J* = 9.0, 6.0 Hz, 1H, $H^{3'}$), 7.47 (dd, *J* = 8.9, 2.2 Hz, 1H, H^{7}), 7.33 – 7.27 (m, 2H, $H^{5,6'}$), 6.95 (ddd, *J* = 8.8, 8.0, 3.0 Hz, 1H, $H^{4'}$).

^{13}C NMR (101 MHz, DMSO-d_6) δ 161.2 (d, *J* = 244.7 Hz, $C^{5'}$), 151.3 (C^{1}), 144.7 (C^{4a}), 143.2 (C^{3}), 140.2 (d, *J* = 10.8 Hz, $C^{1'}$) 136.9 (C^{8a}), 131.5 (d, *J* = 10.0 Hz, $C^{3'}$), 129.0 (C^{8}), 124.0 (C^{6}), 120.8 (C^{7}), 120.5 (d, *J* = 3.3 Hz, $C^{2'}$), 119.2 (C^{4}), 110.5 (d, *J* = 20.9 Hz, $C^{4'}$), 108.5 (d, *J* = 26.0 Hz, $C^{6'}$), 107.7 (C^{5}).

^{19}F NMR (376 MHz, DMSO-d_6) δ −113.1.

HRMS-ESI: m/z: $[M+H]^+$ Calculated for $C_{15}H_{11}N_2Cl_1F_1$; 273.0589, Found 273.0594.

N-(2-chloro-4-methoxyphenyl)quinoxalin-6-amine (**2.42a**)



The reaction was carried out according to general procedure C using 6-bromoquinoxaline (105 mg, 0.50 mmol, 1.0 equiv) and 4-methoxy-2-chloroaniline (95 mg, 0.60 mmol, 1.2 equiv) as starting materials. The crude residue was purified by silica-gel column chromatography, petroleum ether (40 – 60 °C): EtOAc (7: 3) to obtain compound **2.42a** in 87% yield (124 mg, yellow solid).

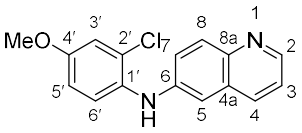
IR $\bar{\nu}_{max}$ (cm^{-1}): 3301 (N-H stretch), 3068 (C-H stretch), 2837 (C-H stretch), 1618 (C=N stretch), 1504 (C=C stretch), 1221 (C-O stretch), 1037 (C-O stretch), 852 (C-Cl stretch).

^{1}H NMR (400 MHz, DMSO-d_6) δ 8.66 (d, *J* = 2.0 Hz, 1H, H^{3}), 8.55 (d, *J* = 2.0 Hz, 1H, H^{2}), 8.42 (s, 1H, -N*H*), 7.87 (d, *J* = 9.1 Hz, 1H, H^{8}), 7.46 (dd, *J* = 9.1, 2.6 Hz, 1H, H^{7}), 7.42 (d, *J* = 8.8 Hz, 1H, $H^{6'}$), 7.20 (d, *J* = 2.9 Hz, 1H, $H^{3'}$), 7.01 (dd, *J* = 8.8, 2.9 Hz, 1H, $H^{5'}$), 6.83 (d, *J* = 2.6 Hz, 1H, H^{5}), 3.82 (s, 3H, -OCH_3).

^{13}C NMR (101 MHz, DMSO-d_6) 157.2 ($C^{4'}$), 147.7 (C^{6}), 145.3 (C^{3}), 144.4 (C^{4a}), 141.0 (C^{2}), 137.4 (C^{8a}), 130.5 ($C^{1'}$), 130.2 (C^{8}), 129.8 ($C^{2'}$), 127.8 ($C^{6'}$), 122.1 (C^{7}), 115.3 ($C^{3'}$), 114.3 ($C^{5'}$), 105.3 (C^{5}), 55.7 (-O*C*H$_3$).

HRMS-ESI: m/z: $[M+H]^+$ Calculated for $C_{15}H_{13}O_1N_3Cl_1$; 286.0742, Found 286.0740.

N-(2-chloro-4-methoxyphenyl)quinolin-6-amine (**2.42b**)



The reaction was carried out according to general procedure C using 6- bromoquinoline (104 mg, 0.50 mmol, 1.0 equiv) and 4-methoxy-2-chloroaniline (93 mg, 0.60 mmol, 1.2 equiv) as starting materials. The crude residue was purified by silica-gel chromatography petroleum ether (40 – 60 °C): EtOAc (7: 3) to obtain compound **2.42b** in 59% yield (84 mg, brown solid).

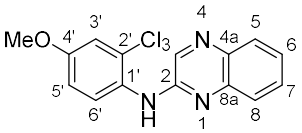
IR $\bar{\nu}_{max}$ (cm^{-1}): 3215 (C-N stretch), 3016 (C-H stretch), 2846 (C-H stretch), 1631 (C=N stretch), 1498 (C=C stretch), 1214 (C-O stretch), 1050 (C-O stretch), 839 (C-Cl stretch).

^{1}H NMR (400 MHz, DMSO-d_6) δ 8.56 (dd, J = 4.2, 1.6 Hz, 1H, H^{2}), 8.03 – 7.97 (m, 2H, -N*H*, H^{4}), 7.82 (d, J = 9.1 Hz, 1H, H^{8}), 7.40 (dd, J = 9.0, 2.6 Hz, 1H, H^{7}), 7.38 (d, J = 8.8 Hz, 1H, $H^{6'}$), 7.31 (dd, J = 8.3, 4.2 Hz, 1H, H^{3}), 7.16 (d, J = 2.8 Hz, 1H, $H^{3'}$), 6.97 (dd, J = 8.8, 2.8 Hz, 1H, $H^{5'}$), 6.85 (d, J = 2.5 Hz, 1H, H^{5}), 3.80 (s, 3H, -OCH_3).

^{13}C NMR (101 MHz, DMSO-d_6) δ 156.4 ($C^{4'}$), 146.3 (C^{2}), 144.1 (C^{6}), 143.0 (C^{8a}), 133.7 (C^{4}), 131.6 (C^{1}), 129.8 (C^{4a}), 129.3 (C^{8}), 129.2 ($C^{2'}$), 126.5 ($C^{6'}$), 121.8 (C^{7}), 121.5 (C^{3}), 115.2 ($C^{3'}$), 114.2 ($C^{5'}$), 105.6 (C^{5}), 55.7 (-O*C*H$_3$).

HRMS-ESI: m/z: $[M+H]^+$ Calculated for $C_{16}H_{14}O_2N_2Cl_1$; 285.0789, Found 285.0793.

N-(2-chloro-4-methoxyphenyl)quinoxalin-2-amine (**2.42c**)



The reaction was carried out according to general procedure C using 2-bromoquinoxaline (105 mg, 0.50 mmol, 1.0 equiv) and 4-methoxy-2-chloroaniline (95 mg, 0.60, 1.2 equiv) as starting materials. The crude residue was purified by silica-gel column chromatography, petroleum ether (40 – 60 °C): EtOAc (85: 15) to obtain compound **2.42c** in 27% yield (38 mg, yellow solid).

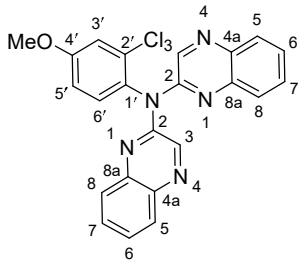
IR $\bar{\nu}_{max}$ (cm^{-1}): 3340 (N-H stretch), 2934 (C-H stretch), 1590 (C=N stretch), 1536 (C=N stretch), 1502 (C=C stretch), 1214 (C-O stretch), 1040 (C-O stretch), 841 (C-Cl stretch).

^{1}H NMR (400 MHz, DMSO-d_6) δ 9.20 (s, 1H, -N*H*), 8.64 (s, 1H, H^3), 7.92 (d, *J* = 8.9 Hz, 1H, $H^{6'}$), 7.84 (dd, *J* = 8.2, 1.2 Hz, 1H, H^8), 7.62 – 7.53 (m, 2H, $H^{5,6}$), 7.46 – 7.41 (m, 1H, H^7), 7.15 (d, *J* = 2.9 Hz, 1H, $H^{3'}$), 7.00 (dd, *J* = 8.9, 2.9 Hz, 1H, $H^{5'}$), 3.81 (s, 3H, -OCH_3).

^{13}C NMR (101 MHz, DMSO-d_6) δ 156.6 ($C^{4'}$), 150.5 (C^2), 140.8 (C^3), 139.8 (C^{8a}), 137.1 (C^{4a}), 129.9 (C^5), 128.9 ($C^{1'}$), 128.4 (C^8), 128.0 ($C^{2'}$), 126.9 ($C^{6'}$), 126.2 (C^6), 124.7 (C^7), 114.6 ($C^{3'}$), 113.6 ($C^{5'}$), 55.7 (-O*C*H$_3$).

HRMS-ESI: m/z: $[M+H]^+$ Calculated for $C_{15}H_{13}O_1N_3Cl_1$; 286.0742, Found 286.0745.

N-(2-chloro-4-methoxyphenyl)-N-(quinoxalin-2-yl)quinoxalin-2-amine (**2.43**)



Preparation 1: The reaction was carried out according to general procedure C using 2-bromoquinoxaline (105 mg, 0.50 mmol, 1.0 equiv) and 4-methoxy-2-chloroaniline (95 mg, 0.60, 1.2 equiv) as starting materials. The crude residue was purified by silica-gel column chromatography, petroleum ether (40 – 60 °C): EtOAc (85: 15) to obtained compound **2.43** in 25 % yield (26 mg, yellow solid).

Preparation 2: The reaction was carried out according to general procedure E using 2-bromoquinoxaline (105 mg, 0.50 mmol, 1.0 equiv) and 4-methoxy-2-chloroaniline (95 mg, 0.60, 1.2 equiv) as starting materials. The crude residue was purified by silica-gel column chromatography, petroleum ether (40 – 60 °C): EtOAc (85: 15) to obtain compound **8** in 61 % yield (63 mg, yellow solid).

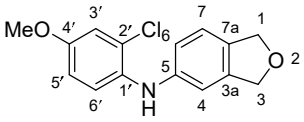
IR $\bar{\nu}_{max}$ (cm^{-1}): 1606 (C=N stretch), 1558 (C=N stretch), 1498 (C=C stretch), 1420 (C=C stretch), 1229 (C-O stretch), 1022 (C-O stretch), 761 (C-Cl stretch).

^{1}H NMR (400 MHz, DMSO-d_6) δ 8.83 (s, 2H, H^3), 8.06 – 8.00 (m, 2H, H^5), 7.76 – 7.68 (m, 6H, $H^{6\text{-}8}$), 7.58 (d, *J* = 8.8 Hz, 1H, $H^{6'}$), 7.32 (d, *J* = 2.9 Hz, 1H, $H^{3'}$), 7.12 (dd, *J* = 8.8, 2.9 Hz, 1H, $H^{5'}$), 3.88 (s, 3H, -OCH_3).

^{13}C NMR (101 MHz, DMSO-d_6) δ 159.6 ($C^{4'}$), 150.4 (C^2), 141.5 (C^3), 140.0 (C^{8a}), 138.8 (C^{4a}), 133.1 ($C^{2'}$), 132.3 ($C^{6'}$), 130.9 ($C^{1'}$), 130.6 ($C^{6/7/8}$), 128.5 (C^5), 128.0 ($C^{6/7/8}$), 127.4 ($C^{6/7/8}$), 115.9 ($C^{3'}$), 115.0 ($C^{5'}$), 55.9 (-O*C*H$_3$).

HRMS-ESI: m/z: $[M+H]^+$ Calculated for $C_{23}H_{17}O_1N_5Cl_1$; 414.1116, Found 414.1115.

N-(2-chloro-4-methoxyphenyl)-1,3-dihydroisobenzofuran-5-amine (**2.42d**)



The reaction was carried out according to general procedure C using 5-bromo-1,3-dihydroisobenzofuran (100 mg, 0.50 mmol, 1.0 equiv) and 4-methoxy-2-chloroaniline (95 mg, 0.60, 1.2 equiv) as starting materials. The crude residue was purified by reverse-phase semi-preparative HPLC over a 5 – 95% gradient B, (solvent A: 0.1% TFA in water, solvent B: 0.1% TFA in acetonitrile) to obtain compound **2.42d** in 18% yield (35 mg, white solid) as the TFA salt.

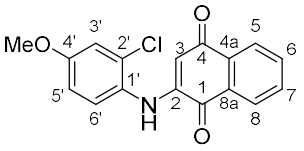
IR $\bar{\nu}_{max}$ (cm^{-1}): 3319 (N-H stretch), 2854 (C-H stretch), 1621 (C=C stretch), 1497 (C=C stretch), 1273 (C-O stretch), 1217 (C-O stretch), 1031 (C-O stretch), 821 (C-Cl stretch).

^{1}H NMR (400 MHz, DMSO-d_6) δ 7.49 (s, 1H, -N*H*), 7.22 (d, *J* = 8.9 Hz, 1H, $H^{6'}$), 7.08 (d, *J* = 2.8 Hz, 1H, $H^{3'}$), 7.07 (d, *J* = 8.4 Hz, 1H, H^{7}), 6.89 (dd, *J* = 8.9, 2.8 Hz, $H^{5'}$), 6.71 (dd, *J* = 8.4, 2.0 Hz, 1H, H^{6}), 6.66 (d, *J* = 2.0 Hz, 1H, H^{4}), 4.88 (s, 4H, 2 × -CH_2), 3.75 (s, 3H, -OCH_3).

^{13}C NMR (101 MHz, DMSO-d_6) δ 155.4 ($C^{4'}$), 144.9 (C^{4a}), 140.0 (C^{3a}), 132.8 ($C^{1'}$), 128.9 (C^{7a}), 127.7 ($C^{2'}$), 124.7 ($C^{6'}$), 121.4 (C^{7}), 115.0 ($C^{3'}$), 114.8 (C^{6}), 114.0 ($C^{5'}$), 107.3 (C^{4}), 72.5 ($C^{1/3}$), 72.3 ($C^{1/3}$), 55.6 (-OCH_3).

HRMS-ESI: m/z: $[M+H]^+$ Calculated for $C_{15}H_{15}O_2N_1Cl_1$; 276.0786, Found 276.0792.

2-((2-chloro-4-methoxyphenyl)amino)naphthalene-1,4-dione (**2.44a**)



The reaction was carried out according to general procedure C using 2-bromo-1,4-napthoquinone (119 mg, 0.50 mmol, 1.0 equiv) and 4-methoxy-2-chloroaniline (95 mg, 0.60 mmol, 1.2 equiv) as starting materials. The crude residue was purified by silica-gel column chromatography, petroleum ether (40 – 60 °C): EtOAc: NEt_3 (100: 8: 1) to obtain compound **2.44a** in 82% yield (129 mg, dark red solid).

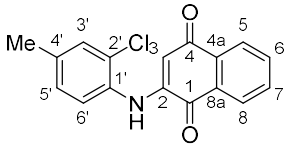
IR $\bar{\nu}_{max}$ (cm^{-1}): 3331 (N-H stretch), 3021 (C-H stretch), 1677 (C=O stretch), 1577 (C=C stretch), 1489 (C=C stretch), 1216 (C-O stretch), 1031 (C-O stretch), 778 (C-Cl stretch).

^{1}H NMR (400 MHz, DMSO-d_6) δ 9.02 (s, 1H, -N*H*), 8.06 (dd, *J* = 7.5, 1.0 Hz, 1H, H^{5}), 7.94 (dd, *J* = 8.8, 1.2 Hz. 1H, H^{8}), 7.86 (ddd, *J* = 7.5, 7.5, 1.4, 1H, H^{6}), 7.79 (ddd, *J* = 7.5, 7.5, 1.4 Hz, 1H, H^{7}), 7.36 (d, *J* = 8.8 Hz, 1H, $H^{6'}$), 7.22 (d, *J* = 2.8 Hz, 1H, $H^{3'}$), 7.04 (dd, *J* = 8.8, 2.8 Hz, 1H, $H^{5'}$), 5.31 (s, 1H, H^{3}), 3.82 (s, 3H, -OCH_3).

^{13}C NMR (101 MHz, DMSO-d_6) δ 182.1 (C^{1}), 181.3 (C^{4}), 158.7 ($C^{4'}$), 147.7 (C^{2}), 135.0 (C^{6}), 132.6 (C^{7}), 131.2 ($C^{1'}$), 130.7 (C^{8a}), 130.3 (C^{4a}), 129.5 ($C^{3'}$), 127.4 ($C^{2'}$), 126.0 (C^{5}), 125.4 (C^{8}), 115.1 ($C^{6'}$), 114.4 ($C^{5'}$), 102.3 (C^{3}), 55.8 (-O*C*H$_3$).

HRMS-ESI: m/z: [M+H]$^+$ Calculated for $C_{17}H_{13}O_3N_1Cl_1$; 314.0578, Found 314.0577.

2-((2-chloro-4-methylphenyl)amino)naphthalene-1,4-dione (**2.44b**)



The reaction was carried out according to general procedure C using 2-bromo-1,4-napthoquinone (119 mg, 0.50 mmol, 1.0 equiv) and 4-methyl-2-chloroaniline (85 mg, 0.60 mmol, 1.2 equiv) as starting materials. The crude residue was purified by silica-gel column chromatography, petroleum ether (40 – 60 °C): EtOAc: NEt$_3$ (90:10:1) to obtain compound **2.44b** in 72% yield (107 mg, red solid).

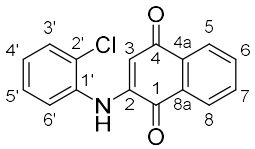
IR $\bar{\nu}_{max}$ (cm^{-1}): 3342 (N-H stretch), 2927 (C-H stretch), 1675 (C=O stretch), 1599 (C=O stretch), 1526 (C=C stretch), 774 (C-Cl).

^{1}H NMR (400 MHz, DMSO-d_6) δ 9.01 (s, 1H, -N*H*), 8.09 – 8.05 (m, 1H, H^{5}), 7.96 – 7.92 (m, 1H, H^{8}), 7.89 – 7.84 (m, 1H, H^{6}), 7.82 – 7.77 (m, 1H, H^{7}), 7.47 (d, J = 1.1 Hz, 1H, $H^{3'}$), 7.35 (d, J = 8.1 Hz, 1H, $H^{6'}$), 7.27 (dd, J = 8.1, 1.3 Hz, $H^{5'}$), 5.41 (s, 1H, H^{3}), 2.35 (s, 3H, -CH_3).

^{13}C NMR (101 MHz, DMSO-d_6) δ 182.3 (C^{4}), 181.2 (C^{1}), 147.0 (C^{2}), 138.5 ($C^{1'}$), 135.0 (C^{6}), 132.7 (C^{4a}), 132.6 (C^{7}), 132.1 ($C^{2'}$), 130.5 (C^{8a}), 130.3 ($C^{3'}$), 129.6 ($C^{4'}$), 129.0 ($C^{5'}$), 127.9 ($C^{6'}$), 126.1 (C^{5}), 125.4 (C^{8}), 102.7 (C^{3}), 20.3 (-*C*H$_3$).

HRMS-ESI: m/z: [M+H]$^+$ Calculated for $C_{17}H_{13}O_2N_1Cl_1$; 298.0629, Found 298.0633.

2-((2-chlorophenyl)amino)naphthalene-1,4-dione (**2.44c**)



The reaction was carried out according to general procedure C using 2-bromo-1,4-napthoquinone (119 mg, 0.50 mmol, 1.0 equiv) and 2-chloroaniline (77 mg, 0.60 mmol, 1.2 equiv) as starting materials. The crude residue was purified by silica-gel column chromatography, petroleum ether (40 – 60 °C): EtOAc (9: 1) to obtain compound **2.44c** in 64% yield (90 mg, brown solid).

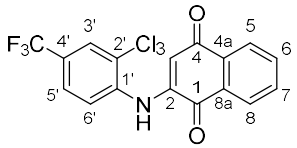
IR $\bar{\nu}_{max}$ (cm^{-1}): 3310 (N-H stretch), 3068 (C-H stretch), 2854 (C-H stretch), 1675 (C=O stretch), 1618 (C=O stretch), 1592 (C=C stretch), 1446 (C=C stretch), 741 (C-Cl stretch).

^{1}H NMR (400 MHz, DMSO-d_6) δ 9.08 (s, 1H, -N*H*), 8.08 (dd, *J* = 7.7, 0.9 Hz, 1H, H^5), 7.95 (dd, *J* = 7.5, 1.1 Hz, 1H, H^8), 7.87 (ddd, *J* = 7.4, 7.4, 1.4 Hz, 1H, H^6), 7.80 (ddd, *J* = 8.0, 6.5, 2.7 Hz, 1H, H^7), 7.64 (dd, *J* = 7.5, 1.1 Hz, 1H, $H^{3'}$), 7.51 – 7.44 (m, 2H, $H^{4',6'}$), 7.38 (ddd, *J* = 8.0, 6.5, 2.7 Hz, 1H, $H^{5'}$), 5.47 (s, 1H, H^3).

^{13}C NMR (101 MHz, DMSO-d_6) δ 182.3 (C^4), 181.2 (C^1), 146.7 (C^2), 135.0 (C^6), 134.2 ($C^{1'}$) 132.8 (C^7), 132.5 (C^{4a}), 130.3 ($C^{3'}$), 129.7 (C^{8a}), 128.4 ($C^{2'}$), 128.3 ($C^{5'}$), 128.0 ($C^{4',6'}$), 126.1 (C^5), 125.4 (C^8), 102.9 (C^3).

HRMS-ESI: m/z: $[M+H]^+$ Calculated for $C_{16}H_{11}O_2N_1Cl_1$; 284.0473, Found 284.0480.

2-((2-chloro-4-(trifluoromethyl)phenyl)amino)naphthalene-1,4-dione (**2.44d**)



The reaction was carried out according to general procedure C using 2-bromo-1,4-napthoquinone (119 mg, 0.50 mmol, 1.0 equiv) and 2-chloro-4-(trifluoromethyl)aniline (117 mg, 0.60 mmol, 1.2 equiv) as starting materials. The crude residue was purified by silica-gel column chromatography, petroleum ether (40 – 60 °C): EtOAc (9: 1) to obtain compound **2.44d** in 69% yield (122 mg, orange solid).

IR $\bar{\nu}_{max}$ (cm^{-1}): 3338 (N-H stretch), 3055 (C-H stretch), 1677 (C=O stretch), 1642 (C=O stretch), 1580 (C=C stretch), 782 (C-Cl stretch).

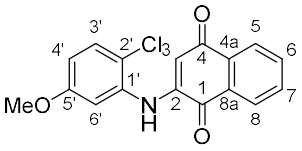
^{1}H NMR (400 MHz, DMSO-d_6) δ 9.10 (s, 1H, -N*H*), 8.08 (dd, *J* = 7.5, 1.1 Hz, 1H, H^8), 8.06 (d, *J* = 1.6 Hz, 1H, $H^{3'}$), 7.96 (dd, *J* = 7.6, 1.2 Hz, 1H, H^5), 7.88 (ddd, *J* = 7.5, 7.5, 1.5 Hz, 1H, H^6), 7.85 – 7.78 (m, 2H, $H^{5',7}$), 7.75 (d, *J* = 8.5 Hz, 1H, $H^{6'}$), 5.77 (s, 1H, H^3).

^{13}C NMR (101 MHz, DMSO-d_6) δ 182.7 (C^4), 181.0 (C^1), 146.0 (C^2), 138.9 ($C^{1'}$), 135.1 (C^6), 133.0 (C^7), 132.3 (C^{4a}), 130.2 (C^{8a}), 129.5 ($C^{2'}$), 127.5 (q, *J* = 32.7 Hz, $C^{4'}$), 127. 4 (q, *J* = 3.8 Hz, $C^{3'}$), 127.2 ($C^{6'}$) 126.2 (C^8), 125.5 (C^5), 125.4 (q, *J* = 3.8 Hz, $C^{5'}$), 123.3 (q, *J* = 272.9 Hz, -CF_3), 104.6 (C^3).

^{19}F NMR (376 MHz, DMSO-d_6) δ −60.85.

HRMS-ESI: m/z: $[M+H]^+$ Calculated for $C_{17}H_{10}O_2N_1Cl_1F_3$; 352.0347, Found 352.0347.

2-((2-chloro-5-methoxyphenyl)amino)naphthalene-1,4-dione (**2.44e**)



The reaction was carried out according to general procedure C using 2-bromo-1,4-napthoquinone (119 mg, 0.50 mmol, 1.0 equiv) and 5-methoxy-2-chloroaniline (95 mg, 0.60 mmol, 1.2 equiv) as starting materials. The crude residue was purified by silica-gel column chromatography, petroleum ether (40 – 60 °C): EtOAc (85: 15) to obtain compound **2.44e** in 59% yield (92 mg, red solid).

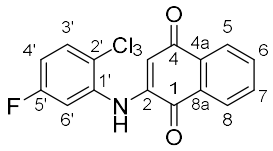
IR $\bar{\nu}_{max}$ (cm^{-1}): 3299 (N-H stretch), 2843 (C-H stretch), 1675 (C=O stretch), 1647 (C=O stretch), 1579 (C=C stretch), 1541 (C=C stretch), 1219 (C-O stretch), 1067 (C-O stretch), 776 (C-Cl stretch).

^{1}H NMR (400 MHz, DMSO-d_6) δ 9.05 (s, 1H, -N*H*), 8.07 (dd, *J* = 7.6, 1.2 Hz, 1H, H^8), 7.95 (dd, *J* = 7.6, 1.2 Hz, 1H, H^5), 7.90 – 7.84 (m, 1H, H^6), 7.83 – 7.77 (m, 1H, H^7), 7.52 (d, *J* = 8.9 Hz, 1H, $H^{3'}$), 7.03 (d, *J* = 3.0 Hz, 1H, $H^{6'}$), 6.97 (dd, *J* = 8.9, 3.0 Hz, 1H, $H^{4'}$), 5.48 (s, 1H, H^3), 3.79 (s, -OCH_3).

^{13}C NMR (101 MHz, DMSO-d_6) δ 182.3 (C^4), 181.2 (C^1), 158.8 ($C^{5'}$), 146.6 (C^2), 135.8 ($C^{1'}$), 135.0 (C^6), 132.8 (C^7), 132.6 (C^{4a}), 130.7 ($C^{3'}$), 130.3 (C^{8a}), 126.1 (C^8), 125.4 (C^5), 120.9 ($C^{2'}$), 114.0 ($C^{4'}$), 113.3 ($C^{6'}$), 103.3 (C^3), 55.7 (-OCH_3).

HRMS-ESI: m/z: $[M+H]^+$ Calculated for $C_{17}H_{13}O_3N_1Cl_1$; 314.0578, Found 314.0586.

2-((2-chloro-5-fluorophenyl)amino)naphthalene-1,4-dione (**2.44f**)



The reaction was carried out according to general procedure C using 2-bromo-1,4-napthoquinone (119 mg, 0.50 mmol, 1.0 equiv) and 2-chloro-5-fluoroaniline (87 mg, 0.60 mmol, 1.2 equiv) as starting materials. The crude residue was purified by silica-gel column chromatography, petroleum ether (40 – 60 °C): EtOAc (9: 1) to obtain compound **2.44f** in 80% yield (120 mg, orange solid).

IR $\bar{\nu}_{max}$ (cm^{-1}): 3310 (N-H stretch), 3074 (C-H stretch), 2858 (C-H stretch), 1675 (C=O stretch), 1647 (C=O stretch), 1599 (C=C stretch), 1541 (C=C stretch), 722 (C-Cl stretch).

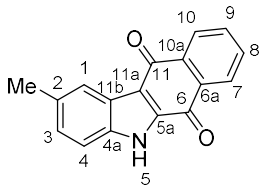
^{1}H NMR (400 MHz, DMSO-d_6) δ 9.08 (s, 1H, -N*H*), 8.10 – 8.06 (m, 1H, H^8), 7.98 – 7.94 (m, 1H, H^5), 7.91 – 7.85 (m, 1H, H^6), 7.85 – 7.79 (m, 1H, H^7), 7.68 (dd, *J* = 9.0, 5.7 Hz, 1H, $H^{3'}$), 7.43 (dd, *J* = 9.5, 3.0 Hz, 1H, $H^{6'}$), 7.26 (ddd, *J* = 8.8, 8.1, 3.0 Hz, 1H, $H^{4'}$), 5.60 (s, 1H, H^3).

^{13}C NMR (101 MHz, DMSO-d_6) δ 182.6 (C^4), 181.0 (C^1), 160.9 (d, J = 246.8 Hz, $C^{5'}$), 146.0 (C^2), 136.4 (d, J = 10.8 Hz, $C^{1'}$), 135.1 (C^6), 132.9 (C^7), 132.4 (C^{4a}), 131.6 (d, J = 9.6 Hz, $C^{3'}$), 130.2 (C^{8a}), 126.2 (C^8), 125.4 (C^5), 125.1 ($C^{2'}$), 115.2 (d, J = 22.8 Hz, $C^{4'}$), 114.8 (d, J = 24.8 Hz, $C^{6'}$), 103.9 (C^3).

^{19}F NMR (376 MHz, DMSO-d_6) δ −112.74.

HRMS-ESI: m/z: $[M+H]^+$ Calculated for $C_{16}H_{10}O_2N_1Cl_1F_1$; 302.0378, Found 302.0380.

2-methyl-5*H*-benzo[*b*]carbazole-6,11-dione (**2.45b**)



The reaction was carried out according to general procedure D using 2-bromonaphthalene-1,4-dione (119 mg, 0.50 mmol, 1.0 equiv) and 4-methyl-2-chloroaniline (85 mg, 0.60 mmol, 1.2 equiv) as starting materials. The crude residue was purified by silica-gel column chromatography, $CHCl_3$ (100%) to obtain compound **2.45b** in 59% yield (77 mg, orange solid).

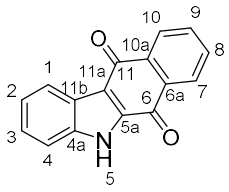
IR $\bar{\nu}_{max}$ (cm^{-1}): 3174 (N-H stretch), 1670 (C=O stretch), 1642 (C=O stretch), 1595 (C=C stretch), 1538 (C=C stretch).

^{1}H NMR (400 MHz, DMSO-d_6) δ 12.98 (s, 1H, -N*H*), 8.15 – 8.06 (m, 2H, $H^{7,10}$), 8.01 (s (app), 1H, H^1), 7.89 – 7.84 (m, 1H, H^9), 7.84 – 7.78 (m, 1H, H^8), 7.50 (d, J = 8.5 Hz, 1H, H^4), 7.29 (d (app), J = 8.5 Hz, 1H, H^3), 2.46 (s, 3H, -CH_3)

^{13}C NMR (101 MHz, DMSO-d_6) δ 180.3 (C^{11}), 177.5 (C^6), 137.1 (C^{5a}), 136.7 (C^{4a}), 134.2 (C^{10a}), 134.1 (C^9), 133.4 (C^2), 133.2 (C^8), 132.7 (C^{6a}), 128.9 (C^3), 126.1 (C^{10}), 126.0 (C^7), 124.2 (C^{11b}), 121.6 (C^1), 116.9 (C^{11a}), 113.5 (C^4), 21.3 (-CH$_3$).

HRMS-ESI: m/z: $[M+H]^+$ Calculated for $C_{17}H_{12}O_2N_1$; 262.0862, Found 262.0861.

5*H*-benzo[*b*]carbazole-6,11-dione (**2.45c**)



The reaction was carried out according to general procedure D using 2-bromonaphthalene-1,4-dione (119 mg, 0.50 mmol, 1.0 equiv) and 2-chloroaniline (77 mg, 0.60 mmol, 1.2 equiv) as starting materials. The crude residue was purified by silica-gel column chromatography, $CHCl_3$ (100%) to obtain compound **2.45c** in 73% yield (90 mg, orange solid).

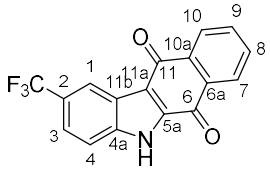
IR $\bar{\nu}_{max}$ (cm^{-1}): 3263 (N-H stretch), 1649 (C=O stretch), 1590 (C=C stretch), 1474 (C=C stretch).

^{1}H NMR (400 MHz, DMSO-d_6) δ 13.08 (s, 1H, -N*H*), 8.22 (d, *J* = 8.0 Hz, 2H, H^{1}), 8.12 (ddd, *J* = 7.4, 7.4, 1.5 Hz, 1H, $H^{7, 10}$), 7.87 (ddd, *J* = 7.4, 7.4, 1.5 Hz, 1H, H^{9}), 7.82 (ddd, *J* = 7.4, 7.4, 1.5 Hz, 1H, H^{8}), 7.61 (d, *J* = 8.3 Hz, 1H, H^{4}), 7.46 (ddd, *J* = 8.3, 7.0, 1.2 Hz, 1H, H^{3}), 7.33 – 7.41 (m, 1H, H^{2}).

^{13}C NMR (101 MHz, DMSO-d_6) δ 180.4 (C^{11}), 177.6 (C^{6}), 138.2 (C^{4a}), 137.2 (C^{5a}), 134.3 (C^{9}), 134.1 (C^{10a}), 133.2 (C^{8}), 132.6 (C^{6a}), 127.0 (C^{3}), 126.1 (C^{10}), 126.0 (C^{7}), 124.0 (C^{11b}), 123.9 (C^{2}), 122.4 (C^{1}), 117.4 (C^{11a}), 113.9 (C^{4}).

HRMS-ESI: m/z: $[M+H]^+$ Calculated for $C_{16}H_{10}O_2N_1$; 248.0706, Found 248.0703.

2-(trifluoromethyl)-5*H*-benzo[*b*]carbazole-6, 11-dione (**2.45d**)



The reaction was carried out according to general procedure D using 2-bromonaphthalene-1,4-dione (119 mg, 0.50 mmol, 1.0 equiv) and 4-trifluoromethyl-2-chloroaniline (117 mg, 0.60 mmol, 1.2 equiv) as starting materials. The crude residue was purified by silica-gel column chromatography, petroleum ether (40 – 60 °C): EtOAc: NEt_3 (100: 20: 4) to obtain compound **2.45d** in 35% yield (54 mg, orange solid).

IR $\bar{\nu}_{max}$ (cm^{-1}): 3234 (N-H stretch), 1655 (C=O stretch), 1631 (C=O stretch), 1586 (C=C stretch), 1541 (C=C stretch).

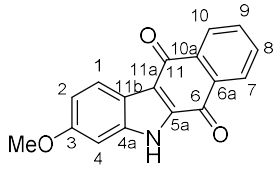
^{1}H NMR (400 MHz, DMSO-d_6) δ 13.44 (s, 1H, -N*H*), 8.49 – 8.45 (m, 1H, H^{1}), 8.16 – 8.08 (m, 2H, $H^{7, 10}$), 7.91 – 7.81 (m, 2H, $H^{8, 9}$), 7.80 – 7.71 (m, 2H, $H^{3, 4}$).

^{13}C NMR (101 MHz, DMSO-d_6) δ 180.3 (C^{11}), 177.5 (C^{6}), 139.5 (C^{4a}), 139.0 (C^{5a}), 134.5 (C^{8}), 133.8 (C^{9}), 133.5 (C^{7a}), 132.5 (C^{10a}), 126.2 ($C^{7, 10}$), 124.7 (q, *J* = 272.9 Hz, -*C*F$_3$), 124.3 (q, *J* = 31.8 Hz, C^{2}), 123.1 (C^{11b}), 123.0 (q, *J* = 3.4 Hz, C^{3}), 119.6 (q, *J* = 4.3 Hz, C^{1}), 117.6 (C^{11a}), 115.1 (C^{4}).

^{19}F NMR (376 MHz, DMSO-d_6) δ −59.7.

HRMS-ESI: m/z: $[M+H]^+$ Calculated for $C_{17}H_8O_2N_1F_3$; 338.0397, Found 338.0394.

3-methoxy-5*H*-benzo[*b*]carbazole-6, 11-dione (**2.45e**)



The reaction was carried out according to general procedure D using 2-bromonaphthalene-1,4-dione (119 mg, 0.5 mmol, 1.0 equiv) and 2-chloro-5-methoxyaniline (95 mg, 0.60 mmol, 1.2 equiv) as starting materials. The crude residue was purified by silica-gel column

chromatography, petroleum ether (40 – 60 °C): EtOAc (9: 1) to obtain compound **2.45e** in 68% yield (94 mg, red solid).

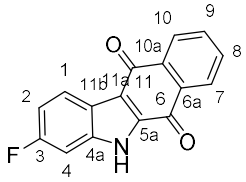
IR $\bar{\nu}_{max}$ (cm^{-1}): 3189 (N-H stretch), 2927 (C-H stretch), 1664 (C=O stretch), 1629 (C=O stretch), 1532 (C=C stretch).

^{1}H NMR (400 MHz, DMSO-d_6) δ 12.89 (s, 1H, -N*H*), 8.11 – 8.03 (m, 3H, $H^{1, 7, 10}$), 7.87 – 7.76 (m, 2H, $H^{8, 9}$), 7.00 (dd, J = 8.8, 2.0 Hz, 1H, H^2), 6.98 (d, J = 2.0 Hz, 1H, H^4), 3.85 (s, 3H, -OCH_3).

^{13}C NMR (101 MHz, DMSO-d_6) δ 180.5 (C^{11}), 176.8 (C^6), 159.4 (C^3), 139.8 (C^{4a}), 136.4 (C^{5a}), 134.0 (C^{6a}), 133.9 (C^8), 133.2 (C^9), 132.7 (C^{10a}), 126.0 ($C^{7/10}$), 125.9 ($C^{7/10}$), 123.2 (C^1), 118.0 ($C^{11a/11b}$), 117.9 ($C^{11a/11b}$), 115.5 (C^2), 95.1 (C^4), 55.4 (-OCH_3).

HRMS-ESI: m/z: [M+H]$^+$ Calculated for $C_{17}H_{12}O_3N_1$; 278.0812, Found 278.0809.

3-fluoro-5*H*-benzo[*b*]carbazole-6, 11-dione (**2.45f**)



The reaction was carried out according to general procedure D using 2-bromonaphthalene-1,4-dione (119 mg, 0.50 mmol, 1.0 equiv) and 5-fluoro-2-chloroaniline (87 mg, 0.60 mmol, 1.2 equiv) as starting materials. The crude residue was purified by silica-gel column chromatography, petroleum ether (40 – 60 °C): EtOAc: NEt_3 (100: 20: 4) to obtain compound **2.45f** in 58% yield (76 mg, orange solid).

IR $\bar{\nu}_{max}$ (cm^{-1}): 3230 (N-H stretch), 2928 (C-H stretch), 1647 (C=O stretch), 1588 (C=C stretch), 1472 (C=C stretch).

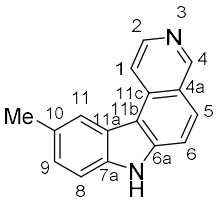
^{1}H NMR (400 MHz, DMSO-d_6) δ 13.12 (s, 1H, -N*H*), 8.19 (dd, J = 8.8, 5.5 Hz, 1H, H^1), 8.11 – 8.05 (m, 2H, $H^{7, 10}$), 7.87 (m, 2H, $H^{8, 9}$), 7.29 (dd, J = 9.4, 2.2 Hz, 1H, H^4), 7.27 – 7.20 (m, 1H, H^2).

^{13}C NMR (101 MHz, DMSO-d_6) δ 180.3 (C^{11}), 177.1 (C^6), 161.5 (d, J = 243.5 Hz, C^3), 138.6 (d, J = 13.2 Hz, C^{4a}), 138.0 (C^{5a}), 134.2 (C^8), 133.8 (C^{6a}), 133.3 (C^9), 132.5 (C^{10a}), 126.0 ($C^{7, 10}$), 124.1 (d, J = 10.5 Hz, C^1), 120.6 ($C^{11a/11b}$), 117.4 ($C^{11a/11b}$), 113.1 (d, J = 25.2 Hz, C^2), 99.6 (d, J = 26.1 Hz, C^4).

HRMS-ESI: m/z: [M+H]$^+$ Calculated for $C_{16}H_9O_2N_1F_1$; 266.0612, Found 266.0609.

^{19}F NMR (376 MHz, DMSO-d_6) δ -113.2.

10-methyl-7*H*-pyrido[3,4-*c*]carbazole (**2.51**)



The reaction was carried out according to general procedure E using 6-bromoisoquinoline (104 mg, 0.50 mmol, 1.0 equiv) and 2-chloro-4-methylaniline (85 mg, 0.60 mmol, 1.2 equiv) as starting materials. The crude residue was purified by silica-gel column chromatography, petroleum ether (40 – 60 °C): EtOAc (1: 1) to obtain compound **2.51** in 54% yield (63 mg, brown solid).

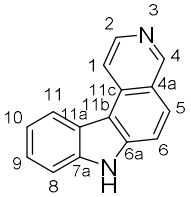
IR $\bar{\nu}_{max}$ (cm^{-1}): 2917 (C-H stretch), 1616 (C=N stretch), 1474 (C=C stretch).

^{1}H NMR (400 MHz, DMSO-d_6) δ 11.97 (s, 1H, -N*H*), 9.31 (s, 1H, H^4), 8.63 (d, J = 5.7 Hz, 1H, H^2), 8.58 (d, J = 5.7 Hz, 1H, H^1), 8.41 (s, 1H, H^{11}), 8.04 (d, J = 8.8 Hz, 1H, H^5), 7.86 (d, J = 8.8 Hz, 1H, H^6), 7.58 (d, J = 8.3 Hz, 1H, H^8), 7.30 (dd, J = 8.3, 1.2 Hz, 1H, H^9), 2.58 (s, 3H, -CH_3).

^{13}C NMR (101 MHz, DMSO-d_6) δ 152.0 (C^4), 143.9 (C^2), 139.7 (C^{6a}), 137.0 (C^{7a}), 132.0 (C^{11c}), 129.0 (C^{10}), 126.1 (C^9), 125.8 (C^5), 123.7 (C^{4a}), 122.9 (C^{11a}), 121.3 (C^{11}), 116.4 (C^1), 114.9 (C^6), 112.2 (C^{11b}), 111.6 (C^8), 21.3 (-CH$_3$).

HRMS-ESI: m/z: [M+H]$^+$ Calculated for $C_{16}H_{13}N_2$; 233.1073, Found 233.1068.

7*H*-pyrido[4,3-*c*]carbazole (**2.52a**)



The reaction was carried out according to general procedure E using 6-bromoisoquinoline (104 mg, 0.50 mmol, 1.0 equiv) and 2-chloroaniline (76 mg, 0.60 mmol, 1.2 equiv) as starting materials. The crude residue was purified by silica-gel column chromatography, hexane: EtOAc (1: 1) to obtain compound **2.52a** in 50% yield (54 mg, brown solid).

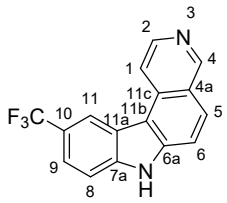
IR $\bar{\nu}_{max}$ (cm^{-1}): 2921 (C-H stretch), 1612 (C=N stretch), 1458 (C=C stretch).

^{1}H NMR (400 MHz, DMSO-d_6) δ 12.10 (s, 1H, -N*H*), 9.33 (s, 1H, H^4), 8.64 (d, J = 5.8 Hz, 1H, H^2), 8.60 (d, J = 8.0 Hz, 1H, H^{11}), 8.58 (d, J = 5.8 Hz, 1H, H^1), 8.07 (d, J = 8.8 Hz, 1H, H^5), 7.89 (d, J = 8.9 Hz, 1H, H^6), 7.69 (d, J = 8.0 Hz, 1H, H^8), 7.48 (ddd, J = 8.0, 7.0, 1.1 Hz, 1H, H^9), 7.36 (ddd, J = 8.9, 7.0, 1.1 Hz, 1H, H^{10}).

^{13}C NMR (101 MHz, DMSO-d_6) δ 152.2 (C^4), 144.1 (C^2), 139.6 (C^{6a}), 138.7 (C^{7a}), 132.0 (C^{11c}), 126.1 (C^5). 124.7 (C^9), 123.8 (C^{4a}), 122.7 (C^{11a}), 121.6 (C^{11}), 120.1 (C^{10}), 116.4 (C^1), 114.9 (C^6), 112.5 (C^8), 111.9 (C^{11b}).

HRMS-ESI: m/z: [M+H]$^+$ Calculated for $C_{15}H_{11}N_2$; 219.0917, Found 219.0922.

10-(trifluoromethyl)-7*H*-pyrido[3,4-*c*]carbazole (**2.52b**)



The reaction was carried out according to general procedure E using 6-bromoisoquinoline (104 mg, 0.50 mmol, 1.0 equiv) and 2-chloro-4-(trifluoromethyl)aniline (117 mg, 0.60 mmol, 1.2 equiv) as starting materials. The crude residue was purified by silica-gel column chromatography, petroleum ether (40 – 60 °C): EtOAc (7: 2) to obtain compound **2.52b** in 25% yield (35 mg, yellow solid).

IR $\bar{\nu}_{max}$ (cm^{-1}): 1638 (C=N stretch), 1618 (C=N stretch), 1463 (C=C stretch), 1420 (C=C stretch).

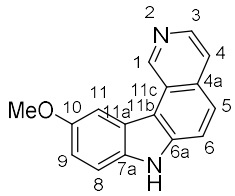
^{1}H NMR (400 MHz, DMSO-d_6) δ 12.53 (s, 1H, -N*H*), 9.38 (s, 1H, H^4), 8.90 (s, 1H, H^{11}), 8.74 – 8.63 (m, 2H, $H^{1, 2}$), 8.17 (d, J = 8.8 Hz, H^5), 7.95 (d, J = 8.8 Hz, 1H, H^6), 7.88 (d, J = 8.6 Hz, 1H, H^8), 7.78 (d, J = 8.6 Hz, 1H, H^9).

^{13}C NMR (101 MHz, DMSO-d_6) δ 152.3 (C^4), 144.6 (C^2), 140.8 (C^{7a}), 140.5 (C^{6a}), 131.8 (C^{11c}), 127.5 (C^5), 125.4 (q, J = 272.6 Hz, -CF$_3$), 124.0 (C^{4a}), 122.2 (C^{11a}), 121.2 (q, J = 4.0 Hz, C^9), 120.8 (q, J = 30.8 Hz, C^{10}), 118.8 (q, J = 4.0 Hz, C^{11}), 116.6 (C^1), 115.0 (C^6), 112.6 (C^8), 112.4 (C^{11b}).

HRMS-ESI: m/z: [M+H]$^+$ Calculated for $C_{16}H_{10}N_2F_3$; 287.0791, Found 287.0805.

^{19}F NMR (376 MHz, DMSO-d_6) δ −58.1.

10-methoxy-7*H*-pyrido[4,3-*c*]carbazole (**2.52d**)



The reaction was carried out according to general procedure E using 7-bromoisoquinoline (104 mg, 0.50 mmol, 1.0 equiv) and 2-chloro-4-methoxyaniline (95 mg, 0.60 mmol, 1.2 equiv) as starting materials. The crude residue was purified by silica gel column chromatography petroleum ether (40 – 60 °C): EtOAc (1: 1) to obtain compound **2.52d** in 83% yield (103 mg, brown solid).

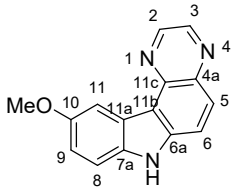
IR $\bar{\nu}_{max}$ (cm^{-1}): 2932 (C-H stretch), 1588 (C=N stretch), 1210 (C-O stretch), 1063 (C-O stretch).

^{1}H NMR (400 MHz, DMSO-d_6) δ 11.89 (s, 1H, -N*H*), 10.14 (s, 1H, H^1), 8.53 (d, J = 5.5 Hz, 1H, H^3), 8.07 (d, J = 2.4 Hz, 1H, H^{11}), 7.99 (d, J = 8.8 Hz, 1H, H^6), 7.96 (d, J = 5.5 Hz, 1H, H^4), 7.91 (d, J = 8.8 Hz, 1H, H^5), 7.61 (d, J = 8.8 Hz, 1H, H^8), 7.14 (dd, J = 8.8, 2.4 Hz, H^9), 3.98 (s, 3H, -OCH_3).

^{13}C NMR (101 MHz, DMSO-d_6) δ 154.0 (C^{10}), 146.7 (C^{1}), 140.5 (C^{3}), 138.3 (C^{6a}), 133.8 (C^{7a}), 131.0 (C^{11b}), 124.7 ($C^{5, 11c}$), 122.1 (C^{11a}), 121.6 (C^{4}), 118.3 (C^{6}), 115.0 (C^{9}), 113.0 (C^{4a}), 112.7 (C^{8}), 104.2 (C^{11}), 55.8 (-O*C*H$_3$).

HRMS-ESI: m/z: [M+H]$^+$ Calculated for $C_{16}H_{13}O_1N_2$; 249.1022, Found 249.1028.

10-methoxy-7*H*-pyrazino[2,3-*c*]carbazole (**2.52e**)



The reaction was carried out according to general procedure E using 6-bromoquinoxaline (105 mg, 0.50 mmol, 1.0 equiv) and 2-chloro-4-methoxyaniline (95 mg, 0.60 mmol, 1.2 equiv) as starting materials. The crude residue was purified by silica-gel column chromatography, petroleum ether (40 – 60 °C): EtOAc (7: 2) to obtain compound **2.52e** in 75% yield (93 mg, yellow solid).

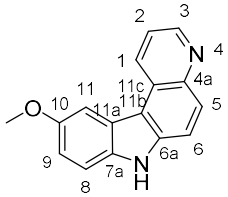
IR $\bar{\nu}_{max}$ (cm^{-1}): 3338 (N-H stretch), 2837 (C-H stretch), 1601 (C=N stretch), 1523 (C=C stretch), 1495 (C=C stretch), 1214 (C-O stretch), 1029 (C-O stretch).

^{1}H NMR (400 MHz, DMSO-d_6) δ 11.96 (s, 1H, -N*H*), 9.04 (d, *J* = 2.0 Hz, 1H, H^{2}), 8.86 (d, *J* = 2.0 Hz, 1H, H^{3}), 8.29 (d, *J* = 2.6 Hz, 1H, H^{11}), 8.05 (d, *J* = 9.1 Hz, 1H, H^{6}), 7.98 (d, *J* = 9.1 Hz, 1H, H^{5}), 7.61 (d, *J* = 8.8 Hz, 1H, H^{8}), 7.13 (dd, *J* = 8.8, 2.6 Hz, 1H, H^{9}), 3.91 (s, 3H, -OCH_3).

^{13}C NMR (101 MHz, DMSO-d_6) δ 154.1 (C^{10}), 144.2 (C^{2}), 141.2 (C^{3}), 140.3 (C^{11c}), 139.5 (C^{6a}), 138.7 (C^{4a}), 133.8 (C^{7a}), 126.5 (C^{5}), 123.3 (C^{11a}), 118.0 (C^{6}), 115.0 (C^{9}), 114.5 (C^{11b}), 112.7 (C^{8}), 104.4 (C^{11}), 55.5 (-O*C*H$_3$).

HRMS-ESI: m/z: [M+H]$^+$ Calculated for $C_{15}H_{12}O_1N_3$; 250.0975, Found 250.0970.

10-methoxy-7*H*-pyrido[2,3-*c*]carbazole (**2.52f**)



The reaction was carried out according to general procedure E using 6-bromoquinoline (104 mg, 0.50 mmol, 1.0 equiv) and 2-chloro-4-methoxyaniline (95 mg, 0.60 mmol, 1.2 equiv) as starting materials. The crude residue was purified by silica gel column chromatography petroleum ether (40 – 60 °C): EtOAc (1: 1) to obtain compound **2.52f** in 65% yield (80 mg, off-white solid).

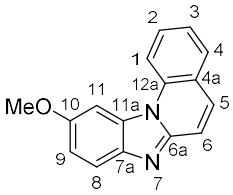
IR $\bar{\nu}_{max}$ (cm^{-1}): 3146 (N-H stretch), 2997 (C-H stretch), 1571 (C=N stretch), 1534 (C=C stretch), 1493 (C=C stretch), 1227 (C-O stretch), 1035 (C-O stretch).

^{1}H NMR (400 MHz, DMSO-d_6) δ 11.77 (s, 1H, -*N*H), 9.17 (d, J = 8.3 Hz, 1H, H^1), 8.82 (dd, J = 4.2, 1.4 Hz, 1H, H^3), 8.02 (d, J = 2.3 Hz, 1H, H^{11}), 7.99 – 7.92 (m, 2H, $H^{5,6}$), 7.67 (dd, J = 8.3, 4.2 Hz, 1H, H^2), 7.58 (d, J = 8.8 Hz, H^8), 7.11 (dd, J = 8.8, 2.3 Hz, H^9), 3.95 (s, 3H, -OCH_3).

^{13}C NMR (101 MHz, DMSO-d_6) δ 153.8 (C^{10}), 146.1 (C^3), 144.2 (C^{4a}), 137.4 (C^{6a}), 133.9 (C^{7a}), 130.8 (C^1), 127.4 (C^5), 124.4 (C^{11c}), 123.1 (C^{11a}), 121.5 (C^2), 116.9 (C^6), 114.2 (C^9), 113.3 (C^{11b}), 112.6 (C^8), 103.9 (C^{11}), 55.8 (-OCH$_3$).

HRMS-ESI: m/z: $[M+H]^+$ Calculated for $C_{16}H_{13}O_1N_2$; 249.1022, Found 249.1026.

10-methoxybenzo[4,5]imidazo[1,2-*a*]quinolone (**2.52g**)



The reaction was carried out according to general procedure E using 2-bromoquinoline (104 mg, 0.50 mmol, 1.0 equiv) and 2-chloro-4-methoxyaniline (95 mg, 0.60 mmol, 1.2 equiv) as starting materials. The crude residue was purified by silica-gel column chromatography, hexane: EtOAc (3: 7) to obtain compound **2.52g** in 25% yield (31 mg, brown solid).

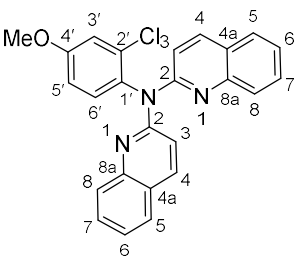
IR $\bar{\nu}_{max}$ (cm^{-1}): 1636 (C=N stretch), 1608 (C=N stretch), 1487 (C=C stretch), 1448 (C=C stretch), 1219 (C-O stretch), 1026 (C-O stretch).

^{1}H NMR (400 MHz, DMSO-d_6) δ 8.78 (d, J = 8.5 Hz, 1H, H^1), 8.08 (d, J = 2.3 Hz, 1H, H^{11}), 8.03 (dd, J = 7.8, 1.5 Hz, 1H, H^4), 7.88 – 7.82 (m, 3H, $H^{2,5,8}$), 7.59 (d, J = 9.5 Hz, 1H, H^6), 7.59 – 7.54 (m, 1H, H^3), 7.21 (dd, J = 8.9, 2.3 Hz, 1H, H^9), 4.00 (s, 3H, -OCH_3).

^{13}C NMR (101 MHz, DMSO-d_6) δ 156.0 (C^{10}), 147.1 (C^{6a}), 138.8 (C^{7a}), 134.8 (C^{12a}), 130.7 (C^{11a}), 130.4 (C^5), 130.0 (C^2), 129.5 (C^4), 124.4 (C^3), 123.0 (C^{4a}), 120.3 (C^8), 117.5 (C^6), 115.6 (C^1), 113.8 (C^9), 98.3 (C^{11}), 56.1 (-OCH$_3$).

HRMS-ESI: m/z: $[M+H]^+$ Calculated for $C_{16}H_{13}O_1N_2$; 249.1022, Found 249.1036.

N-(2-chloro-4-methoxyphenyl)-N-(quinolin-2-yl)quinolin-2-amine (**2.53**)



The reaction was carried out according to general procedure E using 2-bromoquinoline (104 mg, 0.50 mmol, 1.0 equiv) and 2-chloro-4-methoxyaniline (95 mg, 0.60 mmol, 1.2 equiv) as starting materials. The crude residue was purified by silica-gel column chromatography, hexane: EtOAc (3: 7) to obtain compound **2.53** in 26% yield (54 mg, brown solid).

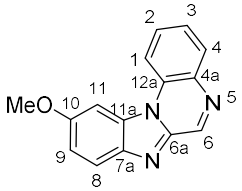
IR $\bar{\nu}_{max}$ (cm^{-1}): 1597 (C=N stretch), 1575 (C=N stretch), 1502 (C=C stretch), 1428 (C=C stretch), 1230 (C-O stretch), 1040 (C-O stretch).

^{1}H NMR (400 MHz, DMSO-d_6) δ 8.22 (d, J = 9.0 Hz, 2H, H^4), 7.88 (d, J = 8.0 Hz, 2H, H^5), 7.66 – 7.59 (m, 4H, $H^{7,8}$), 7.45 (ddd, J = 8.1, 5.5, 2.8 Hz, 2H, H^6), 7.38 (d, J = 8.8 Hz, 1H, $H^{6'}$), 7.28 (d, J = 8.9 Hz, 2H, H^3), 7.24 (d, J = 2.9 Hz, 1H, $H^{3'}$), 7.07 (dd, J = 8.8, 2.9 Hz, 1H, $H^{5'}$), 3.87 (s, 3H, -OCH_3).

^{13}C NMR (101 MHz, DMSO-d_6) δ 158.9 ($C^{4'}$), 155.3 (2×C^2), 146.4 (2×C^{8a}), 137.3 (2×C^4), 133.5 ($C^{1', 2'}$), 132.6 ($C^{6'}$), 129.7 (2×C^7), 127.6 (2×C^5), 127.2 (2×C^8), 125.2 (2×C^{4a}), 124.7 (2×C^6), 116.6 (2×C^3), 115.5 ($C^{3'}$), 114.6 ($C^{5'}$), 55.8 (-OCH$_3$).

HRMS-ESI: m/z: [M+H]$^+$ Calculated for $C_{25}H_{19}O_1N_3Cl_1$; 412.1211, Found 412.1230.

10-methoxybenzo[4,5]imidazo[1,2-*a*]quinoxaline (**2.52h**)



The reaction was carried out according to general procedure E using 2-bromoquinoxaline (105 mg, 0.50 mmol, 1.0 equiv) and 2-chloro-4-methoxyaniline (95 mg, 0.60 mmol, 1.2 equiv) as starting materials. The crude residue was purified by silica-gel column chromatography, hexane: EtOAc (3: 7) to obtain compound **2.52h** in 14% yield (17 mg, white solid).

IR $\bar{\nu}_{max}$ (cm^{-1}): 2843 (C-H stretch), 1580 (C=N stretch), 1590 (C=N stretch), 1463 (C=C stretch), 1225 (C-O stretch), 1026 (C-O stretch).

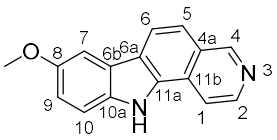
^{1}H NMR (400 MHz, DMSO-d_6) δ 9.23 (s, 1H, H^6), 8.81 (d, J = 8.3 Hz, 1H, H^1), 8.14 (dd, J = 9.0, 1.4 Hz, 1H, H^4), 8.10 (d, J = 2.3 Hz, 1H, H^{11}), 8.00 (d, J = 9.0 Hz, 1H, H^8), 7.87 (ddd, J = 8.3, 7.6, 1.4 Hz, 1H, H^2), 7.69 (ddd, J = 8.0, 7.6, 1.0 Hz, 1H, H^3), 7.33 (dd, J = 9.0, 2.3 Hz, 1H, H^9), 4.04 (s, 3H, -OCH_3).

^{13}C NMR (101 MHz, DMSO-d_6) δ 157.6 (C^{10}), 146.1 (C^6), 140.5 (C^{6a}), 138.5 (C^{7a}), 135.2 (C^{4a}), 130.2 (C^4), 130.0 (2×$C^{2, 11a}$), 129.1 (C^{12a}), 125.7 (C^3), 122.1 (C^8), 116.3 (C^9), 115.9 (C^1), 97.4 (C^{11}), 56.2 (-OCH$_3$).

HRMS-ESI: m/z: [M+H]$^+$ Calculated for $C_{15}H_{12}O_1N_3$; 250.0975, Found 250.0982.

8-methoxy-11H-pyrido[4,3-a]carbazole (**2.52i**)

The reaction was carried out according to general procedure E using 5-bromoisoquinoline (104 mg, 0.50 mmol, 1.0 equiv) and 2-chloro-4- methoxyaniline (95 mg, 0.60 mmol, 1.2 equiv) as



starting materials. The crude residue was purified by silica-gel column chromatography, hexane: EtOAc (3: 7) to obtain compound **2.52i** in 90% yield (111 mg, grey solid).

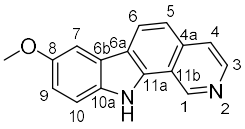
IR $\bar{\nu}_{max}$ (cm^{-1}): 3149 (N-H stretch), 1619 (C=N stretch), 1480 (C=C stretch), 1439 (C=C stretch), 1215 (C-O stretch), 1027 (C-O stretch).

^{1}H NMR (400 MHz, DMSO-d_6) δ 12.30 (s, 1H, -N*H*), 9.36 (s, 1H, H^4), 8.62 (d, J = 5.7 Hz, 1H, H^2), 8.38 (d, J = 8.5 Hz, 1H, H^6), 8.32 (d, J = 5.7 Hz, 1H, H^1), 7.81 (d, J = 2.3 Hz, 1H, H^7), 7.75 (d, J = 8.5 Hz, 1H, H^5), 7.60 (d, J = 8.8 Hz, 1H, H^{10}), 7.13 (dd, J = 8.8, 2.3, 1H, H^9), 3.89 (s, 3H, -OCH_3).

^{13}C NMR (101 MHz, DMSO-d_6) δ 153.7 (C^8), 152.0 (C^4), 142.8 (C^2), 134.1 (C^{10a}), 133.7 (C^{4a}), 126.6 (C^{11a}), 124.1 (C^{11b}), 123.0 (C^{6b}), 121.2 (C^6), 120.3 (C^{6a}), 117.4 (C^5), 115.7 (C^9), 114.9 (C^1), 112.5 (C^{10}), 102.3 (C^7), 55.6 (-O*C*H$_3$).

HRMS-ESI: m/z: [M+H]$^+$ Calculated for $C_{16}H_{13}O_1N_2$; 249.1022, Found 249.1020.

8-methoxy-11*H*-pyrido[3,4-*a*]carbazole (**2.52j**)



The reaction was carried out according to general procedure E using 8-bromoisoquinoline (104 mg, 0.50 mmol, 1.0 equiv) and 2-chloro-4-methoxyaniline (95 mg, 0.60 mmol, 1.2 equiv) as starting materials. The crude residue was purified by silica-gel column chromatography, hexane: EtOAc (3: 7) to obtain **2.52j** in 94% yield (104 mg, grey solid).

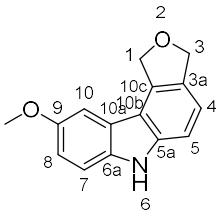
IR $\bar{\nu}_{max}$ (cm^{-1}): 3074 (N-H stretch), 2962 (C-H stretch), 1627 (C=N stretch), 1474 (C=C stretch), 1437 (C=C stretch), 1217 (C-O stretch), 1027 (C-O stretch).

^{1}H NMR (400 MHz, DMSO-d_6) δ 12.39 (s, 1H, -N*H*), 9.86 (s, 1H, H^1), 8.55 (d, J = 5.6 Hz, 1H, H^3), 8.48 (d, J = 8.5 Hz, 1H, H^6), 7.91 (d, J = 5.6 Hz, 1H, H^4), 7.79 (d, J = 2.5 Hz, 1H, H^7), 7.61 (d, J = 8.5 Hz, 1H, H^5), 7.59 (d, J = 8.8 Hz, 1H, H^{10}), 7.10 (dd, J = 8.8, 2.5, 1H, H^9), 3.89 (s, 3H, -OCH_3).

^{13}C NMR (101 MHz, DMSO-d_6) δ 153.8 (C^8), 146.4 (C^1), 142.6 (C^3), 134.7 (C^{4a}), 134.4 (C^{11a}), 133.7 (C^{10a}), 124.6 (C^6), 123.2 (C^{6b}), 121.1 (C^4), 118.8 (C^{6a}), 116.8 (C^{11b}), 116.6 (C^5), 114.9 (C^9), 112.3 (C^{10}), 102.2 (C^7), 55.6 (-O*C*H$_3$).

HRMS-ESI: m/z: [M+H]$^+$ Calculated for $C_{16}H_{13}O_1N_2$; 249.1022, Found 249.1032.

9-methoxy-3,6-dihydro-1*H*-furo[3,4-*c*]carbazole (**2.52k**)



The reaction was carried out according to general procedure D using 5-bromo-1,3-dihydroisobenzofuran (99 mg, 0.50 mmol, 1.0 equiv) and 2-chloro-4-methoxyaniline (95 mg, 0.60 mmol, 1.2 equiv) as starting materials. The crude residue was purified by reverse-phase semi-preparative HPLC over a 5 – 95% gradient B, (solvent A: 0.1% TFA in water, solvent B: 0.1% TFA in acetonitrile) to obtain compound **2.52k** in 10% yield (35 mg, white solid).

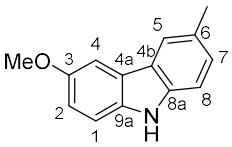
IR $\bar{\nu}_{max}$ (cm^{-1}): 3246 (N-H stretch), 2867 (C-H stretch), 1478 (C=C stretch), 1439 (C=C stretch), 1214 (C-O stretch), 1014 (C-O stretch).

^{1}H NMR (400 MHz, DMSO-d_6) δ 11.15 (s, 1H, -N*H*), 7.41 (d, *J* = 8.8 Hz, 1H, *H*^{7}), 7.38 (d, *J* = 8.3 Hz, 1H, *H*^{5}), 7.30 (d, *J* = 2.6 Hz, 1H, *H*^{10}), 7.29 (d, *J* = 8.3 Hz, 1H, *H*^{4}), 7.06 (dd, *J* = 8.8, 2.6 Hz, 1H, *H*^{8}), 5.52 (t, *J* = 2.2 Hz, 2H, *H*^{1}), 5.14 (t, *J* = 2.2 Hz, 2H, *H*^{3}), 3.84 (s, 3H, -OC*H*$_3$).

^{13}C NMR (101 MHz, DMSO-d_6) δ 153.1 (*C*^{9}), 140.0 (*C*^{5a}), 134.8 (*C*^{6a}), 131.5 (*C*^{10c}), 128.2 (*C*^{3a}), 121.6 (*C*^{10a}), 118.0 (*C*^{4}), 116.0 (*C*^{10b}), 114.6 (*C*^{8}), 111.6 (*C*^{7}), 110.0 (*C*^{5}), 104.2 (*C*^{10}), 72.8 (*C*^{3}), 72.4 (*C*^{1}), 55.7 (-O*C*H$_3$).

HRMS-ESI: m/z: [M+H]$^+$ Calculated for $C_{15}H_{14}O_2N_1$; 240.1019, Found 240.1030.

Glycozoline (**2.26**)[207]



Preparation 1: The reaction was carried out according to general procedure D using 4-bromotoluene (85 mg mg, 0.50 mmol, 1.0 equiv) and 2-chloro-4-methoxyaniline (95 mg, 0.60 mmol, 1.2 equiv) as starting materials. The crude residue was purified by silica-gel column chromatography, petroleum ether (40 – 60 °C): EtOAc (100: 6) to obtain compound **2.26** in 36% yield (38 mg, brown crystalline solid).

Preparation 2: The reaction was carried out according to general procedure D using 4-bromotoluene (85 mg mg, 0.50 mmol, 1.0 equiv) and 2-chloro-4-methoxyaniline (95 mg, 0.60 mmol, 1.2 equiv) as starting materials with the addition of PivOH (15.3 mg, 0.15 mmol, 0.3 equiv). The crude residue was purified by silica-gel column chromatography, petroleum ether (40 – 60 °C): EtOAc (100: 6) to obtain compound **2.26** in 63% yield (66 mg, brown crystalline solid).

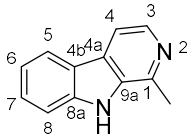
IR $\bar{\nu}_{max}$ (cm^{-1}): 3401 (N-H stretch), 3003 (C-H stretch), 2835 (C-H stretch), 1474 (C=C stretch), 1458 (C=C stretch), 1212 (C-O stretch), 1037 (C-O stretch).

^{1}H NMR (400 MHz, DMSO-d_6) δ 10.85 (s, 1H, -N*H*), 7.87 (d, *J* = 1.0 Hz, 1H, H^5), 7.61 (d, *J* = 2.5 Hz, 1H, H^4), 7.34 (d, *J* = 8.8 Hz, 1H, H^1), 7.32 (d, *J* = 8.3 Hz, 1H, H^8), 7.16 (dd, *J* = 8.3, 1.0 Hz, 1H, H^7), 6.98 (dd, *J* = 8.8, 2.5 Hz, 1H, H^2), 3.83 (s, 3H, -OCH_3), 2.45 (s, 3H, -CH_3).

^{13}C NMR (101 MHz, DMSO-d_6) δ 152.8 (C^3), 138.6 (C^{8a}), 134.8 (C^{9a}), 126.7 ($C^{6,7}$), 126.5 (C^{4a}), 122.5 (C^{4b}), 119.9 (C^5), 114.5 (C^2), 111.5 (C^1), 110.6 (C^8), 102.8 (C^4), 55.5 (-O*C*H$_3$), 21.0 (-*C*H$_3$).

HRMS-ESI: m/z: [M+H]$^+$ Calculated for $C_{14}H_{14}O_1N_1$; 212.1070, Found 212.1079.

Harmane (**2.63**)



The reaction was carried out according to general procedure D using 3-bromo-2-methylpyridine (86 mg, 0.50 mmol, 1.0 equiv) and 2-chloroaniline (77 mg, 0.60 mmol, 1.2 equiv) as starting materials. The crude residue was purified by silica-gel column chromatography, EtOAc (100%) to obtain compound **2.63** in 44% yield (40 mg, purple solid).

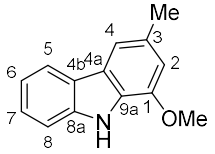
IR $\bar{\nu}_{max}$ (cm^{-1}) 3062 (N-H stretch), 2954 (C-H stretch), 1627 (C=N stretch), 1571 (C=C stretch), 1506 (C=C stretch).

^{1}H NMR (400 MHz, DMSO-d_6) δ 11.53 (s, 1H –N*H*), 8.20 (d, *J* = 5.3 Hz, 1H, H^3), 8.18 (d, *J* = 8.0 Hz, 1H, H^5), 7.92 (d, *J* = 5.3 Hz, 1H, H^4), 7.61 – 7.57 (m, 1H, H^8), 7.52 (ddd, *J* = 8.3, 7.0, 1.2 Hz, 1H, H^7), 7.22 (ddd, *J* = 8.0, 7.0, 1.2 Hz, 1H, H^6), 2.76 (s, 3H, -CH_3).

^{13}C NMR (101 MHz, DMSO-d_6) δ 142.1 (C^1), 140.3 (C^{8a}), 137.5 (C^3), 134.4 (C^{9a}), 127.7 (C^7), 126.8 (C^{4a}), 121.7 (C^5), 121.0 (C^{4b}), 119.1 (C^6), 112.6 (C^4), 111.9 (C^8), 20.4 (-*C*H$_3$).

HRMS-ESI: m/z: [M+H]$^+$ Calculated for $C_{12}H_{11}N_2$; 183.0917, Found 183.0927.

Murrayafoline A (**2.64**)



The reaction was carried out according to general procedure D using 2-bromo-5-methylanisole (101 mg, 0.50 mmol, 1.0 equiv) and 2-chloroaniline (77 mg, 0.60 mmol, 1.2 equiv) as starting materials with the addition of PivOH (15.3 mg, 0.15 mmol, 0.3 equiv). The crude residue was purified by silica-gel column chromatography, hexane: EtOAc (7: 3) to obtain compound **2.64** in 43% yield (45 mg, brown crystalline solid).

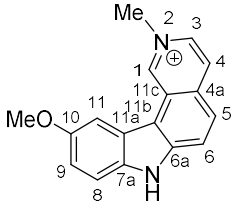
IR $\bar{\nu}_{max}$ (cm^{-1}): 3418 (N-H stretch), 2921 (C-H stretch), 1590 (C=C stretch), 1454 (C=C stretch), 1232 (C-O stretch), 1040 (C-O stretch).

^{1}H NMR (400 MHz, DMSO-d_6) δ 11.12 (s, 1H, -N*H*), 8.00 (d, *J* = 8.0 Hz, 1H, H^5), 7.49 – 7.46 (m, 1H, H^4), 7.45 – 7.41 (m, 1H, H^8), 7.32 (ddd, *J* = 8.3, 7.1, 1.3 Hz, 1H, H^7), 7.09 (ddd, *J* = 8.0, 7.1, 1.1 Hz, 1H, H^6), 6.82 (d, *J* = 1.1 Hz, 1H, H^2), 3.96 (s, 3H, -OCH_3), 2.46 (s, 3H, -CH_3).

^{13}C NMR (101 MHz, DMSO-d_6) δ 145.3 (C^1), 139.7 (C^{8a}), 128.0 (C^{9a}), 127.8 (C^3), 125.0 (C^7), 123.4 ($C^{4a/4b}$), 122.4 ($C^{4a/4b}$), 120.0 (C^5), 118.2 (C^6), 112.2 (C^4), 111.2 (C^8), 107.7 (C^2), 55.2 (-O*C*H$_3$), 21.5 (-*C*H$_3$).

HRMS-ESI: m/z: [M+H]$^+$ Calculated for $C_{14}H_{14}O_1N_1$; 212.1070, Found 212.1082.

10-methoxy-2-methyl-7*H*-pyrido[4,3-*c*]carbazol-2-ium (**2.69**)



To a solution of 10-methoxy-7*H*-pyrido[4,3-*c*]carbazole (**2.52d**) (80 mg, 0.32 mmol, 1.0 equiv) in DMF (1.3 mL) was added MeI (230 mg, 1.61 mmol, 5.3 equiv). The reaction was stirred for 19 h at 50 °C. The resulting yellow precipitate was filtered and washed with cold Et_2O. The resulting solid was recrystallized from hot EtOH twice to yield compound **2.69** in 88% yield (111 mg, yellow solid).

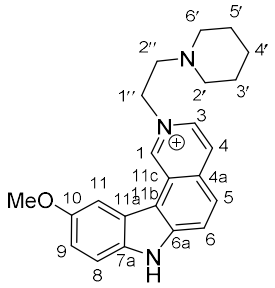
IR $\bar{\nu}_{max}$ (cm^{-1}): 3129 (N-H stretch), 1631 (C=N stretch), 1562 (C=C stretch), 1497 (C=C stretch), 1029 (C-O stretch).

^{1}H NMR (400 MHz, DMSO-d_6) δ 12.50 (s, 1H, -N*H*), 10.28 (s, 1H, H^1), 8.71 (dd, *J* = 6.7, 1.2 Hz, 1H, H^3), 8.67 (d, *J* = 6.7 Hz, 1H, H^4), 8.44 (d, *J* = 8.8 Hz, 1H, H^6), 8.30 (d, *J* = 2.3 Hz, 1H, H^{11}), 8.24 (d, *J* = 8.8 Hz, 1H, H^5), 7.75 (d, *J* = 8.9 Hz, 1H, H^8), 7.32 (dd, *J* = 8.9, 2.4 Hz, 1H, H^9), 4.67 (s, 3H, -NCH_3), 4.00 (s, 3H, -OCH_3).

^{13}C NMR (101 MHz, DMSO-d_6) δ 154.7 (C^{10}), 143.3 (C^1), 139.4 (C^{6a}), 134.4 (C^{7a}), 133.5 (C^3), 133.1 (C^{4a}), 126.0 (C^4), 124.3 (C^5), 124.2 (C^6), 123.4 (C^{11c}), 121.3 (C^{11a}), 116.1 (C^9), 113.7 (C^{11b}), 113.4 (C^8), 105.5 (C^{11}), 56.3 (-O*C*H$_3$), 48.0 (-N*C*H$_3$).

HRMS-ESI: m/z: [M+H]$^+$ Calculated for $C_{17}H_{15}O_1N_2$; 263.1179, Found 263.1198.

10-methoxy-2-(2-(piperidin-1-yl)ethyl)-7*H*-pyrido[4,3-*c*]carbazol-2-ium (**2.70**)



To a solution of 10-methoxy-7*H*-pyrido[4,3-*c*]carbazole (**2.52d**) (60 mg, 0.24 mmol, 1.0 equiv) in DMF (0.5 mL) was added a solution of 1-(2-Chloroethyl)piperidine hydrochloride (178 mg, 1.0 mmol, 4.0 equiv) in a 1:1 mixture of DMF:water (1 mL). The reaction was stirred for 19 h at 80 °C. The resulting yellow precipitate was filtered and washed with cold Et_2O. The resulting solid was recrystallized from hot EtOH three times to yield compound **2.70** in 80% yield (77 mg, yellow solid).

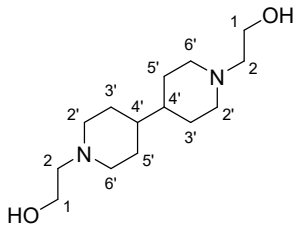
IR $\bar{\nu}_{max}$ (cm^{-1}): 3390 (N-H stretch), 2958 (C-H stretch), 1634 (C=N stretch), 1219 (C-O stretch), 1029 (C-O stretch).

^{1}H NMR (400 MHz, DMSO-d_6) δ 12.61 (s, 1H, -N*H*), 11.00 (s, 1H, -N*H*), 10.46 (s, 1H, H^{l}) 8.86 (d, J = 6.7 Hz, 1H, H^{3}), 8.76 (d, J = 6.7 Hz, 1H, H^{4}), 8.50 (d, J = 8.9 Hz, 1H, H^{6}), 8.41 – 8.34 (m, 1H, H^{11}), 8.26 (d, J = 8.9 Hz, 1H, H^{5}), 7.76 (d, J = 8.9 Hz, 1H, H^{8}), 7.34 (dd, J = 8.9 Hz, 1.9 Hz, 1H, H^{9}), 5.56 – 5.42 (m, 2H, 2×$H^{1''}$), 4.04 (s, 3H, -OCH_3), 3.95 – 3.82 (m, 2H, 2×$H^{2''}$), 3.67 – 3.54 (m, 2H, 2×$H^{2',6'}$), 3.11 – 2.94 (m, 2H, 2×$H^{2',6'}$), 1.90 – 1.77 (m, 4H, $H^{3',5'}$), 1.76 – 1.70 (m, 1H, $H^{4'}$), 1.49 – 1.40 (m, 1H, $H^{4'}$).

^{13}C NMR (101 MHz, DMSO-d_6) δ 154.7 (C^{10}), 143.8 (C^{1}), 139.4 (C^{6a}), 134.5 (C^{7a}), 133.7 (C^{4a}), 132.5 (C^{3}), 126.4 (C^{4}), 124.8 (C^{6}), 124.3 (C^{5}), 123.6 (C^{11c}), 121.3 (C^{11a}), 116.1 (C^{9}), 114.1 (C^{11b}), 113.5 (C^{8}), 105.9 (C^{11}), 56.4 (-O*C*H$_3$), 55.0 (C^{5}), 54.2 ($C^{2''}$), 52.6 (2×$C^{2',6'}$), 22.2 (2×$C^{3',5'}$), 21.2 (2×$C^{4'}$).

HRMS-ESI: m/z: $[M+H]^+$ Calculated for $C_{23}H_{26}O_1N_3$; 360.2070, Found 360.2081.

2,2'-([4,4'-bipiperidine]-1,1'-diyl)bis(ethan-1-ol) (**2.67**)



4,4′-Bipiperidine (300 mg, 1.24 mmol, 1.0 equiv) and K_2CO_3 (1.03 g, 7.47 mmol, 6.0 equiv) was charged to a 10 – 20 mL microwave vial before being sealed, evacuated and purged with Ar (g) three times. DMF (10 mL) was added followed by bromoethanol (528 mg, 4.23 mmol, 3.4 equiv) before being heated for 4 h at 100 °C in a Biotage microwave. The crude residue was purified by silica column chromatography, MeOH: NH_4OH (100: 5) to obtain 2,2'-([4,4'-bipiperidine]-1,1'-diyl)bis(ethan-1-ol) in 70% yield (223 mg, white solid).

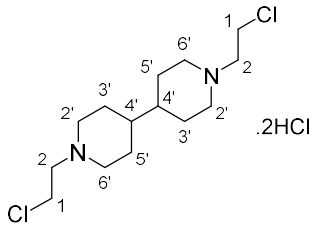
IR $\bar{\nu}_{max}$ (cm^{-1}): 3345 (O-H stretch), 2936 (C-H stretch), 1266 (C-N stretch), 1052 (C-O stretch).

^{1}H NMR (400 MHz, MeOD-d_4) δ 3.80 (t, J = 5.6 Hz, 4H, H^1), 3.40 – 3.33 (m, 4H, $H^{2',6'}$), 2.90 (t, J = 5.6 Hz, 4H, H^2), 2.56 (t, J = 11.8 Hz, 4H, $H^{2',6'}$), 1.90 (d, J = 13.4 Hz, 4H, $H^{3',5'}$), 1.54 – 1.41 (m, 4H, $H^{3',5'}$), 1.39 (m, 2H, $H^{4'}$).

^{13}C NMR (101 MHz, MeOD-d_4) δ 60.5 (C^2), 58.1 (C^1), 54.7 ($C^{2',6'}$), 40.2 ($C^{4'}$), 28.6 ($C^{3',5'}$).

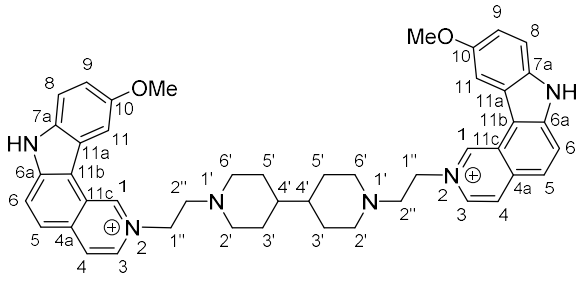
LRMS-ESI: m/z: $[M+H]^+$ Calculated for $C_{14}H_{29}N_2O_2$; 257.2, Found 257.3.

1,1'-bis(2-chloroethyl)-4,4'-bipiperidine (**2.68**)



2,2'-([4,4'-bipiperidine]-1,1'-diyl)bis(ethan-1-ol) (**2.67**) (163 mg, 0.64 mmol, 1.0 equiv) was dissolved in $CHCl_3$ (20 mL) before being evacuated and purged with Ar (g) three times. The reaction was heated to 40 °C and stirred for 30 mins to affect dissolution. $SOCl_2$ (303 mg, 2.54 mmol, 4.0 equiv) was added dropwise and the reaction heated to 70 °C for 8 h. The reaction was cooled to rt and the precipitate isolated through filtration to obtain crude 1,1'-bis(2-chloroethyl)-4,4'-bipiperidine (**2.68**) in 93% yield (216 mg, white solid) to be used directly in the next step without purification.

Ditercalinium (**2.71**)



10-methoxy-7*H*-pyrido[4,3-*c*]carbazole (100 mg, 0.40 mmol, 1.0 equiv) and 1,1'-bis(2-chloroethyl)-4,4'-bipiperidine (89 mg, 0.24 mmol, 0.6 equiv) were charged to a 2 – 5 mL microwave vial which was evacuated and purged with Ar (g) twice. DMF (4 mL) was added and the vial heated to 80 °C for 22 h. H_2O (0.1 mL) was added to further solubilize the starting materials and the reaction heated for a further 24 h at 80 °C. DMF (1 mL) was added to re-dissolve the formation of a yellow precipitate and the reaction heated to 120 °C for a further 24 h. The reaction was cooled and the precipitate isolated by filtration. The precipitate was washed with cold Et_2O and then recrystallized from hot EtOH 5 times to isolate **2.71** in 16% yield (52 mg, yellow solid).

IR $\bar{\nu}_{max}$ (cm^{-1}): 3342 (N-H stretch), 2927 (C-H stretch), 1616 (C=N stretch), 1472 (C=C stretch), 1402 (C=C stretch), 1214 (C-O stretch), 1031 (C-O stretch).

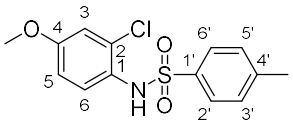
^{1}H NMR (400 MHz, DMSO-d_6) δ 12.69 (s, 2H, -N*H*), 11.63 (s, 2H, -N*H*), 10.51 (s (br), 2H, H^1), 9.00 – 8.78 (s (br), 2H, H^3), 8.77 – 8.67 (d, J = 5.8 Hz, 2H, H^4), 8.49 (d, J = 8.8 Hz, 2H, H^6), 8.45

– 8.29 (s (br), 2H, H^{11}), 8.25 (d, J = 8.9 Hz, 2H, H^{5}), 7.75 (d, J = 8.9 Hz, 2H, H^{8}), 7.31 (dd, J = 9.0, 2.2 Hz, 2H, H^{9}), 5.71 – 5.26 (m, 4H, $H^{1''}$), 4.03, 4.00 – 3.77 (m, 4H, $H^{2''}$), 3.73 – 3.50 (m, 4H, $H^{2',6'}$), 3.11 – 2.91 (m, 4H, $H^{2',6'}$), 2.06 – 1.51 (m, 8H, $H^{3',5'}$), 1.48 – 1.29 (m, 2H, $H^{4'}$).

^{13}C NMR (101 MHz, DMSO-d_6) δ 154.7 (C^{10}), 143.7 (C^{1}), 139.4 (C^{6a}), 134.4 (C^{7a}), 133.6 (C^{4a}), 132.6 (C^{3}), 126.4 (C^{4}), 124.8 (C^{6}), 124.3 (C^{5}), 123.6 (C^{11c}), 121.3 (C^{11a}), 116.3 (C^{9}), 114.1 (C^{11b}), 113.4 (C^{8}), 105.7 (C^{11}), 56.4 (-OCH$_3$), 55.3 (C^{5}), 54.3 ($C^{2''}$), 52.6 (2×$C^{2',6'}$), 37.3 (2×$C^{4'}$), 25.8 (2×$C^{3',5'}$).

HRMS-ESI: m/z: [M+H]$^+$ Calculated for $C_{46}H_{50}O_2N_6$; 359.1992, Found 359.1991.

N-(2-chloro-4-methoxyphenyl)-4-methylbenzenesulfonamide (**2.74**)



2-Chloro-4-methoxyaniline (0.50 g, 3.22 mmol) was stirred in pyridine (16 mL) for 10 mins and then cooled to 0 °C. *p*-Toluenesulfonyl chloride (0.67 g, 3.51 mmol) was added and the reaction stirred for 2 h. The reaction mixture was concentrated *in vacuo* and extracted with DCM. The combined organic layers were washed with water, brine and dried over Na_2SO_4. The filtrate was concentrated *in vacuo* to obtain **2.74** in 98% yield without further purification (0.98 g, purple solid).

IR $\bar{\nu}_{max}$ (cm^{-1}) 3262 (C-N stretch), 2935 (C-H stretch), 2849 (C-H stretch), 1496 (C-H bend).

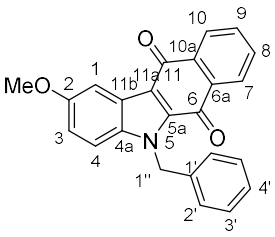
^{1}H NMR (400 MHz, DMSO-d_6) δ 9.65 (s, 1H, -NH), 7.57 – 7.50 (m, 2H, $H^{2',6'}$), 7.37 – 7.31 (m, 1H, $H^{3',5'}$), 7.07 (d, J = 8.9 Hz, 1H, H^{6}), 6.97 (d, J = 2.9 Hz, 1H, H^{3}), 6.85 (dd, J = 8.9, 2.9 Hz, 1H, H^{5}), 3.73 (s, 3H, -OCH_3), 2.37 (s, 3H, -CH_3).

^{13}C NMR (101 MHz, DMSO-d_6) δ 158.2 (C^{4}), 143.0 ($C^{4'}$), 137.6 ($C^{1'}$), 131.3 (C^{2}), 129.7 (C^{6}), 129.5 (2×$C^{3',5'}$), 126.7 (2×$C^{2',5'}$), 126.0 (C^{1}), 114.7 (C^{3}), 113.6 (C^{5}), 55.8 (-OCH$_3$), 20.9 (-CH$_3$),

HRMS-ESI Exact mass calculated for [M + H]$^+$ ($C_{14}H_{14}ClNO_3S$) requires m/z 312.0456, found [M + H]$^+$ m/z 312.0460.

Data corresponds to literature values[208]

5-Benzyl-2-methoxy-5*H*-benzo[*b*]-carbazole-6,11-dione (**2.75a**)



2-Methoxy-5*H*-benzo[*b*]-carbazole-6,11-dione (74 mg, 0.27 mmol) was stirred in anhydrous DMF (8 mL) and cooled to 0 °C. NaH (16 mg, 0.66 mmol) was added and stirred for 1 h. Benzyl bromide (0.078 mL, 0.66 mmol) was added and the reaction stirred for 2 h. The reaction mixture was diluted in EtOAc, washed with 5% w/v LiCl (aq) solution, water, brine, and dried over Na_2SO_4. The filtrate was concentrated *in vacuo* and purified by silica gel flash-column chromatography petroleum ether (40 – 60 °C): EtOAc (10:1) to afford the desired **2.75a** in 83% yield (81 mg, orange solid).

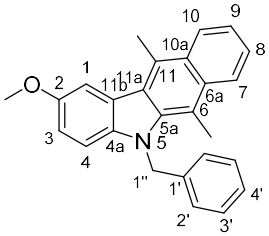
IR $\bar{\nu}_{max}$ (cm^{-1}) 2926 (C-H stretch), 1647 (C=O stretch), 1489 (C-H bend), 1234 (C-O stretch).

^{1}H NMR (500 MHz, DMSO-d_6) δ 8.13 (dd, J = 7.5, 1.1 Hz, 1H, $H^{7/10}$), 8.10 (dd, J = 7.5, 1.2 Hz, 1H, $H^{7/10}$), 7.90 – 7.85 (m, 1H, H^{9}), 7.85 – 7.80 (m, 1H, H^{8}), 7.75 (d, J = 2.5 Hz, 1H, H^{1}), 7.71 (d, J = 9.2 Hz, 1H, H^{4}), 7.33 – 7.28 (m, 2H, 2 × $H^{2'}$), 7.27 – 7.20 (m, 3H, 3 × $H^{3',4'}$), 7.15 (dd, J = 9.2, 2.6 Hz, 1H, H^{3}), 6.04 (s, 2H, -CH_2), 3.88 (s, 3H, -OCH_3).

^{13}C NMR (101 MHz, DMSO-d_6) δ 180.3 (C^{11}), 177.9 (C^{6}), 157.5 (C^{2}), 137.0 ($C^{1'}$), 134.6 (C^{4a}), 134.4 (C^{5a}), 134.2 (C^{9}), 133.5 (C^{8}), 133.3 (C^{10a}), 133.2 (C^{6a}), 128.6 (2×$C^{2'}$), 127.5 ($C^{4'}$), 126.6 (2×$C^{3'}$), 126.3 ($C^{7/10}$), 125.7 ($C^{7/10}$), 124.2 (C^{11b}), 118.8 (C^{3}), 117.7 (C^{11a}), 113.8 (C^{4}), 102.4 (C^{1}), 55.5 (-OCH$_3$), 47.8 (-CH$_2$).

HRMS-ESI Exact mass calculated for $[M + H]^+$ ($C_{24}H_{17}NO_3$) requires m/z 368.1281, found $[M + H]^+$ m/z 368.1284.

5-Benzyl-2-methoxy-6,11-methyl-5*H*-benzo[*b*]-carbazole (**2.76a**)



5-Benzyl-2-methoxy-5*H*-benzo[*b*]-carbazole-6,11-dione (71 mg, 0.19 mmol) was dissolved in anhydrous THF (7 mL) and MeLi (0.55 mL, 0.87 mmol, 1.6 M) was added dropwise over 5 mins. After 3 h, the reaction was quenched with water, and extracted with $CHCl_3$. The combined organic phases were washed with water, brine, dried over Na_2SO_4 and concentrated *in vacuo*. The isolated crude solid was dissolved in THF (5 mL) and added to a solution of $SnCl_2$ (0.37 g, 1.94 mmol) in a mixture of conc. HCl (4.8 mL)/Et_2O (4.8 mL). The reaction mixture was stirred vigorously for 5 h and extracted with $CHCl_3$. The combined organic phases were washed with water, brine, dried over Na_2SO_4, and the filtrate concentrated *in vacuo*. The crude was purified by silica gel flash-column chromatography, petroleum ether (40 – 60 °C): EtOAc (7:3) to afford the desired **2.76a** in 40% yield (28 mg, cream solid).

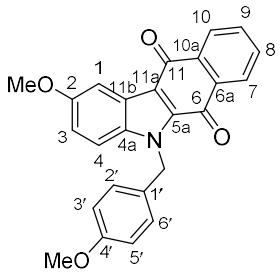
IR $\bar{\nu}_{max}$ (cm^{-1}) 2922 (C-H stretch), 1599 (C=C stretch), 1437 (C-H bend), 1204 (C-O stretch).

^{1}H NMR (400 MHz, DMSO-d_6) δ 8.36 (dd, J = 8.8, 0.8 Hz, 1H, H^{10}), 8.15 (dd, J = 8.9, 0.8 Hz, 1H, H^{7}), 7.92 (d, J = 2.5 Hz, 1H, H^{1}), 7.55 – 7.48 (m, 1H, H^{8}), 7.48 – 7.42 (m, 1H, H^{9}), 7.39 (d, J = 8.8 Hz, 1H, H^{4}), 7.29 (m, 2H, 2 × $H^{3'}$), 7.22 (m, 1H, $H^{4'}$), 7.15 (dd, J = 8.8, 2.5 Hz, 1H, H^{3}), 7.08 (m, 2H, 2 × $H^{2'}$), 5.83 (s, 2H, -CH_2), 3.90 (s, 3H, -OCH_3), 3.20 (s, 3H, C^{11}-CH_3), 2.84 (s, 3H, C^6-CH_3).

^{13}C NMR (101 MHz, DMSO-d_6) δ 153.4 (C^2), 139.5 (C^{4a}), 139.2 (C^{5a}), 139.1 ($C^{1'}$), 131.8 (C^{6a}), 128.7 ($C^{3'}$), 126.9 (2×$C^{4',11a}$), 126.7 (C^{11}), 125.6 ($C^{2'}$), 124.8 (C^{8}), 124.5 (C^{10}), 123.7 (C^{10a}), 123.4 (C^{11b}), 123.3 (C^{7}), 122.2 (C^{9}), 114.4 (C^{3}), 109.8 (C^{4}), 109.6 (C^{6}), 108.2 (C^{1}), 55.8 (-OCH$_3$), 49.0 (-CH$_2$), 15.2 (C^{11}-CH$_3$), 13.6 (C^6-CH$_3$).

HRMS-ESI Exact mass calculated for [M + H]$^+$ ($C_{26}H_{23}NO$) requires m/z 366.1852, found [M + H]$^+$ m/z 366.1854.

2-methoxy-5-(4-methoxybenzyl)-5*H*-benzo[*b*]carbazole-6, 11-dione (**2.75b**)



2-methoxy-5*H*-benzo[*b*]carbazole-6, 11-dione (318 mg, 1.15 mmol, 1.0 equiv), was heated in anhydrous DMF (16 mL) to 30 °C to affect dissolution over 15 min. The reaction was cooled to room temperature and NaH (83 mg, 3.41 mmol, 3.0 equiv) added and stirred for 5 mins. *p*-methoxybenzyl chloride (0.93 mL, 6.0 equiv) was added dropwise and the reaction stirred for 19 h at room temperature. The reaction was quenched with water (20 mL) and extracted with EtOAc (70 mL) thrice. The combined organic layers were swirled gently with water (100 mL) thrice to remove the DMF, washed with brine (70 mL), dried over Na_2SO_4 and then concentrated *in vacuo*. The crude residue was purified by silica-gel column chromatography, DCM: acetone (100: 2) to obtain compound **2.75b** in 85% yield (388 mg, orange solid).

IR $\bar{\nu}_{max}$ (cm^{-1}): 2940 (C-H stretch), 1649 (C=O stretch), 1616 (C=C stretch), 1037 (C-O stretch).

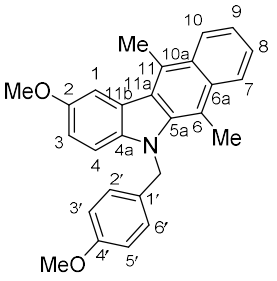
^{1}H NMR (400 MHz, DMSO-d_6) δ 8.09 (dd, J = 7.4, 1.4 Hz, 2H, $H^{7,\ 10}$), 7.86 (ddd, J = 7.4, 7.4, 1.6 Hz, 1H, H^{9}), 7.81 (ddd, J = 7.4, 7.4, 1.4 Hz, 1H, H^{8}), 7.72 (d, J = 9.2 Hz, 1H, H^{4}), 7.70 (d, J = 2.7 Hz, 1H, H^{1}), 7.23 – 7.17 (m, 2H, $H^{2',\ 6'}$), 7.13 (dd, J = 9.2 Hz, 2.6 Hz, 1H, H^{3}), 6.87 – 6.81 (m, 2H, $H^{3',\ 5'}$), 5.93 (s, 2H, -CH_2), 3.86 (s, 3H, Ar-OCH_3), 3.68 (s, 3H, Bn-OCH_3).

^{13}C NMR (101 MHz, DMSO-d_6) δ 180.2 (C^{11}), 177.9 (C^{6}), 158.6 ($C^{4'}$), 157.4 (C^{2}), 134.5 (C^{4a}), 134.2 (C^{5a}), 134.1 (C^{9}), 133.5 (C^{6a}), 133.3 (C^{10a}), 133.3 (C^{8}), 128.9 ($C^{1'}$), 128.3 (2×$C^{2',\ 6'}$), 126.3

(C^{10}), 125.7 (C^{7}), 124.2 (C^{11b}), 118.7 (C^{3}), 117.6 (C^{11a}), 114.0 (2×$C^{3',5'}$), 113.9 (C^{4}), 102.3 (C^{1}), 55.5 (C^{2}-OCH_3), 55.0 ($C^{4'}$-OCH_3) , 47.2 (-CH_2).

HRMS-ESI: m/z: $[M+H]^+$ Calculated for $C_{25}H_{20}O_4N_1$; 398.1387, Found 398.1375.

2-methoxy-5-(4-methoxybenzyl)-6,11-dimethyl-5*H*-benzo[*b*]carbazole (**2.76b**)



2-methoxy-5-(4-methoxybenzyl)-5*H*-benzo[*b*]carbazole-6, 11-dione (80 mg, 0.20 mmol, 1.0 equiv) was dissolved in anhydrous THF (5 mL) and the reaction was sealed and purged three times with nitrogen (g). The reaction was cooled to -80 °C and MeLi (0.6 mL, 1.6 M) was added dropwise over 5 mins. The reaction was stirred at -80 °C for 3 h before a solution of $SnCl_2$:HCl (37%): Et_2O (381 mg: 5 mL: 5mL) was added dropwise and the reaction stirred for a further 30 mins at -80 °C. The reaction was warmed to rt and stirred for 3 h before being quenched with water and extracted with $CHCl_3$ until the aqueous layer was colourless. The combined organic layers were washed with water, brine and dried over Na_2SO_4 before being concentrated *in vacuo*. The crude residue was purified by silica column chromatography, petroleum ether (40 – 60 °C): EtOAc (10:1) to obtain compound **2.76b** in 30% yield (23 mg, yellow solid).

IR $\bar{\nu}_{max}$ (cm^{-1}): 2930 (C-H stretch), 2837 (C-H stretch), 1491 (C-H stretch), 1206 (C-O stretch), 1035 (C-O stretch).

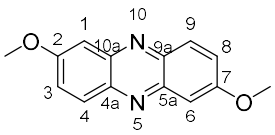
^{1}H NMR (400 MHz, DMSO-d_6) δ 8.36 (dd, J = 8.7, 0.9 Hz, 1H, H^{10}), 8.15 (dd, J = 8.7, 0.9 Hz, 1H, H^{7}), 7.91 (d, J = 2.5 Hz, 1H, H^{1}), 7.52 (ddd, J = 8.6, 6.6, 1.2 Hz, 1H, H^{8}), 7.45 (ddd, J = 8.6, 6.6, 1.2 Hz, 1H, H^{9}), 7.39 (d, J = 9.0 Hz, 1H, H^{4}), 7.15 (dd, J = 9.0, 2.5 Hz, 1H, H^{3}), 7.02 – 6.96 (m, 2H, $H^{3',5'}$), 6.87 – 6.81 (m, 2H, $H^{2',6'}$), 5.75 (s, 2H, -CH_2), 3.90 (s, 3H, Ar-OCH_3), 3.67 (s, 3H, Bn-OCH_3) , 3.19 (s, 3H, C^{11}-CH_3), 2.86 (s, 3H, C^{6}-CH_3).

^{13}C NMR (101 MHz, DMSO-d_6) δ 158.2 ($C^{4'}$), 153.3 (C^{2}), 139.6 (C^{4a}), 139.1 (C^{5a}), 131.7 (C^{6a}), 130.9 ($C^{1'}$), 126.9 (C^{11a}), 126.7 (2×$C^{2',6'}$), 126.6 (C^{11}), 124.8 (C^{8}), 124.4 (C^{10}), 123.7 (C^{10a}), 123.5 (C^{11b}), 123.3 (C^{7}), 122.2 (C^{9}), 114.4 (C^{3}), 114.1 (2×$C^{3',5'}$), 109.9 (C^{6}), 109.6 (C^{4}), 108.2 (C^{1}), 55.8 (Ar-OCH_3), 54.9 (Bn-OCH_3), 48.5 (Bn-CH_2), 15.2 (C^{10}-CH_3), 13.6 (C^{6}-CH_3).

HRMS-ESI: m/z: $[M+H]^+$ Calculated for $C_{27}H_{25}O_2N_1$; 395.1880, Found 395.1872.

6.5.2 Chapter 3: Compound Characterisation

2,7-dimethoxyphenazine (**3.32**)



The reaction was carried out according to general procedure E using isoquinoline (65 mg, 0.50 mmol, 1.0 equiv) and 2-chloro-4-methoxyaniline (95 mg, 0.60 mmol, 1.2 equiv) as starting materials. The crude residue was purified by silica-gel column chromatography, hexane: EtOAc (3: 7) to obtain compound **3.32** in 20% yield (25 mg, brown solid).

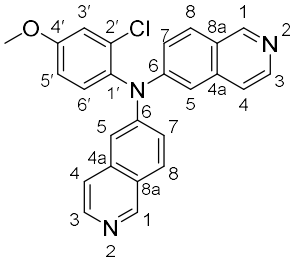
IR $\bar{\nu}_{max}$ (cm^{-1}): 2975 (C-H stretch), 1633 (C=N stretch), 1491 (C=C stretch), 1437 (C=C stretch), 1217 (C-O stretch).

^{1}H NMR (400 MHz, DMSO-d_6) δ 8.06 (d, J = 9.4 Hz, 2H, $H^{4,9}$), 7.60 (dd, J = 9.4, 2.8 Hz, 2H, $H^{3,8}$), 7.50 (d, J = 2.8 Hz, $H^{1,6}$), 4.00 (s, 6H, 2×-OCH_3).

^{13}C NMR (101 MHz, DMSO-d_6) δ 159.8 ($C^{2,7}$), 142.9 ($C^{10a,5a}$), 139.8 ($C^{4a,9a}$), 129.8 ($C^{4,9}$), 125.9 ($C^{3,8}$), 105.1 ($C^{1,6}$), 55.9 (2×-OCH$_3$).

HRMS-ESI: m/z: [M+H]$^+$ Calculated for $C_{14}H_{13}O_2N_2$; 241.0972, Found 241.0976.

N-(2-chloro-4-methoxyphenyl)-N-(isoquinolin-6-yl)isoquinolin-6-amine (**3.33**)



The reaction was carried out according to general procedure E using isoquinoline (65 mg, 0.50 mmol, 1.0 equiv) and 2-chloro-4-methoxyaniline (95 mg, 0.60 mmol, 1.2 equiv) as starting materials. The crude residue was purified by silica-gel column chromatography, hexane: EtOAc (2: 8) to obtain compound **3.33** in 30% yield (60 mg, brown solid).

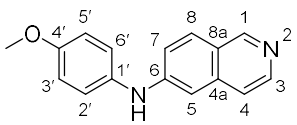
IR $\bar{\nu}_{max}$ (cm^{-1}): 2975 (C-H stretch), 1633 (C=N stretch), 1491 (C=C stretch), 1437 (C=C stretch), 1217 (C-O stretch), 1016 (C-O stretch), 810 (C-Cl stretch).

^{1}H NMR (400 MHz, DMSO-d_6) δ 9.16 (s, 2H, H^1), 8.36 (d, J = 5.8 Hz, 2H, H^3), 8.04 (d, J = 8.9 Hz, 2H, H^8), 7.64 (d, J = 5.8 Hz, 2H, H^4), 7.43 (d, J = 8.8 Hz, 1H, $H^{6'}$), 7.37 (dd, J = 8.9, 2.2 Hz, 2H, H^7), 7.32 (d, J = 2.2 Hz, 2H, $H^{5'}$), 7.28 (d, J = 2.9 Hz, 1H, H^3), 7.09 (dd, J = 8.8, 2.9 Hz, 1H, $H^{5'}$), 3.86 (s, 3H, -OCH_3).

^{13}C NMR (101 MHz, DMSO-d_6) δ 159.0 ($C^{4'}$), 151.5 (2×C^1), 147.3 (2×C^6), 143.4 (2×C^3), 136.6 (2×C^{4a}), 134.6 ($C^{1'}$), 133.3 ($C^{2'}$), 132.4 ($C^{6'}$), 129.2 (2×C^8), 124.8 (2×C^{8a}), 123.1 (2×C^7), 119.6 (2×C^4), 116.1 ($C^{3'}$), 115.4 ($C^{5'}$), 114.0 (2×C^5), 55.9 (-OCH$_3$).

HRMS-ESI: m/z: [M+H]$^+$ Calculated for $C_{25}H_{19}O_1N_3Cl_1$; 412.1211, Found 412.1222.

N-(4-methoxyphenyl)isoquinolin-6-amine (**3.36**)



The reaction was carried out according to general procedure E using 6-bromoisoquinoline (104 mg, 0.50 mmol, 1.0 equiv) and 4-methoxyaniline (74 mg, 0.60 mmol, 1.2 equiv) as starting materials. The crude residue was purified by silica-gel column chromatography, hexane: EtOAc (3: 7) to obtain compound **3.36** in 95% yield (119 mg, brown solid).

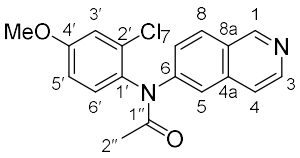
IR $\bar{\nu}_{max}$ (cm^{-1}): 3263 (N-H stretch), 3040 (C-H stretch), 2833 (C-H stretch), 1618 (C=N stretch), 1510 (C=C stretch), 1498 (C=C stretch), 1238 (C-O stretch), 1035 (C-O stretch).

^{1}H NMR (400 MHz, DMSO-d_6) δ 8.93 (s, 1H, H^1), 8.51 (s, 1H, -N*H*), 8.21 (d, J = 5.8 Hz, 1H, H^3), 7.86 (d, J = 8.9 Hz, 1H, H^8), 7.43 (d, J = 5.8 Hz, 1H, H^4), 7.24 (dd, J = 8.9, 2.3 Hz, 1H, H^7), 7.23 – 7.18 (m, 2H, $H^{2',6'}$), 7.08 (d, J = 2.1 Hz, 1H, H^5), 6.99 – 6.94 (m, 2H, $H^{3',5'}$), 3.76 (s, 3H, -OCH_3).

^{13}C NMR (101 MHz, DMSO-d_6) δ 155.2 ($C^{4'}$), 150.9 (C^1), 147.3 (C^6), 143.1 (C^3), 137.5 (C^{4a}), 134.1 ($C^{1'}$), 128.9 (C^8), 122.9 (C^{8a}), 122.7 (2×$C^{2',6'}$), 119.7 (C^7), 118.7 (C^4), 114.7 ($C^{3',5'}$), 102.4 (C^5), 55.2 (-O*C*H$_3$).

HRMS-ESI: m/z: [M+H]$^+$ Calculated for $C_{16}H_{15}O_1N_2$; 251.1179, Found 251.1193.

N-(2-chloro-4-methoxyphenyl)-N-(isoquinolin-6-yl)acetamide (**3.37**)



N-(2-chloro-4-methoxyphenyl)isoquinolin-6-amine (100 mg, 0.35 mmol, 1.0 equiv) was dissolved in acetic anhydride (0.5 mL) and DMAP (4 mg, 0.04 mmol, 10 mol%) was dissolved in acetic anhydride (0.5 mL) before being added to the reaction mixture. The reaction was stirred at r.t. for 19 h before being quenched with H_2O and extracted with EtOAc three times. The combined organic layer was washed with $NaHCO_3$ solution (sat.) four times, washed with brine and then dried over Na_2SO_4. The crude was concentrated *in vacuo* and dry loaded onto silica-gel for purification. The crude residue was purified by silica-gel column chromatography, hexane: EtOAc (3: 7) to obtain compound **3.37** in 28% yield 32 mg, brown oil).

IR $\bar{\nu}_{max}$ (cm^{-1}): 2932 (C-H stretch), 2851 (C-H stretch), 1687 (C=O stretch), 1631 (C=N stretch), 1603 (C=C stretch), 1497 (C=C stretch), 1214 (C-O stretch), 1039 (C-O stretch).

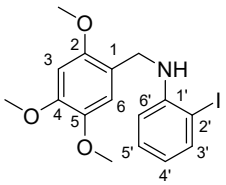
^{1}H NMR (400 MHz, DMSO-d_6) δ 9.26 (s, 1H, H^1), 8.46 (d, J = 5.4 Hz, 1H, H^3), 8.10 (d, J = 8.8 Hz, 1H, H^8), 7.82 – 7.73 overlapping with 7.77 (m (br), 1H, H^5), 7.77 (d, J = 5.4 Hz, 1H, H^4), 7.69 – 7.58 overlapping with 7.66 (m (br), 1H, $H^{6'}$), 7.66 (dd, J = 8.8, 2.1 Hz, 1H, H^7), 7.25 (d, J = 1.5 Hz, 1H, $H^{3'}$), 7.06 (dd, J = 8.5, 1.5 Hz, 1H, $H^{5'}$), 3.82 (s, 3H, -OCH_3), 1.98 (s, 3H, -CH_3).

^{13}C NMR (101 MHz, DMSO-d_6) δ 169.8 ($C^{1''}$), 159.7 ($C^{4'}$), 151.8 (C^{1}), 143.4 (C^{3}), 143.3 (C^{6}), 135.4 (C^{4a}), 133.1 ($C^{1'}$), 132.1 ($C^{6'}$), 128.2 (C^{8}), 126.2 (C^{7}), 126.1 ($C^{2'}$), 121.4 (C^{8a}), 120.2 ($C^{4,5}$), 115.4 ($C^{3'}$), 114.7 ($C^{5'}$), 55.9 (-O*C*H$_3$), 23.2 (-*C*H$_3$).

HRMS-ESI: m/z: $[M+H]^+$ Calculated for $C_{18}H_{16}O_2N_2Cl_1$; 327.0895, Found 327.0912.

6.5.3 Chapter 4: Compound Characterisation

2-iodo-N-(2,4,5-trimethoxybenzyl)aniline (**4.34**)



To a solution of o-iodoaniline (2.00 g, 10.20 mmol) in MeOH (30 mL) was added 2,4,5-trimethoxybenzaldehyde (2.23 g, 10.20 mmol), followed by a solution of AcOH (0.9 mL) in MeOH (5.8 mL) and the reaction stirred at r.t. for 45 mins. Formation of a white precipitate required further addition of MeOH (30 mL). The reaction mixture was cooled to 0 °C and $NaCNBH_3$ (0.90 g, 14.28 mmol) was added and stirred for 30 mins after which the precipitate returned to solution. The reaction was quenched with sat. $NaHCO_3$ (aq) and the organic solvent removed *in vacuo*. The residue was filtered and washed with water to obtain **4.34** in 84% yield without further purification (3.44 g, 84 %, white solid).

IR $\bar{\nu}_{max}$ (cm^{-1}): 3398 (N-H stretch), 2938 (C-H stretch), 2835 (C-H stretch), 1590 (C=C stretch). 1204 (C-O stretch).

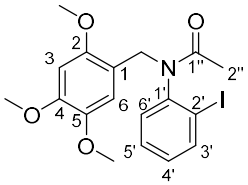
^{1}H NMR (400 MHz, DMSO-d_6) δ 7.60 (dd, J = 7.8, 1.4 Hz, 1H, $H^{2'}$), 7.15 – 7.11 (m, 1H, $H^{5'}$), 6.90 (s, 1H, H^{6}), 6.70 (s, 1H, H^{3}), 6.59 (dd, J = 8.2, 1.2 Hz, 1H, $H^{6'}$), 6.39 – 6.35 (m, 1H, $H^{4'}$), 5.14 (t, J = 6.0 Hz, 1H, -N*H*), 4.25 (d, J = 6.1 Hz, 2H, -CH_2), 3.84 (s, 3H, C^2-OCH_3), 3.78 (s, 3H, C^4-OCH_3), 3.62 (s, 3H, C^5-OCH_3).

^{13}C NMR (101 MHz, DMSO-d_6) δ 151.4 (C^2), 148.7 (C^4), 147.3 ($C^{1'}$), 142.4 (C^5), 138.6 ($C^{3'}$), 129.2 ($C^{5'}$), 118.3 ($C^{4'}$), 117.7 (C^1), 114.1 (C^6), 111.1 ($C^{6'}$), 98.3 (C^3), 85.1 ($C^{2'}$), 56.5 (C^5-OCH_3), 56.2 (C^2-OCH_3), 55.8 (C^4-OCH_3), 42.0 (-CH_2).

LRMS-ESI: m/z: $[M+H]^+$ Calculated for $C_{16}H_{18}INO_2$; 399.0, Found 399.0.

All values correspond to literature values[195]

N-(2-iodophenyl)-N-(2,4,5-trimethoxybenzyl)acetamide (**4.35**)



To a solution of **4.34** (3.00 g, 7.52 mmol), in acetic anhydride (17 mL) was added DMAP (92 mg, 0.75 mmol) and the reaction stirred at r.t. for 19 h under Ar atmosphere. The reaction mixture was diluted with EtOAc and washed with water, brine, dried over Na_2SO_4 and concentrated *in vacuo* to obtain **4.35** in 96% yield without further purification. (3.19 g, white solid).

IR $\bar{\nu}_{max}$ (cm^{-1}): 2936 (C-H stretch), 1655 (C=O stretch), 1614 (C=C stretch), 1521 (C=C stretch), 1210 (C-O stretch), 1031 (C-O stretch).

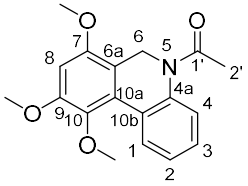
^{1}H NMR (400 MHz, DMSO-d_6) δ 7.95 (d, J = 7.9, 1H, $H^{3'}$), 7.34 – 7.30 (m, 1H, $H^{5'}$), 7.10 – 7.06 (m, 1H, $H^{3'}$), 6.92 (d, J = 7.80, 1H, $H^{6'}$), 6.79 (s, 1H, H^{6}), 6.55 (s, 1H, H^{3}), 5.10 (d, J = 14.2 Hz, 1H, -CH_2), 4.23 (d, J = 14.2 Hz, 1H, -CH_2), 3.74 (s, 3H, C^4-OCH_3), 3.64 (s, 3H, C^5-OCH_3), 3.46 (s, 3H, C^2-OCH_3), 1.68 (s, 3H,-CH_3).

^{13}C NMR (101 MHz, DMSO-d_6) δ 168.7 ($C^{1''}$), 151.8 (C^{2}), 149.2 (C^{4}), 144.2 ($C^{1'}$), 142.3 (C^{5}), 139.4 ($C^{3'}$), 130.4 ($C^{6'}$), 129.8 ($C^{4'}$), 129.2 ($C^{5'}$), 115.5 (C^{1}), 115.2 (C^{6}), 101.1 ($C^{2'}$), 97.9 (C^{3}), 56.3 (C^5-OCH$_3$), 56.0 (C^2-OCH$_3$), 55.7 (C^4-OCH$_3$), 44.4 (-CH$_2$), 22.7 (-CH$_3$).

LRMS-ESI: m/z: [M+H]$^+$ Calculated for $C_{18}H_{20}INO_4$; 442.0, Found 442.0.

All values correspond to literature values[195]

1-(7,9,10-Trimethoxy-5(6*H*)-phenanthridinyl)-ethanone (**4.36**)



N-(2-iodophenyl)-N-(2,4,5-trimethoxybenzyl)acetamide (2.50 g, 5.67 mmol) was stirred in anhydrous DMF (40 mL). Pd(OAc)$_2$ (114 mg, 0.51 mmol), K_2CO_3 (1.14 g, 8.28 mmol) and PPh_3 (445 mg, 1.70 mmol) were added to the reaction mixture and heated to 160 °C for 8 h. The reaction mixture was filtered over Celite© and the cake washed with EtOAc. The combined organic extracts were washed with water, brine, dried over Na_2SO_4. The filtrate was concentrated *in vacuo*. And the crude product purified by silica-gel column chromatography, hexane: EtOAc (7: 3) to obtain compound **4.36** in 80% yield (1.43 g, white solid).

IR $\bar{\nu}_{max}$ (cm^{-1}): 2938 (C-H stretch), 1653 (C=O stretch), 1595 (C=C stretch), 1340 (C-N stretch), 1202 (C-O stretch), 1029 (C-O stretch).

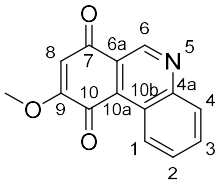
^{1}H NMR (400 MHz, DMSO-d_6) δ 8.30 (dd, J = 7.7, 1.6 Hz, 1H, H^{1}), 7.49 (s (br), 1H, H^{4}), 7.43 – 7.23 (m, 2H, 2 × $H^{2,3}$), 6.78 (s, 1H, H^{8}), 5.04 – 4.25 (s (br), 2H, -CH_2), 3.88 (s, 3H, C^9-OCH_3), 3.86 (s, 3H, C^7-OCH_3), 3.62 (s, 3H, C^{10}-OCH_3), 2.08 (s (br), 3H, -CH_3).

^{13}C NMR (101 MHz, DMSO-d_6) δ 168.1 ($C^{1'}$), 152.7 (C^{9}), 150.8 (C^{7}), 140.0 (C^{10}), 138.5 (C^{4a}), 127.9 (2×$C^{1,2/3}$), 127.4 ($C^{2/3}$), 125.8 ($C^{10a/10b}$), 125.0 (C^{4}), 124.7 ($C^{10a/10b}$), 116.6 (C^{6a}), 97.8 (C^{8}), 60.0 (C^{10}-OCH$_3$), 56.1 (C$^{7/9}$-OCH$_3$), 56.2 (C$^{7/9}$-OCH$_3$), 38.4 (-CH$_2$), 22.0 ($C^{1'}$).

LRMS-ESI: m/z: [M+H]$^+$ Calculated for $C_{18}H_{20}NO_4$; 314.1, Found 314.1.

All values correspond to literature values[195]

9-Methoxy-7,10-Phenanthridinedione (**4.37**)



1-(7,9,10-Trimethoxy-5(6*H*)-phenanthridinyl)-ethanone (0.70 g, 2.24 mmol) was dissolved in a mixture of CH_3CN (172 mL) and $CHCl_3$ (9 mL). A solution of CAN (4.79 g, 8.74 mmol) in H_2O (172 mL) was added to the reaction mixture and heated to reflux for 7 h. The reaction mixture was filtered over and bed of Celite© and the cake washed with EtOAc. The combined organic extracts were washed with water, brine, dried over Na_2SO_4. The filtrate was concentrated *in vacuo* to obtain **4.37** in 90% yield without further purification (481 mg, orange solid).

IR $\bar{\nu}_{max}$ (cm^{-1}) 2953 (C-H stretch), 1690 (C=O stretch), 1647 (C=O stretch), 1619 (C=C stretch), 1338 (C=N stretch). 1016 (C-O stretch).

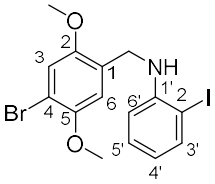
^{1}H NMR (500 MHz, DMSO-d_6) δ 9.48 (s, 1H, H^6), 9.29 (d, J = 8.9 Hz, 1H, H^1), 8.18 (d, J = 8.3 Hz, 1H, H^4), 7.99 – 7.95 (m, 1H, H^3), 7.91 – 7.88 (m, 1H, H^2), 6.41 (s, 1H, H^8), 3.93 (s, 3H, -OCH_3).

^{13}C NMR (126 MHz, DMSO-d_6) δ 184.8 (C^7), 182.1 (C^{10}), 161.0 (C^9), 150.8 (C^{4a}), 147.0 (C^6), 131.8 (C^3), 131.4 (C^{10a}), 130.5 (C^2), 129.9 (C^4), 126.9 (C^1), 122.5 (C^{6a}), 121.6 (C^{10b}), 107.4 (C^8), 56.9 (-OCH$_3$)

LRMS-ESI: m/z: $[M+H]^+$ Calculated for $C_{14}H_{10}NO_3$; 240.1, Found 240.2.

All values correspond to literature values[195]

N-(4-bromo-2,5-dimethoxybenzyl)-2-iodoaniline (**4.41**)



To a solution of *o*-iodoaniline (1.35 g, 6.15 mmol) in MeOH (18 mL), 4-bromo-2,5-dimethoxybenzaldehyde (1.50 g, 6.15 mmol) and AcOH (0.53 mL) in MeOH (4 mL) were added, and the reaction stirred at r.t. for 30 mins. The reaction mixture was cooled to 0 °C and $NaCNBH_3$ (0.54 g, 8.61 mmol) was added and the reaction stirred at 0 °C for 30 mins. The reaction was warmed to r.t. and stirred for 1 h before being quenched with sat. $NaHCO_3$ (aq). The solvent was removed *in vacuo* and the solution filtered. The precipitate was washed with water and pulled dry under vacuum to to obtain **4.41** in 89% yield (2.44 g, white solid).

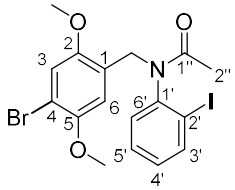
IR $\bar{\nu}_{max}$ (cm^{-1}) 3402 (N-H stretch), 2997 (C-H stretch), 2840 (C-H stretch), 1591 (C=C stretch), 1492 (C=C stretch), 1217 (C-O stretch), 1038 (C-O stretch).

^{1}H NMR (400 MHz, DMSO-d_6) δ 7.62 (dd, J = 9.7, 1.5 Hz, 1H, $H^{6'}$), 7.22 (s, 1H, H^3), 7.14 – 7.10 (m, 1H, $H^{4'}$), 7.03 (s, 1H, H^6), 6.54 (dd, J = 8.2, 1.3 Hz, 1H, $H^{3'}$), 6.40 – 6.36 (m, 1H, $H^{5'}$), 5.33 (t, J = 6.2 Hz, 1H, -N*H*,), 4.31 (d, J = 6.3 Hz, 2H, -CH_2), 3.83 (s, 3H, C^2-OCH_3), 3.68 (s, 3H, C^5-OCH_3).

^{13}C NMR (101 MHz, DMSO-d_6) δ 151.9 (C^2), 149.9 (C^5), 147.6 ($C^{1'}$), 139.3 ($C^{6'}$), 129.7 ($C^{4'}$), 128.0 (C^1), 119.0 ($C^{5'}$), 116.3 (C^3), 113.7 (C^6), 111.7 ($C^{3'}$), 109.3 (C^4), 57.1 (C^5-O*C*H$_3$), 56.8 (C^2-O*C*H$_3$), 42.6 (-*C*H$_2$)

HRMS-ESI Exact mass calculated for [M + H]$^+$ ($C_{15}H_{15}BrINO_2$) requires m/z 447.9404, found 447.9400.

N-(4-bromo-2,5-dimethoxybenzyl)-N-(2-iodophenyl)acetamide (**4.42**)



N-(4-bromo-2,5-dimethoxybenzyl)-2-iodoaniline (2.08 g, 4.64 mmol) was stirred in a solution of acetic anhydride (10 mL) and DMAP (55 mg, 10 mol %) at r.t. for 19 h. The reaction was diluted with water and extracted with DCM. The combined organic phases were washed with water, brine and dried over Na_2SO_4. The filtrate was concentrated *in vacuo* to obtain **4.42** in 87% yield (1.98 g, white solid).

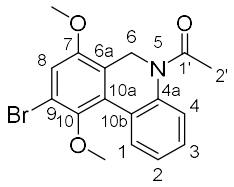
IR $\bar{\nu}_{max}$ (cm^{-1}) 2925 (C-H stretch), 2826 (C-H stretch), 1649 (C=O stretch), 1510 (C=C stretch), 1469 (C=C stretch), 1047 (C-O stretch).

^{1}H NMR (400 MHz, DMSO-d_6) δ 7.96 (dd, J = 7.9, 1.3 Hz, 1H, $H^{3'}$), 7.38 – 7.33 (m, 1H, $H^{5'}$), 7.12 – 7.08 (m, 2H, 2 × $H^{3',3}$), 7.04 (dd, J = 7.8, 1.5 Hz, 1H, $H^{6'}$), 6.96 (s, 1H, H^6), 5.10 (d, J = 14.5 Hz, 1H, -CH_2), 4.28 (d, J = 14.5 Hz, 1H, -CH_2), 3.74 (s, 3H, C^5-OCH_3), 3.49 (s, 3H, C^2-OCH_3), 1.71 (s, 3H, -CH_3).

^{13}C NMR (101 MHz, DMSO-d_6) δ 169.0 ($C^{1''}$), 151.6 (C^2), 149.2 (C^5), 144.2 ($C^{1'}$), 139.6 ($C^{3'}$), 130.4 ($C^{6'}$), 129.9 ($C^{4'}$), 129.3 ($C^{5'}$), 124.9 (C^1), 115.9 (C^3), 114.9 (C^6), 109.8 (C^4), 101.0 ($C^{2'}$), 56.6 (C^5-O*C*H$_3$), 56.0 (C^2-O*C*H$_3$), 45.1 (-*C*H$_2$), 22.6 ($C^{1''}$-*C*H$_3$).

HRMS-ESI Exact mass calculated for [M + H]$^+$ ($C_{17}H_{17}BrINO_3$) requires m/z 489.9509, found 489.9502.

1-(9-bromo-7,10-dimethoxyphenanthridin-5(6*H*)-yl)ethan-1-one (**4.43**)



N-(4-bromo-2,5-dimethoxybenzyl)-N-(2-iodophenyl)acetamide (488 mg, 1.00 mmol) was dissolved in dry DMF (10 mL) in a 10 – 20 mL microwave vial. $Pd(OAc)_2$ (22 mg, 0.10 mmol), K_2CO_3 (276 mg, 2.00 mmol), and PPh_3 (78 mg, 0.30 mmol) were charged and the vial was capped, evacuated and purged with argon 3 times and heated at 160 °C for 1 h under microwave irradiation in a Biotage® Microwave. The crude mixture was diluted with EtOAc and washed with LiCl (5% w/v, aq), brine and dried over Na_2SO_4. The filtrate was concentrated *in vacuo* and the crude residue was purified by silica-gel column chromatography, petroleum ether (40 – 60 °C): EtOAc (85: 15) to obtain compound **4.43** in 46% yield (170 mg, white solid).

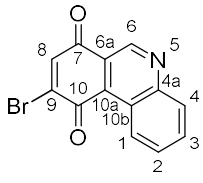
IR $\bar{\nu}_{max}$ (cm^{-1}): 2932 (C-H stretch), 2846 (C-H stretch), 1659 (C=O stretch), 1450 (C=C stretch), 1243 (C-O stretch), 1033 (C-O stretch).

^{1}H NMR (400 MHz, DMSO-d_6) δ 8.34 (dd, J = 7.9, 1.5 Hz, 1H, H^1), 7.55 (d, J = 5.4 Hz, 1H, H^4), 7.46 – 7.32 (m, 2H, $H^{2,3}$), 7.29 (s, 1H, H^8), 5.18 – 4.33 (s (br), 2H, -CH_2), 3.85 (s, 3H, C^7-OCH_3), 3.53 (s, 3H, C^{10}-OCH_3), 2.09 (s, 3H, -CH_3).

^{13}C NMR (101 MHz, DMSO-d_6) δ 168.4 ($C^{1''}$), 151.4 (C^7), 147.6 (C^{10}), 138.4 (C^{4a}), 128.8 ($C^{2/3}$), 127.4 (C^1), 126.7 (C^{6a}), 126.3 ($C^{2/3}$), 126.2 ($C^{10a/10b}$), 126.0 ($C^{10a/10b}$), 125.2 (C^4), 116.9 (C^9), 114.8 (C^8), 60.3 (C^{10}-OCH$_3$), 56.4 (C^7-OCH$_3$), 38.4 (-CH$_2$), 22.0 ($C^{1'}$).

HRMS-ESI Exact mass calculated for $[M + H]^+$ ($C_{17}H_{17}O_3NBr$) requires m/z 362.0386, found 362.0392.

9-bromophenanthridine-7,10-dione (**4.44**)



1-(9-bromo-7,10-dimethoxyphenanthridin-5(6H)-yl)ethan-1-one (400 mg, 1.11 mmol) was dissolved in CH_3CN (11 mL) and $CHCl_3$ (2 mL) and heated to 50 °C. A solution of CAN (4.86 g, 8.86 mmol), in H_2O (84 mL) was added and he reaction heated to reflux for 14 h. The reaction was cooled and extracted with $CHCl_3$ before being washed with water, brine and dried over Na_2SO_4. The filtrate was concentrated *in vacuo* and the crude residue was purified by silica-gel column chromatography, petroleum ether (40 – 60 °C): EtOAc (90: 10) to obtain compound **4.44** in 78% yield (248 mg, orange solid).

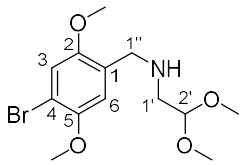
IR $\bar{\nu}_{max}$ (cm^{-1}) 2923 (C-H stretch), 1675 (C=O stretch), 1655 (C=O stretch), 1601 (C=N stretch).

^{1}H NMR (400 MHz, DMSO-d_6) δ 9.45 (s, 1H, H^6), 9.28 (d, J = 8.7 Hz, 1H, H^1), 8.20 (d, J = 8.5 Hz, 1H, H^4), 8.03 – 7.97 (m, 1H, H^3), 7.95 – 7.88 (m, 1H, H^2), 7.80 (s, 1H, H^8).

^{13}C NMR (101 MHz, DMSO-d_6) δ 183.0 (C^{10}), 180.1 (C^7), 150.9 (C^{4a}), 147.0 (C^6), 140.4 (C^9), 137.7 (C^8), 132.2 (C^{10a}), 132.0 (C^4), 130.6 (C^2), 130.0 (C^4), 127.1 (C^1), 122.8 (C^{6a}), 121.8 (C^{10b}).

HRMS-ESI Exact mass calculated for $[M + H]^+$ ($C_{13}H_7O_2NBr$) requires m/z 287.9655, found 287.9670.

N-(4-bromo-2,5-dimethoxybenzyl)-2,2-dimethoxyethan-1-amine (**4.50**)



To a solution of aminoacetaldehyde dimethyl acetal (0.67 mL, 6.15 mmol) in MeOH (18 mL), 4-bromo-2,5-dimethoxybenzaldehyde (1.50 g, 6.15 mmol) and AcOH (0.53 mL) in MeOH (4 mL) were added, and the reaction stirred at rt for 30 mins. The reaction mixture was cooled to 0 °C and $NaCNBH_3$ (0.54 g, 8.61 mmol) was added and the reaction stirred at 0 °C for 30 mins. The reaction was warmed to r.t. and stirred for 1 h before being quenched with sat. $NaHCO_3$ (aq). The solvent was removed *in vacuo* and the solution filtered. The filtrate was washed with water, brine, dried over Na_2SO_4 and concentrated *in vacuo* to obtain **4.50** in 74% yield without further purification (1.51 g, yellow oil).

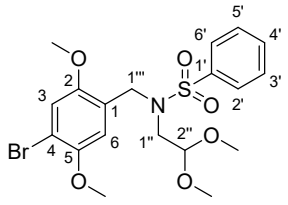
IR $\bar{\nu}_{max}$ (cm^{-1}) 2943 (C-H stretch), 2840 (C-H stretch), 1496 (C=C stretch), 1460 (C=C stretch), 1213 (C-O stretch), 1038 (C-O stretch).

^{1}H NMR (400 MHz, DMSO-d_6) δ 7.15 (s, 1H, H^3), 7.13 (s, 1H, H^6), 4.39 (t, J = 5.4 Hz, 1H, $H^{2'}$), 3.79 (s, 3H, C^5-OCH_3), 3.75 (s, 3H, C^2-OCH_3), 3.64 (s, 2H, $H^{1''}$), 3.24 (s, 6H, 2 ×C$^{2''}$-OCH_3), 2.57 (d, J = 5.4 Hz, 2H, $H^{1''}$).

^{13}C NMR (101 MHz, DMSO-d_6) δ 151.4 (C^2), 149.3 (C^5), 129.2 (C^1), 115.5 (C^3), 113.7 (C^6), 108.2 (C^4), 103.5 ($C^{2'}$), 56.5 (C^5-OCH$_3$), 56.1 (C^2-OCH$_3$), 53.1 (2 ×-OCH$_3$), 50.0 ($C^{1'}$), 47.2 ($C^{1''}$).

HRMS-ESI Exact mass calculated for $[M + H]^+$ ($C_{13}H_{20}BrNO_4$) requires m/z 334.0648, found $[M + H]^+$ m/z 334.0654.

N-(4-bromo-2,5-dimethoxybenzyl)-N-(2,2-dimethoxyethyl)benzenesulfonamide (**4.51**)



To a solution of compound **4.50** (1.00 g, 3.00 mmol) dissolved in THF (30 mL) was added 2.5 % Na_2CO_3 (16 mL) and benzenesulfonyl chloride (0.39 mL, 3.0 mmol) and the reaction was stirred at r.t. for 19 h. The reaction mixture was extracted with DCM and washed with

water, brine and dried over Na_2SO_4. The filtrate was concentrated *in vacuo* and purified by silica gel flash-column chromatography, petroleum ether (40 – 60 °C): EtOAc (85: 15) to obtain compound **4.51** in 95% yield (1.35 g, colourless oil).

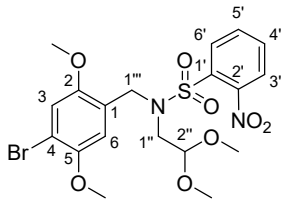
IR $\bar{\nu}_{max}$ (cm^{-1}) 2943 (C-H stretch), 2826 (C=H stretch), 1451 (C=C stretch), 1343 (S=O stretch), 1217 (S=O stretch), 1047 (C-O stretch).

^{1}H NMR (400 MHz, DMSO-d_6) δ 7.82 – 7.78 (m, 2H, 2 × $H^{2',6'}$), 7.70 – 7.65 (m, 1H, $H^{4'}$), 7.62 – 7.57 (m, 2H, 2 ×$H^{3',5'}$), 7.14 (s, 1H, H^3), 6.93 (s, 1H, H^6), 4.34 (s, 2H, $H^{1''}$), 4.33 (t, J = 5.6 Hz, 1H, $H^{2''}$), 3.69 (s, 3H, $C^{2/5}$-OCH_3), 3.68 (s, 3H, $C^{2/5}$-OCH_3), 3.26 (d, J = 4.3 Hz, 2H, $H^{2''}$), 3.16 (s, 6H, 2 × -OCH_3).

^{13}C NMR (101 MHz, DMSO-d_6) δ 151.1 (C^2), 149.2 (C^5), 139.4 ($C^{1'}$), 132.8 (2×$C^{5',3'}$), 129.3 ($C^{4'}$), 126.9 (2×$C^{2',6'}$), 124.9 (C^1), 115.6 (C^3), 113.6 (C^6), 109.5 (C^4), 102.7 ($C^{2''}$), 56.5 ($C^{2/5}$-OCH$_3$), 56.1 ($C^{2/5}$-OCH$_3$), 53.7 (2×$C^{2''}$-OCH$_3$), 49.8 ($C^{1''}$), 47.2 ($C^{1'''}$).

HRMS-ESI Exact mass calculated for $[M + H]^+$ ($C_{19}H_{25}BrNO_6S$) requires m/z 474.0580, found $[M + H]^+$ m/z 474.0570.

N-(4-bromo-2,5-dimethoxybenzyl)-N-(2,2-dimethoxyethyl)-2-nitrobenzenesulfonamide (**4.58**)



4.50 (0.50 g, 1.50 mmol) was dissolved in anhydrous DCM (12 mL). 10 % Na_2CO_3 (aq) (8 mL) was added and the solution stirred for 1 h. 2-Nitrophenylsulfonyl chloride (0.22 g, 1.27 mmol) was added dropwise and the reaction stirred for a further 19 h at r.t. The reaction mixture was washed with water, brine, dried over Na_2SO_4 and the filtrate concentrated *in vacuo*. The crude residue was purified by silica gel flash-column chromatography, petroleum ether (40 – 60 °C): EtOAc (80: 20) to obtain compound **4.58** in 75% yield (0.58 g, yellow solid).

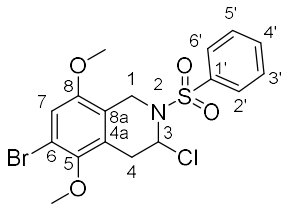
IR $\bar{\nu}_{max}$ (cm^{-1}) 2934 (C-H stretch), 1537 (C-N stretch), 1501 (C=C stretch), 1447 (C=C stretch), 1213 (C-O stretch), 1060 (C-O stretch).

^{1}H NMR (500 MHz, DMSO-d_6) δ 7.98 – 7.95 (m, 2H, 2 × $H^{3',6'}$), 7.89 – 7.83 (m, 1H, $H^{4'}$), 7.79 – 7.75 (m, 1H, $H^{5'}$), 7.16 (s, 1H, H^6), 6.82 (s, 1H, H^3), 4.52 (s, 2H, $H^{1''}$), 4.40 (t, J = 5.3 Hz, 1H, $H^{2''}$), 3.69 (s, 3H, C^2-OCH_3), 3.64 (s, 3H, C^5-OCH_3), 3.37 (d, J = 5.3 Hz, 2H, $H^{1''}$), 3.20 (s, 6H, 2 × $C^{2''}$-OCH_3).

^{13}C NMR (126 MHz, DMSO-d_6) δ 151.7 (C^{2}), 149.7 (C^{5}), 134.9 ($C^{1'}$), 132.8 ($C^{5'}$), 132.7 ($C^{4'}$), 130.4 ($C^{6'}$), 124.7 (C^{1}), 124.3 ($C^{3'}$), 116.3 (C^{6}), 113.8 (C^{3}), 110.3 (C^{4}), 103.2 ($C^{2''}$), 56.8 ($C^{2/5}$-OCH_3), 56.6 ($C^{2/5}$-OCH_3), 54.6 (2 × $C^{2''}$-OCH_3), 49.8 ($C^{1''}$), 47.3 ($C^{1'''}$).

LRMS-ESI: m/z: $[M+H]^+$ Calculated for $C_{19}H_{23}N_2BrO_8S$; 519.0, Found 519.0

6-Bromo-3-chloro-5,8-dimethoxy-2-(phenylsulfonyl)-1,2,3,4-tetrahydroisoquinoline (**4.61**)



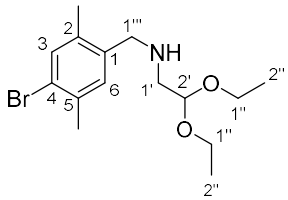
To a cooled solution (– 78 °C) of **4.51** (0.11 g, 0.23 mmol) in anhydrous DCM (2 mL) was slowly added a cooled solution (– 78 °C) of chlorosulfonic acid (0.12 mL) in DCM (0.52 mL). The reaction was stirred at – 78 °C under Ar for 1 h and allowed to warm to r.t. of 2 h. The reaction was quenched with water, washed with sat. $NaHCO_3$ (aq), brine, dried over Na_2SO_4 and the filtrate concentrated *in vacuo*. The crude residue was purified by silica gel flash-column chromatography, petroleum ether (40 – 60 °C): EtOAc (70: 30) to obtain compound **4.61** in 70% yield (72 mg, cream solid).

^{1}H NMR (400 MHz, DMSO-d_6) δ 7.87 – 7.82 (m, 2H, 2 × $H^{2',6'}$), 7.76 – 7.71 (m, 1H, $H^{4'}$), 7.70 – 7.64 (m, 2H, 2 × $H^{3',5'}$), 7.26 (s, 1H, H^{7}), 5.53 – 5.51 (m, 1H, H^{3}), 4.50 (d, J = 17.2 Hz, 1H, H^{1}), 4.10 (d, J = 12.4 Hz, 1H, H^{4}), 3.84 (s, 3H, C^{5}-OCH_3), 3.81 (s, 3H, C^{8}-OCH_3), 3.51 (d, J = 16.4 Hz, 1H, H^{1}), 3.11 (dd, J = 13.4, 2.2 Hz, 1H, H^{4}).

^{13}C NMR (126 MHz, DMSO-d_6) δ 151.8 (C^{8}), 148.1 (C^{5}), 135.8 ($C^{1'}$), 133.5 ($C^{4'}$), 129.7 (2×$C^{3',5'}$), 129.5 (C^{4a}), 127.4 (2×$C^{2',6'}$), 120.7 (C^{8a}), 115.3 (C^{7}), 114.7 (C^{6}), 61.5 (C^{5}-OCH_3), 56.3 (C^{8}-OCH_3), 50.6 (C^{3}), 50.0 (C^{4}), 42.4 (C^{1}).

HRMS-ESI Exact mass calculated for $[M + H]^+$ ($C_{17}H_{18}BrClNO_4S$) requires m/z 445.9823, found 445.9781.

N-(4-bromo-2,5-dimethylbenzyl)-2,2-diethoxyethan-1-amine (**4.66**)[209]



Aminoacetaldehyde diethyl acetal (1.78 mL, 12.25 mmol), 4-bromo-2,5-dimethylbenzaldehyde (0.52 g, 2.45 mmol) and $NaCNBH_3$ (0.20 g, 3.19 mmol) were charged to a 2 – 5 mL microwave vial and EtOH (5 mL) added. The vial was sealed and heated in a Biotage© Microwave to 130 °C for 10 mins. The solvent was removed *in vacuo* and the crude residue purified by silica gel flash-column chromatography, petroleum ether (40 – 60 °C): EtOAc (80: 20) to obtain compound **4.66** in 60% yield (0.49 g, colourless oil).

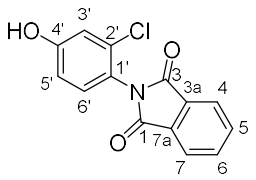
IR $\bar{\nu}_{max}$ (cm^{-1}) 2979 (C-H stretch), 1491 (C=C stretch), 1376 (C-H bend), 1117 (C-O stretch), 1061 (C-O stretch).

^{1}H NMR (400 MHz, DMSO-d_6) δ 7.34 (s, 1H, H^3), 7.25 (s, 1H, H^6), 4.52 (t, J = 5.6 Hz, 1H, $H^{2'}$), 3.61 (s, 2H, $H^{1'}$), 3.57 (q, J = 7.1 Hz, 2H, $H^{1''}$), 3.46 (q, J = 7.1 Hz, 2H, $H^{1''}$), 2.58 (d, J = 5.6 Hz, 2H, $H^{1'}$), 2.28 (s, 3H, C^5-CH_3), 2.22 (s, 3H, C^2-CH_3), 1.10 (t, J = 7.1 Hz, 6H, $H^{2''}$).

^{13}C NMR (101 MHz, DMSO-d_6) δ 138.4 (C^2), 136.1 (C^1), 133.9 (C^5), 133.0 (C^3), 131.0 (C^6), 121.8 (C^4), 101.8 ($C^{2'}$), 61.6 ($C^{1''}$), 51.3 ($C^{1'}$), 50.0 ($C^{1''}$), 22.0 (C^5-CH_3), 17.7 (C^2-CH_3), 15.4 (2×$C^{2''}$).

LRMS-ESI m/z: $[M+H]^+$ Calculated for ($C_{15}H_{25}BrNO_2$); 330.1, Found 330.2.

2-(2-chloro-4-hydroxyphenyl)isoindoline-1,3-dione (**4.70**)



4-Amino-3-chlorophenol (10.0 g, 69.65 mmol) and 1, 2-benzenedicarboxylic anhydride (13.4 g, 90.55 mmol) were heated in acetic acid (400 mL) to 120 °C for 19 h. The reaction mixture was quenched with water and the precipitate isolated by filtration to obtain **4.70** in 93% yield (17.8 g, purple solid).

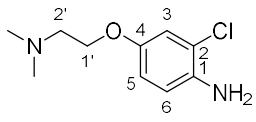
IR $\bar{\nu}_{max}$ (cm^{-1}) 3505 (O-H stretch), 2889 (C-H stretch), 2777 (C-H stretch), 1721 (C=O stretch), 1694 (C=O stretch), 1384 (C-H bend), 1096 (C-O stretch).

^{1}H NMR (500 MHz, MeOD-d_4) δ 10.33 (s, 1H, -O*H*), 7.99 – 7.90 (m, 4H, 4 × H^{5-7}) 7.25 (d, J = 8.7, 1H, $H^{6'}$) 7.03 (d, J = 2.6 Hz, 1H, $H^{3'}$), 6.88 (dd, J = 8.7, 2.7 Hz, 1H, $H^{5'}$).

^{13}C NMR (125 MHz, MeOD-d_4) δ 168.7 ($C^{1,3}$), 160.7 ($C^{4'}$), 135.9 ($C^{3a,7a}$), 134.8 ($C^{2'}$), 133.2 ($C^{1'}$), 132.7 (2×$C^{5,6}$), 124.7 (2×$C^{4,7}$), 122.0 ($C^{6'}$), 117.5 ($C^{3'}$), 115.9 ($C^{5'}$).

HRMS-ESI Exact mass calculated for $[M + H]^+$ ($C_{14}H_8ClNO_3$) requires m/z 274.0265 , found $[M + H]^+$ m/z 274.0269.

2-Chloro-4-[2-(dimethylamino)ethoxy]aniline (**4.71**)



2-Chloro-N,N-dimethylethylamine hydrochloride (10.0 g, 69.43 mmol) was stirred vigorously in a mixture of water (43 mL), toluene (15 mL) and NaOH aq (30% w/v, 8 mL) for 1 h. The organic layer was extracted for use in the next step. To a solution of compound **4.70** (2.00g, 7.31 mmol), K_2CO_3 (3.03 g, 21.92 mmol) and TBAB (25 mg, 0.08 mmol) in EtOAc (30 mL), 2-Chloro-N,N-dimethylethylamine in

toluene (8 mL) was added and the reaction heated to 80 °C for 4 h. The reaction mixture was concentrated *in vacuo* and passed through a silica plug to obtain the alkylated intermediate without further purification. A portion of the crude residue (1.2 g, 3.48 mmol) obtained was re-dissolved in a solution of EtOH (20 mL) and DCM (4 mL) before hydrazine monohydrate (0.33 mL) was added. The reaction was stirred at r.t. for 2 h and the reaction was filtered. The filtrate was concentrated *in vacuo* to obtain **4.71** in 75% overall yield (0.71 g, yellow oil).

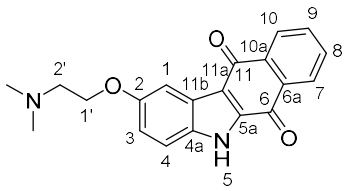
IR $\bar{\nu}_{max}$ (cm^{-1}) 3334 (N-H stretch), 3198 (N-H stretch), 2947 (C-H stretch), 2778 (C-H stretch), 1605 (N-H stretch), 1504 (N-H stretch), 1212 (C-O stretch), 1039 (C-O stretch).

^{1}H NMR (400 MHz, DMSO-d_6) δ 6.83 (d, J = 2.8 Hz, 1H, H^3), 6.74 (d, J = 8.5 Hz, 1H, H^6), 6.69 (dd, J = 8.5, 2.6 Hz, 1H, H^5), 4.83 (s, 2H, -NH_2), 3.91 (t, J = 5.9 Hz, 2H, $H^{1'}$), 2.55 (t, J = 5.9 Hz, 2H, $H^{2'}$), 2.33 (s, 6H, 2 × -CH_3).

^{13}C NMR (125 MHz, MeOD-d_4) δ 153.0 (C^4), 139.1 (C^1), 120.8 (C^2), 118.3 (C^6), 116.5 (C^5), 116.0 (C^3), 67.5 ($C^{1'}$), 59.2 ($C^{2''}$), 44.4 (2 × -CH$_3$).

HRMS-ESI Exact mass calculated for $[M + H]^+$ ($C_{10}H_{15}ClN_2O$) requires m/z 215.0946, found $[M + H]^+$ m/z 215.0947.

2-(2-(dimethylamino)ethoxy)-5*H*-benzo[*b*]carbazole-6,11-dione (**4.72**)



The reaction was carried out according to general procedure D using 2-bromonaphthalene-1,4-dione (119 mg, 0.50 mmol, 1 equiv) and 2-chloro-4-[2-(dimethylamino)ethoxy]aniline (0.124 g, 0.60 mmol) as starting materials. The crude residue was purified by silica-gel column chromatography, DCM: MeOH (100: 8) to obtain compound **4.72** in 63% yield (108 mg, orange solid).

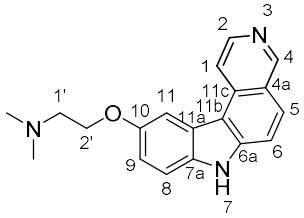
IR $\bar{\nu}_{max}$ (cm^{-1}) 3541 (N-H stretch), 2928 (C-H stretch), 2876 (C-H stretch), 1712 (C=O stretch), 1643 (C=O stretch), 1596 (C=C stretch), 1223 (C-O stretch).

^{1}H NMR (400 MHz, DMSO-d_6) δ 13.1 (s, 1H, -NH), 8.14 – 8.08 (m, 2H, 2 × $H^{7,10}$), 7.91 – 7.85 (m, 1H, H^9), 7.85 – 7.82 (m, 1H, H^8), 7.72 (d, J = 2.4 Hz, 1H, H^1), 7.56 (d, J = 9.0 Hz, 1H, H^4), 7.18 (dd, J = 9.0, 2.5 Hz, 1H, H^3), 4.42 (t, J = 5.0 Hz, 2H, $H^{1'}$), 2.74 (t, J = 5.0 Hz, 2H, $H^{2'}$), 2.29 (s, 6H, 2 × -CH_3).

^{13}C NMR (101 MHz, DMSO-d_6) δ 180.2 (C^{11}), 177.4 (C^{6}), 155.2 (C^{2}), 137.5 (C^{5a}), 134.4 (C^{9}) 134.2 (C^{10a}), 133.8 (C^{8}), 133,4 (C^{4a}), 132.8 (C^{6a}), 126.2 (2×$C^{7,10}$), 124.7 (C^{11b}), 118.4 (C^{3}), 117.1 (C^{11a}), 115.2 (C^{4}), 104.0 (C^{1}), 62.7 ($C^{1'}$), 57.7 ($C^{2'}$), 45.6 (2 × -CH$_3$) .

HRMS-ESI Exact mass calculated for [M + H]$^+$ ($C_{20}H_{18}N_2O_3$) requires m/z 335.1390, found [M + H]$^+$ m/z 335.1394.

2-((7*H*-pyrido[3,4-*c*]carbazol-10-yl)oxy)-N,N-dimethylethan-1-amine (**4.73**)



The reaction was carried out according to general procedure D using 6-bromoisoquinoline (104 mg, 0.50 mmol), and 2-chloro-4-[2-(dimethylamino)ethoxy]aniline (124 mg, 0.60 mmol) as starting materials. The crude residue was purified by silica-gel column chromatography, DCM: MeOH (85: 15) to obtain compound **4.73** in 28% yield (108 mg, cream solid).

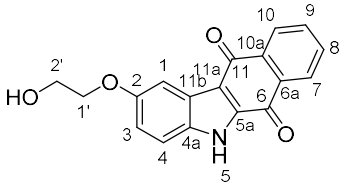
IR $\bar{\nu}_{max}$ (cm^{-1}) 2921 (C-H stretch), 1616 (C=N stretch), 1459 (C=C stretch), 1031 (C-O stretch).

^{1}H NMR (400 MHz, DMSO-d_6) δ 12.00 (s, 1H, -N*H*), 9.30 (s, 1H, H^{4}), 8.67 – 8.55 (m, 2H, $H^{1,2}$), 8.05 (d, J = 2.1 Hz, 1H, H^{11}), 8.03 (d, J = 9.0 Hz, 1H, H^{5}), 7.85 (d, J = 9.0 Hz, 1H, H^{6}), 7.60 (d, J = 8.8 Hz, 1H, H^{8}), 7.13 (dd, J = 8.8, 2.1 Hz, 1H, H^{9}), 4.30 (t, J = 5.7 Hz, 1H, $H^{2'}$), 2.83 (t, J = 5.7 Hz, 1H, $H^{1'}$), 2.37 (s, 6H, 2×-CH_3).

^{13}C NMR (101 MHz, DMSO-d_6) δ 153.2 (C^{10}), 152.1 (C^{4}), 144.2 (C^{1}), 140.1 (C^{6a}), 133.7 (C^{7a}), 132.2 (C^{11c}), 126.0 (C^{5}), 123.7 (C^{11b}), 123.1 (C^{11a}), 116.6 (C^{2}), 115.1 (C^{6}), 114.9 (C^{9}), 112.7 (C^{8}), 112.3 (C^{4a}), 104.9 (C^{11}), 66.2 ($C^{2'}$), 57.8 ($C^{1'}$), 45.4 (2×-CH$_3$).

HRMS-ESI Exact mass calculated for [M + H]$^+$ ($C_{19}H_{20}O_1N_3$) requires m/z 306.1601, Found 306.1608.

2-(2-hydroxyethoxy)-5*H*-benzo[*b*]carbazole-6,11-dione (**4.75**)



The reaction was carried out according to general procedure D using 2-bromonaphthalene-1,4-dione (119 mg, 0.50 mmol, 1 equiv) and 2-(4-amino-3-chlorophenoxy)ethan-1-ol (0.112 g, 0.60 mmol) as starting materials. The crude residue was purified by silica-gel column chromatography, DCM: MeOH (100: 1) to obtain compound **4.75** in 30% yield (46 mg, red solid).

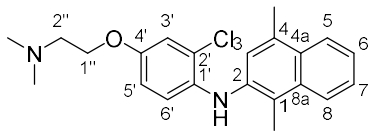
IR $\bar{\nu}_{max}$ (cm^{-1}) 3461 (O-H stretch), 3230 (N-H stretch), 2938 (C-H stretch), 1640 (C=O stretch), 1588 (C=O stretch), 1242 (C-O stretch), 1018 (C-O stretch).

^{1}H NMR (400 MHz, DMSO-d_6) δ 13.04 (s, 1H, -N*H*), 8.14 – 8.07 (m, 2H, $H^{7,10}$), 7.90 – 8.84 (m, 1H, H^{9}), 7.84 – 7.78 (m, 1H, H^{8}), 7.62 (d, J = 2.5 Hz, 1H, H^{1}), 7.50 (d, J = 9.0 Hz, 1H, H^{4}), 7.11 (dd, J = 9.0, 2.5 Hz, 1H, H^{3}), 4.94 (t, J = 5.6 Hz, 1H, -O*H*), 4.07 (t, J = 5.6 Hz, 1H, $H^{1'}$), 3.82 – 3.73 (m, 2H, $H^{2'}$).

^{13}C NMR (101 MHz, DMSO-d_6) δ 180.4 (C^{11}), 177.3 (C^{6}), 156.4 (C^{2}), 137.1 (C^{5a}), 134.3 (2×$C^{9,10a}$), 133.5 (C^{8}), 133,4 (C^{4a}), 132.8 (C^{6a}), 126.2 (2×$C^{7,10}$), 124.9 (C^{11b}), 118.4 (C^{3}), 117.1 (C^{11a}), 115.2 (C^{4}), 104.0 (C^{1}), 70.0 ($C^{2'}$), 59.6 ($C^{1'}$).

HRMS-ESI Exact mass calculated for $[M + H]^+$ ($C_{18}H_{14}O_4N$) requires m/z 308.0917, Found 308.0916.

N-(2-chloro-4-(2-(dimethylamino)ethoxy)phenyl)-1,4-dimethylnaphthalen-2-amine (**4.78**)



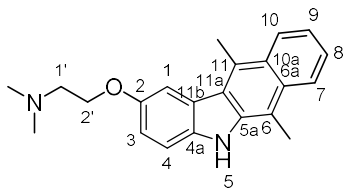
2-bromo-1,4-dimethylnaphthalene (255 mg, 1.09 mmol), 2-chloro-4-[2-(dimethylamino)ethoxy]aniline (280 mg, 1.30 mmol), $Pd(OAc)_2$ (12 mg, 0.05 mmol), $HP^tBu_3BF_4$ (32 mg, 0.11 mmol), and NaO^tBu (208 mg, 2.17 mmol), were charged to a 10 – 20 mL microwave vial and 1,4-dioxane (11 mL) added. The vial was sealed, purged with Ar (g) three times and heated to 120 °C for 1 h. The reaction was concentrated *in vacuo* and the crude residue purified by silica-gel column chromatography, DCM: MeOH (100: 8) to obtain compound **4.78** in 85% yield (340 mg, brown oil).

^{1}H NMR (400 MHz, DMSO-d_6) δ 7.97 (d, J = 8.4 Hz, 1H, H^{5}), 7.92 (d, J = 8.2 Hz, 1H, H^{8}), 7.54 – 7.47 (m, 1H, H^{7}), 7.44 – 7.37 (m, 1H, H^{6}), 7.08 (d, J = 2.8 Hz, 1H, $H^{3'}$), 7.03 (s, 1H, -N*H*), 6.94 (s, 1H, H^{3}), 6.80 (dd, J = 8.9, 2.8 Hz, 1H, $H^{5'}$), 6.67 (d, J = 8.9, 2.8 Hz, 1H, $H^{6'}$), 4.00 (t, J = 5.8 Hz, 2H, $H^{1''}$), 2.59 (t, J = 5.8 Hz, 1H, $H^{2''}$), 2.53 (s, 3H, C^4-CH_3), 2.40 (s, 3H, C^1-CH_3), 2.20 (s, 6H, 2×-CH_3).

^{13}C NMR (101 MHz, DMSO-d_6) δ 153.0 ($C^{4'}$), 138.6 (C^{2}), 135.4 ($C^{1'}$), 133.6 (C^{8a}), 132.4 (C^{1}), 128.9 (C^{4a}), 126.0 (C^{7}), 124.5 (C^{8}), 124.1 ($C^{2'}$), 124.0 (C^{5}), 123.5 (C^{6}), 122.5 (C^{3}), 120.7 ($C^{6'}$), 120.0 (C^{4}), 115.6 ($C^{3'}$), 114.6 ($C^{5'}$), 66.4 ($C^{1''}$), 57.7 ($C^{2''}$), 45.6 (2×-NCH_3), 19.1 (C^4-CH_3), 12.8 (C^1-CH_3).

HRMS-ESI Exact mass calculated for $[M + H]^+$ ($C_{22}H_{26}ON_2Cl$) requires m/z 369.1728, Found 369.1728.

2-((6,11-dimethyl-5*H*-benzo[*b*]carbazol-2-yl)oxy)-N,N-dimethylethan-1-amine (**4.68**)



Compound **4.78** (180 mg, 0.49 mmol), was dissolved in DMSO (30 mL) and NaO^{t}Bu (94 mg, 0.98 mmol) was added. The mixture was separated into six vials (5 mL) and submitted to UV-irradiation (400 W UV-A flood lamp, 320 nm – 400 nm) for 1 h. The vials were combined and the reaction mixture passed through a RP-silica plug to obtain **4.68** in 19% yield without further purification (30 mg, white solid).

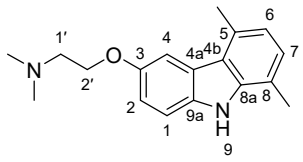
IR $\bar{\nu}_{max}$ (cm^{-1}) 3422 (N-H stretch), 2949 (C-H stretch), 2828 (C-H stretch), 1629 (C-N stretch), 1478 (C=C stretch) 1563 (C=C stretch), 1227 (C-O stretch), 1029 (C-O stretch).

^{1}H NMR (400 MHz, DMSO-d_6) δ 10.87 (s, -N*H*), 8.32 (d, *J* = 8.5 Hz, 1H, *H*^{10}), 8.10 (d, *J* = 8.6 Hz, 1H, *H*^{7}), 7.86 (d, *J* = 2.3 Hz, 1H, *H*^{1}), 7.54 – 7.48 (m, 1H, *H*^{8}), 7.43 – 7.37 (m, 1H, *H*^{9}), 7.42 (d, *J* = 8.6 Hz, 1H, *H*^{4}), 7.15 (dd, *J* = 8.6, 2.3 Hz), 4.17 (t, *J* = 5.9 Hz, 2H, *H*$^{2'}$), 3.16 (s, 3H, C^{11}-C*H*$_3$), 2.80 (s, 3H, C^6-C*H*$_3$), 2.67 (t, *J* = 5.9 Hz, 2H, *H*$^{1'}$), 2.26 (s, 6H, 2×-NC*H*$_3$).

^{13}C NMR (101 MHz, DMSO-d_6) δ 151.9 (*C*^{2}), 138.9 (*C*^{5a}), 137.5 (*C*^{4a}), 130.7 (*C*^{6a}), 126.4 (*C*^{10a}), 125.9 (*C*^{11}), 124.6 (*C*^{10}), 124.4 (*C*^{8}), 123.8 (*C*^{11b}), 123.4 (*C*^{7}), 122.8 (*C*^{11a}), 121.6 (*C*^{9}), 115.3 (*C*^{3}), 110.8 (C^4), 108.9 (*C*^{1}), 108.7 (*C*^{6}), 66.8 (*C*$^{2'}$), 58.1 (*C*$^{1'}$), 45.7 (2×-N*C*H$_3$), 15.1 (C^{11}-*C*H$_3$), 12.7 (C^6-*C*H$_3$).

HRMS-ESI Exact mass calculated for [M + H]$^+$ ($C_{22}H_{25}ON_2$) requires m/z 333.1961, Found 333.1966.

2-((5,8-dimethyl-9*H*-carbazol-3-yl)oxy)-N,N-dimethylethan-1-amine (**4.82**)



The reaction was carried out according to general procedure D using 2-bromo-*p*-xylene (93 mg, 0.50 mmol, 1.0 equiv) and 2-chloro-4-(2-(dimethylamino)ethoxy)aniline (128 mg, 0.60 mmol, 1.2 equiv) as starting materials and HP^{t}Bu$_3$BF$_4$ (14.5 mg, 10 mol%). The crude residue was purified by silica-gel column chromatography, DCM: MeOH (100:3) to obtain compound **4.82** in 22% yield (31 mg, brown solid).

IR $\bar{\nu}_{max}$ (cm^{-1}): 3857 (N-H stretch), 2925 (C-H stretch), 1523 (C=C stretch), 1465 (C-H stretch), 1057 (C-O stretch).

^{1}H NMR (400 MHz, DMSO-d_6) δ 11.04 (s, -N*H*), 7.67 (d, *J* = 2.4 Hz, 1H, *H*^{4}), 7.46 (d, *J* = 8.7 Hz, 1H, *H*^{1}), 7.12 (dd, *J* = 8.7, 2.4 Hz), 7.06 (d, *J* = 7.2 Hz, 1H, *H*^{7}), 6.82 (d, *J* = 7.2 Hz, 1H, *H*^{6}),

4.40 (t, J = 5.1 Hz, 2H, $H^{2'}$), 3.44 (t, J = 5.1 Hz, 2H, $H^{1'}$), 2.82 (s, 6H, -N(CH_3)$_2$), 2.77 (s, 3H, C^5-CH_3), 2.50 (s, 3H, C^8-CH_3).

^{13}C NMR (101 MHz, DMSO-d_6) δ 151.1 (C^3), 139.8 (C^{8a}), 135.2 (C^{9a}), 129.6 (C^5), 125.8 (C^7), 123.6 (C^{4a}), 120.3 (C^{4b}), 119.6 (C^6), 117.5 (C^8), 114.1 (C^2), 111.4 (C^1), 107.0 (C^4) 63.7 ($C^{2'}$), 56.0 ($C^{1'}$), 41.2 ((-NCH$_3$)$_2$), 20.2 (C^5-CH$_3$), 16.7 (C^8-CH$_3$).

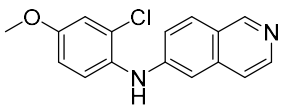
HRMS-ESI: m/z: $[M+H]^+$ Calculated for $C_{18}H_{23}O_1N_2$; 283.1805, Found 283.1812.

6.6 DFT Experimental

All the calculations are carried out with Gaussian 09 program and visualized in Gaussview v05. All calculations were carried out with the DFT B3LYP method with the 6-31G+G(d,p) basis set and optimized to a minimum.

6.6.1 Compound 7a

E = -1262.49949229 a.u.



HOMO = -0.20496 eV **LUMO** = -0.05912 eV

Row	Symbol	X	Y	Z
1	C	1.670868	-0.93267	0.486367
2	C	1.416851	0.408982	0.166901
3	C	2.53866	1.206679	-0.14782
4	C	3.829314	0.697554	-0.15984
5	C	4.048663	-0.65599	0.128385
6	C	2.959309	-1.47128	0.454537
7	H	0.843682	-1.56767	0.782962
8	H	4.67236	1.33442	-0.40047
9	H	3.09454	-2.51611	0.705869
10	N	0.136562	0.972618	0.204509
11	H	0.097455	1.952115	0.44821
12	C	-1.09291	0.342981	0.013535
13	C	-2.23548	0.891807	0.58484
14	C	-1.21284	-0.81598	-0.81541
15	C	-3.50986	0.319757	0.359823
16	H	-2.1528	1.770184	1.220596

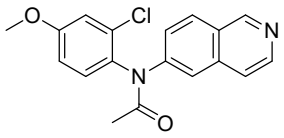
17	C	-2.44105	-1.39222	-1.03314
18	H	-0.33014	-1.22011	-1.29722
19	C	-4.71634	0.828073	0.914101
20	C	-3.61906	-0.85058	-0.45315
21	H	-2.52128	-2.2665	-1.67426
22	C	-5.90672	0.187833	0.649345
23	H	-4.69806	1.71403	1.542787
24	C	-4.90858	-1.41073	-0.64906
25	H	-6.83818	0.562711	1.066209
26	H	-5.00794	-2.30142	-1.27037
27	N	-6.02066	-0.92661	-0.12781
28	Cl	2.309373	2.916655	-0.50783
29	O	5.350167	-1.06979	0.069698
30	C	5.639431	-2.4328	0.35648
31	H	5.132655	-3.10519	-0.34726
32	H	6.71892	-2.53714	0.242766
33	H	5.355122	-2.69474	1.383425

Table S17. DFT atom list compound 9a.

6.6.2 Compound 16

E= -1415.15310016 a.u.

HOMO = -0.23190 eV **LUMO** = -0.07160 eV



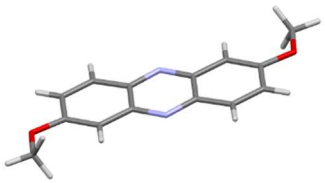
	Atom	X	Y	Z
1	C	2.087934	-0.02024	1.335721
2	C	1.381352	0.504475	0.252491
3	C	1.835685	0.189781	-1.03967
4	C	2.932943	-0.6387	-1.23894
5	C	3.622557	-1.1594	-0.13503
6	C	3.200476	-0.84403	1.163213
7	H	1.764458	0.239047	2.338704
8	H	3.274739	-0.87691	-2.23908

9	H	3.721309	-1.2224	2.03382
10	N	0.237845	1.345086	0.472083
11	C	-1.06133	0.796111	0.212024
12	C	-1.97166	1.493718	-0.63163
13	C	-1.4128	-0.4319	0.740856
14	C	-3.21741	0.973492	-0.89475
15	H	-1.66028	2.427875	-1.08475
16	C	-2.68546	-0.99733	0.469597
17	H	-0.71151	-0.97399	1.36725
18	C	-3.60638	-0.27903	-0.35196
19	H	-3.90663	1.508523	-1.54266
20	C	0.465027	2.624827	0.991
21	O	4.688404	-1.95407	-0.43322
22	C	5.462273	-2.4879	0.636923
23	H	4.860341	-3.14762	1.273818
24	H	6.257337	-3.06643	0.165838
25	H	5.903171	-1.68917	1.245462
26	N	-5.2628	-2.03273	-0.11125
27	C	-3.11625	-2.24944	0.983824
28	H	-2.45556	-2.83745	1.614615
29	C	-4.37717	-2.70888	0.674703
30	H	-4.72747	-3.66374	1.057803
31	C	-4.87726	-0.86925	-0.59684
32	H	-5.5935	-0.33939	-1.22516
33	O	1.603665	3.055943	1.110761
34	Cl	1.033825	0.856597	-2.44926
35	C	-0.73275	3.445815	1.436573
36	H	-1.07757	4.084886	0.617479
37	H	-1.57606	2.842863	1.778266
38	H	-0.38843	4.097469	2.241273

Table S18. DFT atom list compound 16.

6.7 Crystallographic Data

6.7.1 Compound 11



Identification code	burley_wee_org	
Empirical formula	C14 H12 N2 O2	
Formula weight	240.26	
Temperature	100(2) K	
Wavelength	1.54184 Å	
Crystal system	Monoclinic	
Space group	P 21/n	
Unit cell dimensions	a = 3.82700(10) Å	α= 90°.
	b = 18.3658(7) Å	β= 98.847(3)°.
	c = 7.9201(3) Å	γ= 90°.
Volume	550.05(3) Å3	
Z	2	
Density (calculated)	1.451 Mg/m3	
Absorption coefficient	0.807 mm-1	
F(000)	252	
Crystal size	0.30 x 0.04 x 0.02 mm3	
Theta range for data collection	4.816 to 71.339°.	
Index ranges	-4<=h<=3, -22<=k<=22, -9<=l<=9	
Reflections collected	5007	
Independent reflections	[R(int) = 0.0510]	
Completeness to theta = 70.000°	100.00%	

Absorption correction	Semi-empirical from equivalents	
Max. and min. transmission	1.00000 and 0.29887	
Refinement method	Full-matrix least-squares on F2	
Data / restraints / parameters	1067 / 0 / 83	
Goodness-of-fit on F2	1.049	
Final R indices [I>2sigma(I)]	R1 = 0.0446, wR2 = 0.1256	
R indices (all data)	R1 = 0.0507, wR2 = 0.1307	
Extinction coefficient	n/a	
Largest diff. peak and hole	0.194 and -0.296 e.Å-3	

Table S19. General Crystallographic information for compound 11.

	x	y	z	U(eq)
O(1)	1875(2)	7708(1)	6928(1)	23(1)
N(1)	-911(3)	9433(1)	11082(1)	20(1)
C(1)	205(3)	9286(1)	9584(2)	19(1)
C(2)	444(4)	8547(1)	9077(2)	20(1)
C(3)	1551(3)	8392(1)	7556(2)	20(1)
C(4)	2479(4)	8960(1)	6474(2)	22(1)
C(5)	2293(3)	9669(1)	6936(2)	21(1)
C(6)	1119(3)	9861(1)	8508(2)	20(1)
C(7)	846(4)	7118(1)	7936(2)	24(1)

Table S20. Atomic coordinates (x 104) and equivalent isotropic displacement parameters (Å2x 103) for burley_wee_org_auto. U(eq) is defined as one third of the trace of the orthogonalized Uij tensor.

O(1)-C(3)	1.3643(16)
O(1)-C(7)	1.4354(16)
N(1)-C(6)#1	1.3417(17)
N(1)-C(1)	1.3488(18)
C(1)-C(2)	1.4221(19)
C(1)-C(6)	1.4340(19)
C(2)-C(3)	1.367(2)
C(2)-H(2)	0.95
C(3)-C(4)	1.430(2)
C(4)-C(5)	1.3559(18)
C(4)-H(4)	0.95
C(5)-C(6)	1.4312(19)
C(5)-H(5)	0.95
C(7)-H(7A)	0.98
C(7)-H(7B)	0.98
C(7)-H(7C)	0.98
C(3)-O(1)-C(7)	116.34(10)
C(6)#1-N(1)-C(1)	116.40(12)
N(1)-C(1)-C(2)	118.79(13)
N(1)-C(1)-C(6)	121.00(13)
C(2)-C(1)-C(6)	120.20(12)
C(3)-C(2)-C(1)	119.36(13)
C(3)-C(2)-H(2)	120.3
C(1)-C(2)-H(2)	120.3
O(1)-C(3)-C(2)	124.88(12)
O(1)-C(3)-C(4)	114.16(12)
C(2)-C(3)-C(4)	120.95(13)
C(5)-C(4)-C(3)	120.73(13)
C(5)-C(4)-H(4)	119.6
C(3)-C(4)-H(4)	119.6

C(4)-C(5)-C(6)	120.54(13)
C(4)-C(5)-H(5)	119.7
C(6)-C(5)-H(5)	119.7
N(1)#1-C(6)-C(5)	119.19(13)
N(1)#1-C(6)-C(1)	122.59(13)
C(5)-C(6)-C(1)	118.21(13)
O(1)-C(7)-H(7A)	109.5
O(1)-C(7)-H(7B)	109.5
H(7A)-C(7)-H(7B)	109.5
O(1)-C(7)-H(7C)	109.5
H(7A)-C(7)-H(7C)	109.5
H(7B)-C(7)-H(7C)	109.5

Table S21. Bond lengths [Å] and angles [°] for burley_wee_org_auto.

Symmetry transformations used to generate equivalent atoms:

#1 -x,-y+2,-z+2

	U11	U22	U33	U23	U13	U12
O(1)	26(1)	16(1)	27(1)	-1(1)	7(1)	1(1)
N(1)	18(1)	19(1)	24(1)	0(1)	3(1)	0(1)
C(1)	15(1)	19(1)	23(1)	0(1)	2(1)	0(1)
C(2)	19(1)	16(1)	25(1)	2(1)	2(1)	-1(1)
C(3)	16(1)	18(1)	26(1)	-2(1)	0(1)	1(1)
C(4)	20(1)	23(1)	22(1)	0(1)	5(1)	1(1)
C(5)	20(1)	21(1)	23(1)	1(1)	4(1)	-1(1)
C(6)	16(1)	17(1)	24(1)	0(1)	2(1)	0(1)
C(7)	25(1)	18(1)	29(1)	1(1)	6(1)	0(1)

Table S22. Anisotropic displacement parameters (Å2x 103)for burley_wee_org_auto. The anisotropic displacement factor exponent takes the form: -2□2[h2a*2U11 + ... + 2 h k a* b* U12]

	x	y	z	U(eq)
H(2)	-160	8166	9788	24
H(4)	3234	8841	5420	26
H(5)	2946	10040	6210	26
H(7A)	2257	7133	9078	36
H(7B)	1246	6654	7385	36
H(7C)	-1666	7165	8032	36

Table S23. Hydrogen coordinates (x 104) and isotropic displacement parameters (Å2x 103)

for burley_wee_org_auto.C(6)#1-N(1)-C(1)-C(2)	-179.41(11)
C(6)#1-N(1)-C(1)-C(6)	0.2(2)
N(1)-C(1)-C(2)-C(3)	179.62(11)
C(6)-C(1)-C(2)-C(3)	0.0(2)
C(7)-O(1)-C(3)-C(2)	2.20(19)
C(7)-O(1)-C(3)-C(4)	-177.69(11)
C(1)-C(2)-C(3)-O(1)	-179.72(11)
C(1)-C(2)-C(3)-C(4)	0.2(2)
O(1)-C(3)-C(4)-C(5)	-179.86(11)
C(2)-C(3)-C(4)-C(5)	0.2(2)
C(3)-C(4)-C(5)-C(6)	-0.8(2)
C(4)-C(5)-C(6)-N(1)#1	-178.99(12)
C(4)-C(5)-C(6)-C(1)	0.9(2)
N(1)-C(1)-C(6)-N(1)#1	-0.2(2)
C(2)-C(1)-C(6)-N(1)#1	179.39(11)
N(1)-C(1)-C(6)-C(5)	179.85(11)
C(2)-C(1)-C(6)-C(5)	-0.53(19)

Table S24. Torsion angles [°] for burley_wee_org_auto.

Symmetry transformations used to generate equivalent atoms: #1 -x,-y+2,-z+2

References

(1) Yip, K. W.; Reed, J. C. Bcl-2 Family Proteins and Cancer. *Oncogene* **2008**, *27* (50), 6398–6406. https://doi.org/10.1038/onc.2008.307.

(2) Sivaramakrishnan, M.; McCarthy, K. D.; Campagne, S.; Huber, S.; Meier, S.; Augustin, A.; Heckel, T.; Meistermann, H.; Hug, M. N.; Birrer, P.; Moursy, A.; Khawaja, S.; Schmucki, R.; Berntenis, N.; Giroud, N.; Golling, S.; Tzouros, M.; Banfai, B.; Duran-Pacheco, G.; Lamerz, J.; Hsiu Liu, Y.; Luebbers, T.; Ratni, H.; Ebeling, M.; Cléry, A.; Paushkin, S.; Krainer, A. R.; Allain, F. H. T.; Metzger, F. Binding to SMN2 Pre-MRNA-Protein Complex Elicits Specificity for Small Molecule Splicing Modifiers. *Nat. Commun.* **2017**, *8* (1). https://doi.org/10.1038/s41467-017-01559-4.

(3) Weldon, C.; Behm-Ansmant, I.; Hurley, L. H.; Burley, G. A.; Branlant, C.; Eperon, I. C.; Dominguez, C. Identification of G-Quadruplexes in Long Functional RNAs Using 7-Deazaguanine RNA. *Nat. Chem. Biol.* **2017**, *13* (1), 18–20. https://doi.org/10.1038/nchembio.2228.

(4) Pucci, C.; Martinelli, C.; Ciofani, G. Innovative Approaches for Cancer Treatment: Current Perspectives and New Challenges. *Ecancermedicalscience* **2019**, *13*, 1–26. https://doi.org/10.3332/ecancer.2019.961.

(5) Cancer https://www.who.int/health-topics/cancer#tab=tab_1.

(6) Okamoto, R.; Maeda, Y.; Sasaki, T. Hepatotoxicity of Chemotherapy. *Gan To Kagaku Ryoho.* **2003**, *30* (6), 772–778. https://doi.org/10.1634/theoncologist.6-2-162.

(7) Shaikh, A. Y.; Shih, J. A. Chemotherapy-Induced Cardiotoxicity. *Curr. Heart Fail. Rep.* **2012**, *9* (2), 117–127. https://doi.org/10.1007/s11897-012-0083-y.

(8) Srinivasarao, M.; Galliford, C. V.; Low, P. S. Principles in the Design of Ligand-Targeted Cancer Therapeutics and Imaging Agents. *Nat. Rev. Drug Discov.* **2015**, *14* (3), 203–219. https://doi.org/10.1038/nrd4519.

(9) Surget, S.; Khoury, M. P.; Bourdon, J. C. Uncovering the Role of P53 Splice Variants in Human Malignancy: A Clinical Perspective. *Onco. Targets. Ther.* **2013**, *7*, 57–67. https://doi.org/10.2147/OTT.S53876.

(10) Stevens, M.; Oltean, S. Modulation of the Apoptosis Gene Bcl-x Function Through Alternative Splicing. *Front. Genet.* **2019**, *10* (804), 1–9.

https://doi.org/10.3389/fgene.2019.00804.

(11) Crick, F. H. C. On Protein Synthesis. In Symposia of the Society for Experimental Biology, Number XII: The Biological Replication of Macromolecules, F.K. Sanders. Cambridge University Press 1958.

(12) Crick, F. H. C. Central Dogma of Molecular Biology. *Nature* **1970**, *227* (5258), 561–563. https://doi.org/10.1038/227561a0.

(13) Baltimore, D. Viral RNA-Dependent DNA Polymerase: RNA-Dependent DNA Polymerase in Virions of RNA Tumour Viruses. *Nature*. 1970, pp 1209–1211. https://doi.org/10.1038/2261209a0.

(14) Egli, M.; Flavell, A.; Pyle, A. M.; Wilson, W. D.; Haq, S. I.; Luisi, B.; Fisher, J.; Laughton, C.; Allen, S.; Engels, J.; Blackburn, G. M.; Gait, M. J.; Loakes, D.; Williams, D. M. *Nucleic Acids in Chemistry and Biology*; The Royal Society of Chemistry, 2006. https://doi.org/10.1039/9781847555380.

(15) Nikolova, E. N.; Kim, E.; Wise, A. A.; O'Brien, P. J.; Andricioaei, I.; Al-Hashimi, H. M. Transient Hoogsteen Base Pairs in Canonical Duplex DNA. *Nature* **2011**, *470* (7335), 498–504. https://doi.org/10.1038/nature09775.

(16) Bang, I. Untersuchungen Über Die Guanylsäure. *Biochem. Z.* **1910**, *26*, 293–311.

(17) Gellert, M.; Lipsett, M. N.; Davies, D. R. Helix Formation by Guanylic Acid. *Proc. Natl. Acad. Sci. U. S. A.* **1962**, *48*, 2013–2018. https://doi.org/10.1073/pnas.48.12.2013.

(18) Siddiqui-Jain, A.; Hurley, L. H. Visualizing the Quadruplex. *Nat. Chem.* **2013**, *5*, 153.

(19) Sen, D.; Gilbert, W. A Sodium-Potassium Switch in the Formation of Four-Stranded G4-DNA. *Nature* **1990**, *344* (6265), 410–414. https://doi.org/10.1038/344410a0.

(20) Balasubramanian, S.; Hurley, L. H. UKPMC Funders Group Targeting G-Quadruplexes in Gene Promoters : A Novel Anticancer Strategy? *Nat. Rev. Drug Discov.* **2011**, *10* (4), 261–275. https://doi.org/10.1038/nrd3428.

(21) Bugaut, A.; Balasubramanian, S. A Sequence-Independent Study of the Influence of Short Loop Lengths on the Stability and Topology of Intramolecular DNA G-Quadraplexes. *Biochemistry* **2008**, *47* (2), 689–697. https://doi.org/10.1021/bi701873c.

(22) Patel, D. J.; Phan, A. T.; Kuryavyi, V. Human Telomere, Oncogenic Promoter and 5′-UTR

G-Quadruplexes: Diverse Higher Order DNA and RNA Targets for Cancer Therapeutics. *Nucleic Acids Res.* **2007**, *35* (22), 7429–7455. https://doi.org/10.1093/nar/gkm711.

(23) Burge, S.; Parkinson, G. N.; Hazel, P.; Todd, A. K.; Neidle, S. Quadruplex DNA: Sequence, Topology and Structure. *Nucleic Acids Res.* **2006**, *34* (19), 5402–5415. https://doi.org/10.1093/nar/gkl655.

(24) Monchaud, D.; Teulade-Fichou, M. P. A Hitchhiker's Guide to G-Quadruplex Ligands. *Org. Biomol. Chem.* **2008**, *6* (4), 627–636. https://doi.org/10.1039/b714772b.

(25) Dexheimer, T. S.; Sun, D.; Hurley, L. H. Deconvoluting the Structureal and Drug-Recognition Complexity of the G-Quadruplex-Forming Region Upstream of the Bcl-2 P1 Promoter. *J. Am. Chem. Soc.* **2006**, 5404–5415.

(26) Siddiqui-Jain, A.; Grand, C. L.; Bearss, D. J.; Hurley, L. H. Direct Evidence for a G-Quadruplex in a Promoter Region and Its Targeting with a Small Molecule to Repress c-MYC Transcription. *Proc. Natl. Acad. Sci. U. S. A.* **2002**, *99* (18), 11593–11598. https://doi.org/10.1073/pnas.182256799.

(27) Cogoi, S.; Xodo, L. E. G-Quadruplex Formation within the Promoter of the KRAS Proto-Oncogene and Its Effect on Transcription. *Nucleic Acids Res.* **2006**, *34* (9), 2536–2549. https://doi.org/10.1093/nar/gkl286.

(28) Rankin, S.; Reszka, A. P.; Huppert, J.; Zloh, M.; Parkinson, G. N.; Todd, A. K.; Ladame, S.; Balasubramanian, S.; Neidle, S. Putative DNA Quadruplex Formation within Th Human C-Kit Oncogene. *J. Am. Chem. Soc.* **2005**, *127* (30), 10584–10589.

(29) Sun, D.; Guo, K.; Rusche, J. J.; Hurley, L. H. Facilitation of a Structural Transition in the Polypurine/Polypyrimidine Tract within the Proximal Promoter Region of the Human VEGF Gene by the Presence of Potassium and G-Quadruplex-Interactive Agents. *Nucleic Acids Res.* **2005**, *33* (18), 6070–6080. https://doi.org/10.1093/nar/gki917.

(30) Guo, J. U.; Bartel, D. P. RNA G-Quadruplexes Are Globally Unfolded in Eukaryotic Cells and Depleted in Bacteria. *Science (80-.).* **2016**, *353* (6306), 1–8. https://doi.org/10.1126/science.aaf5371.

(31) Chambers, V. S.; Marsico, G.; Boutell, J. M.; Di Antonio, M.; Smith, G. P.; Balasubramanian, S. High-Throughput Sequencing of DNA G-Quadruplex Structures in the Human Genome. *Nat. Biotechnol.* **2015**, *33* (8), 877–881. https://doi.org/10.1038/nbt.3295.

(32) Marsico, G.; Chambers, V. S.; Sahakyan, A. B.; McCauley, P.; Boutell, J. M.; Antonio, M. Di; Balasubramanian, S. Whole Genome Experimental Maps of DNA G-Quadruplexes in Multiple Species. *Nucleic Acids Res.* **2019**, *47* (8), 3862–3874. https://doi.org/10.1093/nar/gkz179.

(33) Huppert, J. L.; Balasubramanian, S. G-Quadruplexes in Promoters throughout the Human Genome. *Nucleic Acids Res.* **2007**, *35* (2), 406–413. https://doi.org/10.1093/nar/gkl1057.

(34) De Cian, A.; Lacroix, L.; Douarre, C.; Temime-Smaali, N.; Trentesaux, C.; Riou, J. F.; Mergny, J. L. Targeting Telomeres and Telomerase. *Biochimie* **2008**, *90*, 131–155. https://doi.org/10.1016/j.biochi.2007.07.011.

(35) Varshney, D.; Spiegel, J.; Zyner, K.; Tannahill, D.; Balasubramanian, S. The Regulation and Functions of DNA and RNA G-Quadruplexes. *Nat. Rev. Mol. Cell Biol.* **2020**, *21* (8), 459–474. https://doi.org/10.1038/s41580-020-0236-x.

(36) Savva, L.; Georgiades, S. N. Recent Developments in Small-Molecule Ligands of Medicinal Relevance for Harnessing the Anticancer Potential of g-Quadruplexes. *Molecules* **2021**, *26*, 1–27. https://doi.org/10.3390/molecules26040841.

(37) Shay, J. W.; Wright, W. E. Telomeres and Telomerase: Three Decades of Progress. *Nat. Rev. Genet.* **2019**, *20* (5), 299–309. https://doi.org/10.1038/s41576-019-0099-1.

(38) Hwang, H.; Buncher, N.; Opresko, P. L.; Myong, S. POT1-TPP1 Regulated Telomeric Overhang Structural Dynamics. *Struct. Des.* **2012**, *20* (11), 1872–1880. https://doi.org/10.1016/j.str.2012.08.018.

(39) Zahler, A. M.; Williamson, J. R.; Cech, T. R.; Prescott, D. M. Inhibition of Telomerase by G-Quartet DMA Structures. *Nature* **1991**, *350* (6320), 718–720. https://doi.org/10.1038/350718a0.

(40) Oganesian, L.; Bryan, T. M. Physiological Relevance of Telomeric G-Quadruplex Formation : A Potential Drug Target. *BioEssays* **2007**, *29*, 155–165. https://doi.org/10.1002/bies.20523.

(41) Kelland, L. Targeting the Limitless Replicative Potential of Cancer : The Telomerase / Telomere Pathway. *Mol. Pathways* **2007**, *13* (17), 4960–4964. https://doi.org/10.1158/1078-0432.CCR-07-0422.

(42) Clark, G. R.; Pytel, P. D.; Squire, C. J.; Neidle, S. Structure of the First Parallel DNA

Quadruplex-Drug Complex. *J. Am. Chem. Soc.* **2003**, *125* (14), 4066–4067. https://doi.org/10.1021/ja0297988.

(43) Rodriguez, R.; Müller, S.; Yeoman, J. A.; Trentesaux, C.; Riou, J. F.; Balasubramanian, S. A Novel Small Molecule That Alters Shelterin Integrity and Triggers a DNA-Damage Response at Telomeres. *J. Am. Chem. Soc.* **2008**, *130* (47), 15758–15759. https://doi.org/10.1021/ja805615w.

(44) Mergny, J. L.; Lacroix, L.; Teulade-Fichou, M. P.; Hounsou, C.; Guittat, L.; Hoarau, M.; Arimondo, P. B.; Vigneron, J. P.; Lehn, J. M.; Riou, J. F.; Garestier, T.; Hélène, C. Telomerase Inhibitors Based on Quadruplex Ligands Selected by a Fluorescence Assay. *Proc. Natl. Acad. Sci. U. S. A.* **2001**, *98* (6), 3062–3067. https://doi.org/10.1073/pnas.051620698.

(45) Hounsou, C.; Guittat, L.; Monchaud, D.; Jourdan, M.; Saettel, N.; Mergny, J.; Teulade-fichou, M. G-Quadruplex Recognition by Quinacridines : A SAR , NMR , and Biological Study. *ChemMedChem* **2007**, *2*, 655–666. https://doi.org/10.1002/cmdc.200600286.

(46) Simonsson, T.; Pecinka, P.; Kubista, M. DNA Tetraplex Formation in the Control Region of C-Myc. *Nucleic Acids Res.* **1998**, *26* (5), 1167–1172.

(47) Brooks, T. A.; Hurley, L. H. Targeting MYC Expression through G-Quadruplexes. *Genes Cancer* **2010**, *1* (6), 641–649. https://doi.org/10.1177/1947601910377493.

(48) Brown, R. V.; Danford, F. L.; Gokhale, V.; Hurley, L. H.; Brooks, T. A. Demonstration That Drug-Targeted down-Regulation of MYC in Non-Hodgkins Lymphoma Is Directly Mediated through the Promoter G-Quadruplex. *J. Biol. Chem.* **2011**, *286* (47), 41018–41027. https://doi.org/10.1074/jbc.M111.274720.

(49) Grand, C. L.; Han, H.; Mũnoz, R. M.; Weitman, S.; Von Hoff, D. D.; Hurley, L. H.; Bearss, D. J. The Cationic Porphyrin TMPyP4 Down-Regulates c-MYC and Human Telomerase Reverse Transcriptase Expression and Inhibits Tumor Growth in Vivo. *Mol. Cancer Ther.* **2002**, *1* (8), 565–573.

(50) Izbicka, E.; Wheelhouse, R. T.; Raymond, E.; Davidson, K. K.; Lawrence, R. A.; Sun, D.; Windle, B. E.; Hurley, L. H.; Von Hoff, D. D. Effects of Cationic Porphyrins as G-Quadruplex Interactive Agents in Human Tumor Cells. *Cancer Res.* **1999**, *59* (3), 639–644.

(51) Han, F. X.; Wheelhouse, R. T.; Hurley, L. H. Interactions of TMPyP4 and TMPyP2 with

Quadruplex DNA. Structural Basis for the Differential Effects on Telomerase Inhibition. *J. Am. Chem. Soc.* **1999**, *121* (15), 3561–3570. https://doi.org/10.1021/ja984153m.

(52) Qin, Y.; Hurley, L. H. Structures, Folding Patterns, and Functions of Intramolecular DNA G-Quadruplexes Found in Eukaryotic Promoter Regions. *Biochimie* **2008**, *90* (8), 1149–1171. https://doi.org/10.1016/j.biochi.2008.02.020.

(53) Han, H.; Langley, D. R.; Rangan, A.; Hurley, L. H. Selective Interactions of Cationic Porphyrins with G-Quadruplex Structures. *J. Am. Chem. Soc.* **2001**, *123* (37), 8902–8913. https://doi.org/10.1021/ja002179j.

(54) Seenisamy, J.; Bashyam, S.; Gokhale, V.; Vankayalapati, H.; Sun, D.; Siddiqui-Jain, A.; Streiner, N.; Shin-ya, K.; White, E.; Wilson, W. D.; Hurley, L. H. Design and Synthesis of an Expanded Porphyrin That Has Selectivity for the C-MYC G-Quadruplex Structure. *J. Am. Chem. Soc.* **2005**, *127* (9), 2944–2959. https://doi.org/10.1021/ja0444482.

(55) Cian, A. De; Cristofari, G.; Reichenbach, P.; Lemos, E. De; Monchaud, D.; Teulade-fichou, M.; Shin-ya, K.; Lacroix, L.; Lingner, J.; Mergny, J. Reevaluation of Telomerase Inhibition by Quadruplex Ligands and Their Mechanisms of Action. *PNAS* **2007**, *104* (44), 17347–17352.

(56) Monchaud, D.; Allain, C.; Teulade-Fichou, M. P. Development of a Fluorescent Intercalator Displacement Assay (G4-FID) for Establishing Quadruplex-DNA Affinity and Selectivity of Putative Ligands. *Bioorganic Med. Chem. Lett.* **2006**, *16* (18), 4842–4845. https://doi.org/10.1016/j.bmcl.2006.06.067.

(57) Bombard, S.; Monchaud, D.; Bertrand, H.; Teulade-Fichou, M. P. A Platinum – Quinacridine Hybrid as a G-Quadruplex Ligand. *J. Biol. Inorg. Chem.* **2007**, 1003–1014. https://doi.org/10.1007/s00775-007-0273-3.

(58) Dixon, I. M.; Tejera, A. M.; Esteve, J.; Blasco, M. A.; Meunier, B. A G-Quadruplex Ligand with 10000-Fold Selectivity over Duplex DNA. *J. Am. Chem. Soc.* **2007**, *129*, 1502–1503.

(59) De Cian, A.; Guittat, L.; Shin-ya, K.; Riou, J. F.; Mergny, J.-L. Affinity and Selectivity of G4 Ligand Measured by FRET. *Nucleic Acids Symp. Ser.* **2005**, *49*, 235–236.

(60) Kim, M. Y.; Gleason-Guzman, M.; Izbicka, E.; Nishioka, D.; Hurley, L. H. The Different Biological Effects of Telomestatin and TMPyP4 Can Be Attributed to Their Selectivity for Interaction with Intramolecular or Intermolecular G-Quadruplex Structures. *Cancer*

Res. **2003**, *63* (12), 3247–3256.

(61) Doi, T.; Yoshida, M.; Shin-ya, K.; Takahashi, T. Total Synthesis of (R) -Telomestatin. *Org. Lett.* **2006**, *6*, 12–14.

(62) Xu, Y.; Kaminaga, K.; Komiyama, M. G-Quadruplex Formation by Human Telomeric Repeats-Containing RNA in Na + Solution. *J. Am. Chem. Soc.* **2008**, *130* (33), 11179–11184. https://doi.org/10.1021/ja8031532.

(63) Martadinata, H.; Phan, A. T. Structure of Propeller-Type Parallel-Stranded RNA G-Quadruplexes, Formed by Human Telomeric RNA Sequences in K+ Solution. *J. Am. Chem. Soc.* **2009**, *131* (7), 2570–2579. https://doi.org/10.1021/ja806592z.

(64) Joachimi, A.; Benz, A.; Hartig, J. S. A Comparison of DNA and RNA Quadruplex Structures and Stabilities. *Bioorganic Med. Chem.* **2009**, *17* (19), 6811–6815. https://doi.org/10.1016/j.bmc.2009.08.043.

(65) Tao, Y.; Zheng, Y.; Zhai, Q.; Wei, D. Recent Advances in the Development of Small Molecules Targeting RNA G-Quadruplexes for Drug Discovery. *Bioorg. Chem.* **2021**, *110* (February), 104804. https://doi.org/10.1016/j.bioorg.2021.104804.

(66) Ryan, D. P.; Hong, T. S.; Bardeesy, N. Pancreatic Adenocarcinoma. *N. Engl. J. Med.* **2014**, 1039–1049. https://doi.org/10.1056/NEJMra1404198.

(67) Miglietta, G.; Cogoi, S.; Marinello, J.; Capranico, G.; Tikhomirov, A. S.; Shchekotikhin, A.; Xodo, L. E. RNA G-Quadruplexes in Kirsten Ras (KRAS) Oncogene as Targets for Small Molecules Inhibiting Translation. *J. Med. Chem.* **2017**, *60* (23), 9448–9461. https://doi.org/10.1021/acs.jmedchem.7b00622.

(68) Zuker, M. Mfold Web Server for Nucleic Acid Folding and Hybridization Prediction. *Nucleic Acids Res.* **2003**, *31* (13), 3406–3415. https://doi.org/10.1093/nar/gkg595.

(69) Biffi, G.; Tannahill, D.; McCafferty, J.; Balasubramanian, S. Quantitative Visualization of DNA G-Quadruplex Structures in Human Cells. *Nat. Chem.* **2013**, *5* (3), 182–186. https://doi.org/10.1038/nchem.1548.

(70) G-quadruplex, S. T.; Yangyuoru, P. M.; Antonio, M. Di; Ghimire, C.; Biffi, G. Dual Binding of an Antibody and a Small Molecule Increases The. *Angew. Commun.* **2015**, 910–913. https://doi.org/10.1002/anie.201408113.

(71) Kumari, S.; Bugaut, A.; Huppert, J. L.; Balasubramanian, S. An RNA G-Quadruplex in

the 5′ UTR of the NRAS Proto-Oncogene Modulates Translation. *Nat. Chem. Biol.* **2007**, *3* (4), 218–221. https://doi.org/10.1038/nchembio864.

(72) Bugaut, A.; Rodriguez, R.; Kumari, S.; Hsu, S. T. D.; Balasubramanian, S. Small Molecule-Mediated Inhibition of Translation by Targeting a Native RNA G-Quadruplex. *Org. Biomol. Chem.* **2010**, *8* (12), 2771–2776. https://doi.org/10.1039/c002418j.

(73) Katsuda, Y.; Sato, S. I.; Asano, L.; Morimura, Y.; Furuta, T.; Sugiyama, H.; Hagihara, M.; Uesugi, M. A Small Molecule That Represses Translation of G-Quadruplex-Containing MRNA. *J. Am. Chem. Soc.* **2016**, *138* (29), 9037–9040. https://doi.org/10.1021/jacs.6b04506.

(74) Morris, M. J.; Wingate, K. L.; Silwal, J.; Leeper, T. C.; Basu, S. The Porphyrin TmPyP4 Unfolds the Extremely Stable G-Quadruplex in MT3-MMP MRNA and Alleviates Its Repressive Effect to Enhance Translation in Eukaryotic Cells. *Nucleic Acids Res.* **2012**, *40* (9), 4137–4145. https://doi.org/10.1093/nar/gkr1308.

(75) Asamitsu, S.; Obata, S.; Yu, Z.; Bando, T.; Sugiyama, H. Recent Progress of Targeted G-Quadruplex-Preferred Ligands toward Cancer Therapy. *Molecules* **2019**, *24* (3). https://doi.org/10.3390/molecules24030429.

(76) Sainsbury, S.; Bernecky, C.; Cramer, P. Structural Basis of Transcription Initiation by RNA Polymerase II. *Nat. Publ. Gr.* **2015**, *16*, 129–143. https://doi.org/10.1038/nrm3952.

(77) Boeger, H.; Bushnell, D. A.; Davis, R.; Griesenbeck, J.; Lorch, Y.; Strattan, J. S.; Westover, K. D.; Kornberg, R. D. Structural Basis of Eukaryotic Gene Transcription. *FEBS Lett.* **2005**, *579*, 899–903. https://doi.org/10.1016/j.febslet.2004.11.027.

(78) Tazi, J.; Bakkour, N.; Stamm, S. Alternative Splicing and Disease. *Biochim. Biophys. Acta* **2009**, *1792* (1), 14–26. https://doi.org/10.1016/j.bbadis.2008.09.017.

(79) Proudfoot, N. J.; Furger, A.; Dye, M. J.; William, S. Integrating MRNA Processing with Transcription. *Cell* **2002**, *108*, 501–512.

(80) Proudfoot, N. J. Connecting Transcription to Messenger RNA Processing. *Trends Biochem. Sci.* **2000**, *25* (6), 290–293. https://doi.org/10.1016/S0968-0004(00)01591-7.

(81) Scotti, M. M.; Swanson, M. S. RNA Mis-Splicing in Disease. *Nat. Rev. Genet.* **2015**, *17*, 19.

(82) Goodall, G. J.; Wickramasinghe, V. O. RNA in Cancer. *Nat. Rev. Cancer* **2021**, *21*, 22–

36. https://doi.org/10.1038/s41568-020-00306-0.

(83) Taladriz-Sender, A.; Campbell, E.; Burley, G. A. Splice-Switching Small Molecules: A New Therapeutic Approach to Modulate Gene Expression. *Methods* **2019**, *167* (February), 134–142. https://doi.org/10.1016/j.ymeth.2019.06.011.

(84) Wahl, M. C.; Will, C. L.; Lührmann, R. The Spliceosome: Design Principles of a Dynamic RNP Machine. *Cell* **2009**, *136* (4), 701–718. https://doi.org/10.1016/j.cell.2009.02.009.

(85) Chen, M.; Manley, J. L. Mechanisms of Alternative Splicing Regulation: Insights from Molecular and Genomics Approaches. *Nat. Rev. Mol. Cell Biol.* **2009**, *10* (11), 741–754. https://doi.org/10.1038/nrm2777.

(86) Yang, H.; Beutler, B.; Zhang, D. Emerging Roles of Spliceosome in Cancer and Immunity. *Protein Cell* **2021**. https://doi.org/10.1007/s13238-021-00856-5.

(87) Keren, H.; Lev-Maor, G.; Ast, G. Alternative Splicing and Evolution: Diversification, Exon Definition and Function. *Nat. Rev. Genet.* **2010**, *11* (5), 345–355. https://doi.org/10.1038/nrg2776.

(88) Kornblihtt, A. R.; Schor, I. E.; Alló, M.; Dujardin, G.; Petrillo, E.; Muñoz, M. J. Alternative Splicing: A Pivotal Step between Eukaryotic Transcription and Translation. *Nat. Rev. Mol. Cell Biol.* **2013**, *14*, 153.

(89) Fairbrother, W. G.; Yeh, R.-F.; Sharp, P. A.; Burge, C. B. Predictive Identification of Exonic Splicing Enhancers in Human Genes. *Science (80-.).* **2014**, *1007* (2002), 1001–1013. https://doi.org/10.1126/science.1073774.

(90) Cartegni, L.; Chew, S. L.; Krainer, A. R. Listening to Silence and Understanding Nonesense: Exonic Mutations That Affect Splicing. *Nat. Rev. Genet.* **2002**, *3* (April), 285–298. https://doi.org/10.1038/nrg775.

(91) Manning, K. S.; Cooper, T. A. The Roles of RNA Processing in Translating Genotype to Phenotype. *Nat. Rev. Mol. Cell Biol.* **2017**, *18*, 102–114. https://doi.org/10.1038/nrm.2016.139.

(92) Makarova, O. V. The Evolution of Cellular Machines: Spliceosome: The Unravelling Complexity. *Biochem. (Lond).* **2014**, *36* (5), 46–52.

(93) Barta, A.; Jantsch, M. F. RNA in Disease and Development. *RNA Biol.* **2017**, *14* (5), 457–459. https://doi.org/10.1080/15476286.2017.1316929.

(94) Pan, Q.; Shai, O.; Lee, L. J.; Frey, B. J.; Blencowe, B. J. Deep Surveying of Alternative Splicing Complexity in the Human Transcriptome by High-Throughput Sequencing. *Nat. Genet.* **2008**, *40*, 1413–1415.

(95) Schoch, K. M.; Miller, T. M. Antisense Oligonucleotides: Translation from Mouse Models to Human Neurodegenerative Diseases. *Neuron* **2017**, *94* (6), 1056–1070. https://doi.org/10.1016/j.neuron.2017.04.010.

(96) Rinaldi, C.; Wood, M. J. A. Antisense Oligonucleotides: The next Frontier for Treatment of Neurological Disorders. *Nat. Rev. Neurol.* **2018**, *14* (1), 9–22. https://doi.org/10.1038/nrneurol.2017.148.

(97) Hua, Y.; Sahashi, K.; Hung, G.; Rigo, F.; Passini, M. A.; Bennett, C. F.; Krainer, A. R. Antisense Correction of SMN2 Splicing in the CNS Rescues Necrosis in a Type III SMA Mouse Model. *Genes Dev.* **2010**, *24* (15), 1634–1644. https://doi.org/10.1101/gad.1941310.

(98) Wan, L.; Dreyfuss, G. Splicing-Correcting Therapy for SMA. *Cell* **2017**, *170* (1), 5. https://doi.org/10.1016/j.cell.2017.06.028.

(99) Lally, C.; Jones, C.; Farwell, W.; Reyna, S. P.; Cook, S. F.; Flanders, W. D. Indirect Estimation of the Prevalence of Spinal Muscular Atrophy Type I, II, and III in the United States. *Orphanet J. Rare Dis.* **2017**, *12* (1), 1–6. https://doi.org/10.1186/s13023-017-0724-z.

(100) Singh, R. N.; Ottesen, E. W.; Singh, N. N. The First Orally Deliverable Small Molecule for the Treatment of Spinal Muscular Atrophy. *Neurosci. Insights* **2020**, *15*. https://doi.org/10.1177/2633105520973985.

(101) Buratti, E.; Baralle, M.; Baralle, F. E. Defective Splicing , Disease and Therapy : Searching for Master Checkpoints in Exon Definition. *Nucleic Acids Res.* **2006**, *34* (12), 3494–3510. https://doi.org/10.1093/nar/gkl498.

(102) Chiriboga, C. A.; Swoboda, K. J.; Darras, B. T.; Iannaccone, S. T.; Montes, J.; De Vivo, D. C.; Norris, D. A.; Bennett, C. F.; Bishop, K. M. Results from a Phase 1 Study of Nusinersen (ISIS-SMN(Rx)) in Children with Spinal Muscular Atrophy. *Neurology* **2016**, *86* (10), 890–897. https://doi.org/10.1212/WNL.0000000000002445.

(103) (FDA), F. and D. A. FDA approves first drug for spinal muscular atrophy https://www.fda.gov/newsevents/newsroom/pressannouncements/ucm534611.htm

(accessed 2016 -08 -08). https://doi.org/10.1016/j.clinph.2007.10.014.

(104) Naryshkin, N. A.; Babiak, J.; Almstead, N. G.; Peltz, S. W.; Eng, L. A.; Chen, K. S.; Mull, J. L.; Lynes, M. S.; Rubin, L. L.; Fontoura, P.; Santarelli, L.; Haehnke, D.; Mccarthy, K. D.; Schmucki, R.; Ebeling, M.; Sivaramakrishnan, M.; Ko, C.; Paushkin, S. V; Ratni, H. SMN2 Splicing Modifiers Improve Motor Function and Longevity in Mice with Spinal Muscular Atrophy. *Science (80-.).* **2014**, *345* (6197), 688–692. https://doi.org/10.1126/science.1250127.

(105) Palacino, J.; Swalley, S. E.; Song, C.; Cheung, A. K.; Shu, L.; Zhang, X.; Van Hoosear, M.; Shin, Y.; Chin, D. N.; Keller, C. G.; Beibel, M.; Renaud, N. A.; Smith, T. M.; Salcius, M.; Shi, X.; Hild, M.; Servais, R.; Jain, M.; Deng, L.; Bullock, C.; McLellan, M.; Schuierer, S.; Murphy, L.; Blommers, M. J. J.; Blaustein, C.; Berenshteyn, F.; Lacoste, A.; Thomas, J. R.; Roma, G.; Michaud, G. A.; Tseng, B. S.; Porter, J. A.; Myer, V. E.; Tallarico, J. A.; Hamann, L. G.; Curtis, D.; Fishman, M. C.; Dietrich, W. F.; Dales, N. A.; Sivasankaran, R. SMN2 Splice Modulators Enhance U1-Pre-MRNA Association and Rescue SMA Mice. *Nat. Chem. Biol.* **2015**, *11* (7), 511–517. https://doi.org/10.1038/nchembio.1837.

(106) Ratni, H.; Karp, G. M.; Weetall, M.; Naryshkin, N. A.; Paushkin, S. V.; Chen, K. S.; McCarthy, K. D.; Qi, H.; Turpoff, A.; Woll, M. G.; Zhang, X.; Zhang, N.; Yang, T.; Dakka, A.; Vazirani, P.; Zhao, X.; Pinard, E.; Green, L.; David-Pierson, P.; Tuerck, D.; Poirier, A.; Muster, W.; Kirchner, S.; Mueller, L.; Gerlach, I.; Metzger, F. Specific Correction of Alternative Survival Motor Neuron 2 Splicing by Small Molecules: Discovery of a Potential Novel Medicine to Treat Spinal Muscular Atrophy. *J. Med. Chem.* **2016**, *59* (13), 6086–6100. https://doi.org/10.1021/acs.jmedchem.6b00459.

(107) Ratni, H.; Ebeling, M.; Baird, J.; Bendels, S.; Bylund, J.; Chen, K. S.; Denk, N.; Feng, Z.; Green, L.; Guerard, M.; Jablonski, P.; Jacobsen, B.; Khwaja, O.; Kletzl, H.; Ko, C. P.; Kustermann, S.; Marquet, A.; Metzger, F.; Mueller, B.; Naryshkin, N. A.; Paushkin, S. V.; Pinard, E.; Poirier, A.; Reutlinger, M.; Weetall, M.; Zeller, A.; Zhao, X.; Mueller, L. Discovery of Risdiplam, a Selective Survival of Motor Neuron-2 (SMN2) Gene Splicing Modifier for the Treatment of Spinal Muscular Atrophy (SMA). *J. Med. Chem.* **2018**, *61* (15), 6501–6517. https://doi.org/10.1021/acs.jmedchem.8b00741.

(108) Wang, J.; Schultz, P. G.; Johnson, K. A. Mechanistic Studies of a Small-Molecule Modulator of SMN2 Splicing. *Proc. Natl. Acad. Sci. U. S. A.* **2018**, *115* (20), E4604–

E4612. https://doi.org/10.1073/pnas.1800260115.

(109) Campagne, S.; Boigner, S.; Rüdisser, S.; Moursy, A.; Gillioz, L.; Knörlein, A.; Hall, J.; Ratni, H.; Cléry, A.; Allain, F. H. T. Structural Basis of a Small Molecule Targeting RNA for a Specific Splicing Correction. *Nat. Chem. Biol.* **2019**, *15* (12), 1191–1198. https://doi.org/10.1038/s41589-019-0384-5.

(110) Hardwick, J. M.; Soane, L. Multiple Functions of BCL-2 Family Proteins. *Cold Spring Harb. Perspect. Biol.* **2013**, *5* (2), a008722–a008722. https://doi.org/10.1101/cshperspect.a008722.

(111) Willimott, S.; Merriam, T.; Wagner, S. D. Apoptosis Induces Bcl-XS and Cleaved Bcl-XL in Chronic Lymphocytic Leukaemia. *Biochem. Biophys. Res. Commun.* **2011**, *405* (3), 480–485. https://doi.org/10.1016/j.bbrc.2011.01.057.

(112) Hossini, A. M.; Eberle, J.; Fecker, L. F.; Orfanos, C. E.; Geilen, C. C. Conditional Expression of Exogenous Bcl-XStriggers Apoptosis in Human Melanoma Cells in Vitro and Delays Growth of Melanoma Xenografts. *FEBS Lett.* **2003**, *553* (3), 250–256. https://doi.org/10.1016/S0014-5793(03)01017-2.

(113) Boddupally, P. V. L.; Hahn, S.; Beman, C.; De, B.; Brooks, T. A.; Gokhale, V.; Hurley, L. H. Anticancer Activity and Cellular Repression of C-MYC by the G-Quadruplex-Stabilizing 11-Piperazinylquindoline Is Not Dependent on Direct Targeting of the G-Quadruplex in the c-MYC Promoter. *J. Med. Chem.* **2012**, *55* (13), 6076–6086. https://doi.org/10.1021/jm300282c.

(114) Chen, B.-J.; Wu, Y.-L.; Tanaka, Y.; Zhang, W. Small Molecules Targeting C-Myc Oncogene: Promising Anti-Cancer Therapeutics. *Int. J. Biol. Sci.* **2014**, *10* (10), 1084–1096. https://doi.org/10.7150/ijbs.10190.

(115) Weldon, C.; Dacanay, J. G.; Gokhale, V.; Boddupally, P. V. L.; Behm-Ansmant, I.; Burley, G. A.; Branlant, C.; Hurley, L. H.; Dominguez, C.; Eperon, I. C. Specific G-Quadruplex Ligands Modulate the Alternative Splicing of Bcl-X. *Nucleic Acids Res.* **2017**, 1–11. https://doi.org/10.1093/nar/gkx1122.

(116) Rutherford, Olivia, I. Splice Switching Small Molecules as Inducers of Apoptosis, University of Strathclyde, 2018.

(117) Kochi, J. K.; Tamura, M. Vinylation of Grignard Reagents. Catalysis by Iron. *J. Am. Chem. Soc.* **1968**, *497* (I), 1968–1970.

(118) Campeau, L. C.; Thansandote, P.; Fagnou, K. High-Yielding Intramolecular Direct Arylation Reactions with Aryl Chlorides. *Org. Lett.* **2005**, *7* (9), 1857–1860. https://doi.org/10.1021/ol050501v.

(119) Miyaura, N.; Yamada, K.; Suzuki, A. A New Stereospecific Cross-Coupling by the Palladium-Catalyzed Reaction of 1-Alkenylboranes with 1-Alkenyl or 1-Alkynl Halides. *Tetrahedron Lett.* **1979**, *36*, 3437–3440.

(120) King, A. O.; Okukado, N.; Negishi, E. Highly General Stereo- , Regio- , and Chemo-Selective Synthesis of Terminal and Internal Conjugated Enynes by the Pd -Catalysed Reaction of Alkynylzinc Reagents with Alkenyl Halides. *J. Chem. Soc.* **1977**, 683–684.

(121) Heck, R. F. The Mechanism of Arylation and Carbomethoxylation of Olefins with Organopalladium Compounds / C = CC. *J. Am. Chem. Soc.* **1968**, *5518* (1), 6707–6714.

(122) Larsen, R. D.; King, A. O.; Chen, C. Y.; Corley, E. G.; Foster, B. S.; Roberts, F. E.; Yang, C.; Lieberman, D. R.; Reamer, R. A.; Tschaen, D. M.; Verhoeven, T. R.; Reider, P. J.; Lo, Y. S.; Rossano, L. T.; Brookes, A. S.; Meloni, D.; Moore, J. R.; Arnett, J. F. Efficient Synthesis of Losarían , A Nonpeptide Angiotensin II Receptor Antagonist. *J. Org. Chem.* **1994**, *59* (21), 6391–6394. https://doi.org/https://doi.org/10.1021/jo00100a048.

(123) Campeau, L.-C.; Thansandote, P.; Fagnou, K. High-Yielding Intramolecular Direct Arylation Reactions with Aryl Chlorides. *Org. Lett.* **2005**, *7* (9), 1857–1860. https://doi.org/10.1021/ol050501v.

(124) Ruiz-Castillo, P.; Buchwald, S. L. Applications of Palladium-Catalyzed C-N Cross-Coupling Reactions. *Chem. Rev.* **2016**, *116* (19), 12564–12649. https://doi.org/10.1021/acs.chemrev.6b00512.

(125) Biffis, A.; Centomo, P.; Del Zotto, A.; Zecca, M. Pd Metal Catalysts for Cross-Couplings and Related Reactions in the 21st Century: A Critical Review. *Chem. Rev.* **2018**, *118* (4), 2249–2295. https://doi.org/10.1021/acs.chemrev.7b00443.

(126) Paul, F.; Patt, J.; Hartwig, J. F. Palladium-Catalyzed Formation of Carbon-Nitrogen Bonds. Reaction Intermediates and Catalyst Improvements in the Hetero Cross-Coupling of Aryl Halides and Tin Amides. *J. Am. Chem. Soc.* **1994**, *116* (13), 5969–5970.

(127) Buchwald, S. L.; Guram, A. S. Palladium-Catalyzed Aromatic Aminations with in Situ Generated Aminostannanes. *J. Am. Chem. Soc.* **1994**, *116* (10), 7901–7902.

(128) Biscoe, M. R.; Fors, B. P.; Buchwald, S. L. A New Class of Easily Activated Palladium Precatalysts for Facile C - N Cross-Coupling Reactions and the Low Temperature Oxidative Addition of Aryl Chlorides. *J. Am. Chem. Soc.* **2008**, *130*, 6686–6687.

(129) Fleckenstein, C. A.; Plenio, H. Sterically Demanding Trialkylphosphines for Palladium-Catalyzed Cross Coupling Reactions — Alternatives to P t Bu 3. *Chem. Soc. Rev.* **2010**, *39*, 694–711. https://doi.org/10.1039/b903646f.

(130) Dı, S.; Marion, N.; Nolan, S. P. N-Heterocyclic Carbenes in Late Transition Metal Catalysis. *Chem. Rev.* **2009**, *109*, 3612–3676.

(131) Kantchev, E. A. B.; Brien, C. J. O.; Organ, M. G. Palladium Catalysis Palladium Complexes of N-Heterocyclic Carbenes as Catalysts for Cross-Coupling Reactions — A Synthetic Chemist s Perspective Angewandte. *Angew. Chemie - Int. Ed.* **2007**, *46*, 2768–2813. https://doi.org/10.1002/anie.200601663.

(132) Herrmann, W. A. N-Heterocyclic Carbenes : A New Concept in Organometallic Catalysis. *Angew. Chemie Int. Ed.* **2002**, *41*, 1290–1309.

(133) Zim, D.; Buchwald, S. L. An Air and Thermally Stable One-Component Catalyst for the Amination of Aryl Chlorides. *Org. Lett.* **2003**, *5* (14), 2413–2415. https://doi.org/10.1021/ol034561h.

(134) Valente, C.; Pompeo, M.; Sayah, M.; Organ, M. G. Carbon − Heteroatom Coupling Using Pd-PEPPSI Complexes. *Org. Process Res. Dev.* **2014**, *18*, 180–190.

(135) Tsang, W. C. P.; Zheng, N.; Buchwald, S. L. Combined C-H Functionalization/C-N Bond Formation Route to Carbazoles. *J. Am. Chem. Soc.* **2005**, *127* (42), 14560–14561. https://doi.org/10.1021/ja055353i.

(136) Jerphagnon, T.; Gabriella, M.; Feringa, B. L. Bite Angle Effects of Diphosphines in C – C and C – X Bond Forming Cross Coupling Reactions. *Chem. Soc. Rev.* **2009**, *38* (4). https://doi.org/10.1039/b806211k.

(137) Mc Glacken, G. P.; Bateman, L. M. Recent Advances in Aryl–Aryl Bond Formation by Direct Arylation. *Chem. Soc. Rev.* **2009**, *38* (8), 2447–2464. https://doi.org/10.1039/b805701j.

(138) Constable, D. J. C.; Dunn, P. J.; Hayler, J. D.; Humphrey, G. R.; Leazer, J. L.; Linderman, R. J.; Lorenz, K.; Manley, J.; Pearlman, B. A.; Wells, A.; Zhang, T. Y. Key Green

Chemistry Research Areas — a Perspective from Pharmaceutical Manufacturers. *Green Chem.* **2007**, *9*, 411–420. https://doi.org/10.1039/b703488c.

(139) Alberico, D.; Scott, M. E.; Lautens, M. Aryl-Aryl Bond Formation by Transition-Metal-Catalyzed Direct Arylation. *Chem. Rev.* **2007**, *107* (1), 174–238. https://doi.org/10.1021/cr0509760.

(140) Schmidt, A. W.; Reddy, K. R.; Knölker, H. J. Occurrence, Biogenesis, and Synthesis of Biologically Active Carbazole Alkaloids. *Chem. Rev.* **2012**, *112* (6), 3193–3328. https://doi.org/10.1021/cr200447s.

(141) Bedford, R. B.; Cazin, C. S. J. A Novel Catalytic One-Pot Synthesis of Carbazoles via Consecutive Amination and C-H Activation. *Chem. Commun.* **2002**, *2* (20), 2310–2311. https://doi.org/10.1039/b207712b.

(142) Ames, D. E.; Opalko, A. Palladium-Catalysed Cyclisation of 2-Substituted Halogenoarenes by Dehydrohalogenation. *Tetrahedron* **1984**, *40* (10), 1919–1925. https://doi.org/10.1016/S0040-4020(01)91149-4.

(143) Iwaki, T.; Yasuhara, A.; Sakamoto, T. Novel Synthetic Strategy of Carbolines via Palladium-Catalyzed Amination and Arylation Reaction. *J. Chem. Soc. - Perkin Trans. 1* **1999**, No. 11, 1505–1510. https://doi.org/10.1039/a901088b.

(144) Bedford, R. B.; Betham, M. N-H Carbazole Synthesis from 2-Chloroanilines via Consecutive Amination and C-H Activation. *J. Org. Chem.* **2006**, *71* (25), 9403–9410. https://doi.org/10.1021/jo061749g.

(145) Ackermann, L.; Althammer, A.; Mayer, P. Palladium-Catalyzed Direct Arylation-Based Domino Synthesis of Annulated N-Heterocycles Using Alkenyl or (Hetero)Aryl 1,2-Dihalides. *Synthesis (Stuttg).* **2009**, No. 20, 3493–3503. https://doi.org/10.1055/s-0029-1216977.

(146) Liu, Z.; Larock, R. C. Synthesis of Carbazoles and Dibenzofurans via Cross-Coupling of o-Iodoanilines and o-Iodophenols with Silylaryl Triflates and Subsequent Pd-Catalyzed Cyclization. *Tetrahedron* **2007**, *63* (2), 347–355. https://doi.org/10.1016/j.tet.2006.10.071.

(147) Dalton, L. K.; Demerac, S.; Elmes, B. C.; Loder, J. W.; Swan, J. M.; Teitei, T. Synthesis of the Tumour-Inhibitory Alkaloids, Ellipticine, 9-Methoxyellipticine, and Related Pyrido[4,3-b]Carbazoles. *Aust. J. Chem.* **1967**, *20* (12), 2715–2727.

(148) Gribble, G. W.; Saulnier, M. G.; Obaza-Nutaitis, J. A.; Ketcha, D. M. A Versatile and Efficient Construction of the 6H-Pyrido[4,3-b]Carbazole Ring System. Syntheses of the Antitumor Alkaloids Ellipticine, 9-Methoxyellipticine, and Olivacine and Their Analogues. *J. Org. Chem.* **1992**, *57* (22), 5891–5899. https://doi.org/10.1021/jo00048a022.

(149) Boogaard, A. T.; Pandit, U. K.; Koomen, G.-J. Ring D Modifications of Ellipticine. Part 2. Chlorination of Ellipticine via Its N-Oxide and Synthesis and Selective Acetylation of 5,5,11-Trimethyl-5H-Benzo[b]Carbazole. *Tetrahedron* **1994**, *50* (16), 4811–4828. https://doi.org/10.1016/S0040-4020(01)85018-3.

(150) Deane, F. M.; O'Sullivan, E. C.; Maguire, A. R.; Gilbert, J.; Sakoff, J. A.; McCluskey, A.; McCarthy, F. O. Synthesis and Evaluation of Novel Ellipticines as Potential Anti-Cancer Agents. *Org. Biomol. Chem.* **2013**, *11* (8), 1334–1344. https://doi.org/10.1039/c2ob27186a.

(151) Nishigaichi, Y.; Orimi, T.; Koyachi, K.; Ohmuro, Y.; Suzuki, M. Photochemically Assisted Introduction of a Benzyl Unit into Isoquinolines Using Benzyltrifluoroborates. *Chem. Lett.* **2016**, *45* (12), 1382–1384. https://doi.org/10.1246/cl.160762.

(152) Sridharan, V.; Antonia Martín, M.; Carlos Menéndez, J. Acid-Free Synthesis of Carbazoles and Carbazolequinones by Intramolecular Pd-Catalyzed, Microwave-Assisted Oxidative Biaryl Coupling Reactions Efficient Syntheses of Murrayafoline A, 2-Methoxy-3-Methylcarbazole, and Glycozolidine. *European J. Org. Chem.* **2009**, No. 27, 4614–4621. https://doi.org/10.1002/ejoc.200900537.

(153) Guchhait, S. K.; Saini, M. Chan-Lam: N -Arylation and C-H Amination with Heteroaromatic Ring-NH: An Approach to Access Extended-Fused Imidazo[1,2- a] -Pyridines/Pyrazines. *New J. Chem.* **2019**, *44* (2), 308–312. https://doi.org/10.1039/c9nj04966e.

(154) Lafrance, M.; Fagnou, K. Palladium-Catalyzed Benzene Arylation: Incorporation of Catalytic Pivalic Acid as a Proton Shuttle and a Key Element in Catalyst Design. *J. Am. Chem. Soc.* **2006**, *128* (51), 16496–16497. https://doi.org/10.1021/ja067144j.

(155) Mandal, T.; Chakraborti, G.; Karmakar, S.; Dash, J. Divergent and Orthogonal Approach to Carbazoles and Pyridoindoles from Oxindoles via Indole Intermediates. *Org. Lett.* **2018**, *20* (16), 4759–4763. https://doi.org/10.1021/acs.orglett.8b01827.

(156) Chakraborti, G.; Paladhi, S.; Mandal, T.; Dash, J. "on Water" Promoted Ullmann-Type C-N Bond-Forming Reactions: Application to Carbazole Alkaloids by Selective N-Arylation of Aminophenols. *J. Org. Chem.* **2018**, *83* (14), 7347–7359. https://doi.org/10.1021/acs.joc.7b03020.

(157) Pelaprat, D.; Oberlin, R.; Guen, I. Le; Roques, B. P.; Le Pecq, J. B. DNA Intercalating Compounds as Potential Antitumor Agents. 2. Preparation and Properties of 7H-Pyridocarbazole Dimers. *J. Med. Chem.* **1980**, *23* (12), 1336–1343. https://doi.org/10.1021/jm00186a010.

(158) Léon, P.; Garbay-Jaureguiberry, C.; Roques, B. P.; Lambert, B.; Pecq, J. B. L. Asymmetrical Bisintercalators as Potential Antitumor Agents. *J. Med. Chem.* **1988**, *31* (5), 1021–1026. https://doi.org/10.1021/jm00400a023.

(159) Ramkumar, N.; Nagarajan, R. Formal Total Synthesis of Calothrixin B and Its N-Benzyl Analogues. *RSC Adv.* **2015**, *5* (107), 87838–87840. https://doi.org/10.1039/c5ra18120h.

(160) Guo, S.; Tipparaju, S. K.; Pegan, S. D.; Wan, B.; Mo, S.; Orjala, J.; Mesecar, A. D.; Franzblau, S. G.; Kozikowski, A. P. Natural Product Leads for Drug Discovery: Isolation, Synthesis and Biological Evaluation of 6-Cyano-5-Methoxyindolo[2,3-a]Carbazole Based Ligands as Antibacterial Agents. *Bioorganic Med. Chem.* **2009**, *17* (20), 7126–7130. https://doi.org/10.1016/j.bmc.2009.08.061.

(161) Miki, Y.; Tada, Y.; Matsushita, K. Reaction of 1-Benzylindole-2,3-Dicarboxylic Anhydride with 3-Bromo-4-Lithiopyridine: Formal Synthesis of Ellipticine. *Heterocycles* **1998**, *48*, 1998.

(162) Shiotani, A.; Itatani, H. Dibenzofurans by Intramolecular Ring Closure Reactions. *Angew. Chemie Int. Ed. English* **1974**, *13* (7), 471–472. https://doi.org/10.1002/anie.197404711.

(163) Ackermann, L.; Vicente, R.; Kapdi, A. R. Transition-Metal-Catalyzed Direct Arylation of (Hetero)Arenes by C-H Bond Cleavage. *Angew. Chemie - Int. Ed.* **2009**, *48* (52), 9792–9826. https://doi.org/10.1002/anie.200902996.

(164) Lapointe, D.; Fagnou, K. Overview of the Mechanistic Work on the Concerted Metallation-Deprotonation Pathway. *Chem. Lett.* **2010**, *39*, 1118-. https://doi.org/10.1246/cl.2010.1118.

(165) Mueller, J. A.; Goller, C. P.; Sigman, M. S. Elucidating the Significance of β-Hydride Elimination and the Dynamic Role of Acid/Base Chemistry in a Palladium-Catalyzed

Aerobic Oxidation of Alcohols. *J. Am. Chem. Soc.* **2004**, *126* (31), 9724–9734. https://doi.org/10.1021/ja047794s.

(166) Yamakawa, M.; Ito, H.; Noyori, R. The Metal-Ligand Bifunctional Catalysis: A Theoretical Study on the Ruthenium(II)-Catalyzed Hydrogen Transfer between Alcohols and Carbonyl Compounds. *J. Am. Chem. Soc.* **2000**, *122* (7), 1466–1478. https://doi.org/10.1021/ja991638h.

(167) Davidson, M.; Triggs, C. Reaction of Metal Ion Complexes with Hydrocarbons. *J. Chem. Soc.* **1968**, *5* (1324), 1324–1330.

(168) Parisien, M.; Valette, D.; Fagnou, K. Direct Arylation Reactions Catalyzed by Pd(OH)2/C: Evidence for a Soluble Palladium Catalyst. *J. Org. Chem.* **2005**, *70* (19), 7578–7584. https://doi.org/10.1021/jo051039v.

(169) Leblanc, M.; Fagnou, K. Allocolchicinoid Synthesis via Direct Arylation. *Org. Lett.* **2005**, *7* (14), 2849–2852. https://doi.org/10.1021/ol0505959.

(170) Campeau, L. C.; Parisien, M.; Jean, A.; Fagnou, K. Catalytic Direct Arylation with Aryl Chlorides, Bromides, and Iodides: Intramolecular Studies Leading to New Intermolecular Reactions. *J. Am. Chem. Soc.* **2006**, *128* (2), 581–590. https://doi.org/10.1021/ja055819x.

(171) Campeau, L.-C.; Parisien, M.; Jean, A.; Fagnou, K. Catalytic Direct Arylation with Aryl Chlorides, Bromides, and Iodides: Intramolecular Studies Leading to New Intermolecular Reactions. *J. Am. Chem. Soc.* **2006**, *128* (2), 581–590. https://doi.org/10.1021/ja055819x.

(172) Wang, X.; Lane, B. S.; Sames, D. Direct C-Arylation of Free (NH)-Indoles and Pyrroles Catalyzed by Ar-Rh(III) Complexes Assembled in Situ. *J. Am. Chem. Soc.* **2005**, *127* (14), 4996–4997. https://doi.org/10.1021/ja050279p.

(173) Campo, M. A.; Huang, Q.; Yao, T.; Tian, Q.; Larock, R. C. 1,4-Palladium Migration via C-H Activation, Followed by Arylation: Synthesis of Fused Polycycles. *J. Am. Chem. Soc.* **2003**, *125* (38), 11506–11507. https://doi.org/10.1021/ja035121o.

(174) García-Cuadrado, D.; Braga, A. A. C.; Maseras, F.; Echavarren, A. M. Proton Abstraction Mechanism for the Palladium-Catalyzed Intramolecular Arylation. *J. Am. Chem. Soc.* **2006**, *128* (4), 1066–1067. https://doi.org/10.1021/ja056165v.

(175) Campeau, L. C.; Parisien, M.; Leblanc, M.; Fagnou, K. Biaryl Synthesis via Direct Arylation: Establishment of an Efficient Catalyst for Intramolecular Processes. *J. Am.*

Chem. Soc. **2004**, *126* (30), 9186–9187. https://doi.org/10.1021/ja049017y.

(176) Lafrance, M.; Blaquière, N.; Fagnou, K. Direct Intramolecular Arylation of Unactivated Arenes: Application to the Synthesis of Aporphine Alkaloids. *Chem. Commun.* **2004**, *2004* (24), 2874–2875. https://doi.org/10.1039/b410394g.

(177) Mota, A. J.; Dedieu, A.; Bour, C.; Suffert, J. Cyclocarbopalladation Involving an Unusual 1,5-Palladium Vinyl to Aryl Shift as Termination Step: Theoretical Study of the Mechanism. *J. Am. Chem. Soc.* **2005**, *127* (19), 7171–7182. https://doi.org/10.1021/ja050453+.

(178) Lapointe, D.; Fagnou, K. Overview of the Mechanistic Work on the Concerted Metallation-Deprotonation Pathway. *Chem. Lett.* **2010**, *39* (11), 1118–1126. https://doi.org/10.1246/cl.2010.1118.

(179) Sambiagio, C.; Schönbauer, D.; Blieck, R.; Dao-Huy, T.; Pototschnig, G.; Schaaf, P.; Wiesinger, T.; Zia, M. F.; Wencel-Delord, J.; Besset, T.; Maes, B. U. W.; Schnürch, M. A Comprehensive Overview of Directing Groups Applied in Metal-Catalysed C-H Functionalisation Chemistry. *Chem. Soc. Rev.* **2018**, *47* (17), 6603–6743. https://doi.org/10.1039/c8cs00201k.

(180) Yang, Z.; Qiu, F. C.; Gao, J.; Li, Z. W.; Guan, B. T. Palladium-Catalyzed Oxidative Arylation of Tertiary Benzamides: Para-Selectivity of Monosubstituted Arenes. *Org. Lett.* **2015**, *17* (17), 4316–4319. https://doi.org/10.1021/acs.orglett.5b02135.

(181) Kohn, K. W.; Waring, M. J.; Glaubiger, D.; Friedman, C. A. Intercalative Binding of Ellipticine to DNA Intercalative Binding of Ellipticine to DNA ’. **1975**, No. January, 71–76.

(182) Khayat, D.; Borel, C.; Azab, M.; Paraisot, D.; Malaurie, E.; Bouloux, C.; Weil, M. Phase I Study of Datelliptium Chloride, Hydrochloride given by 24-h Continuous Intravenous Infusion. *Cancer Chemother. Pharmacol.* **1992**, *30* (3), 226–228. https://doi.org/10.1007/BF00686318.

(183) Ahomadegbe, J.; Multon, E.; Riou, J.-F.; Riout, G.; Lefevere, D. Topoisomerase II-Mediated DNA Cleavage Activity Induced by Ellipticines on the Human Tumor Cell Line N417. *Biochem. Pharmacol.* **1989**, *38* (13), 2077–2086. https://doi.org/https://doi.org/10.1016/0006-2952(89)90060-9.

(184) Paoletti, C.; Le Pecq, J.-B.; Dat-Xuong, N.; Juret, P.; Garnier, H.; Amiel, J.-L.; Rouesse,

J. Antitumor Activity, Pharmacology, and Toxicity of Ellipticines, Ellipticinium, and 9-Hydroxy Derivatives: Preliminary Clinical Trials of 2-Methyl-9-Hydroxy Ellipticinium (NSC 264-137) BT - Cancer Chemo- and Immunopharmacology: 1. Chemopharmacology; Mathé, G., Muggia, F. M., Eds.; Springer Berlin Heidelberg: Berlin, Heidelberg, 1980; pp 107–123. https://doi.org/10.1007/978-3-642-81488-4_15.

(185) Stiborová, M.; Poljaková, J.; Martínková, E.; Bořek-Dohalská, L.; Eckschlager, T.; Kizek, R.; Frei, E. Ellipticine Cytotoxicity to Cancer Cell Lines-a Comparative Study. *Interdiscip. Toxicol.* **2011**, *4* (2), 98–105. https://doi.org/10.2478/v10102-011-0017-7.

(186) Kizek, R.; Adam, V.; Hrabeta, J.; Eckschlager, T.; Smutny, S.; Burda, J. V; Frei, E.; Stiborova, M. Anthracyclines and Ellipticines as DNA-Damaging Anticancer Drugs: Recent Advances. *Pharmacol. Ther.* **2012**, *133* (1), 26–39. https://doi.org/https://doi.org/10.1016/j.pharmthera.2011.07.006.

(187) Canals, A.; Purciolas, M.; Aymamí, J.; Coll, M. The Anticancer Agent Ellipticine Unwinds DNA by Intercalative Binding in an Orientation Parallel to Base Pairs. *Acta Crystallogr. Sect. D Biol. Crystallogr.* **2005**, *61* (7), 1009–1012. https://doi.org/10.1107/S0907444905015404.

(188) Stiborova, M.; Stiborova, M.; Bor, L.; Wiessler, M.; Frei, E. Rat Microsomes Activating the Anticancer Drug Ellipticine to Species Covalently Binding to Deoxyguanosine in DNA Are a Suitable Model Mimicking Ellipticine Bioactivation in Humans. *Chem. Res. Toxicol.* **2003**, *16*, 38–47.

(189) Stiborová, M.; Sejbal, J.; Bor, L.; Aimova, D.; Poljakova, J.; Forsterova, K.; Wiessler, M.; Frei, E. The Anticancer Drug Ellipticine Forms Covalent DNA Adducts , Mediated by Human Cytochromes P450 , through Metabolism to 13-Hydroxyellipticine and Ellipticine N 2 -Oxide. *Cancer Res.* **2004**, No. 1, 8374–8380.

(190) Deane, F. M.; Miller, C. M.; Maguire, A. R.; McCarthy, F. O. Modifications to the Vilsmeier-Haack Formylation of 1,4-Dimethylcarbazole and Its Application to the Synthesis of Ellipticines. *J. Heterocycl. Chem.* **2011**, *48* (April), 814–823. https://doi.org/10.1002/jhet.598.

(191) Cranwell, P. A.; Sacton, J. E. A Synthesis of Ellipticine. *J. Chem. Soc.* **1962**, *683*, 3482–3487.

(192) Powers, J.; Bossinger, O.; Rose, D.; Strome, S.; Saxton, W. A Nematode Kinesin Required

for Cleavage Furrow Advancement. *Curr. Biol.* **1998**, *8* (20), 1133–1136. https://doi.org/10.1016/S0960-9822(98)70470-1.

(193) T. Parvatkar, P. Recent Progress Towards the Total Synthesis and Biological Studies of Calothrixin A and B. *Curr. Org. Chem.* **2015**, *20* (8), 839–855. https://doi.org/10.2174/1385272819666150803235103.

(194) Khan, Q. A.; Lu, J.; Hecht, S. M. Calothrixins, a New Class of Human DNA Topoisomerase i Poisons. *J. Nat. Prod.* **2009**, *72* (3), 438–442. https://doi.org/10.1021/np8007232.

(195) Xu, S.; Nguyen, T.; Pomilio, I.; Vitale, M. C.; Velu, S. E. Total Synthesis of Calothrixins A and B via Oxidative Radical Reaction of Cyclohexenone with Aminophenanthridinedione. *Tetrahedron* **2014**, *70* (35), 5928–5933. https://doi.org/10.1016/j.tet.2014.06.021.

(196) Bernini, R.; Cacchi, S.; Fabrizi, G.; Sferrazza, A. A Simple General Approach to Phenanthridinones via Palladium-Catalyzed Intramolecular Direct Arene Arylation. *Synthesis (Stuttg).* **2008**, No. 5, 729–738. https://doi.org/10.1055/s-2008-1032169.

(197) Kaliyaperumal, S. A.; Banerjee, S.; Syam Kumar, U. K. Palladium Mediated Intramolecular Multiple C-X/C-H Cross Coupling and C-H Activation: Synthesis of Carbazole Alkaloids Calothrixin B and Murrayaquinone A. *Org. Biomol. Chem.* **2014**, *12* (32), 6105–6113. https://doi.org/10.1039/c4ob00493k.

(198) Bernardo, P. H.; Fitriyanto, W.; Chai, C. L. L. Palladium-Mediated Synthesis of Calothrixin B. *Synlett* **2007**, No. 12, 1935–1939. https://doi.org/10.1055/s-2007-984520.

(199) Naciuk, F. F.; Milan, J. C.; Andreão, A.; Miranda, P. C. M. L. Exploitation of a Tuned Oxidation with N -Haloimides in the Synthesis of Caulibugulones A-D. *J. Org. Chem.* **2013**, *78* (10), 5026–5030. https://doi.org/10.1021/jo302772t.

(200) Reimann, E.; Hertel, R.; Krauss, J. Synthesis of 6-Methyl-8H-Dibenzo[a,g]Quinolizin-8-Imines via Reissert Compounds. *Monatshefte fur Chemie* **2008**, *139* (6), 673–684. https://doi.org/10.1007/s00706-007-0826-8.

(201) Boogard, A. T.; Pandit, U. K.; Kooman, G.-J. Ring D Modifications of Ellipticine. Part 2. Chlorination of Ellipticine via N-Oxide and Synthesis and Selective Acetylation of 5,6,11-Trimethyl-5H-Benzo[b]Carbazole. *Tetrahedron* **1994**, *50* (16), 4811–4828.

(202) Wu, R.; Jiang, K.; An, D.; Cui, Y.; Men, L. Process for Preparing Itopride Hydrochloride. WO2006051079A1, 2006.

(203) Aricò, F.; Chiurato, M.; Peltier, J.; Tundo, P. Sulfur and Nitrogen Mustard Carbonate Analogues. *European J. Org. Chem.* **2012**, No. 17, 3223–3228. https://doi.org/10.1002/ejoc.201200321.

(204) Martín-Matute, B.; Mateo, C.; Cárdenas, D. J.; Echavarren, A. M. Intramolecular C-H Activation by Alkylpalladium(II) Complexes: Insights into the Mechanism of the Palladium-Catalyzed Arylation Reaction. *Chem. - A Eur. J.* **2001**, *7* (11), 2341–2348. https://doi.org/10.1002/1521-3765(20010601)7:11<2341::AID-CHEM23410>3.0.CO;2-S.

(205) Budén, M. E.; Vaillard, V. A.; Martin, S. E.; Rossi, R. A. Synthesis of Carbazoles by Intramolecular Arylation of Diarylamide Anions. *J. Org. Chem.* **2009**, *74*, 4490–4498. https://doi.org/10.1021/jo9006249.

(206) Morgan, E. . Vogel's Textbook of Practical Organic Chemistry. 5th Edn. *Endeavour*. 1990, pp 1–1287. https://doi.org/10.1016/0160-9327(90)90017-l.

(207) Yan, Q.; Gin, E.; Wasinska-Kalwa, M.; Banwell, M. G.; Carr, P. D. A Palladium-Catalyzed Ullmann Cross-Coupling/Reductive Cyclization Route to the Carbazole Natural Products 3-Methyl-9H-Carbazole, Glycoborine, Glycozoline, Clauszoline K, Mukonine, and Karapinchamine A. *J. Org. Chem.* **2017**, *82* (8), 4148–4159. https://doi.org/10.1021/acs.joc.7b00044.

(208) Yin, Z.; Zhang, J.; Wu, J.; Green, R.; Li, S.; Zheng, S. Synthesis of O-Chlorophenols via an Unexpected Nucleophilic Chlorination of Quinone Monoketals Mediated by N,N′-Dimethylhydrazine Dihydrochloride. *Org. Biomol. Chem.* **2014**, *12* (18), 2854–2858. https://doi.org/10.1039/c4ob00391h.

(209) Oliveira-campos, A. M. F.; Shannon, P. V. R.; Pereira, A. M. B.; Raposo, M. M. M. Studies on 5-Bromo-4,7-Dimethylindene, an Intermediate in the Synthesis of 6-Bromo-5,8-Dimethylisoquinoline. *J. Chem. Res.* **1999**, *567* (466), 466–467.

Appendix

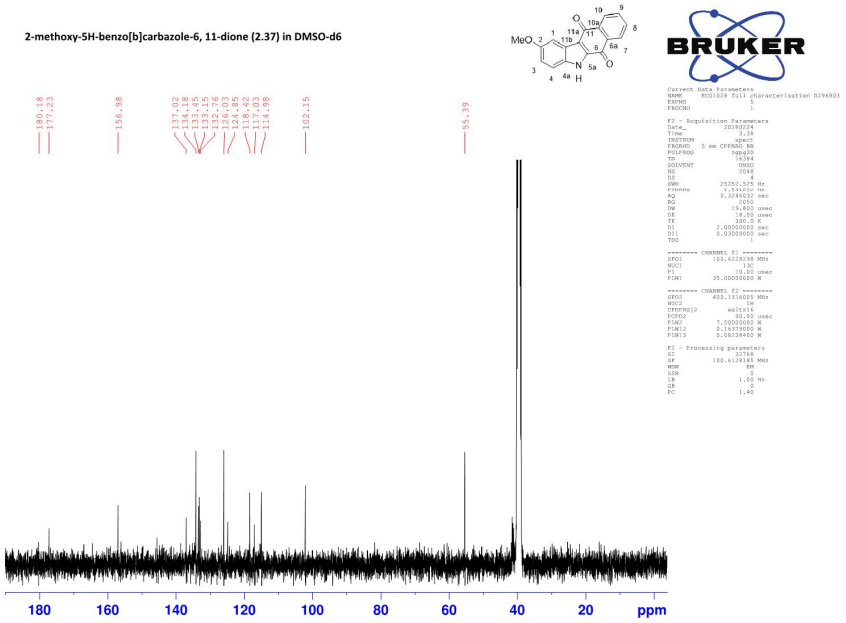


Figure 79. ^{13}C NMR spectra of 2-methoxy-5*H*-benzo[*b*]carbazole-6, 11-dione (**2.37**).

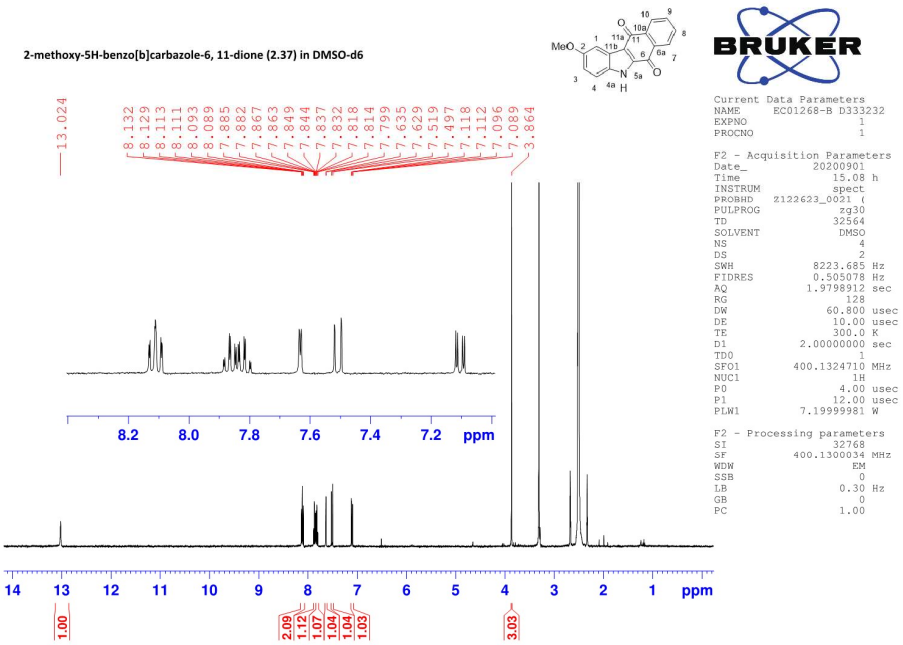


Figure 80. [1]H NMR spectra of 2-methoxy-5*H*-benzo[*b*]carbazole-6, 11-dione (**2.37**).

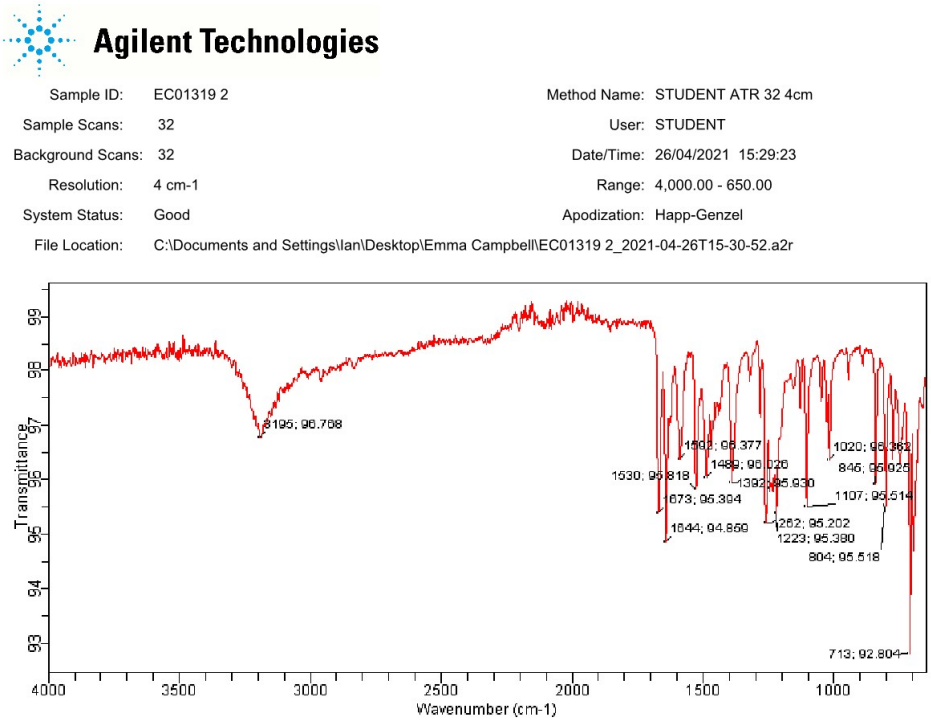


Figure 81. FT-IR spectra of 2-methoxy-5H-benzo[b]carbazole-6, 11-dione (**2.37**).

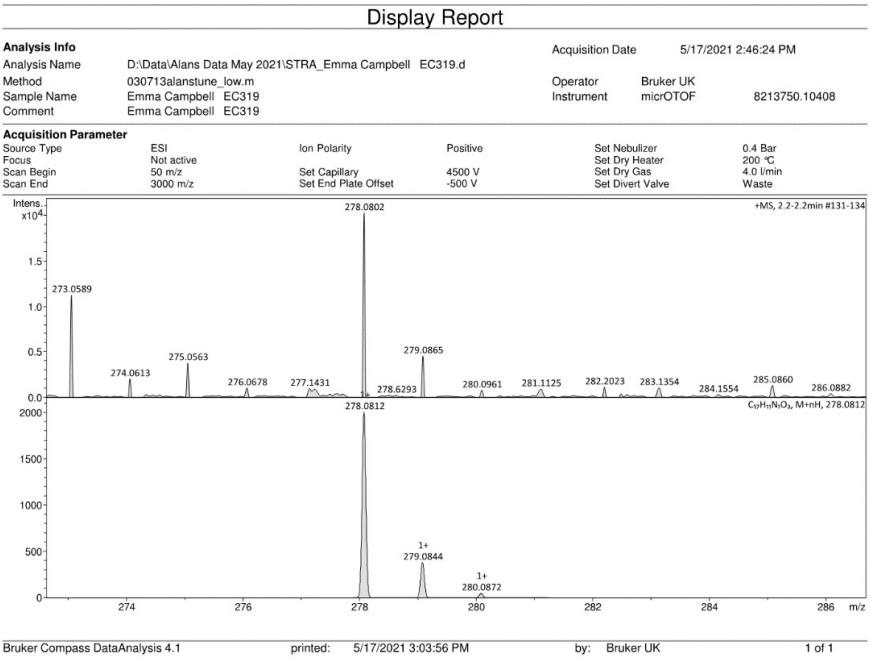


Figure 82. HRMS spectra of 2-methoxy-5H-benzo[b]carbazole-6, 11-dione (**2.37**).

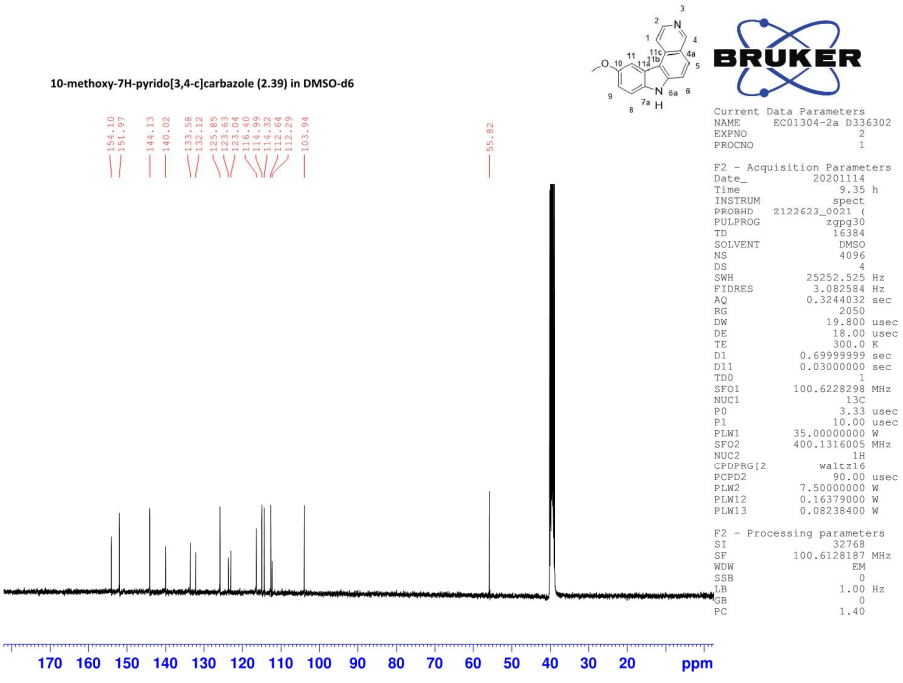


Figure 83. ^{13}C NMR spectra of 10-methoxy-7H-pyrido[3,4-*c*]carbazole (**2.39**).

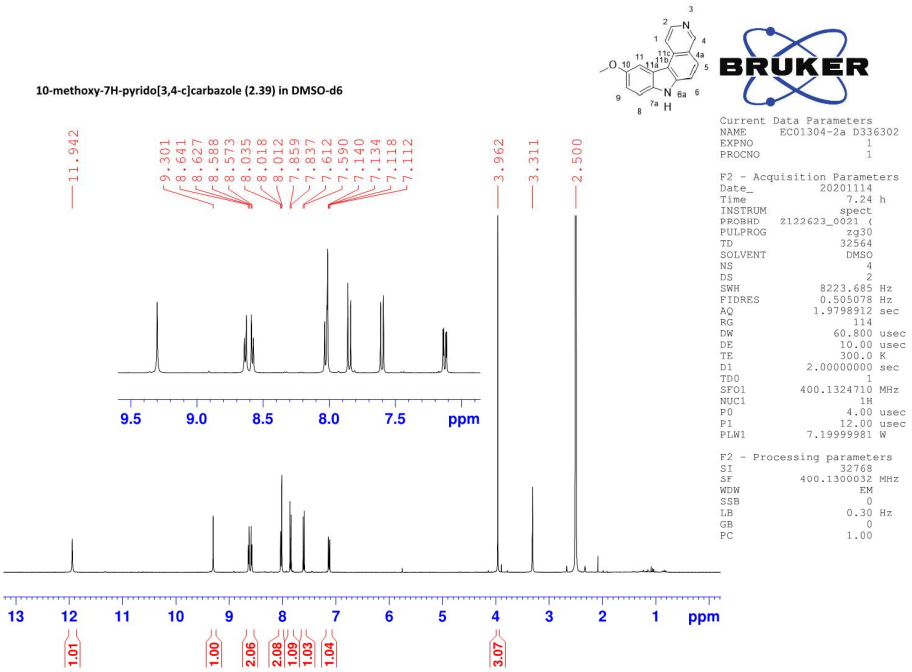


Figure 84. [1]H NMR spectra of 10-methoxy-7H-pyrido[3,4-c]carbazole (**2.39**).

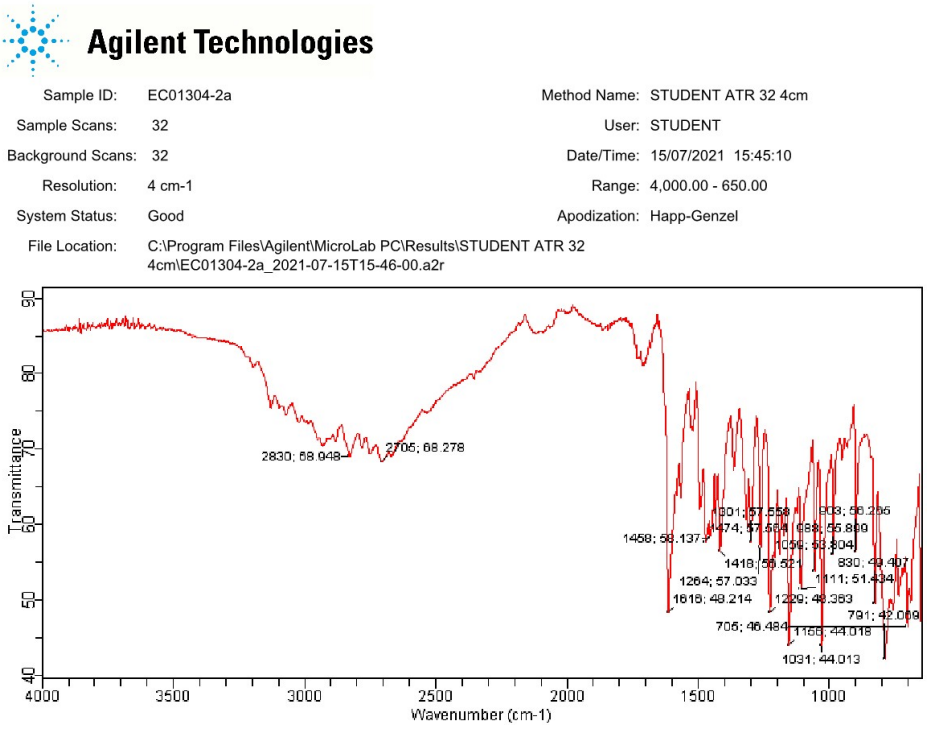


Figure 85. FT-IR spectra of 10-methoxy-7H-pyrido[3,4-*c*]carbazole (**2.39**).

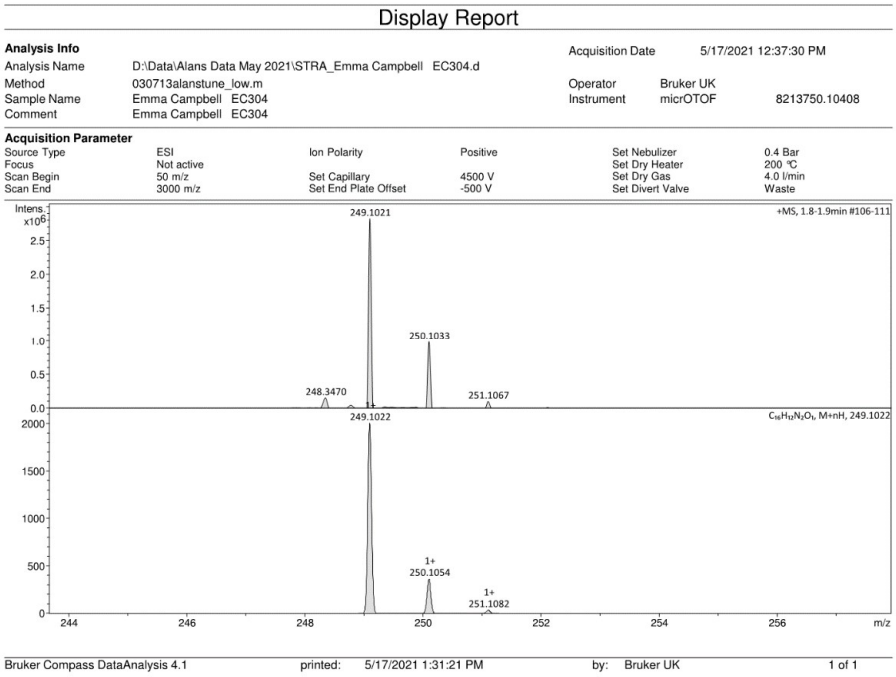


Figure 86. HRMS spectra of 10-methoxy-7H-pyrido[3,4-*c*]carbazole (**2.39**).

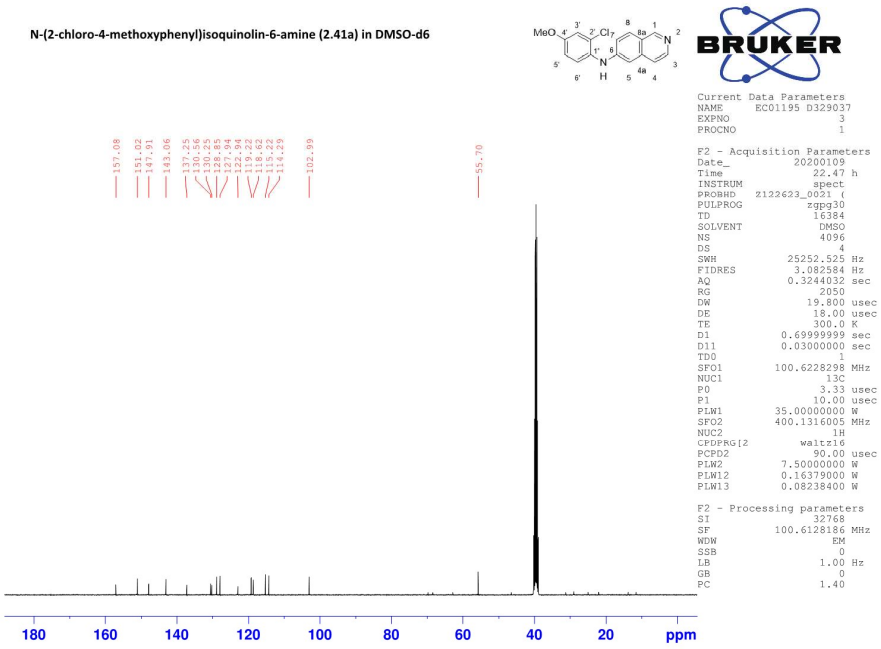


Figure 87. ^{13}C NMR spectra of N-(2-*c*hloro-4-methoxyphenyl)isoquinolin-6-amine (**2.41a**).

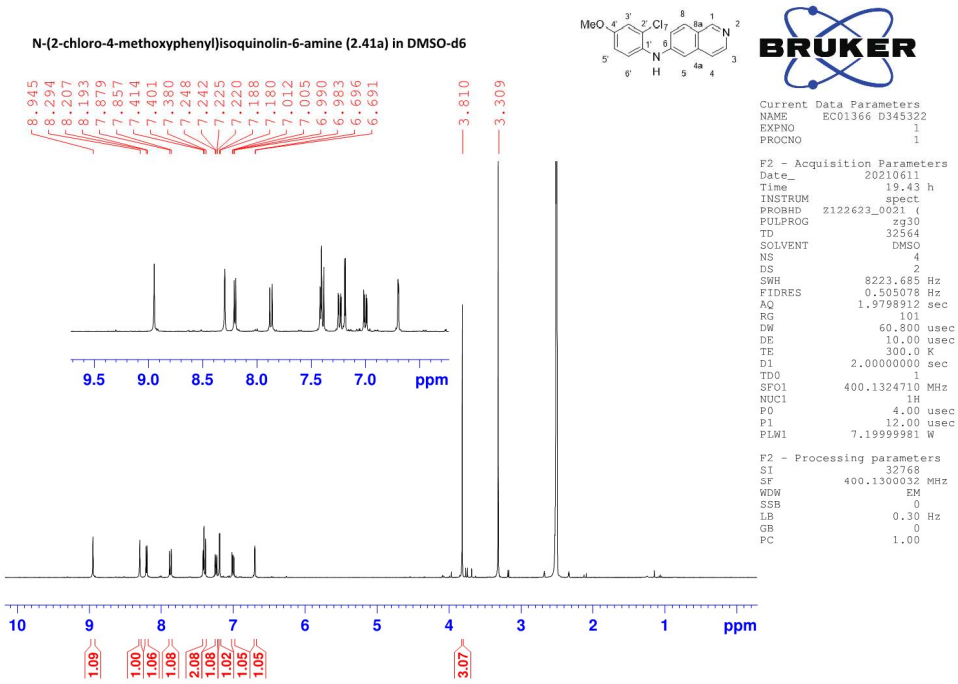


Figure 88. ^{1}H NMR spectra of N-(2-chloro-4-methoxyphenyl)isoquinolin-6-amine (**2.41a**).

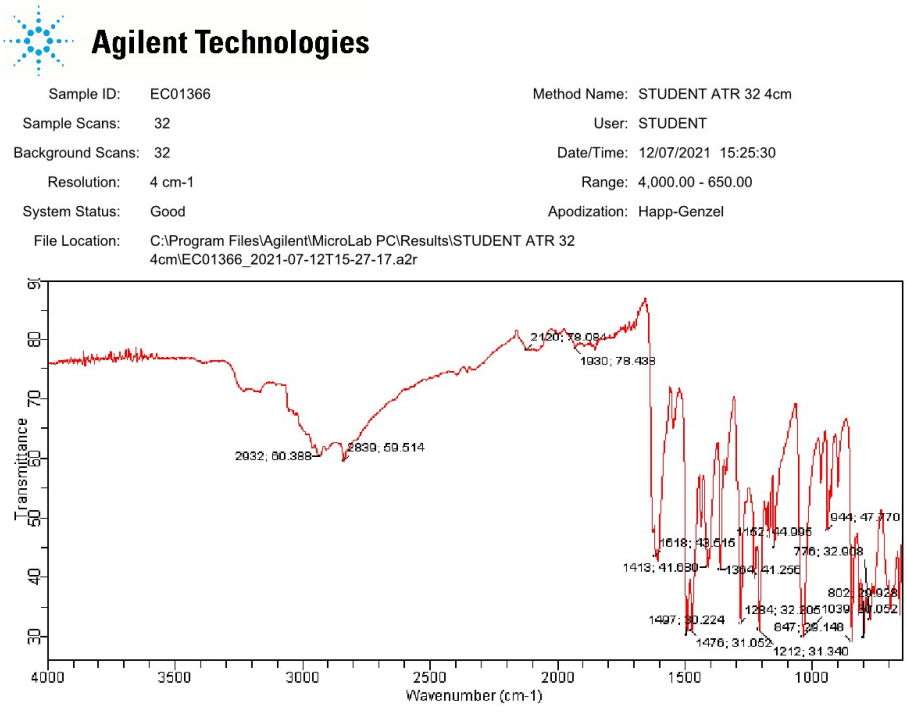


Figure 89. FT-IR spectra of N-(2-chloro-4-methoxyphenyl)isoquinolin-6-amine (**2.41a**).

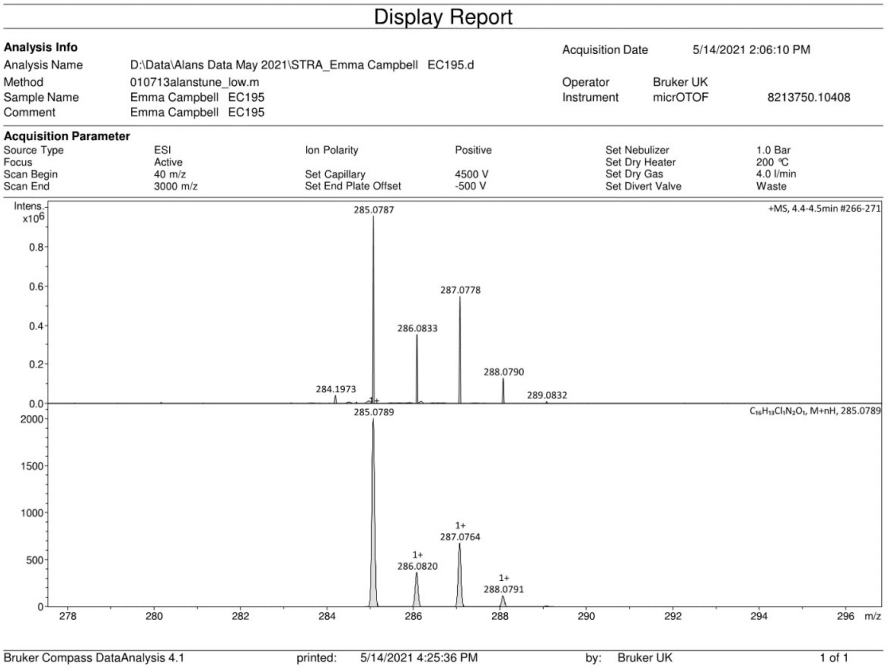


Figure 90. HRMS spectra of N-(2-chloro-4-methoxyphenyl)isoquinolin-6-amine (**2.41a**).

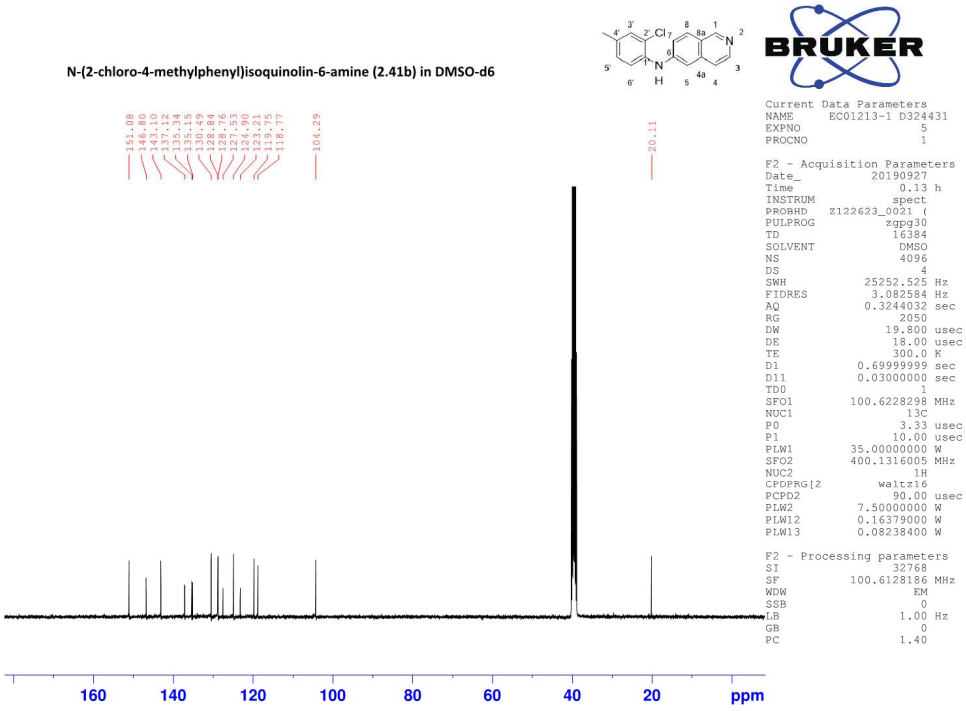


Figure 91. ^{13}C NMR spectra of N-(2-chloro-4-methylphenyl)isoquinolin-6-amine (**2.41b**).

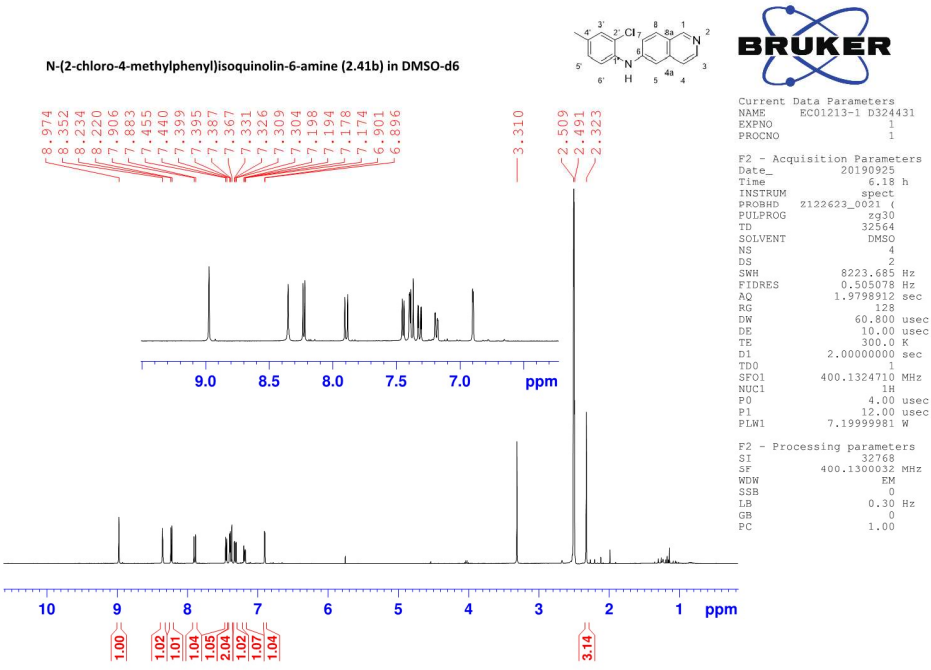


Figure 92. ^{1}H NMR spectra of N-(2-chloro-4-methylphenyl)isoquinolin-6-amine (**2.41b**)

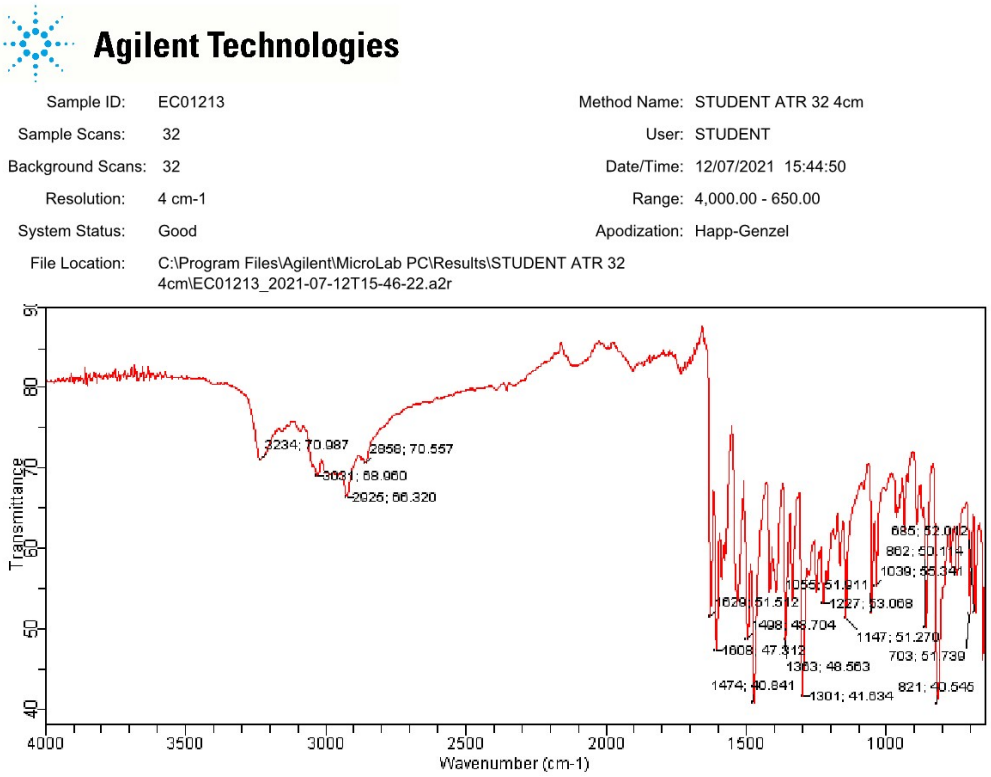


Figure 93. FT-IR spectra of N-(2-chloro-4-methylphenyl)isoquinolin-6-amine (**2.41b**).

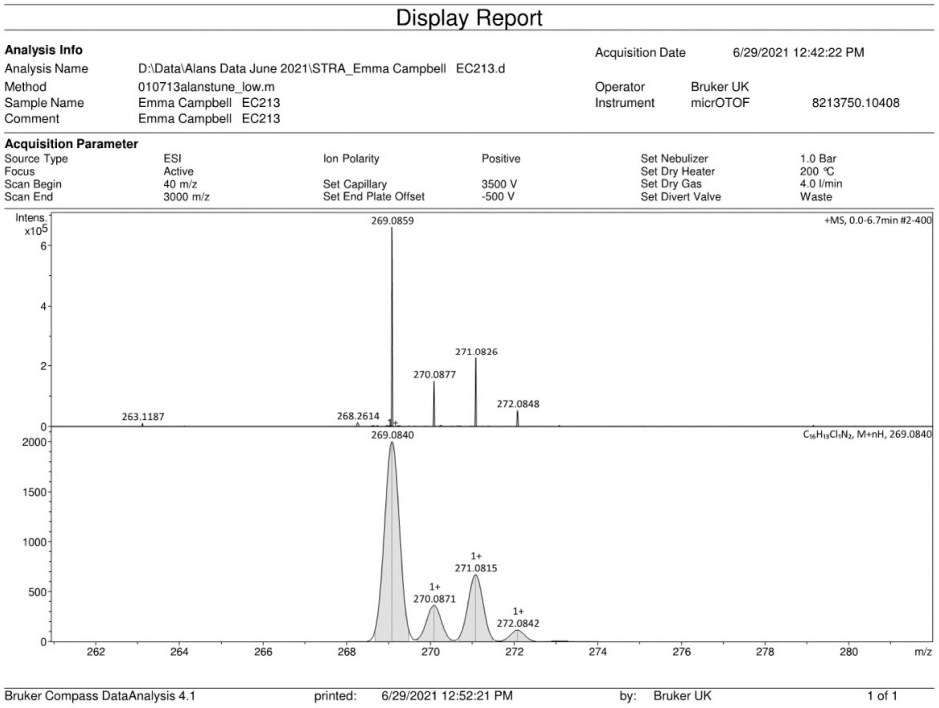


Figure 94. HRMS spectra of N-(2-chloro-4-methylphenyl)isoquinolin-6-amine (**2.41b**).

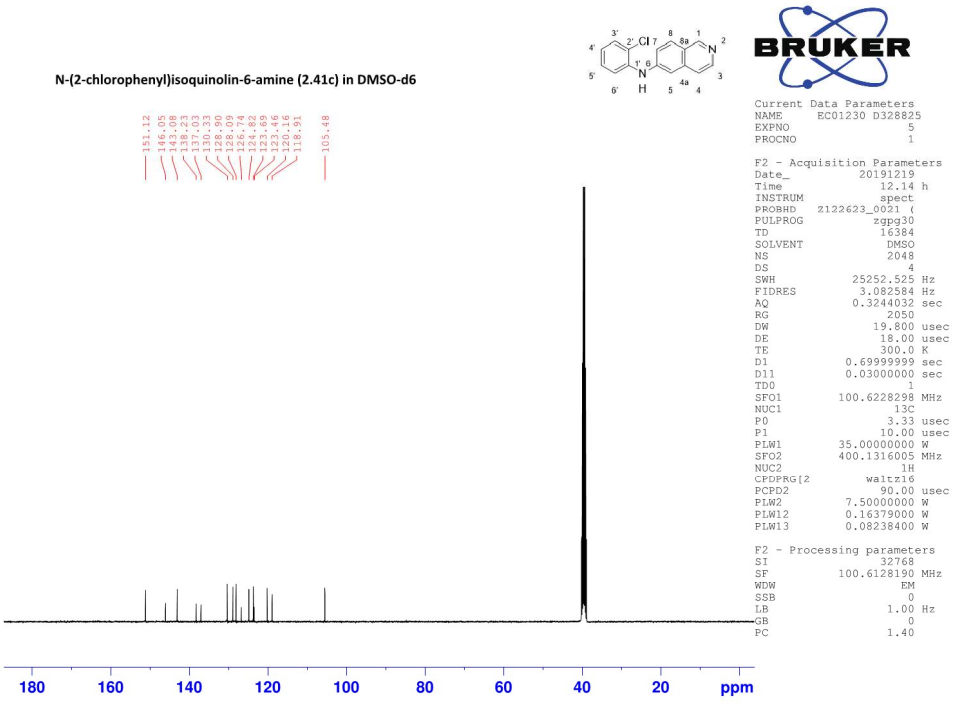


Figure 95. ^{13}C NMR spectra of N-(2-chlorophenyl)isoquinolin-6-amine (**2.41c**).

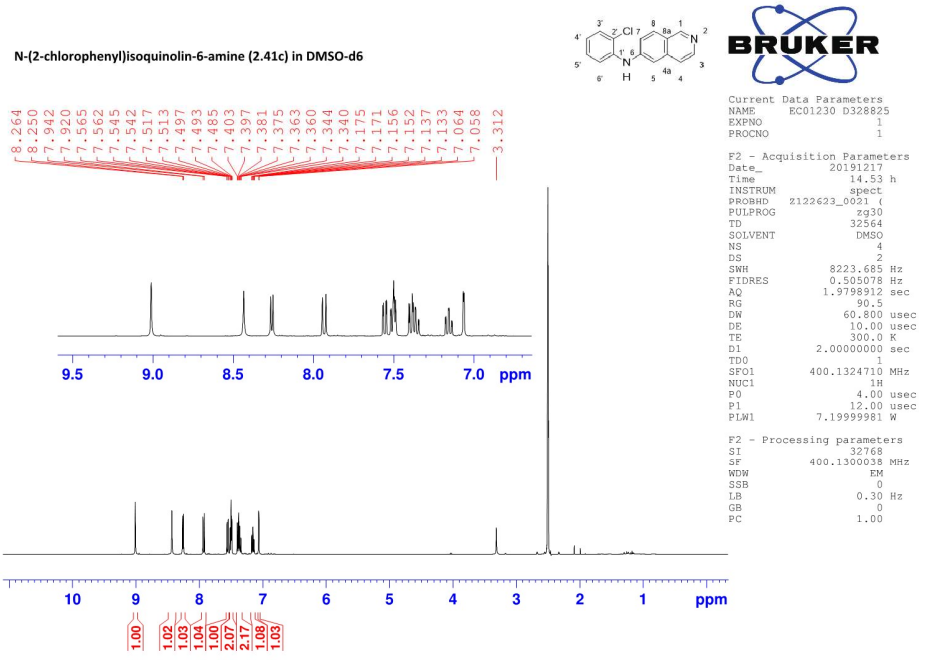


Figure 96. ^{1}H NMR spectra of N-(2-chlorophenyl)isoquinolin-6-amine (**2.41c**).

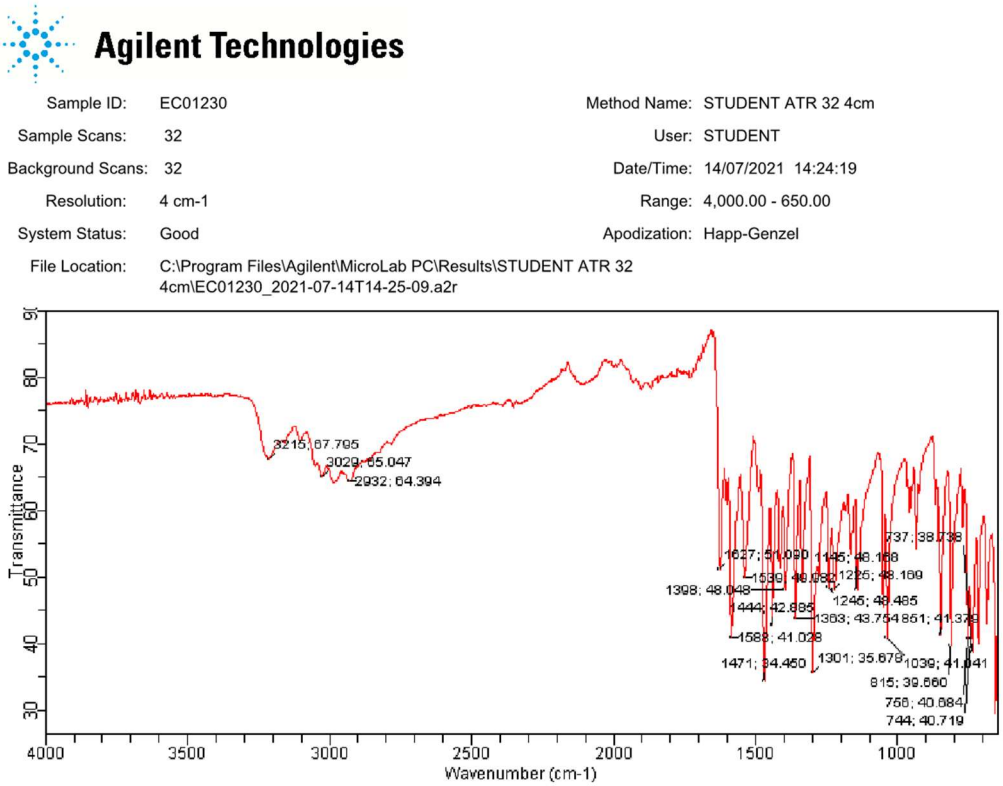


Figure 97. FT-IR spectra of N-(2-chlorophenyl)isoquinolin-6-amine (**2.41c**).

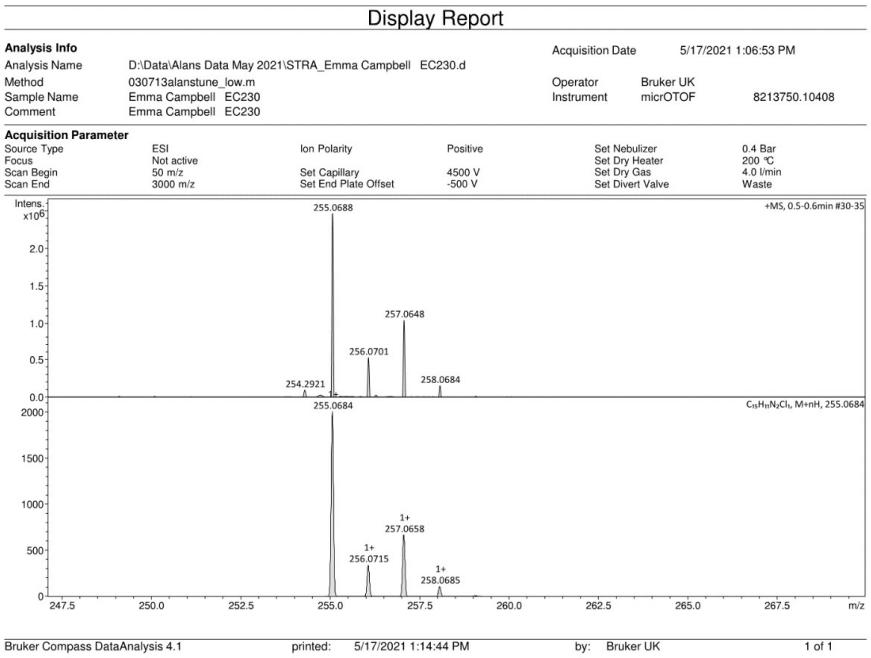


Figure 98. HRMS spectra of N-(2-chlorophenyl)isoquinolin-6-amine (**2.41c**).

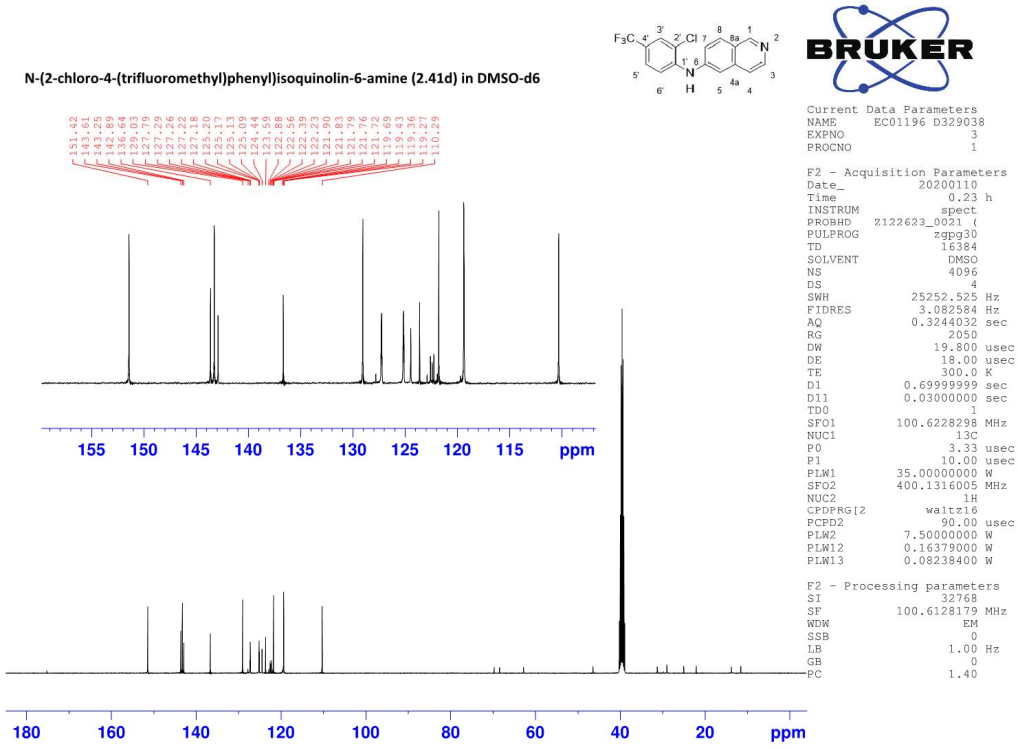


Figure 99. ^{13}C NMR spectra of N-(2-chloro-4-(trifluoromethyl)phenyl)isoquinolin-6-amine (**2.41d**).

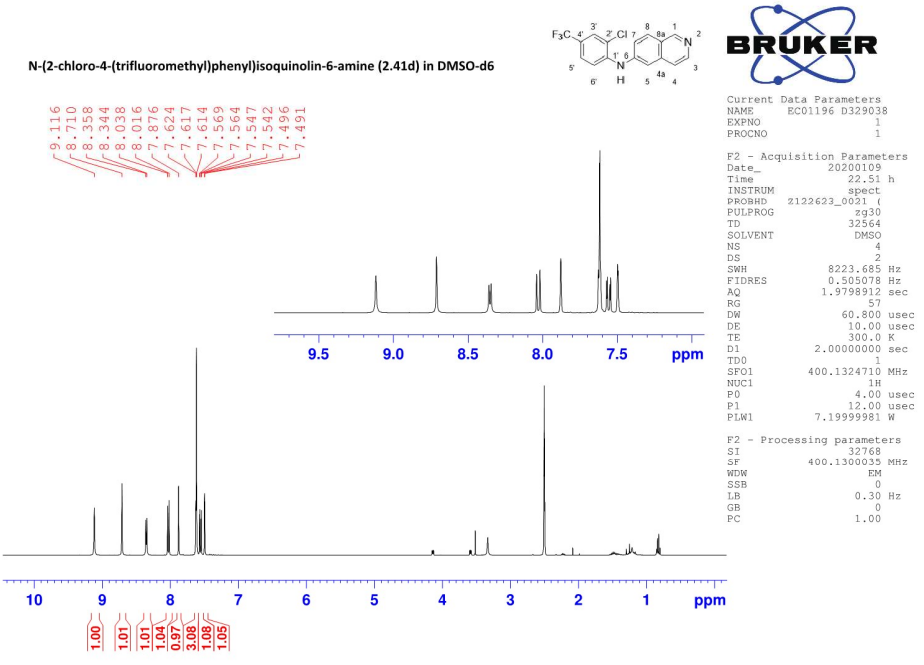


Figure 100. ^{1}H NMR spectra of N-(2-chloro-4-(trifluoromethyl)phenyl)isoquinolin-6-amine (**2.41d**).

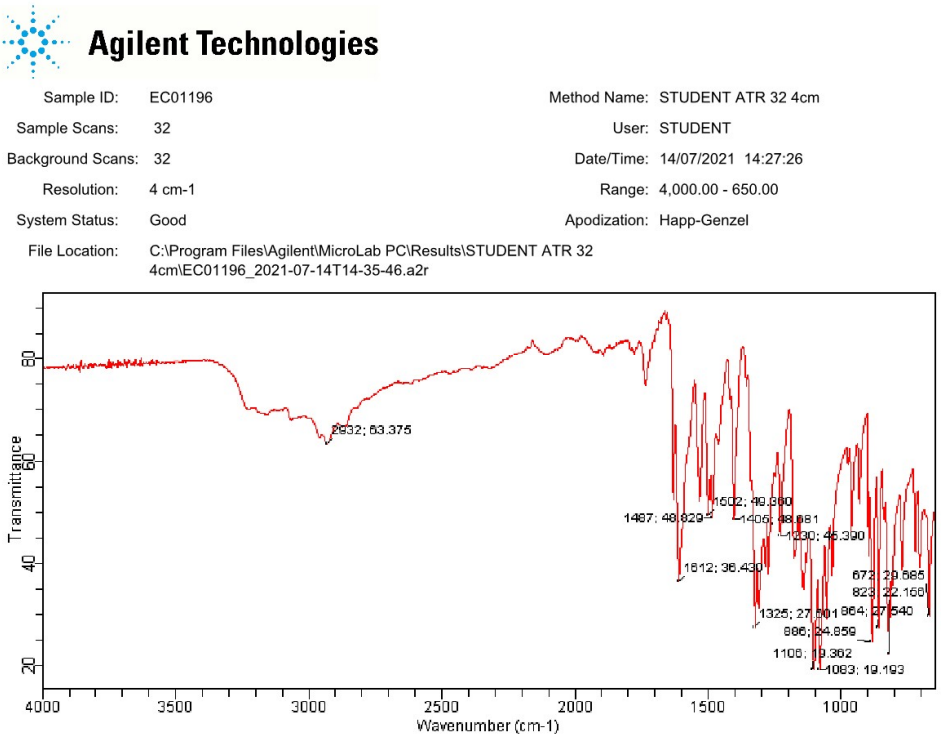


Figure 101. FT-IR spectra of N-(2-chloro-4-(trifluoromethyl)phenyl)isoquinolin-6-amine (**2.41d**).

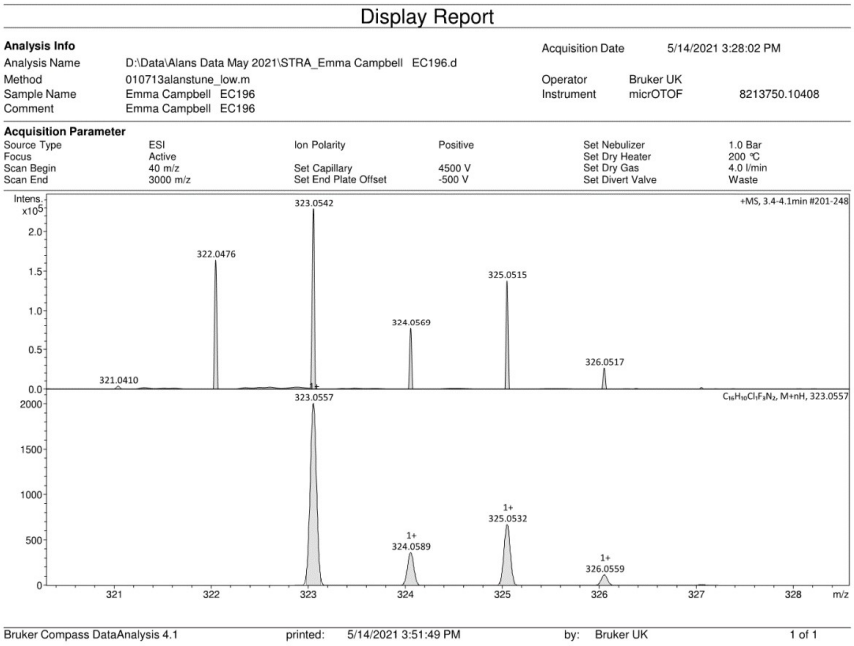


Figure 102. HRMS spectra of N-(2-chloro-4-(trifluoromethyl)phenyl)isoquinolin-6-amine (**2.41d**).

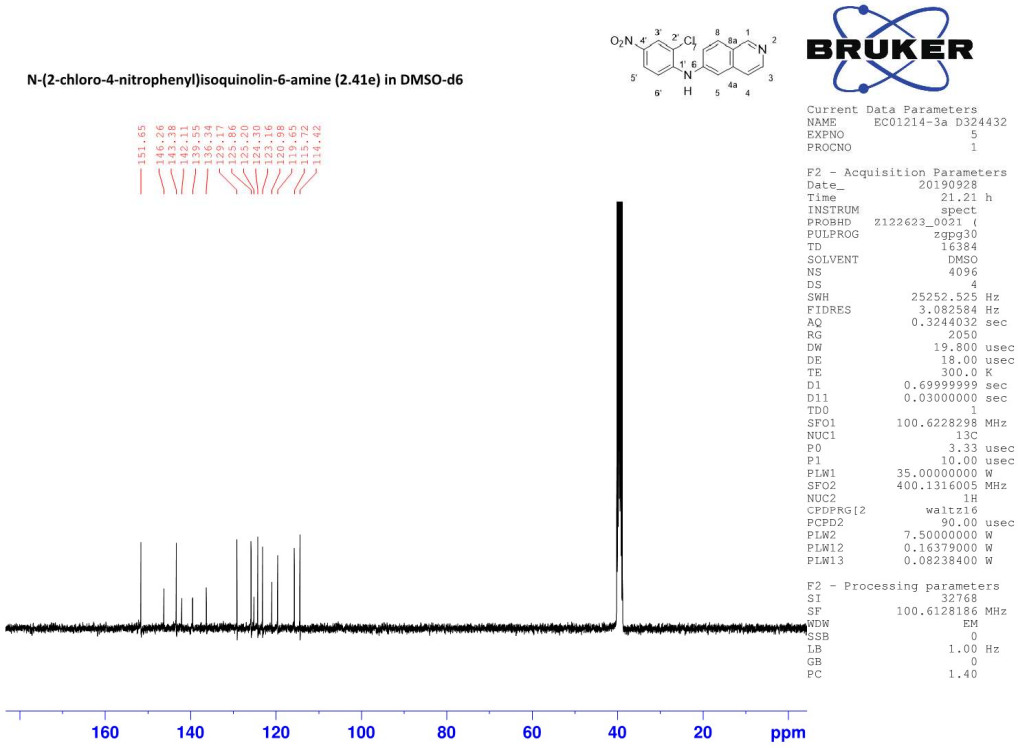


Figure 103. ^{13}C NMR spectra of N-(2-chloro-4-nitrophenyl)isoquinolin-6-amine (**2.41e**).

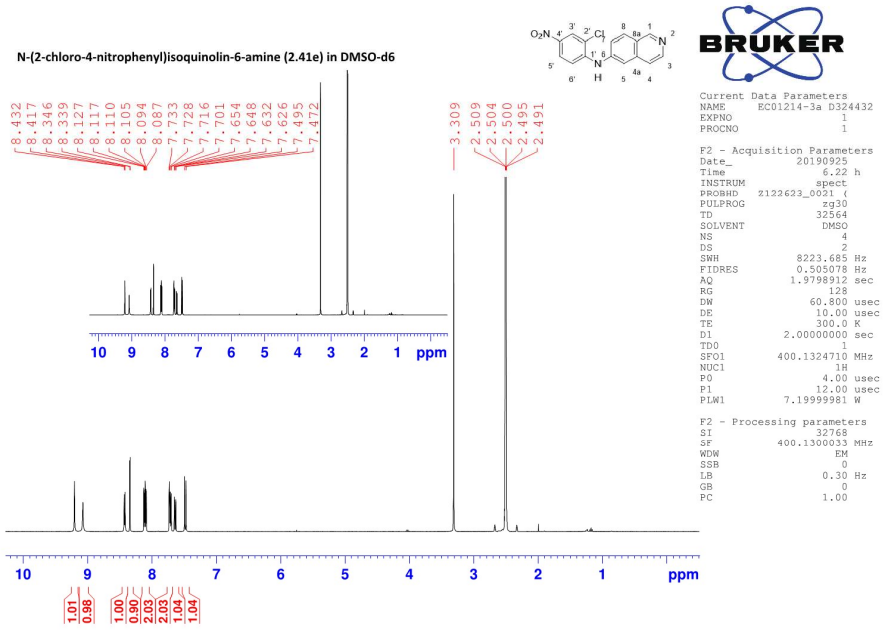


Figure 104. ^{1}H NMR spectra of N-(2-chloro-4-nitrophenyl)isoquinolin-6-amine (**2.41e**).

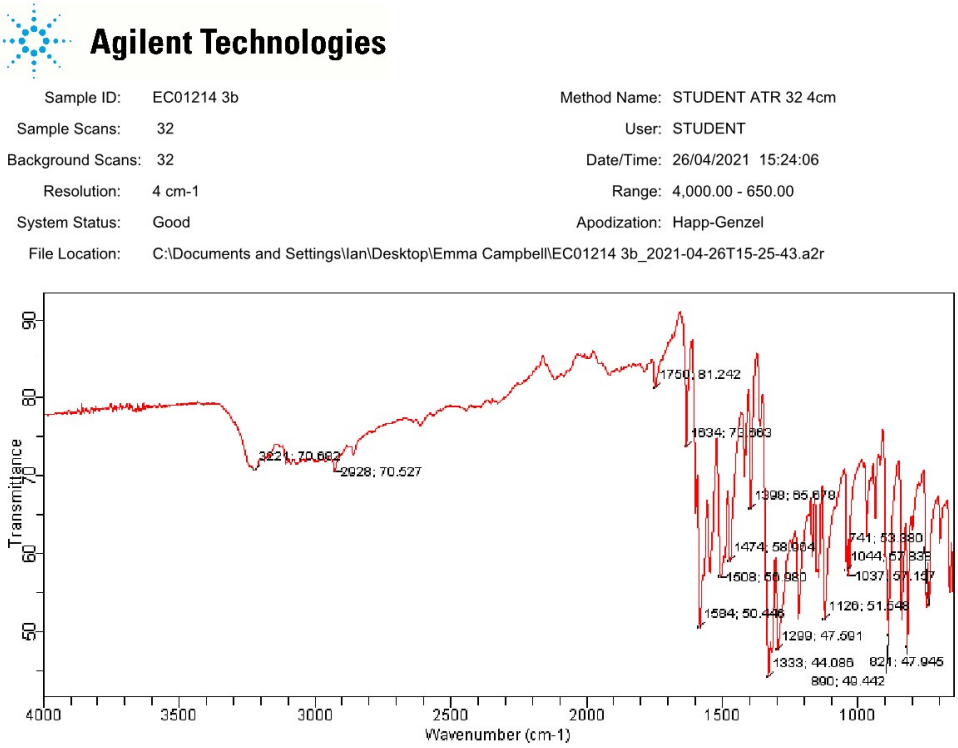


Figure 105. FT-IR spectra of N-(2-chloro-4-nitrophenyl)isoquinolin-6-amine (**2.41e**).

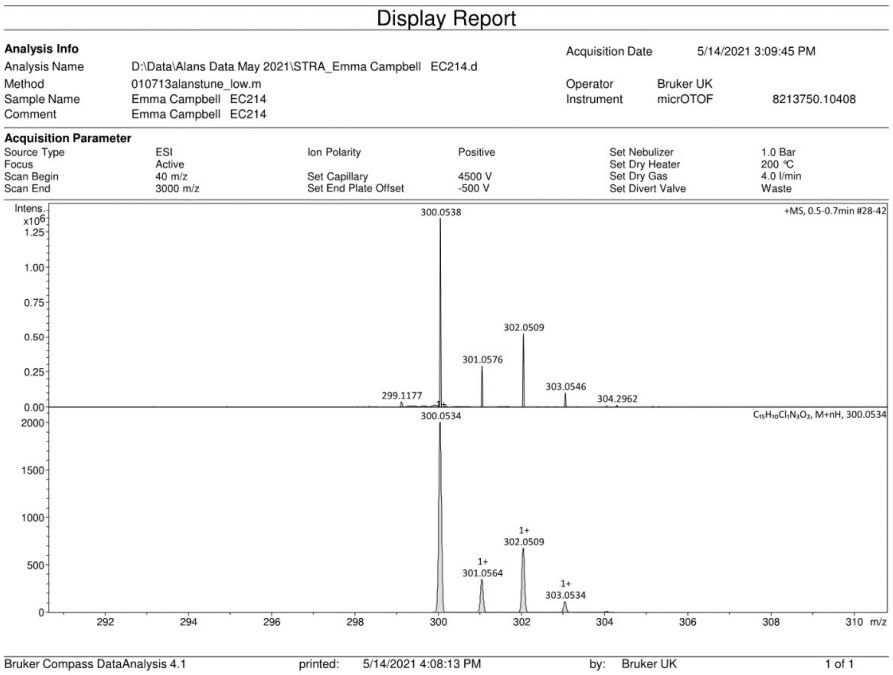


Figure 106. HRMS spectra of N-(2-chloro-4-nitrophenyl)isoquinolin-6-amine (**2.41e**).

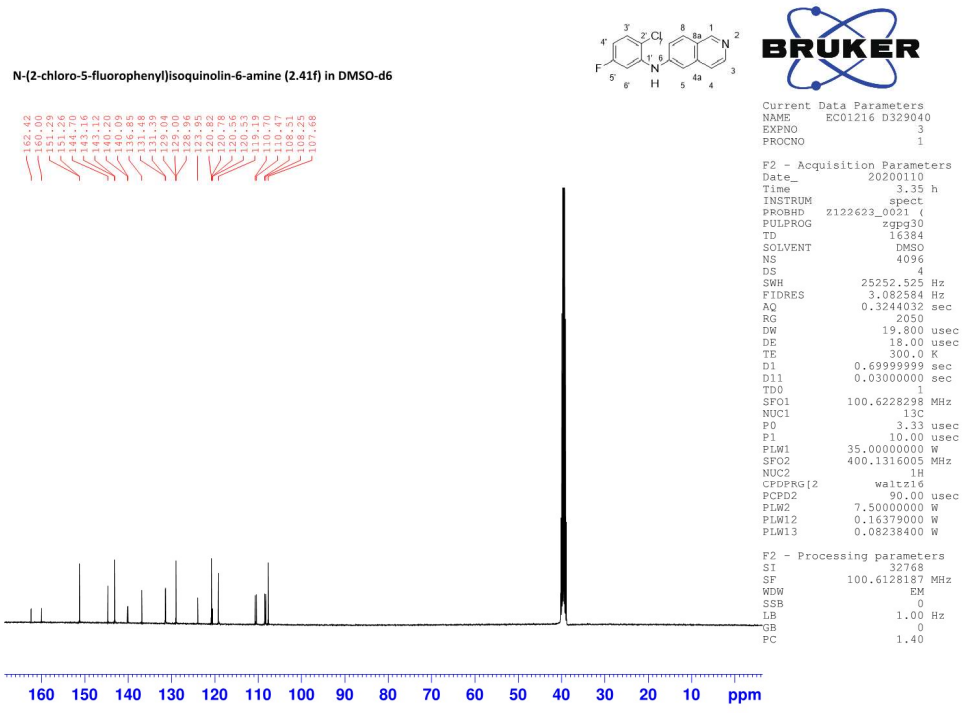


Figure 107. ^{13}C NMR spectra of N-(2-chloro-5-fluorophenyl)isoquinolin-6-amine (**2.41f**).

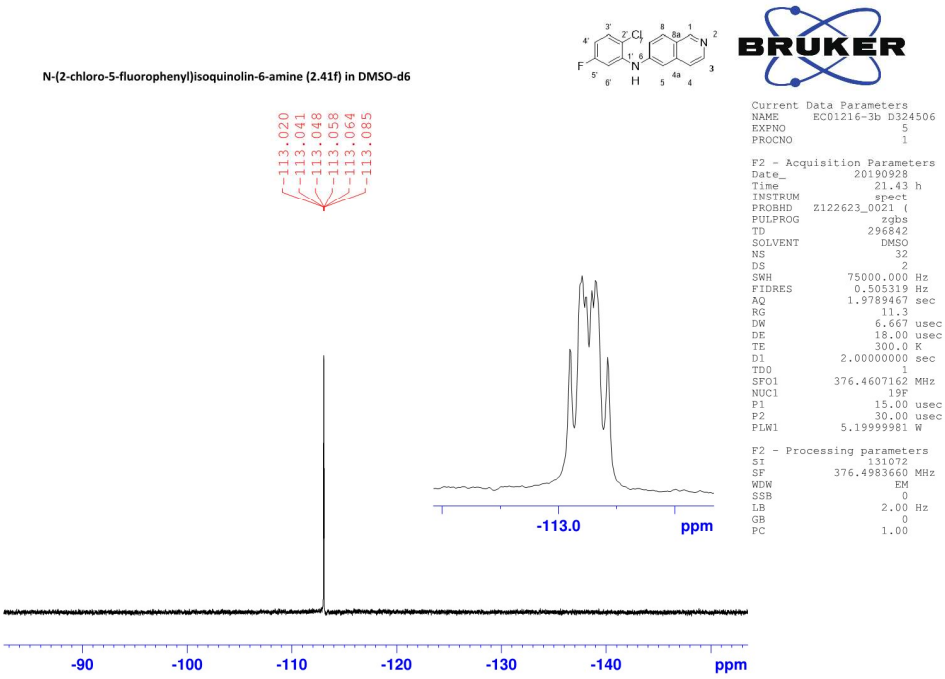


Figure 108. ^{19}F NMR spectra of N-(2-chloro-5-fluorophenyl)isoquinolin-6-amine (**2.41f**).

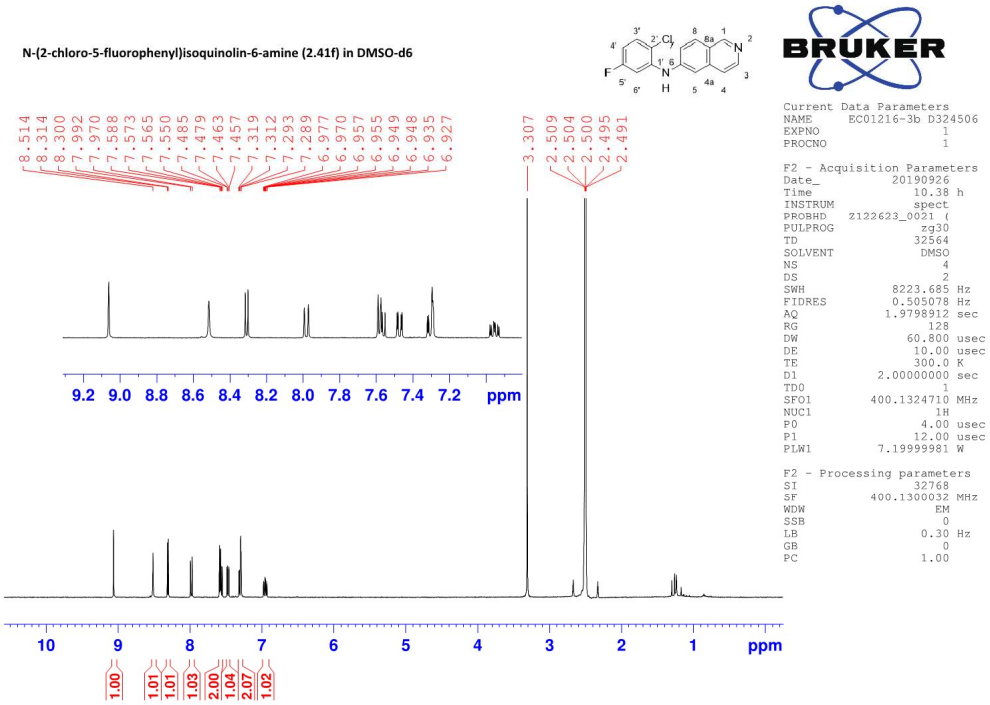


Figure 109. ^{1}H NMR spectra of N-(2-chloro-5-fluorophenyl)isoquinolin-6-amine (**2.41f**).

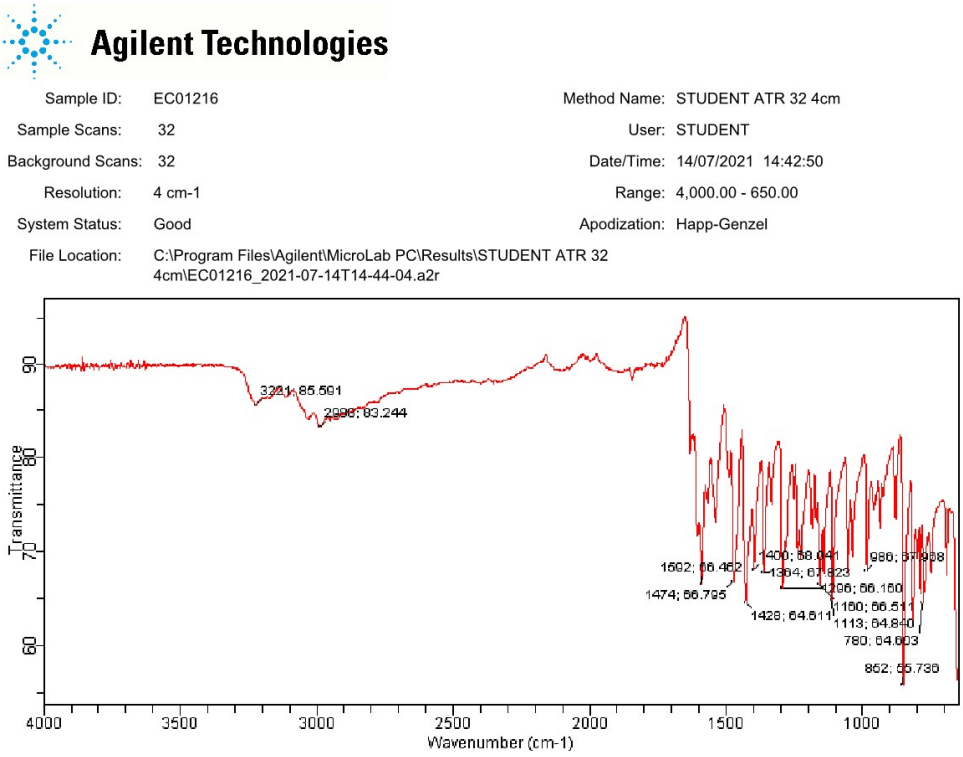


Figure 110. FT-IR spectra of N-(2-chloro-5-fluorophenyl)isoquinolin-6-amine (**2.41f**).

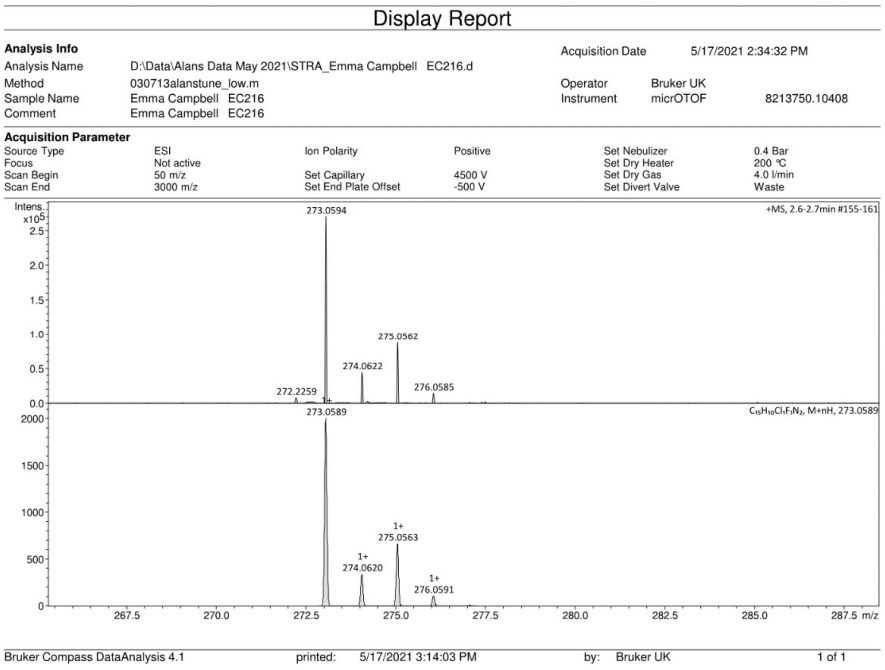


Figure 111. HRMS spectra of N-(2-chloro-5-fluorophenyl)isoquinolin-6-amine (**2.41f**).

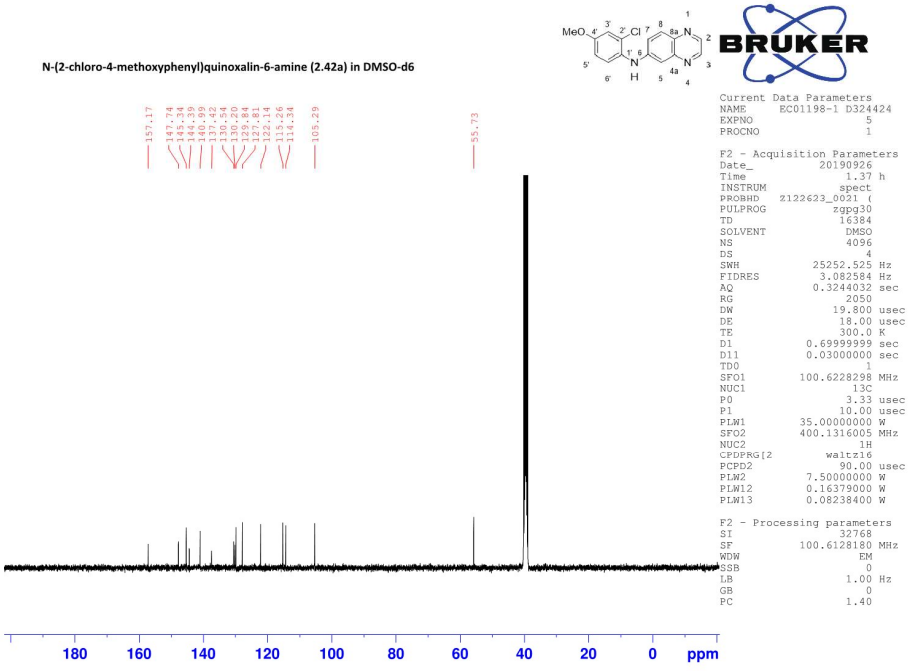


Figure 112. ^{13}C NMR spectra of N-(2-chloro-4-methoxyphenyl)quinoxalin-6-amine (**2.42a**).

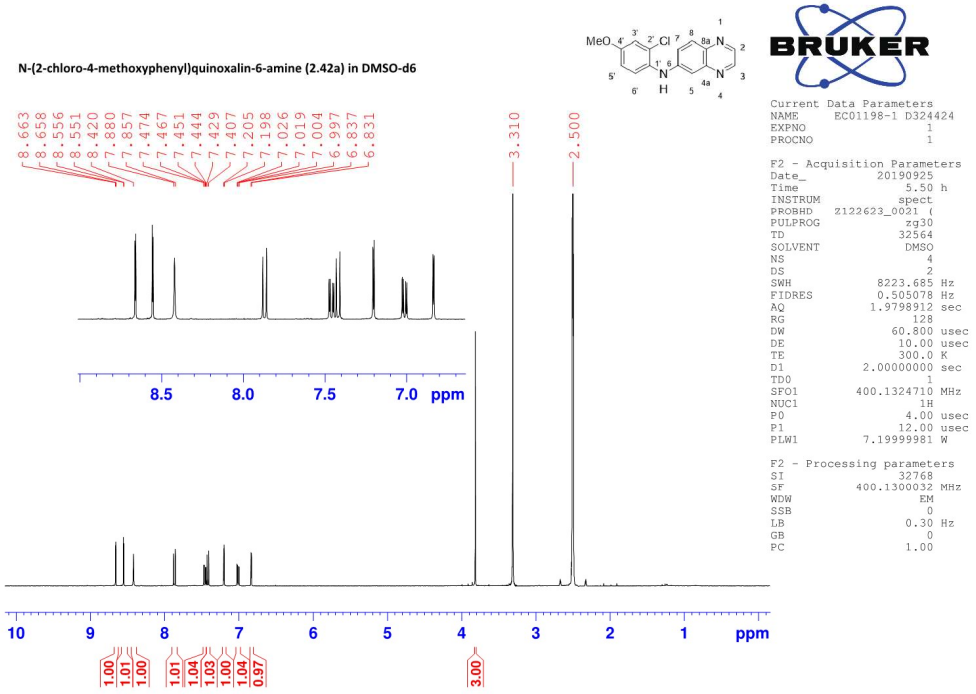


Figure 113. [1]H NMR spectra of N-(2-chloro-4-methoxyphenyl)quinoxalin-6-amine (**2.42a**).

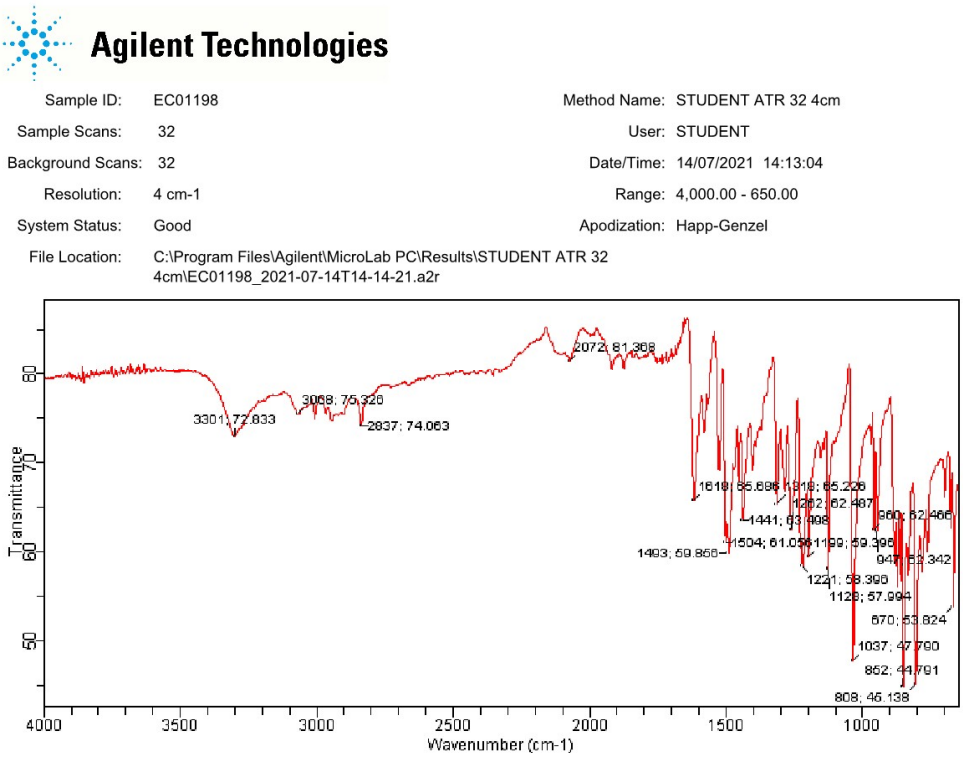


Figure 114. FT-IR spectra of N-(2-chloro-4-methoxyphenyl)quinoxalin-6-amine (**2.42a**).

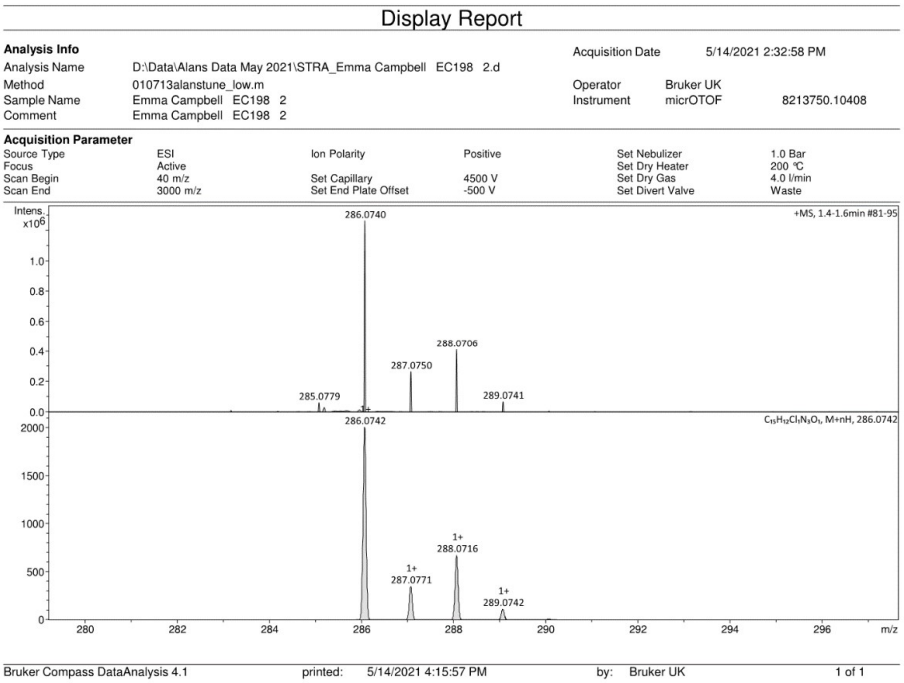


Figure 115. HRMS spectra of N-(2-chloro-4-methoxyphenyl)quinoxalin-6-amine (**2.42a**).

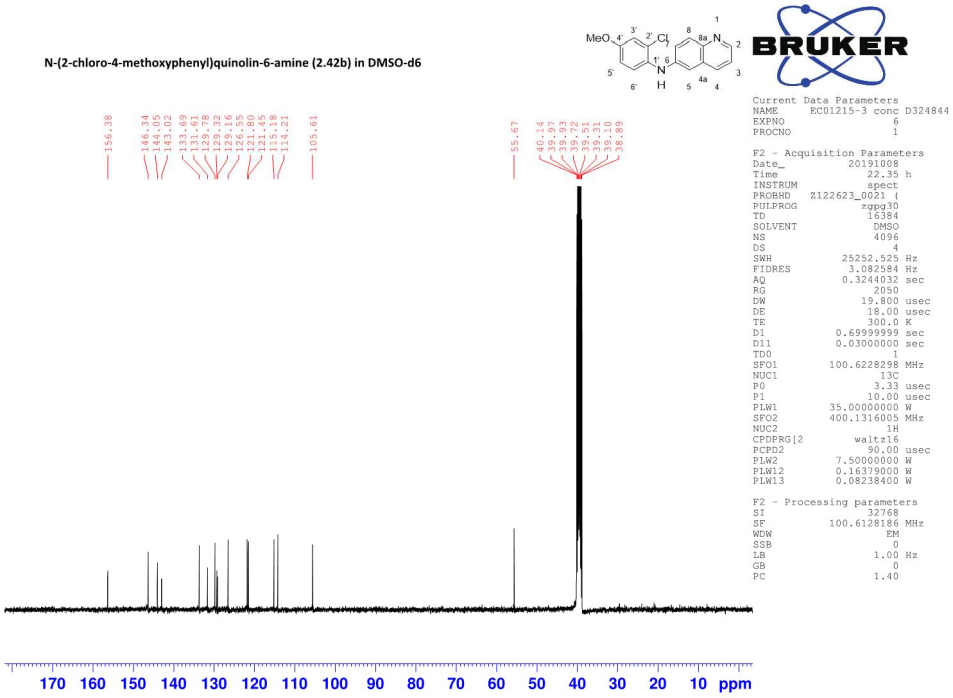


Figure 116. ^{13}C NMR spectra of N-(2-chloro-4-methoxyphenyl)quinolin-6-amine (**2.42b**).

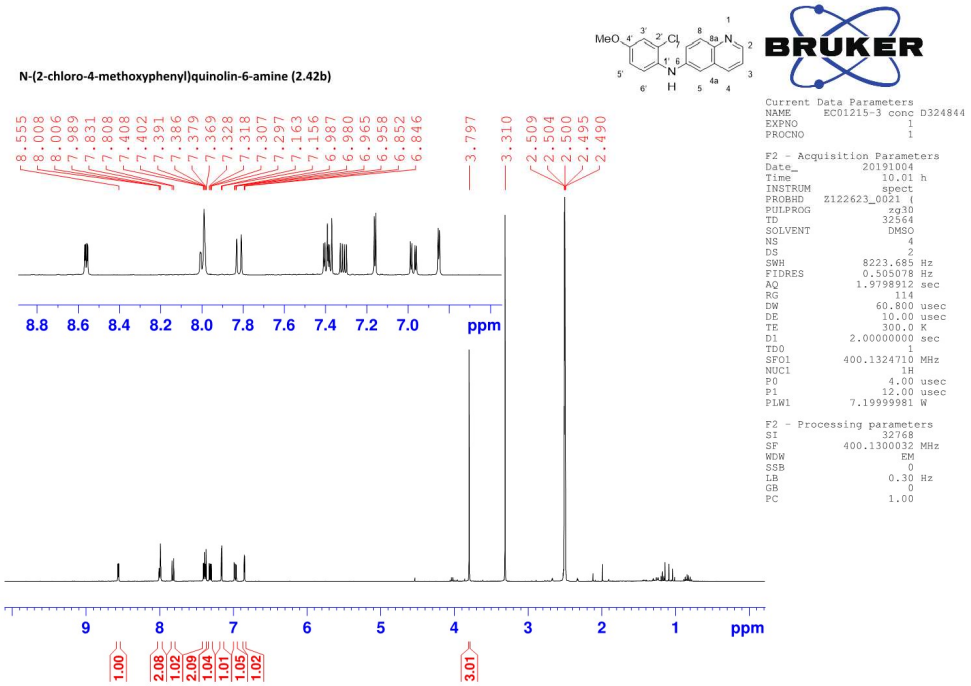


Figure 117. [1]H NMR spectra of N-(2-chloro-4-methoxyphenyl)quinolin-6-amine (**2.42b**).

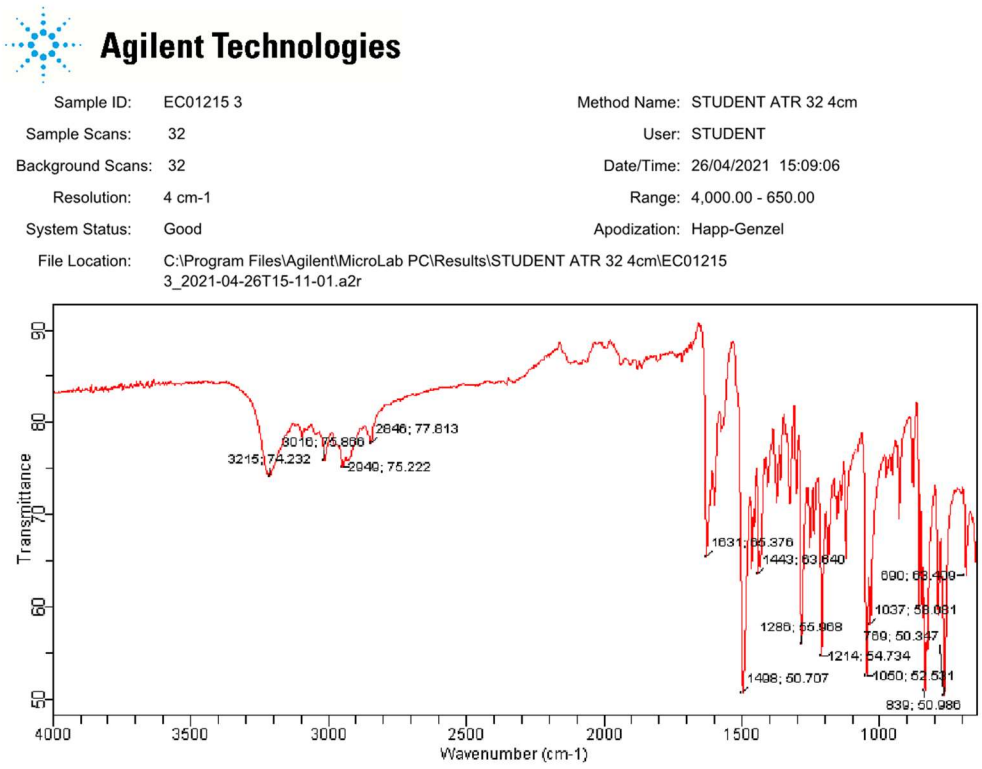


Figure 118. FT-IR spectra of N-(2-chloro-4-methoxyphenyl)quinolin-6-amine (**2.42b**).

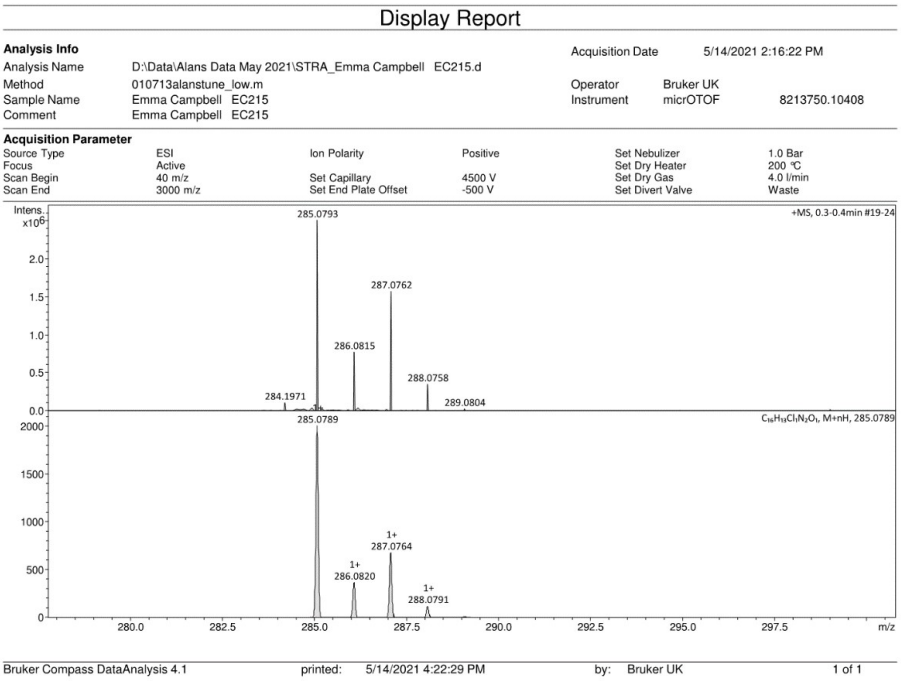


Figure 119. HRMS spectra of N-(2-chloro-4-methoxyphenyl)quinolin-6-amine (**2.42b**).

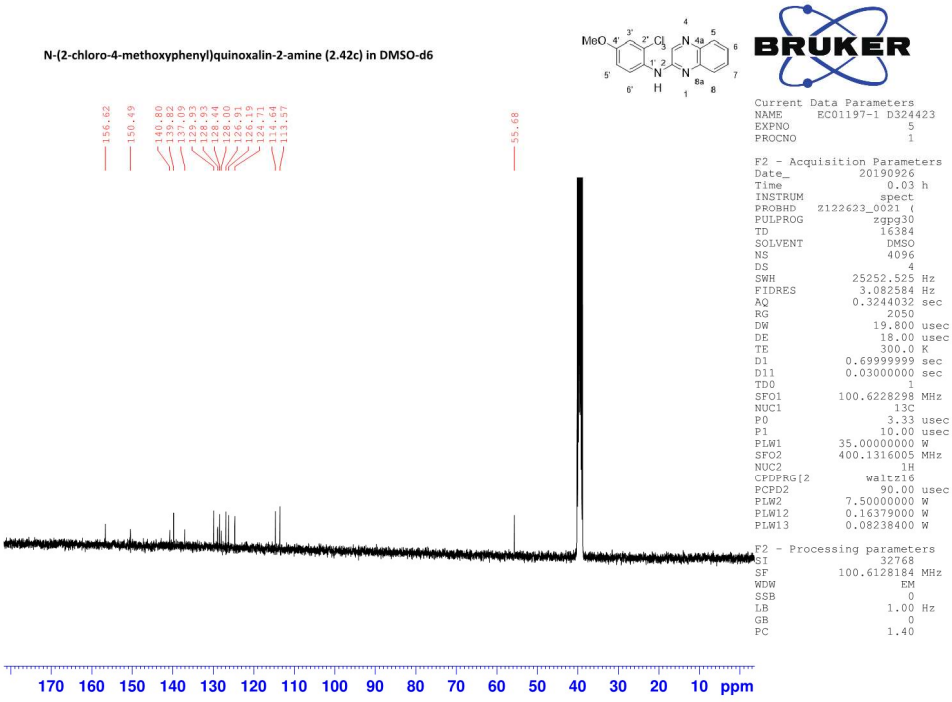


Figure 120. ^{13}C NMR spectra of N-(2-chloro-4-methoxyphenyl)quinoxalin-2-amine (**2.42c**).

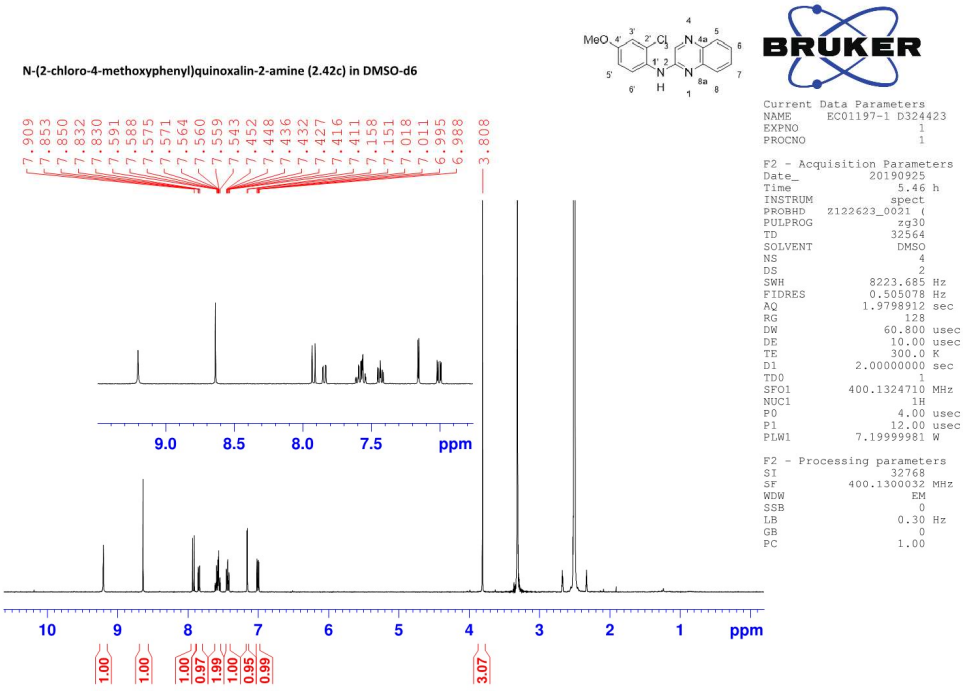


Figure 121. [1]H NMR spectra of N-(2-chloro-4-methoxyphenyl)quinoxalin-2-amine (**2.42c**) .

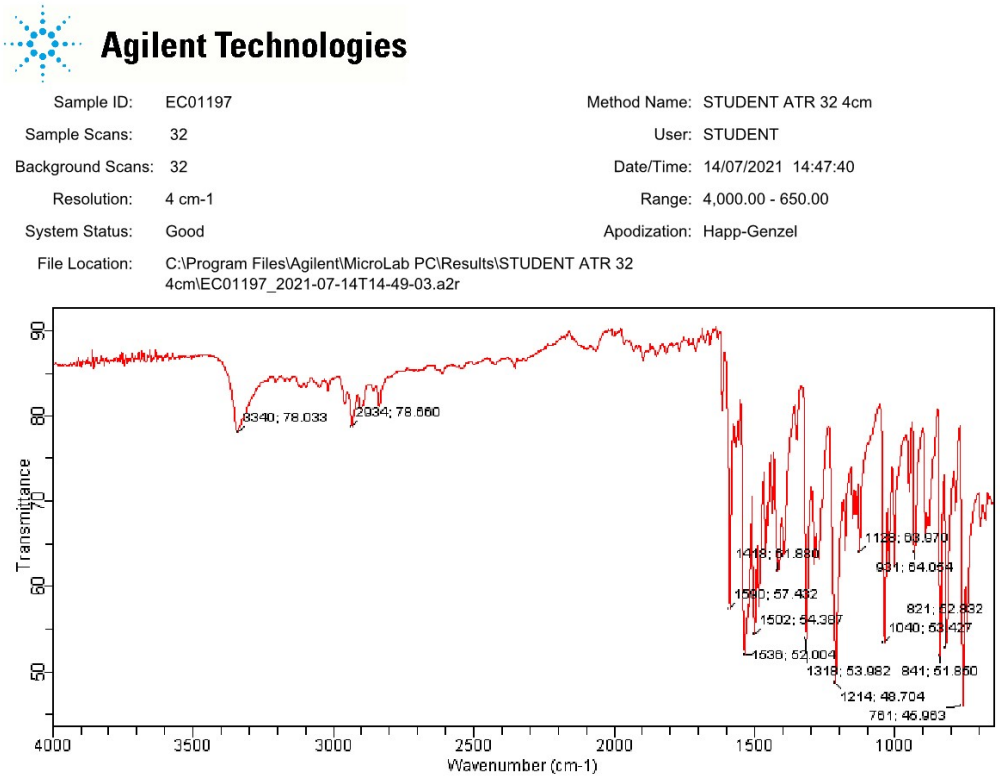


Figure 122. FT-IR spectra of N-(2-chloro-4-methoxyphenyl)quinoxalin-2-amine (**2.42c**).

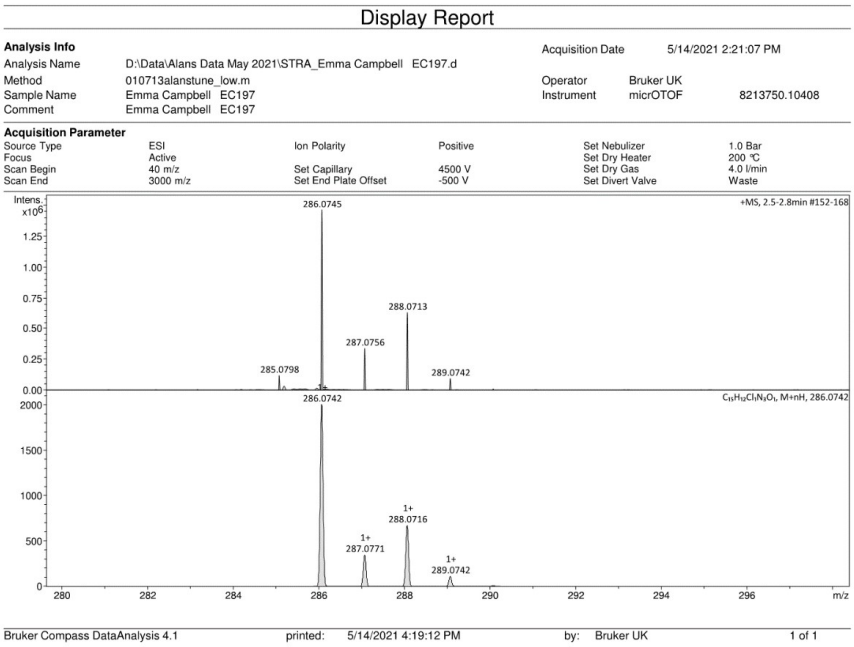


Figure 123. HRMS spectra of N-(2-chloro-4-methoxyphenyl)quinoxalin-2-amine (**2.42c**).

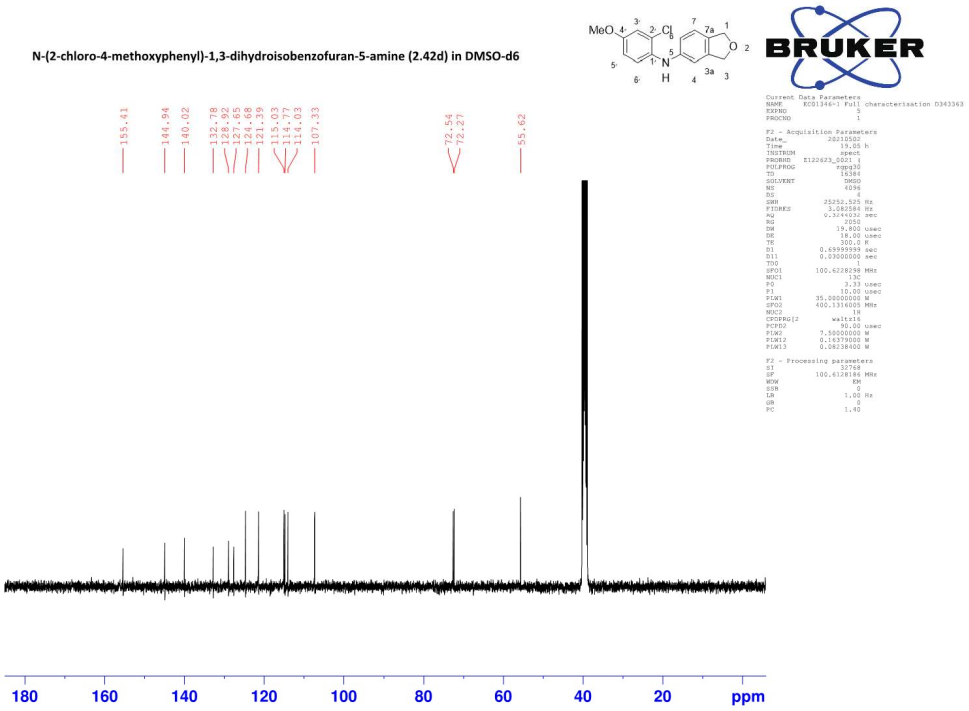


Figure 124. ^{13}C NMR spectra of N-(2-chloro-4-methoxyphenyl)-1,3-dihydroisobenzofuran-5-amine (**2.42d**).

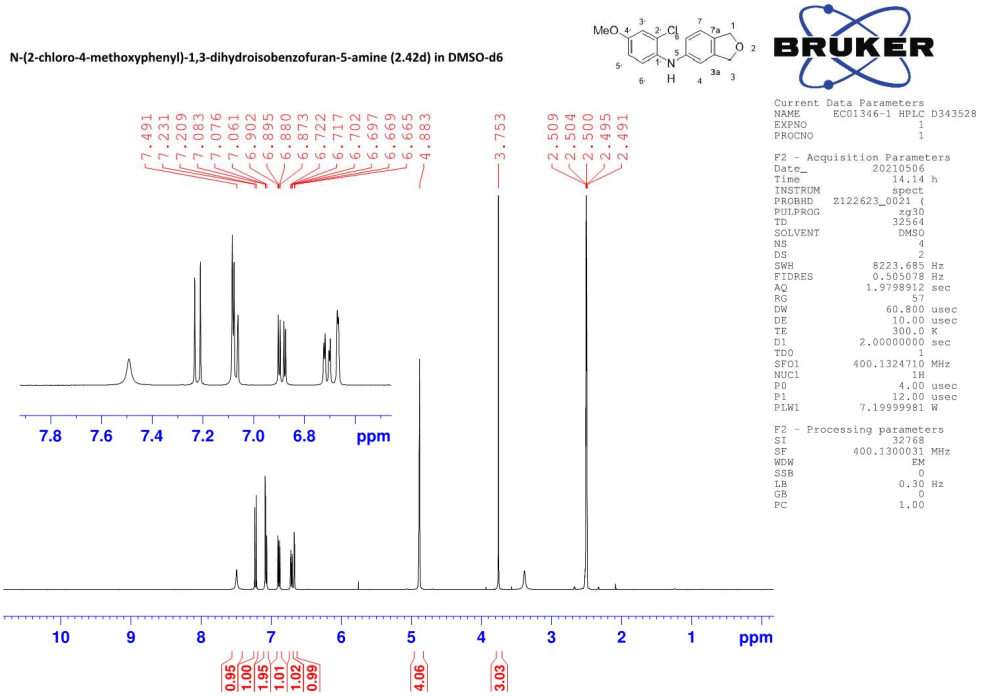


Figure 125. [1]H NMR spectra of N-(2-chloro-4-methoxyphenyl)-1,3-dihydroisobenzofuran-5-amine (**2.42d**).

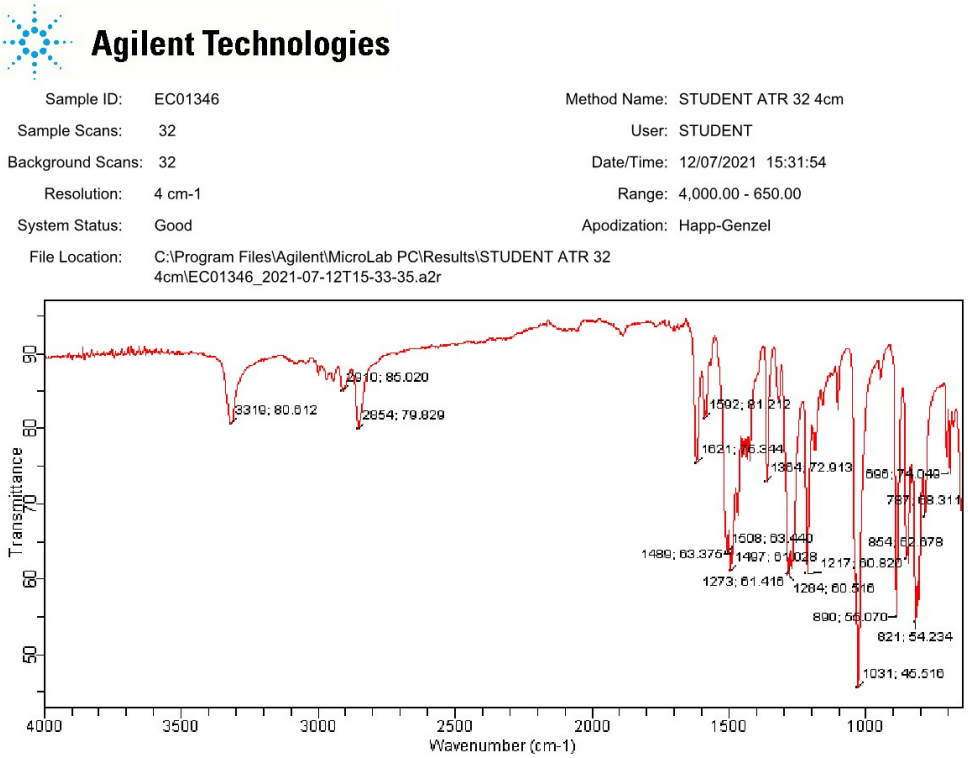


Figure 126. FT-IR spectra of N-(2-chloro-4-methoxyphenyl)-1,3-dihydroisobenzofuran-5-amine (**2.42d**).

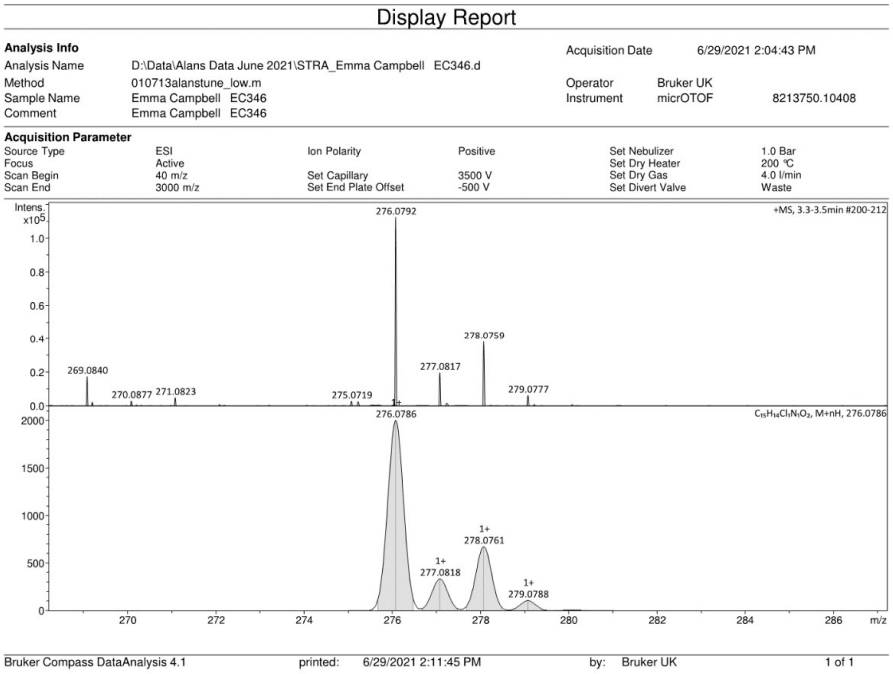


Figure 127. HRMS spectra of N-(2-chloro-4-methoxyphenyl)-1,3-dihydroisobenzofuran-5-amine (**2.42d**).

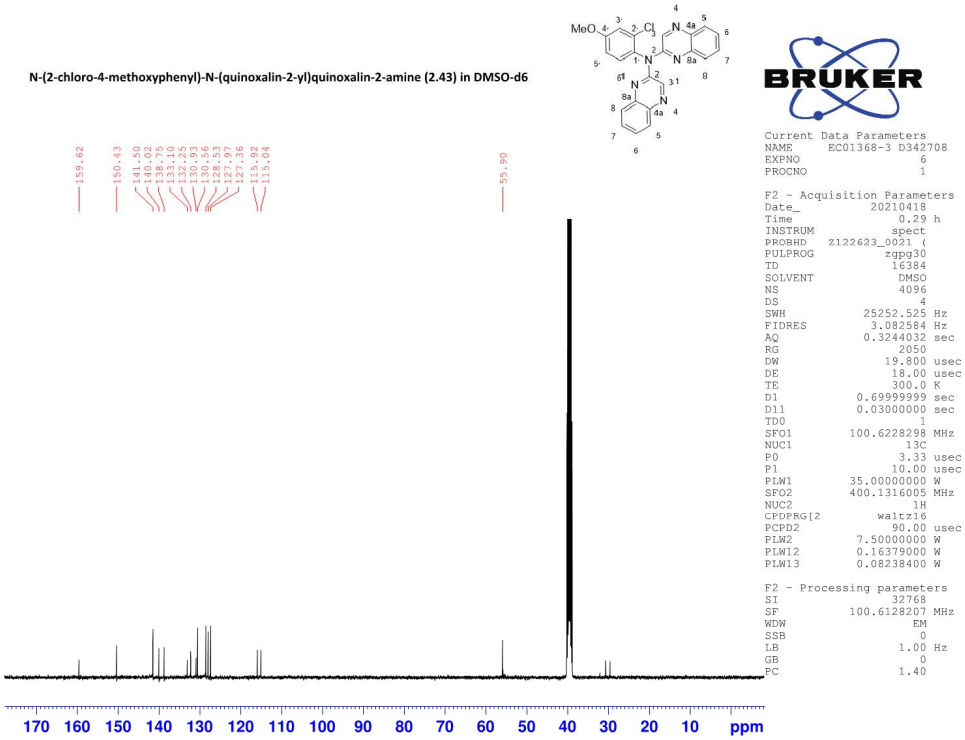


Figure 128. ^{13}C NMR spectra of N-(2-chloro-4-methoxyphenyl)-N-(quinoxalin-2-yl)quinoxalin-2-amine (**2.43**).

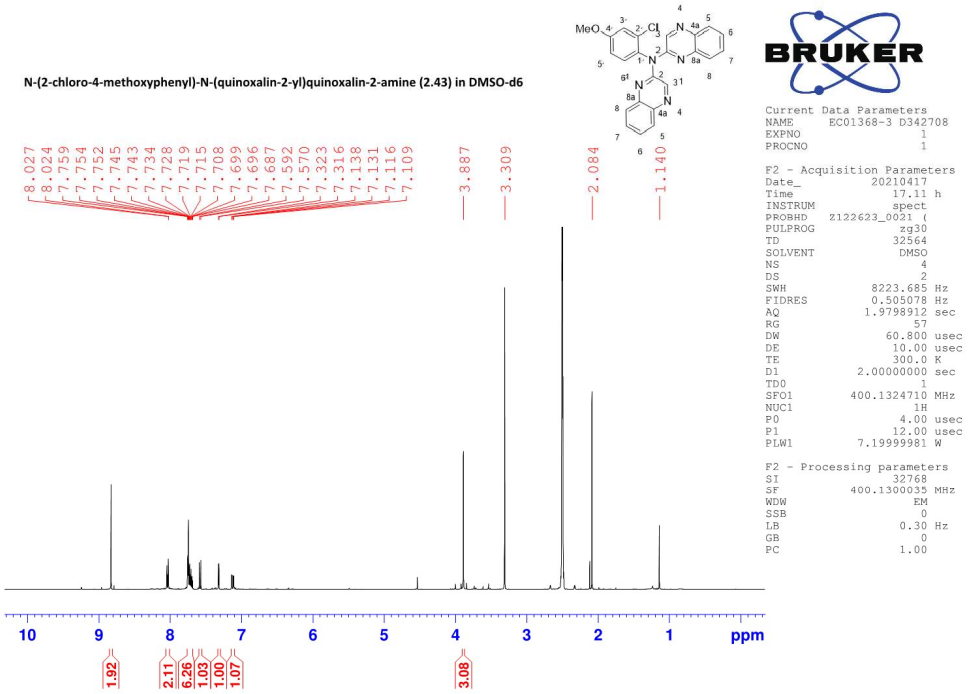


Figure 129. [1]H NMR spectra of N-(2-chloro-4-methoxyphenyl)-N-(quinoxalin-2-yl)quinoxalin-2-amine (**2.43**).

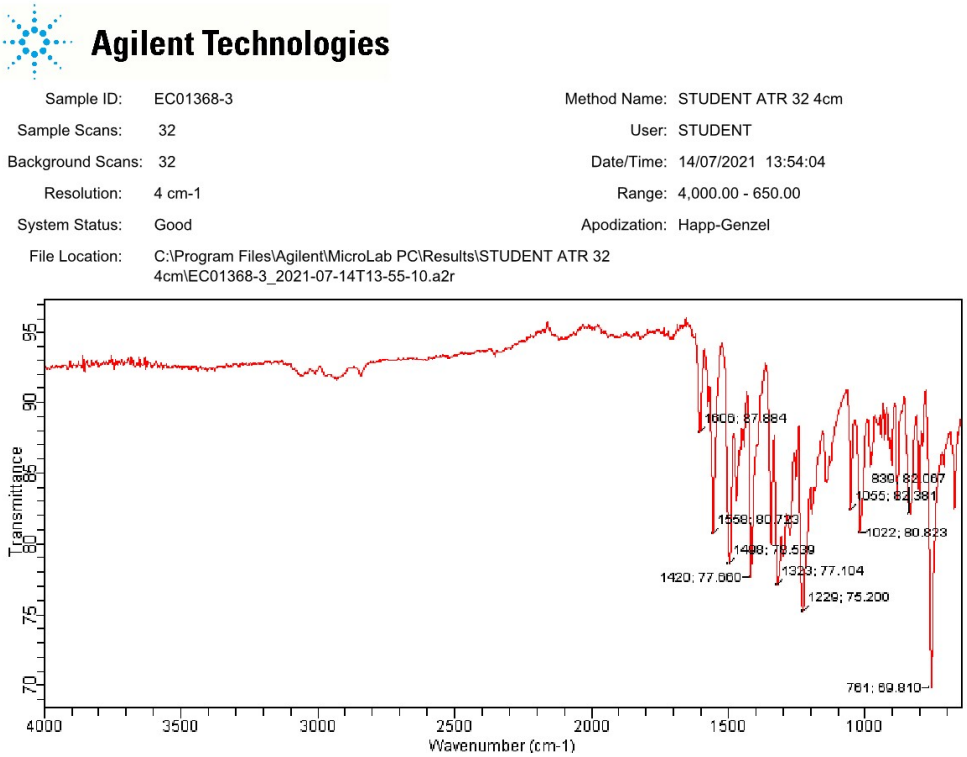


Figure 130. FT-IR spectra of N-(2-chloro-4-methoxyphenyl)-N-(quinoxalin-2-yl)quinoxalin-2-amine (**2.43**).

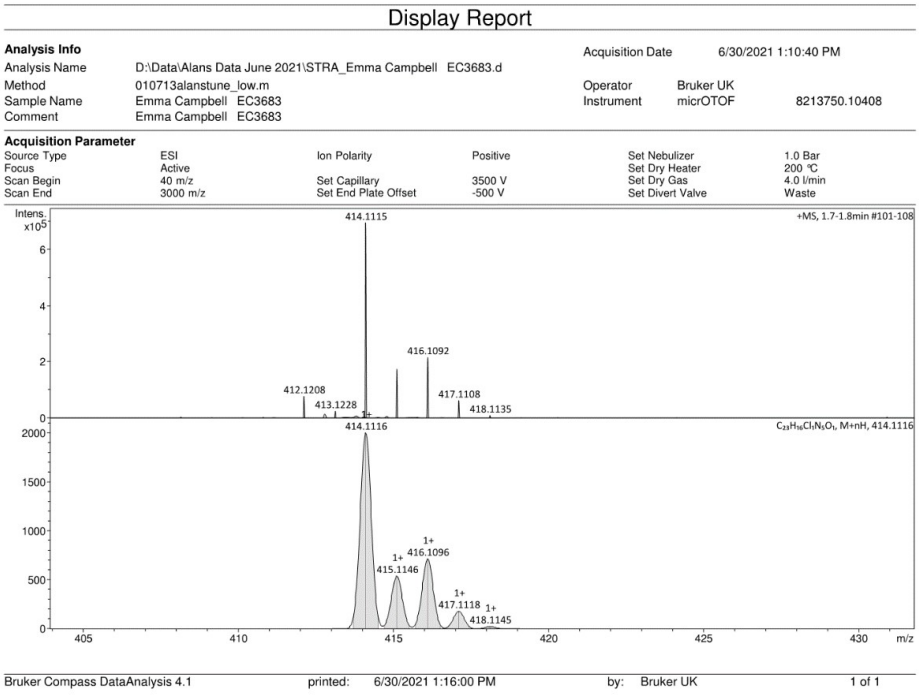


Figure 131. HRMS spectra of N-(2-chloro-4-methoxyphenyl)-N-(quinoxalin-2-yl)quinoxalin-2-amine (**2.43**).

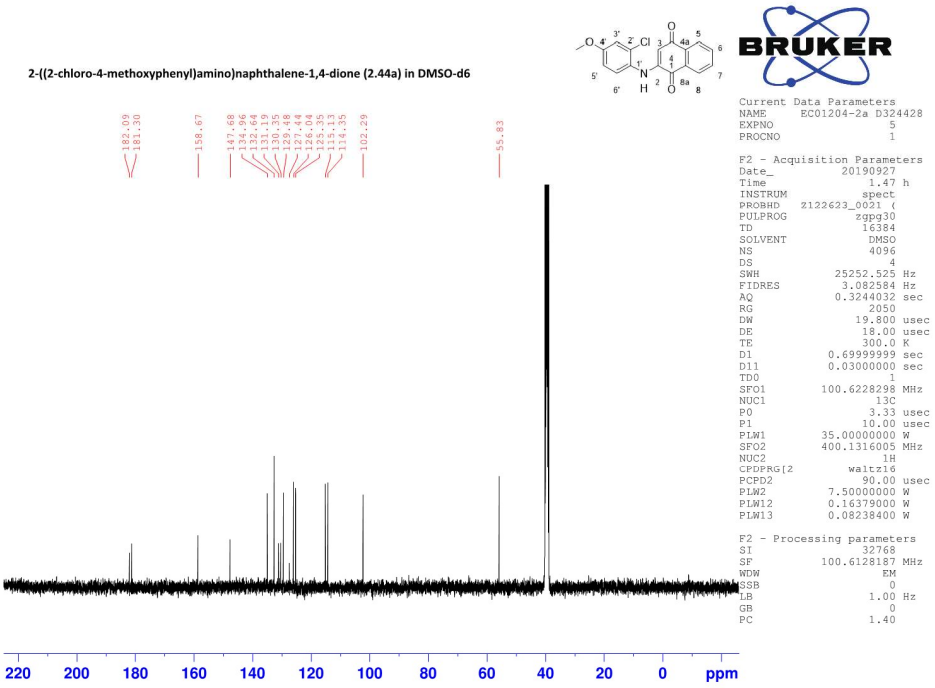


Figure 132. ^{13}C NMR spectra of 2-((2-chloro-4-methoxyphenyl)amino)naphthalene-1,4-dione (**2.44a**).

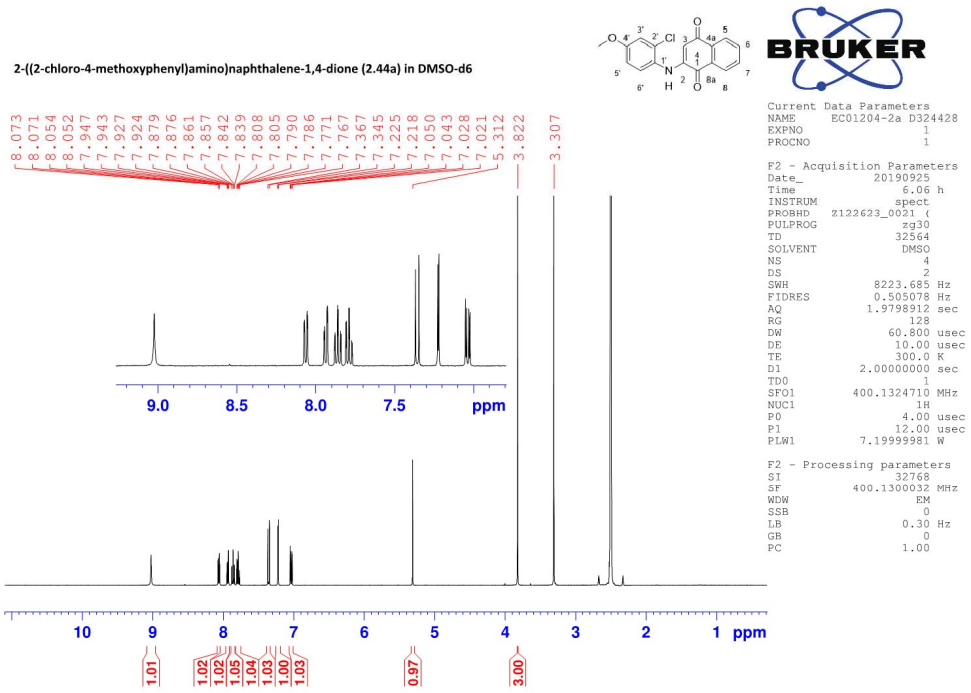


Figure 133. ^{1}H NMR spectra of 2-((2-chloro-4-methoxyphenyl)amino)naphthalene-1,4-dione (**2.44a**).

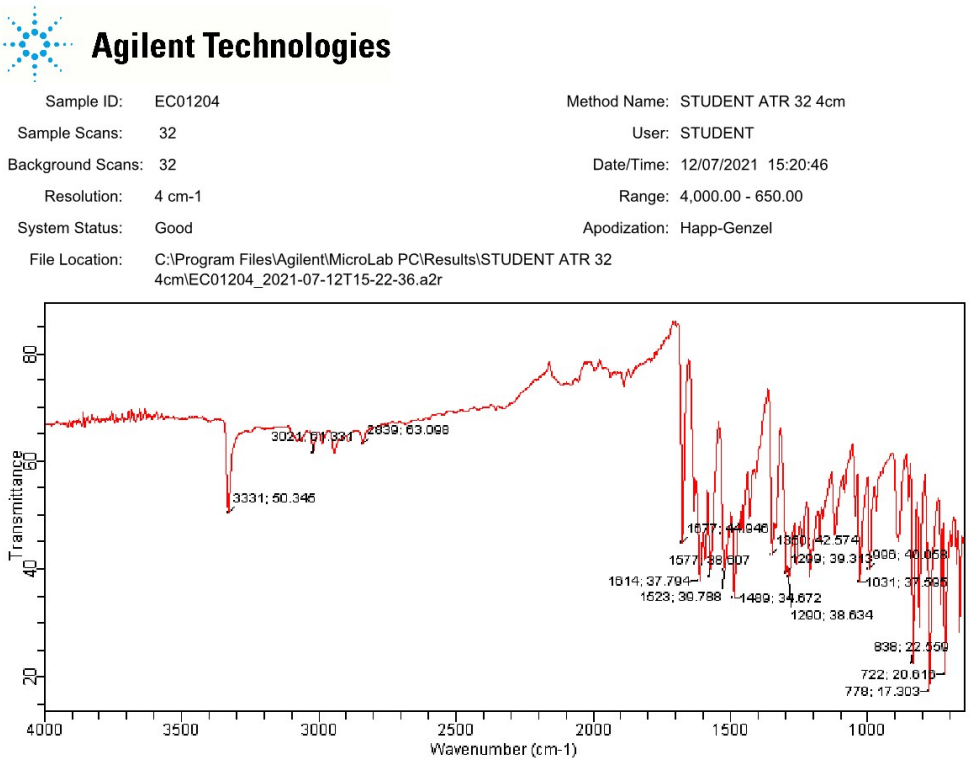


Figure 134. FT-IR spectra of 2-((2-chloro-4-methoxyphenyl)amino)naphthalene-1,4-dione (**2.44a**).

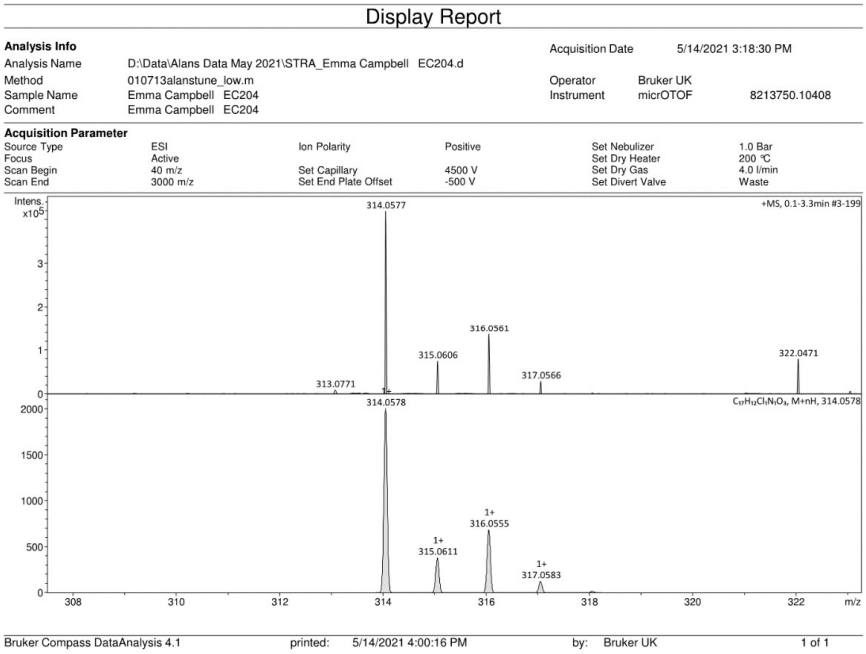


Figure 135. HRMS spectra of 2-((2-chloro-4-methoxyphenyl)amino)naphthalene-1,4-dione (**2.44a**).

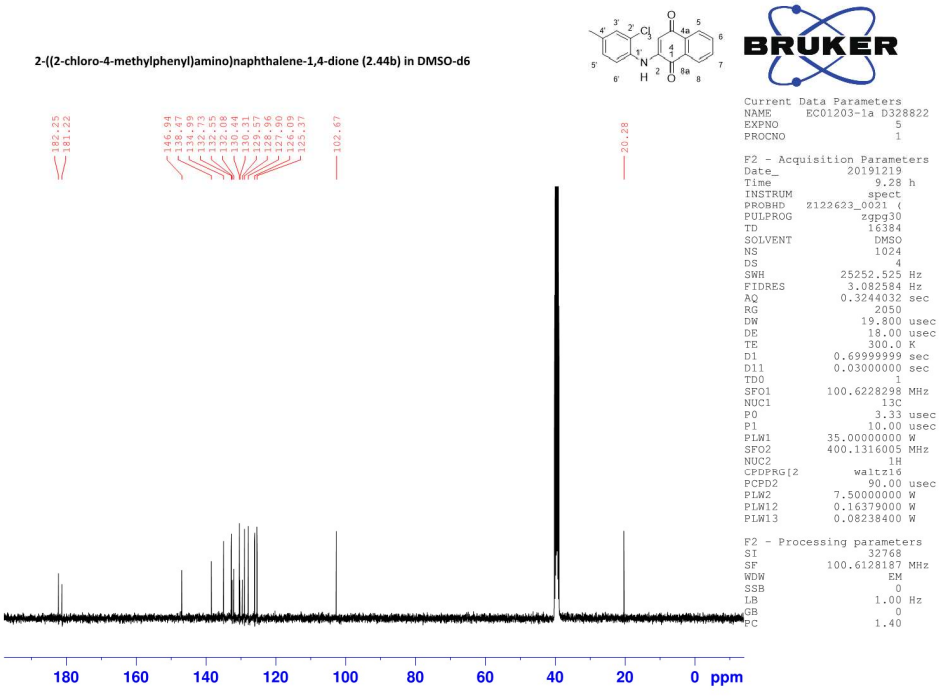


Figure 136. ^{13}C NMR spectra of 2-((2-chloro-4-methylphenyl)amino)naphthalene-1,4-dione (**2.44b**).

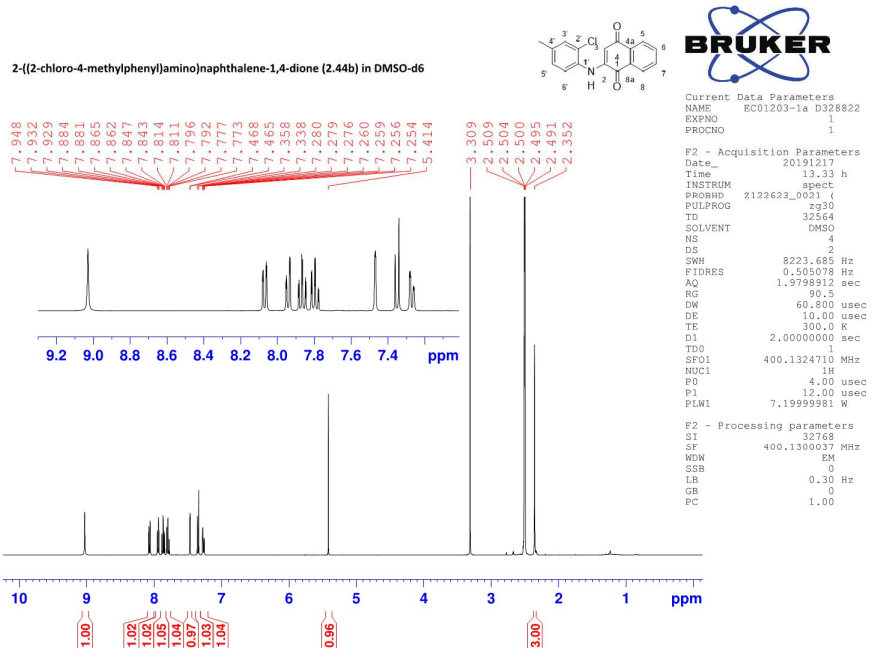


Figure 137. ^{1}H NMR spectra of 2-((2-chloro-4-methylphenyl)amino)naphthalene-1,4-dione (**2.44b**).

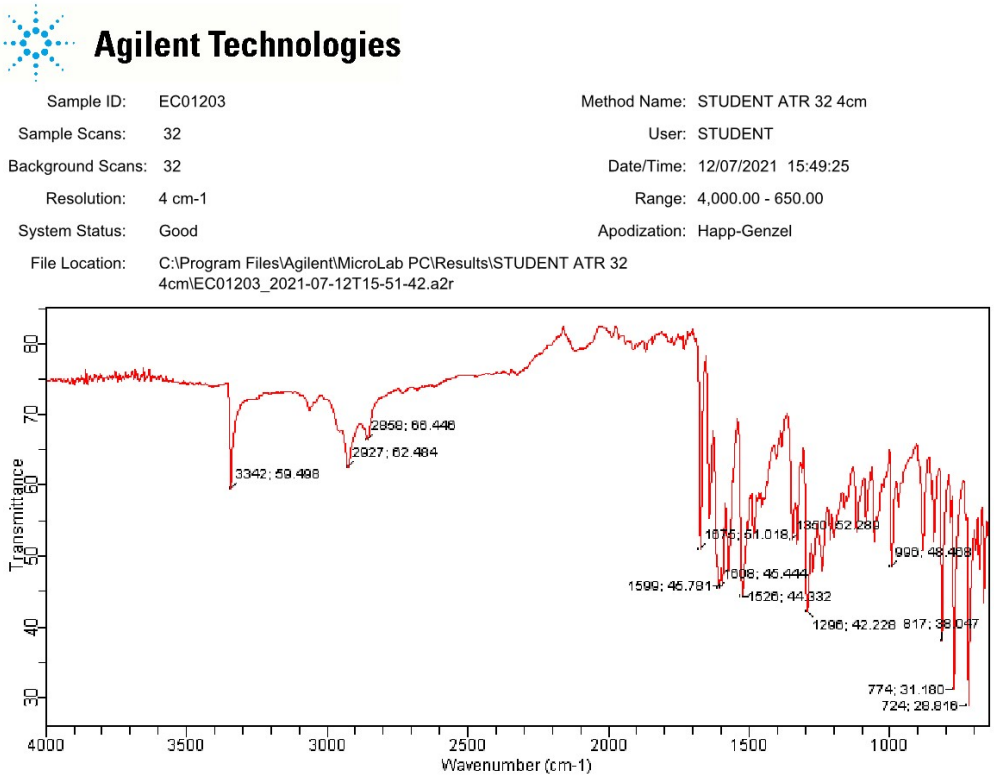


Figure 138. FT-IR spectra of 2-((2-chloro-4-methylphenyl)amino)naphthalene-1,4-dione (**2.44b**).

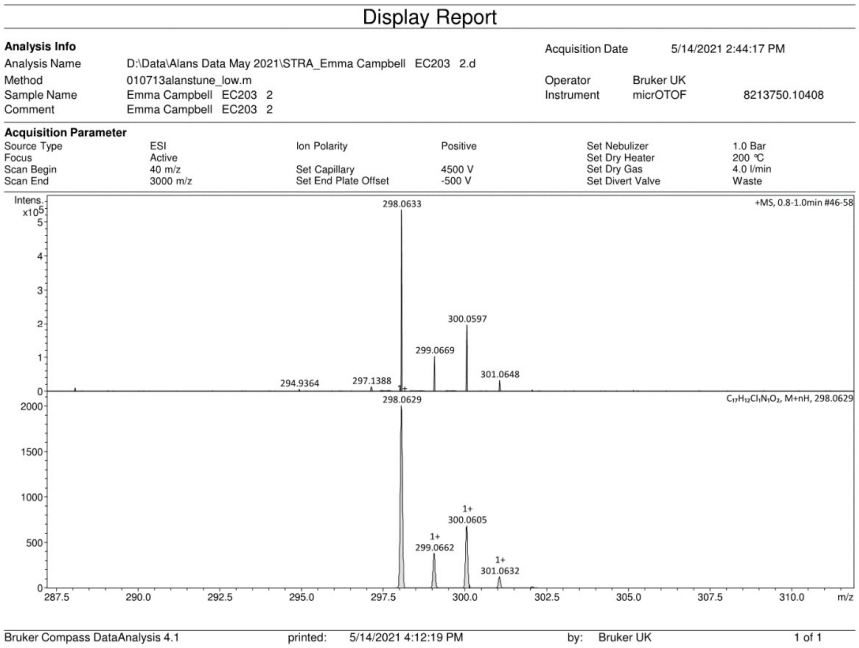


Figure 139. HRMS spectra of 2-((2-chloro-4-methylphenyl)amino)naphthalene-1,4-dione (**2.44b**).

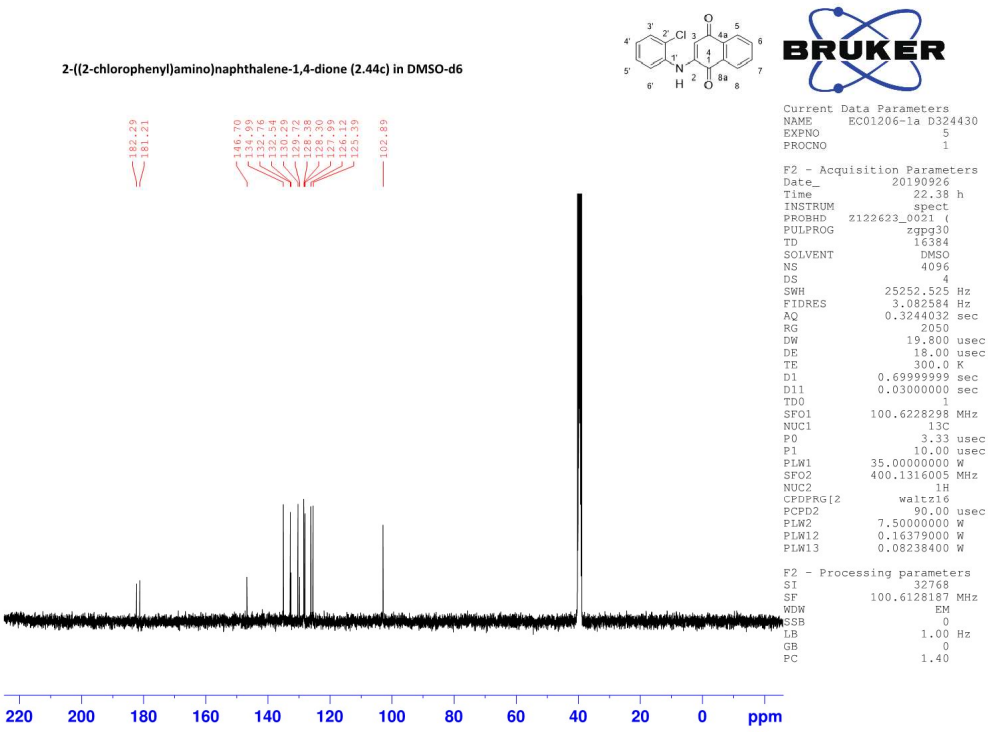


Figure 140. ^{13}C NMR spectra of 2-((2-chlorophenyl)amino)naphthalene-1,4-dione (**2.44c**).

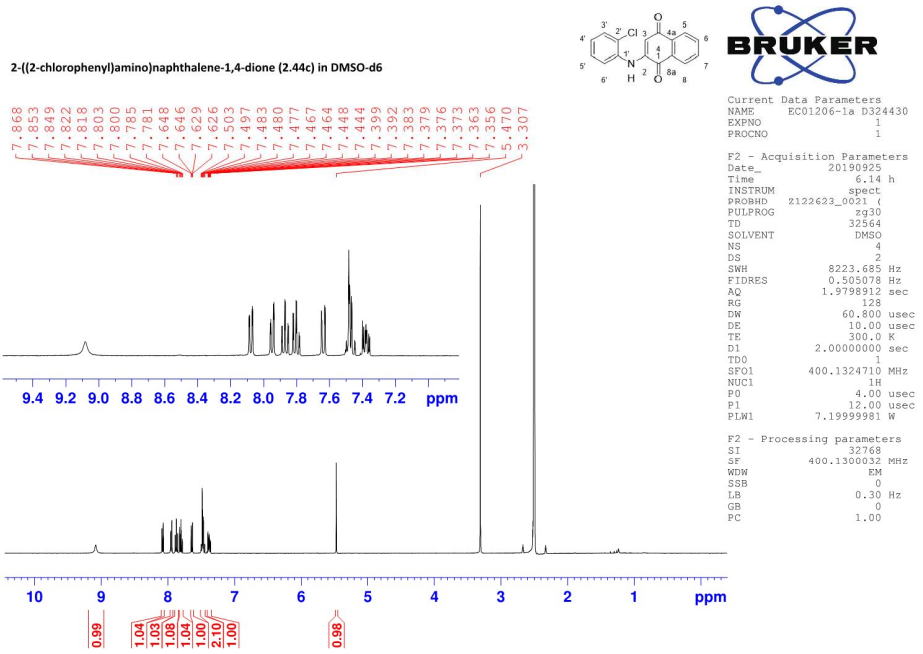


Figure 141. ^{1}H NMR spectra of2-((2-chlorophenyl)amino)naphthalene-1,4-dione (**2.44c**).

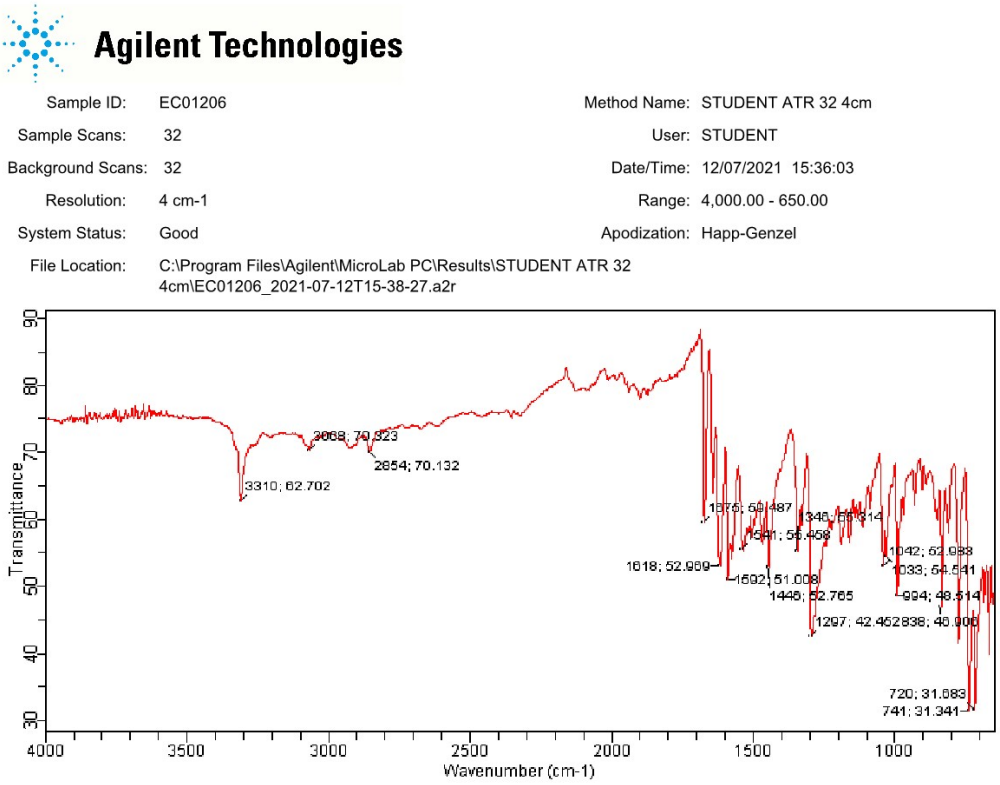


Figure 142. FT-IR spectra of 2-((2-chlorophenyl)amino)naphthalene-1,4-dione (**2.44c**).

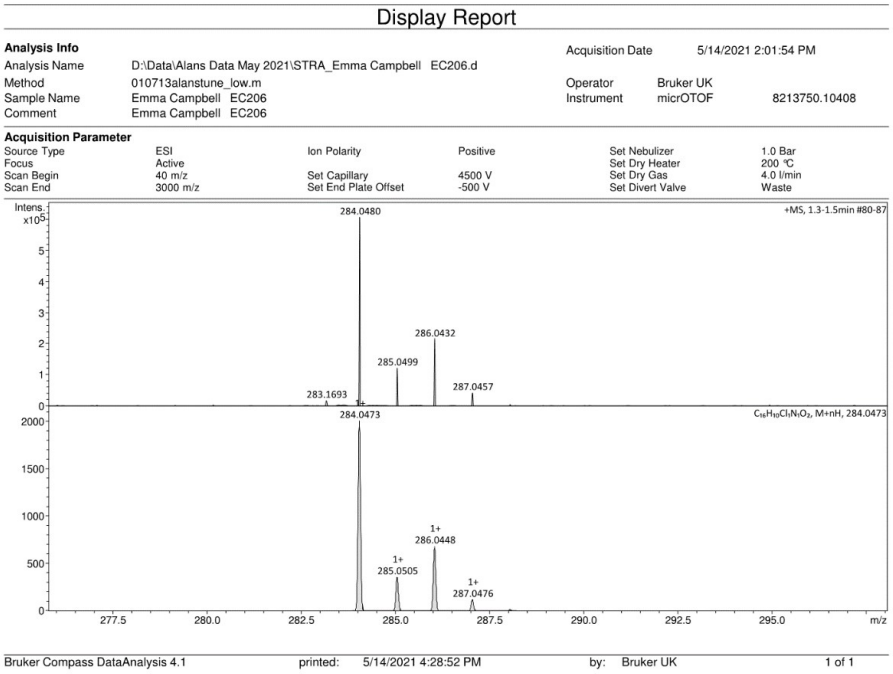


Figure 143. HRMS spectra of 2-((2-chlorophenyl)amino)naphthalene-1,4-dione (**2.44c**).

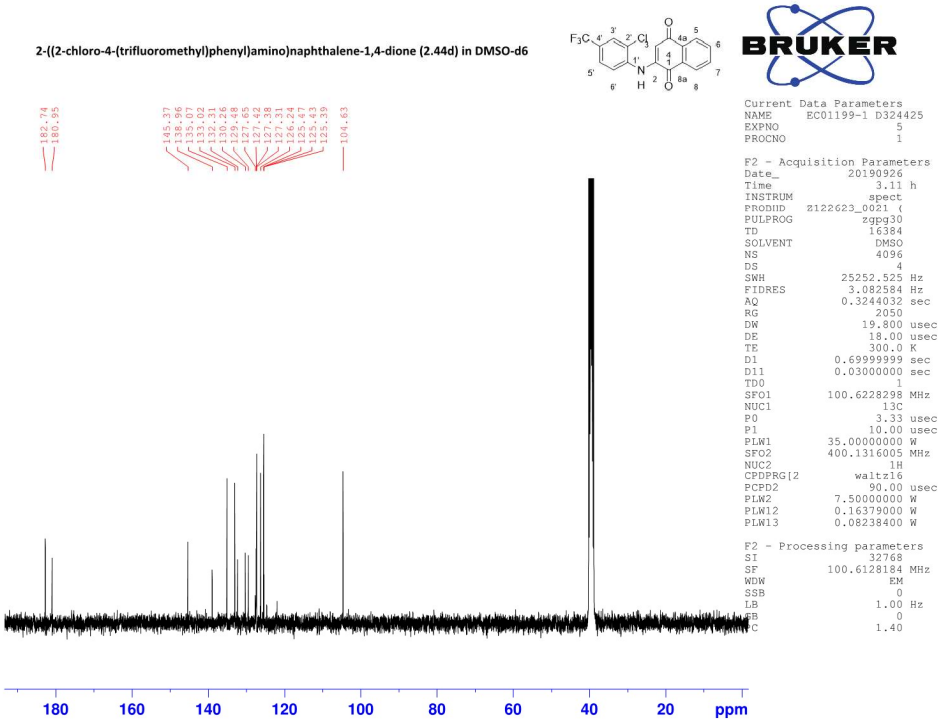


Figure 144. ^{13}C NMR spectra of 2-((2-chloro-4-(trifluoromethyl)phenyl)amino)naphthalene-1,4-dione (**2.44d**).

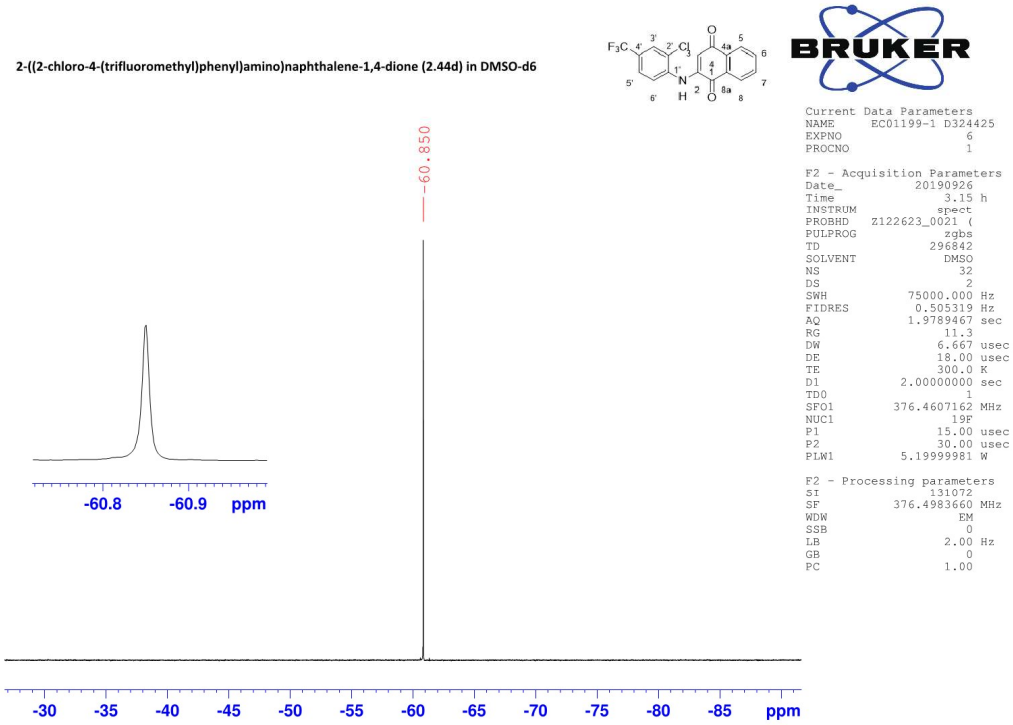


Figure 145. ^{19}F NMR spectra of 2-((2-chloro-4-(trifluoromethyl)phenyl)amino)naphthalene-1,4-dione (**2.44d**).

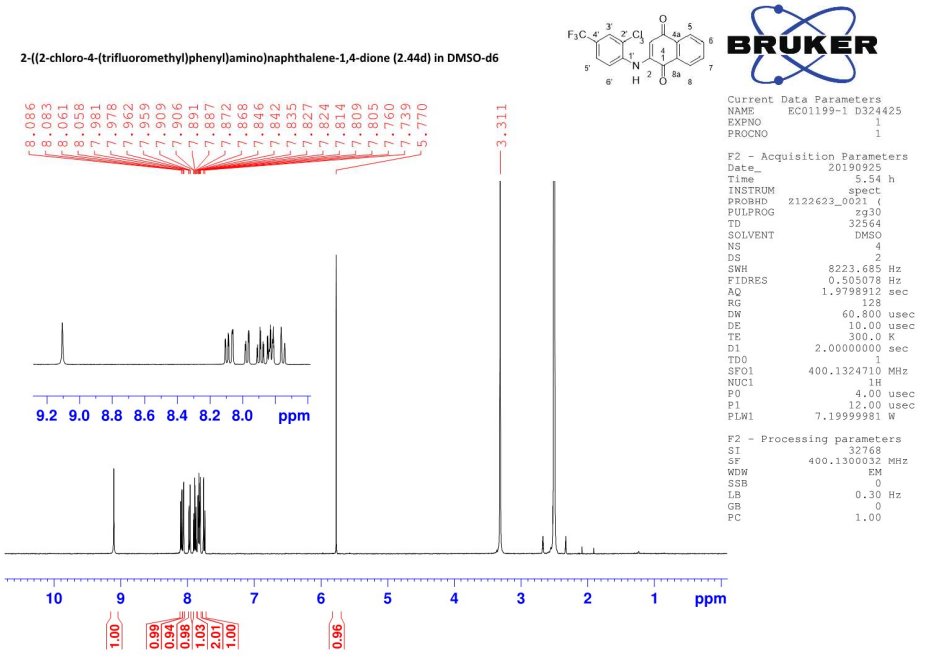


Figure 146. ^{1}H NMR spectra of 2-((2-chloro-4-(trifluoromethyl)phenyl)amino)naphthalene-1,4-dione (**2.44d**).

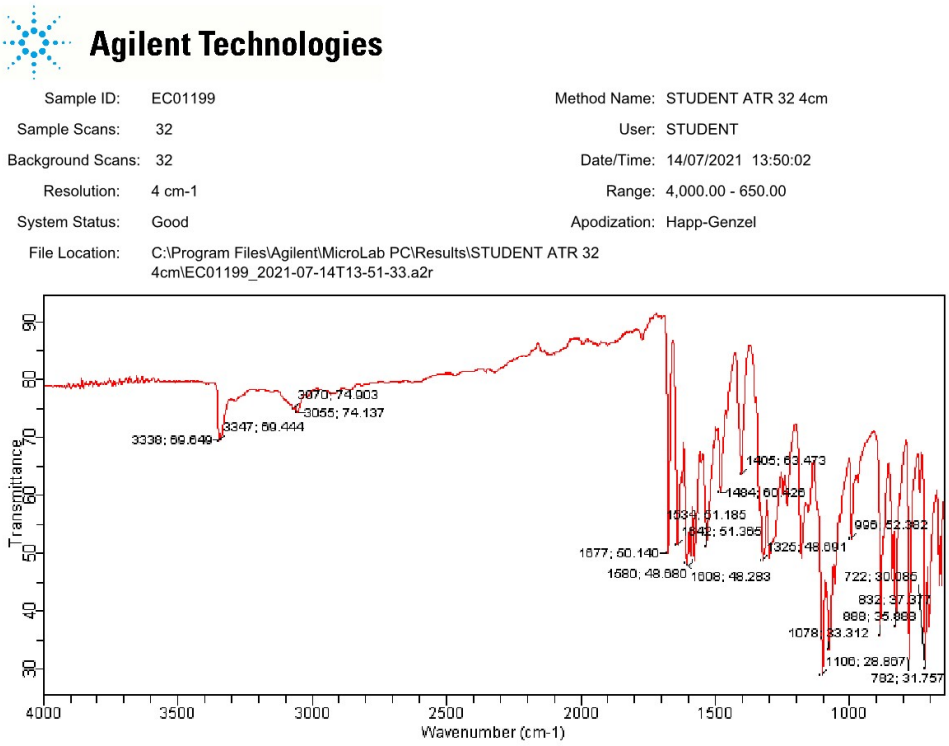


Figure 147. FT-IR spectra of 2-((2-chloro-4-(trifluoromethyl)phenyl)amino)naphthalene-1,4-dione (**2.44d**).

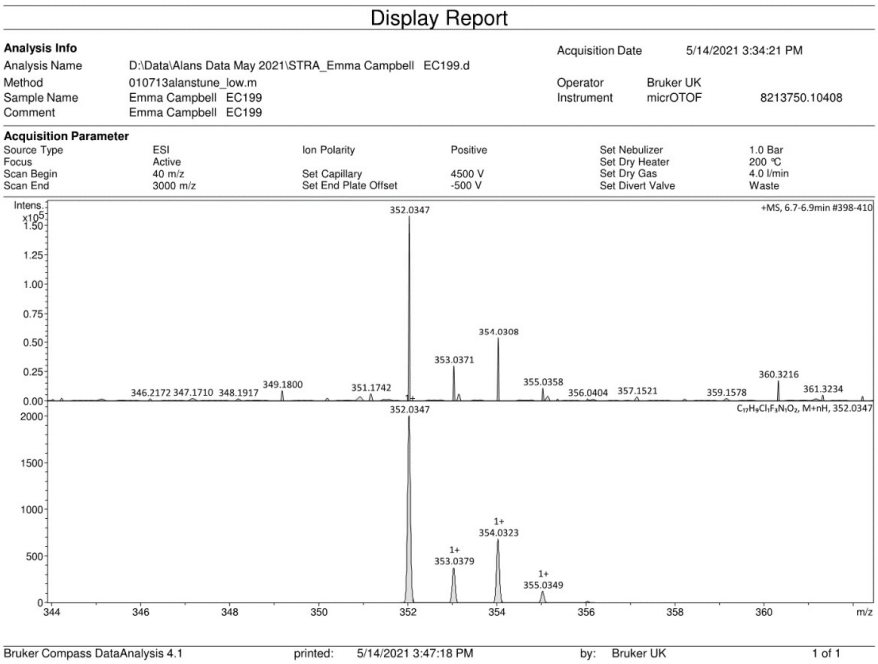


Figure 148. HRMS spectra of 2-((2-chloro-4-(trifluoromethyl)phenyl)amino)naphthalene-1,4-dione (**2.44d**).

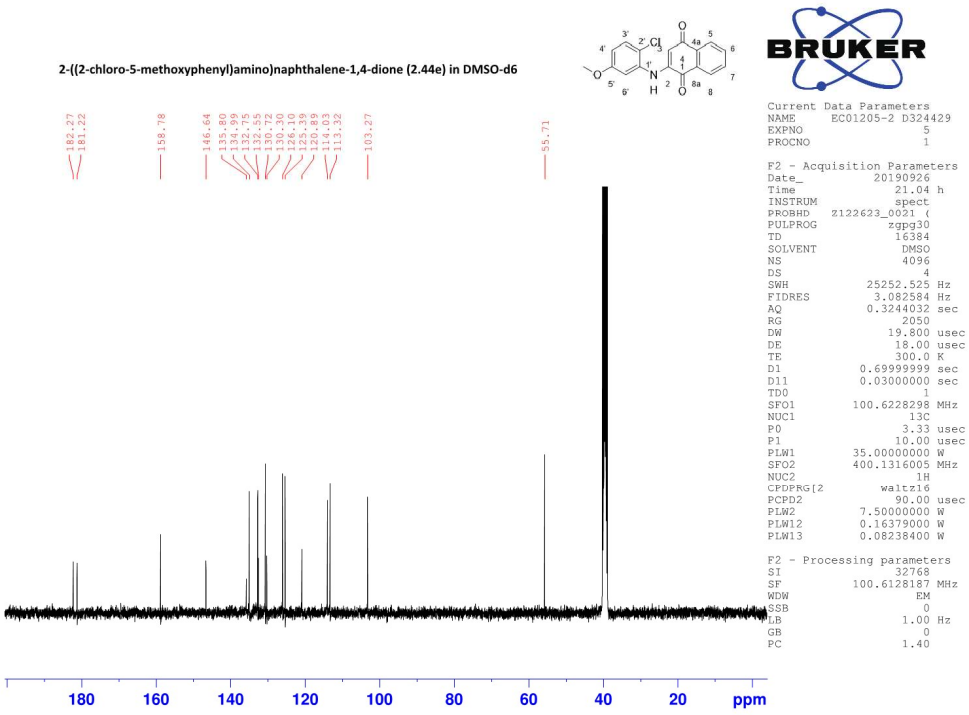


Figure 149. ^{13}C NMR spectra of 2-((2-chloro-5-methoxyphenyl)amino)naphthalene-1,4-dione (**2.44e**).

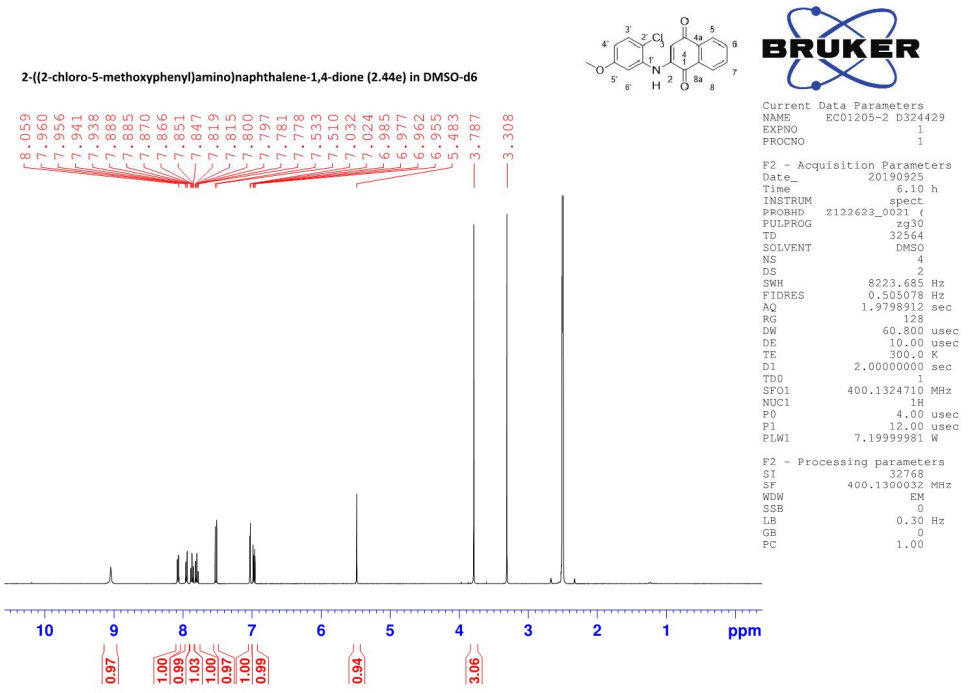


Figure 150. ^{1}H NMR spectra of 2-((2-chloro-5-methoxyphenyl)amino)naphthalene-1,4-dione (**2.44e**).

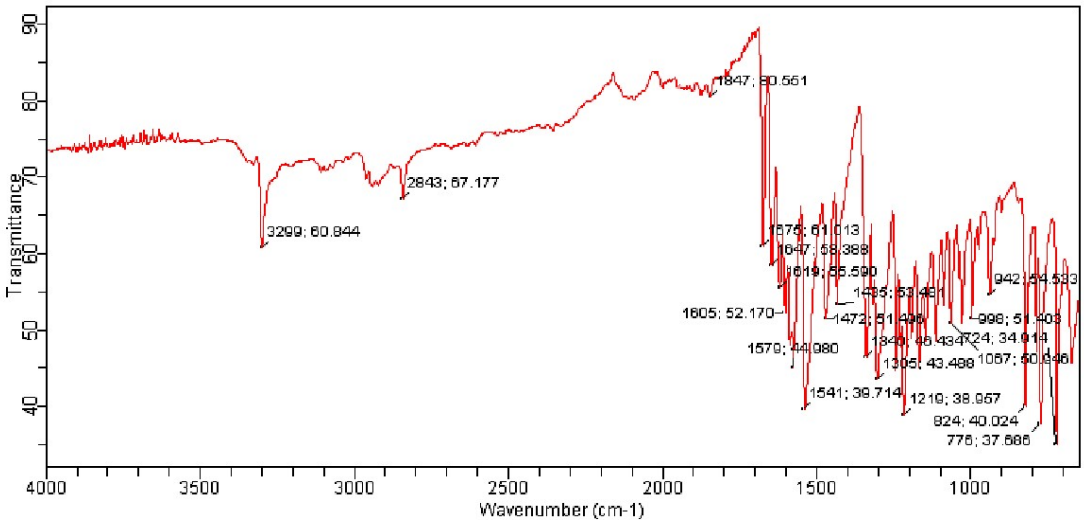


Figure 151. FT-IR spectra of 2-((2-chloro-5-methoxyphenyl)amino)naphthalene-1,4-dione (**2.44e**)

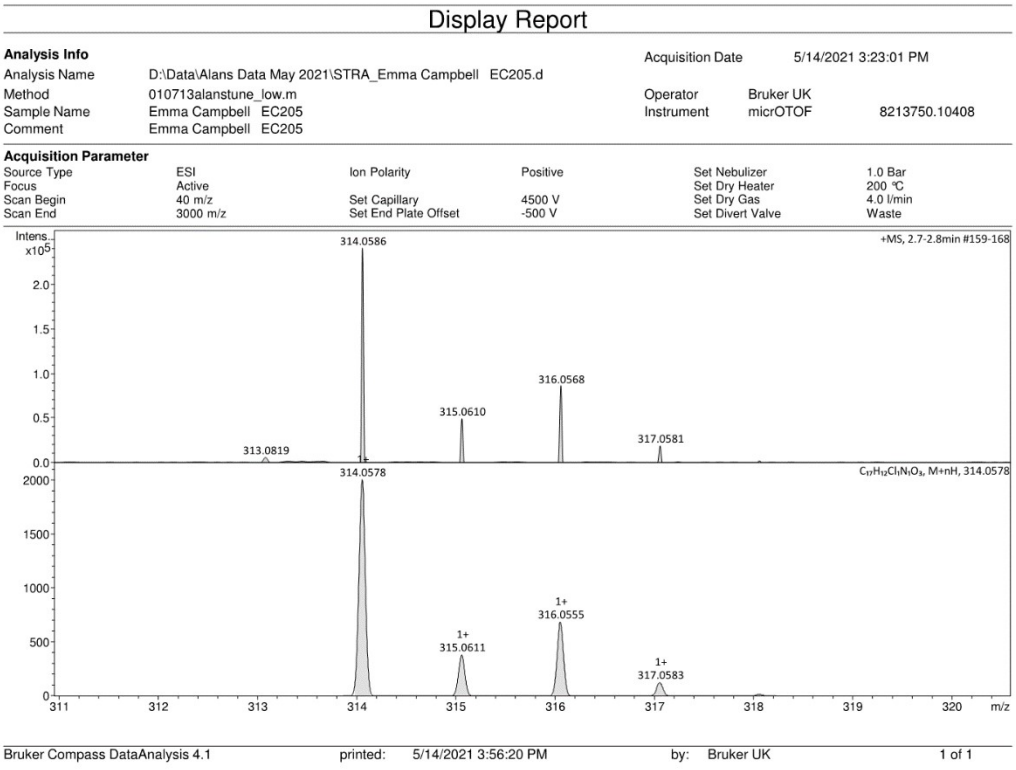


Figure 152. HRMS spectra of 2-((2-chloro-5-methoxyphenyl)amino)naphthalene-1,4-dione (**2.44e**).

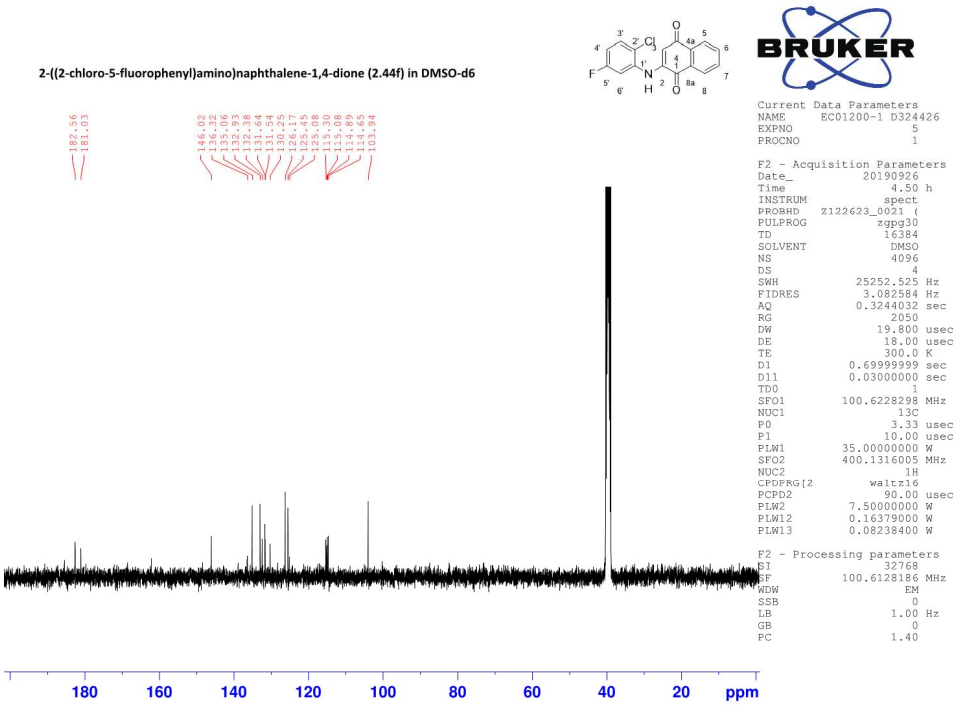


Figure 153. ^{13}C NMR spectra of 2-((2-chloro-5-fluorophenyl)amino)naphthalene-1,4-dione (**2.44f**).

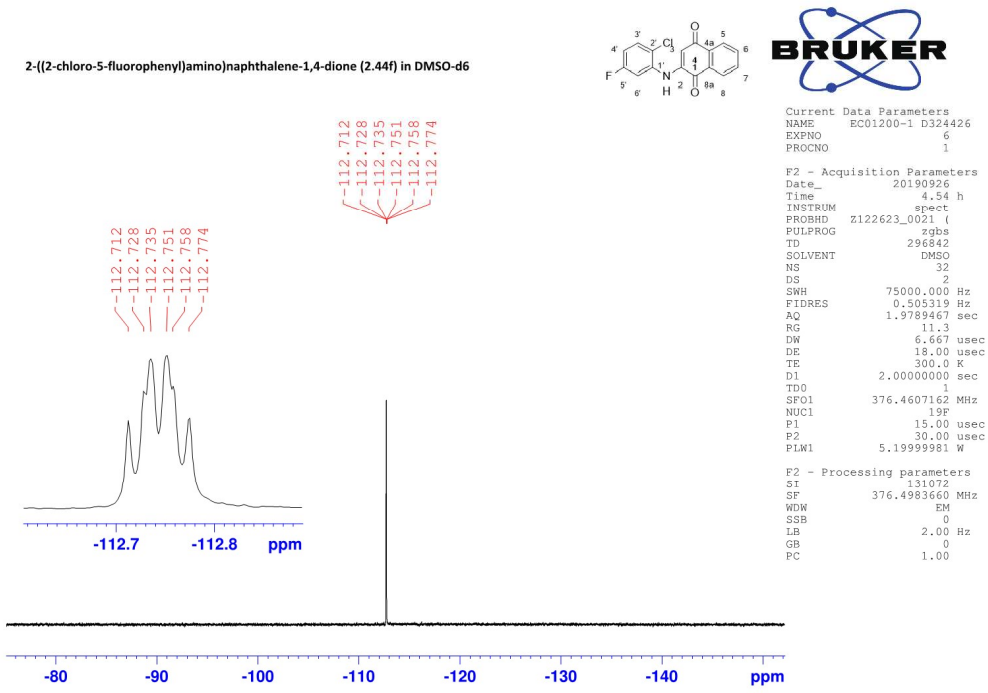


Figure 154. ^{19}F NMR spectra of 2-((2-chloro-5-fluorophenyl)amino)naphthalene-1,4-dione (**2.44f**).

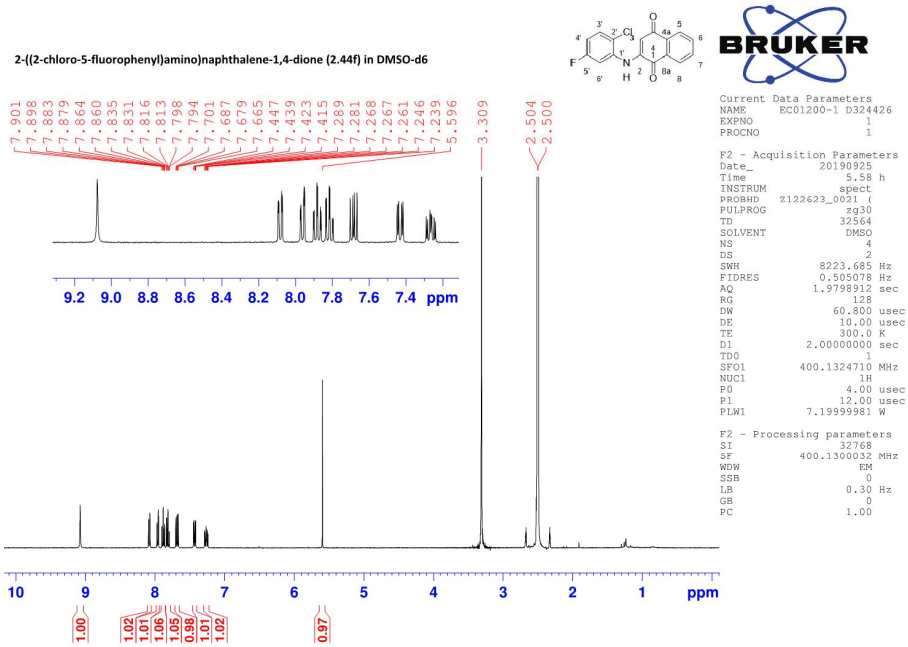


Figure 155. ^{1}H NMR spectra of 2-((2-chloro-5-fluorophenyl)amino)naphthalene-1,4-dione (**2.44f**).

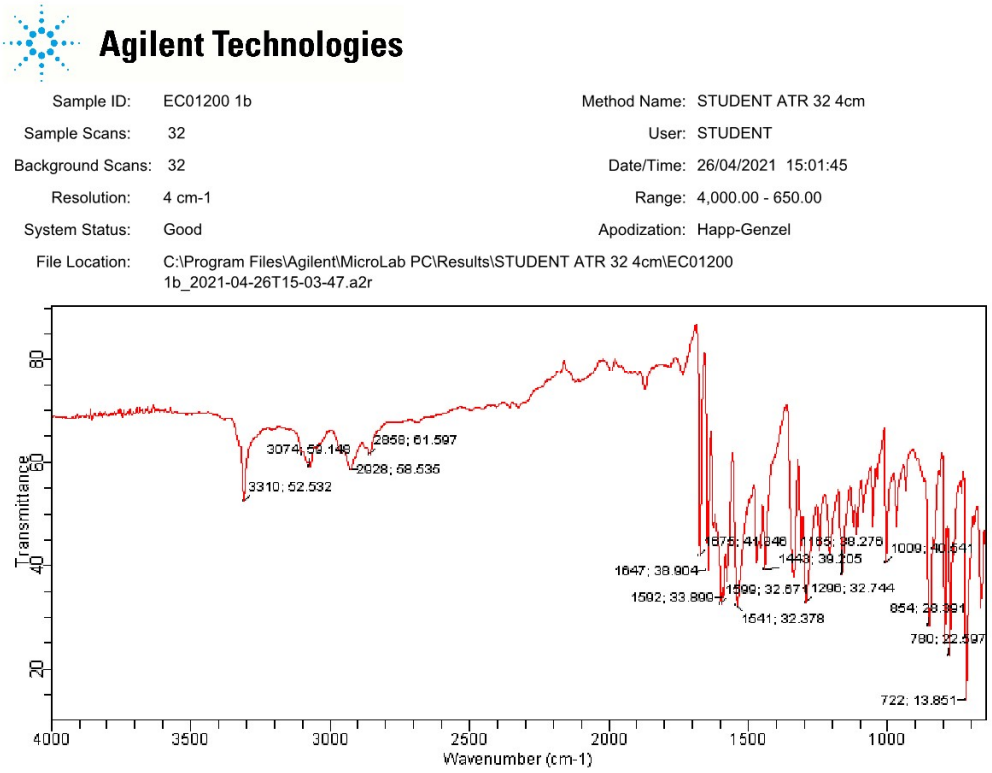


Figure 156. FT-IR spectra of 2-((2-chloro-5-fluorophenyl)amino)naphthalene-1,4-dione (**2.44f**).

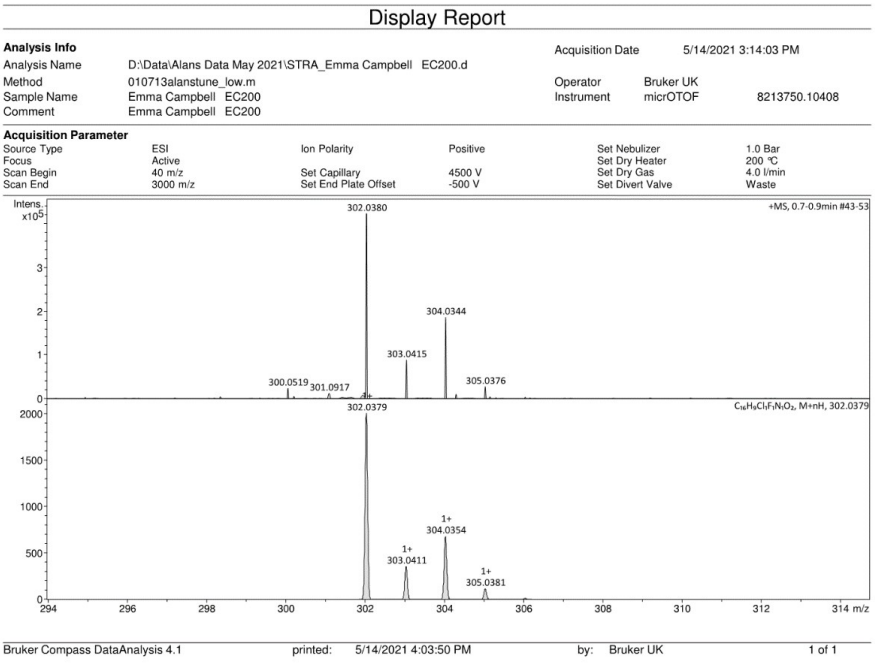


Figure 157. HRMS spectra of 2-((2-chloro-5-fluorophenyl)amino)naphthalene-1,4-dione (**2.44f**).

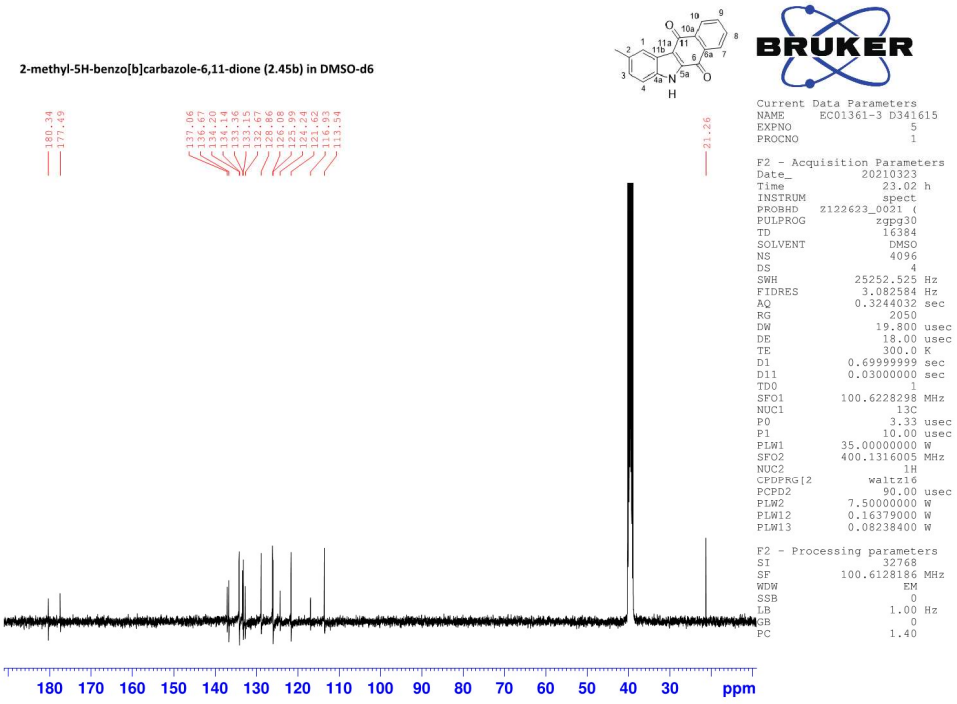


Figure 158. ^{13}C NMR spectra of 2-methyl-5H-benzo[b]carbazole-6,11-dione (**2.45b**).

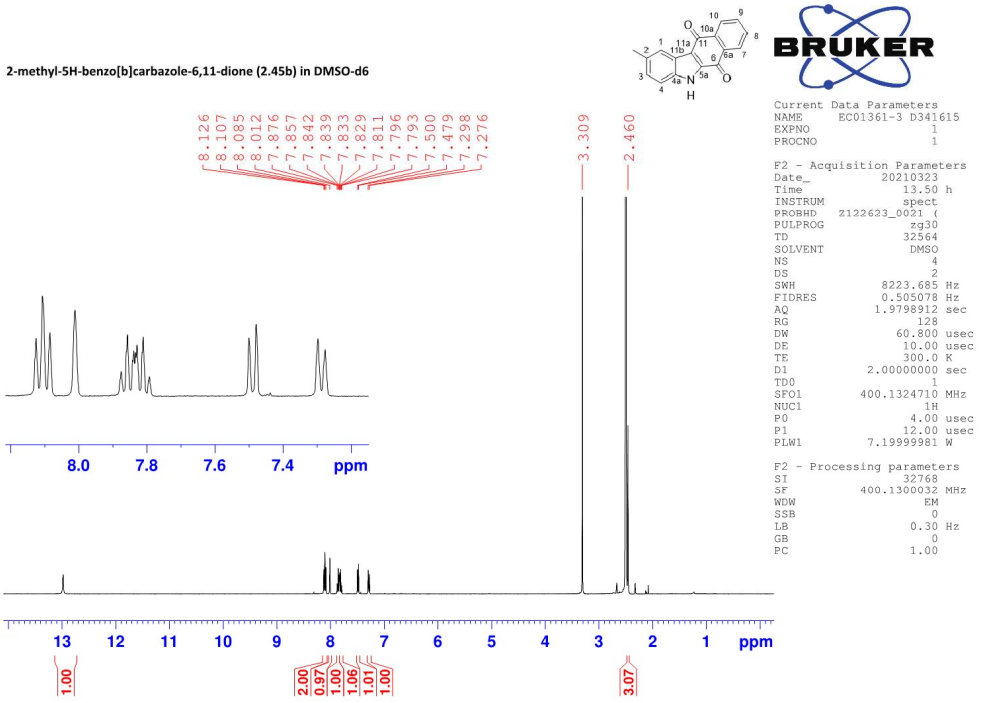


Figure 159. [1]H NMR spectra of 2-methyl-5H-benzo[b]carbazole-6,11-dione (**2.45b**).

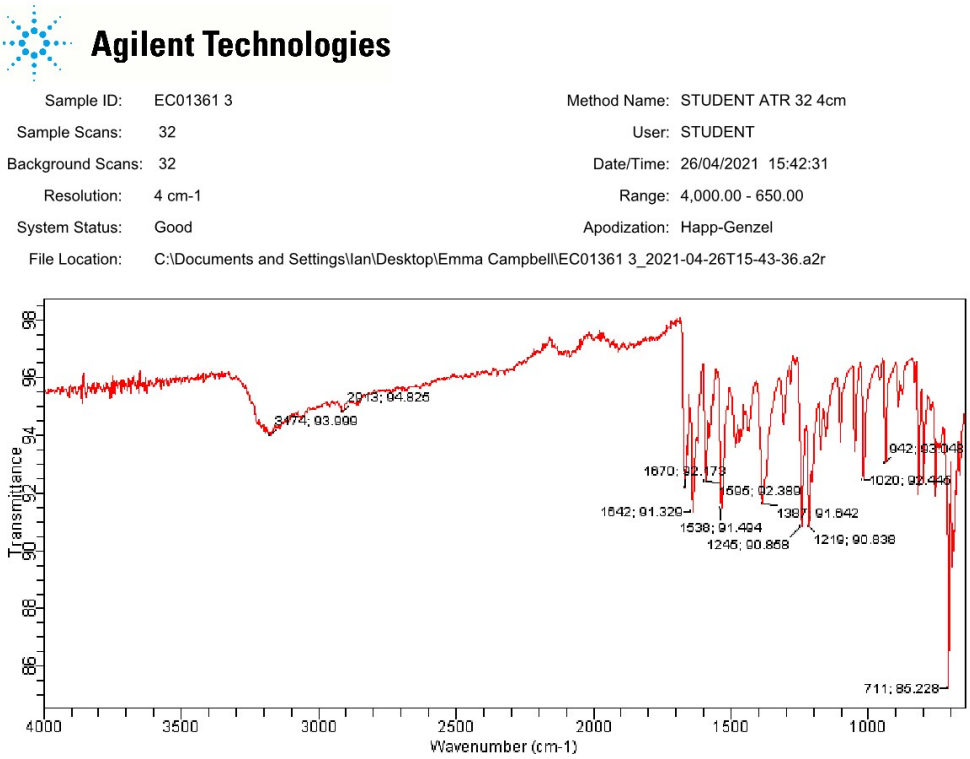


Figure 160. FT-IR spectra of 2-methyl-5H-benzo[b]carbazole-6,11-dione (**2.45b**).

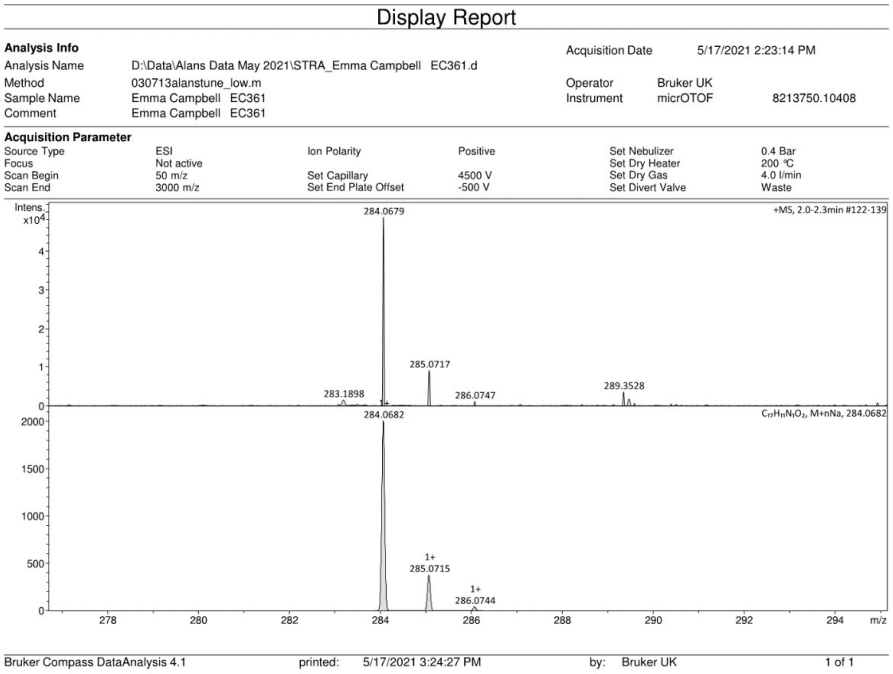


Figure 161. HRMS spectra of 2-methyl-5H-benzo[b]carbazole-6,11-dione (**2.45b**).

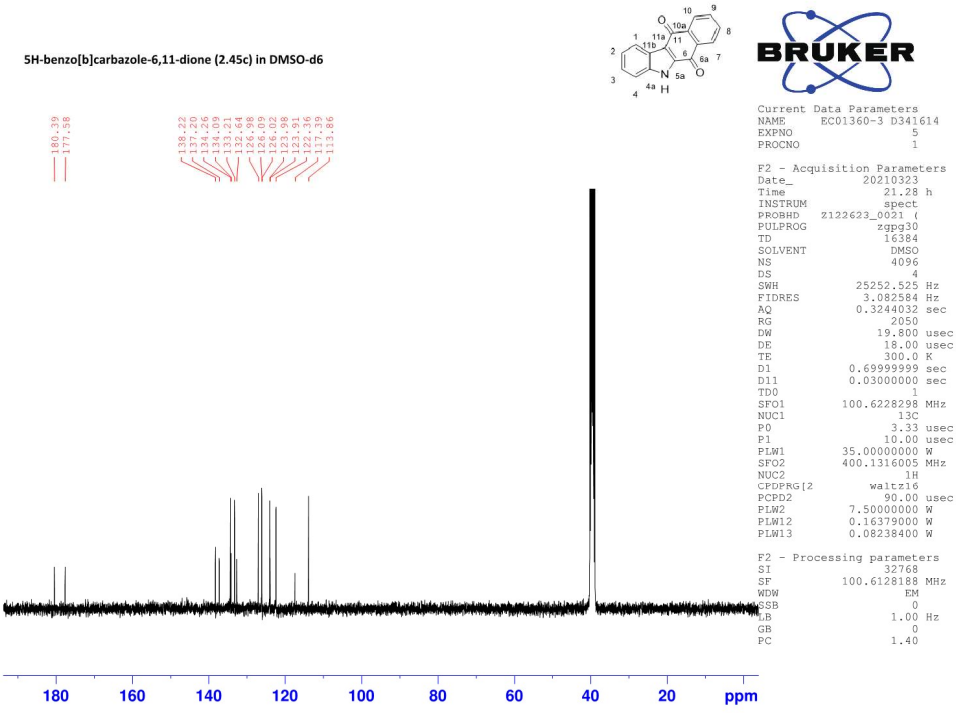


Figure 162. ^{13}C NMR spectra of 5H-benzo[b]carbazole-6,11-dione (**2.45c**).

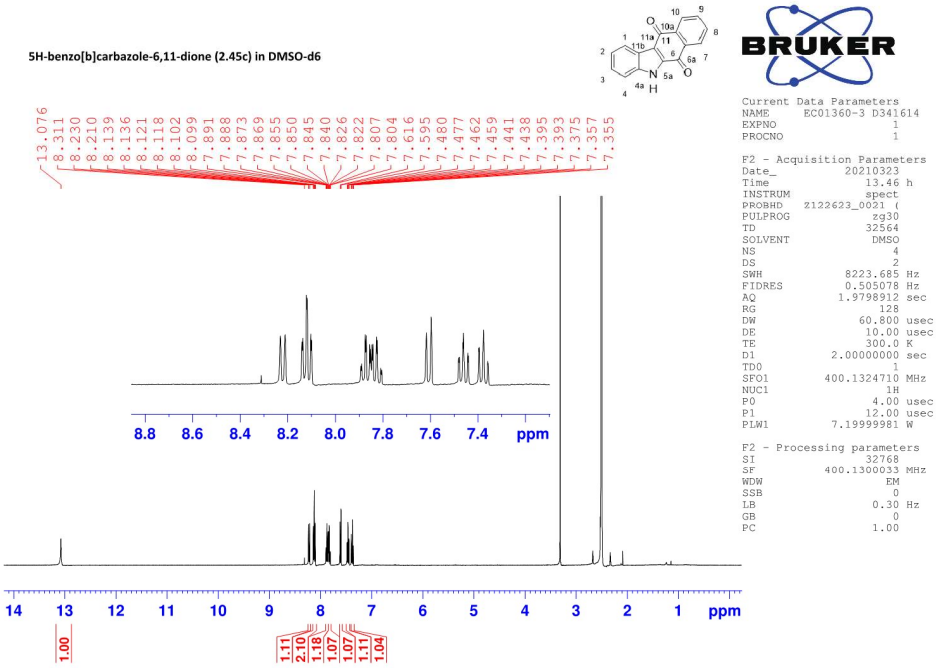


Figure 163. ^{1}H NMR spectra of 5H-benzo[b]carbazole-6,11-dione (**2.45c**).

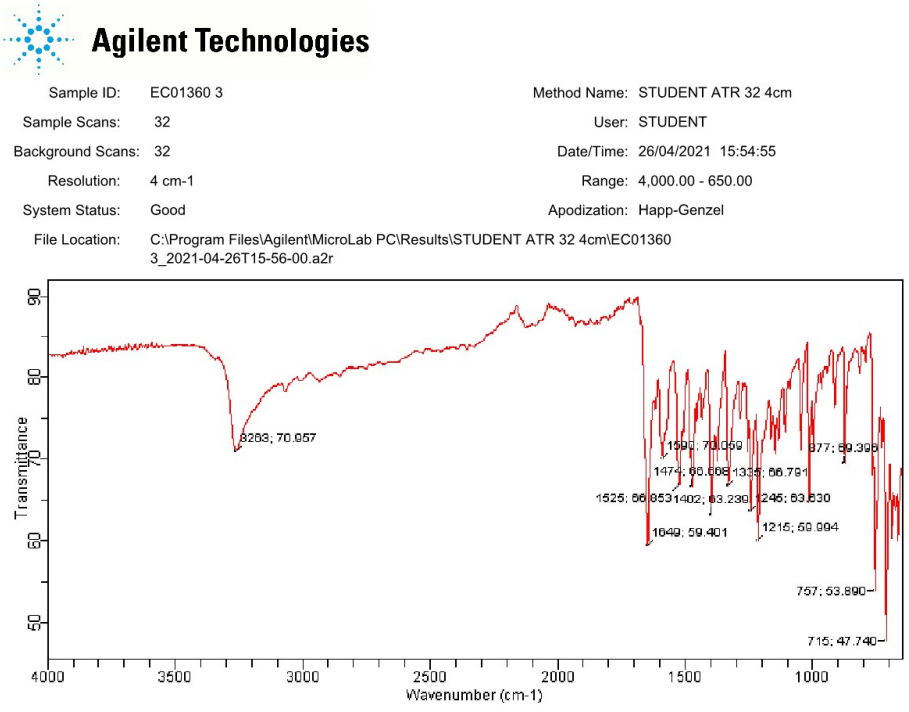


Figure 164. FT-IR spectra of 5H-benzo[b]carbazole-6,11-dione (**2.45c**).

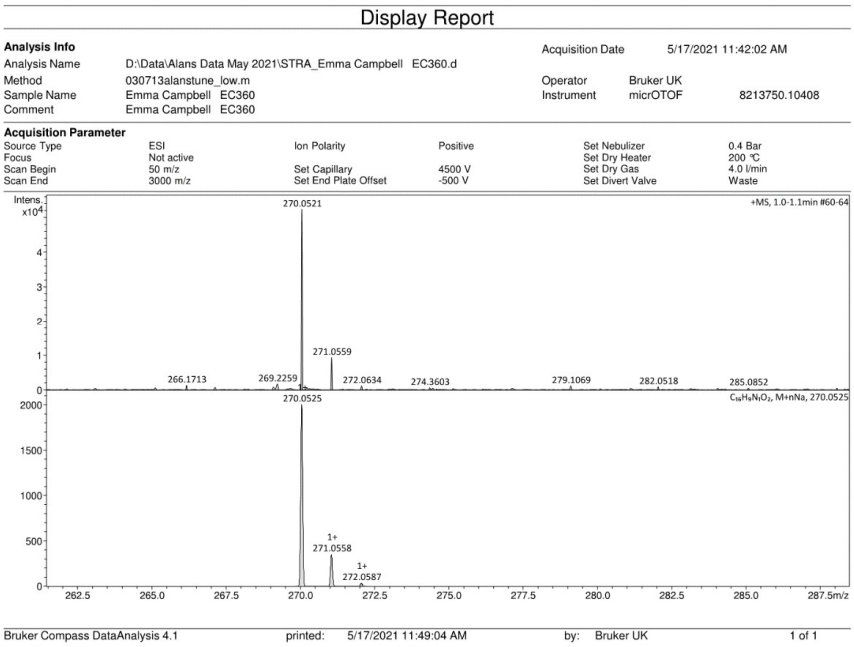


Figure 165. HRMS spectra of 5H-benzo[b]carbazole-6,11-dione (**2.45c**).

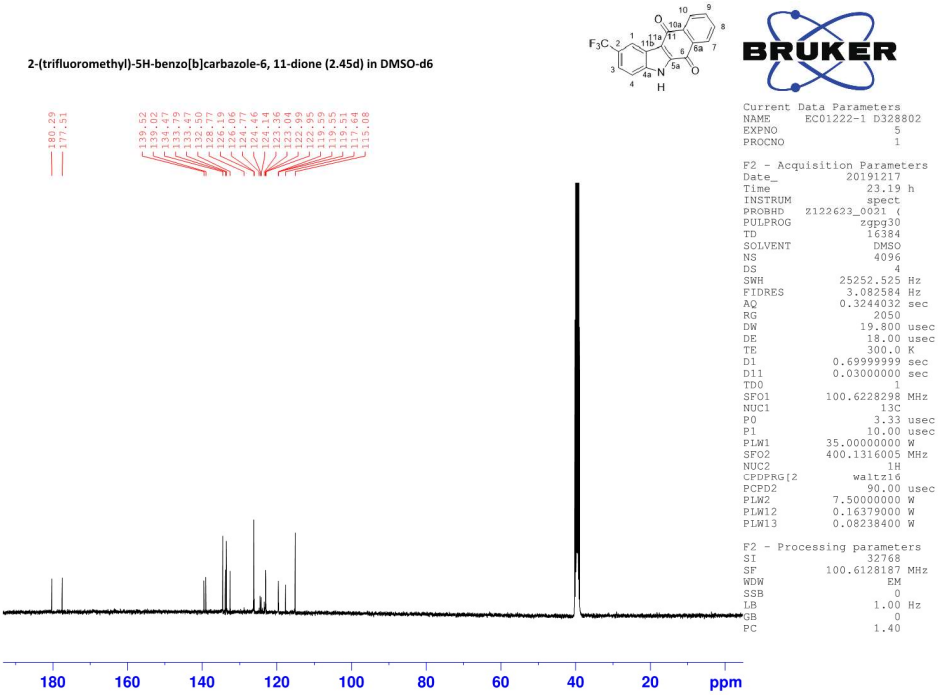


Figure 166. ^{13}C NMR spectra of 2-(trifluoromethyl)-5H-benzo[b]carbazole-6, 11-dione (**2.45d**).

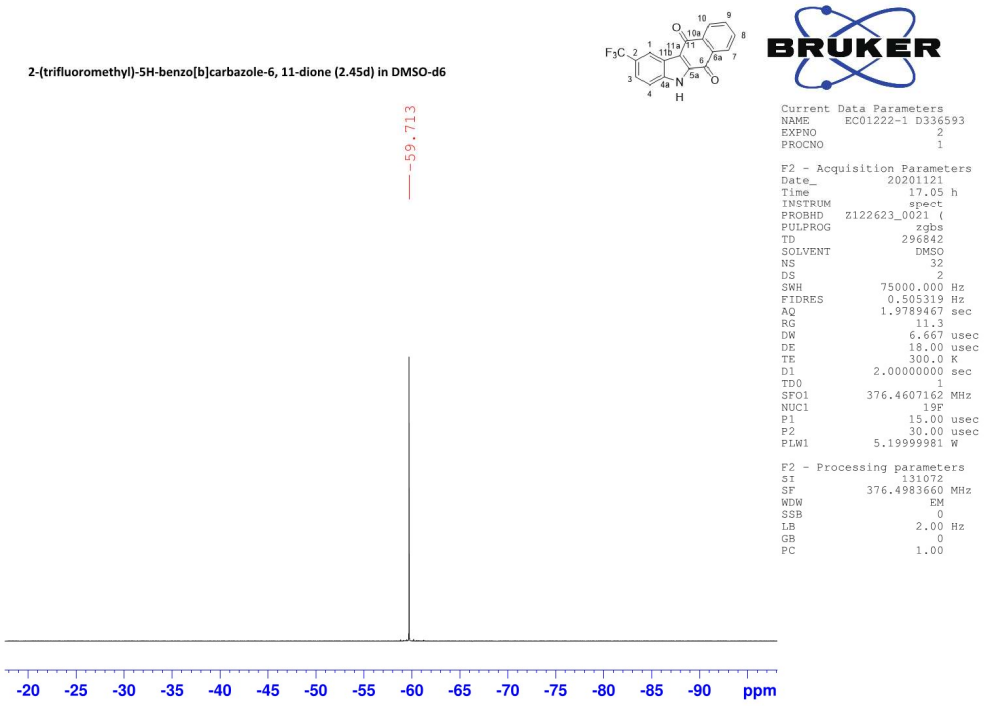


Figure 167. ^{19}F NMR spectra of 2-(trifluoromethyl)-5H-benzo[b]carbazole-6, 11-dione (**2.45d**).

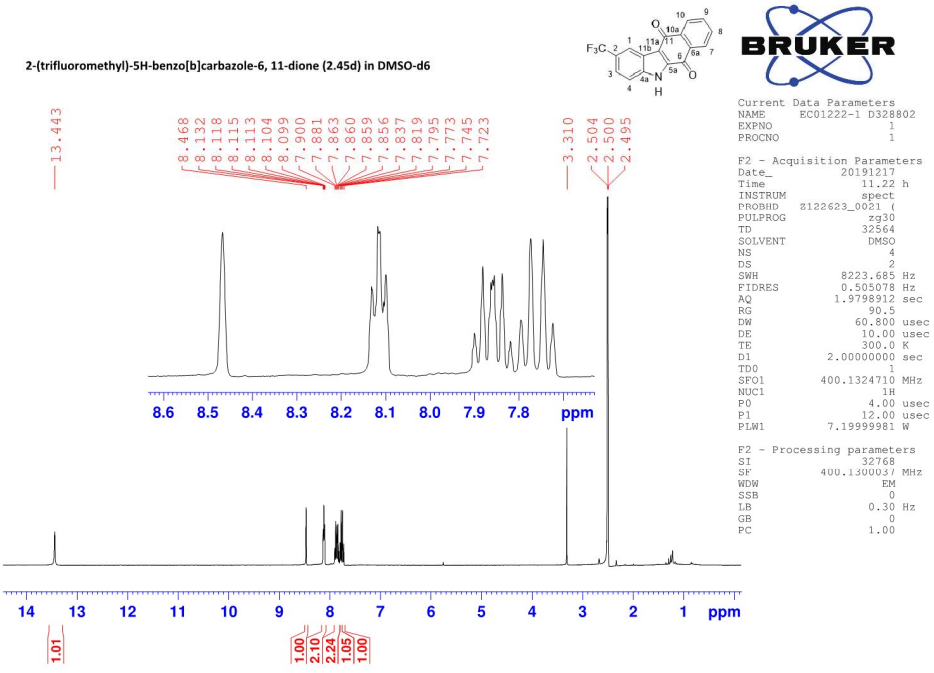


Figure 168. ^{1}H NMR spectra of 2-(trifluoromethyl)-5H-benzo[b]carbazole-6, 11-dione (**2.45d**).

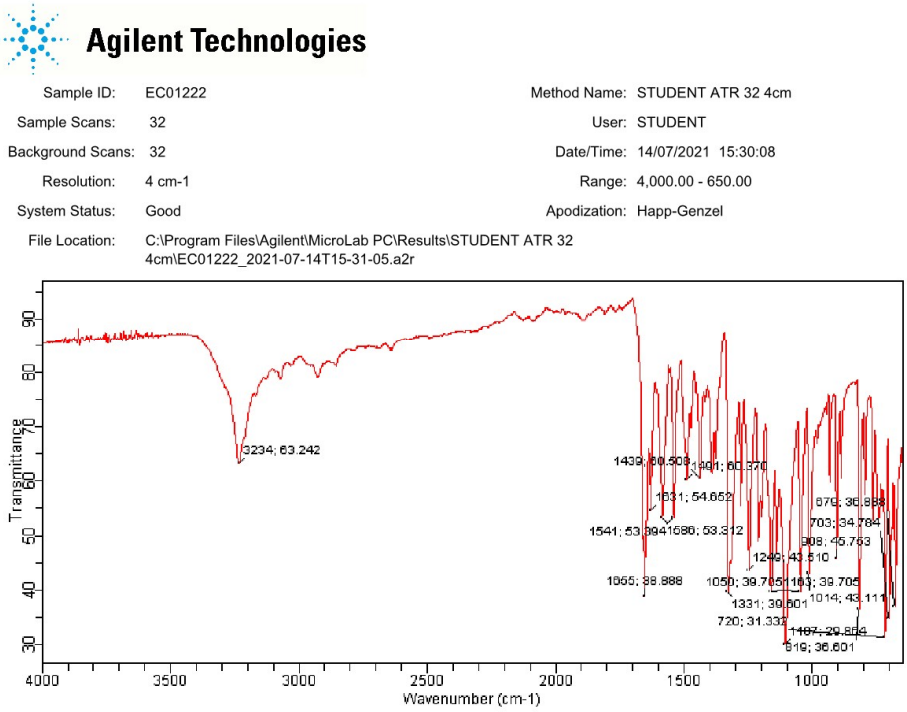


Figure 169. FT-IR spectra of 2-(trifluoromethyl)-5H-benzo[b]carbazole-6, 11-dione (**2.45d**).

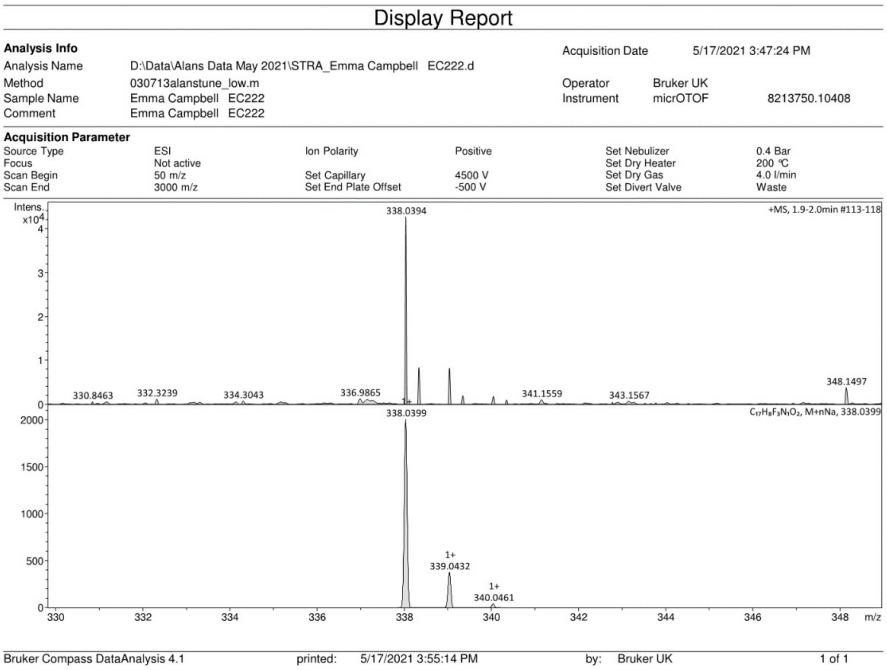


Figure 170. HRMS spectra of 2-(trifluoromethyl)-5H-benzo[b]carbazole-6, 11-dione (**2.45d**).

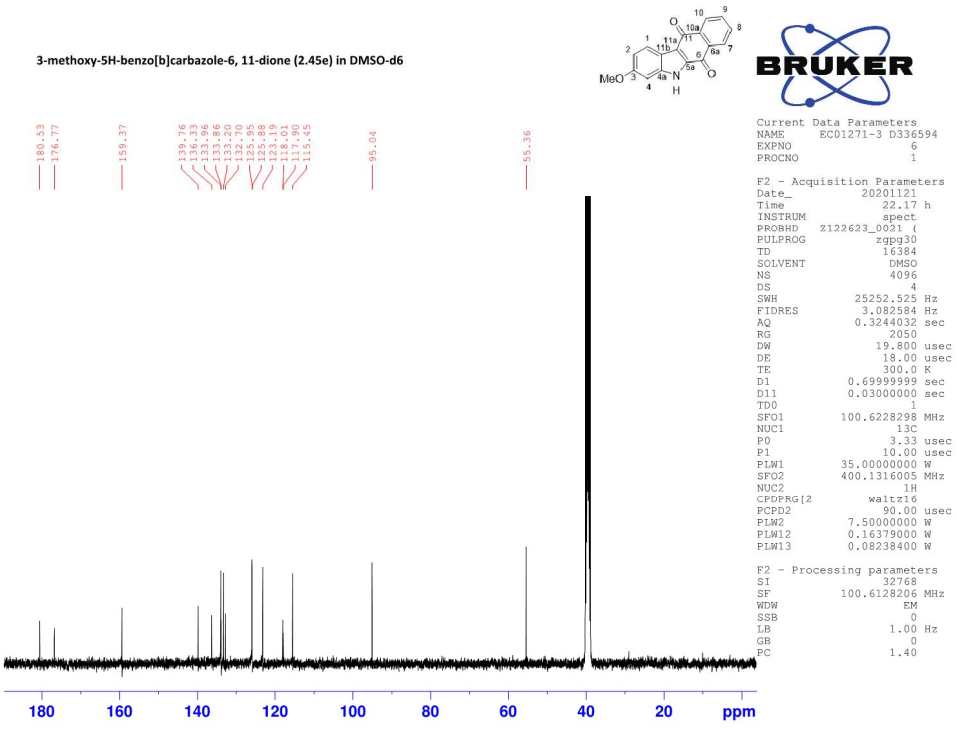


Figure 171. ^{13}C NMR spectra of 3-methoxy-5H-benzo[b]carbazole-6, 11-dione (**2.45e**).

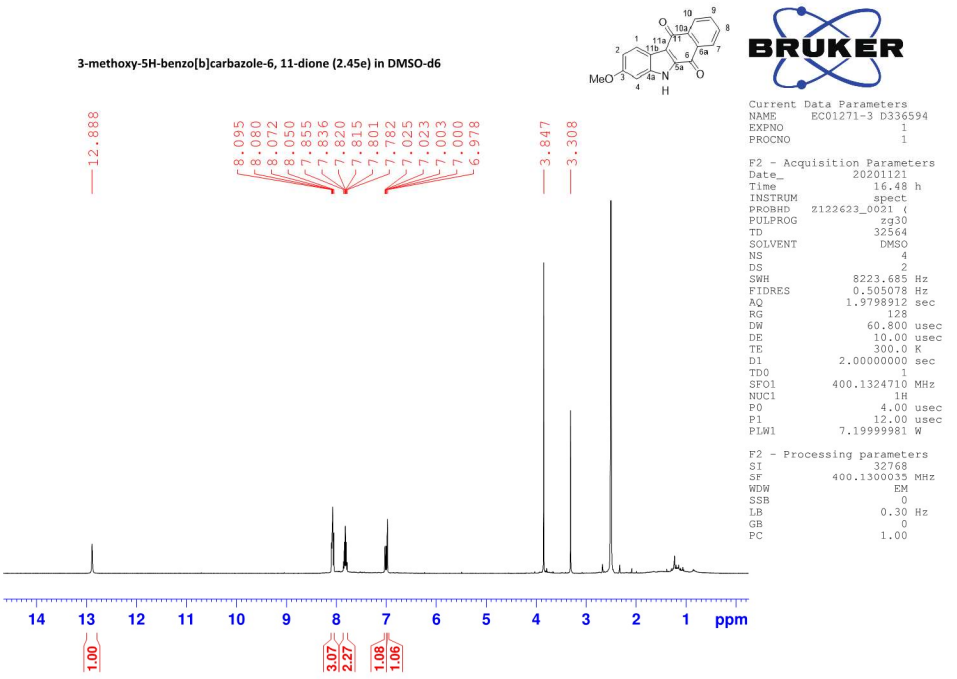


Figure 172. ^{1}H NMR spectra of 3-methoxy-5H-benzo[b]carbazole-6, 11-dione (**2.45e**).

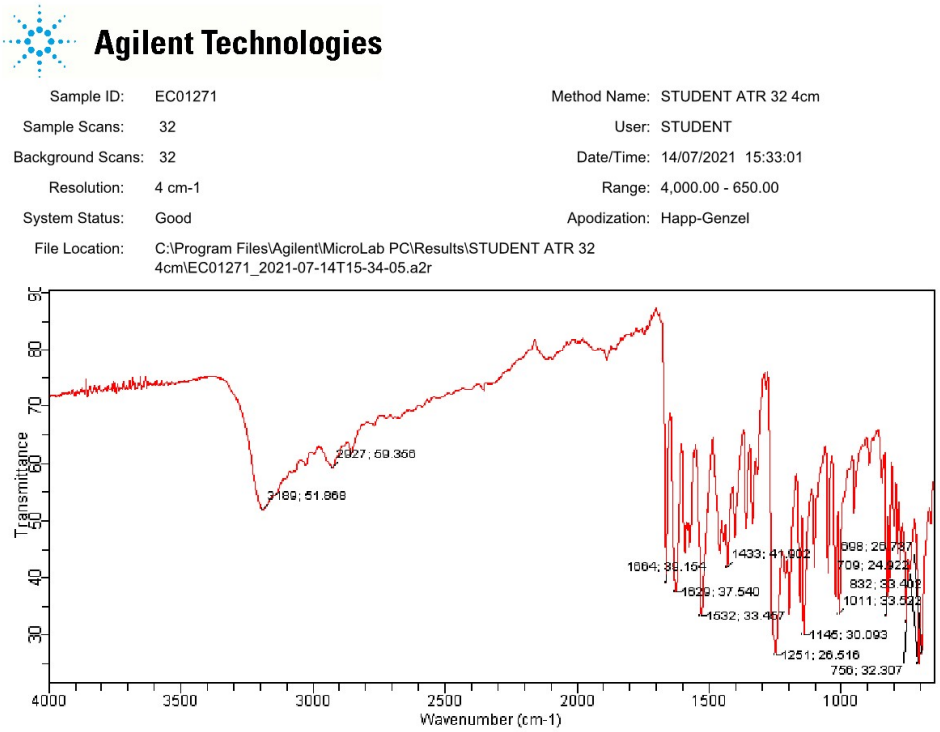


Figure 173. FT-IR spectra of 3-methoxy-5H-benzo[b]carbazole-6, 11-dione (**2.45e**).

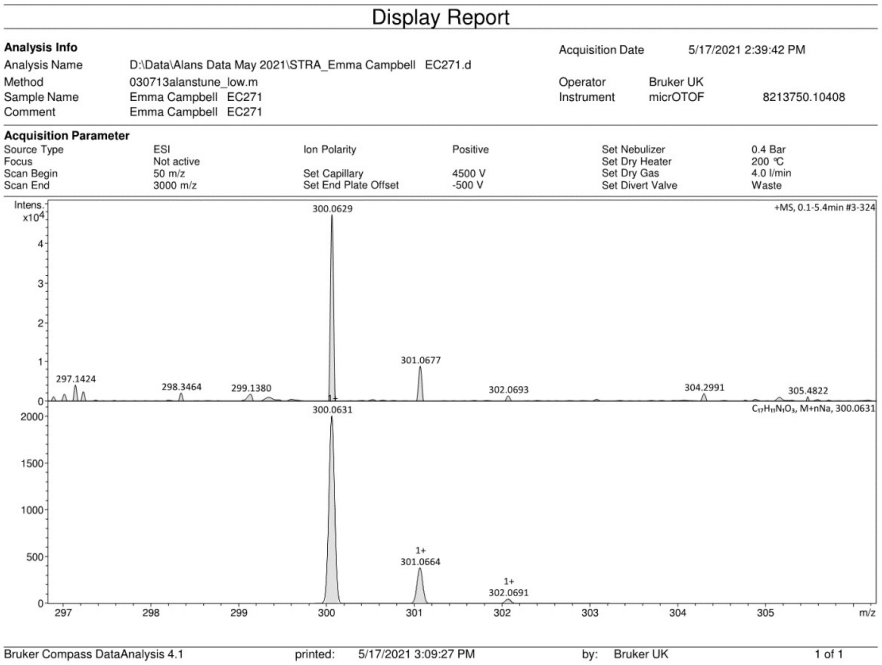


Figure 174. HRMS spectra of 3-methoxy-5H-benzo[b]carbazole-6, 11-dione (**2.45e**).

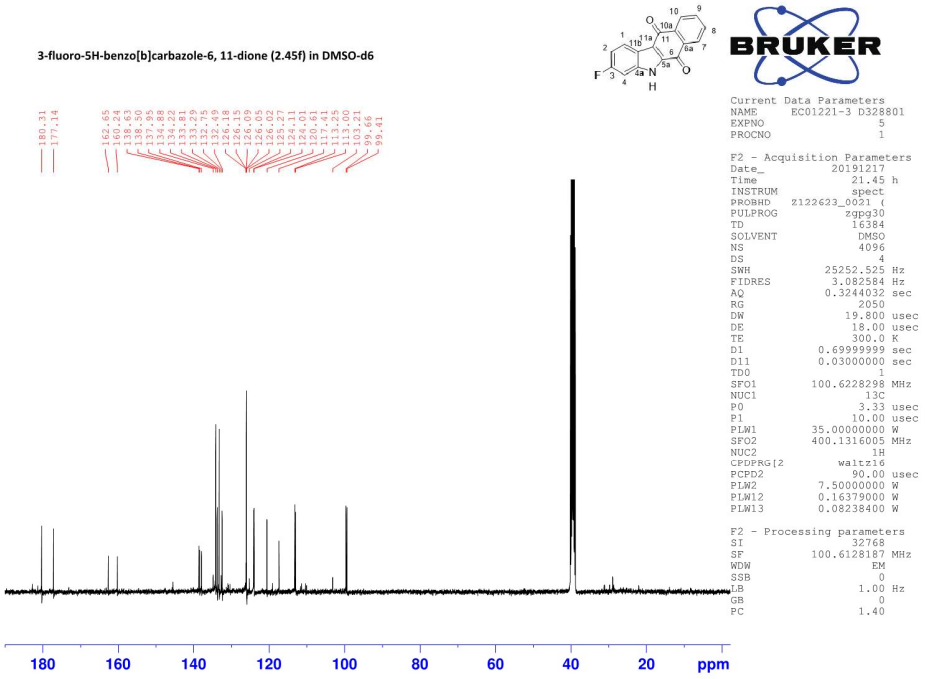


Figure 175. ^{13}C NMR spectra of 3-fluoro-5H-benzo[b]carbazole-6, 11-dione (**2.45f**).

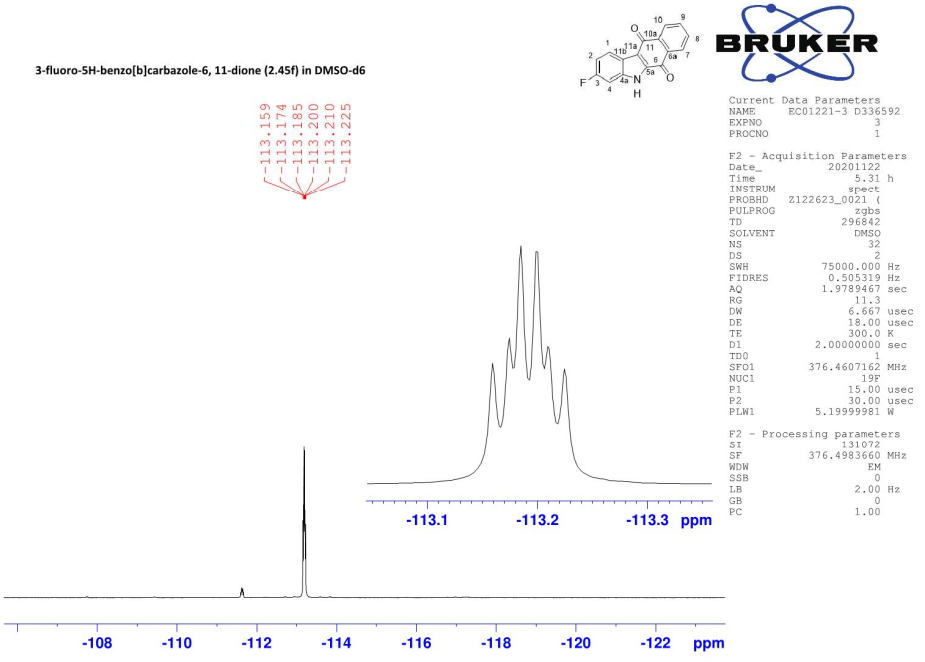


Figure 176. ^{19}F NMR spectra of 3-fluoro-5H-benzo[b]carbazole-6, 11-dione (**2.45f**).

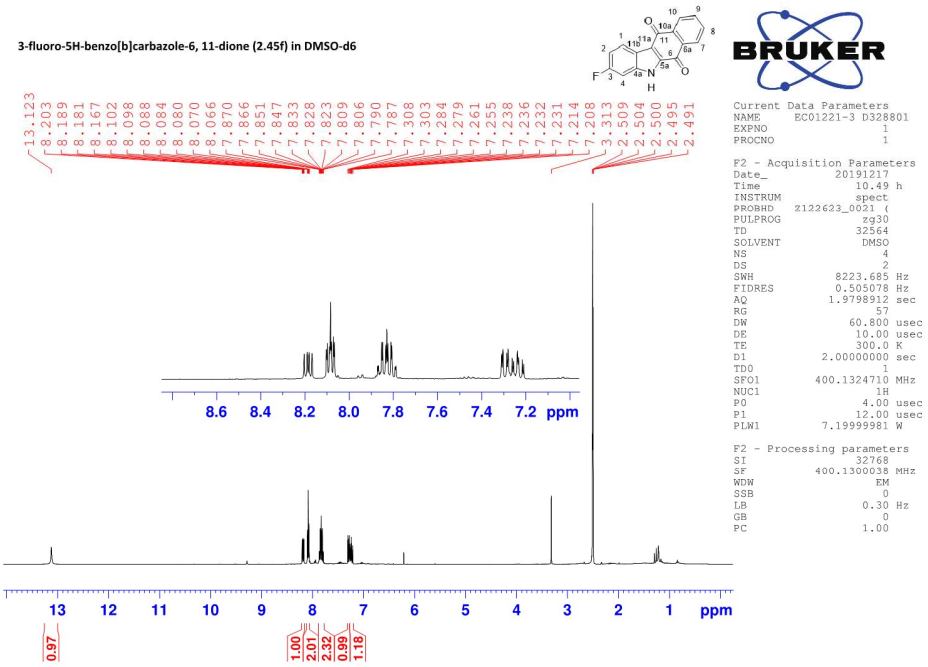


Figure 177. ^{1}H NMR spectra of 3-fluoro-5H-benzo[b]carbazole-6, 11-dione (**2.45f**).

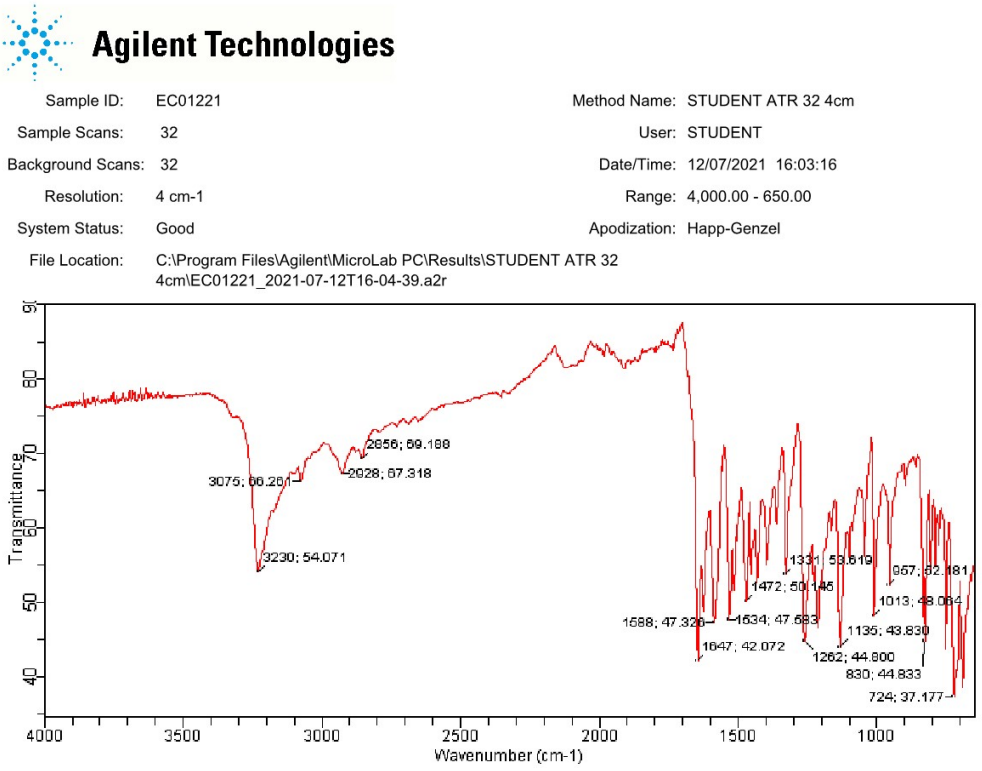


Figure 178. FT-IR spectra of 3-fluoro-5H-benzo[b]carbazole-6, 11-dione (**2.45f**).

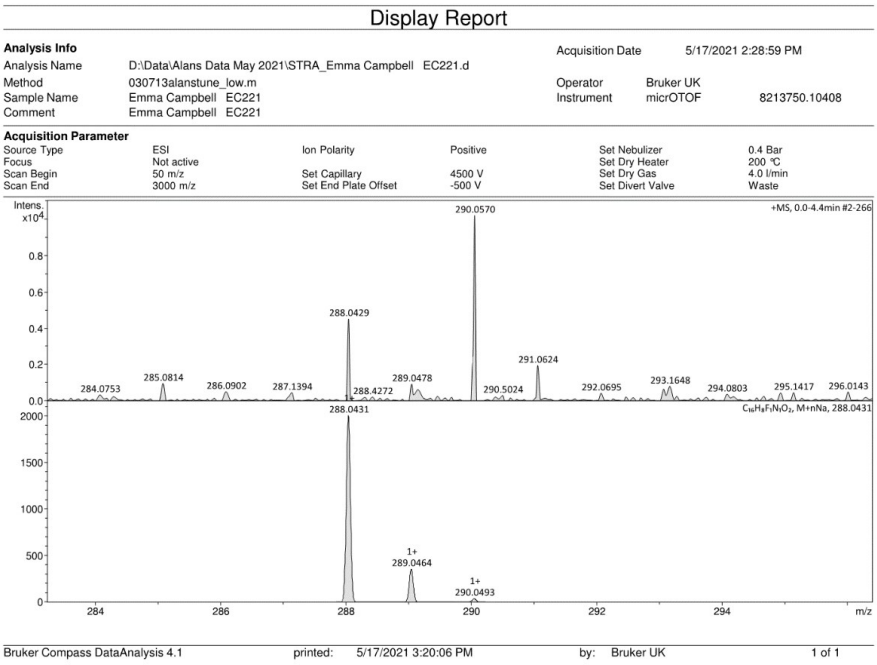


Figure 179. HRMS spectra of 3-fluoro-5H-benzo[b]carbazole-6, 11-dione (**2.45f**).

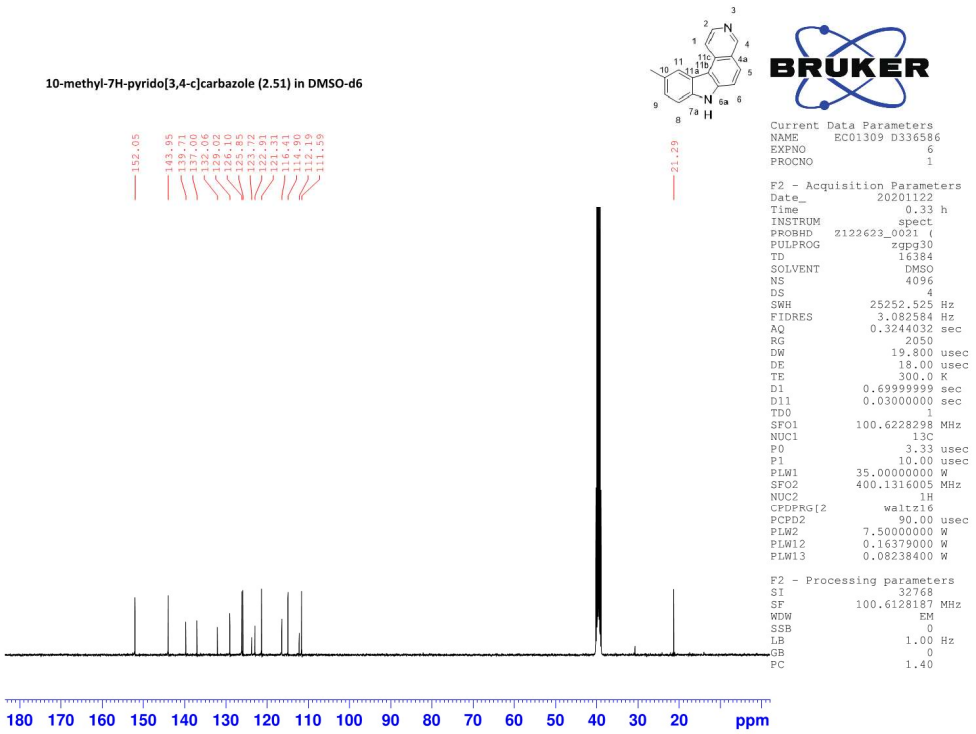


Figure 180. ^{13}C NMR spectra of 10-methyl-7H-pyrido[3,4-c]carbazole (**2.51**).

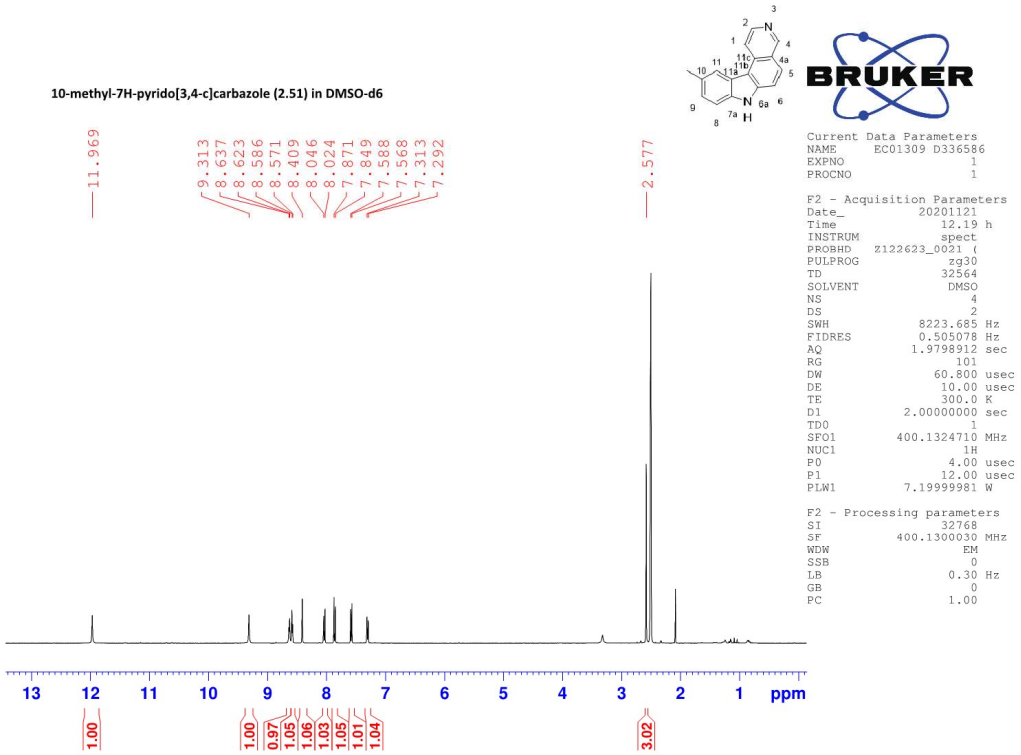


Figure 181. ^{1}H NMR spectra of 10-methyl-7H-pyrido[3,4-c]carbazole (**2.51**).

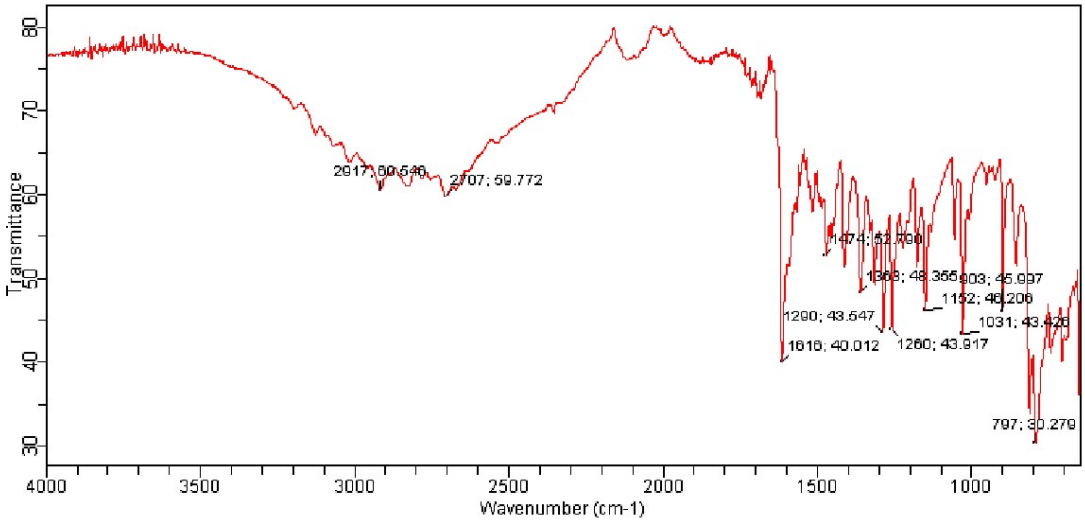


Figure 182. FT-IR spectra of 10-methyl-7H-pyrido[3,4-c]carbazole (**2.51**).

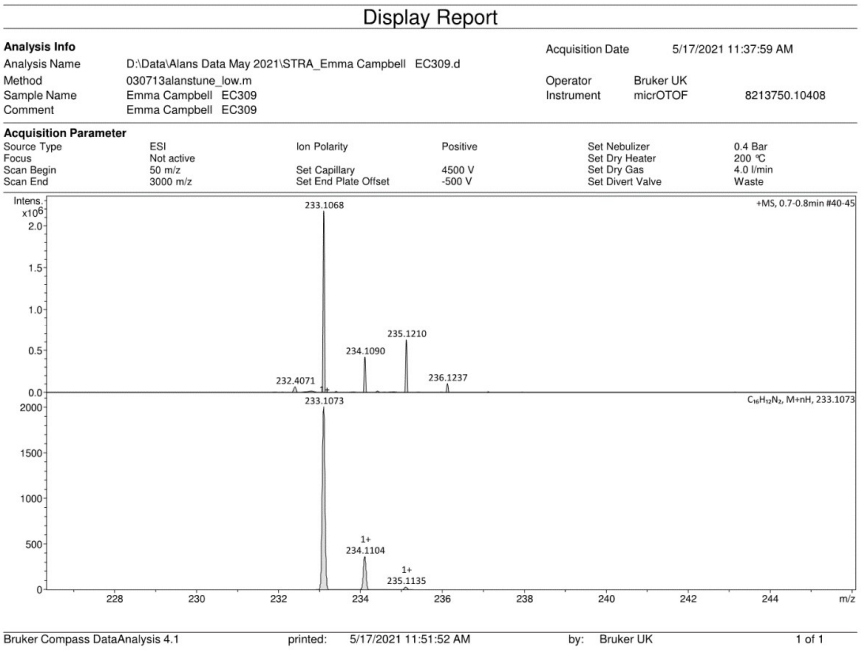


Figure 183. HRMS spectra of 10-methyl-7H-pyrido[3,4-c]carbazole (**2.51**).

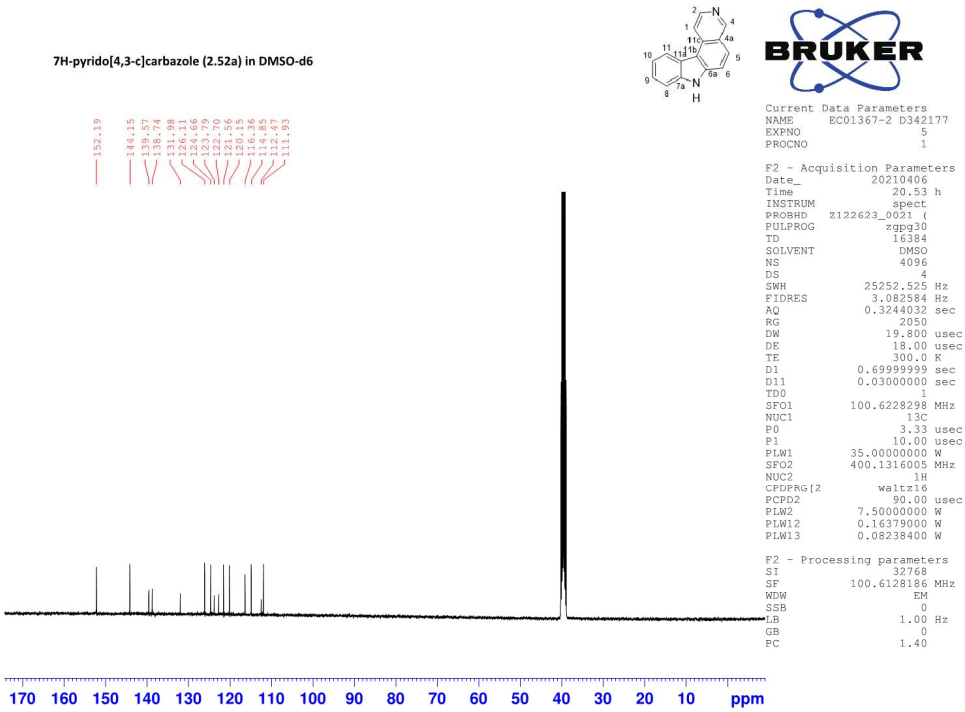


Figure 184. ^{13}C NMR spectra of 7H-pyrido[4,3-c]carbazole (**2.52a**).

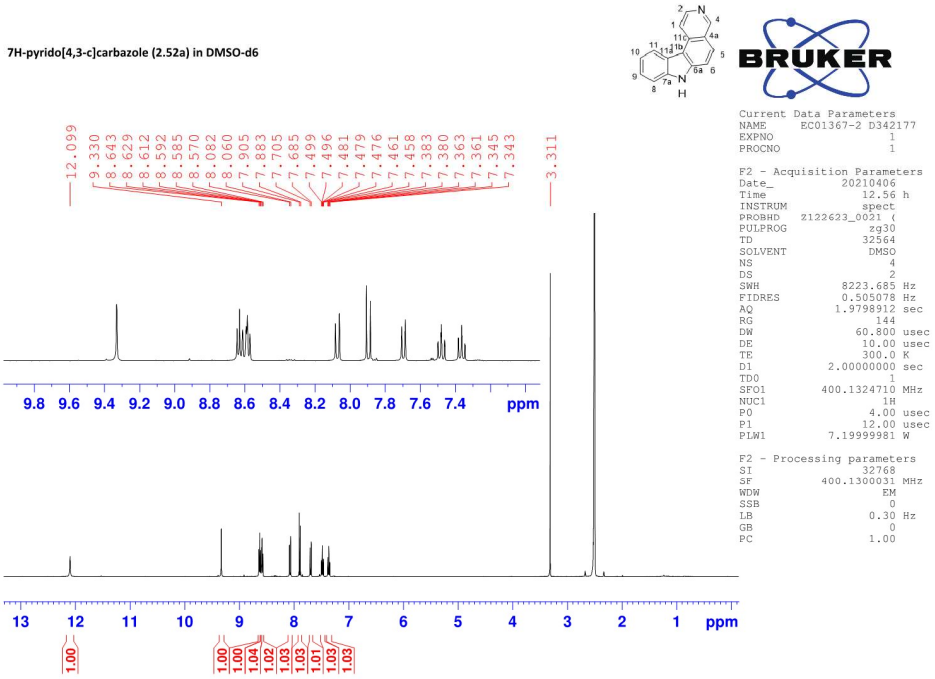


Figure 185. [1]H NMR spectra of 7H-pyrido[4,3-c]carbazole (**2.52a**).

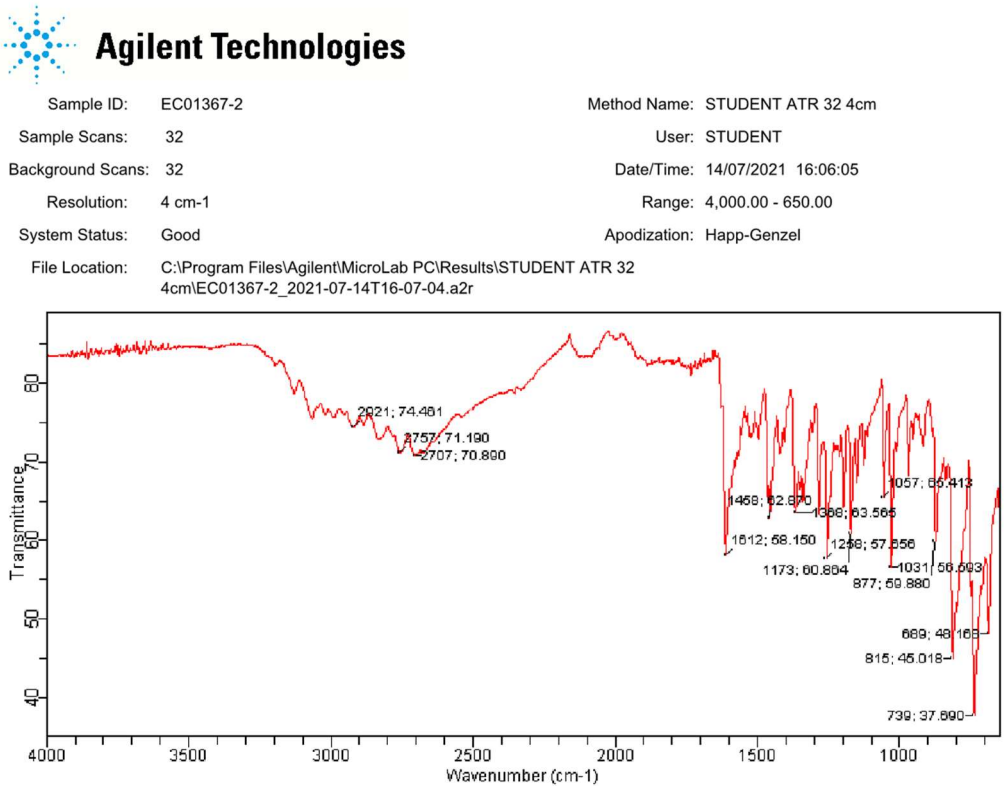


Figure 186. FT-IR spectra of 7H-pyrido[4,3-c]carbazole (**2.52a**).

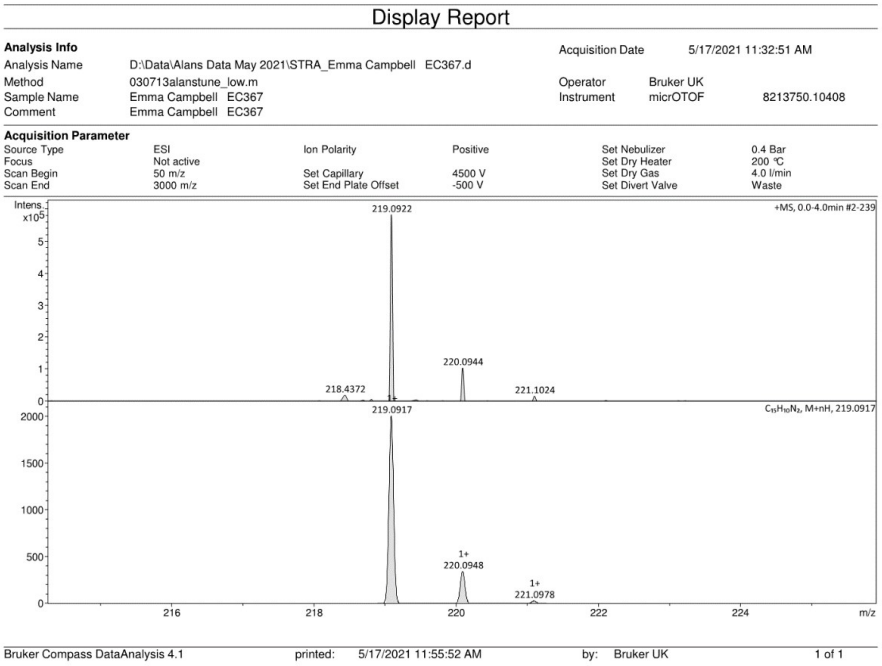


Figure 187. HRMS spectra of 7H-pyrido[4,3-c]carbazole (**2.52a**).

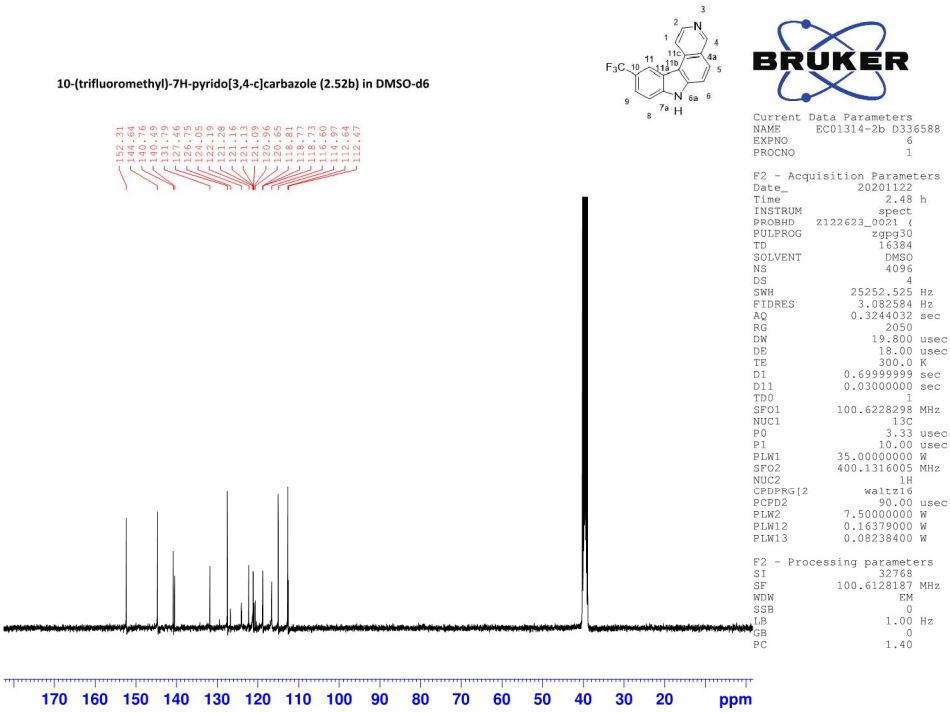


Figure 188. ^{13}C NMR spectra of 10-(trifluoromethyl)-7H-pyrido[3,4-c]carbazole (**2.52b**).

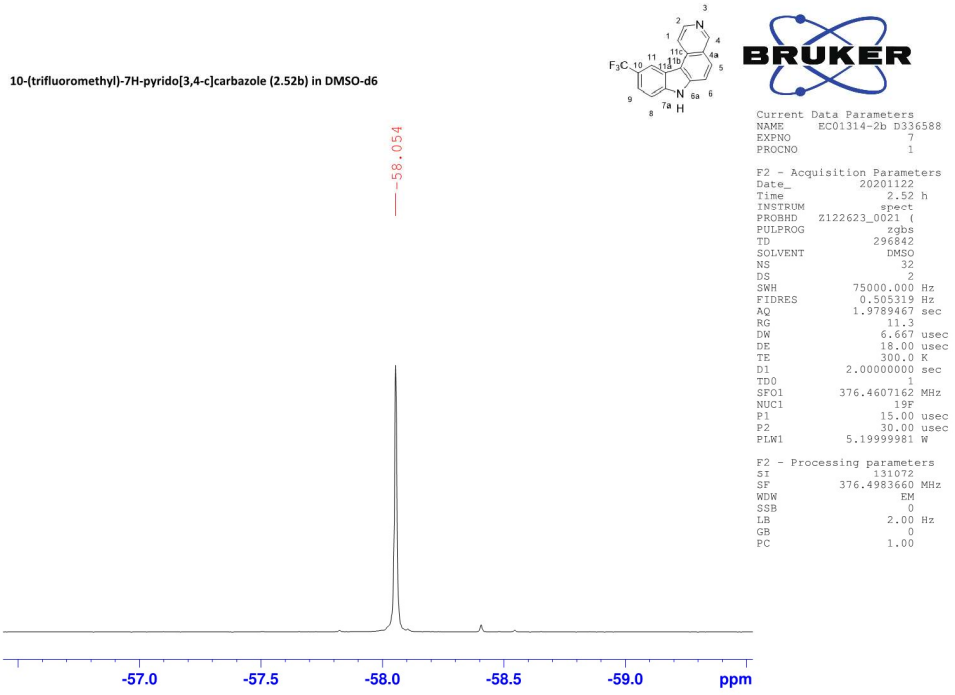


Figure 189. ^{19}F NMR spectra of 10-(trifluoromethyl)-7H-pyrido[3,4-c]carbazole (**2.52b**).

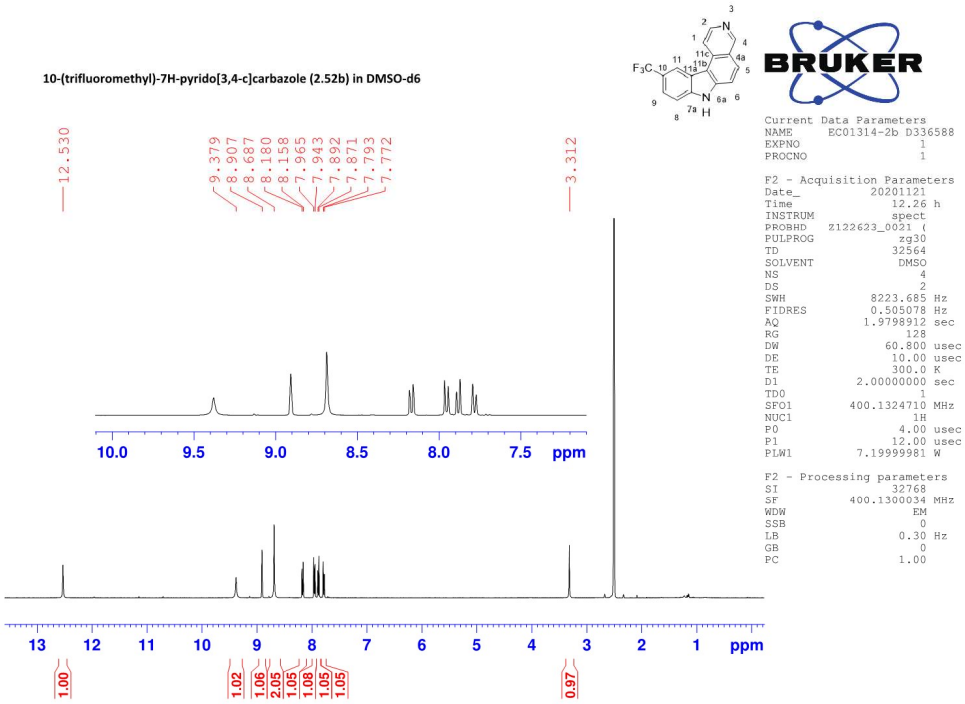


Figure 190. ^{1}H NMR spectra of 10-(trifluoromethyl)-7H-pyrido[3,4-c]carbazole (**2.52b**).

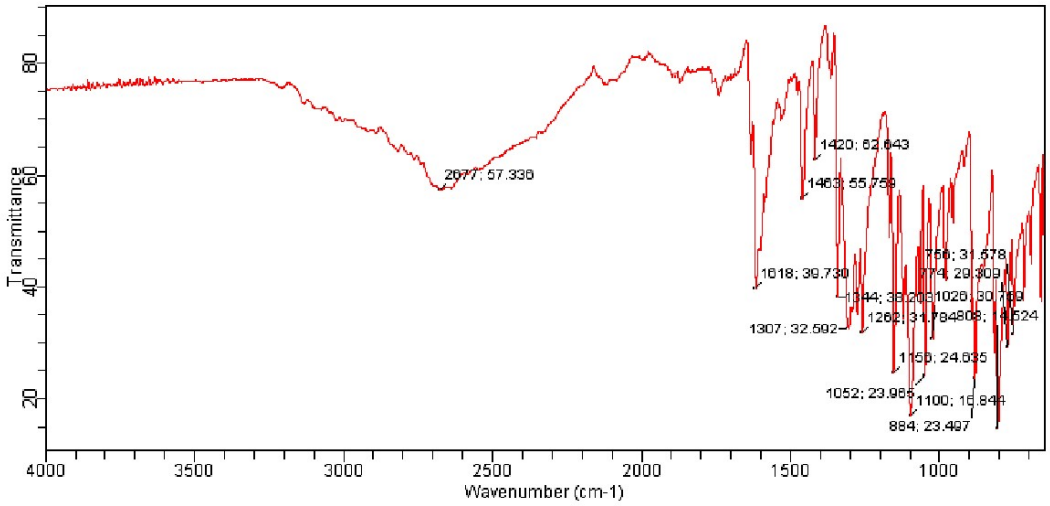


Figure 191. FT-IR spectra of 10-(trifluoromethyl)-7H-pyrido[3,4-c]carbazole (**2.52b**).

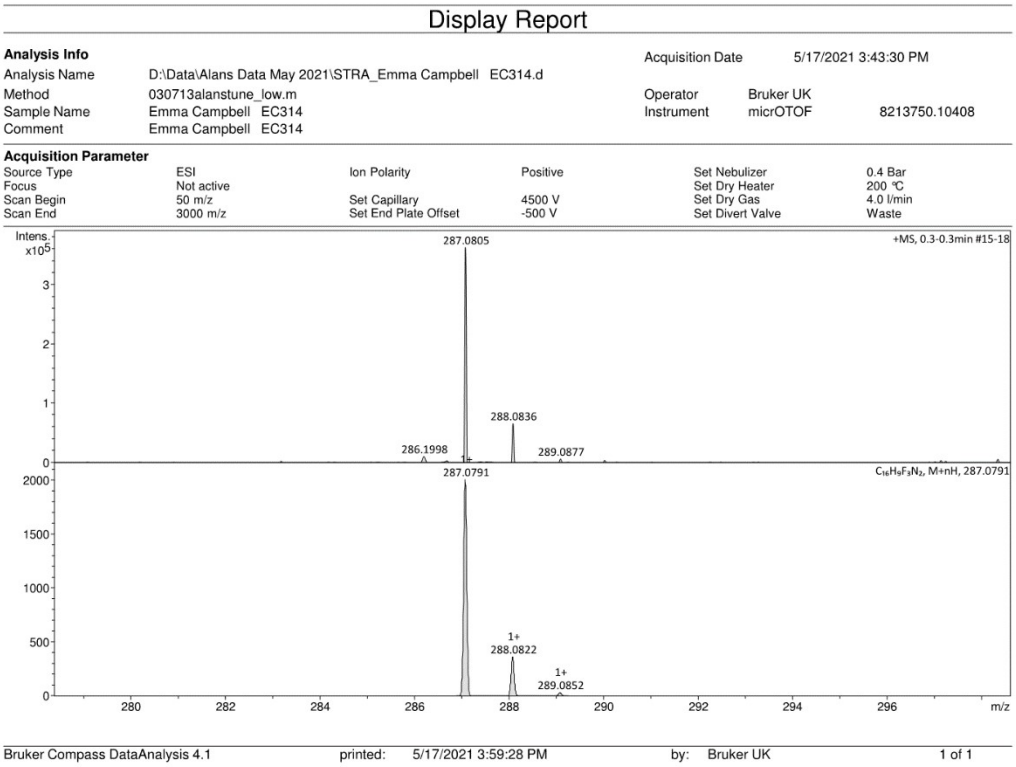


Figure 192. HRMS spectra of 10-(trifluoromethyl)-7H-pyrido[3,4-c]carbazole (**2.52b**).

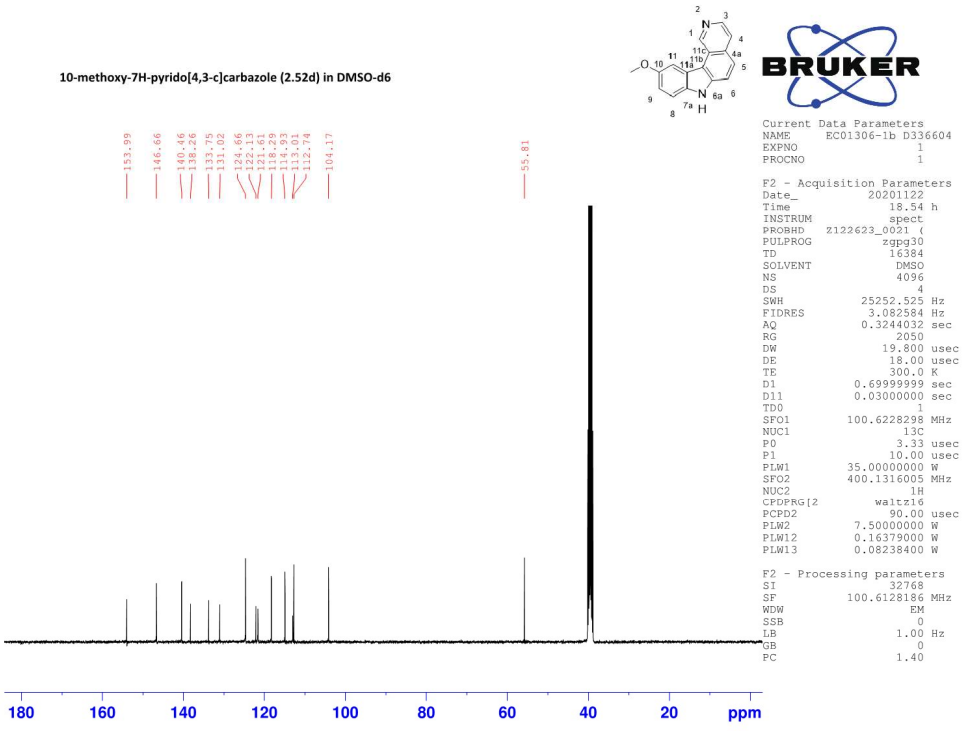


Figure 193. ^{13}C NMR spectra of 10-methoxy-7H-pyrido[4,3-c]carbazole (**2.52d**).

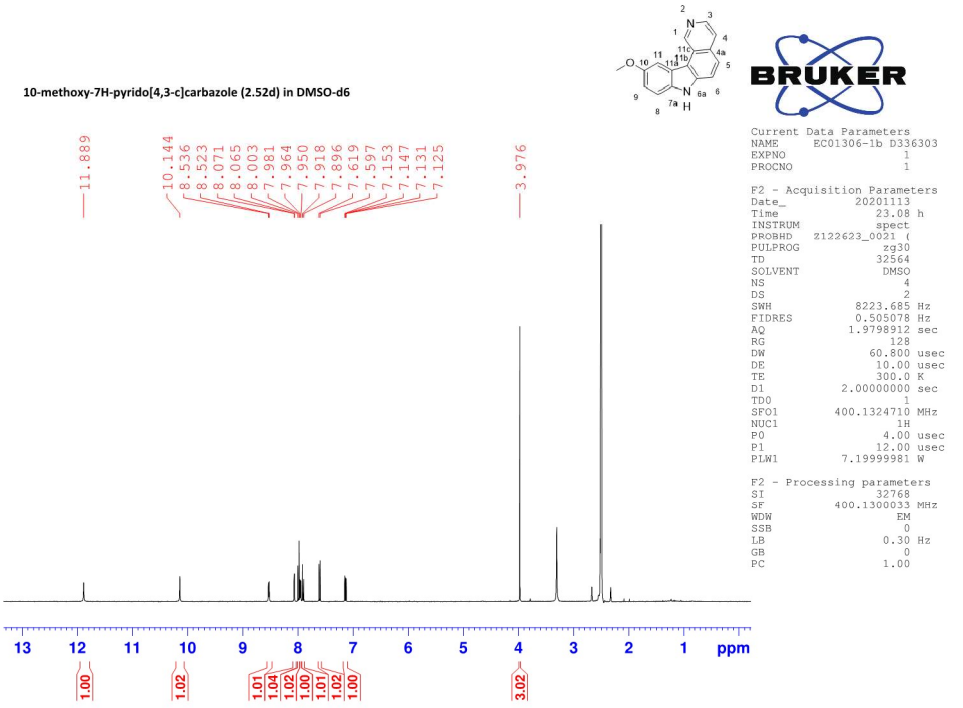


Figure 194. ^{1}H NMR spectra of 10-methoxy-7H-pyrido[4,3-c]carbazole (**2.52d**).

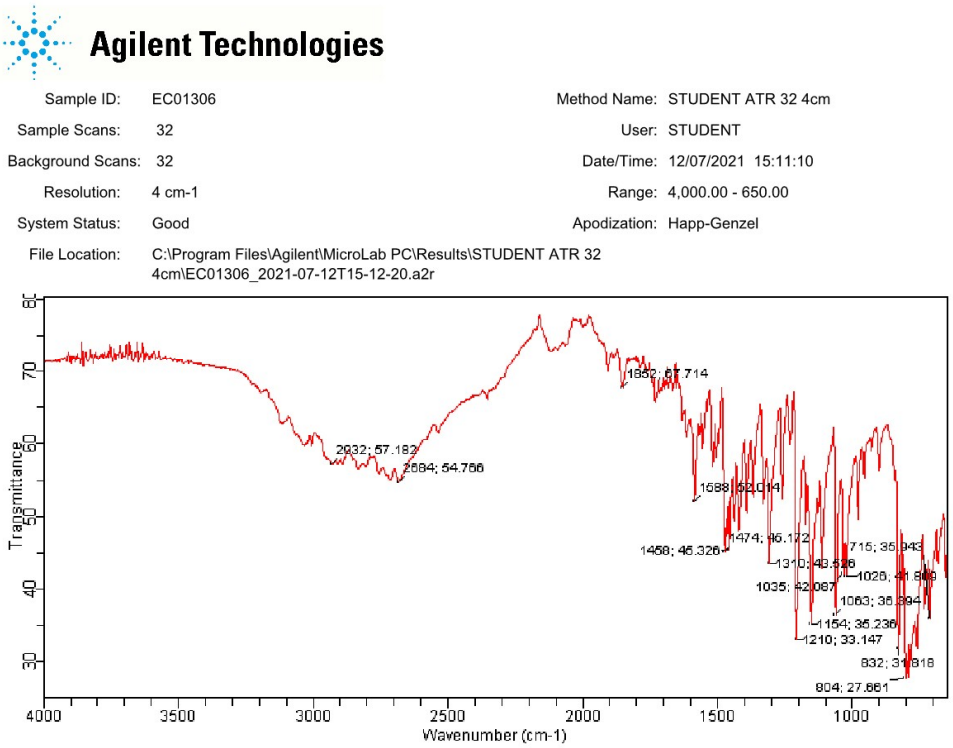


Figure 195. FT-IR spectra of 10-methoxy-7H-pyrido[4,3-c]carbazole (**2.52d**).

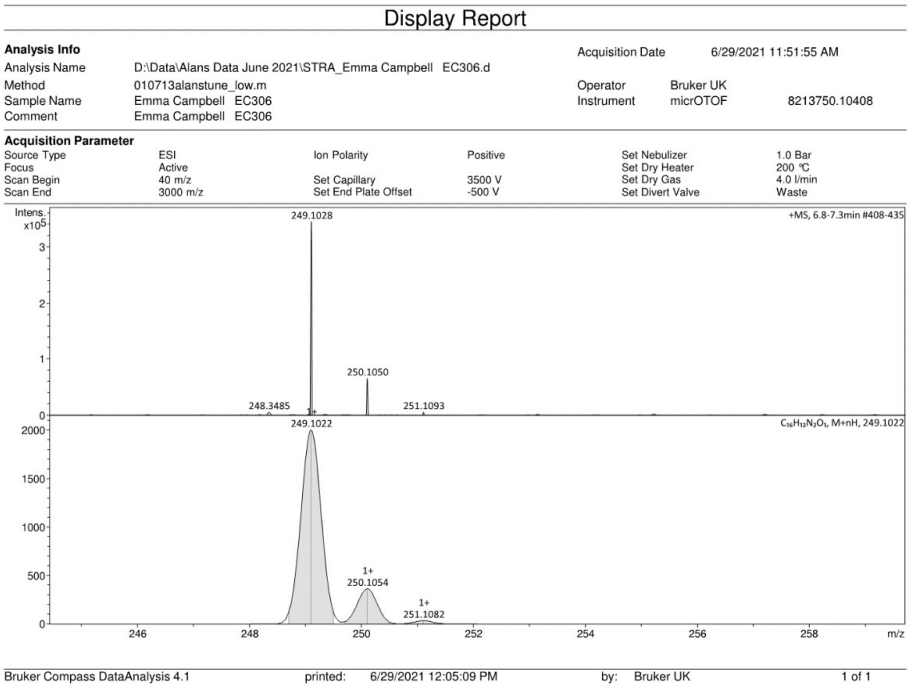


Figure 196. HRMS spectra of 10-methoxy-7H-pyrido[4,3-c]carbazole (**2.52d**).

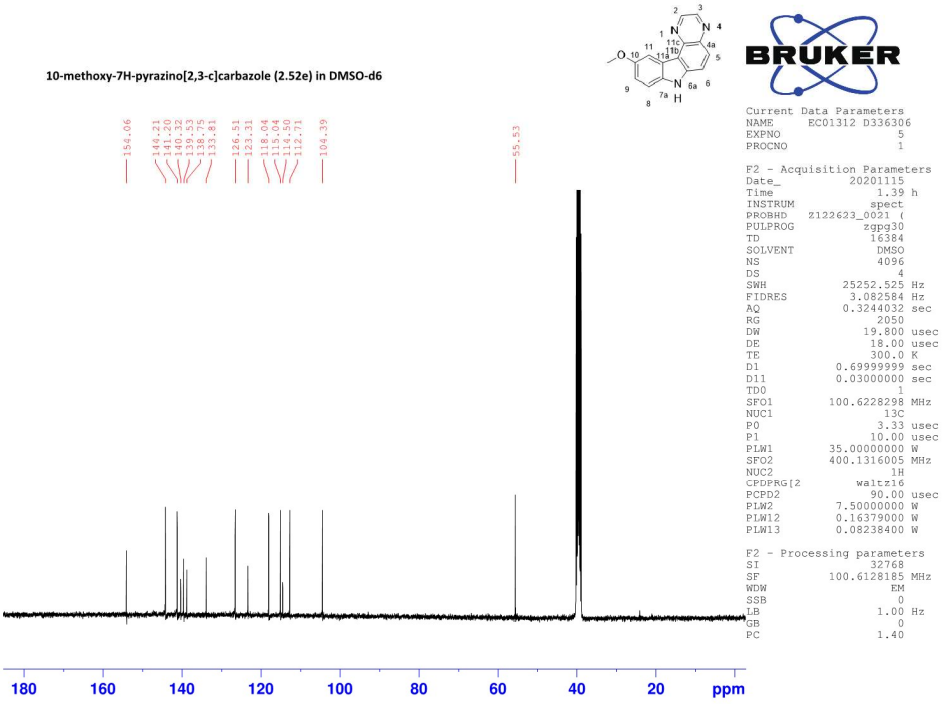


Figure 197. ^{13}C NMR spectra of 10-methoxy-7H-pyrazino[2,3-c]carbazole (**2.52e**).

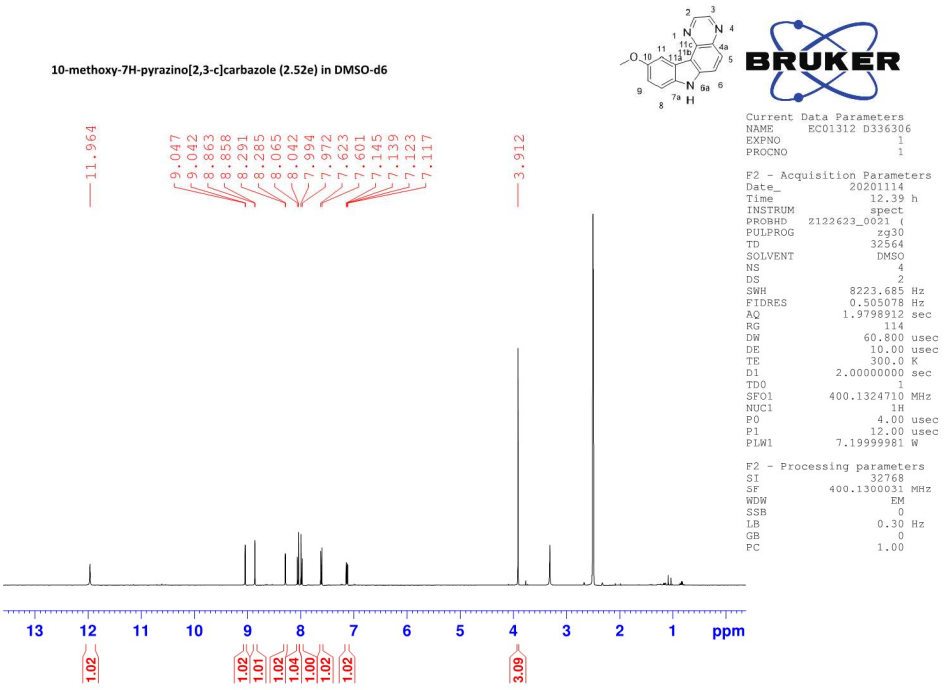


Figure 198. ^{1}H NMR spectra of 10-methoxy-7H-pyrazino[2,3-c]carbazole (**2.52e**).

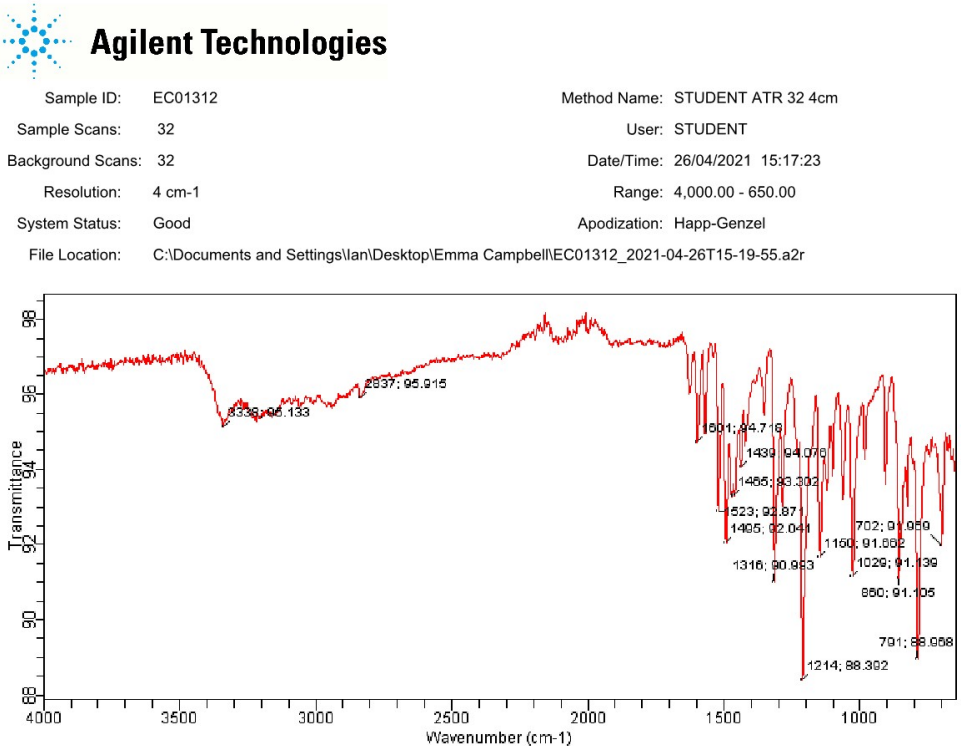


Figure 199. FT-IR spectra of 10-methoxy-7H-pyrazino[2,3-c]carbazole (**2.52e**).

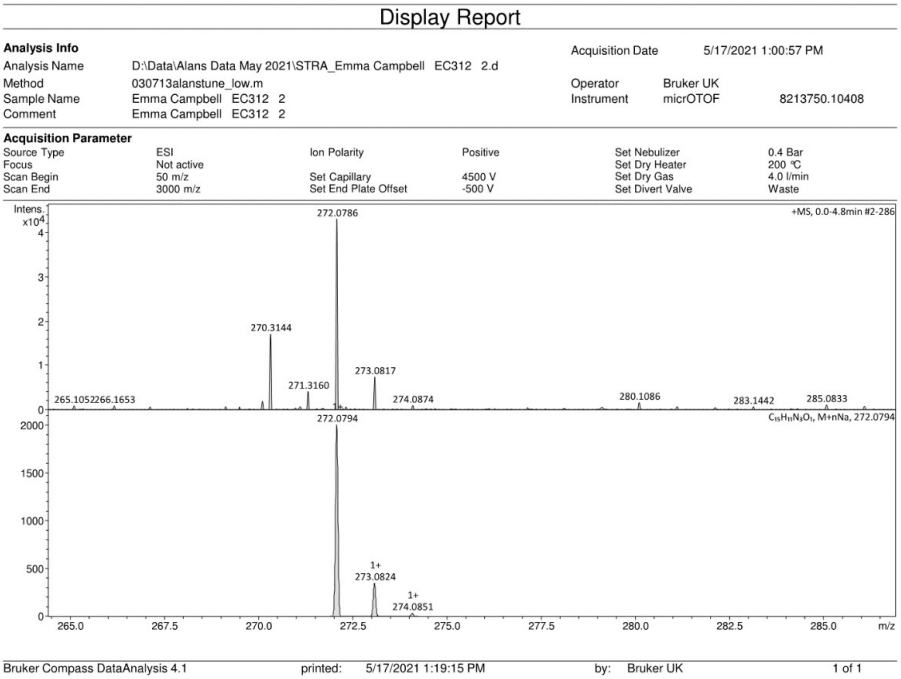


Figure 200. HRMS spectra of 10-methoxy-7H-pyrazino[2,3-c]carbazole (**2.52e**).

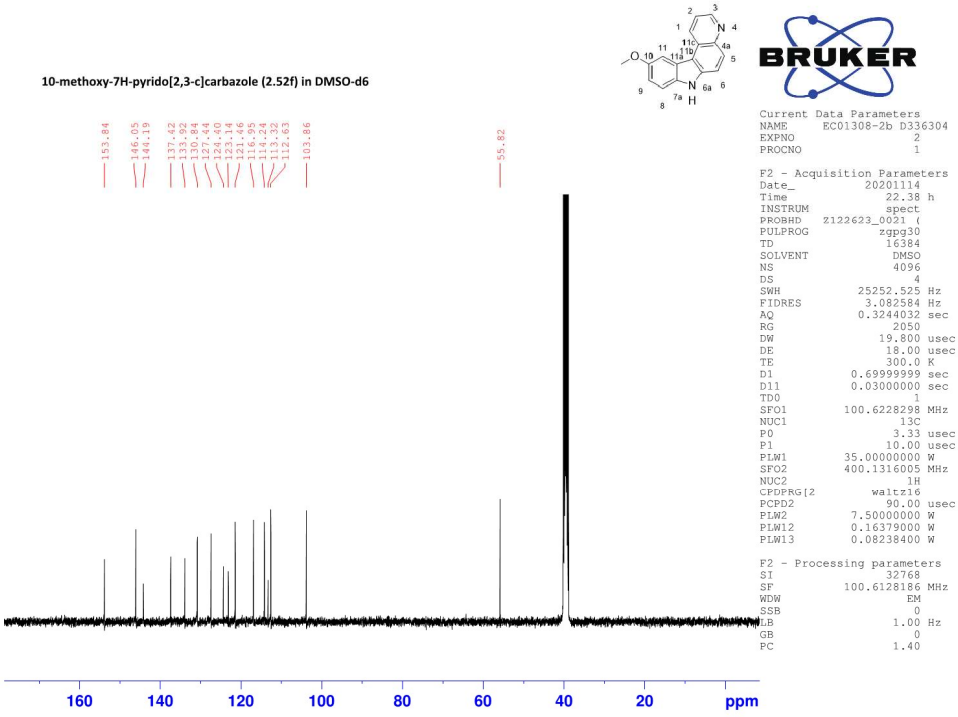


Figure 201. ^{13}C NMR spectra of 10-methoxy-7H-pyrido[2,3-c]carbazole (**2.52f**).

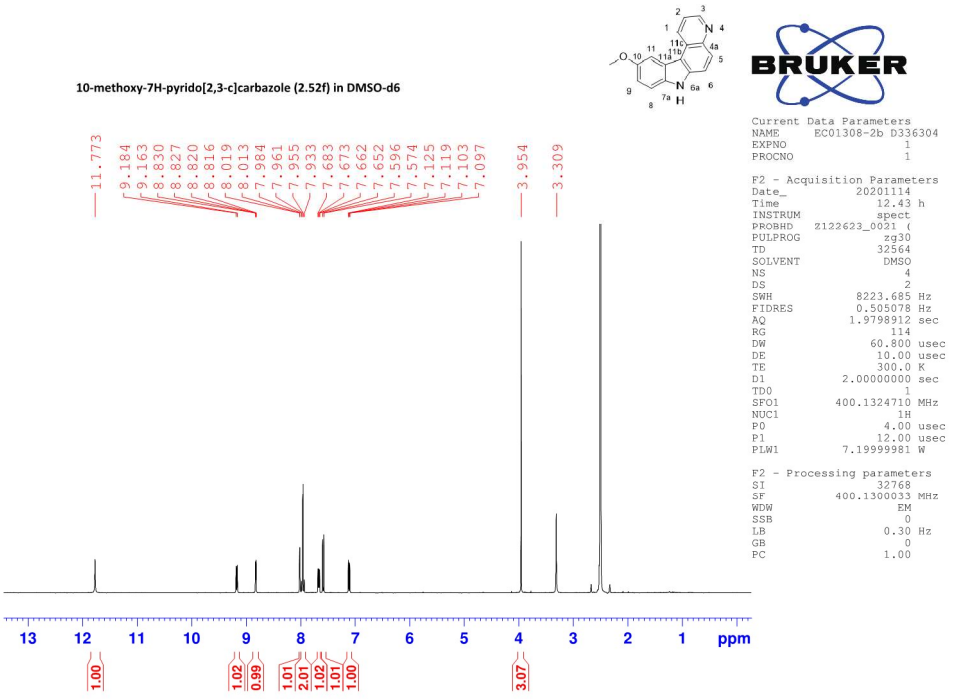


Figure 202. ^{1}H NMR spectra of 10-methoxy-7H-pyrido[2,3-c]carbazole (**2.52f**).

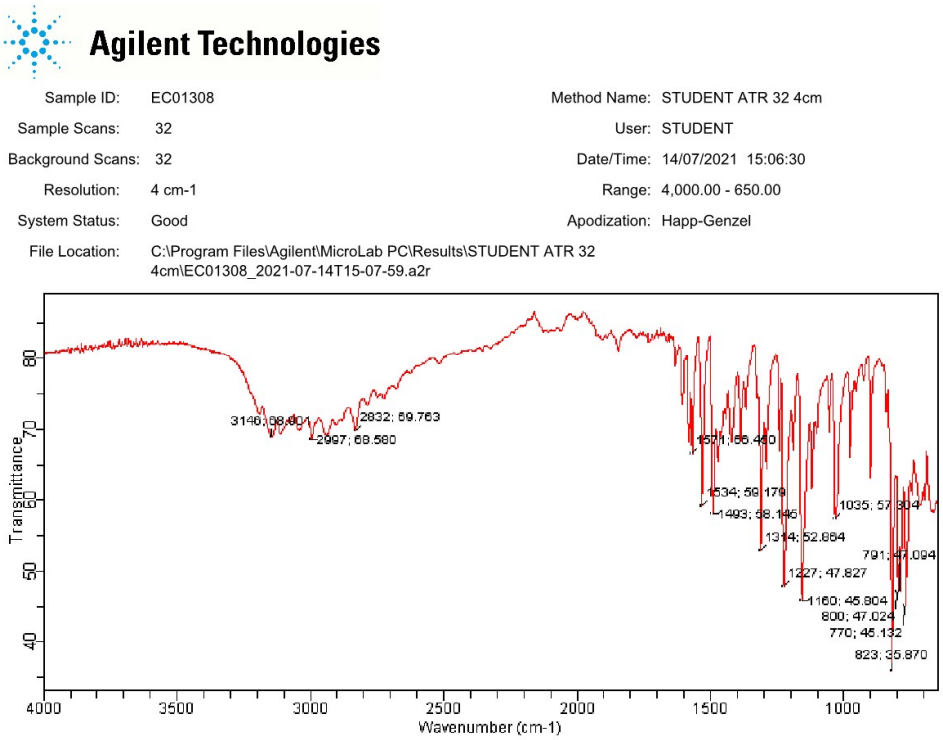


Figure 203. FT-IR spectra of 10-methoxy-7H-pyrido[2,3-c]carbazole (**2.52f**).

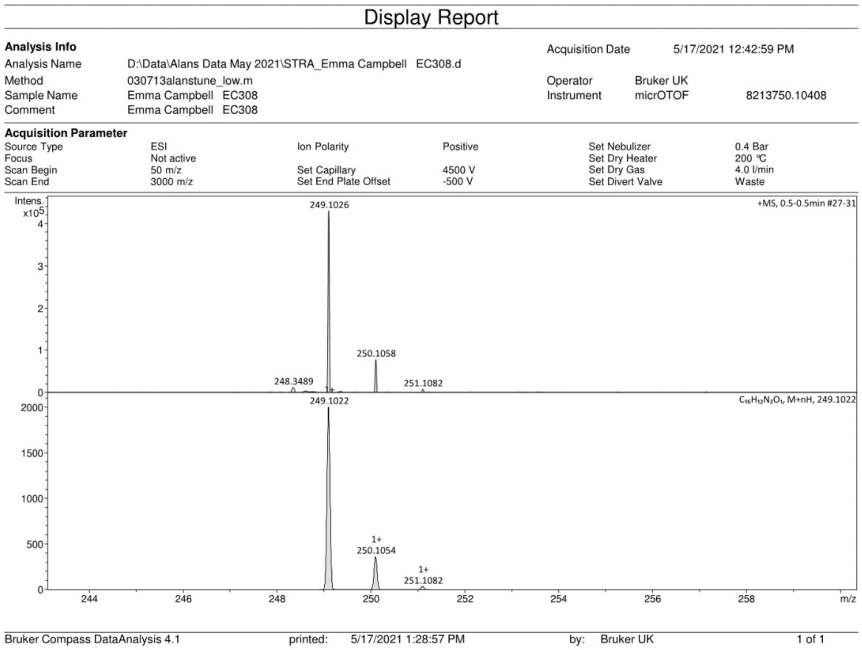


Figure 204. HRMS spectra of 10-methoxy-7H-pyrido[2,3-c]carbazole (**2.52f**).

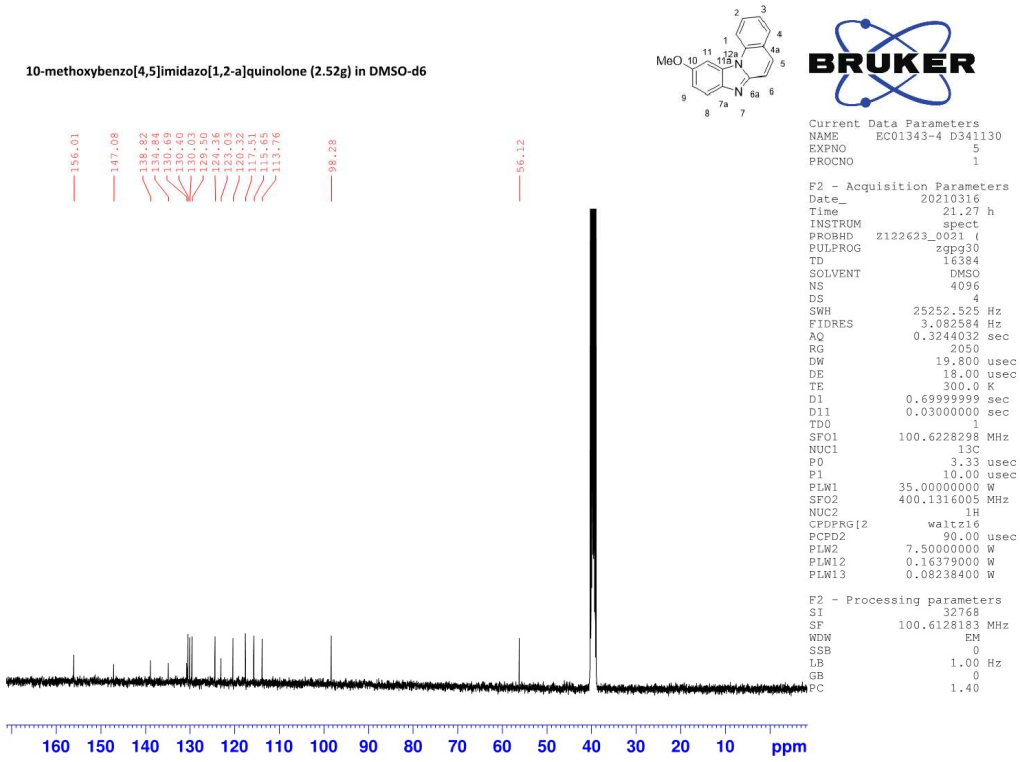


Figure 205. ^{13}C NMR spectra of 10-methoxybenzo[4,5]imidazo[1,2-a]quinolone (**2.52g**).

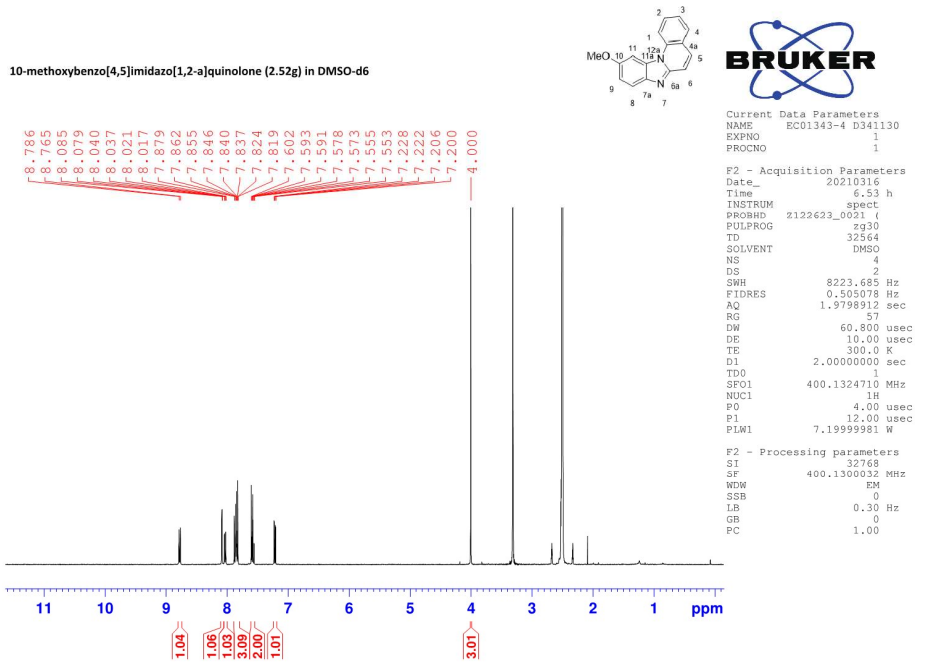


Figure 206. ^{1}H NMR spectra of 10-methoxybenzo[4,5]imidazo[1,2-a]quinolone (**2.52g**).

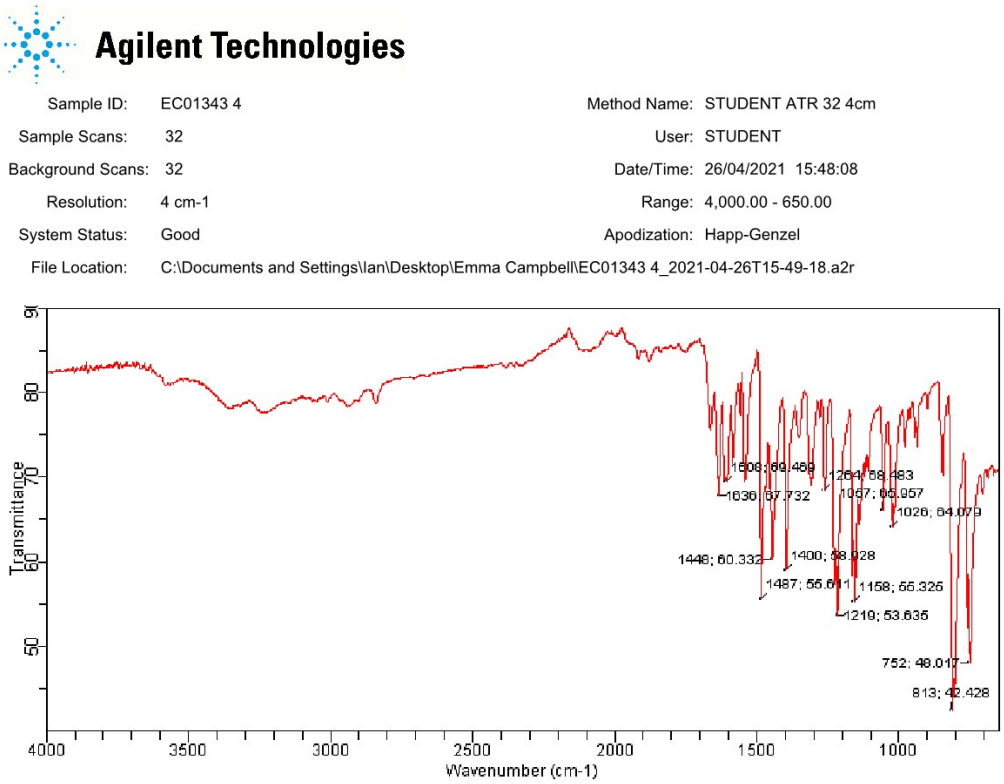


Figure 207. FT-IR spectra of 10-methoxybenzo[4,5]imidazo[1,2-a]quinolone (**2.52g**).

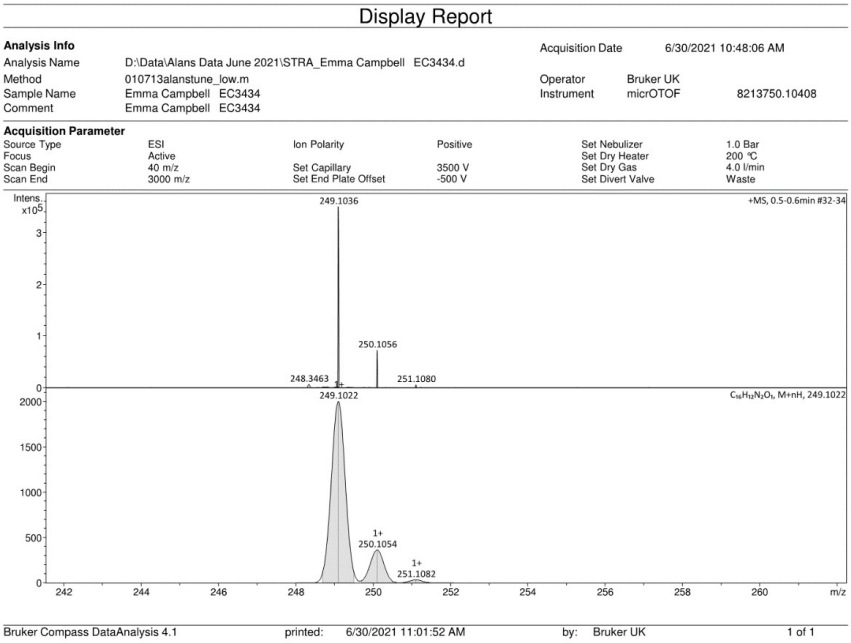


Figure 208. HRMS spectra of 10-methoxybenzo[4,5]imidazo[1,2-a]quinolone (**2.52g**).

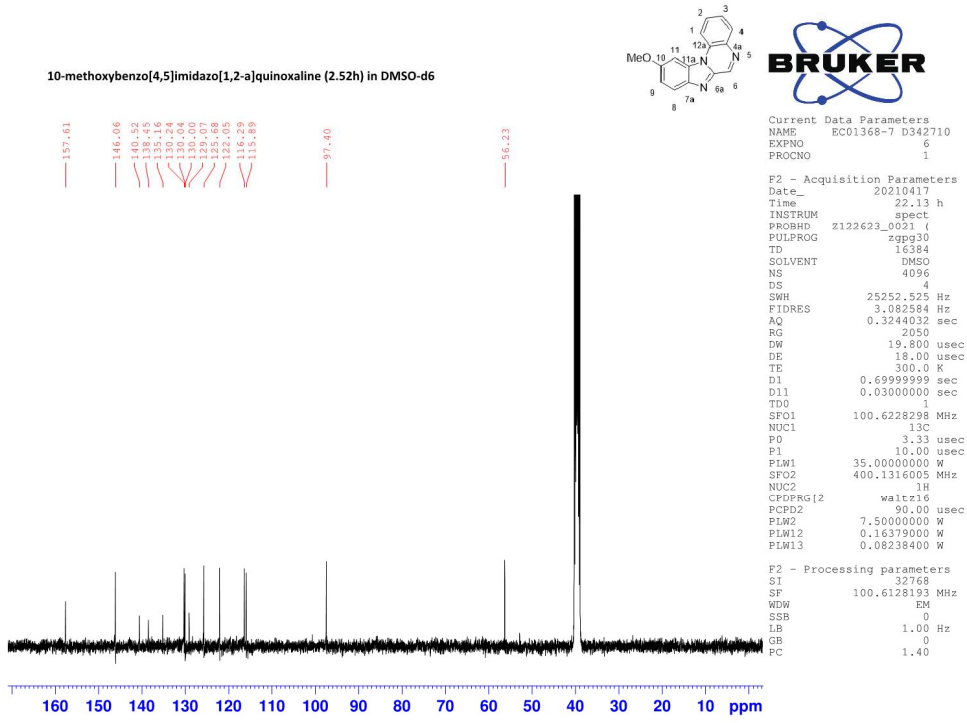


Figure 209. ^{13}C NMR spectra of 10-methoxybenzo[4,5]imidazo[1,2-a]quinoxaline (**2.52h**).

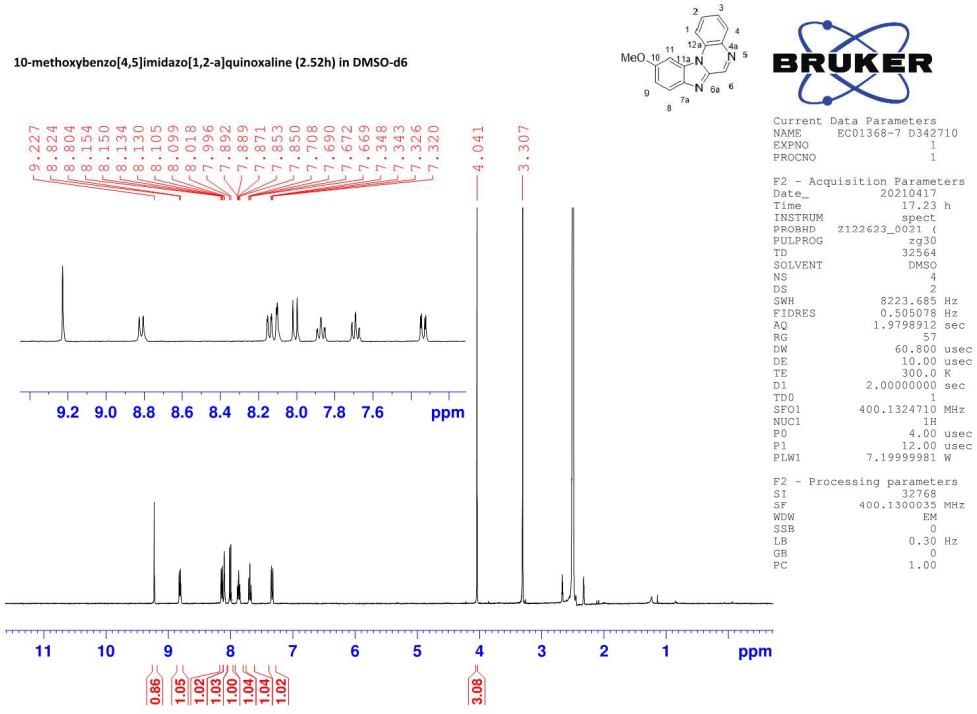


Figure 210. ^{1}H NMR spectra of 10-methoxybenzo[4,5]imidazo[1,2-a]quinoxaline (**2.52h**).

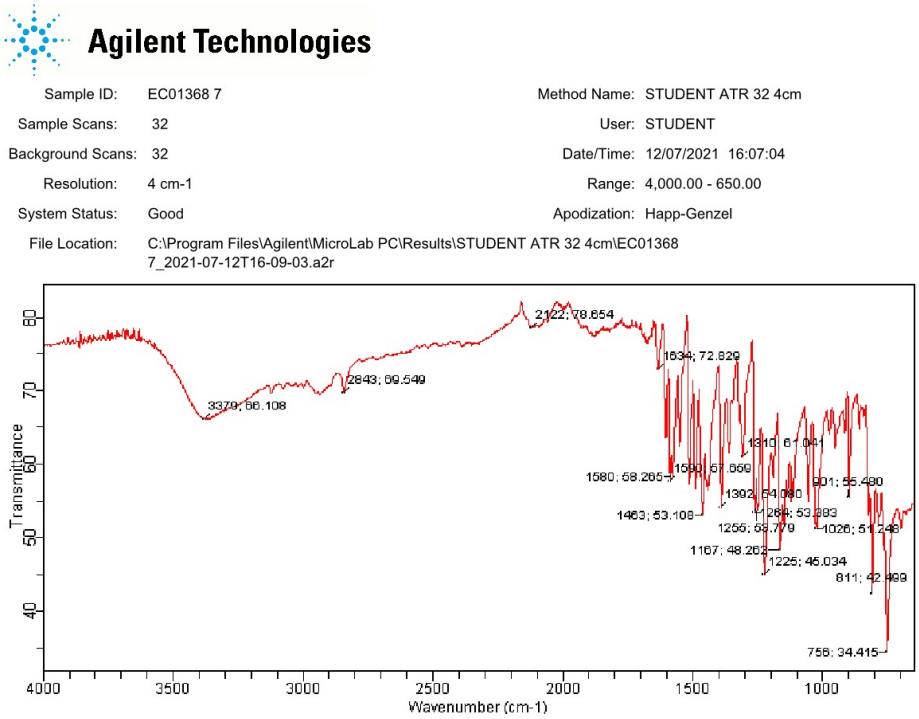


Figure 211. FT-IR spectra of 10-methoxybenzo[4,5]imidazo[1,2-a]quinoxaline (**2.52h**).

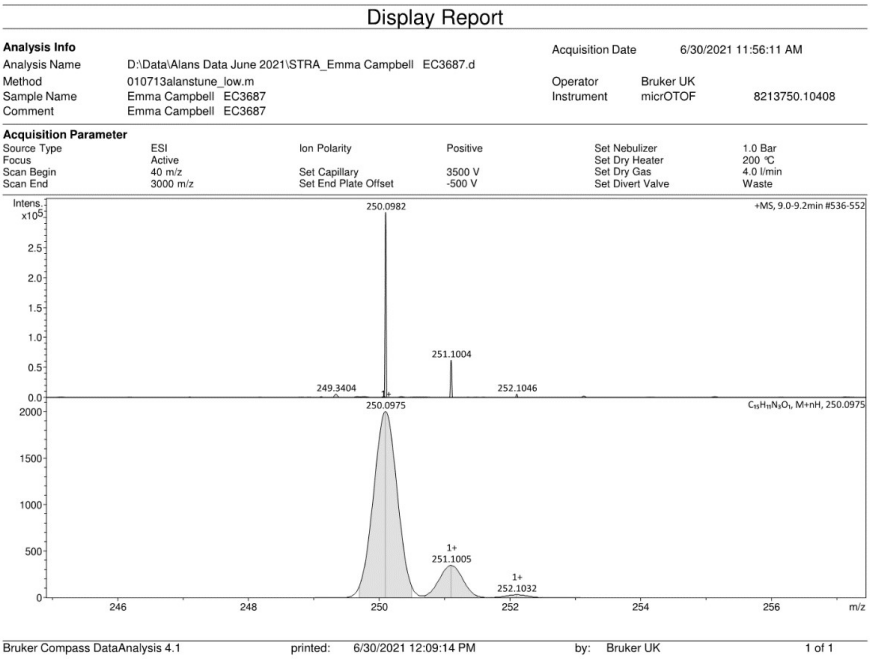


Figure 212. HRMS spectra of 10-methoxybenzo[4,5]imidazo[1,2-a]quinoxaline (**2.52h**).

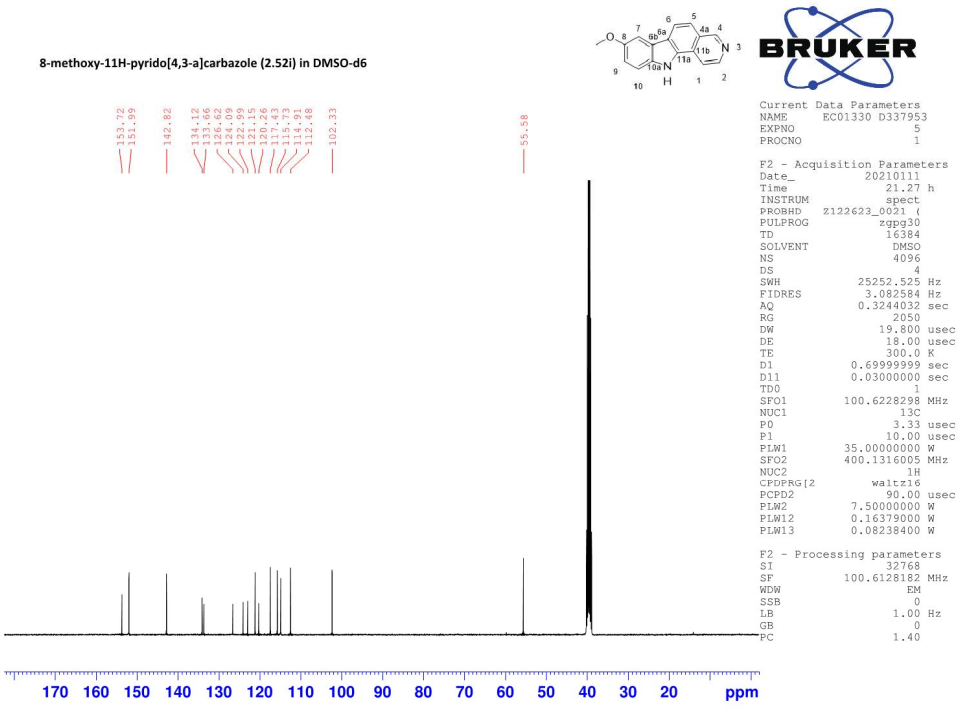


Figure 213. ^{13}C NMR spectra of 8-methoxy-11H-pyrido[4,3-a]carbazole (**2.52i**).

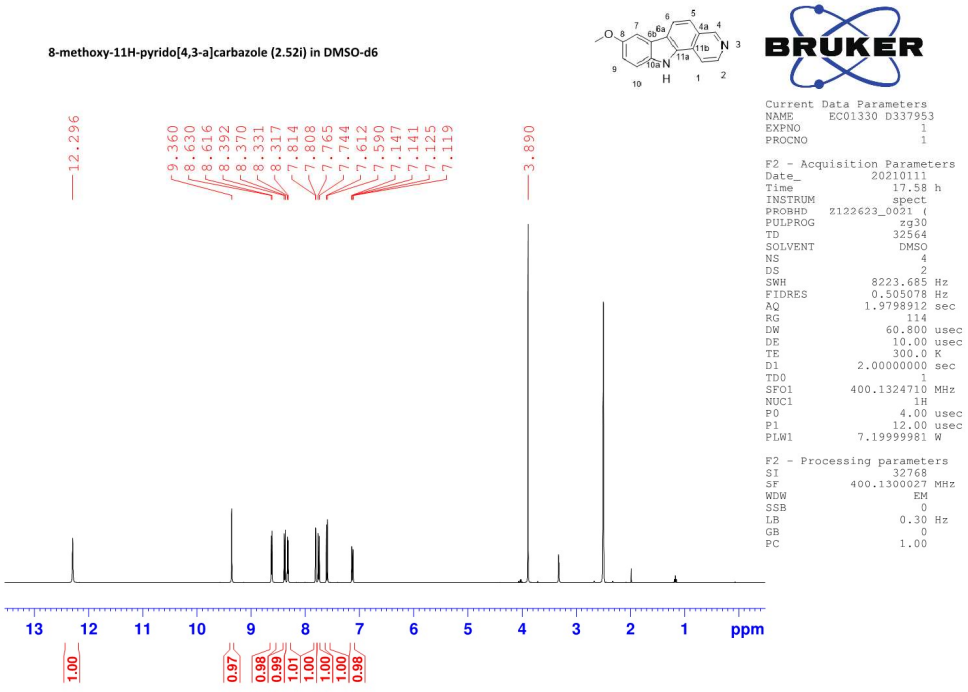


Figure 214. ^{1}H NMR spectra of 8-methoxy-11H-pyrido[4,3-a]carbazole (**2.52i**).

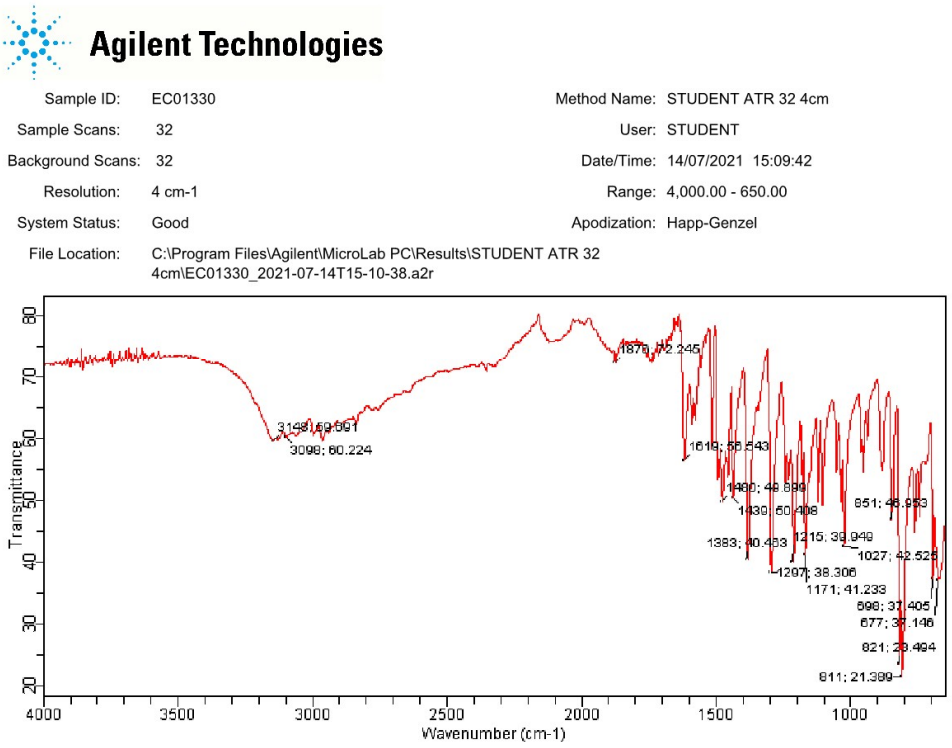


Figure 215. FT-IR spectra of 8-methoxy-11H-pyrido[4,3-a]carbazole (**2.52i**).

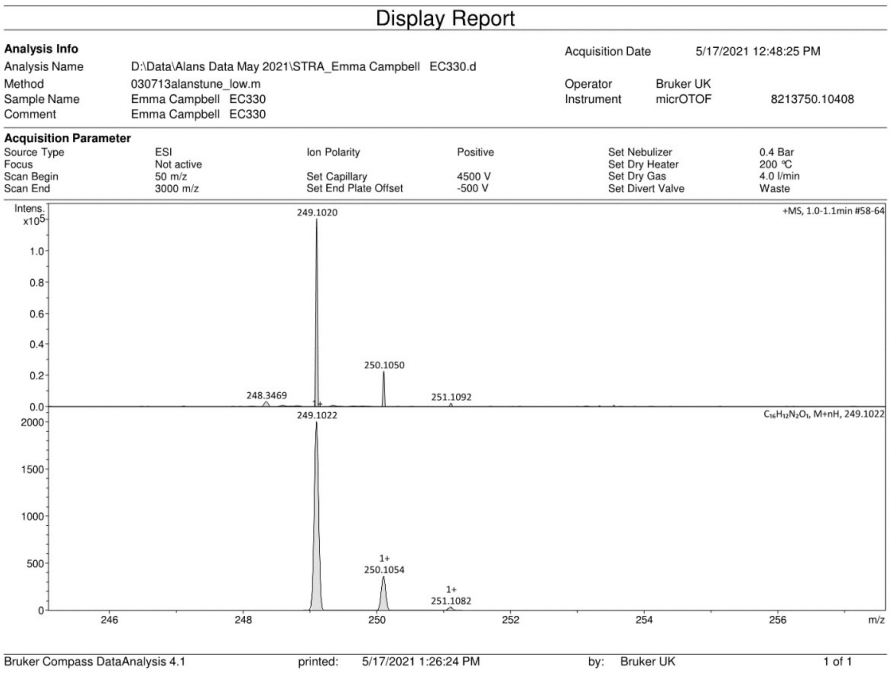


Figure 216. HRMS spectra of 8-methoxy-11H-pyrido[4,3-a]carbazole (**2.52i**).

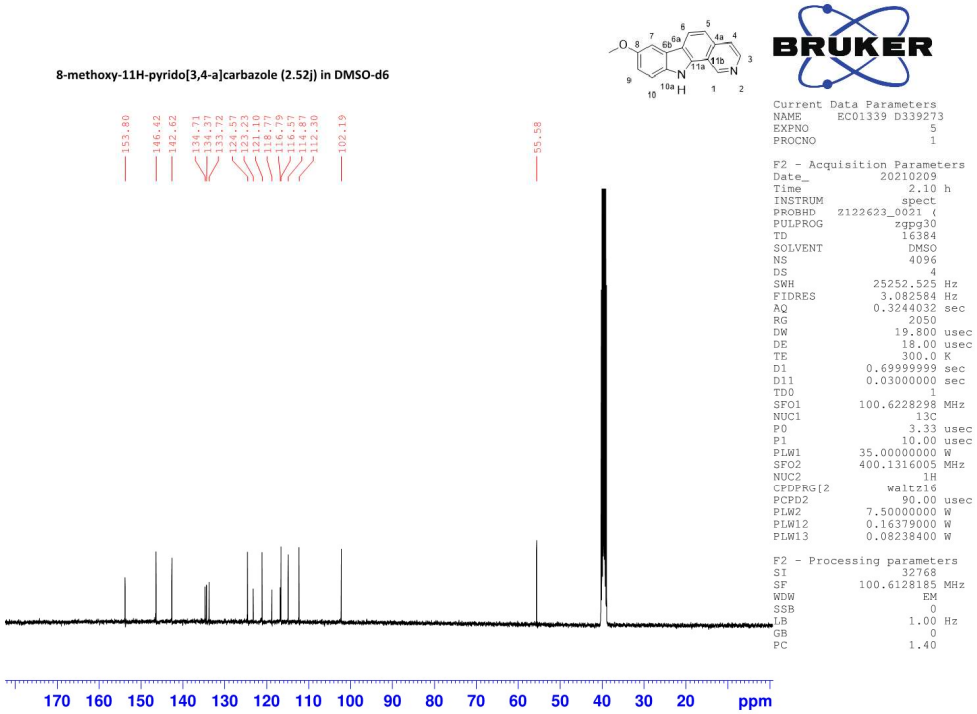


Figure 217. ^{13}C NMR spectra of 8-methoxy-11H-pyrido[3,4-a]carbazole (**2.52j**).

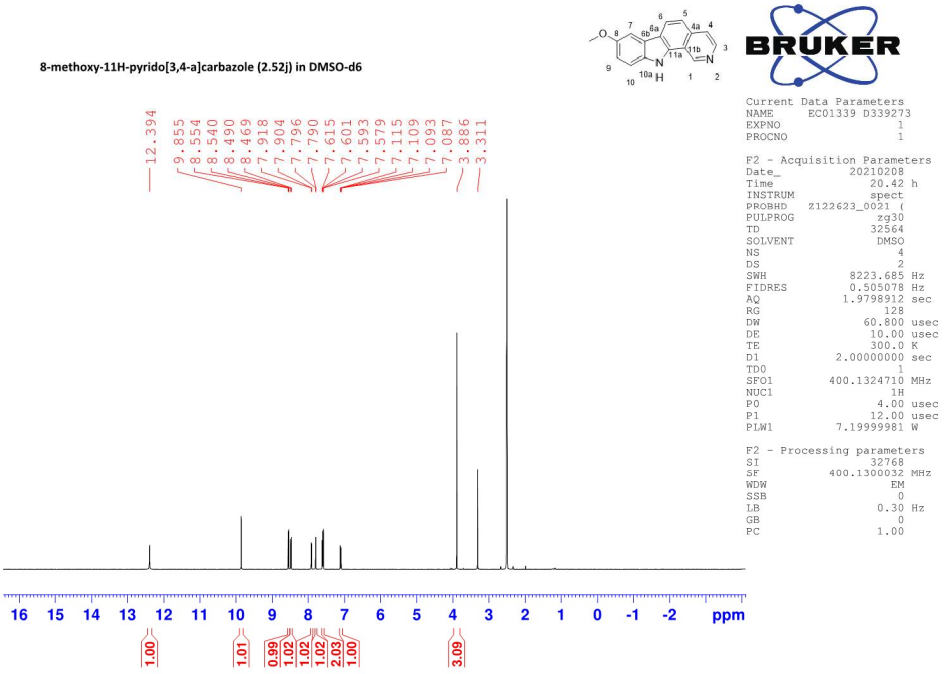


Figure 218. ^{1}H NMR spectra of 8-methoxy-11H-pyrido[3,4-a]carbazole (**2.52j**).

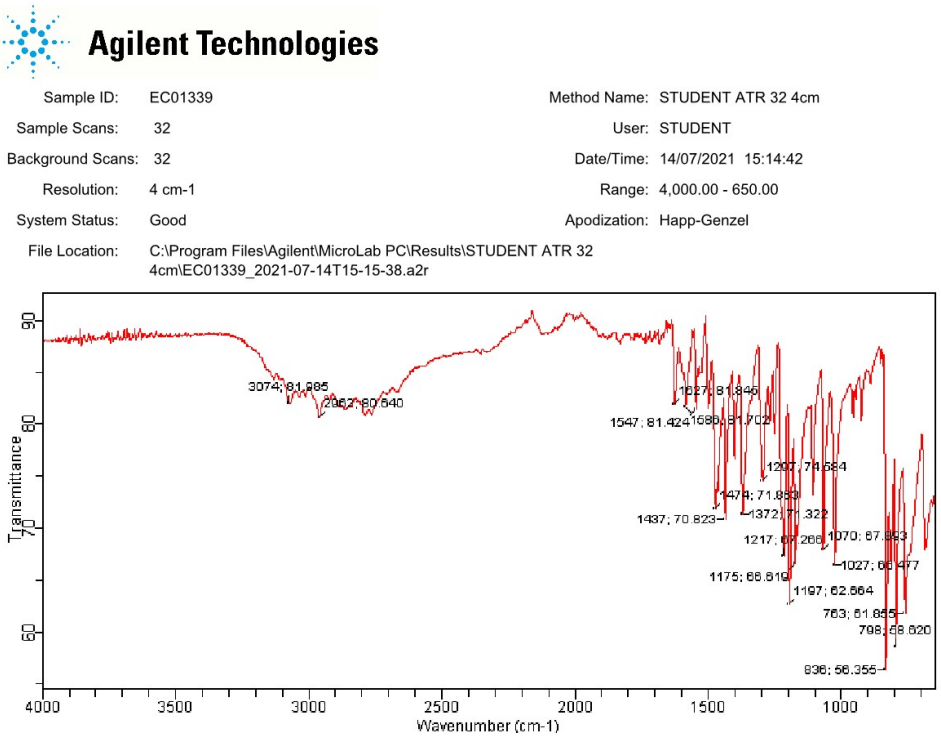


Figure 219. FT-IR spectra of 8-methoxy-11H-pyrido[3,4-a]carbazole (**2.52j**).

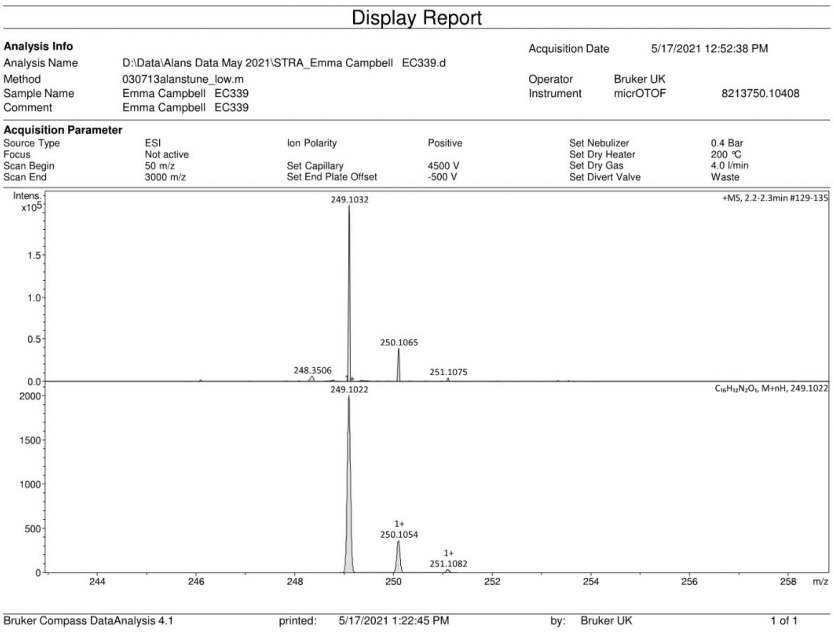


Figure 220. HRMS spectra of 8-methoxy-11H-pyrido[3,4-a]carbazole (**2.52j**).

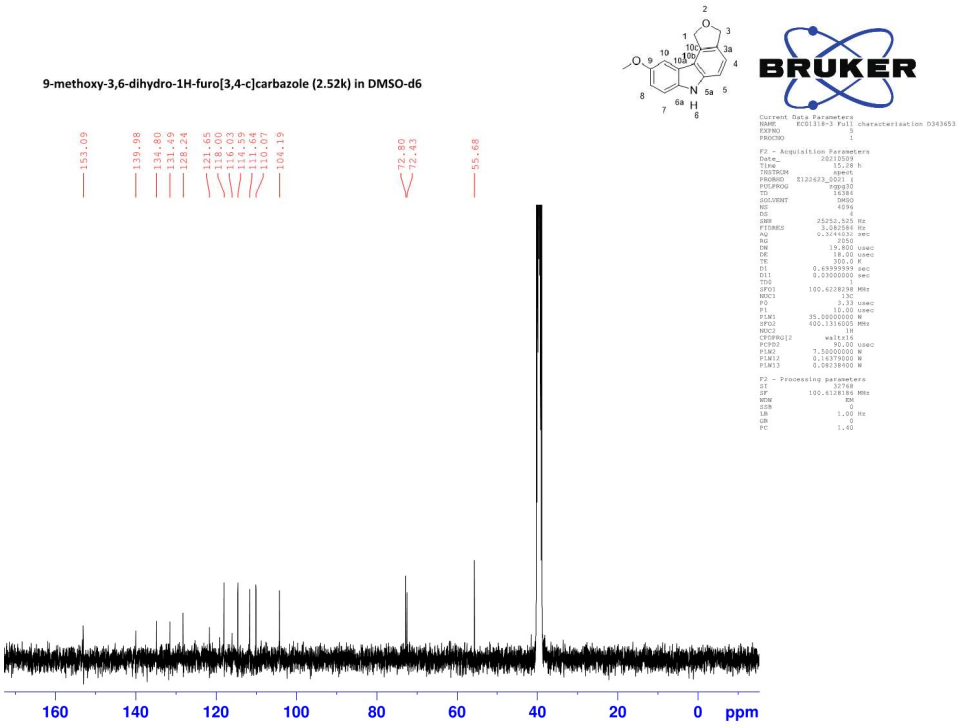


Figure 221. ^{13}C NMR spectra of 9-methoxy-3,6-dihydro-1H-furo[3,4-c]carbazole (**2.52k**).

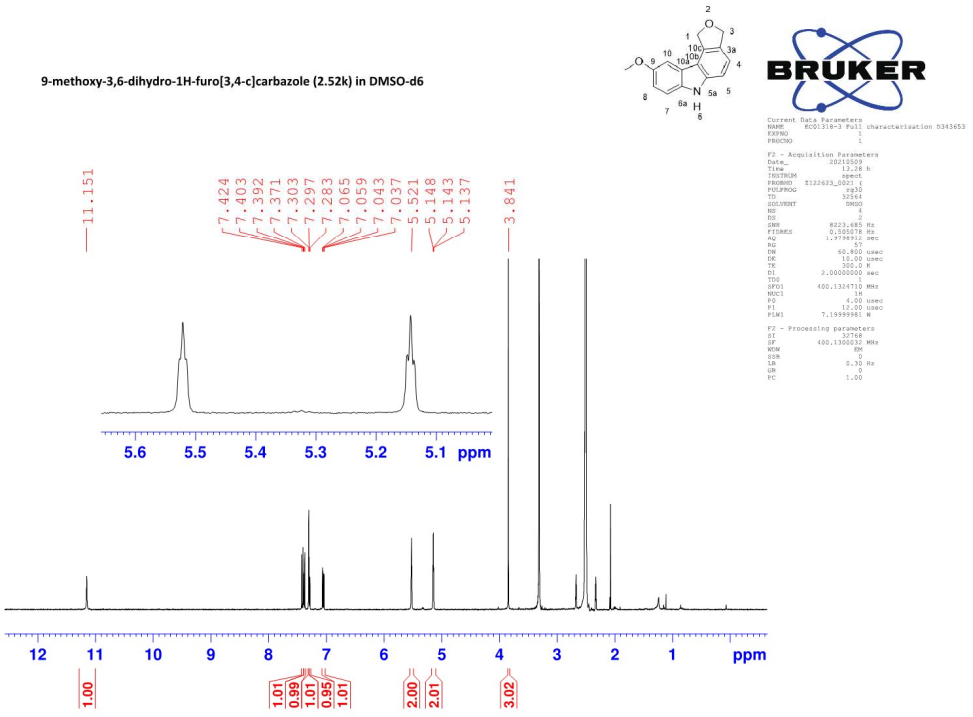


Figure 222. ^{1}H NMR spectra of 9-methoxy-3,6-dihydro-1H-furo[3,4-c]carbazole (**2.52k**).

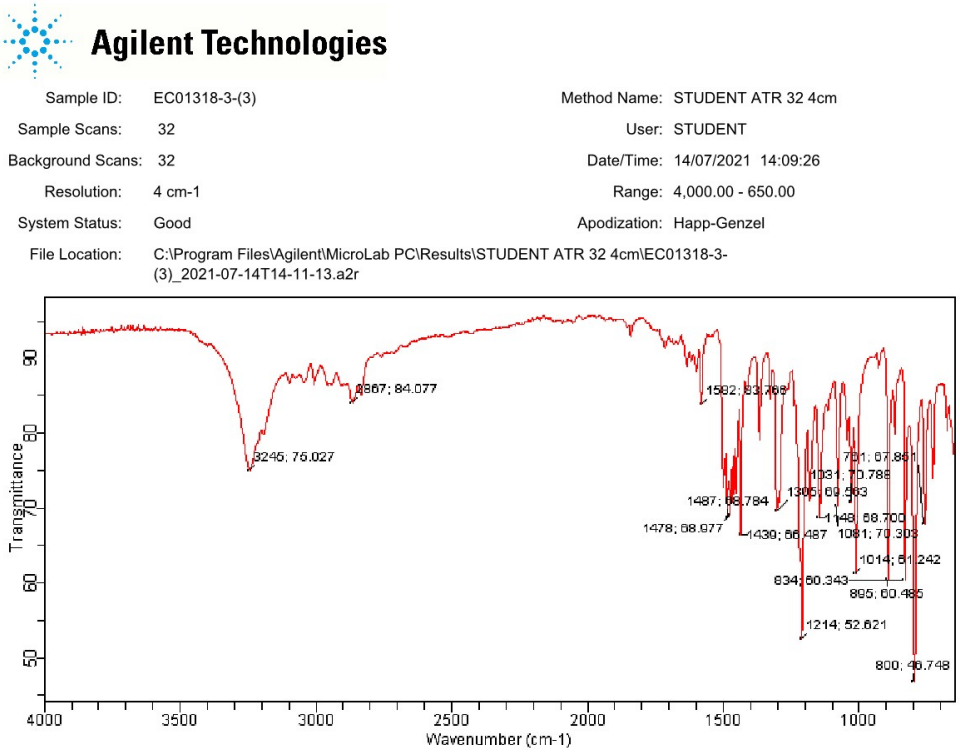


Figure 223. FT-IR spectra of 9-methoxy-3,6-dihydro-1H-furo[3,4-c]carbazole (**2.52k**).

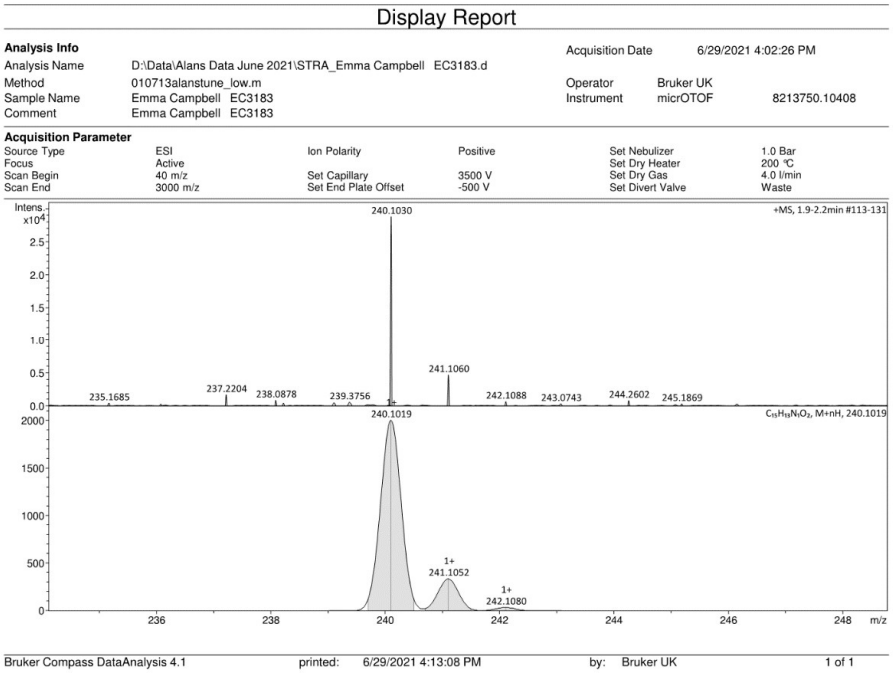


Figure 224. HRMS spectra of 9-methoxy-3,6-dihydro-1H-furo[3,4-c]carbazole (**2.52k**).

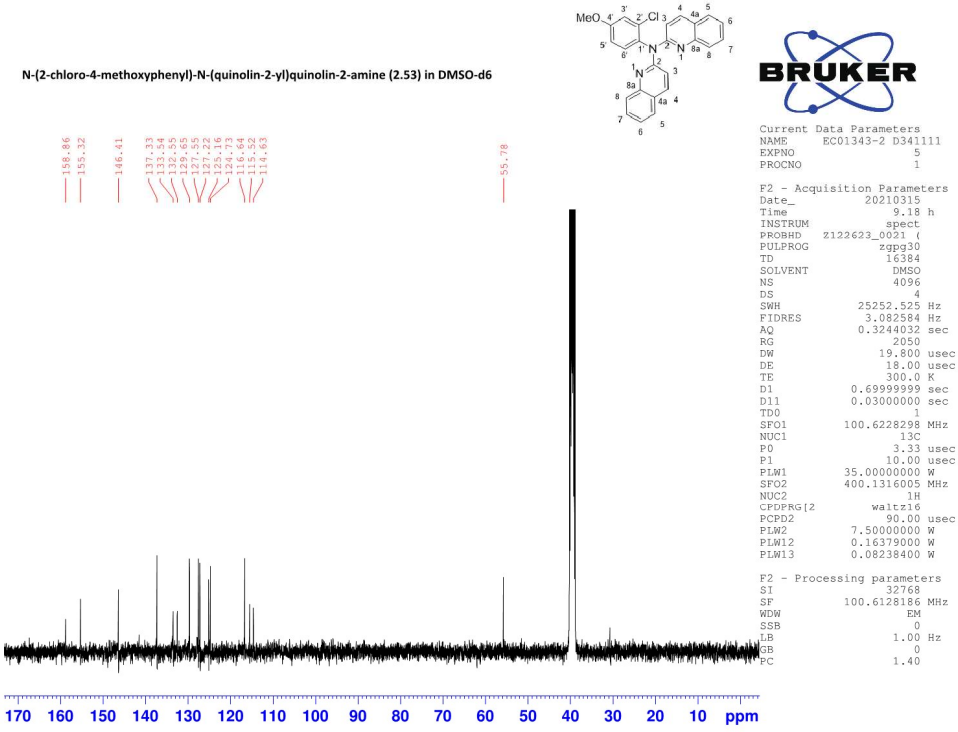


Figure 225. ^{13}C NMR spectra of N-(2-chloro-4-methoxyphenyl)-N-(quinolin-2-yl)quinolin-2-amine (**2.53**).

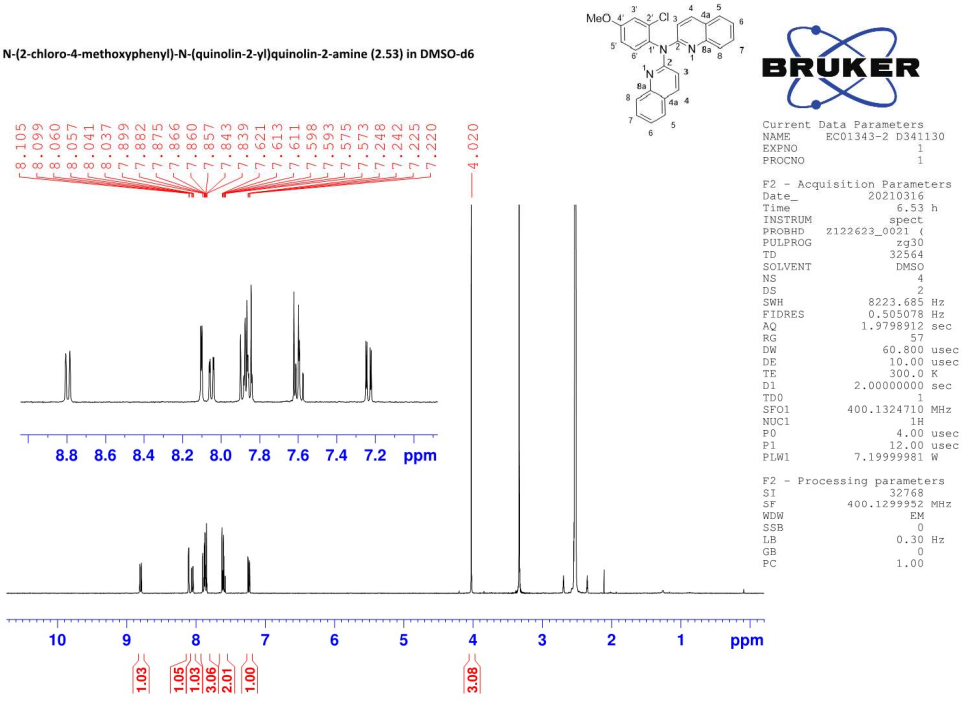


Figure 226. ^{1}H NMR spectra of N-(2-chloro-4-methoxyphenyl)-N-(quinolin-2-yl)quinolin-2-amine (**2.53**).

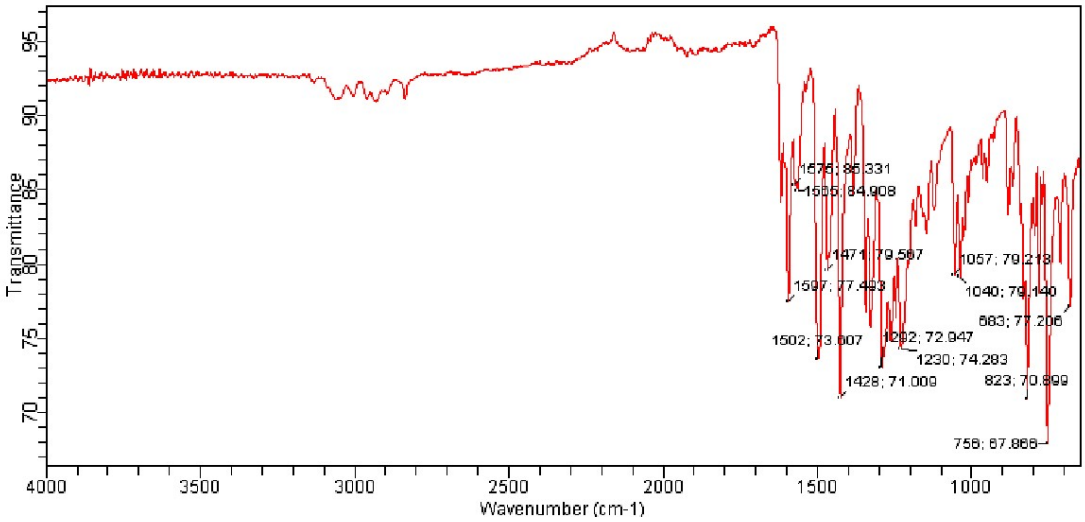


Figure 227. FT-IR spectra of N-(2-chloro-4-methoxyphenyl)-N-(quinolin-2-yl)quinolin-2-amine (**2.53**).

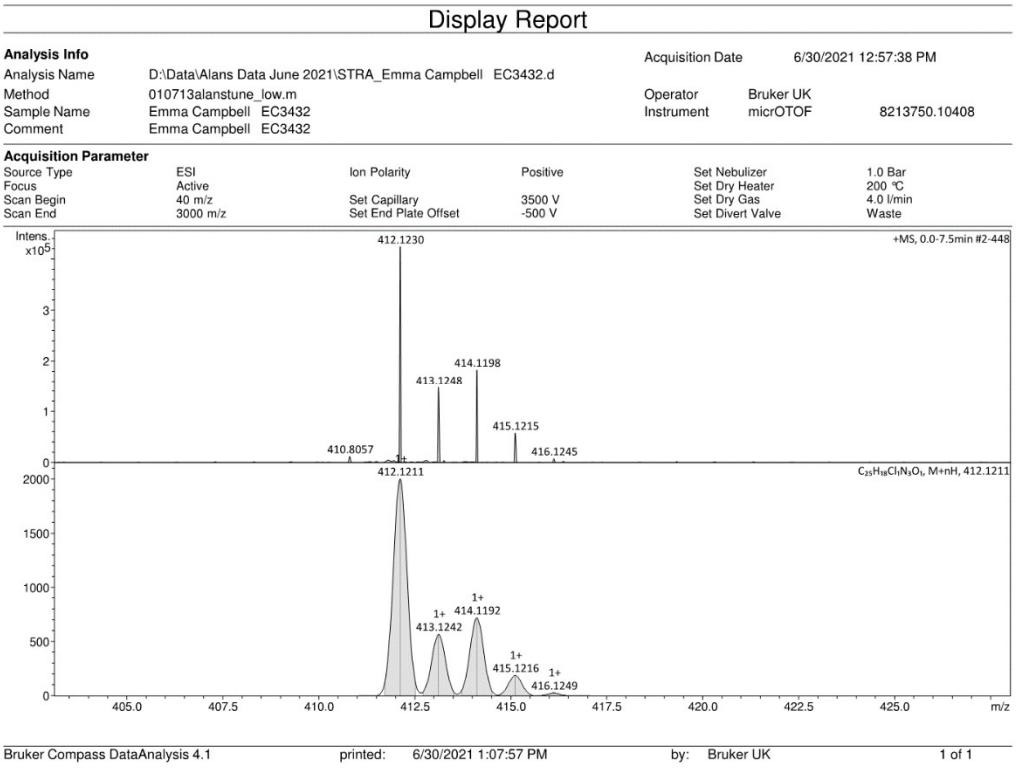


Figure 228. HRMS spectra of N-(2-chloro-4-methoxyphenyl)-N-(quinolin-2-yl)quinolin-2-amine (**2.53**).

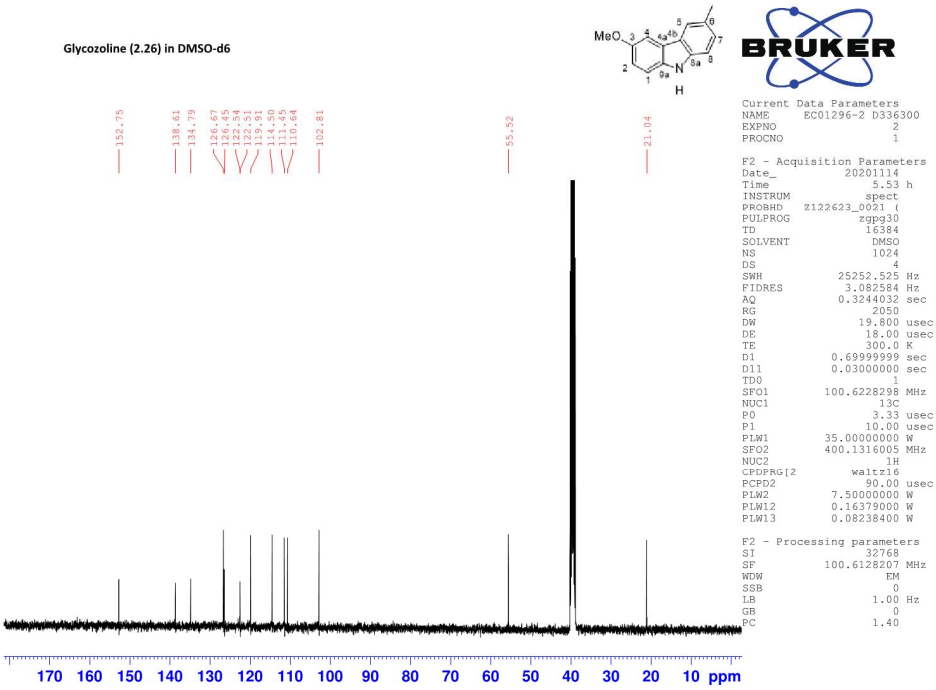


Figure 229. ^{13}C NMR spectra of Glycozoline (**2.26**).

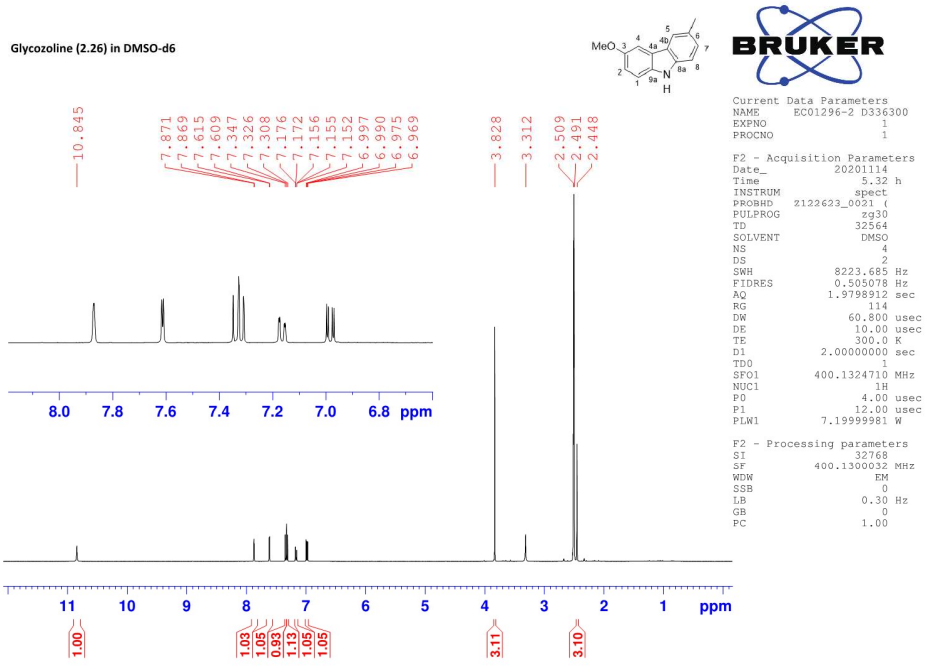


Figure 230. ^{1}H NMR spectra of Glycozoline (**2.26**).

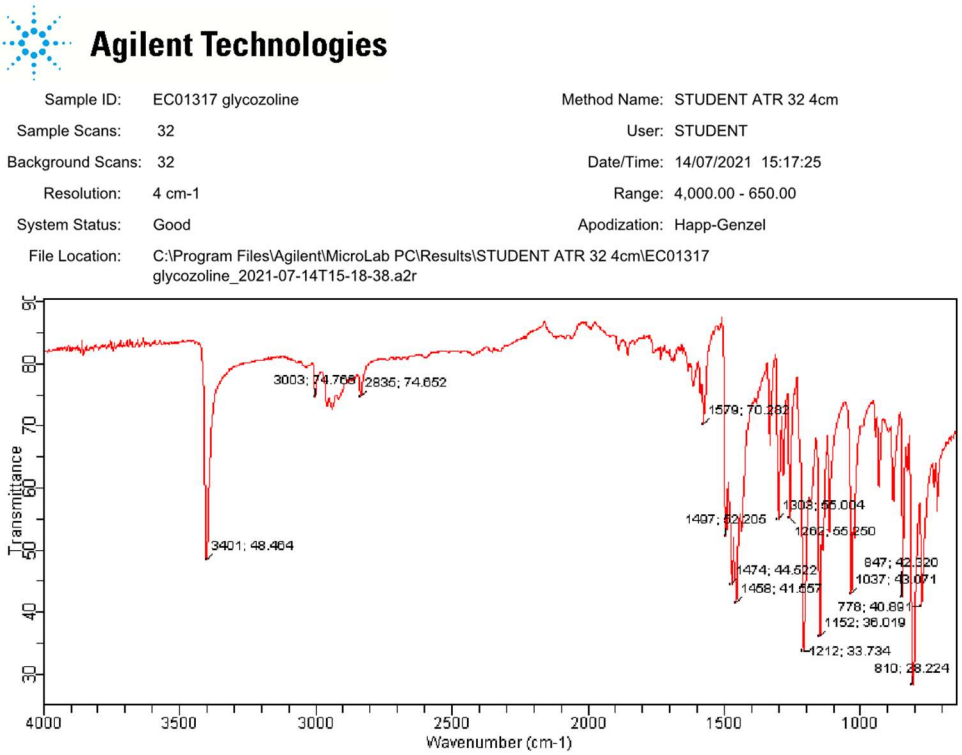


Figure 231. FT-IR spectra of Glycozoline (**2.26**).

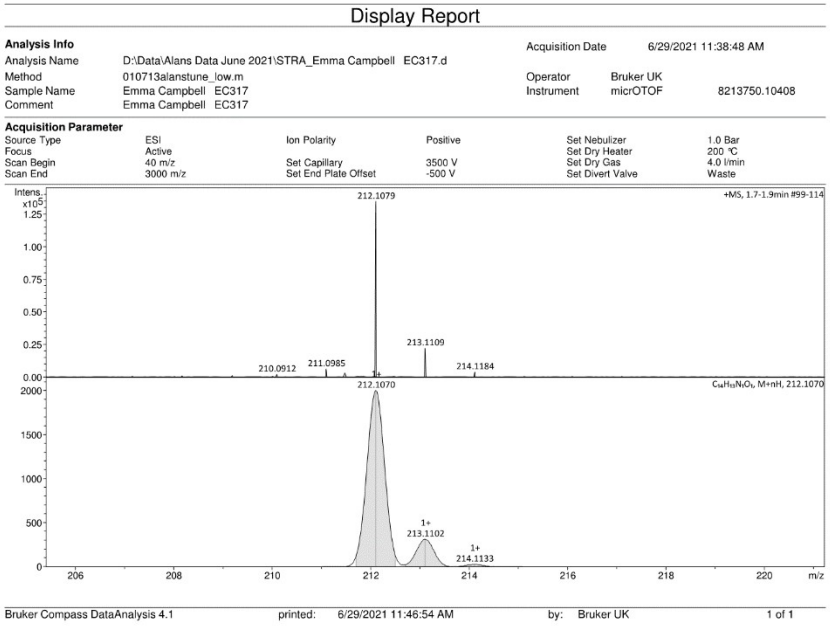


Figure 232. HRMS spectra of Glycozoline (**2.26**).

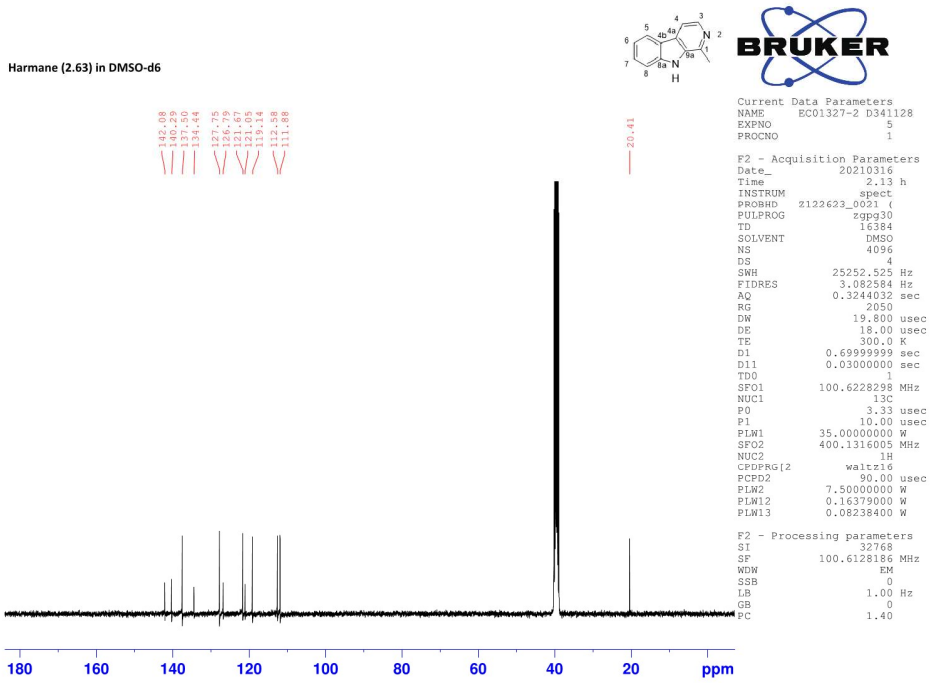


Figure 233. ^{13}C NMR spectra of Harmane (**2.63**).

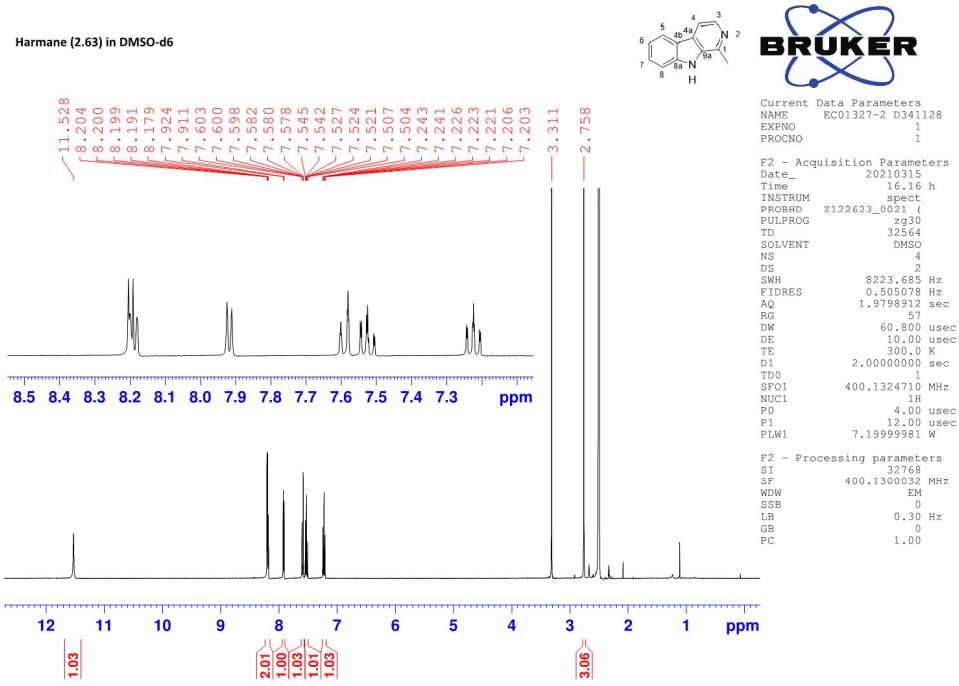


Figure 234. ^{1}H NMR spectra of Harmane (**2.63**).

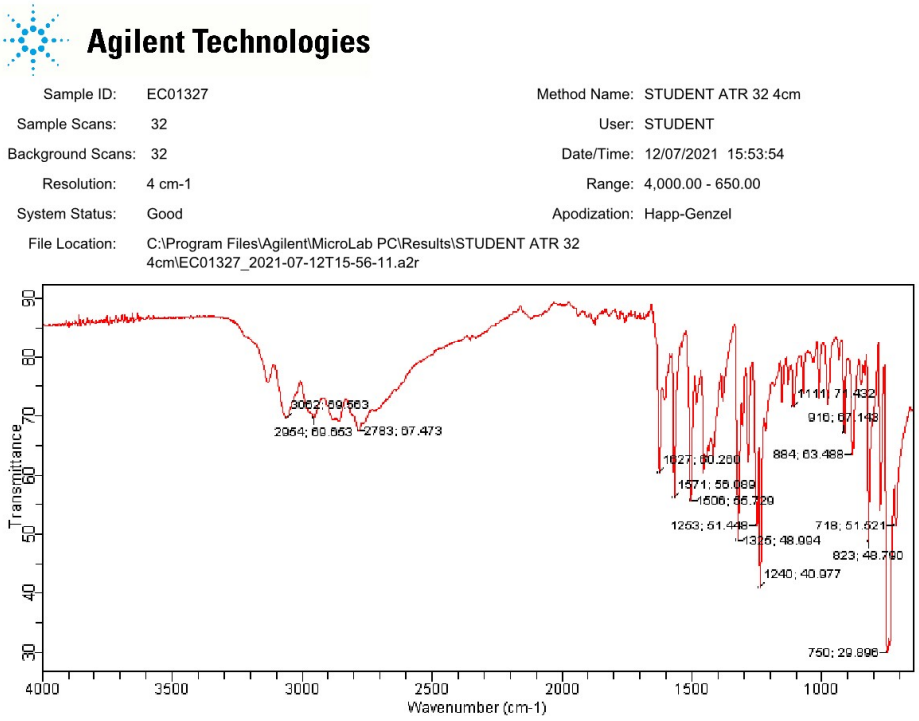


Figure 235. FT-IR spectra of Harmane (**2.63**).

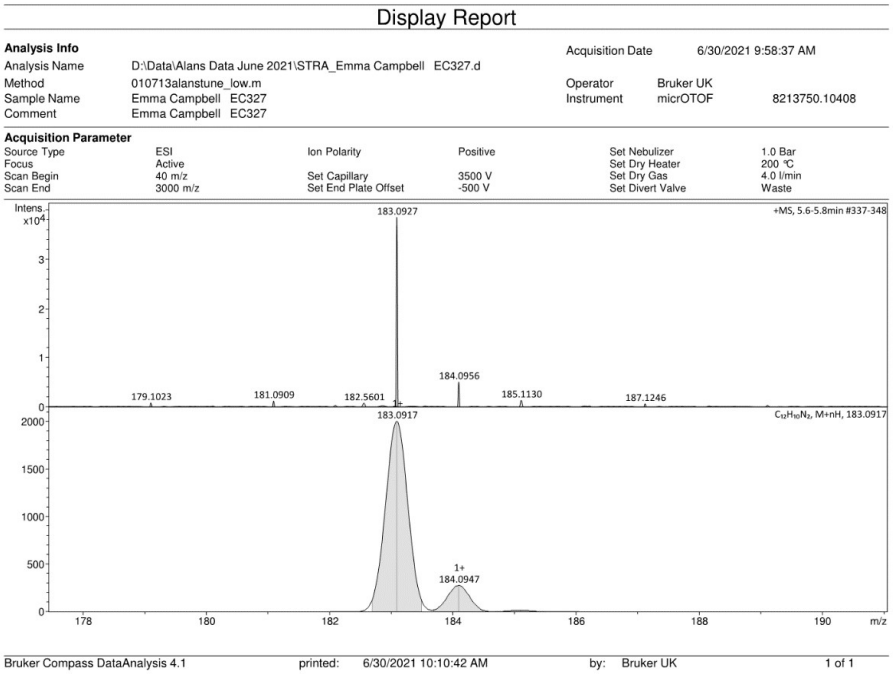


Figure 236. HRMS spectra of Harmane (**2.63**).

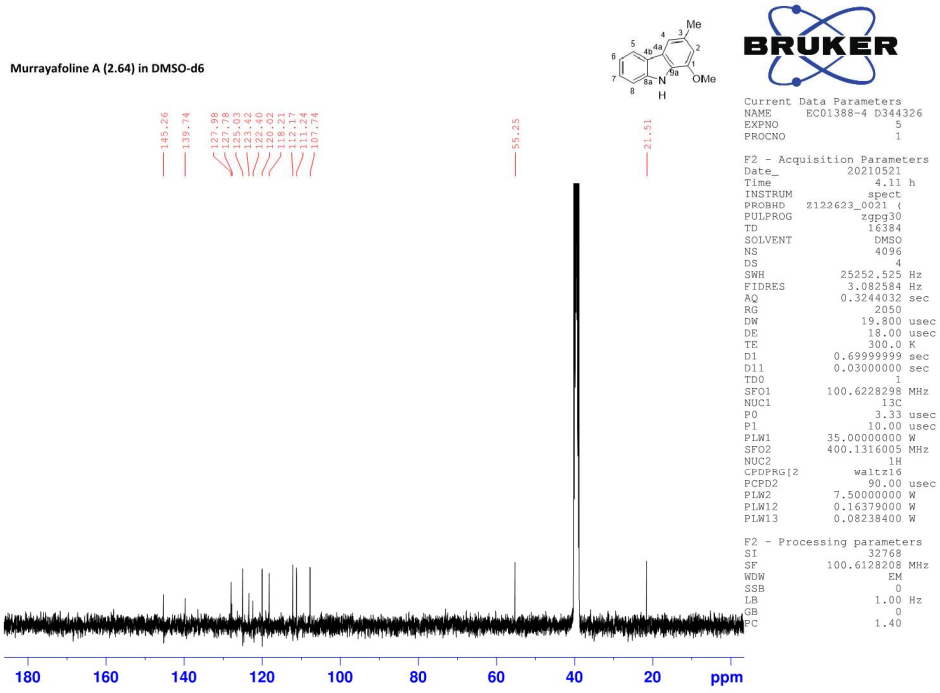


Figure 237. ^{13}C NMR spectra of Murrayafoline A (**2.64**).

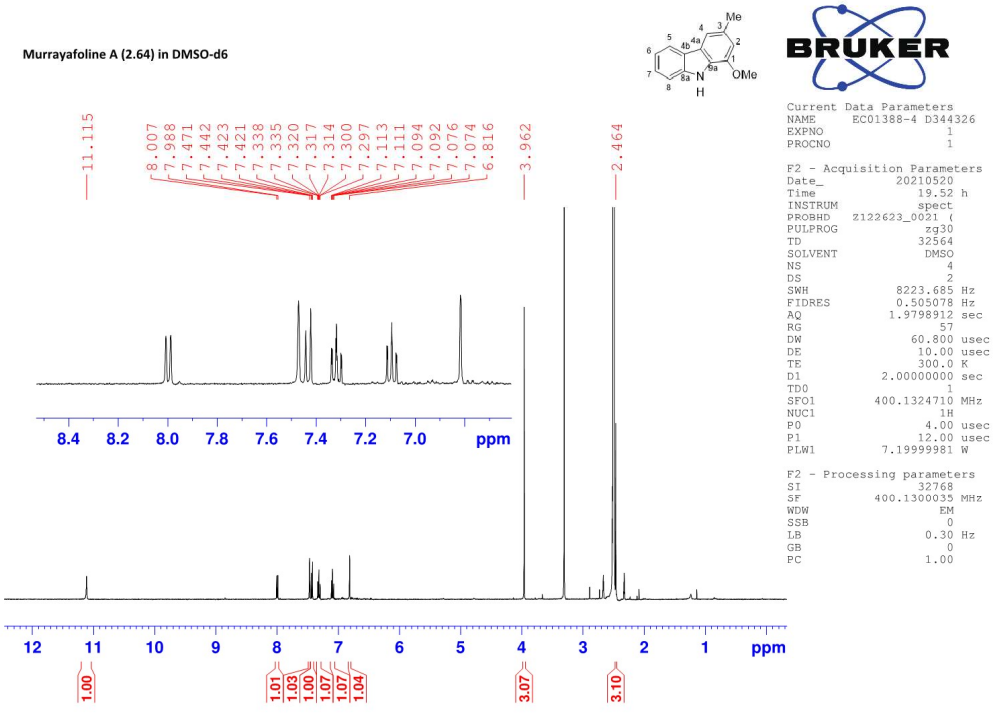


Figure 238. ^{1}H NMR spectra of Murrayafoline A (**2.64**).

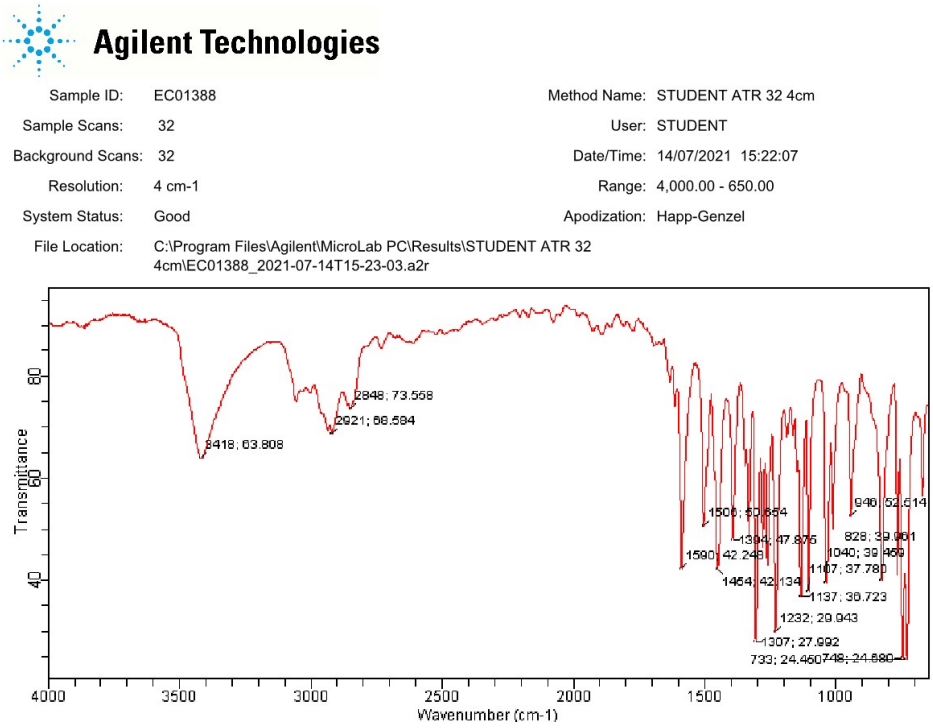


Figure 239. FT-IR spectra of Murrayafoline A (**2.64**).

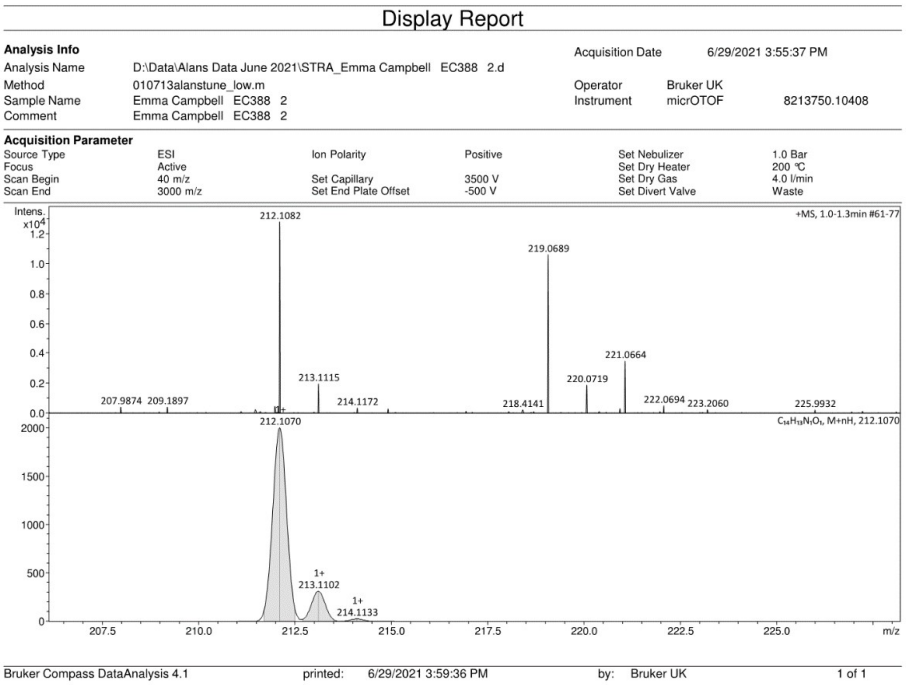


Figure 240. HRMS spectra of Murrayafoline A (**2.64**).

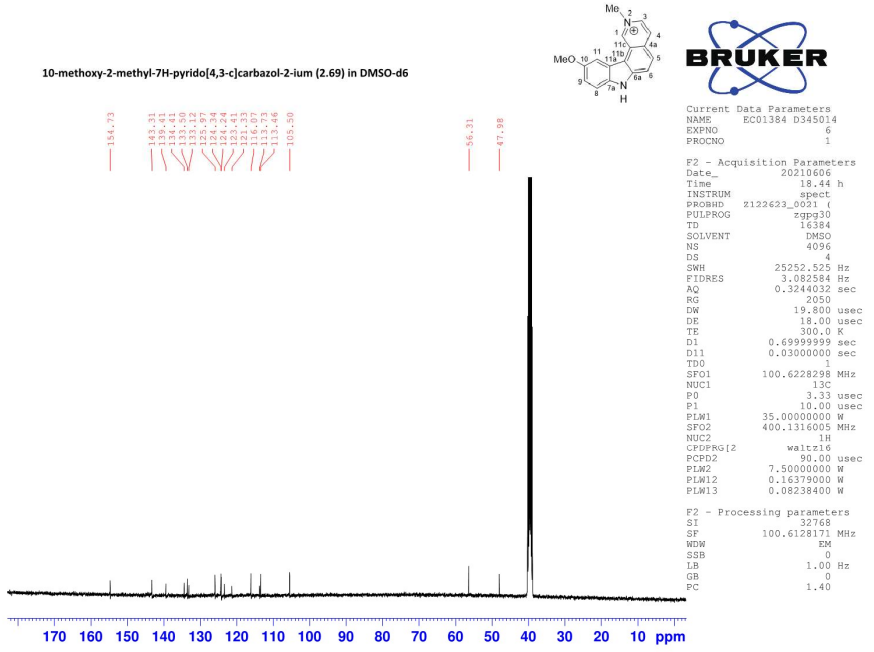


Figure 241. ^{13}C NMR spectra of 10-methoxy-2-methyl-7H-pyrido[4,3-c]carbazol-2-ium (**2.69**).

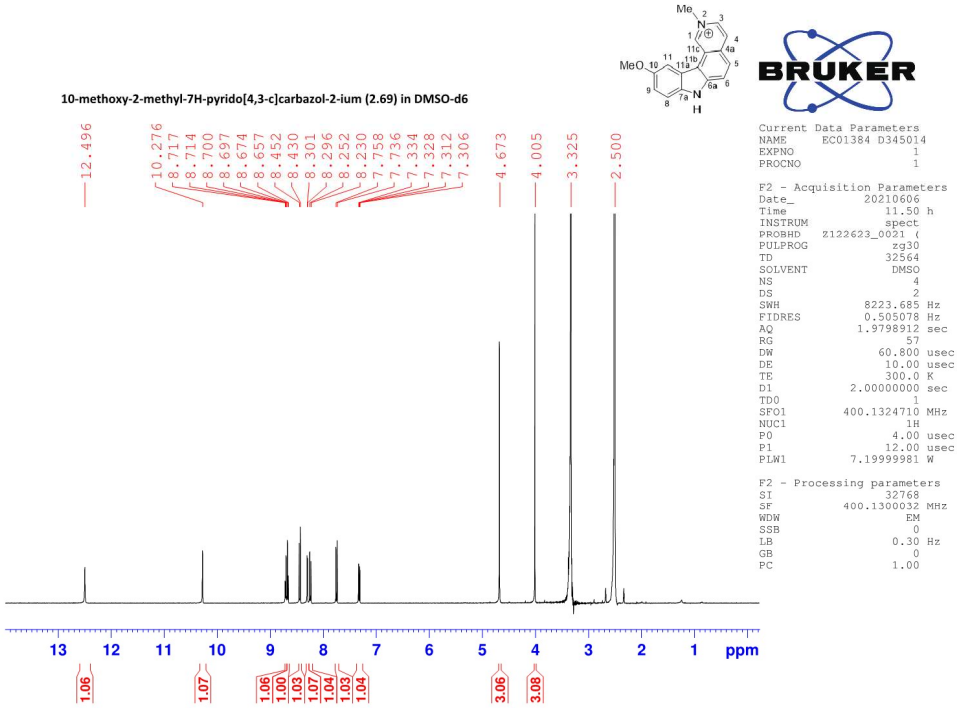


Figure 242. ^{1}H NMR spectra of 10-methoxy-2-methyl-7H-pyrido[4,3-c]carbazol-2-ium (**2.69**).

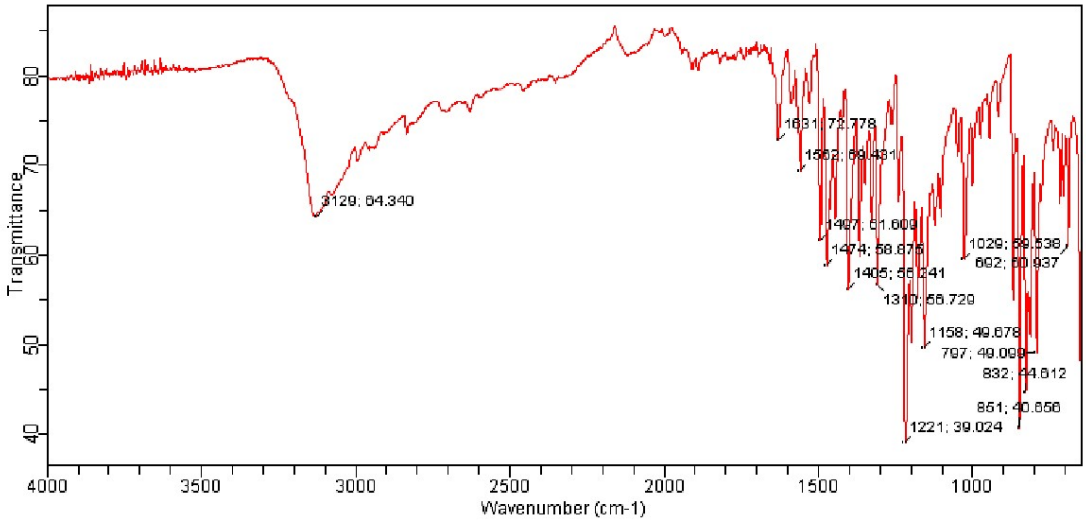


Figure 243. FT-IR spectra of 10-methoxy-2-methyl-7H-pyrido[4,3-c]carbazol-2-ium (**2.69**).

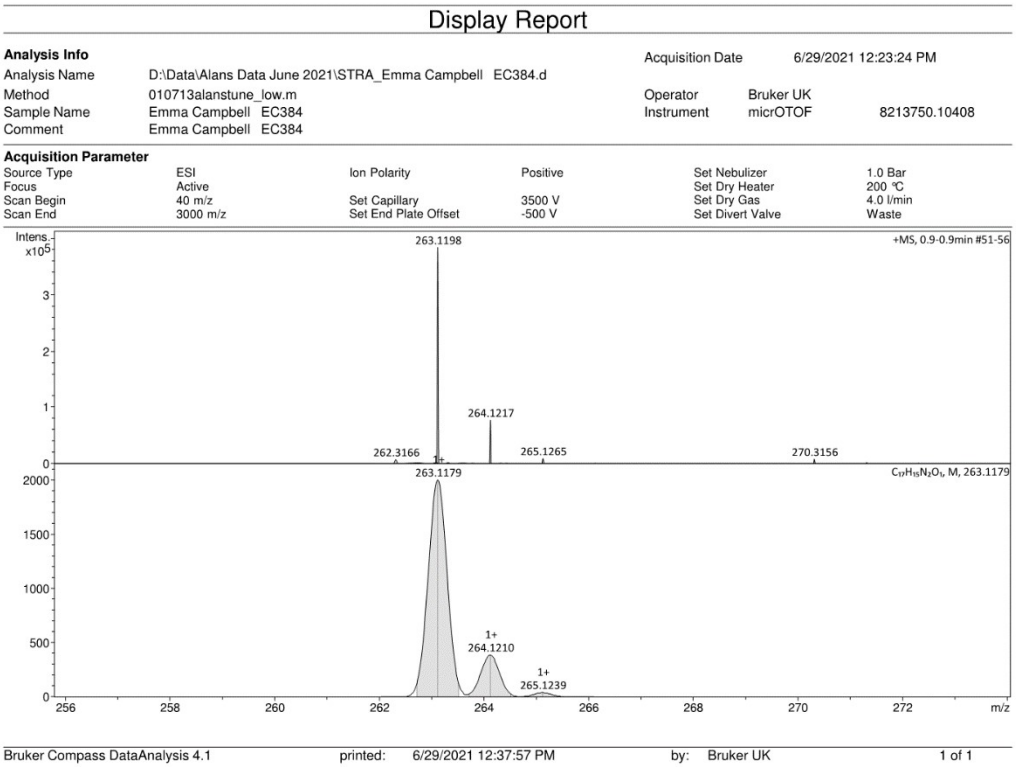


Figure 244. HRMS spectra of 10-methoxy-2-methyl-7H-pyrido[4,3-c]carbazol-2-ium (**2.69**).

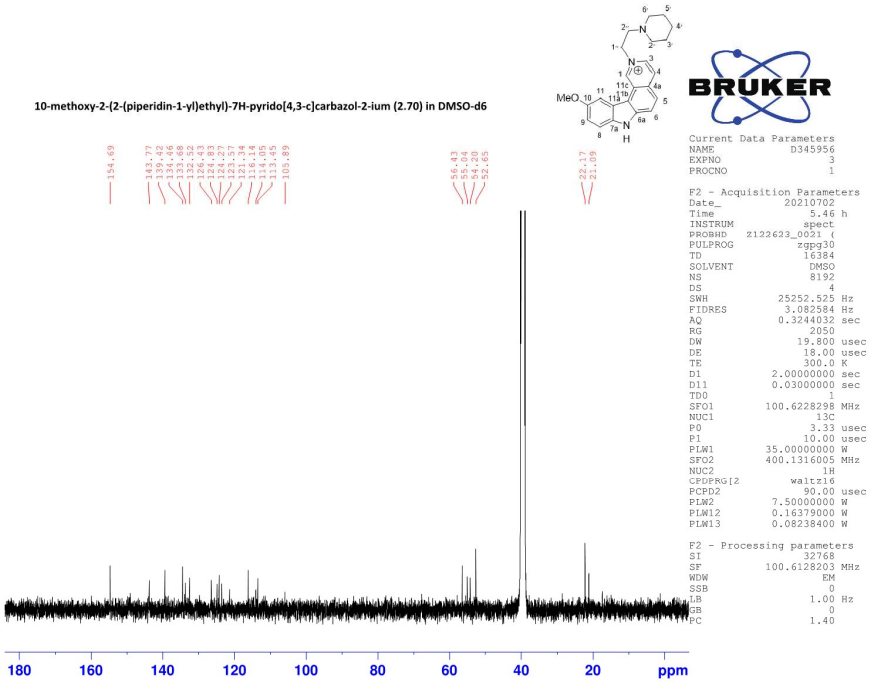


Figure 245. ^{13}C NMR spectra of 10-methoxy-2-(2-(piperidin-1-yl)ethyl)-7H-pyrido[4,3-c]carbazol-2-ium (**2.70**).

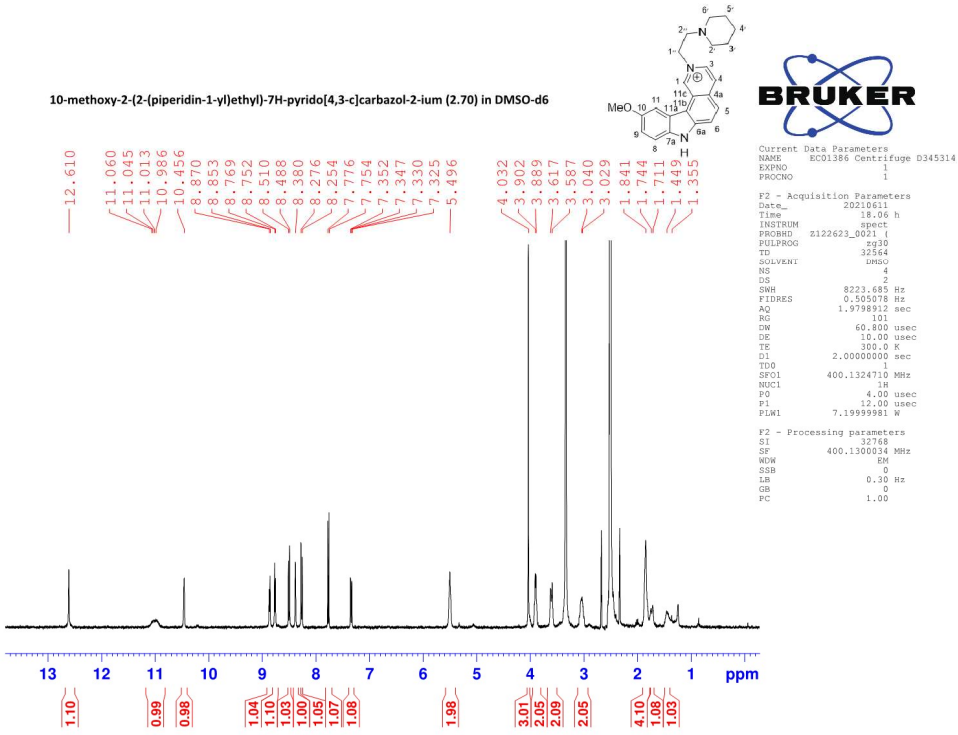


Figure 246. ^{1}H NMR spectra of 10-methoxy-2-(2-(piperidin-1-yl)ethyl)-7H-pyrido[4,3-c]carbazol-2-ium (**2.70**).

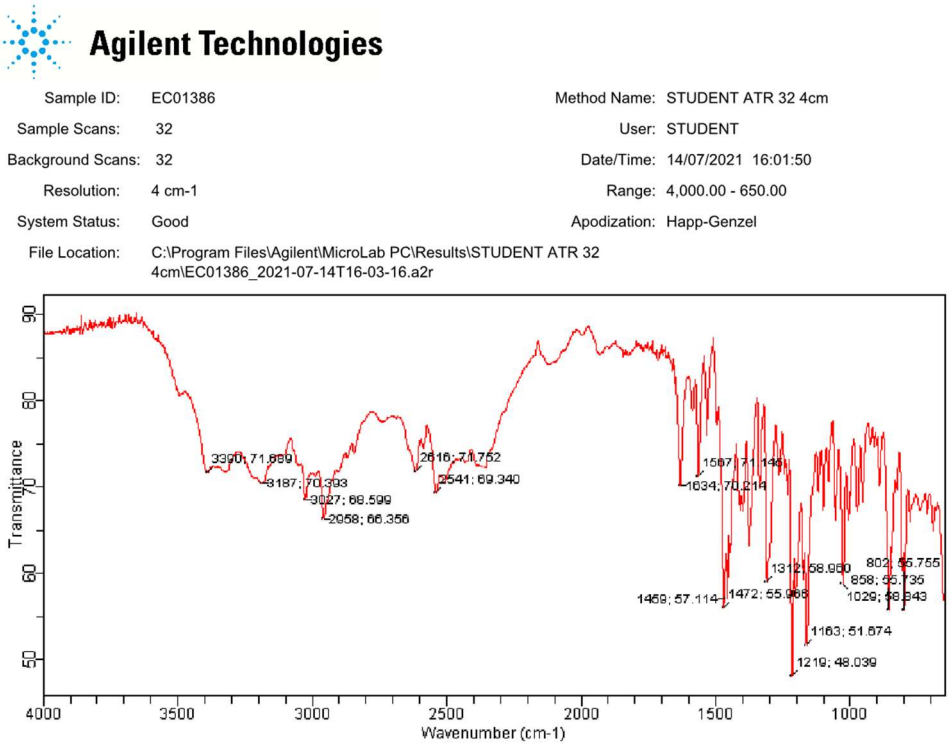


Figure 247. FT-IR spectra of 10-methoxy-2-(2-(piperidin-1-yl)ethyl)-7H-pyrido[4,3-c]carbazol-2-ium (**2.70**).

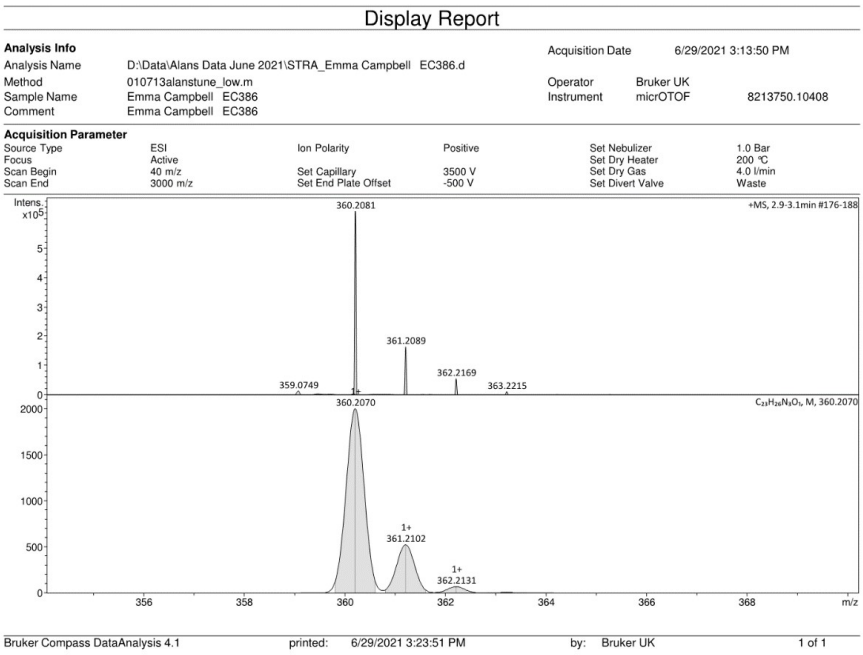


Figure 248. HRMS spectra of 10-methoxy-2-(2-(piperidin-1-yl)ethyl)-7H-pyrido[4,3-c]carbazol-2-ium (**2.70**).

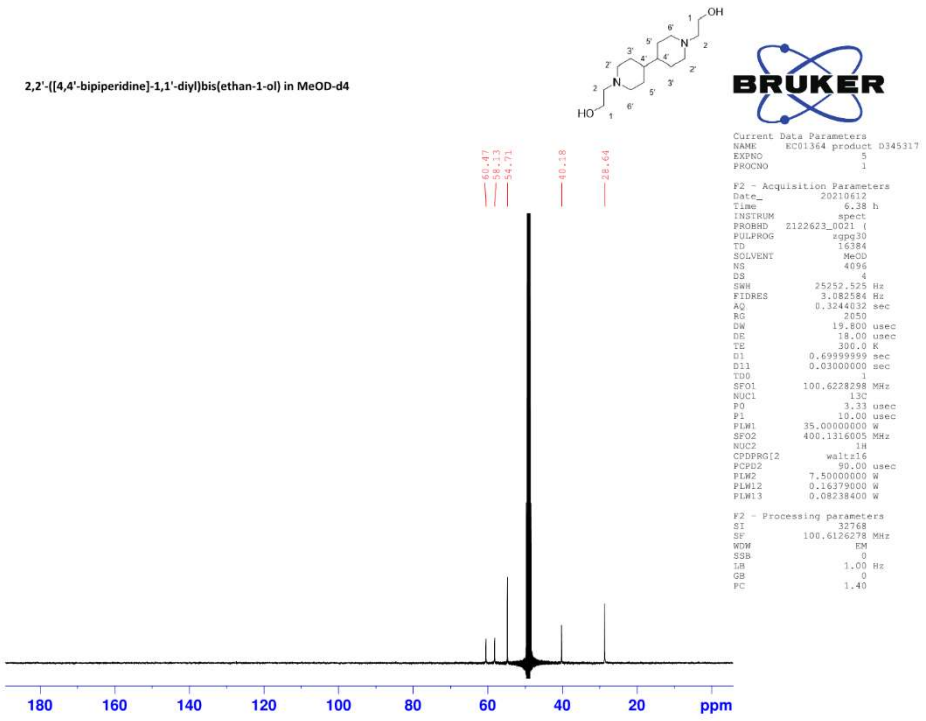


Figure 249. ^{13}C NMR spectra of 2,2'-([4,4'-bipiperidine]-1,1'-diyl)bis(ethan-1-ol) (**2.67**).

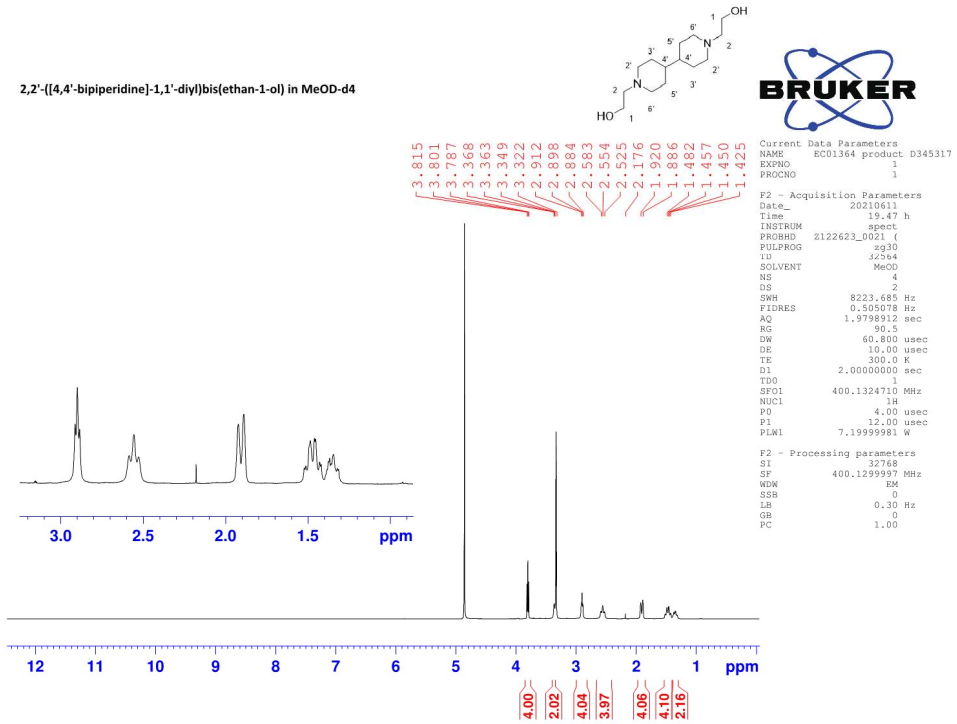


Figure 250. ^{1}H NMR spectra of 2,2'-([4,4'-bipiperidine]-1,1'-diyl)bis(ethan-1-ol) (**2.67**).

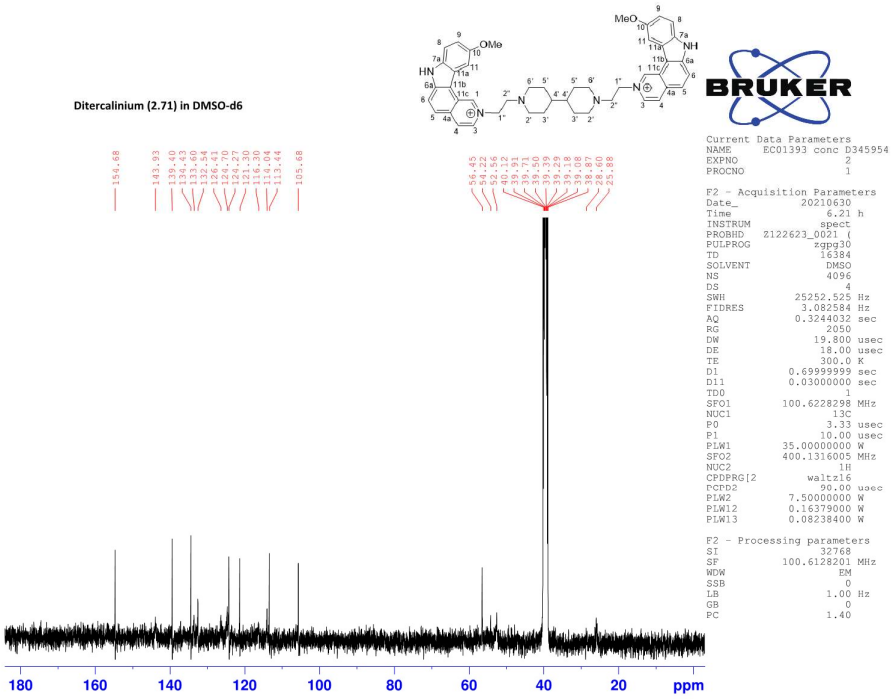


Figure 251. ^{13}C NMR spectra of Ditercalinium (**2.71**).

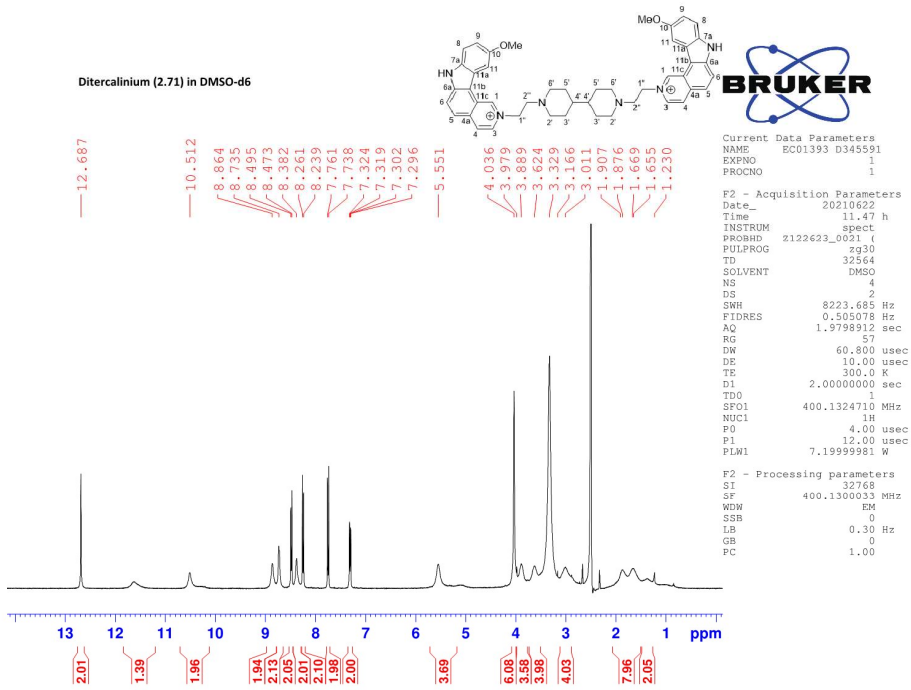


Figure 252. ^{1}H NMR spectra of Ditercalinium (**2.71**).

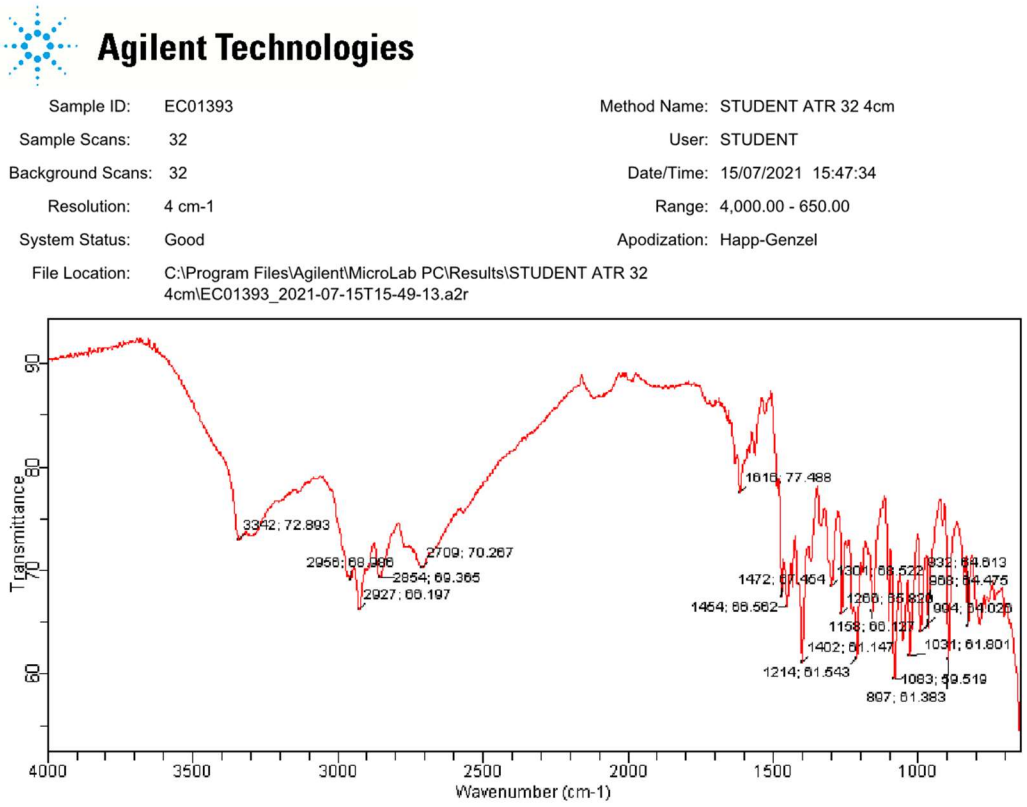


Figure 253. FT-IR spectra of Ditercalinium (**2.71**).

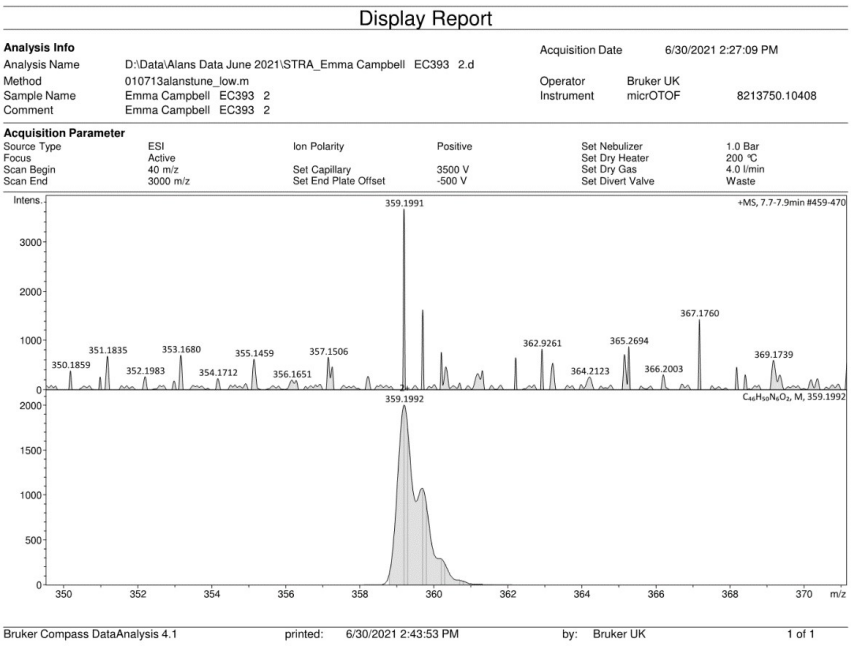


Figure 254. HRMS spectra of Ditercalinium (**2.71**).

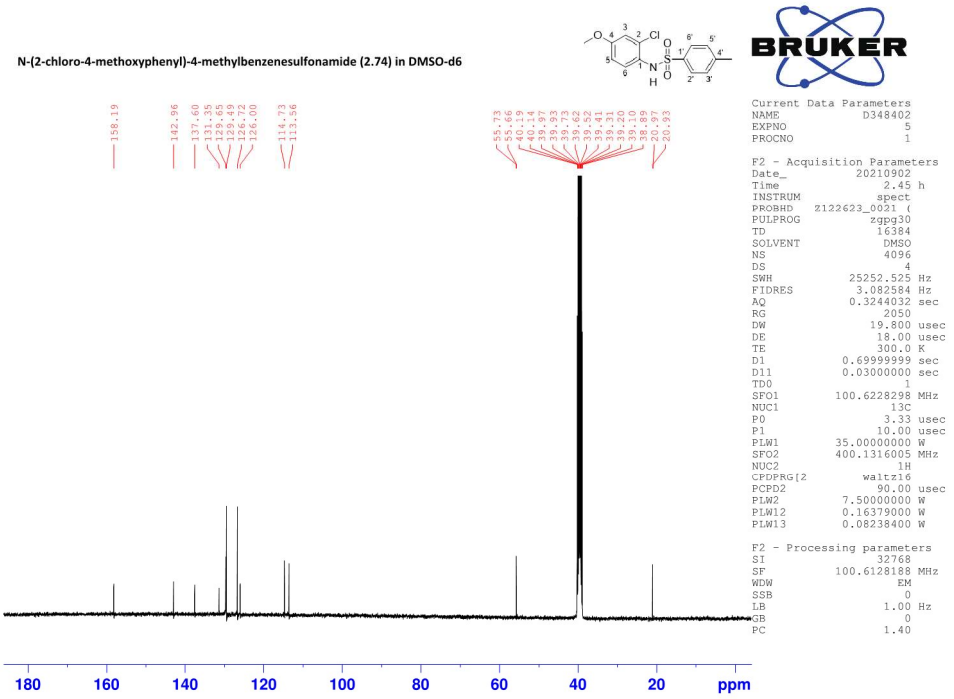


Figure 255. ^{13}C NMR spectra of N-(2-chloro-4-methoxyphenyl)-4-methylbenzenesulfonamide (**2.74**).

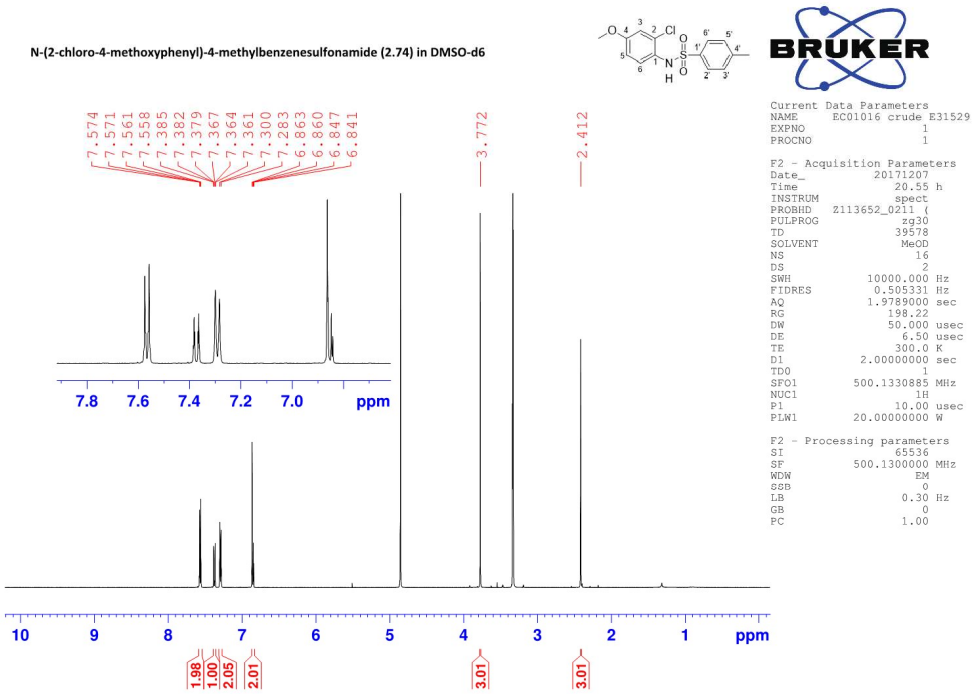


Figure 256. ^{1}H NMR spectra of N-(2-chloro-4-methoxyphenyl)-4-methylbenzenesulfonamide (**2.74**).

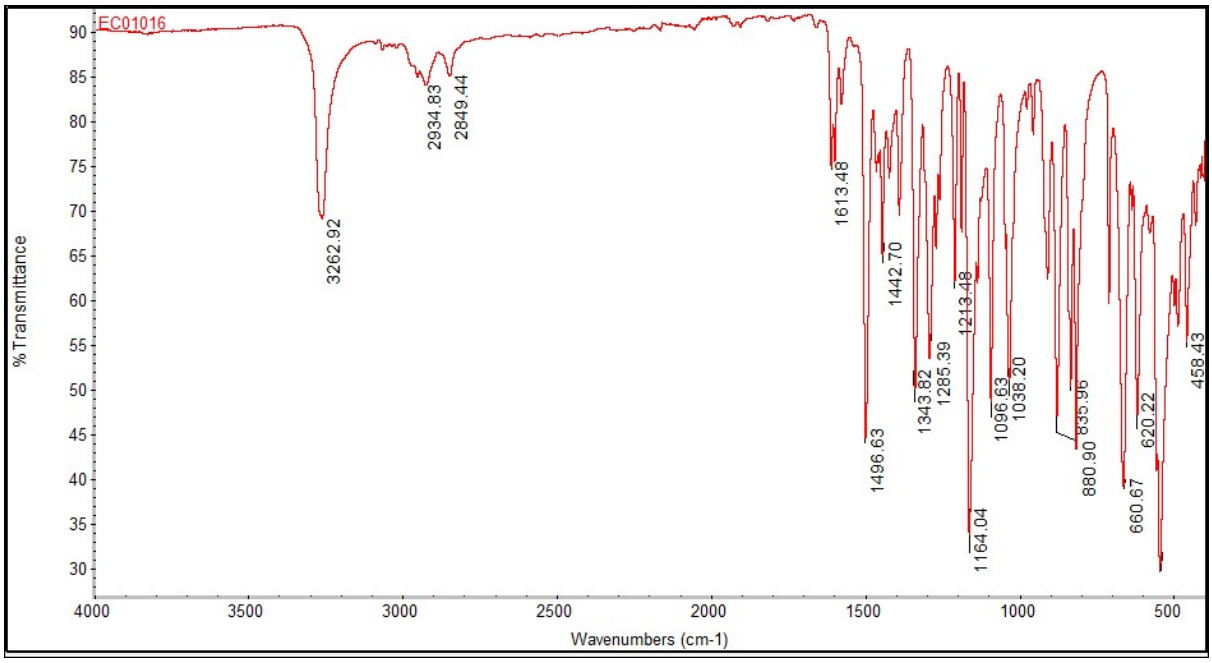


Figure 257. FT-IR spectra of N-(2-chloro-4-methoxyphenyl)-4-methylbenzenesulfonamide (**2.74**).

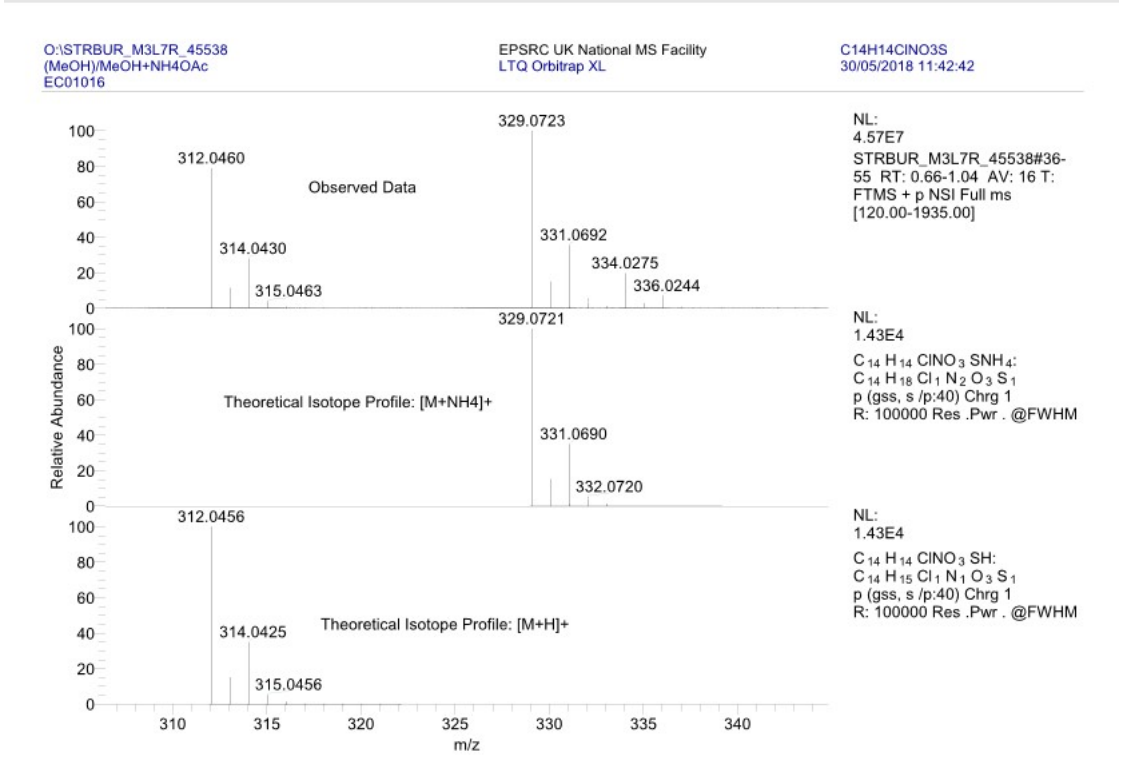


Figure 258. HRMS spectra of N-(2-chloro-4-methoxyphenyl)-4-methylbenzenesulfonamide (**2.74**).

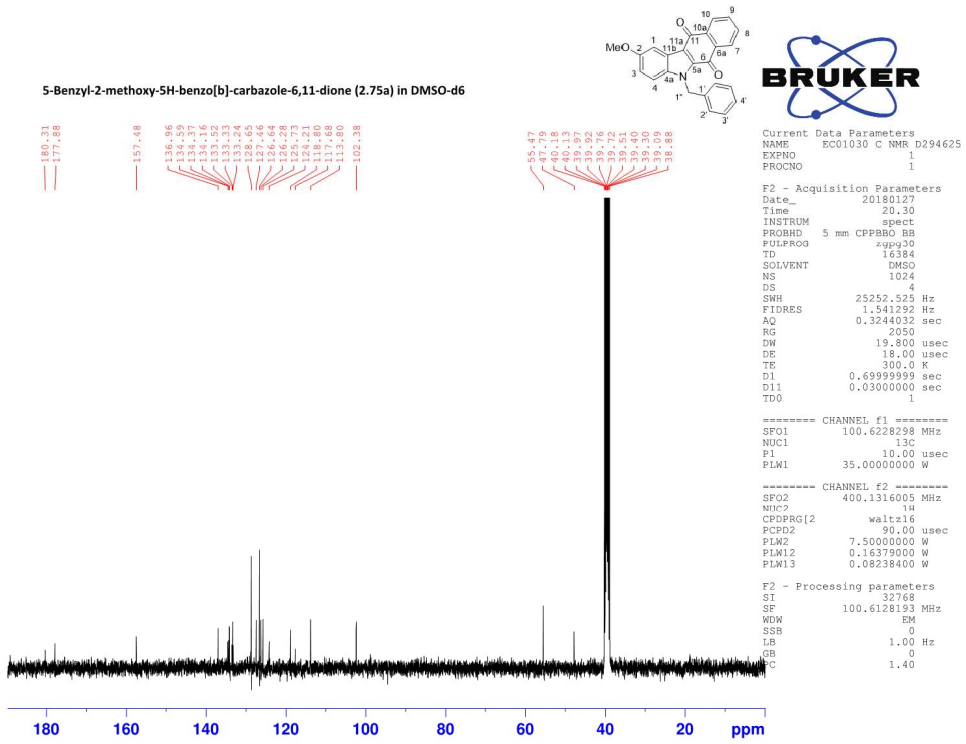


Figure 259. ^{13}C NMR spectra of 5-Benzyl-2-methoxy-5H-benzo[b]-carbazole-6,11-dione (**2.75a**).

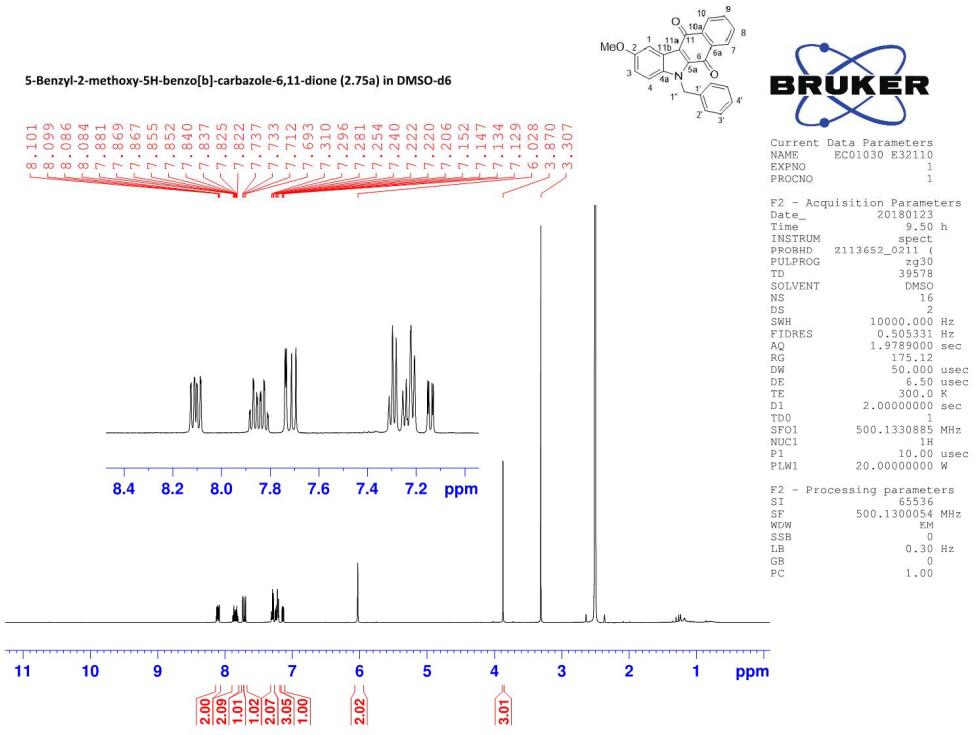


Figure 260. ^{1}H NMR spectra of 5-Benzyl-2-methoxy-5H-benzo[b]-carbazole-6,11-dione (**2.75a**).

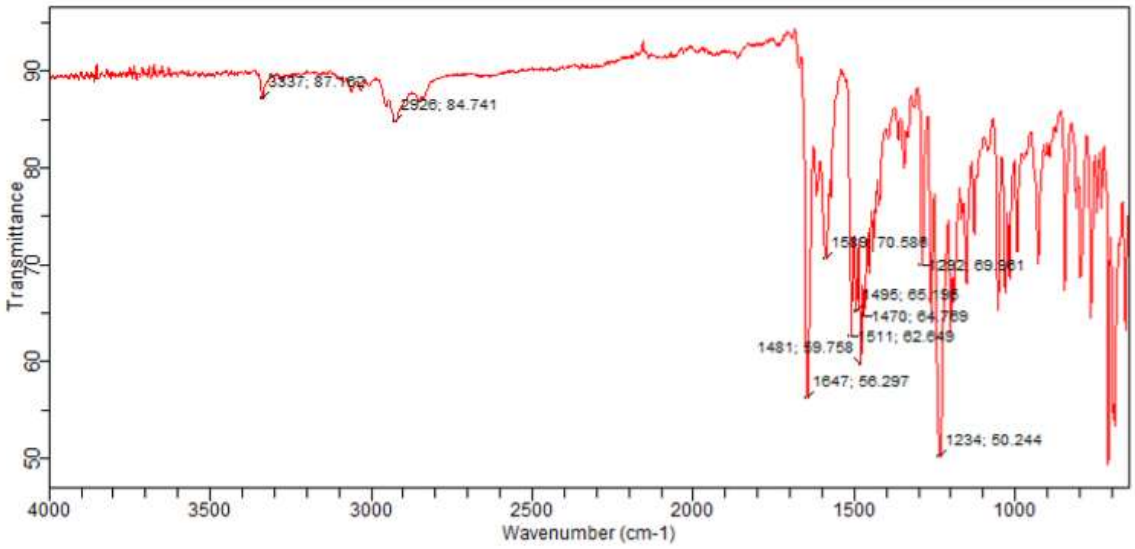


Figure 261. FT-IR spectra of 5-Benzyl-2-methoxy-5H-benzo[b]-carbazole-6,11-dione (**2.75a**).

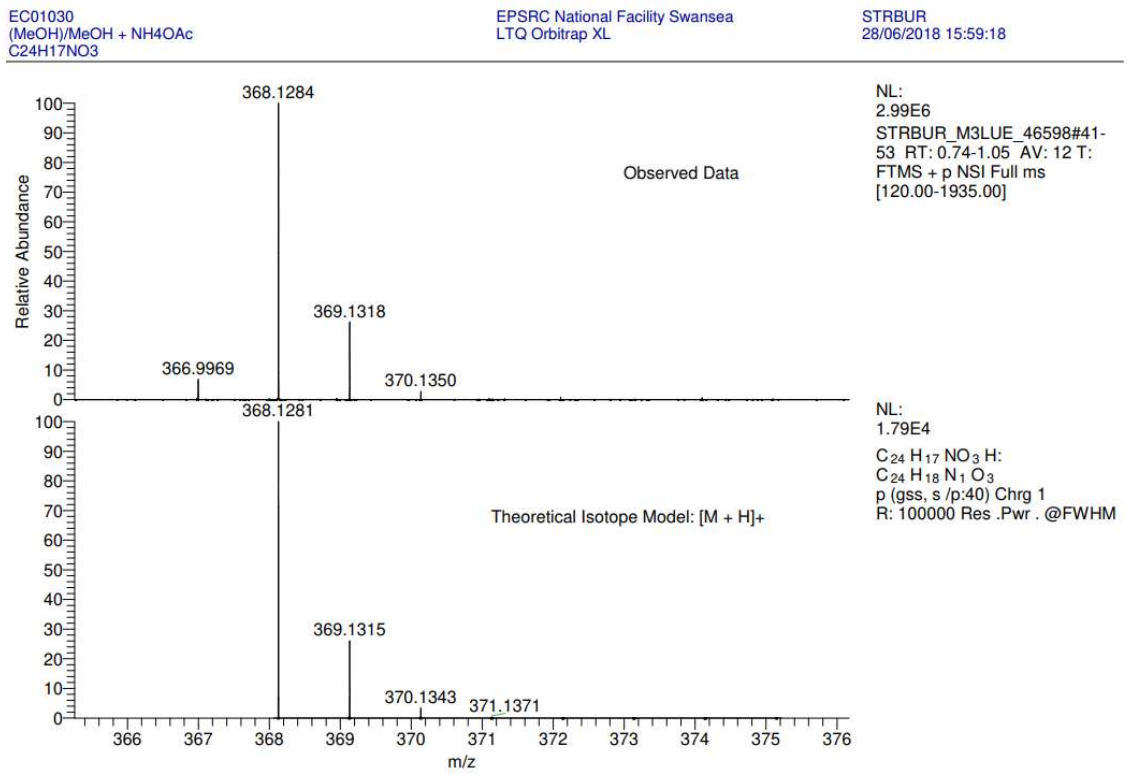


Figure 262. HRMS spectra of 5-Benzyl-2-methoxy-5H-benzo[b]-carbazole-6,11-dione (**2.75a**).

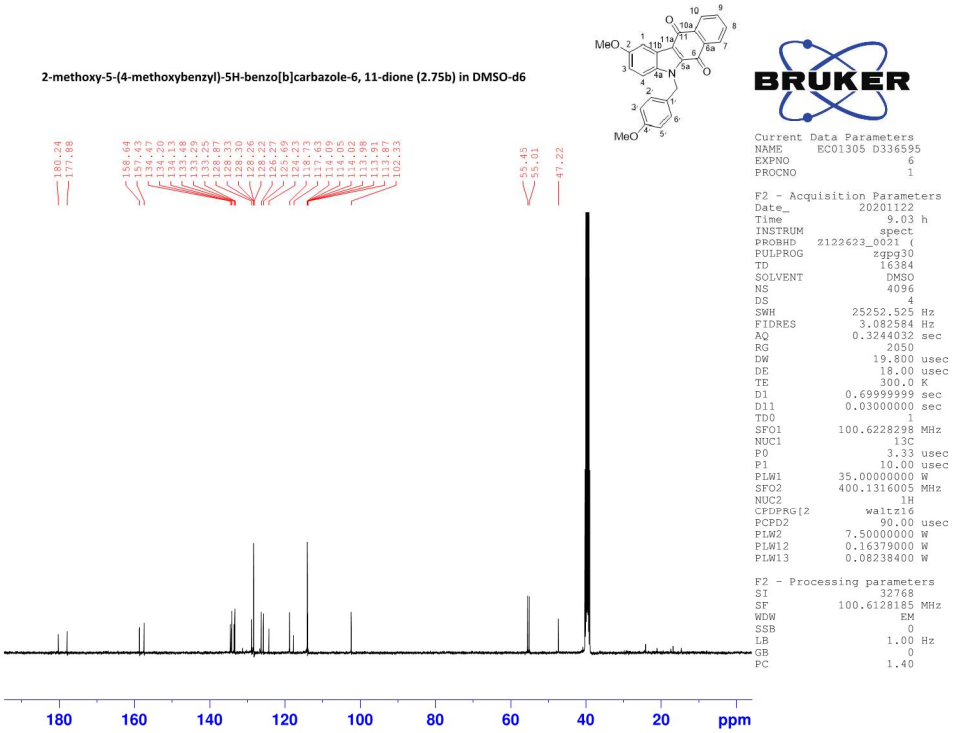


Figure 263. ^{13}C NMR spectra of 2-methoxy-5-(4-methoxybenzyl)-5H-benzo[b]carbazole-6, 11-dione (**2.75b**).

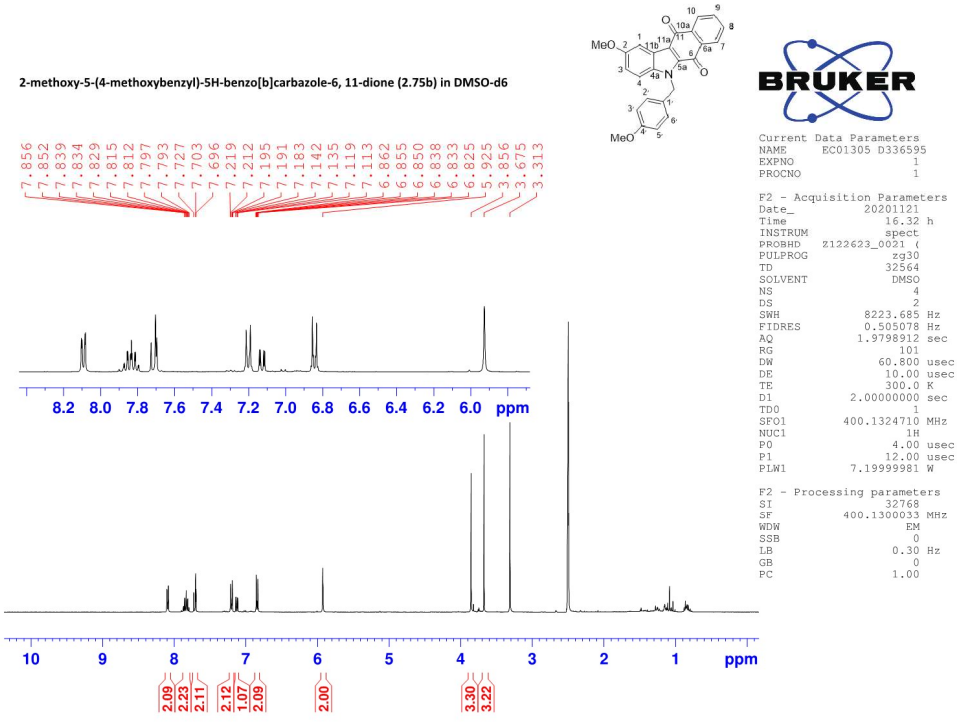


Figure 264. ^{1}H NMR spectra of 2-methoxy-5-(4-methoxybenzyl)-5H-benzo[b]carbazole-6, 11-dione (**2.75b**).

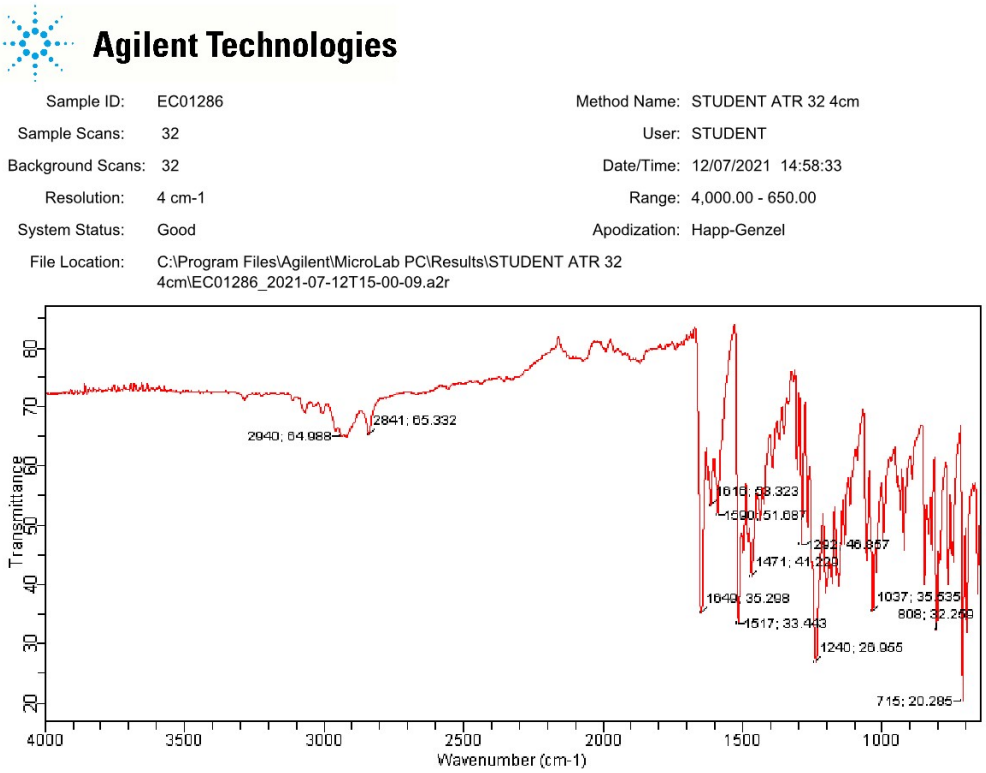


Figure 265. FT-IR spectra of 2-methoxy-5-(4-methoxybenzyl)-5H-benzo[b]carbazole-6, 11-dione (**2.75b**).

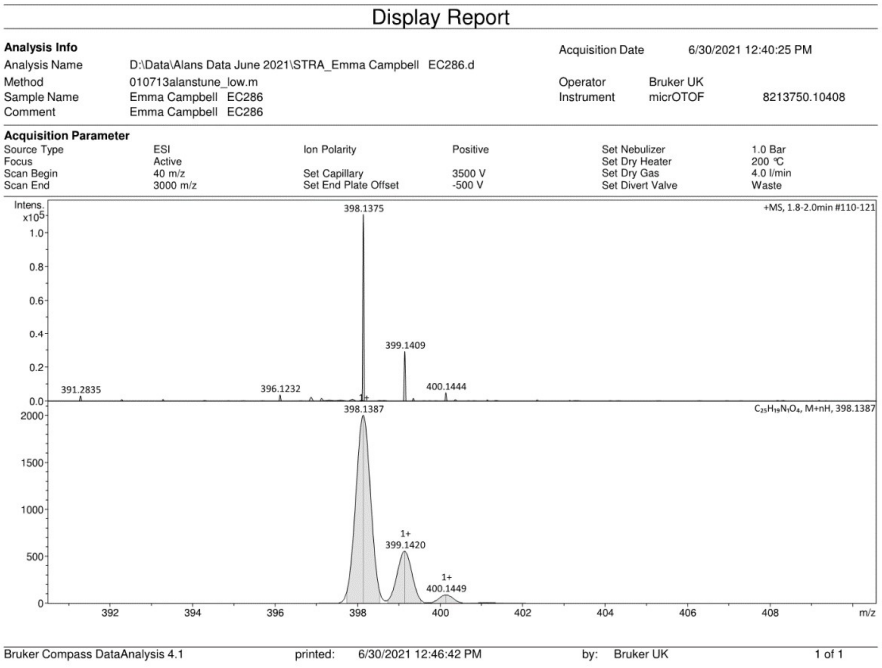


Figure 266. HRMS spectra of 2-methoxy-5-(4-methoxybenzyl)-5H-benzo[b]carbazole-6, 11-dione (**2.75b**).

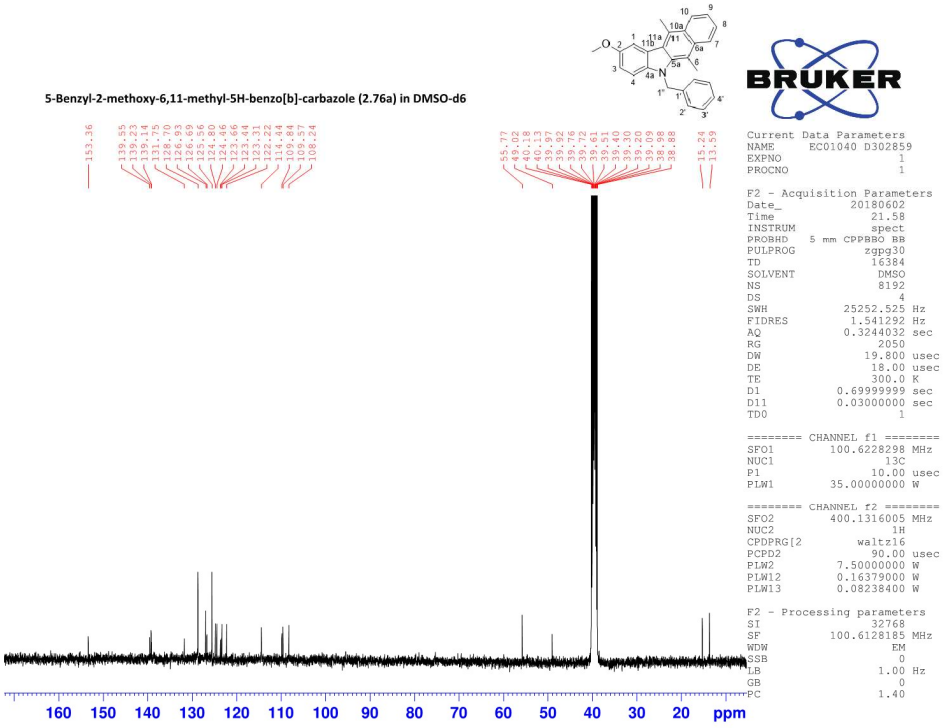


Figure 267. ^{13}C NMR spectra of 5-Benzyl-2-methoxy-6,11-methyl-5H-benzo[b]-carbazole (**2.76a**).

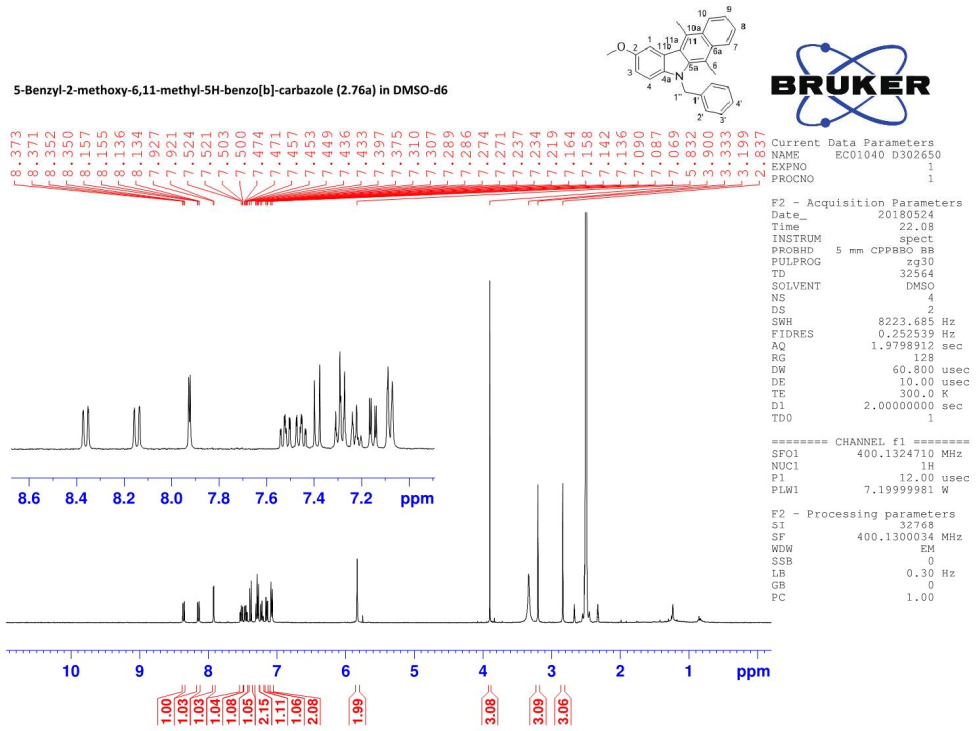


Figure 268. ^{1}H NMR spectra of 5-Benzyl-2-methoxy-6,11-methyl-5H-benzo[b]-carbazole (**2.76a**).

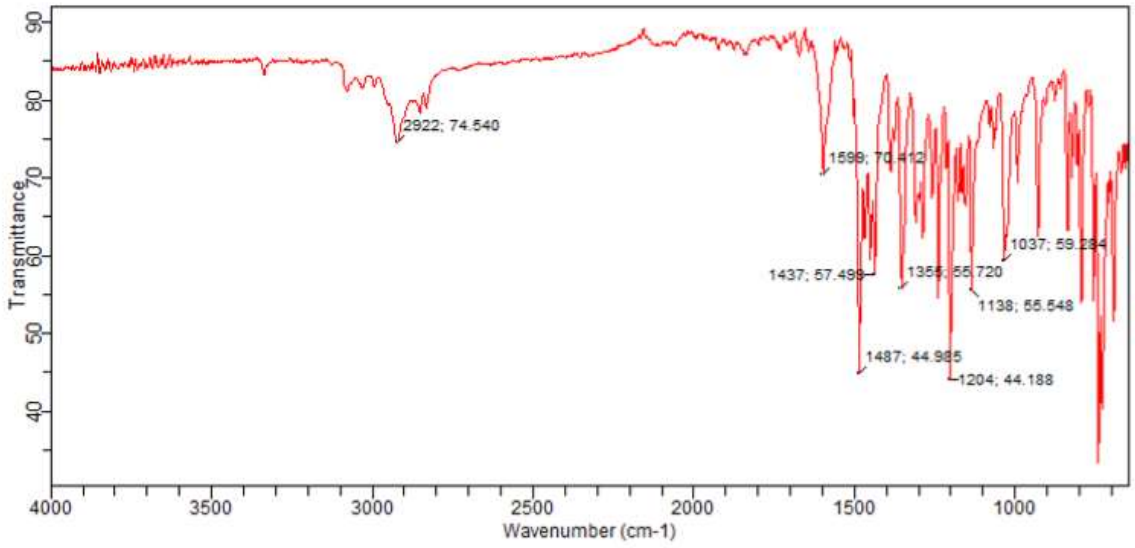


Figure 269. FT-IR spectra of 5-Benzyl-2-methoxy-6,11-methyl-5H-benzo[b]-carbazole (**2.76a**).

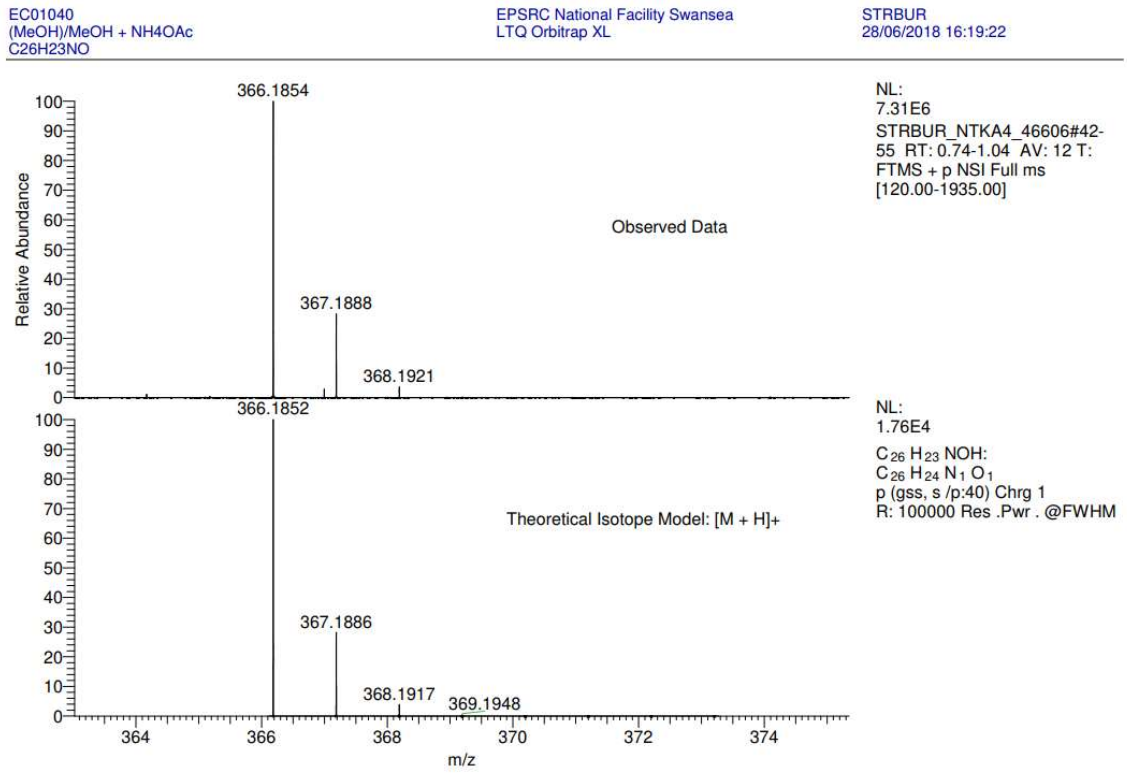


Figure 270. HRMS spectra of 5-Benzyl-2-methoxy-6,11-methyl-5H-benzo[b]-carbazole (**2.76a**).

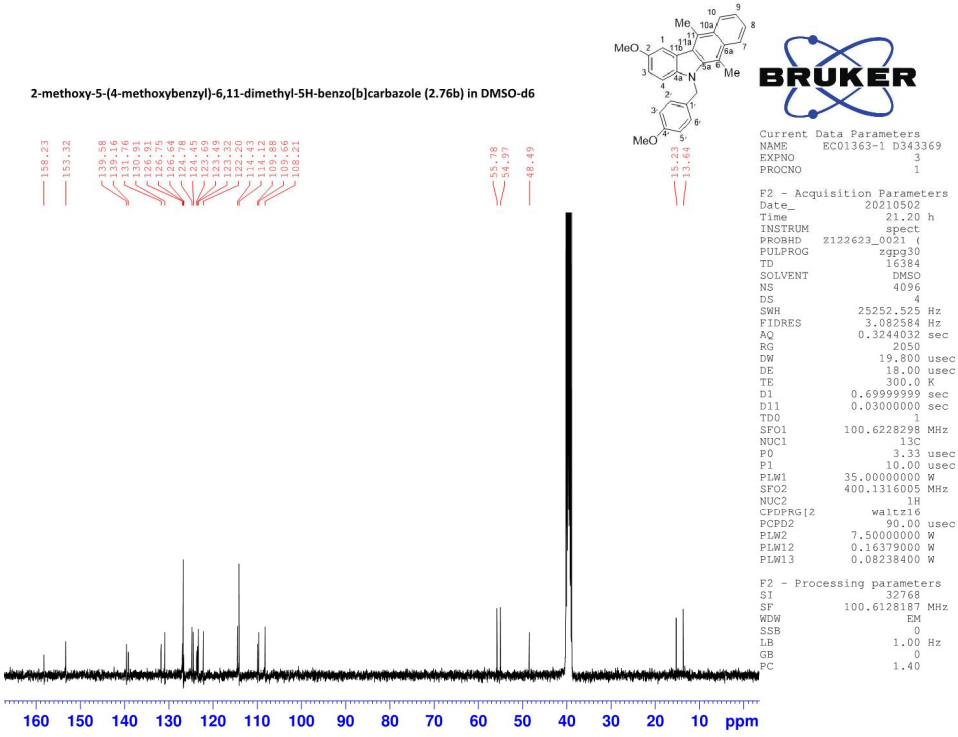


Figure 271. ^{13}C NMR spectra of 2-methoxy-5-(4-methoxybenzyl)-6,11-dimethyl-5H-benzo[b]carbazole (**2.76b**).

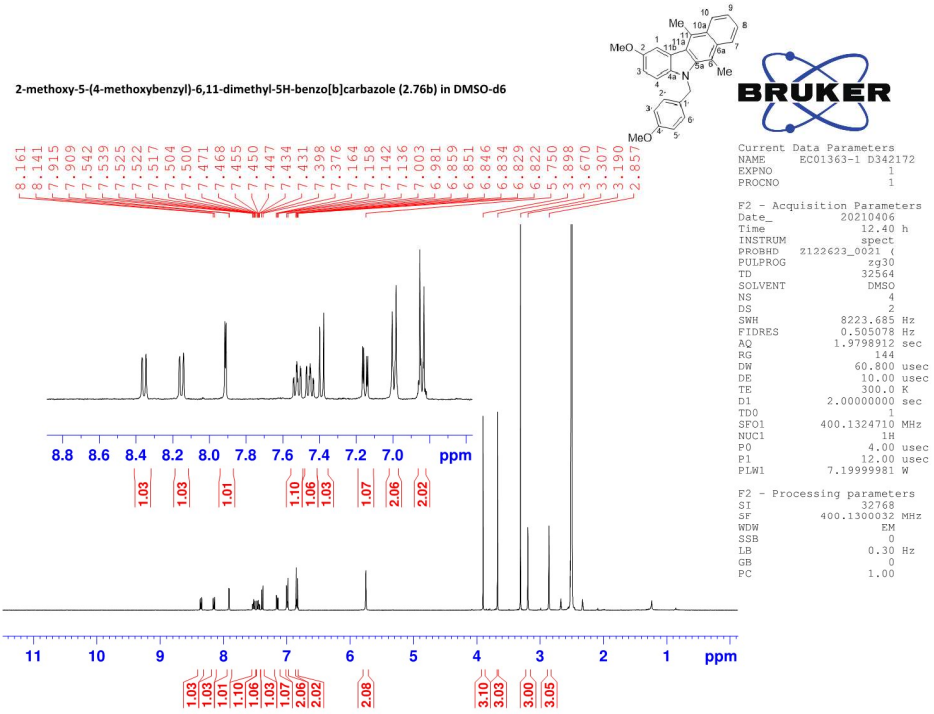


Figure 272. ^{1}H NMR spectra of 2-methoxy-5-(4-methoxybenzyl)-6,11-dimethyl-5H-benzo[b]carbazole (**2.76b**).

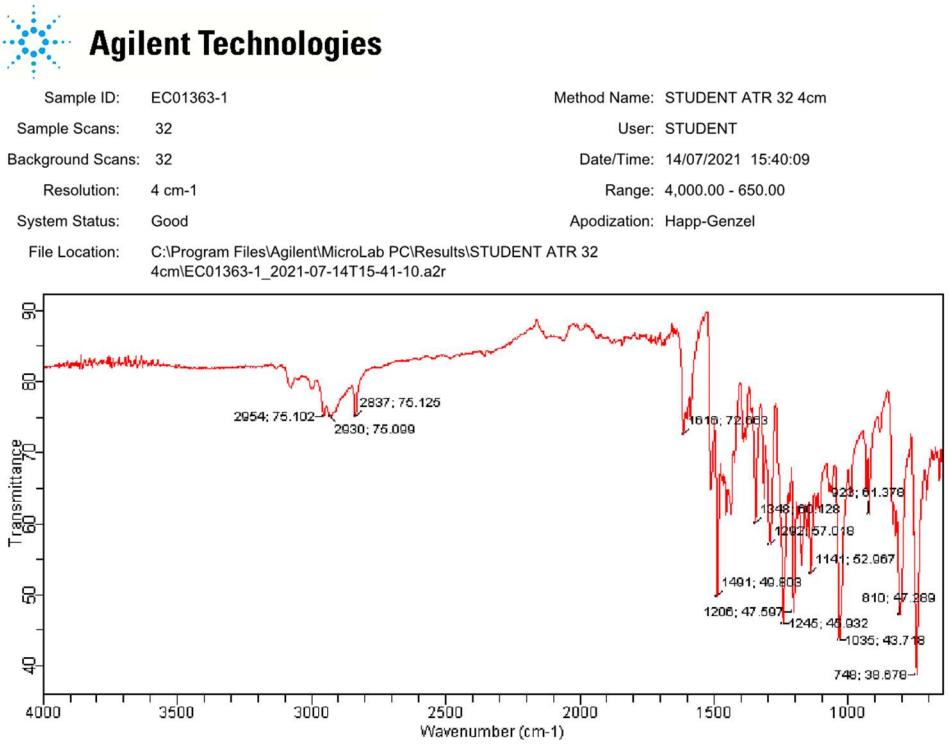


Figure 273. FT-IR spectra of 2-methoxy-5-(4-methoxybenzyl)-6,11-dimethyl-5H-benzo[b]carbazole (**2.76b**).

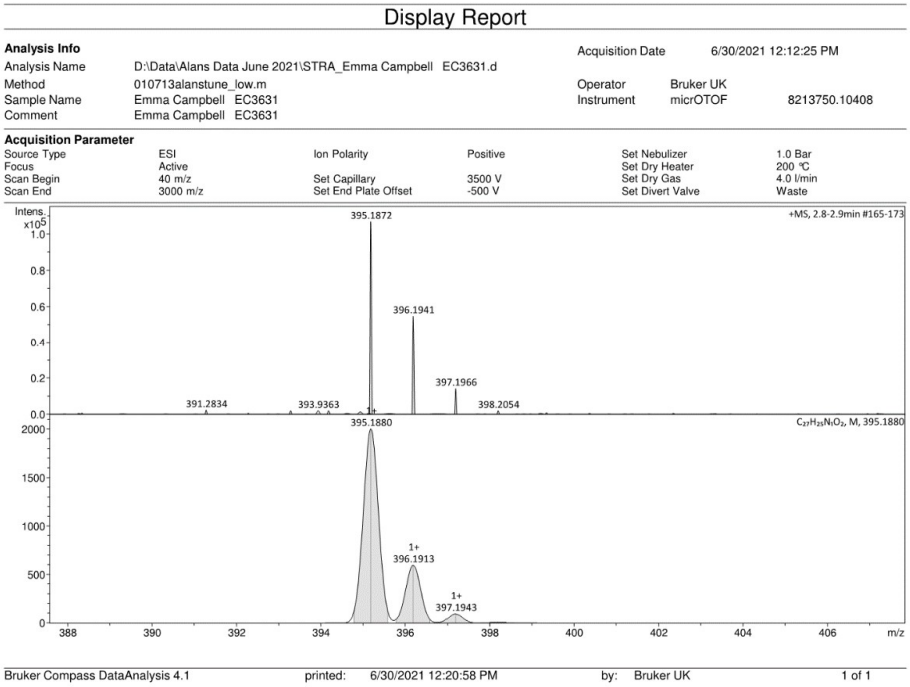


Figure 274. HRMS spectra of 2-methoxy-5-(4-methoxybenzyl)-6,11-dimethyl-5H-benzo[b]carbazole (**2.76b**).

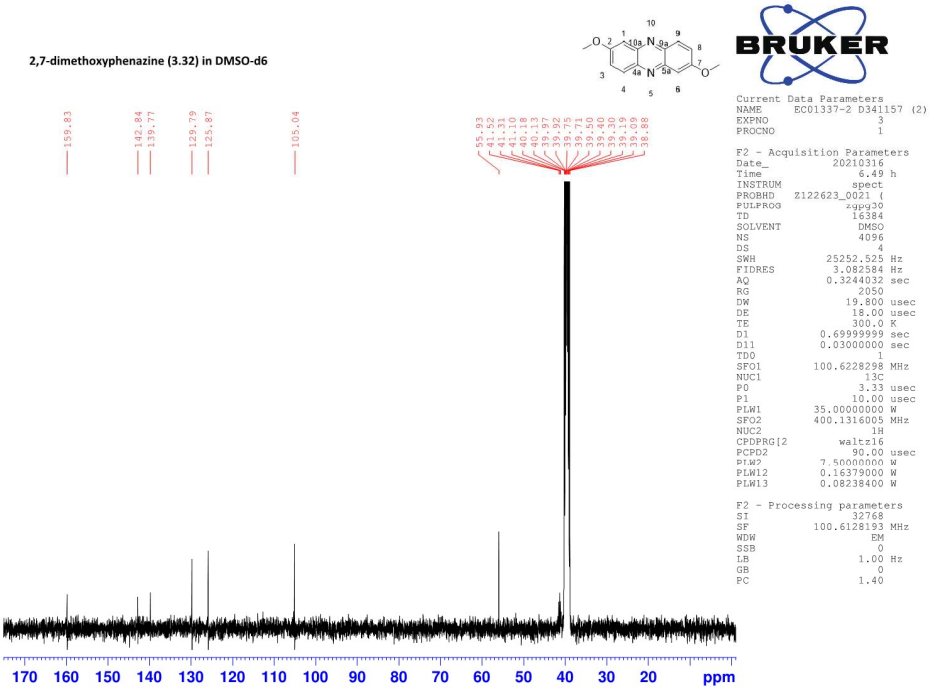


Figure 275. ^{13}C NMR spectra of 2,7-dimethoxyphenazine (**3.32**).

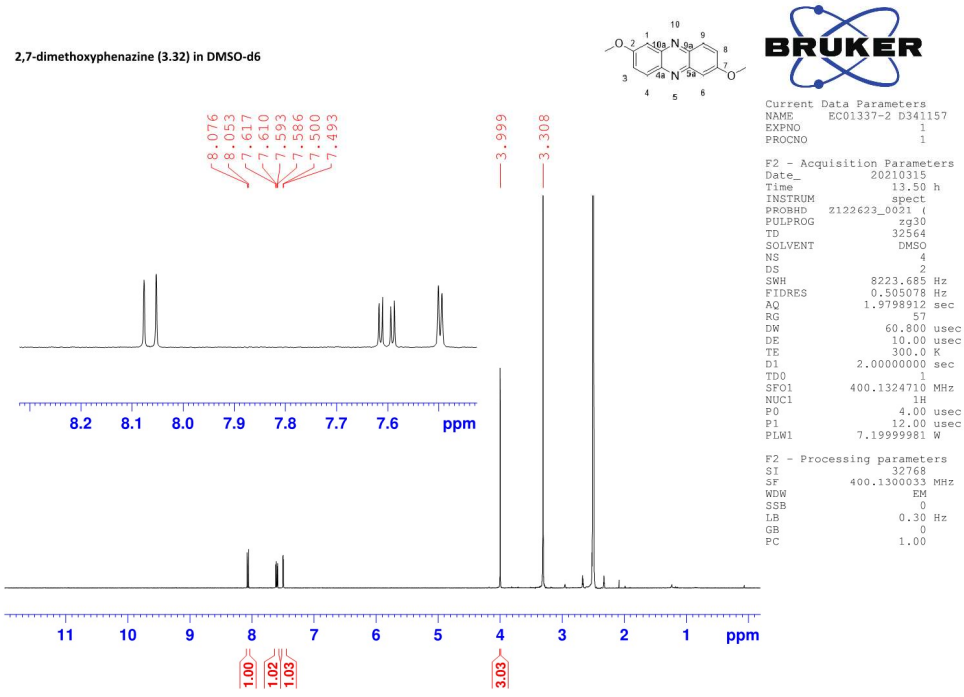


Figure 276. ^{1}H NMR spectra of 2,7-dimethoxyphenazine (**3.32**).

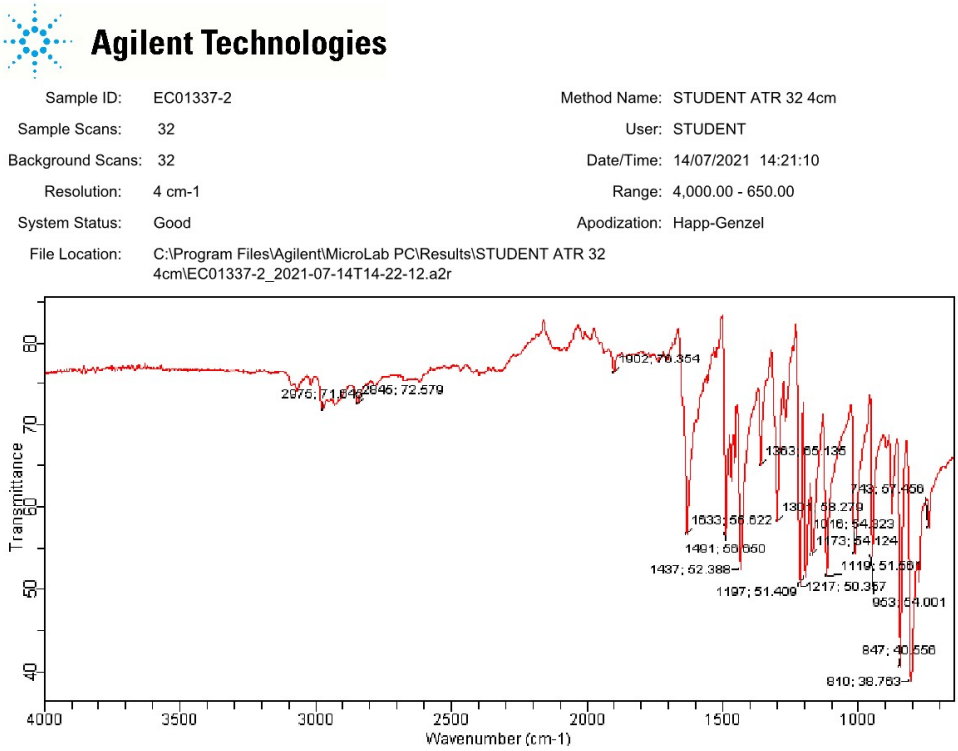


Figure 277. FT-IR spectra of 2,7-dimethoxyphenazine (**3.32**).

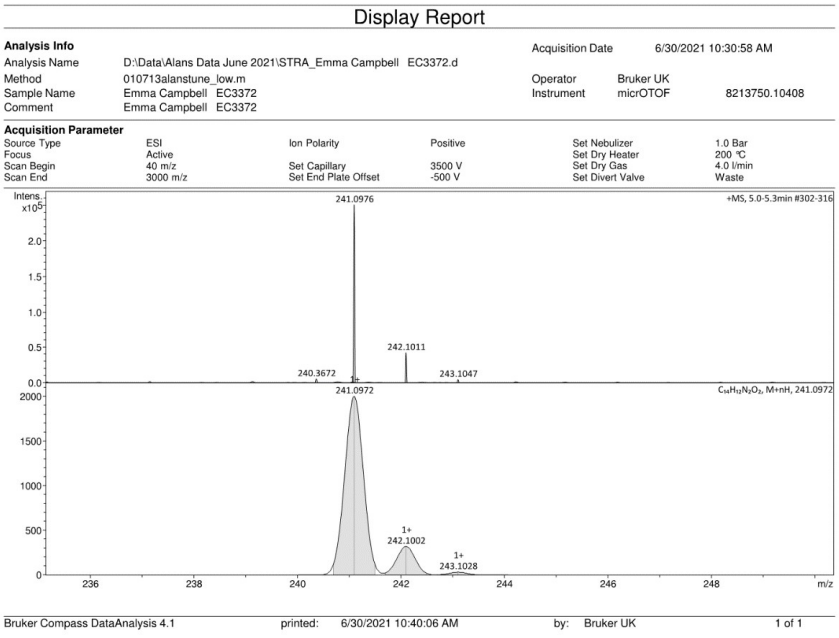


Figure 278. HRMS spectra of 2,7-dimethoxyphenazine (**3.32**).

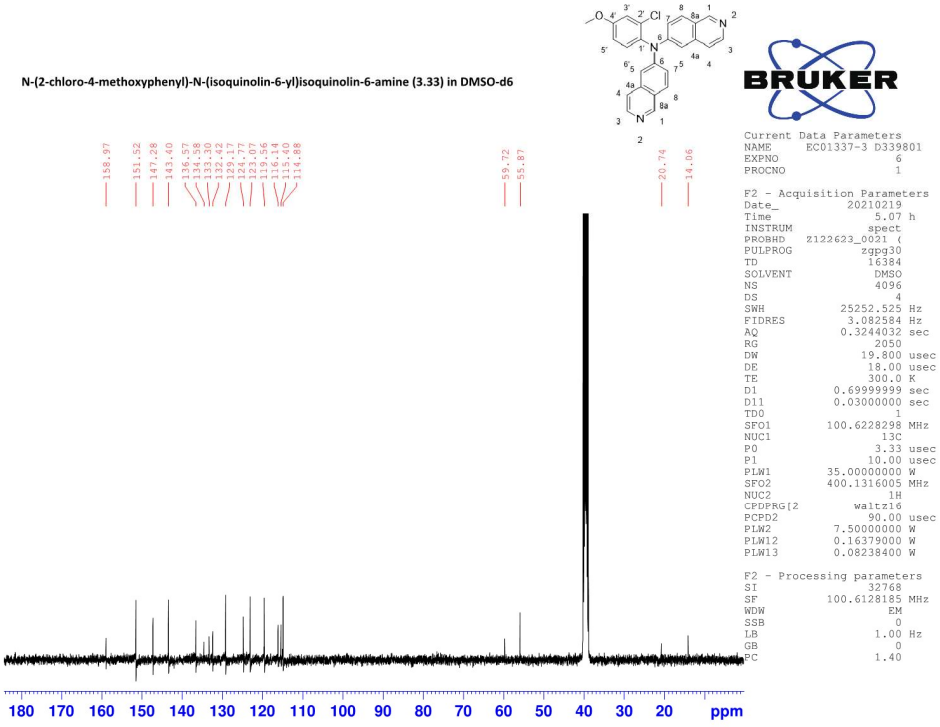


Figure 279. ^{13}C NMR spectra of N-(2-chloro-4-methoxyphenyl)-N-(isoquinolin-6-yl)isoquinolin-6-amine (**3.33**).

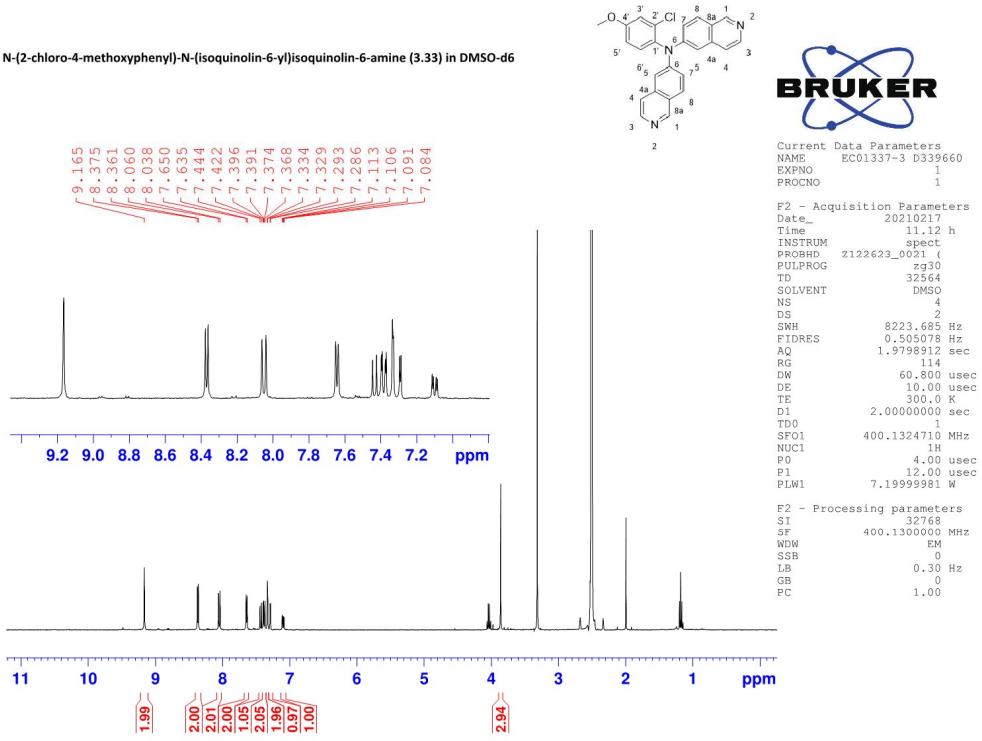


Figure 280. ^{1}H NMR spectra of N-(2-chloro-4-methoxyphenyl)-N-(isoquinolin-6-yl)isoquinolin-6-amine (**3.33**).

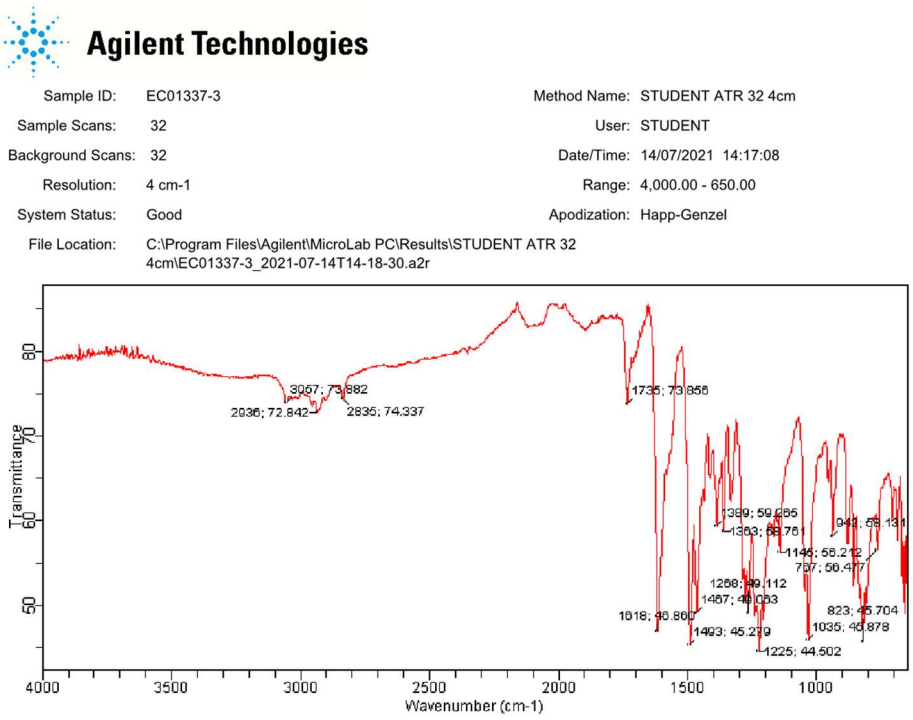


Figure 281. FT-IR spectra of N-(2-chloro-4-methoxyphenyl)-N-(isoquinolin-6-yl)isoquinolin-6-amine (**3.33**).

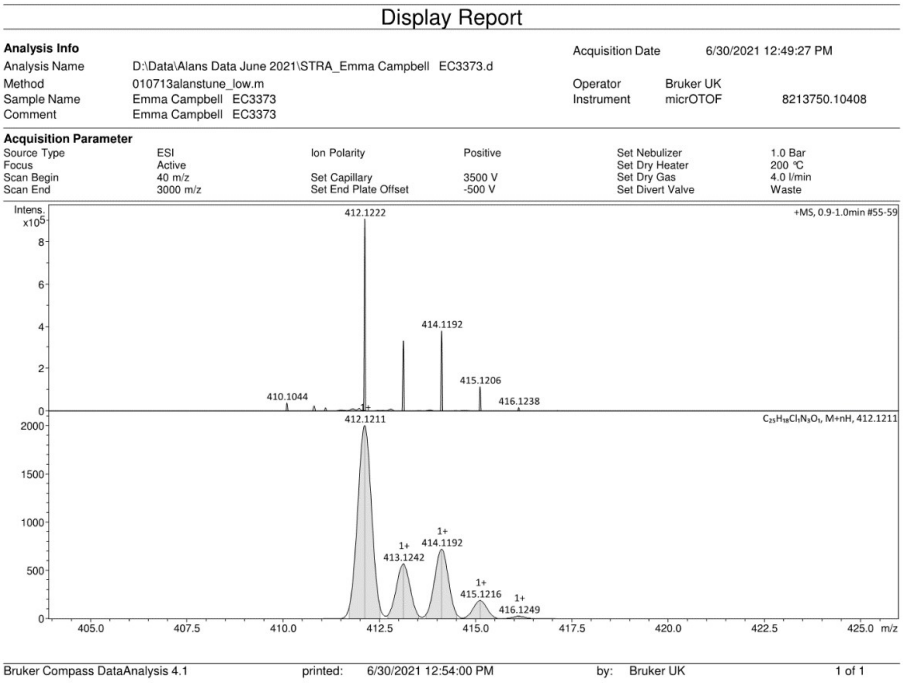


Figure 282. HRMS spectra of N-(2-chloro-4-methoxyphenyl)-N-(isoquinolin-6-yl)isoquinolin-6-amine (**3.33**).

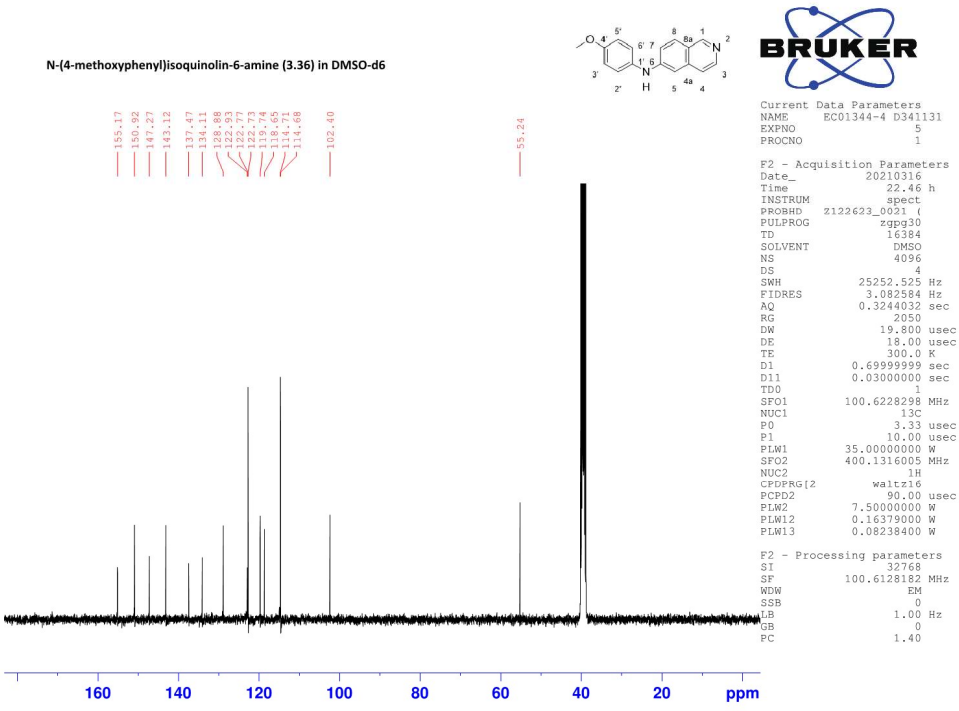


Figure 283. ^{13}C NMR spectra of N-(4-methoxyphenyl)isoquinolin-6-amine (**3.36**).

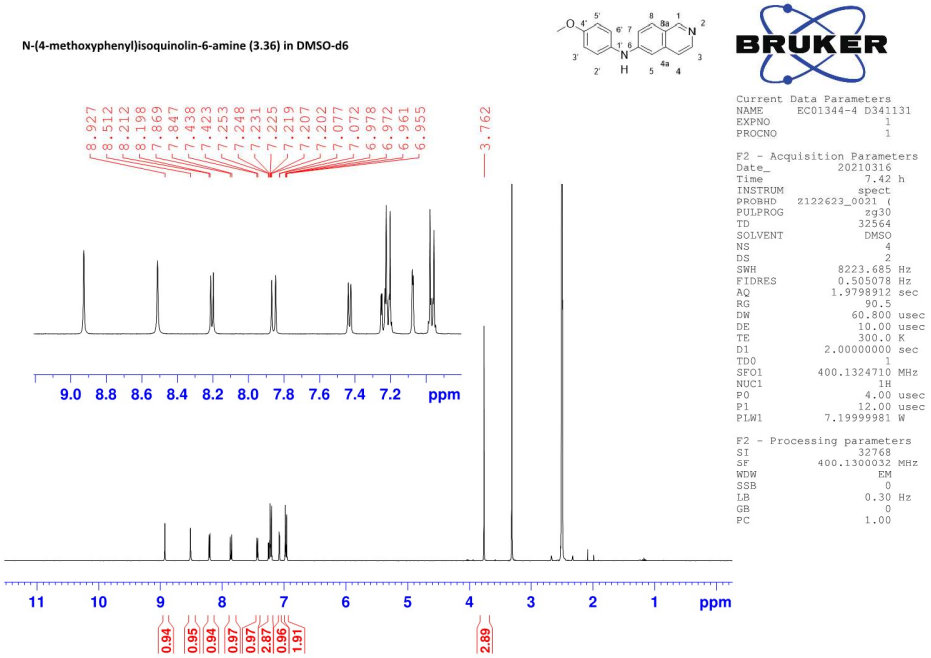


Figure 284. ^{1}H NMR spectra of N-(4-methoxyphenyl)isoquinolin-6-amine (**3.36**).

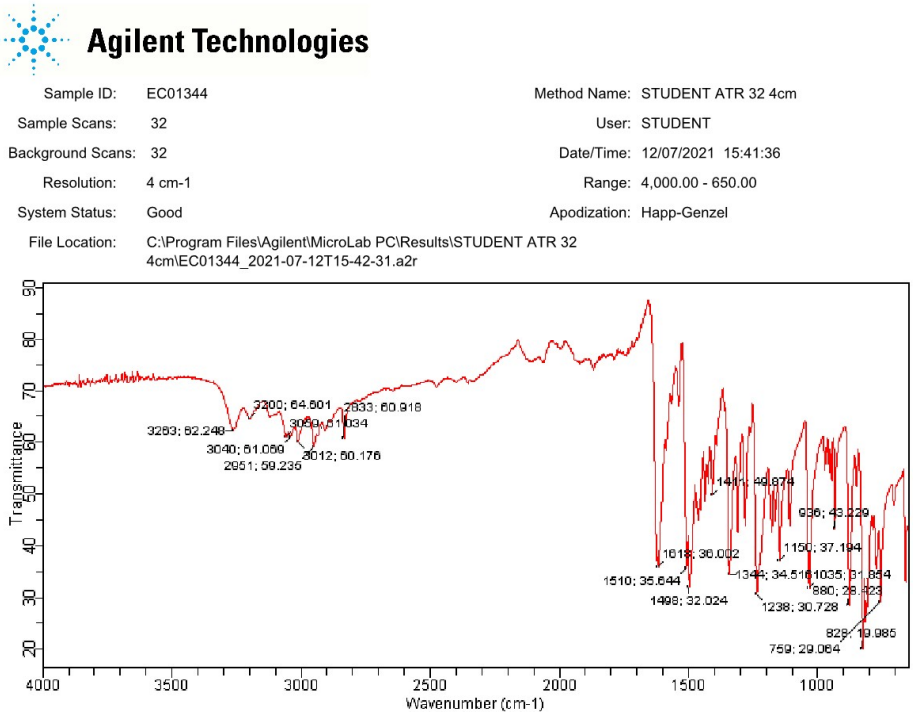


Figure 285. FT-IR spectra of N-(4-methoxyphenyl)isoquinolin-6-amine (**3.36**).

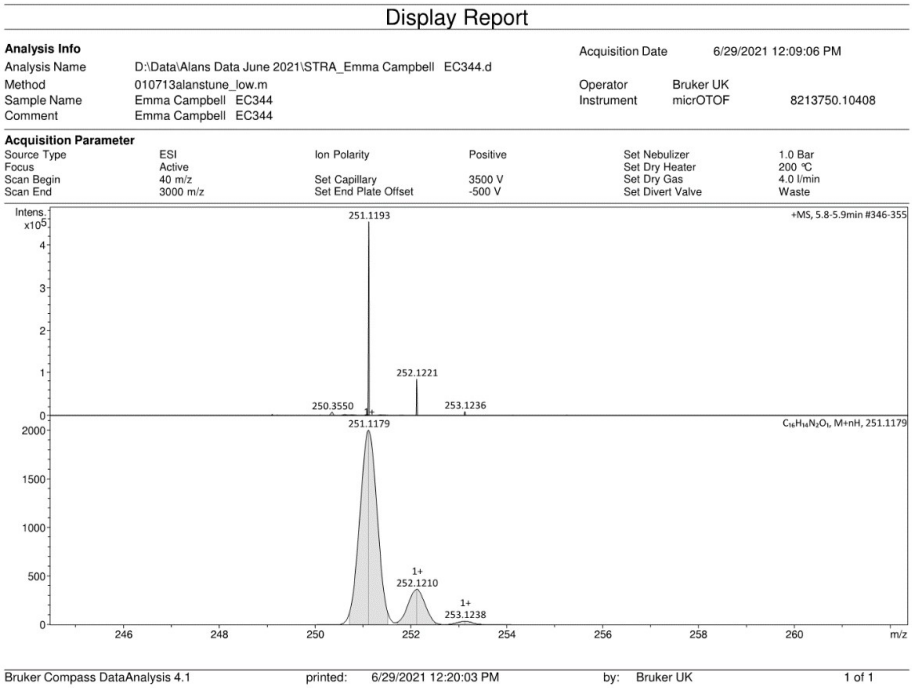


Figure 286. HRMS spectra of N-(4-methoxyphenyl)isoquinolin-6-amine (**3.36**).

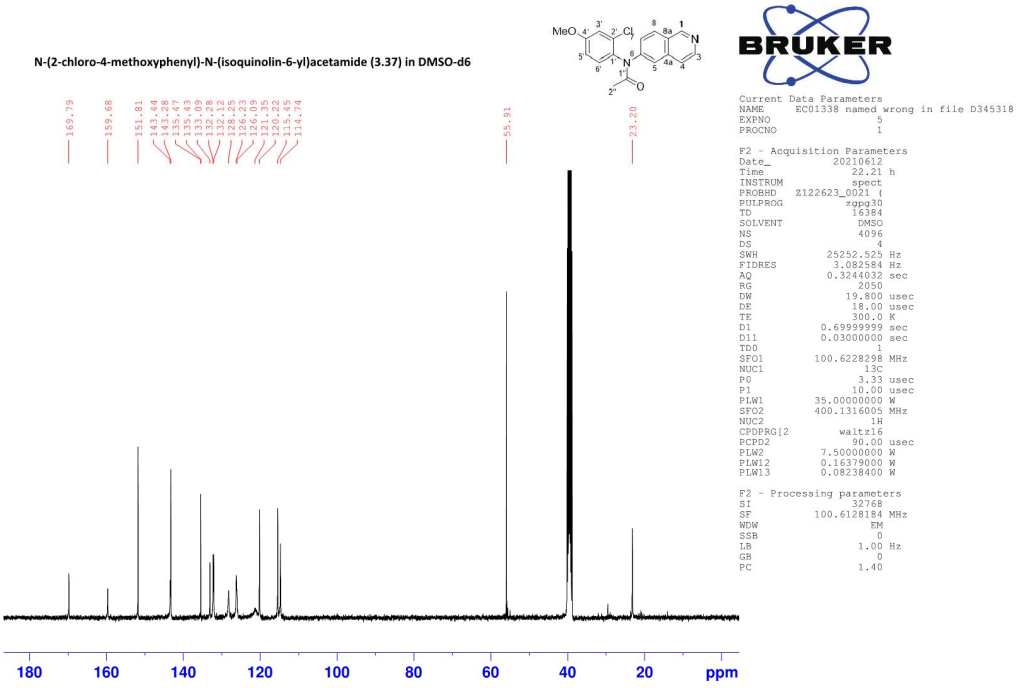


Figure 287. ^{13}C NMR spectra of N-(2-chloro-4-methoxyphenyl)-N-(isoquinolin-6-yl)acetamide (**3.37**).

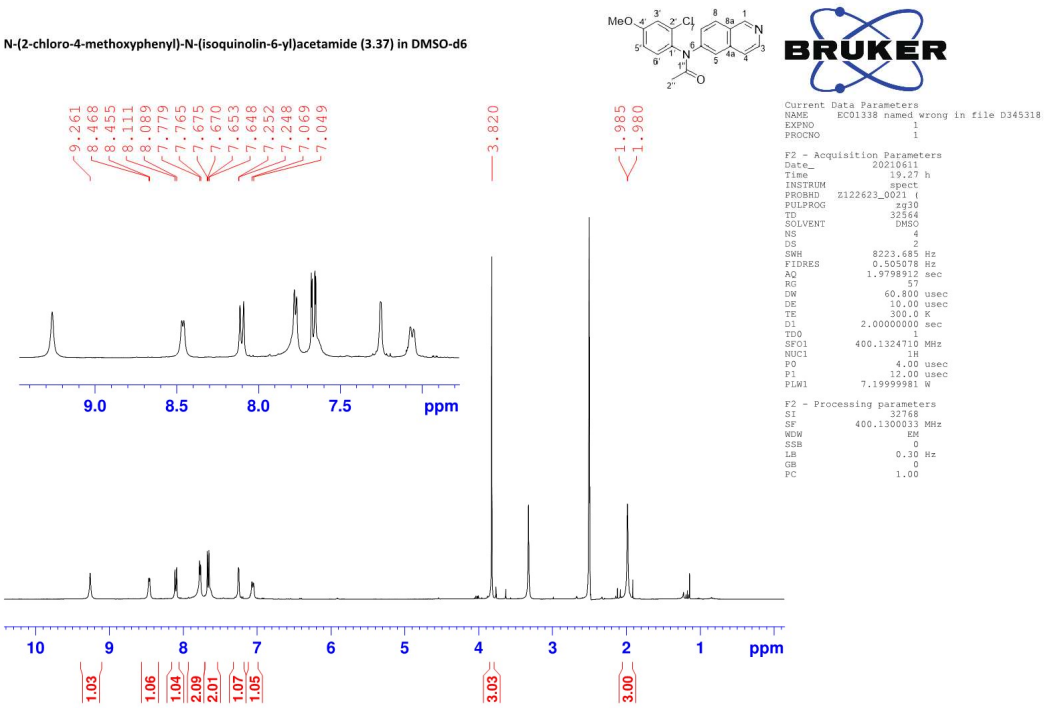


Figure 288. ^{1}H NMR spectra of N-(2-chloro-4-methoxyphenyl)-N-(isoquinolin-6-yl)acetamide (**3.37**).

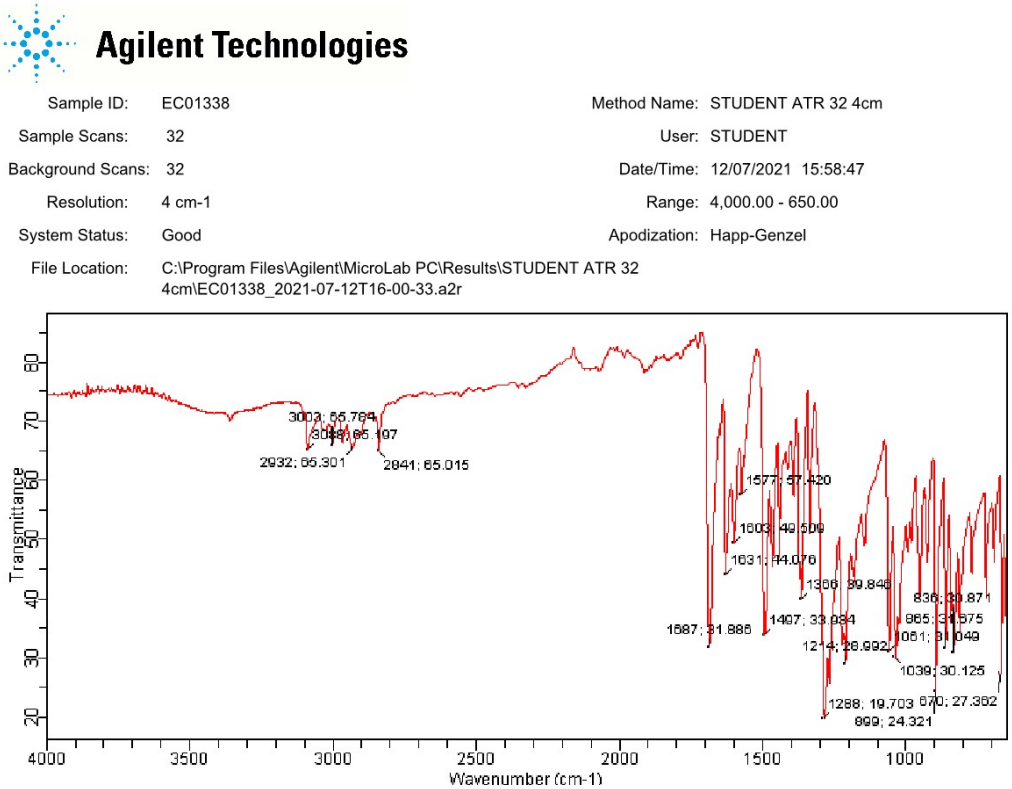


Figure 289. FT-IR spectra of N-(2-chloro-4-methoxyphenyl)-N-(isoquinolin-6-yl)acetamide (**3.37**).

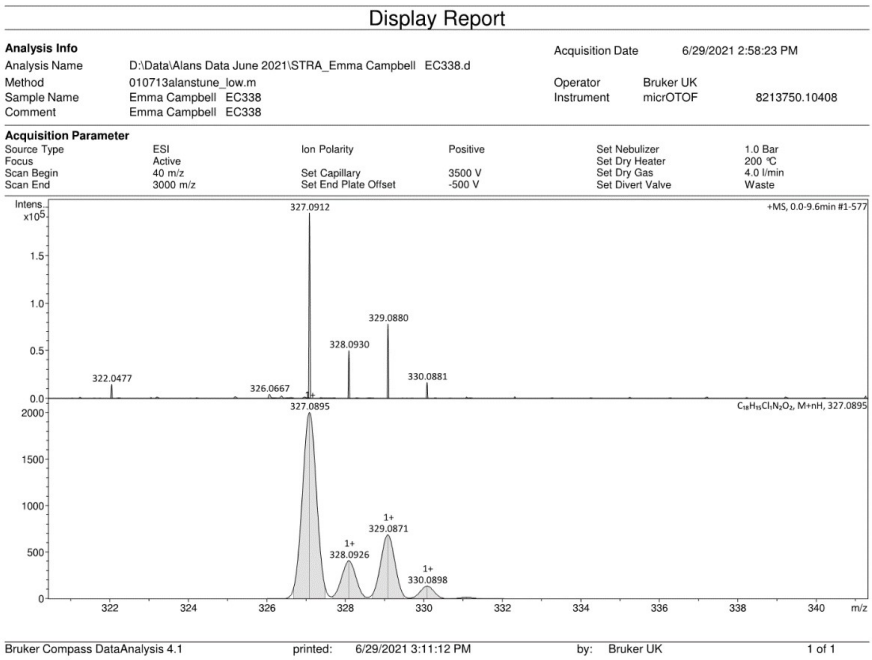


Figure 290. HRMS spectra of N-(2-chloro-4-methoxyphenyl)-N-(isoquinolin-6-yl)acetamide (**3.37**).

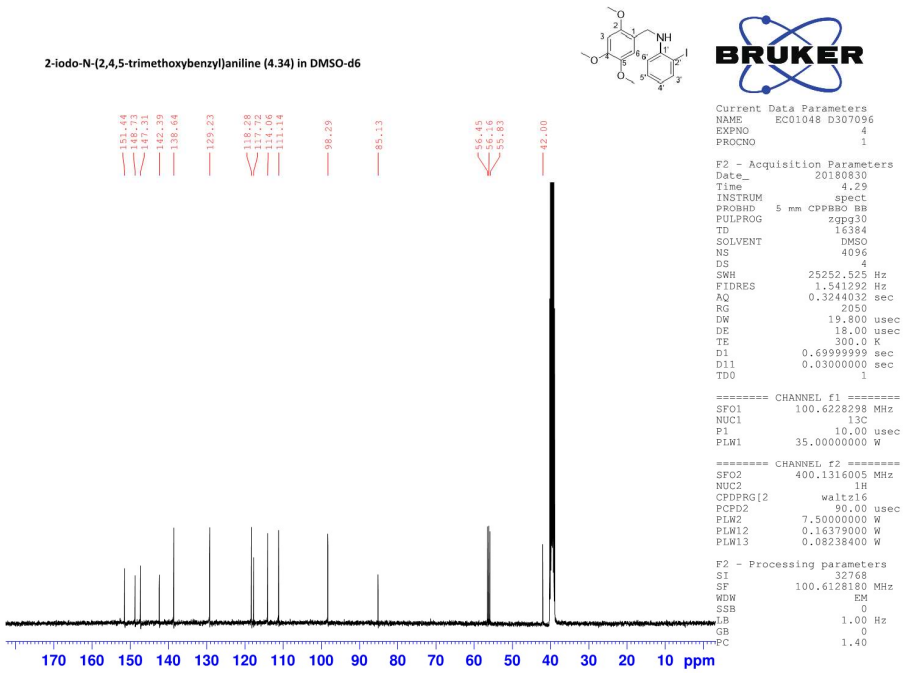


Figure 291. ^{13}C NMR spectra of 2-iodo-N-(2,4,5-trimethoxybenzyl)aniline (**4.34**).

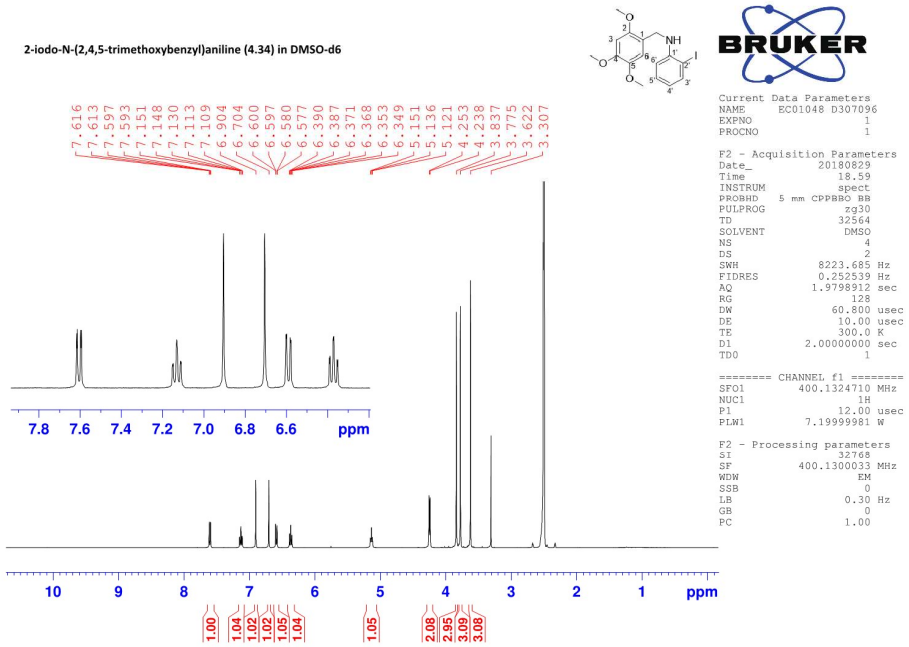


Figure 292. ^{1}H NMR spectra of 2-iodo-N-(2,4,5-trimethoxybenzyl)aniline (**4.34**).

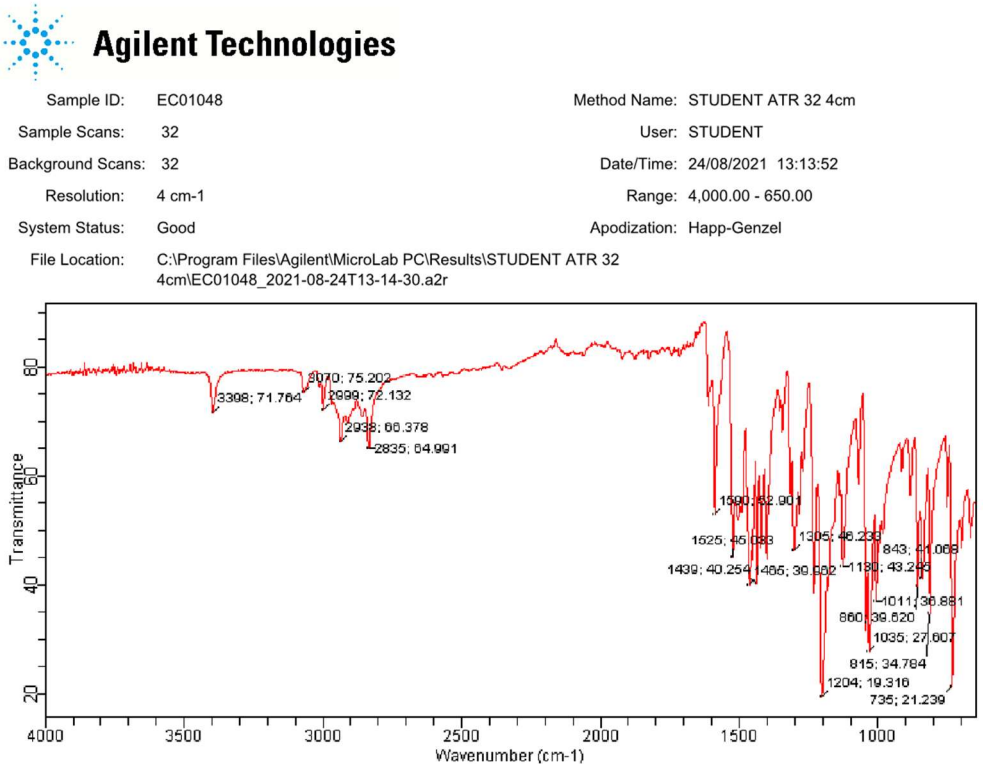


Figure 293. FT-IR spectra of 2-iodo-N-(2,4,5-trimethoxybenzyl)aniline (**4.34**)

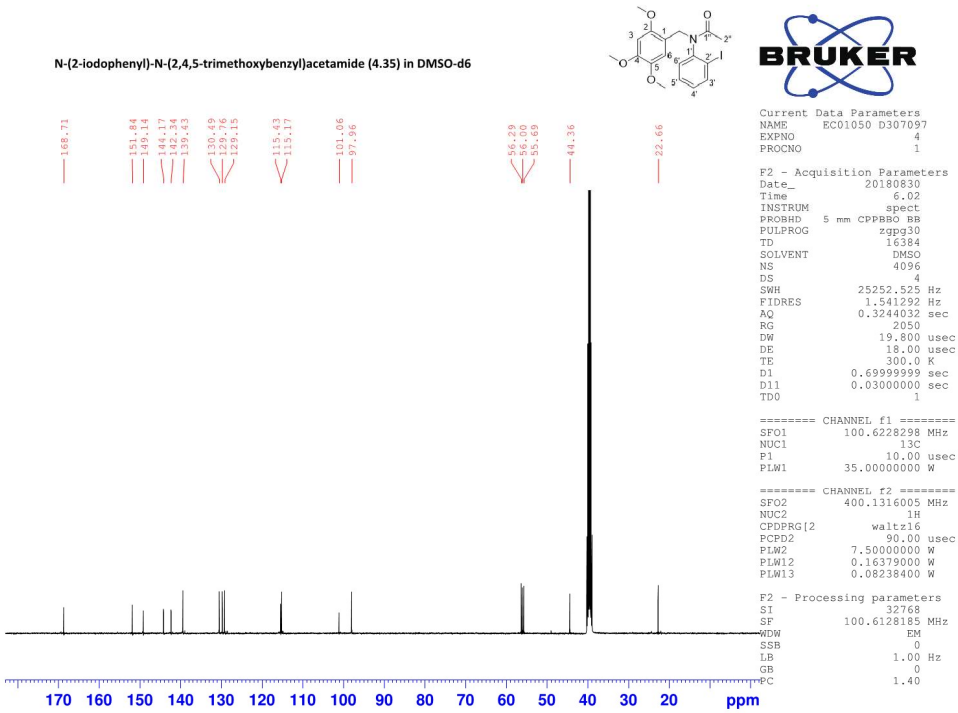


Figure 294. ^{13}C NMR spectra of N-(2-iodophenyl)-N-(2,4,5-trimethoxybenzyl)acetamide (**4.35**).

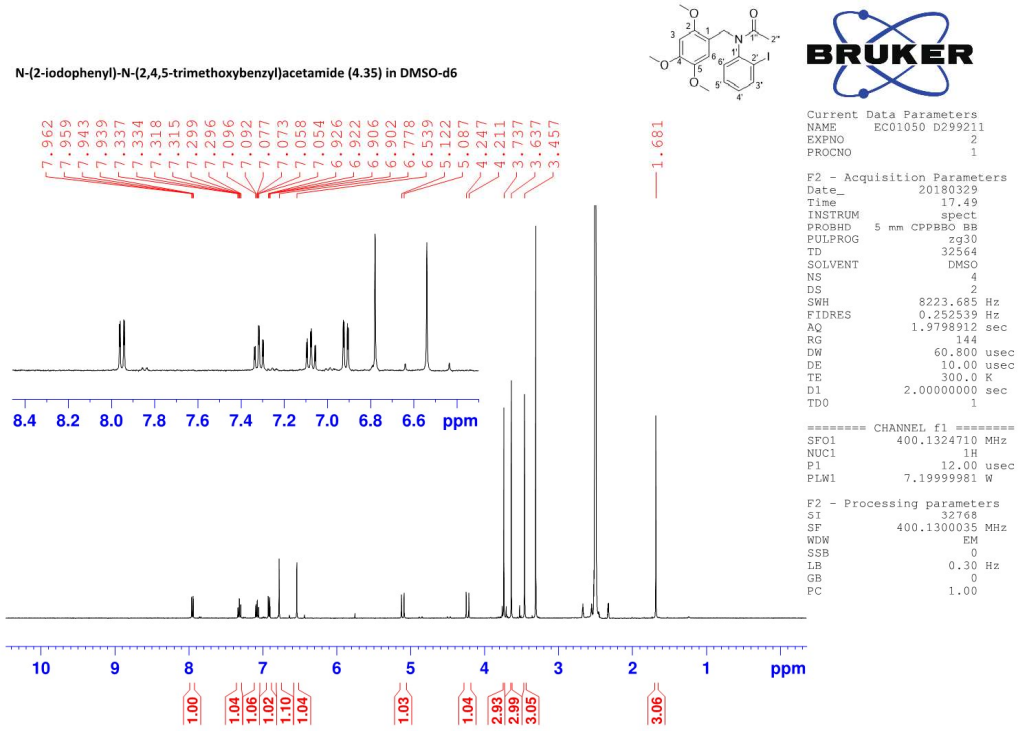


Figure 295. ^{1}H NMR spectra of N-(2-iodophenyl)-N-(2,4,5-trimethoxybenzyl)acetamide (**4.35**).

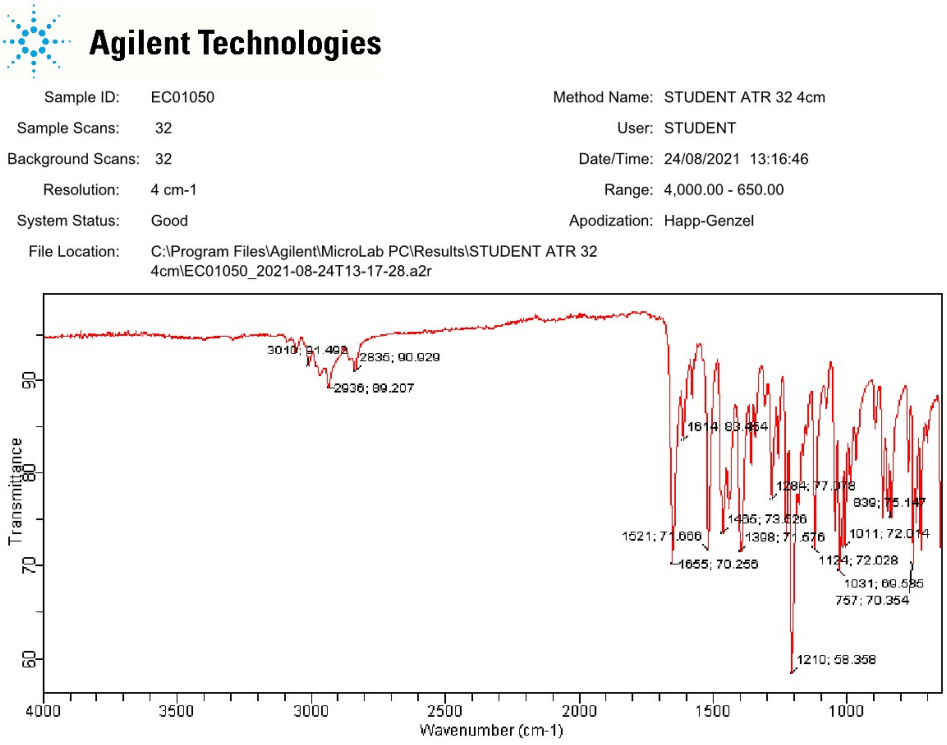


Figure 296. FT-IR spectra of N-(2-iodophenyl)-N-(2,4,5-trimethoxybenzyl)acetamide (**4.35**).

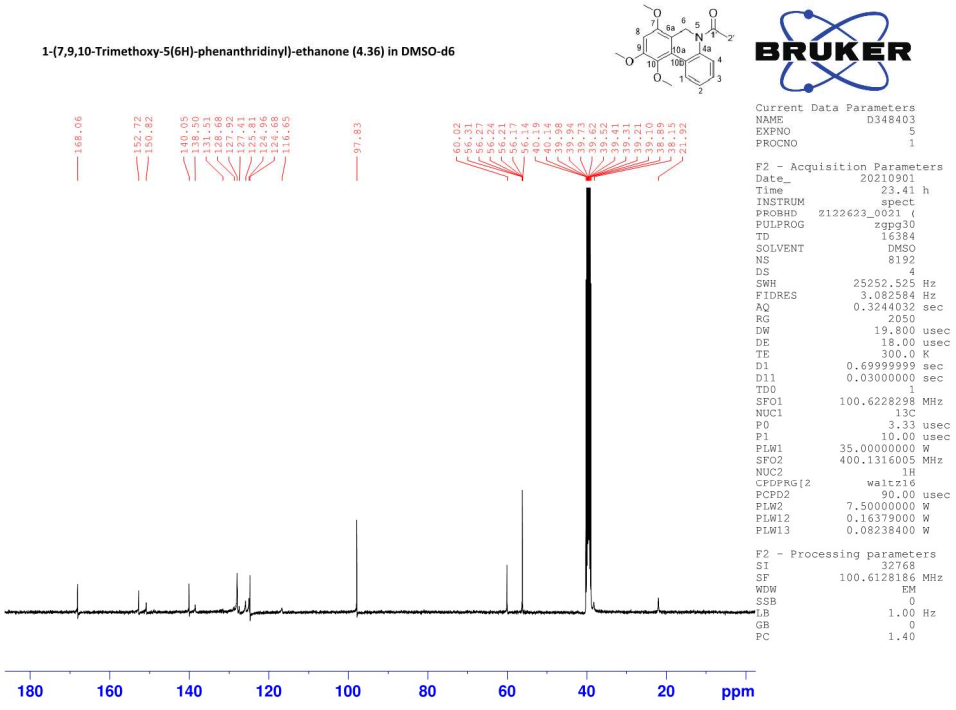


Figure 297. ^{13}C NMR spectra of 1-(7,9,10-Trimethoxy-5(6H)-phenanthridinyl)-ethanone (**4.36**).

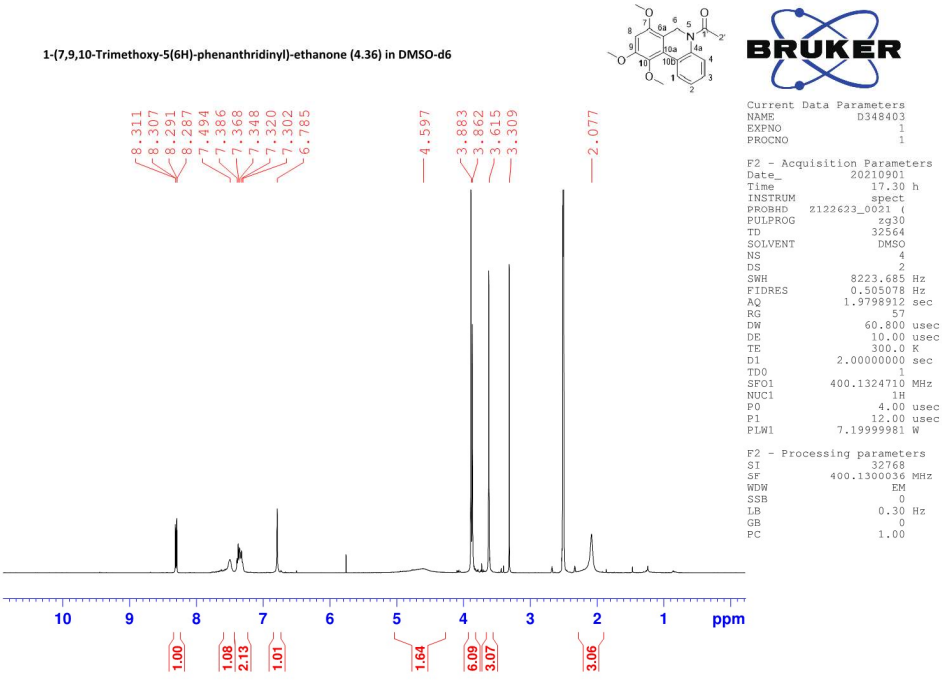


Figure 298. ^{1}H NMR spectra of 1-(7,9,10-Trimethoxy-5(6H)-phenanthridinyl)-ethanone (**4.36**).

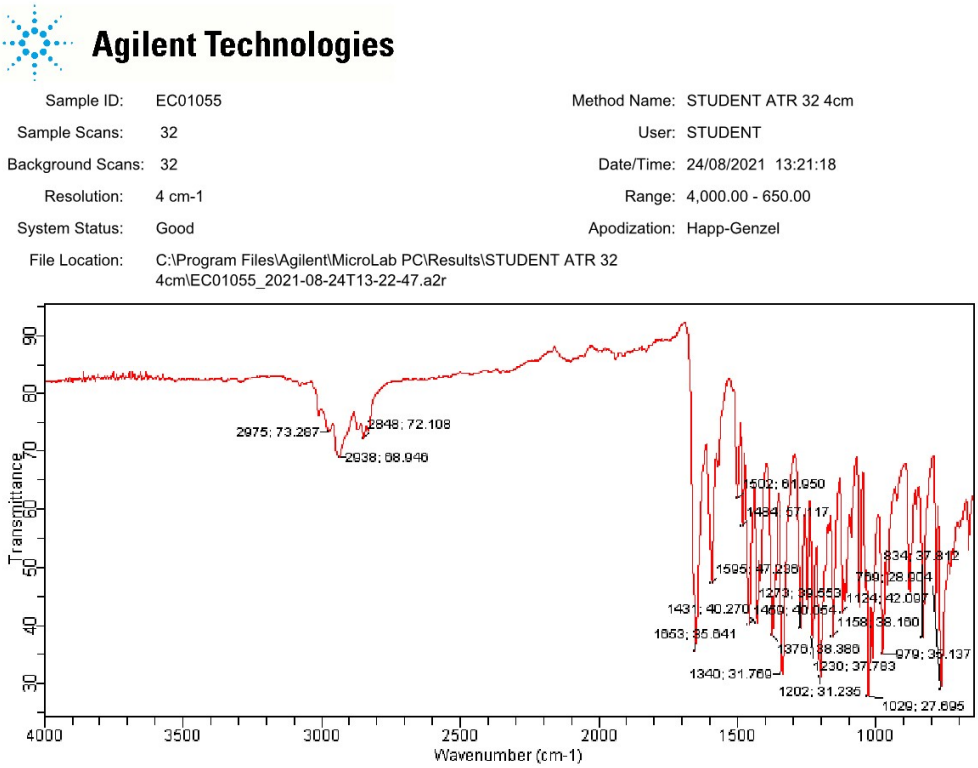


Figure 299. FT-IR spectra of 1-(7,9,10-Trimethoxy-5(6H)-phenanthridinyl)-ethanone (**4.36**).

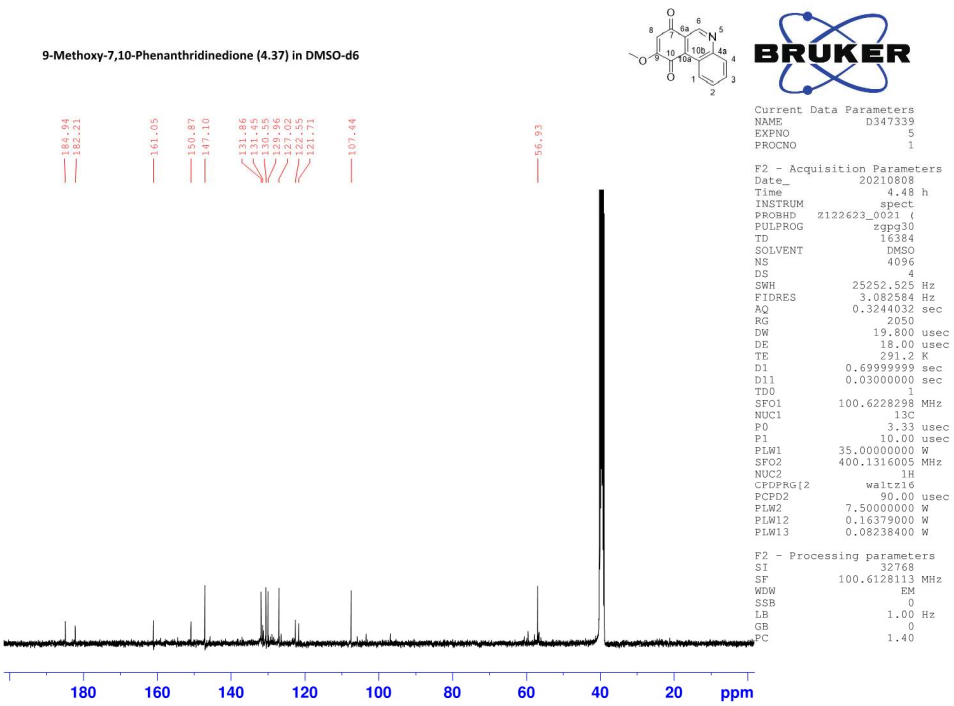


Figure 300. ^{13}C NMR spectra of 9-Methoxy-7,10-Phenanthridinedione (**4.37**).

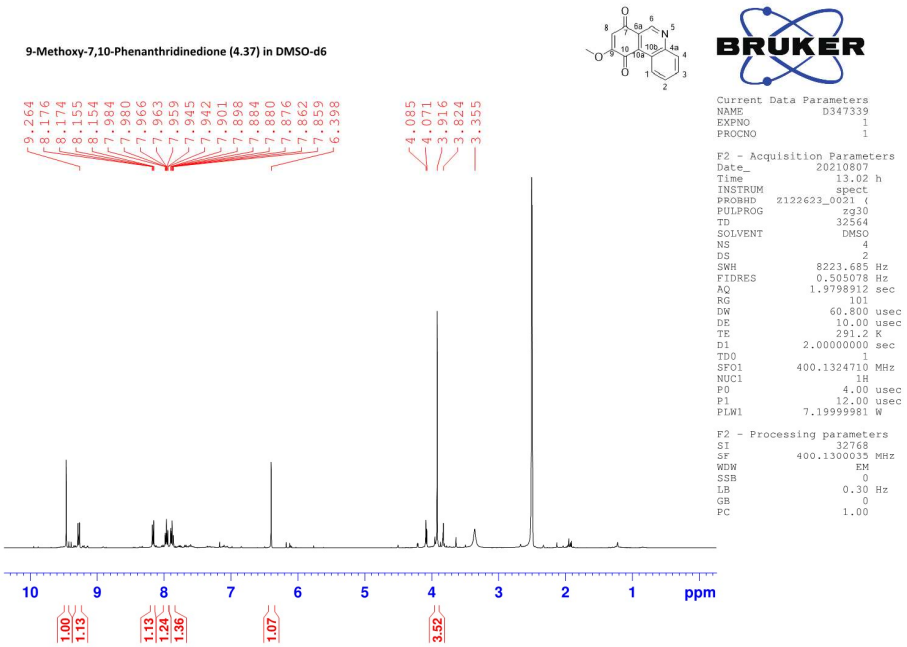


Figure 301. [1]H NMR spectra of 9-Methoxy-7,10-Phenanthridinedione (**4.37**).

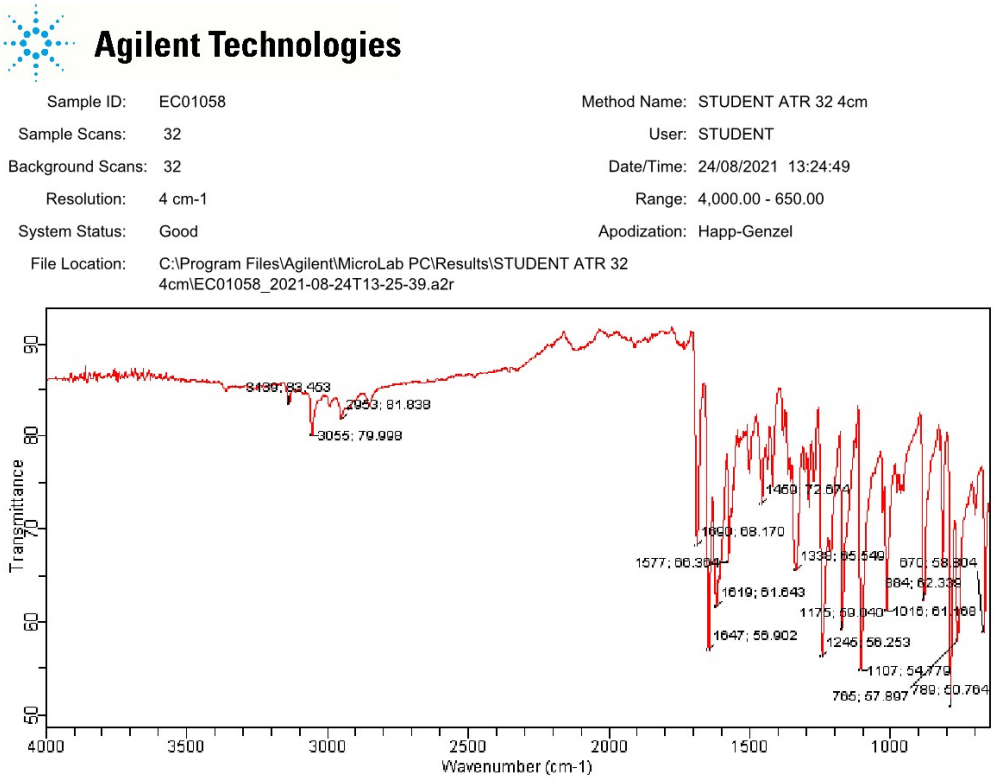


Figure 302. FT-IR spectra of 9-Methoxy-7,10-Phenanthridinedione (**4.37**).

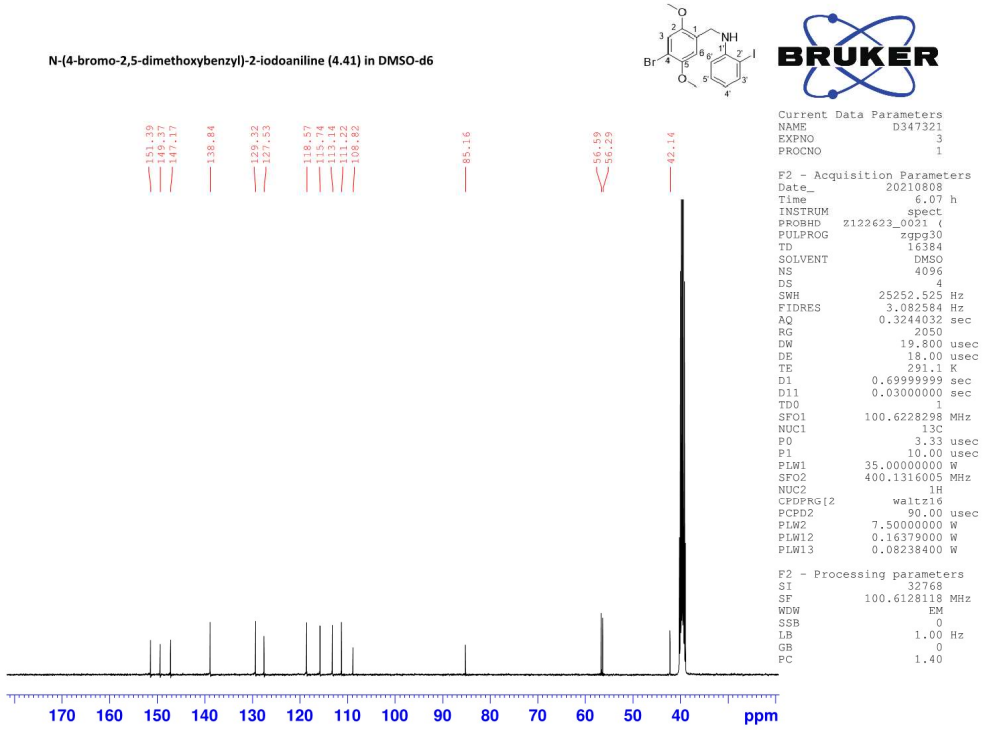


Figure 303. ^{13}C NMR spectra of N-(4-bromo-2,5-dimethoxybenzyl)-2-iodoaniline (**4.41**).

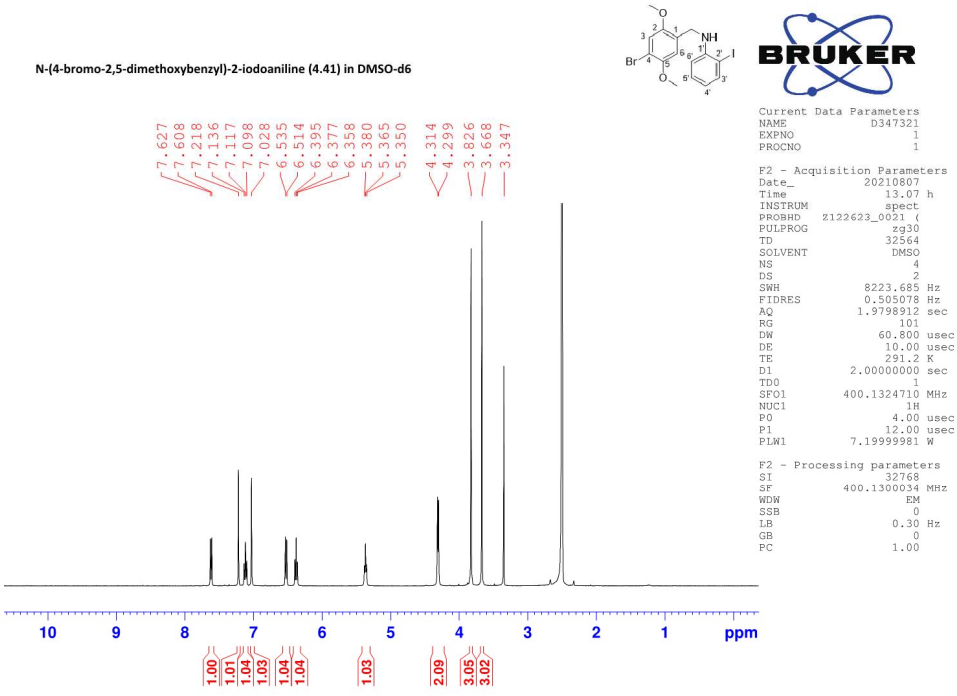


Figure 304. ^{1}H NMR spectra of N-(4-bromo-2,5-dimethoxybenzyl)-2-iodoaniline (**4.41**).

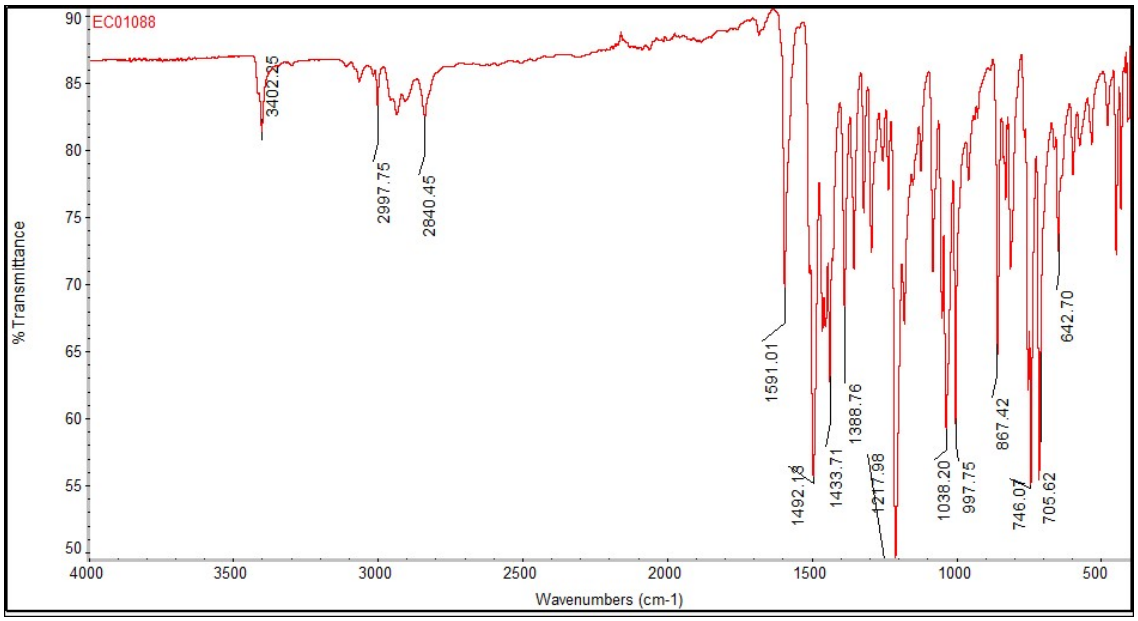


Figure 305. FT-IR spectra of N-(4-bromo-2,5-dimethoxybenzyl)-2-iodoaniline (**4.41**).

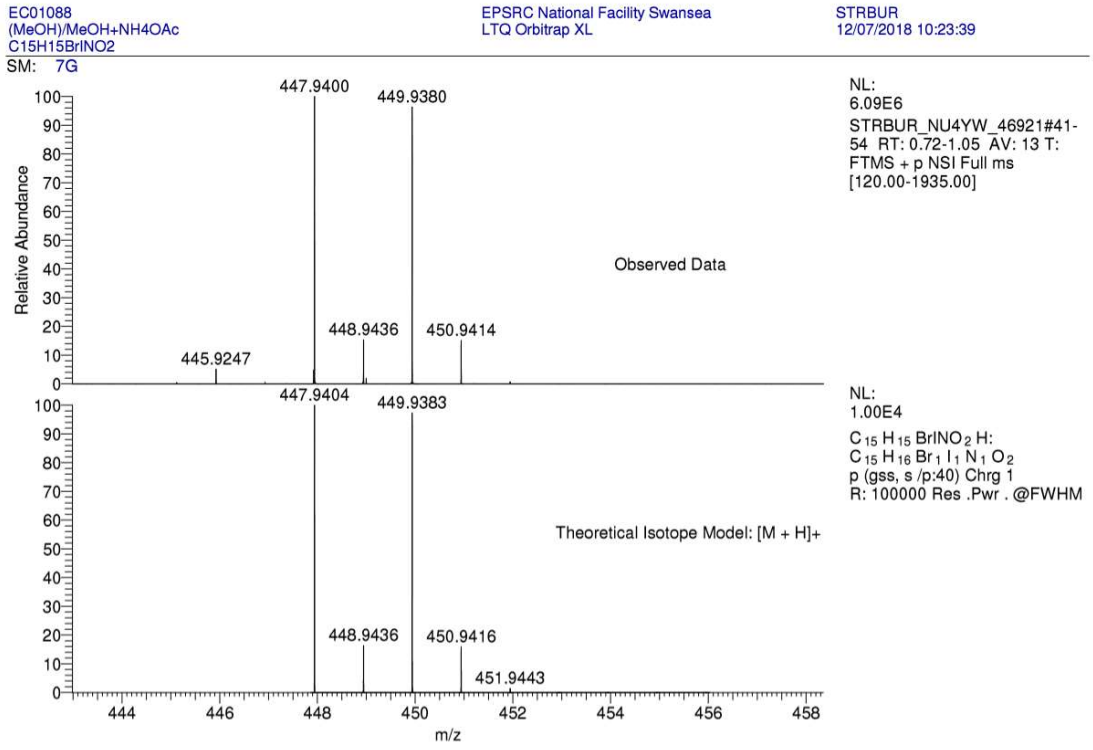


Figure 306. HRMS spectra of N-(4-bromo-2,5-dimethoxybenzyl)-2-iodoaniline (**4.41**).

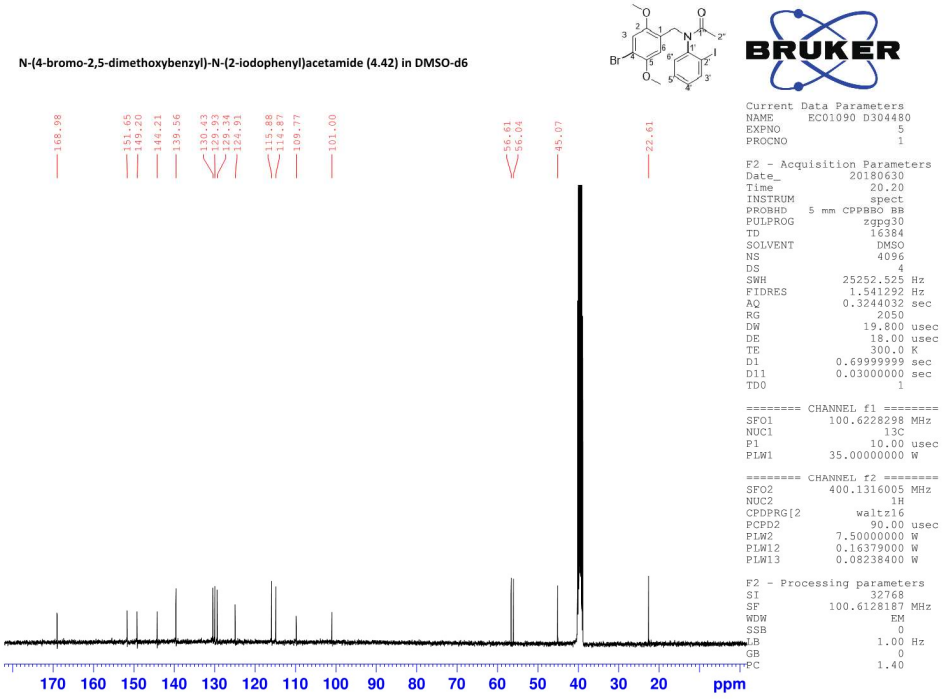


Figure 307. ^{13}C NMR spectra of N-(4-bromo-2,5-dimethoxybenzyl)-N-(2-iodophenyl)acetamide (**4.42**).

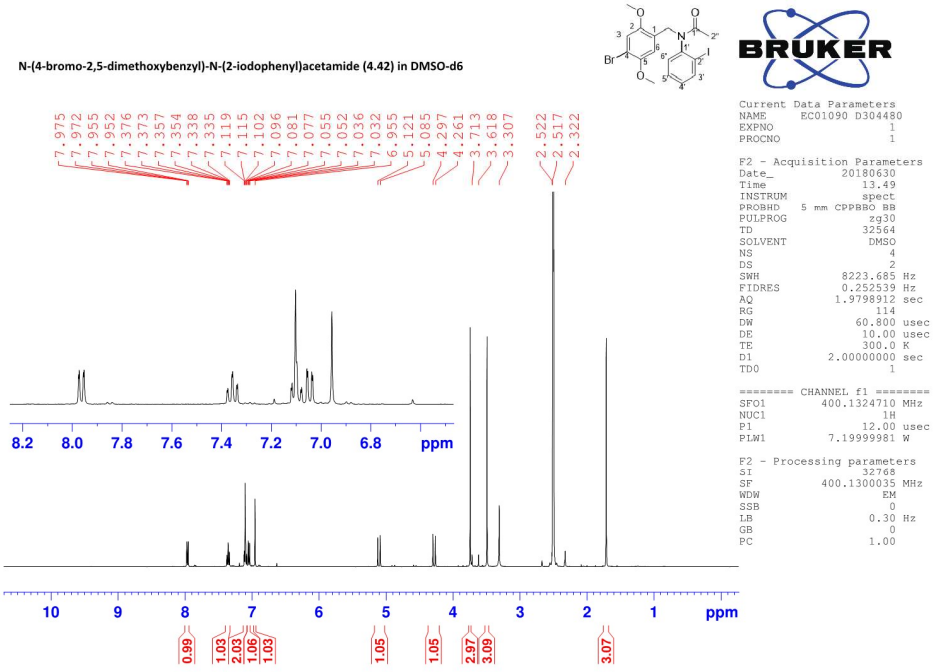


Figure 308. ^{1}H NMR spectra of N-(4-bromo-2,5-dimethoxybenzyl)-N-(2-iodophenyl)acetamide (**4.42**).

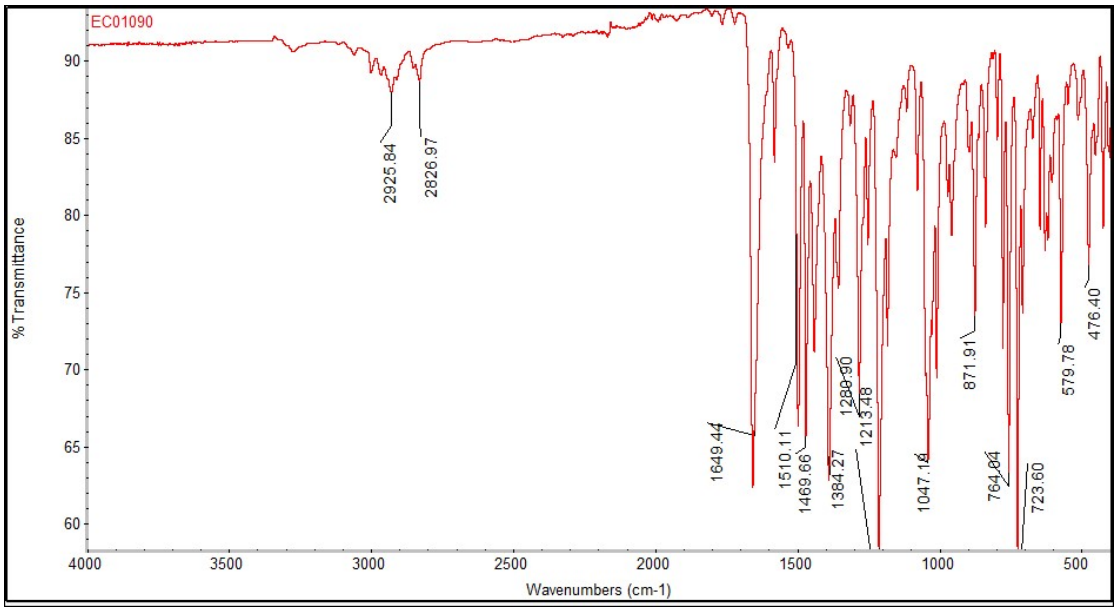


Figure 309. FT-IR spectra of N-(4-bromo-2,5-dimethoxybenzyl)-N-(2-iodophenyl)acetamide (**4.42**).

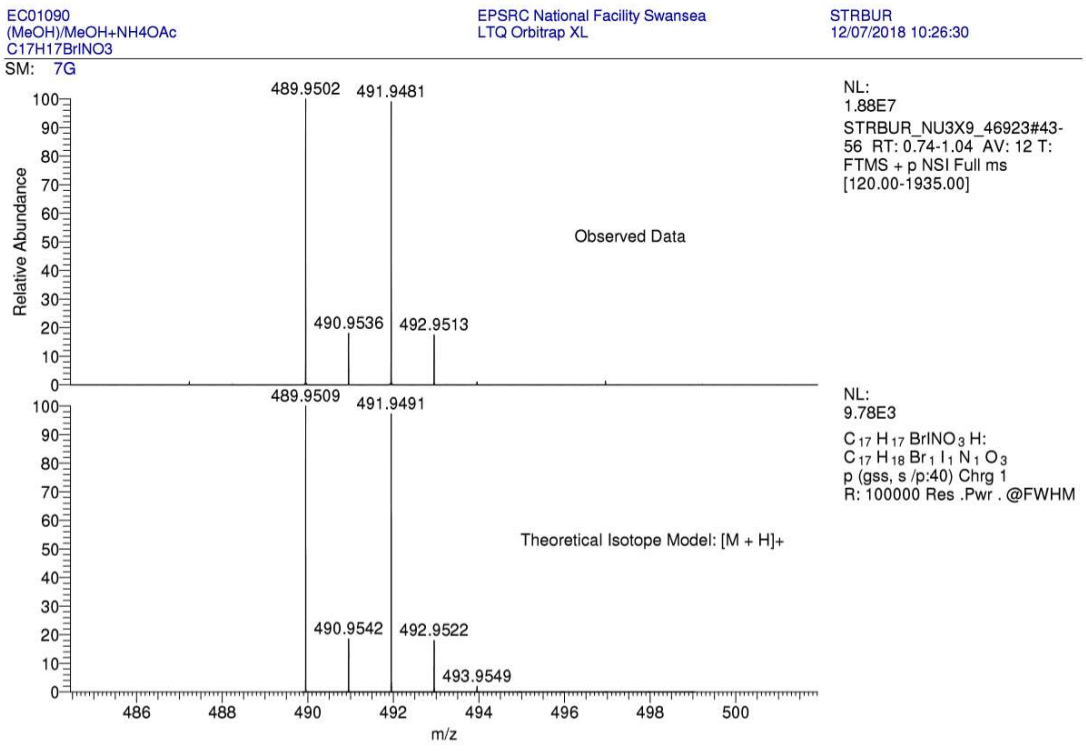


Figure 310. HRMS spectra of N-(4-bromo-2,5-dimethoxybenzyl)-N-(2-iodophenyl)acetamide (**4.42**).

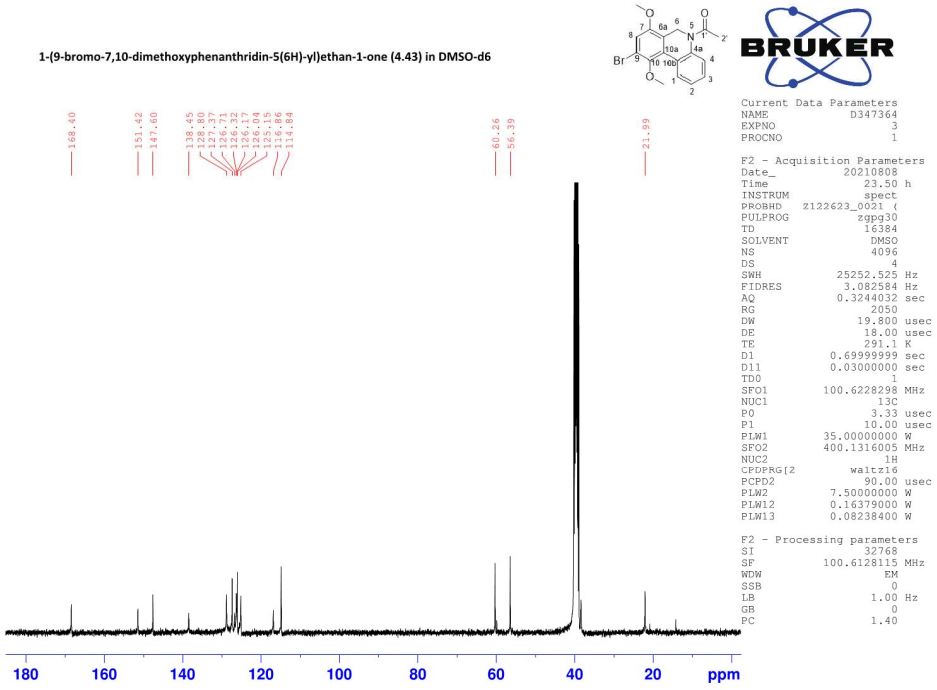


Figure 311. ^{13}C NMR spectra of 1-(9-bromo-7,10-dimethoxyphenanthridin-5(6H)-yl)ethan-1-one (**4.43**).

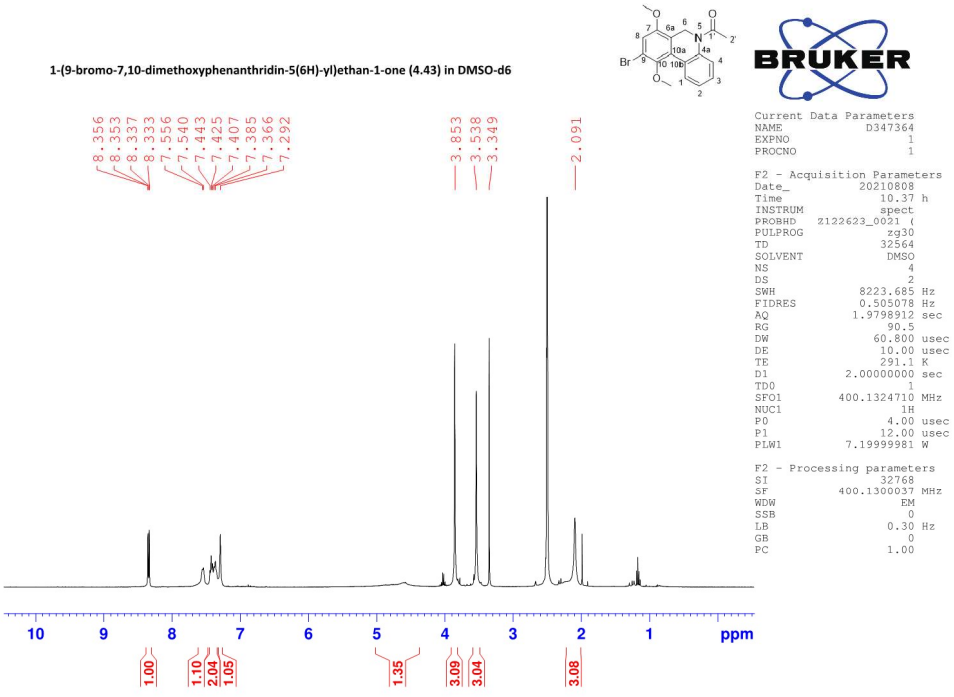


Figure 312. ^{1}H NMR spectra of 1-(9-bromo-7,10-dimethoxyphenanthridin-5(6H)-yl)ethan-1-one (**4.43**).

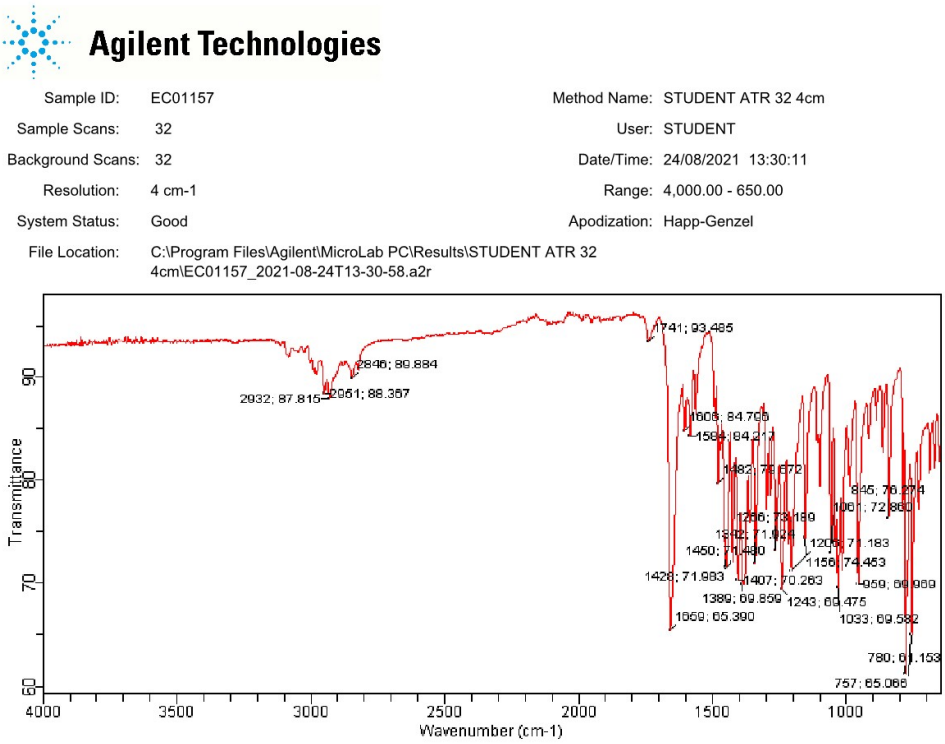


Figure 313. FT-IR spectra of 1-(9-bromo-7,10-dimethoxyphenanthridin-5(6H)-yl)ethan-1-one (**4.43**).

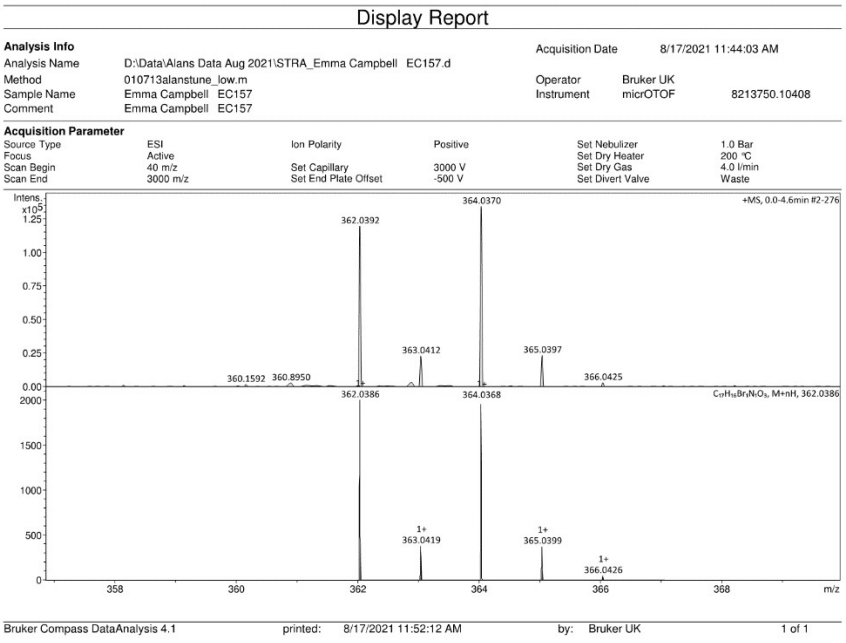


Figure 314. HRMS spectra of 1-(9-bromo-7,10-dimethoxyphenanthridin-5(6H)-yl)ethan-1-one (**4.43**).

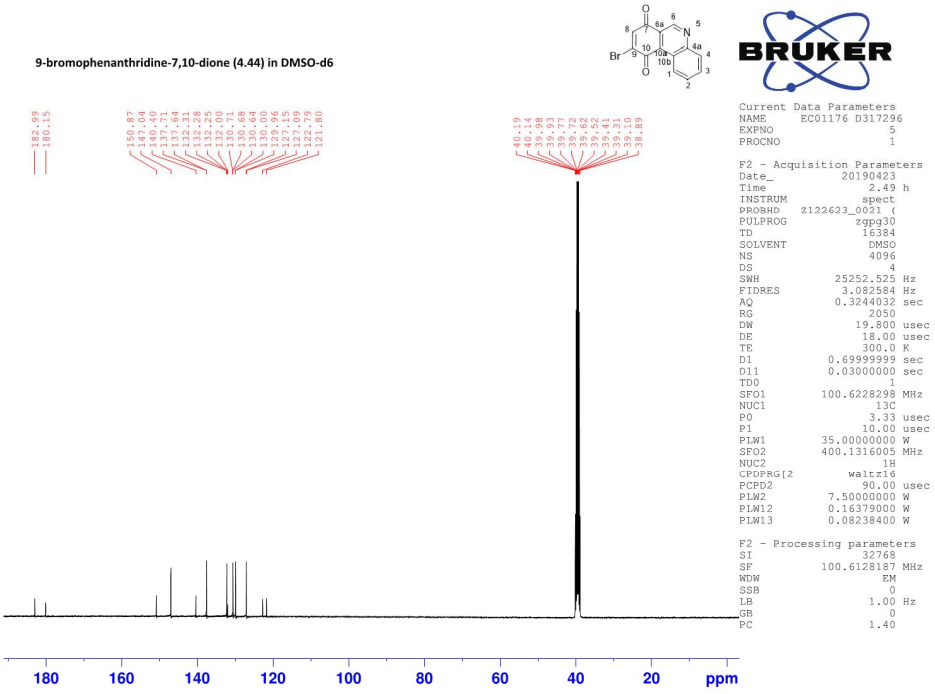


Figure 315. ^{13}C NMR spectra of 9-bromophenanthridine-7,10-dione (**4.44**).

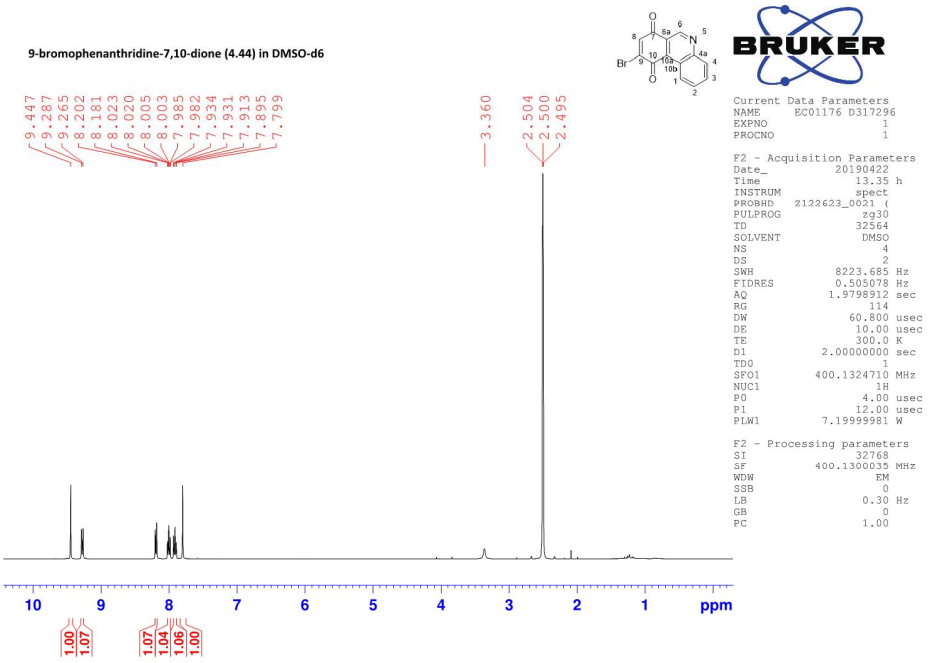


Figure 316. ^{1}H NMR spectra of 9-bromophenanthridine-7,10-dione (**4.44**).

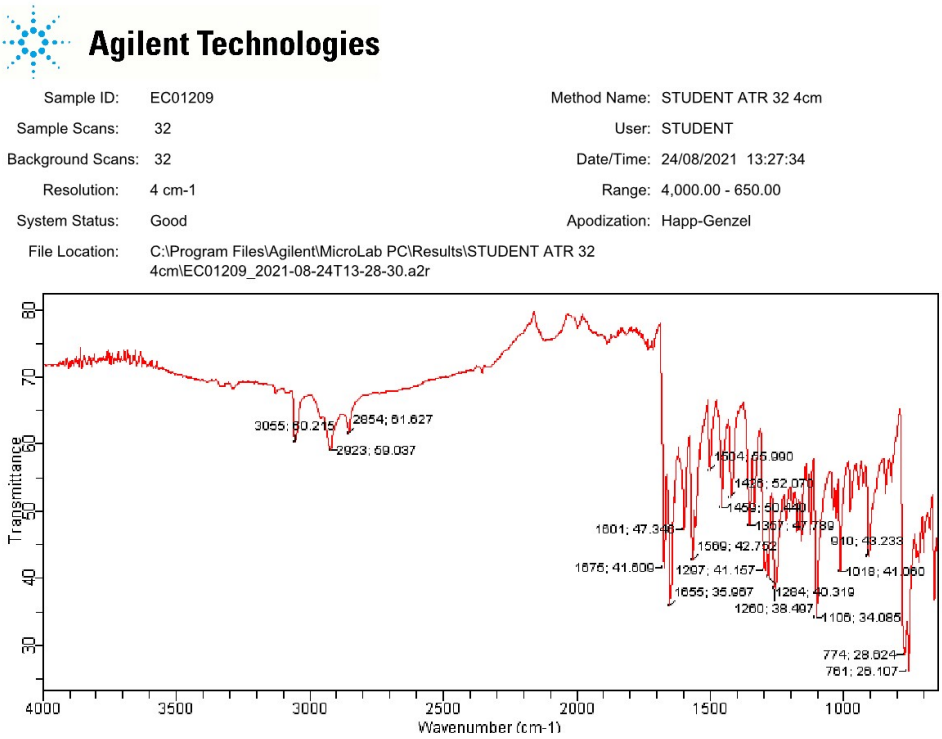


Figure 317. FT-IR spectra of 9-bromophenanthridine-7,10-dione (**4.44**).

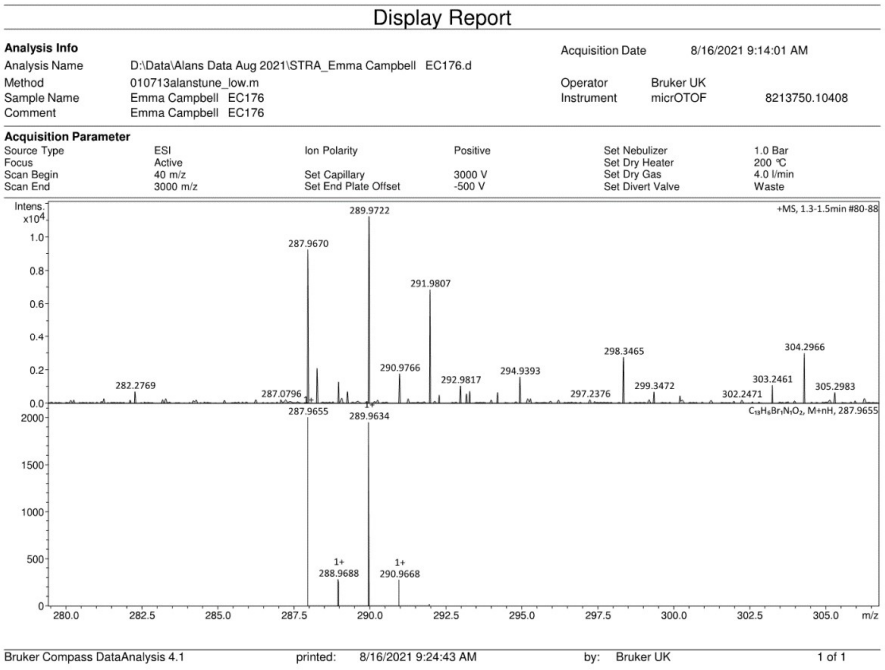


Figure 318. HRMS spectra of 9-bromophenanthridine-7,10-dione (**4.44**).

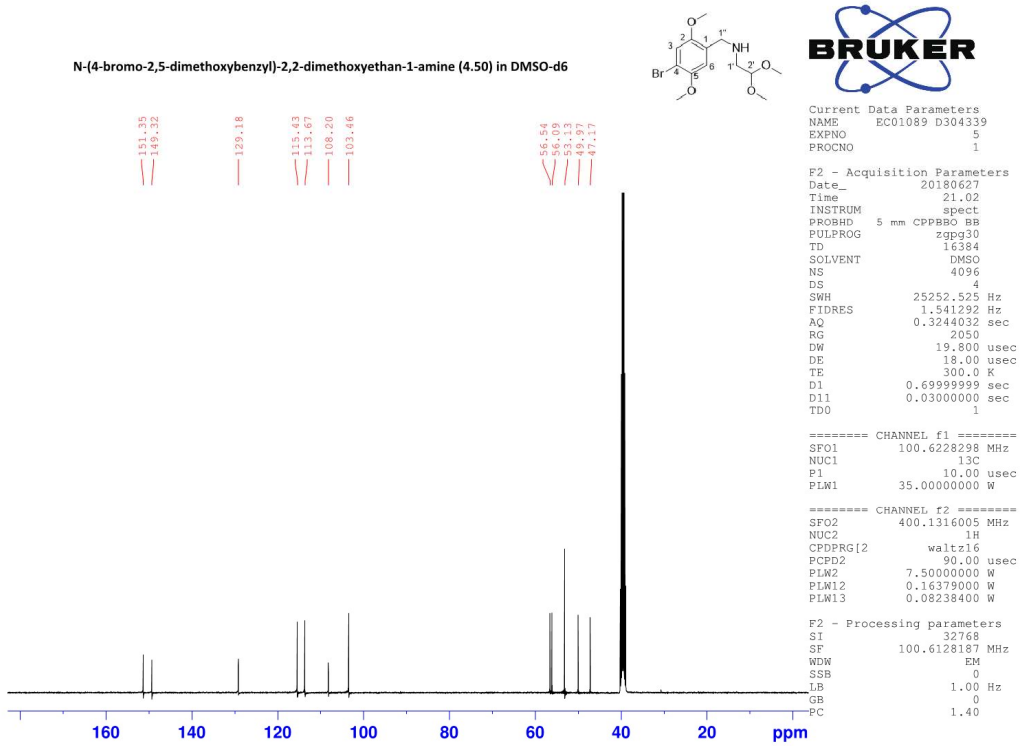


Figure 319. ^{13}C NMR spectra of N-(4-bromo-2,5-dimethoxybenzyl)-2,2-dimethoxyethan-1-amine (**4.50**).

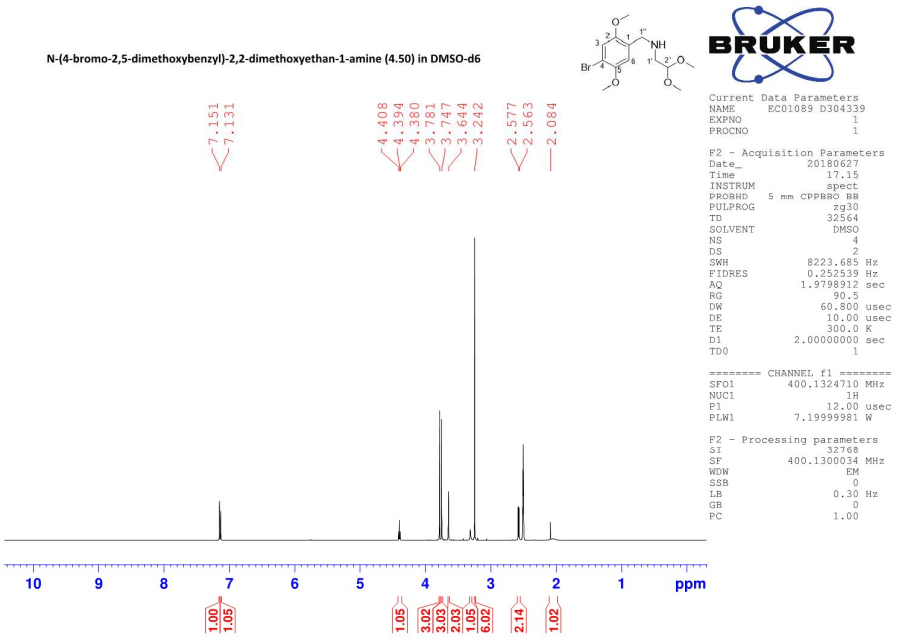


Figure 320. ^{1}H NMR spectra of N-(4-bromo-2,5-dimethoxybenzyl)-2,2-dimethoxyethan-1-amine (**4.50**).

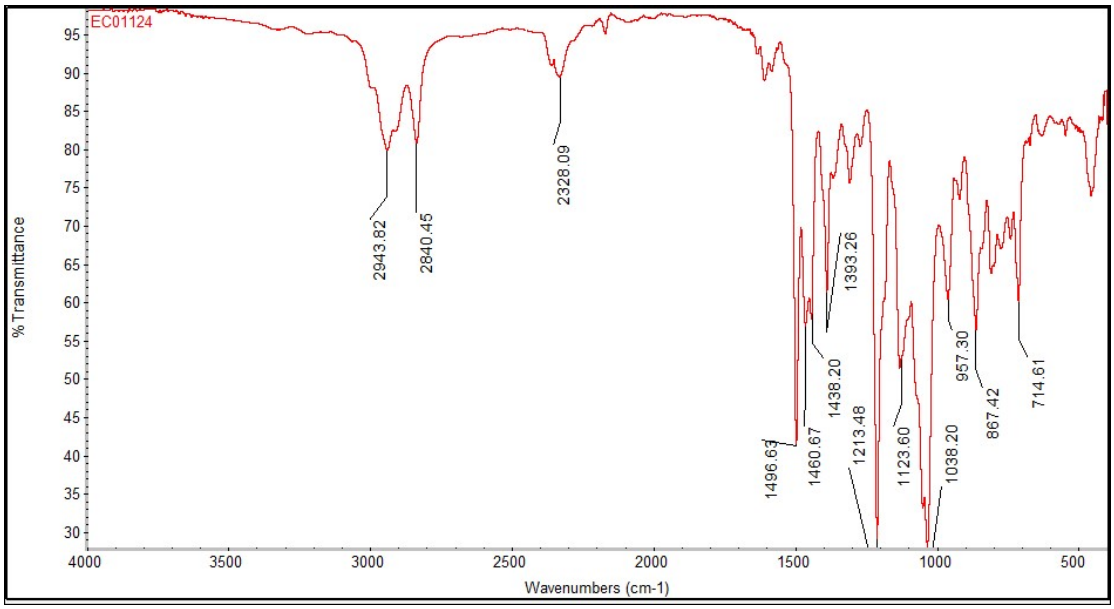


Figure 321. FT-IR spectra of N-(4-bromo-2,5-dimethoxybenzyl)-2,2-dimethoxyethan-1-amine (**4.50**).

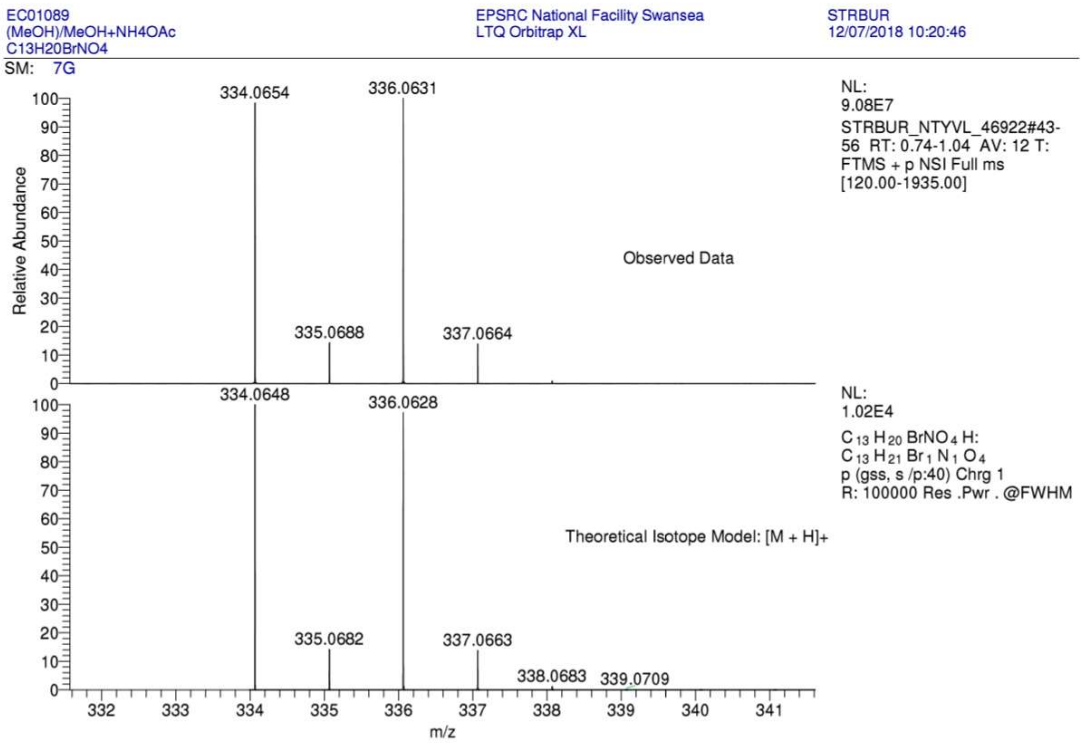


Figure 322. HRMS spectra of N-(4-bromo-2,5-dimethoxybenzyl)-2,2-dimethoxyethan-1-amine (**4.50**).

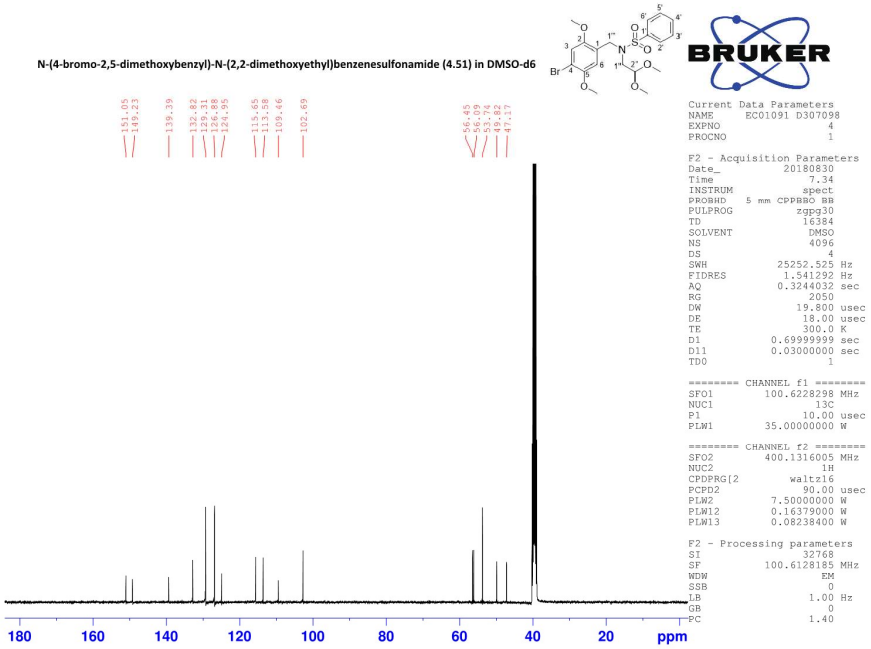


Figure 323. ^{13}C NMR spectra of N-(4-bromo-2,5-dimethoxybenzyl)-N-(2,2-dimethoxyethyl)benzenesulfonamide (**4.51**).

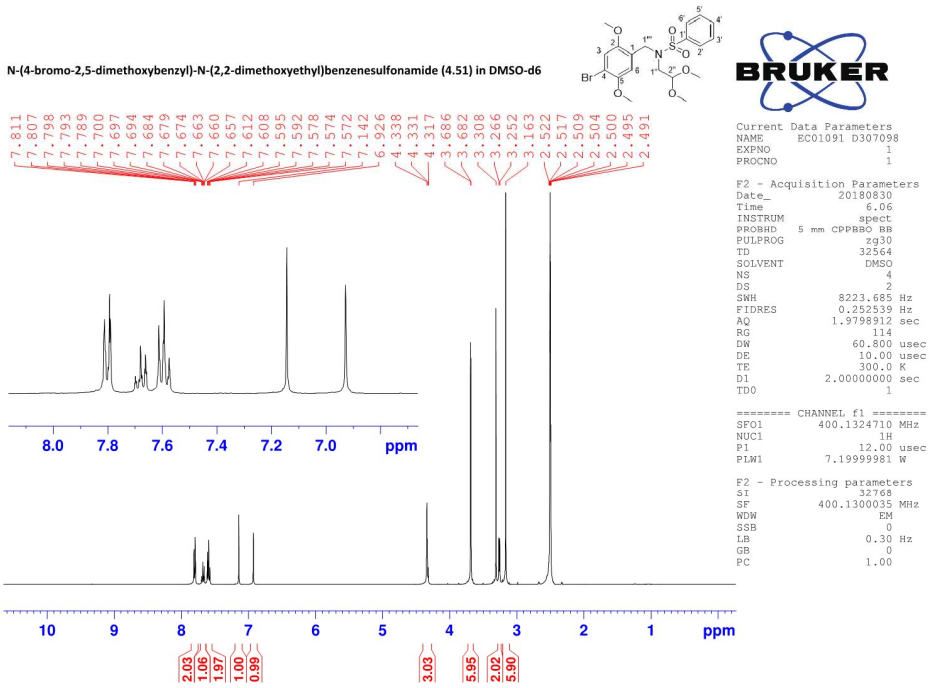


Figure 324. ^{1}H NMR spectra of N-(4-bromo-2,5-dimethoxybenzyl)-N-(2,2-dimethoxyethyl)benzenesulfonamide (**4.51**).

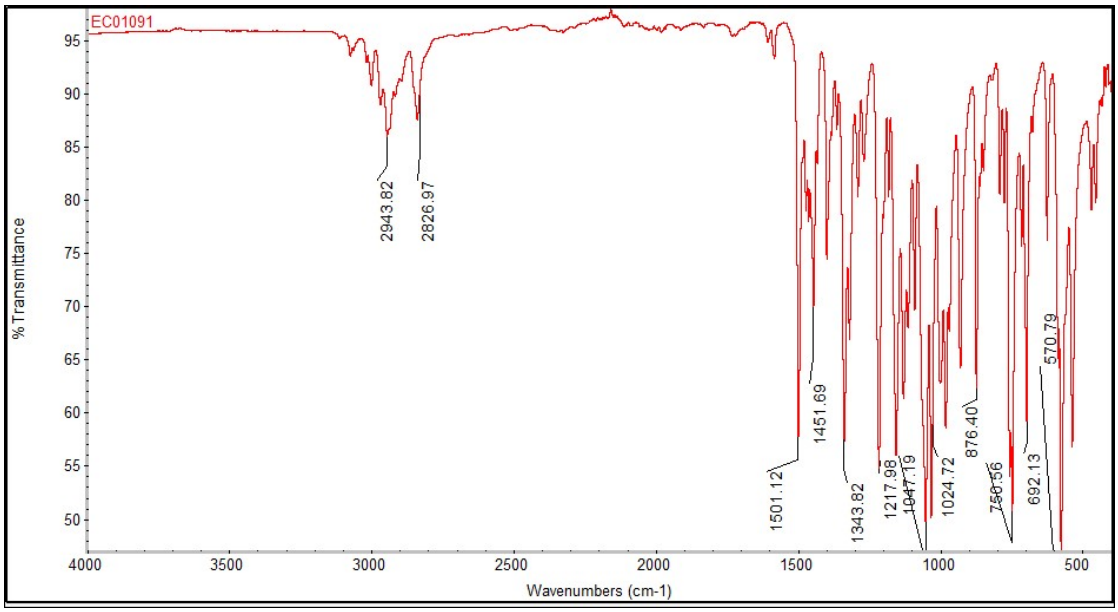


Figure 325. FT-IR spectra of N-(4-bromo-2,5-dimethoxybenzyl)-N-(2,2-dimethoxyethyl)benzenesulfonamide (**4.51**).

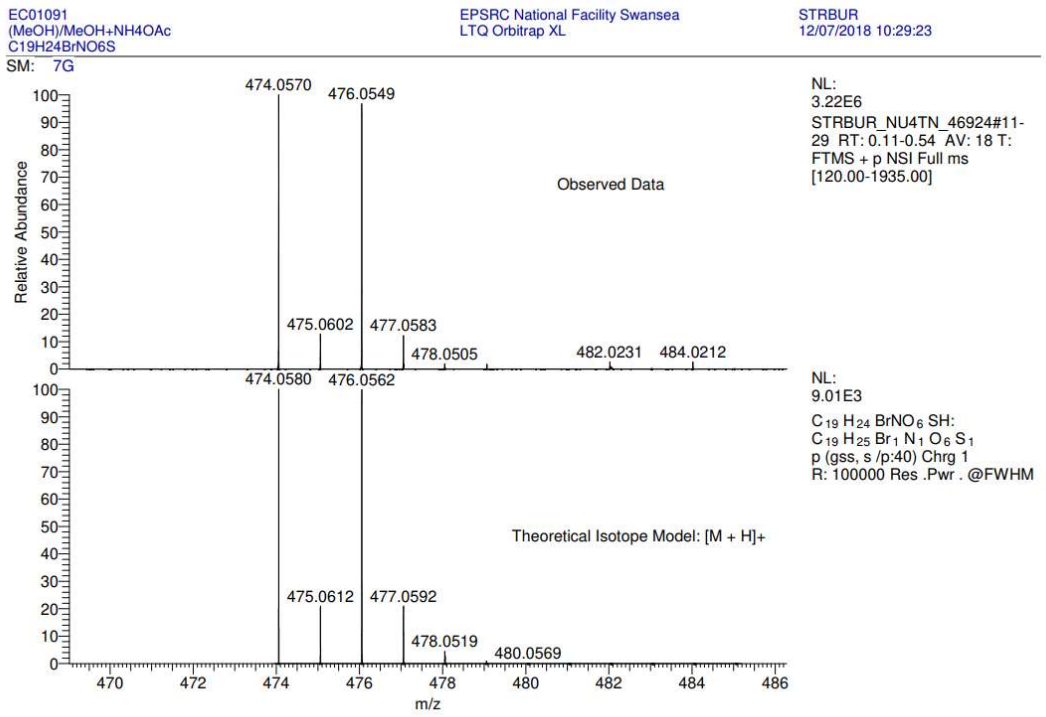


Figure 326. HRMS spectra of N-(4-bromo-2,5-dimethoxybenzyl)-N-(2,2-dimethoxyethyl)benzenesulfonamide (**4.51**).

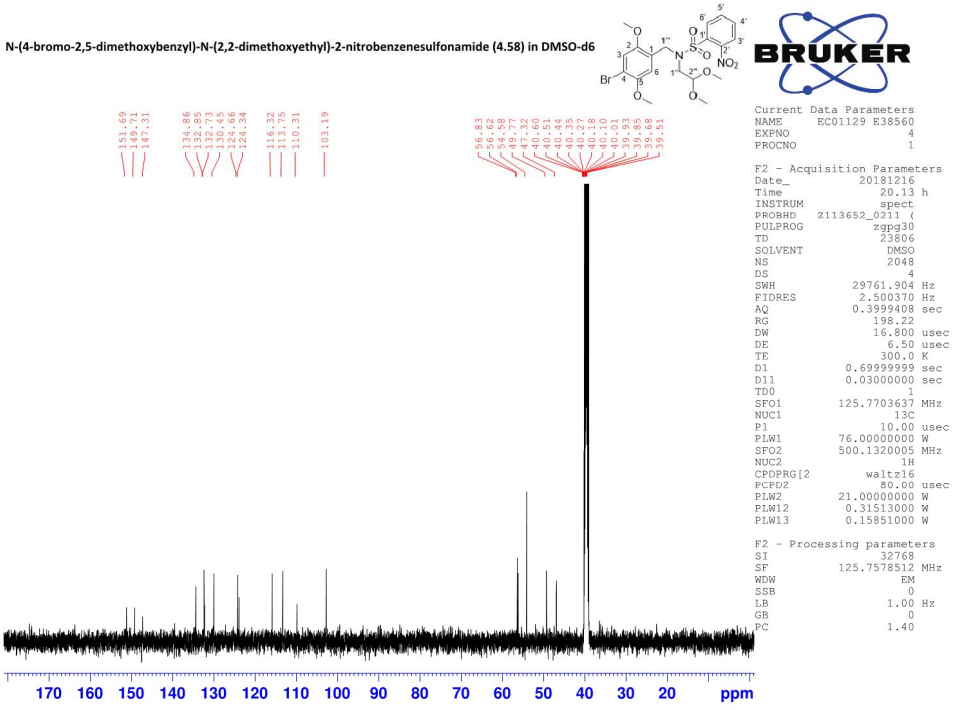


Figure 327. ^{13}C NMR spectra of N-(4-bromo-2,5-dimethoxybenzyl)-N-(2,2-dimethoxyethyl)-2-nitrobenzenesulfonamide (**4.58**).

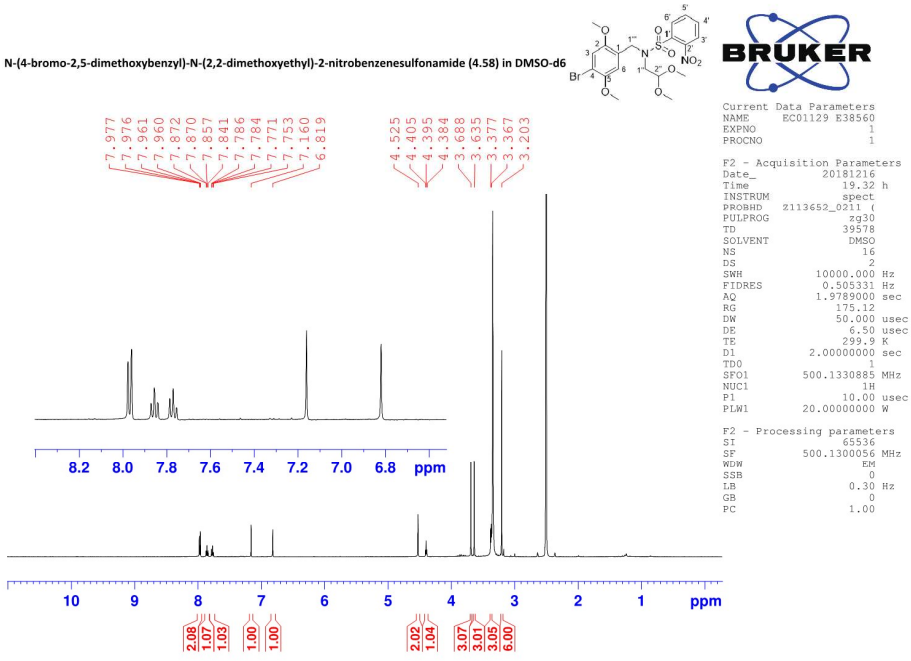


Figure 328. ^{1}H NMR spectra of N-(4-bromo-2,5-dimethoxybenzyl)-N-(2,2-dimethoxyethyl)-2-nitrobenzenesulfonamide (**4.58**).

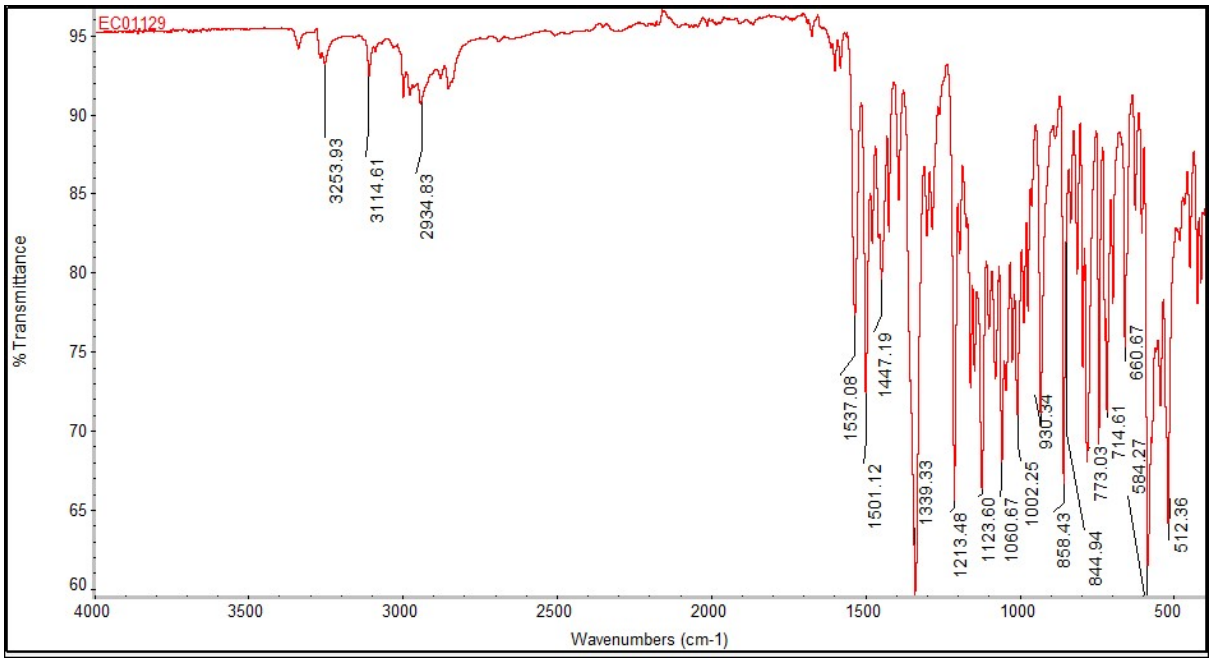


Figure 329. FT-IR spectra of N-(4-bromo-2,5-dimethoxybenzyl)-N-(2,2-dimethoxyethyl)-2-nitrobenzenesulfonamide (**4.58**).

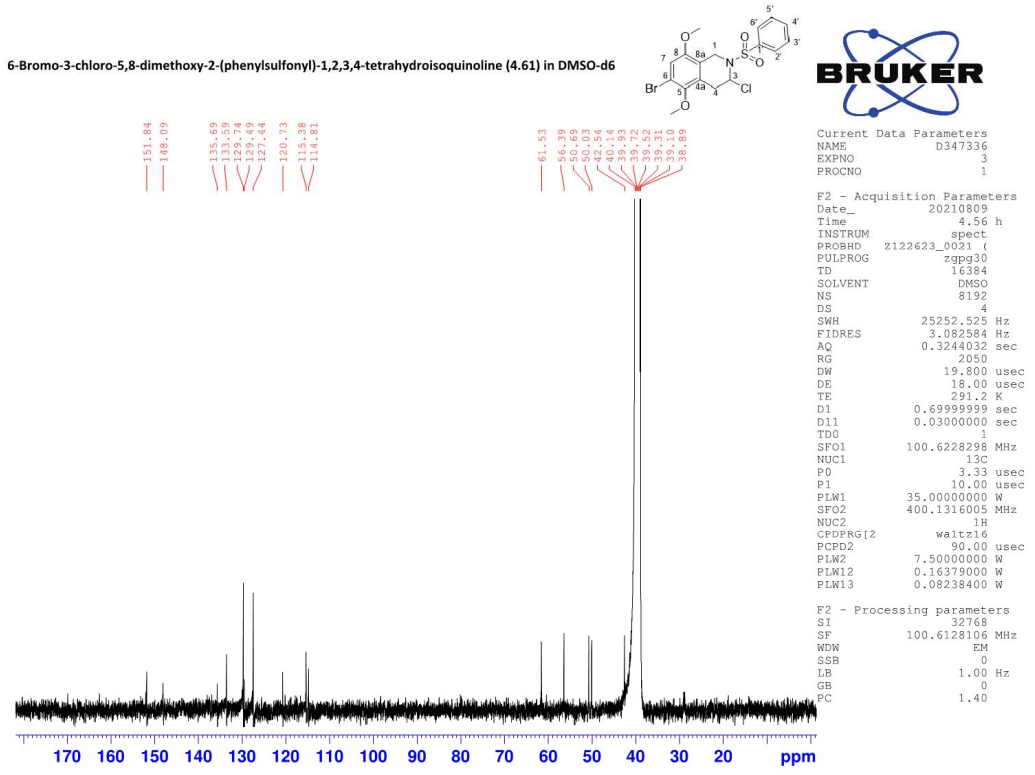


Figure 330. ^{13}C NMR spectra of 6-Bromo-3-chloro-5,8-dimethoxy-2-(phenylsulfonyl)-1,2,3,4-tetrahydroisoquinoline (**4.61**).

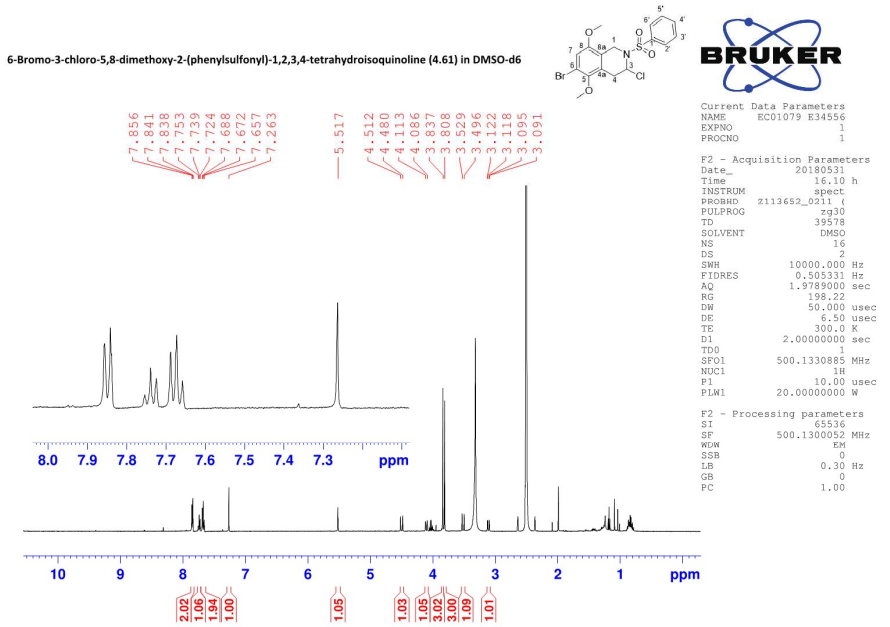


Figure 331. [1]H NMR spectra of 6-Bromo-3-chloro-5,8-dimethoxy-2-(phenylsulfonyl)-1,2,3,4-tetrahydroisoquinoline (**4.61**).

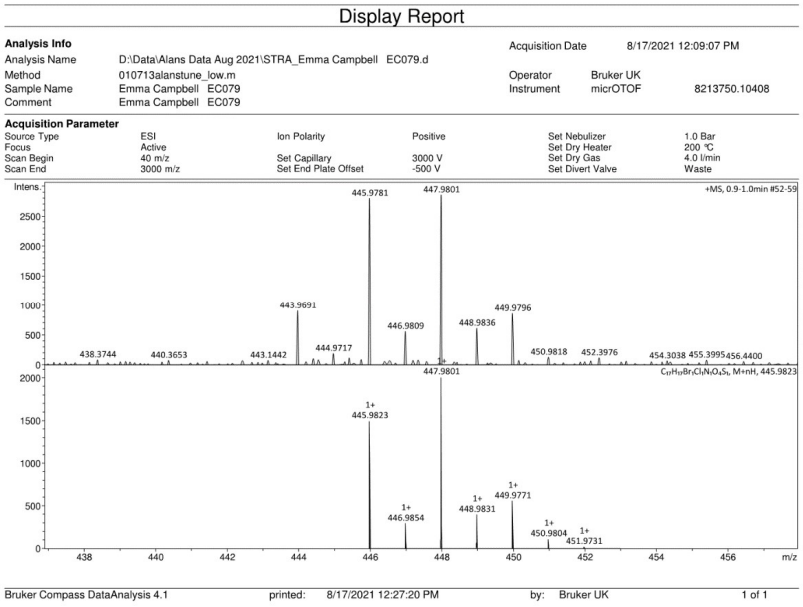


Figure 332. HRMS spectra of 6-Bromo-3-chloro-5,8-dimethoxy-2-(phenylsulfonyl)-1,2,3,4-tetrahydroisoquinoline (**4.61**).

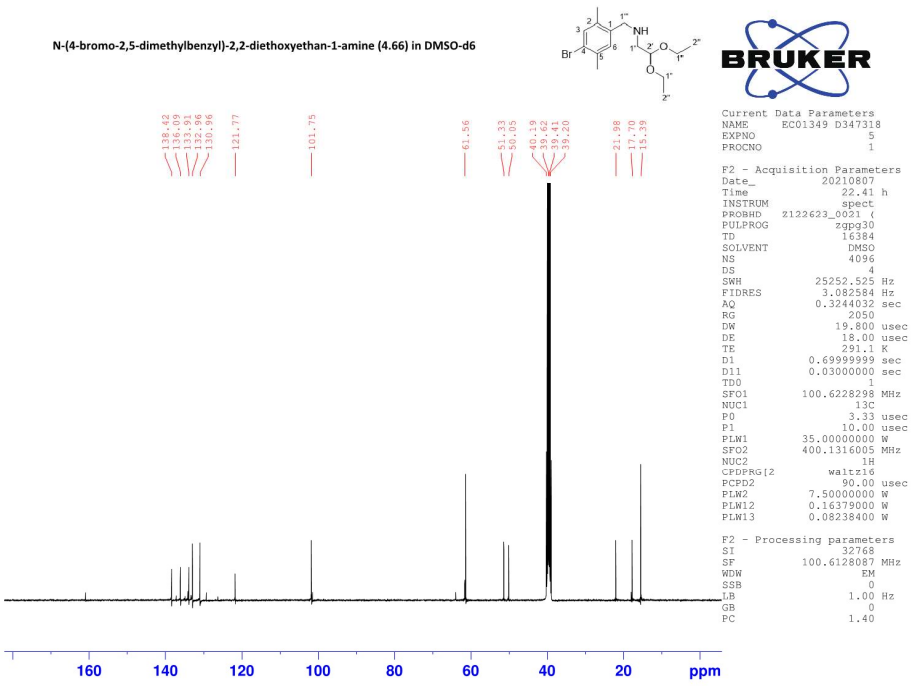


Figure 333. ^{13}C NMR spectra of N-(4-bromo-2,5-dimethylbenzyl)-2,2-diethoxyethan-1-amine (**4.66**).

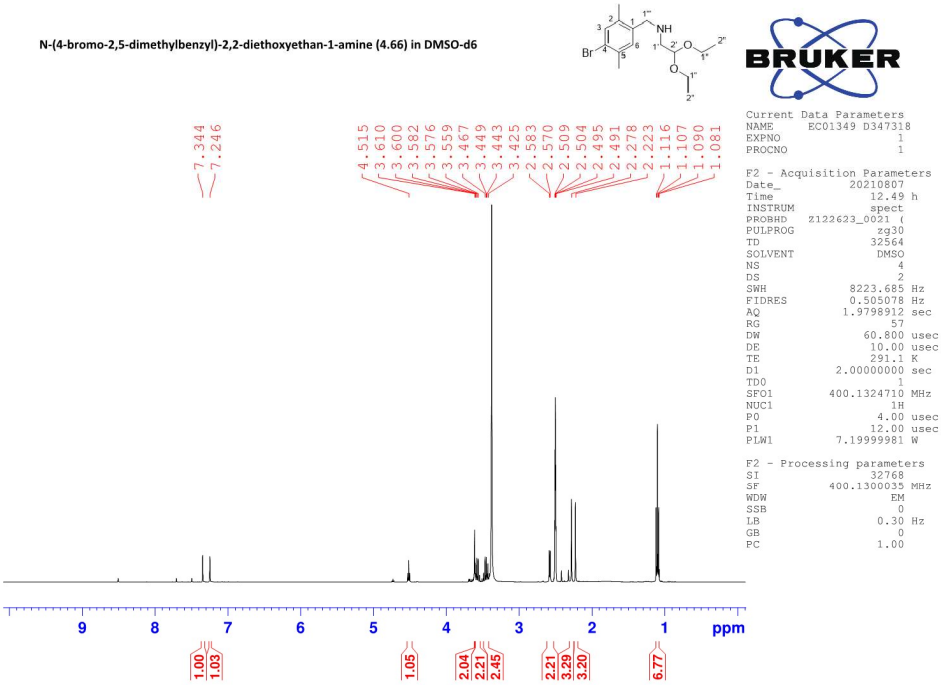


Figure 334. ^{1}H NMR spectra of N-(4-bromo-2,5-dimethylbenzyl)-2,2-diethoxyethan-1-amine (**4.66**).

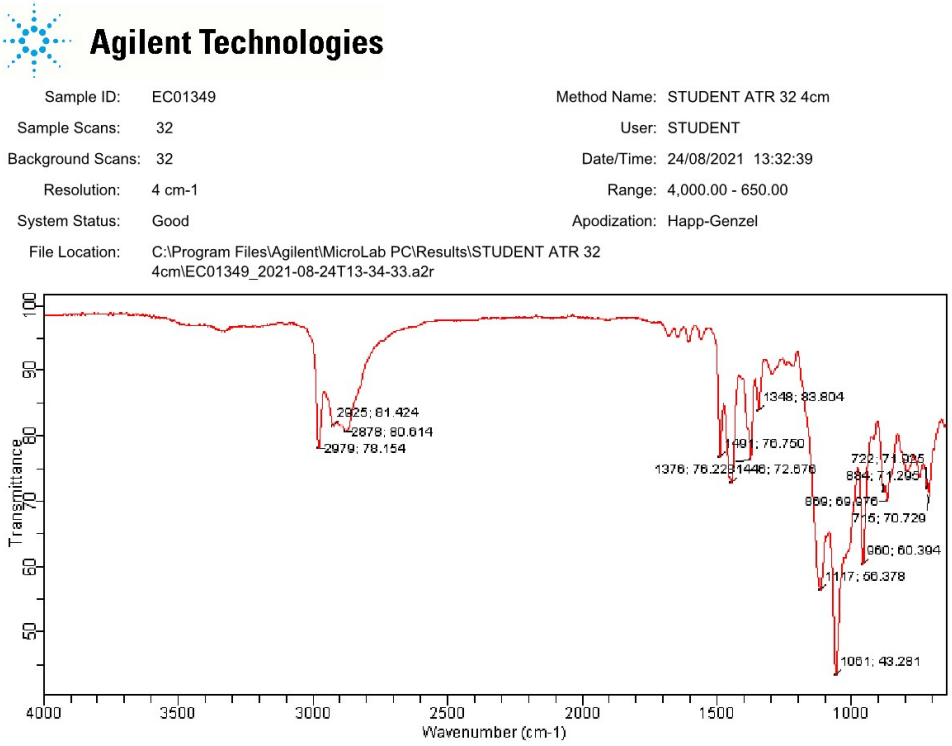


Figure 335. FT-IR spectra of N-(4-bromo-2,5-dimethylbenzyl)-2,2-diethoxyethan-1-amine (**4.66**).

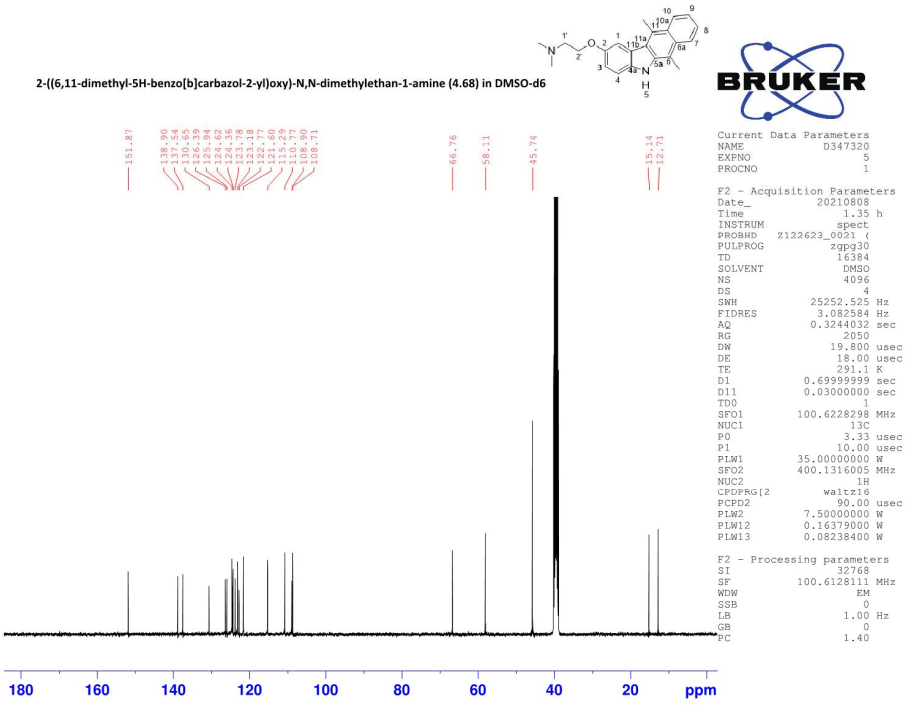


Figure 336. ^{13}C NMR spectra of 2-((6,11-dimethyl-5H-benzo[b]carbazol-2-yl)oxy)-N,N-dimethylethan-1-amine (**4.68**).

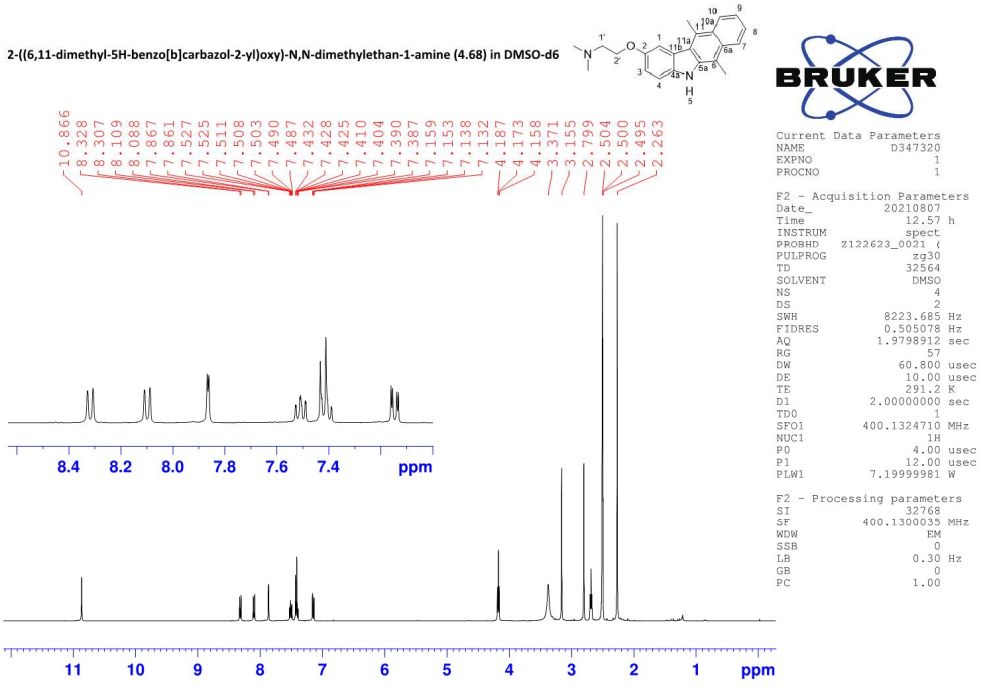


Figure 337. ^{1}H NMR spectra of 2-((6,11-dimethyl-5H-benzo[b]carbazol-2-yl)oxy)-N,N-dimethylethan-1-amine (**4.68**).

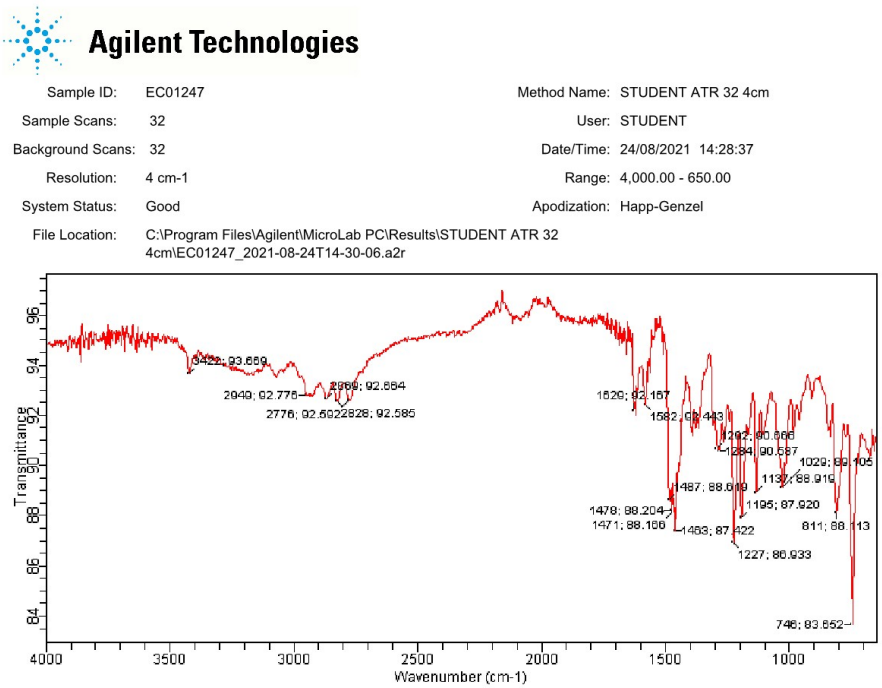


Figure 338. FT-IR spectra of 2-((6,11-dimethyl-5H-benzo[b]carbazol-2-yl)oxy)-N,N-dimethylethan-1-amine (**4.68**).

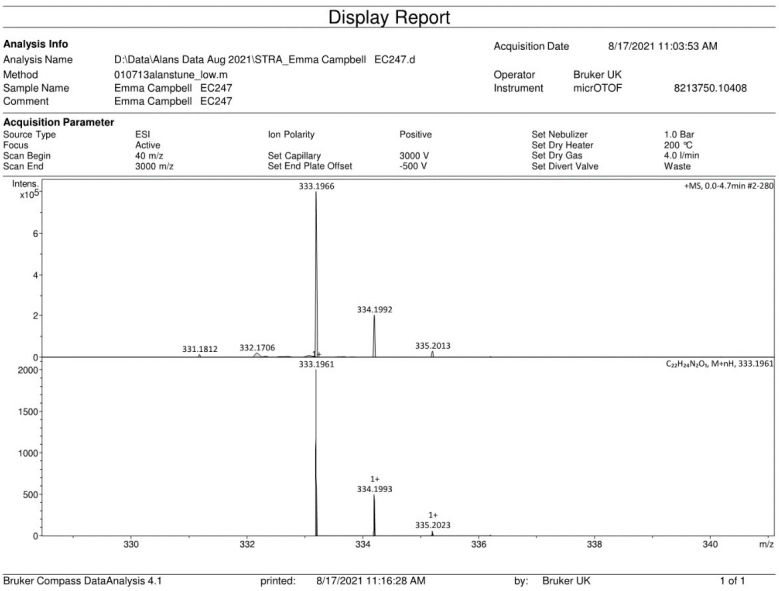


Figure 339. HRMS spectra of 2-((6,11-dimethyl-5H-benzo[b]carbazol-2-yl)oxy)-N,N-dimethylethan-1-amine (**4.68**).

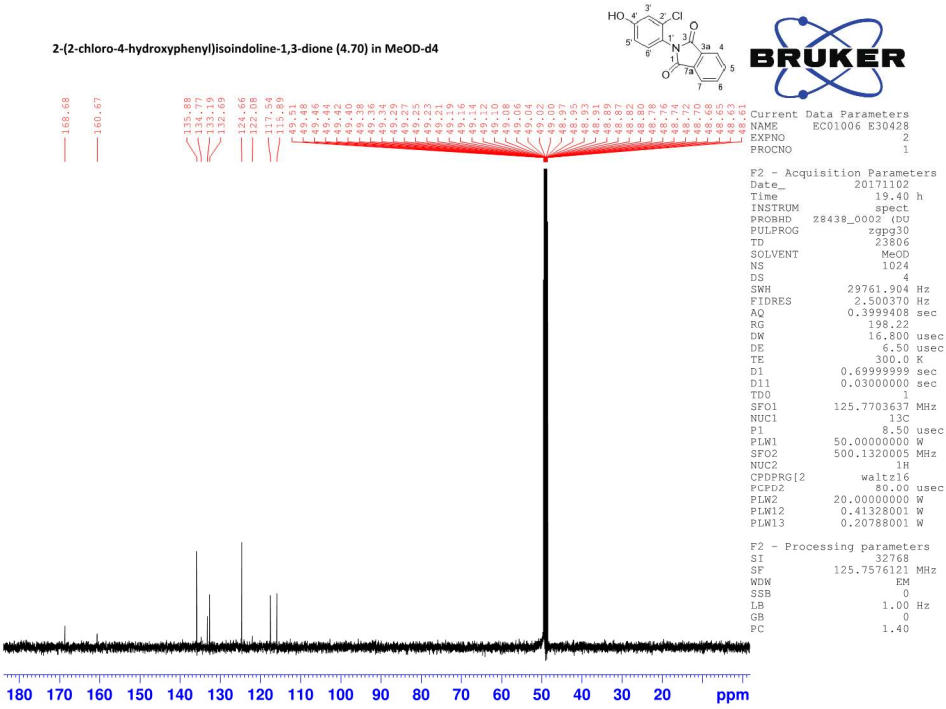


Figure 340. ^{13}C NMR spectra of 2-(2-chloro-4-hydroxyphenyl)isoindoline-1,3-dione (**4.70**).

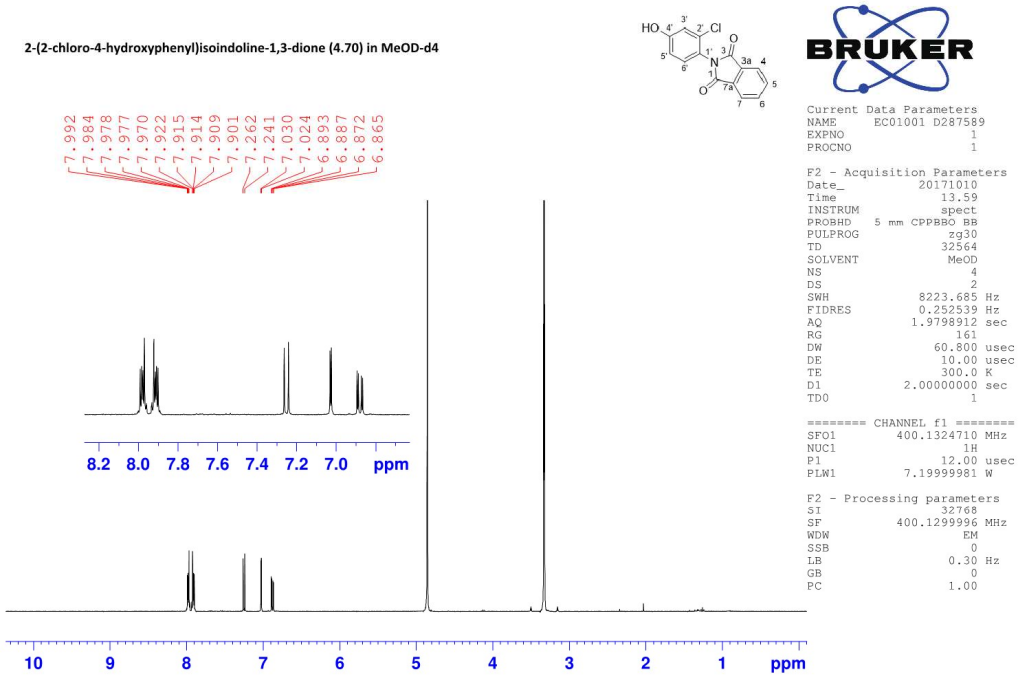


Figure 341. ^{1}H NMR spectra of 2-(2-chloro-4-hydroxyphenyl)isoindoline-1,3-dione (**4.70**).

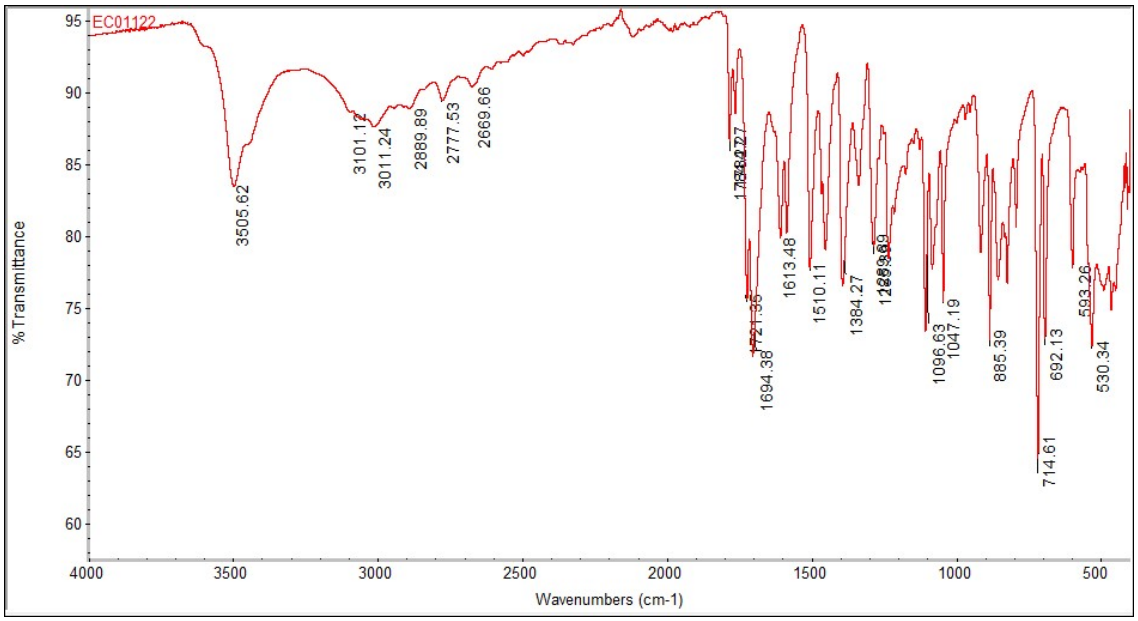


Figure 342. FT-IR spectra of 2-(2-chloro-4-hydroxyphenyl)isoindoline-1,3-dione (**4.70**).

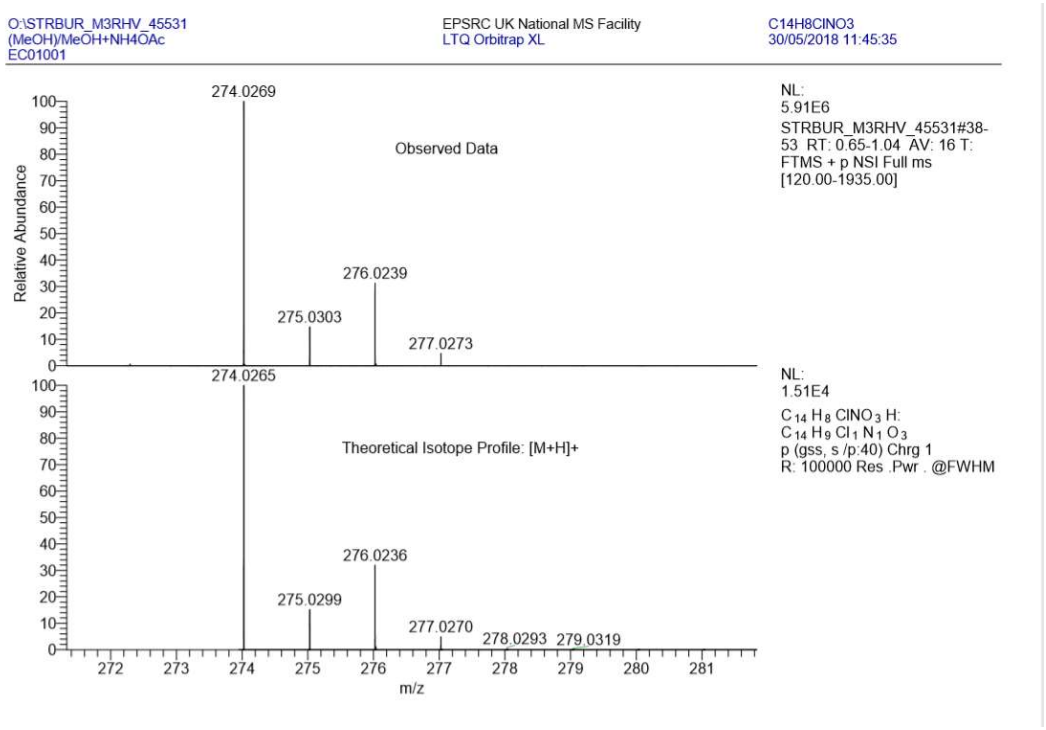


Figure 343. HRMS spectra of 2-(2-chloro-4-hydroxyphenyl)isoindoline-1,3-dione (**4.70**).

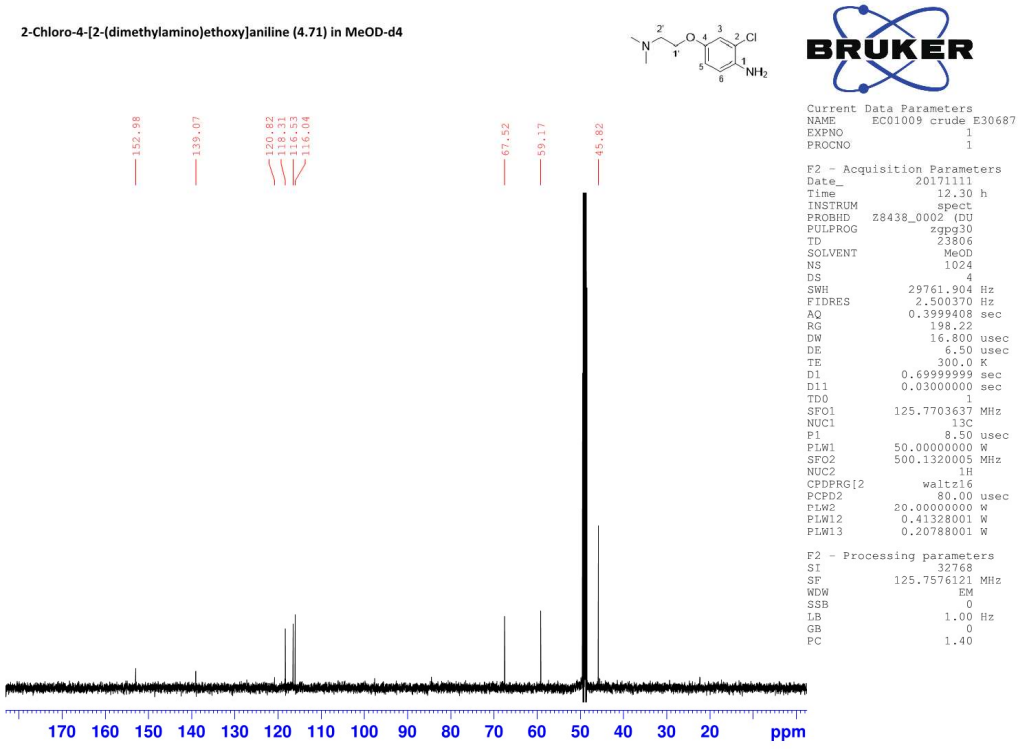


Figure 344. ^{13}C NMR spectra of 2-Chloro-4-[2-(dimethylamino)ethoxy]aniline (**4.71**).

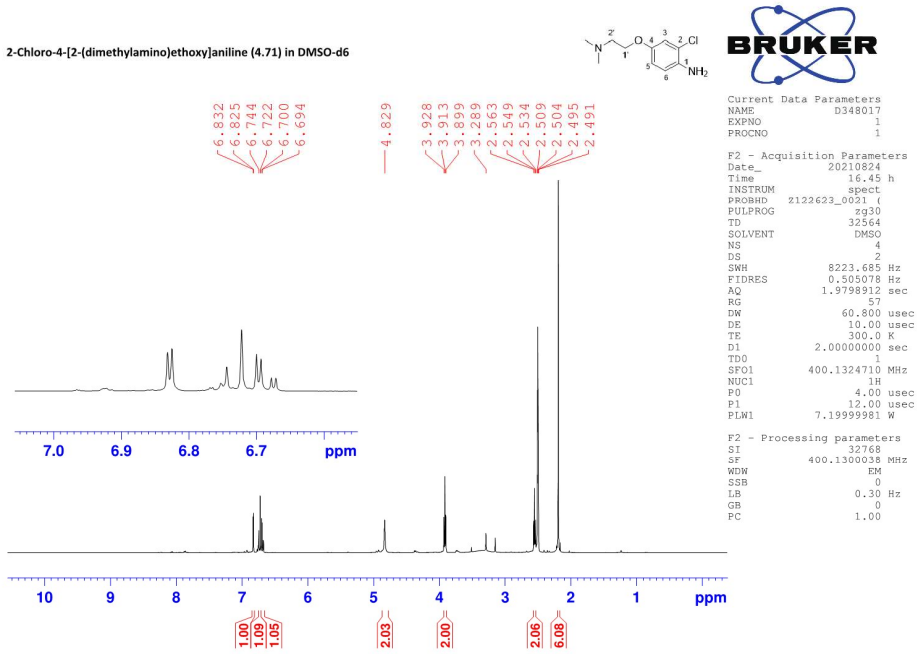


Figure 345. ^{1}H NMR spectra of 2-Chloro-4-[2-(dimethylamino)ethoxy]aniline (**4.71**).

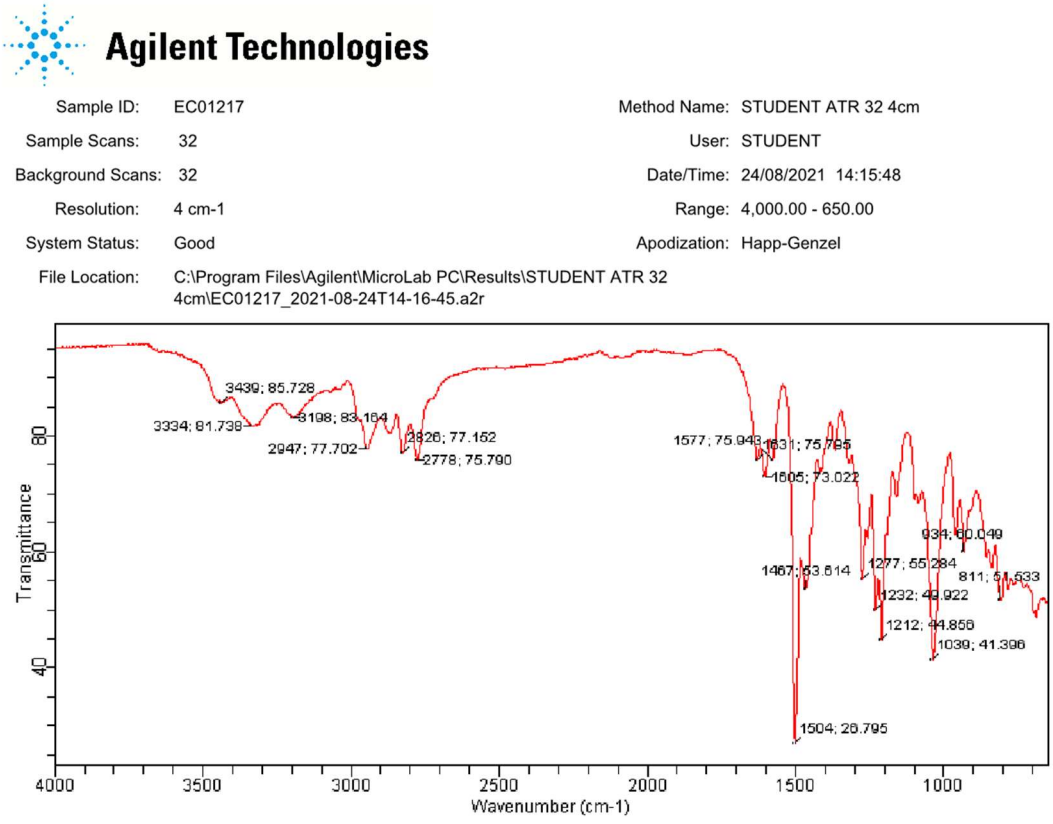


Figure 346. FT-IR spectra of 2-Chloro-4-[2-(dimethylamino)ethoxy]aniline (**4.71**).

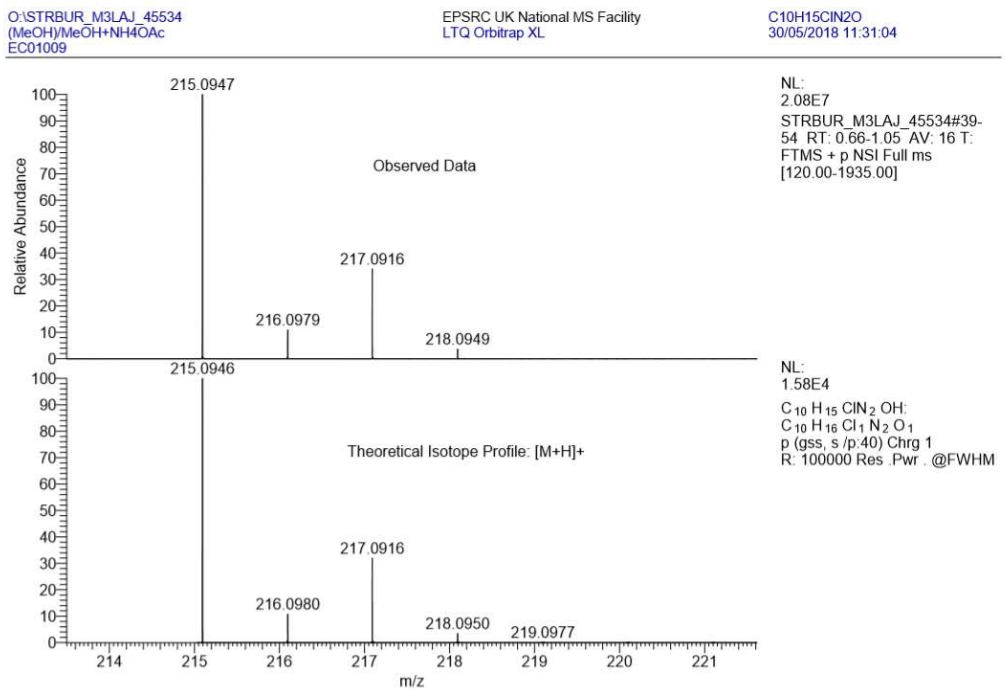


Figure 347. HRMS spectra of 2-Chloro-4-[2-(dimethylamino)ethoxy]aniline (**4.71**).

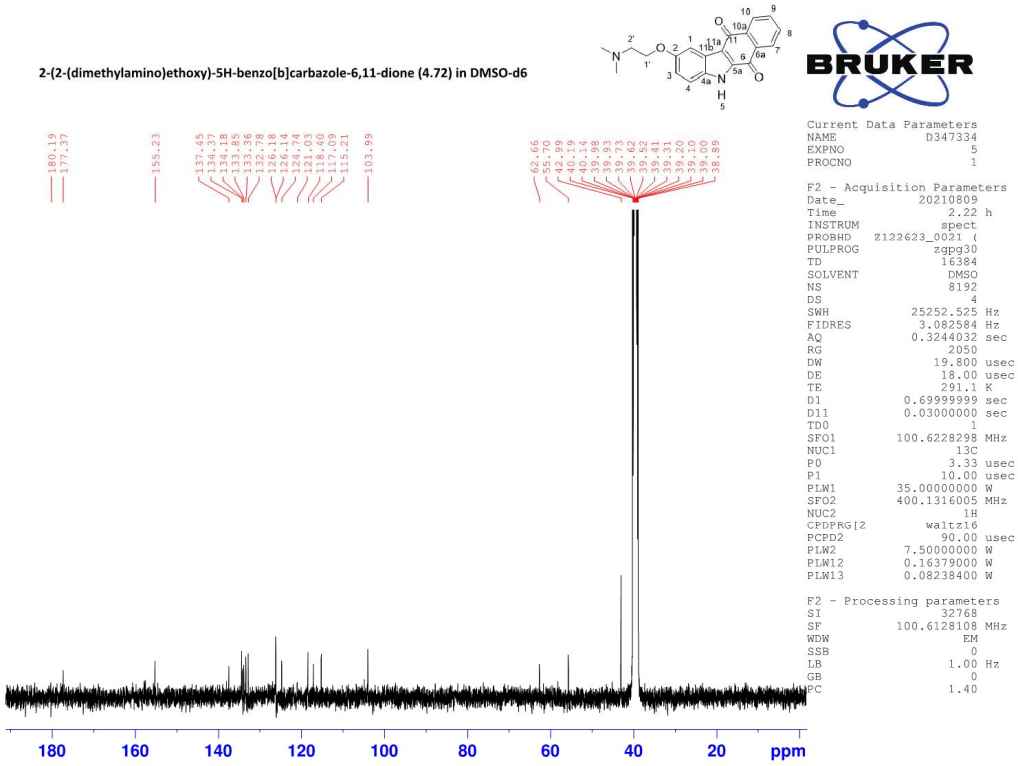


Figure 348. ^{13}C NMR spectra of 2-(2-(dimethylamino)ethoxy)-5H-benzo[b]carbazole-6,11-dione (**4.72**).

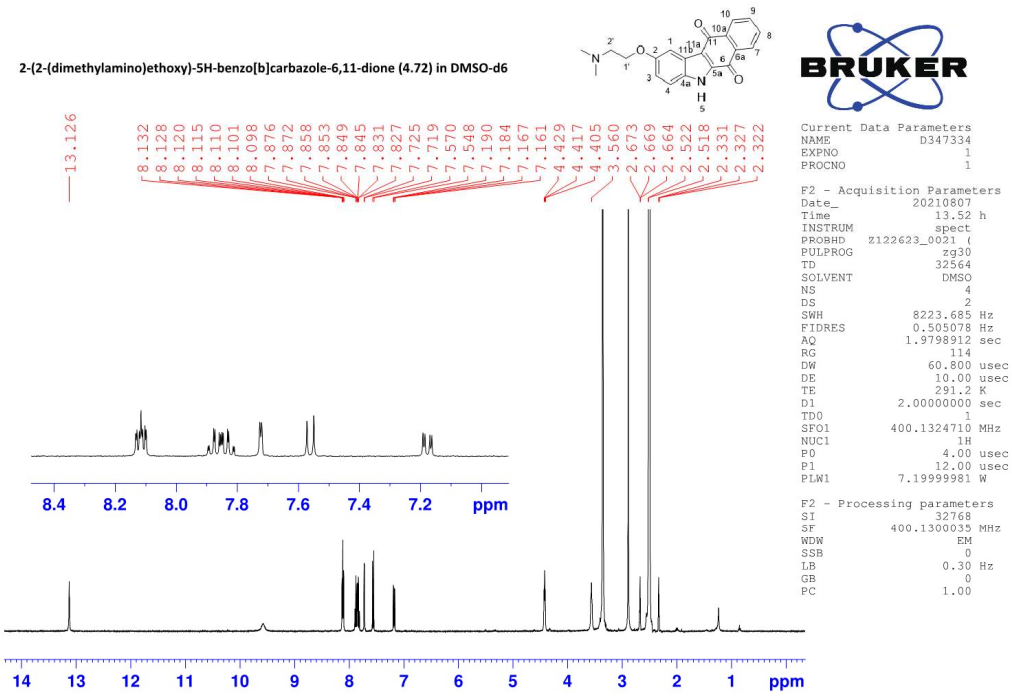


Figure 349. ^{1}H NMR spectra of 2-(2-(dimethylamino)ethoxy)-5H-benzo[b]carbazole-6,11-dione (**4.72**).

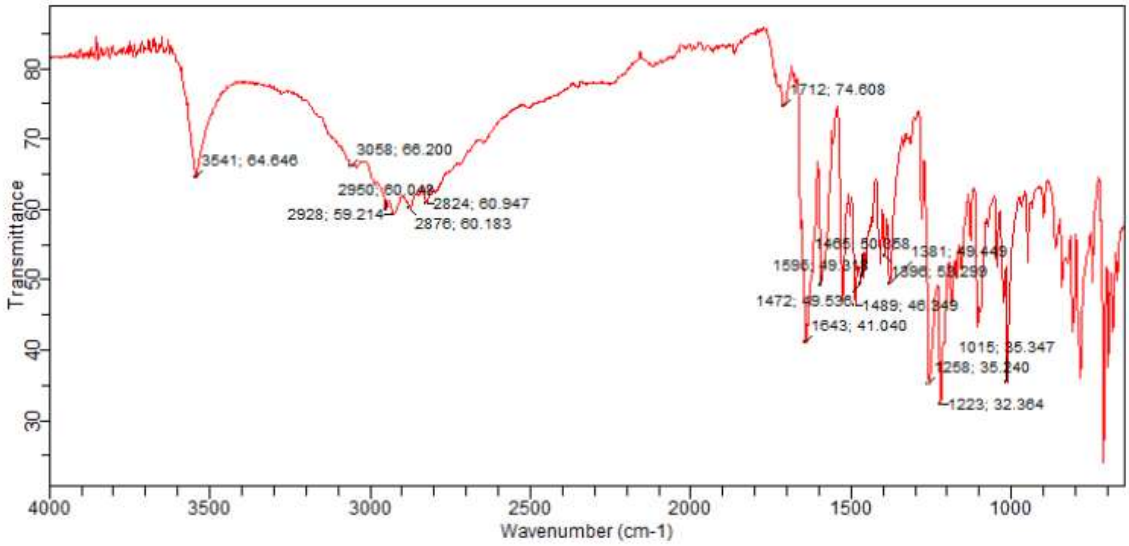


Figure 350. FT-IR spectra of 2-(2-(dimethylamino)ethoxy)-5H-benzo[b]carbazole-6,11-dione (**4.72**).

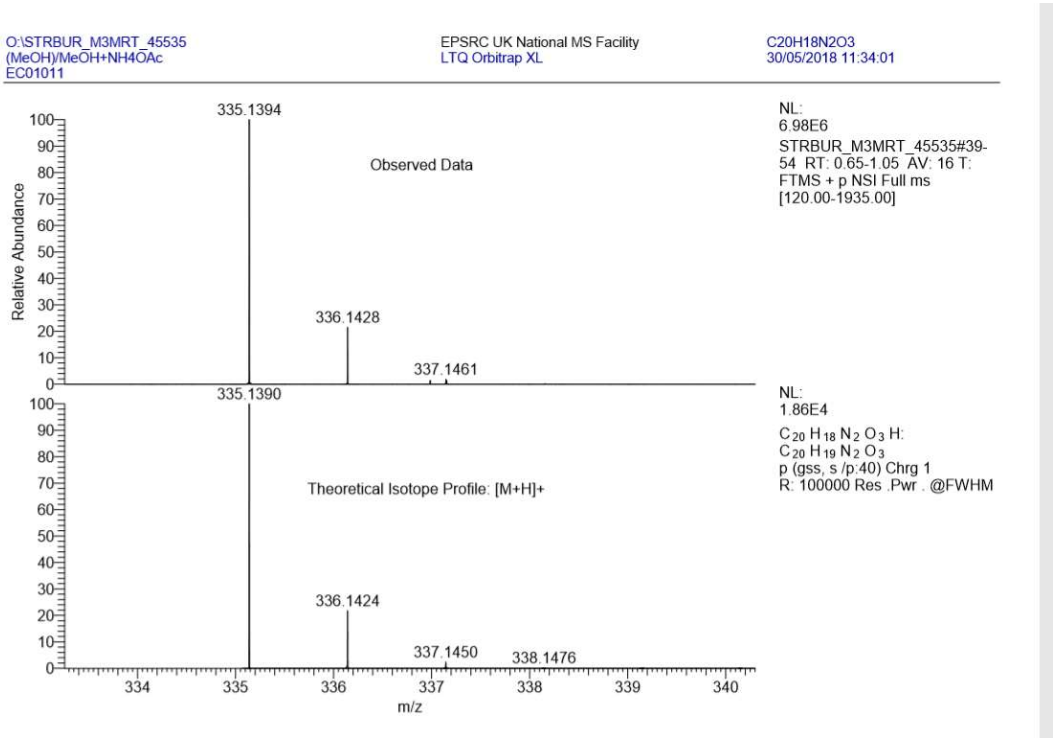


Figure 351. HRMS spectra of 2-(2-(dimethylamino)ethoxy)-5H-benzo[b]carbazole-6,11-dione (**4.72**).

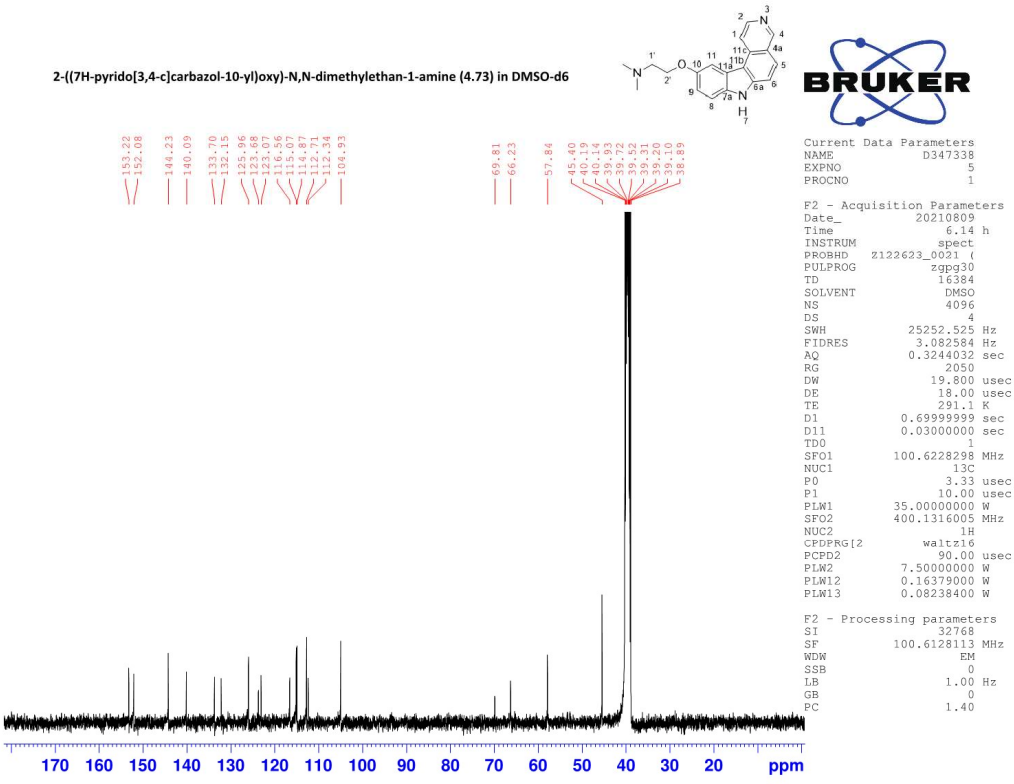


Figure 352. ^{13}C NMR spectra of 2-((7H-pyrido[3,4-c]carbazol-10-yl)oxy)-N,N-dimethylethan-1-amine (**4.73**).

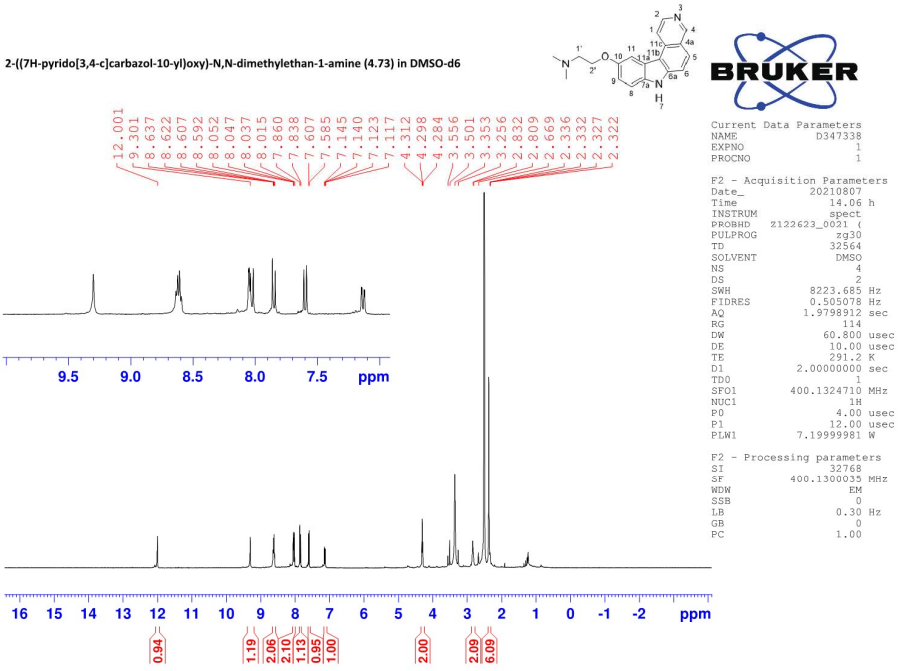


Figure 353. [1]H NMR spectra of 2-((7H-pyrido[3,4-c]carbazol-10-yl)oxy)-N,N-dimethylethan-1-amine (**4.73**).

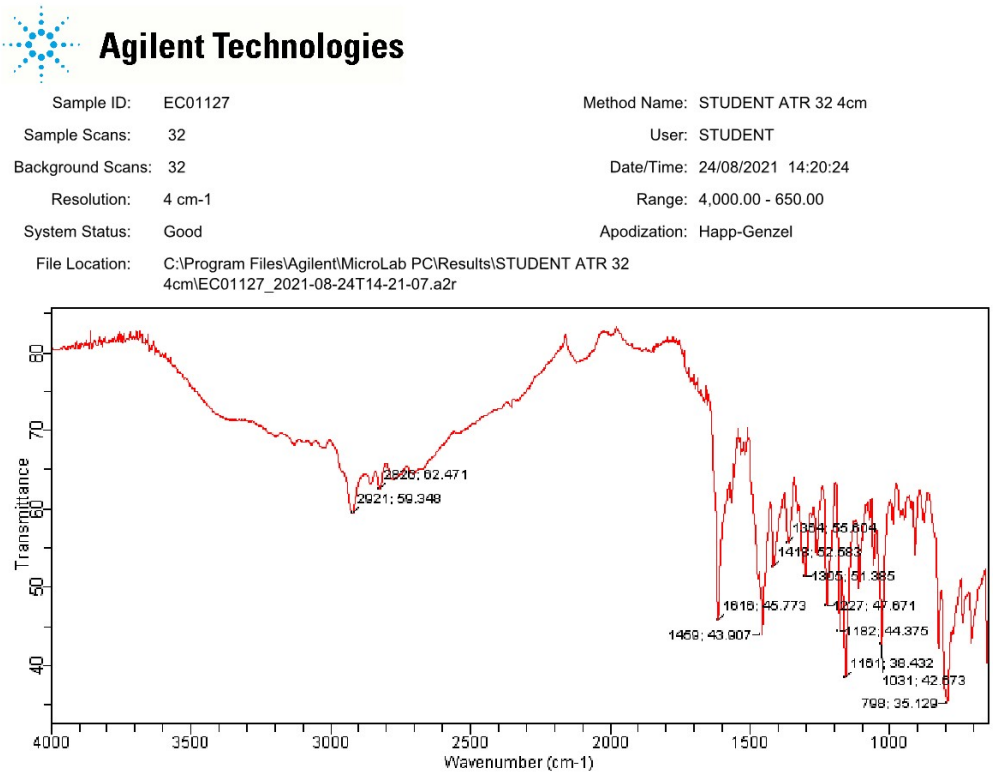


Figure 354. FT-IR spectra of 2-((7H-pyrido[3,4-c]carbazol-10-yl)oxy)-N,N-dimethylethan-1-amine (**4.73**).

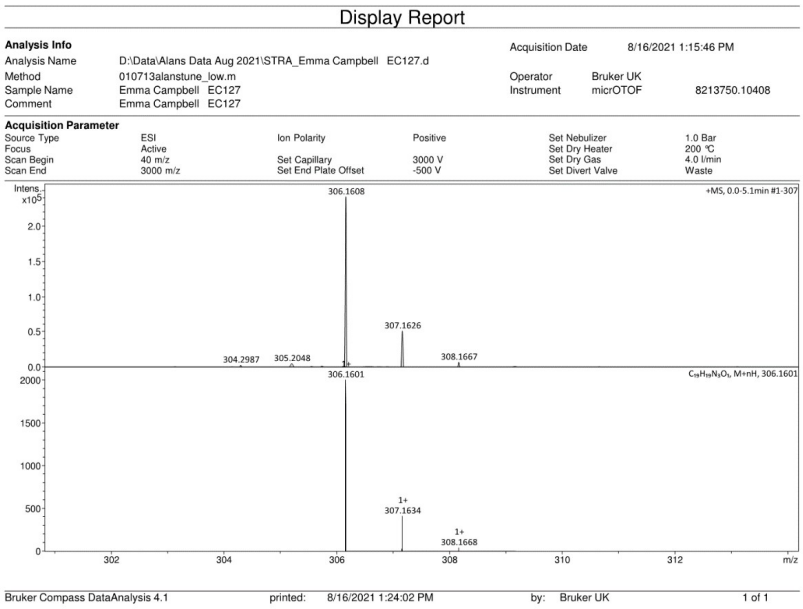


Figure 355. HRMS spectra of 2-((7H-pyrido[3,4-c]carbazol-10-yl)oxy)-N,N-dimethylethan-1-amine (**4.73**).

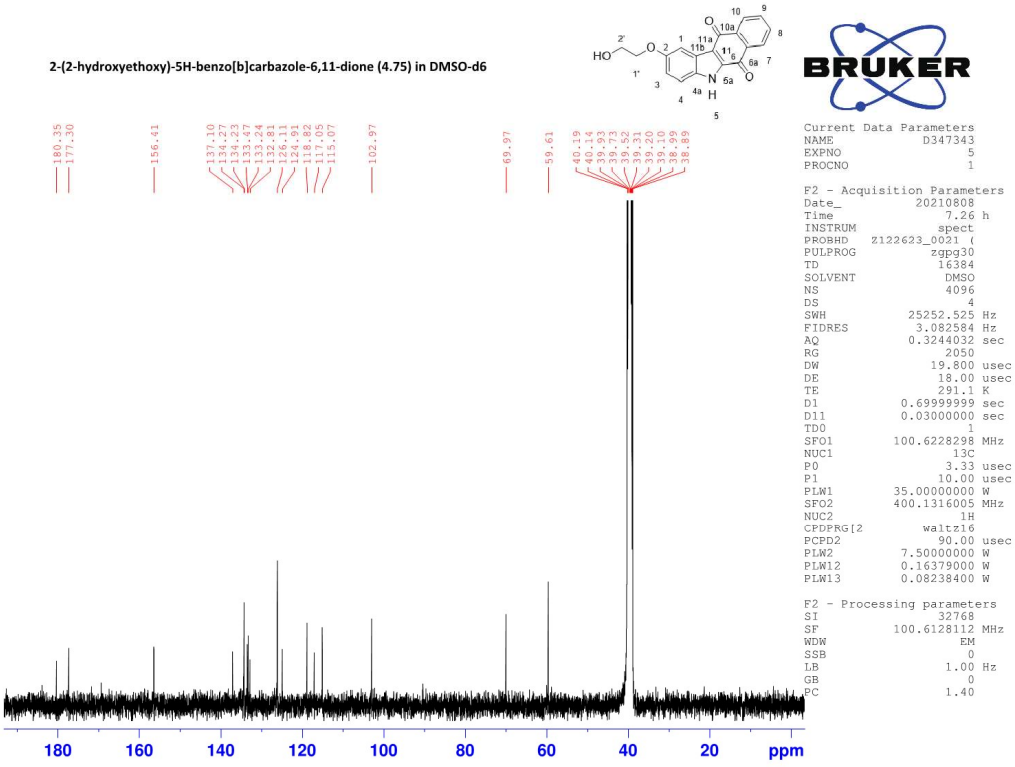


Figure 356. ^{13}C NMR spectra of 2-(2-hydroxyethoxy)-5H-benzo[b]carbazole-6,11-dione (**4.75**).

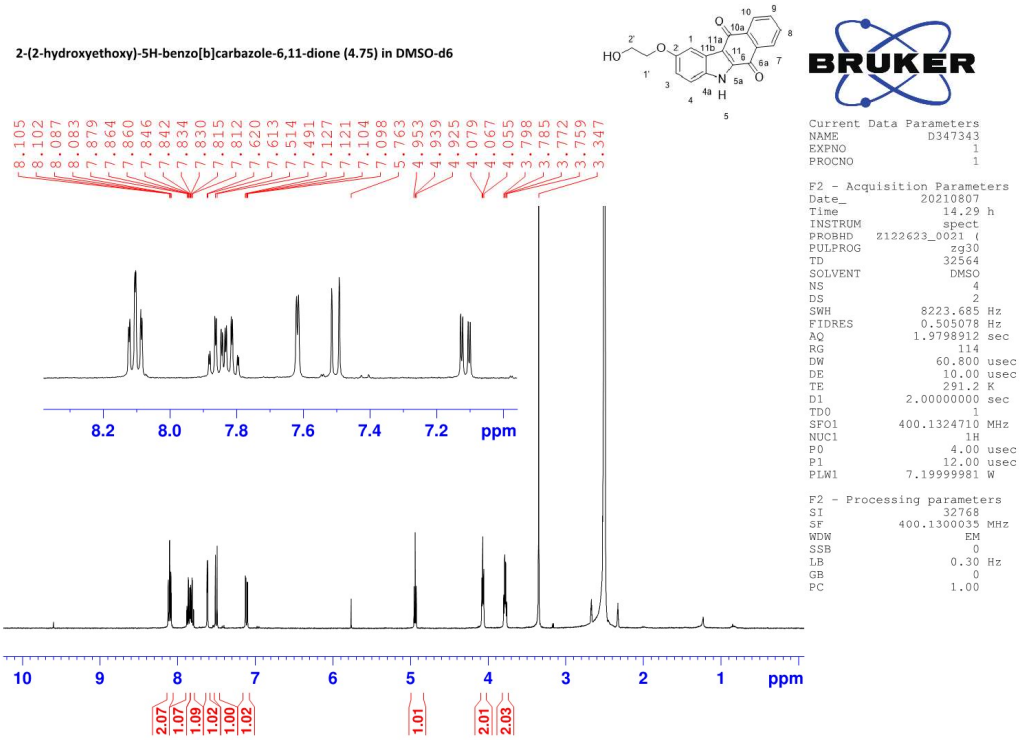


Figure 357. [1]H NMR spectra of 2-(2-hydroxyethoxy)-5H-benzo[b]carbazole-6,11-dione (**4.75**).

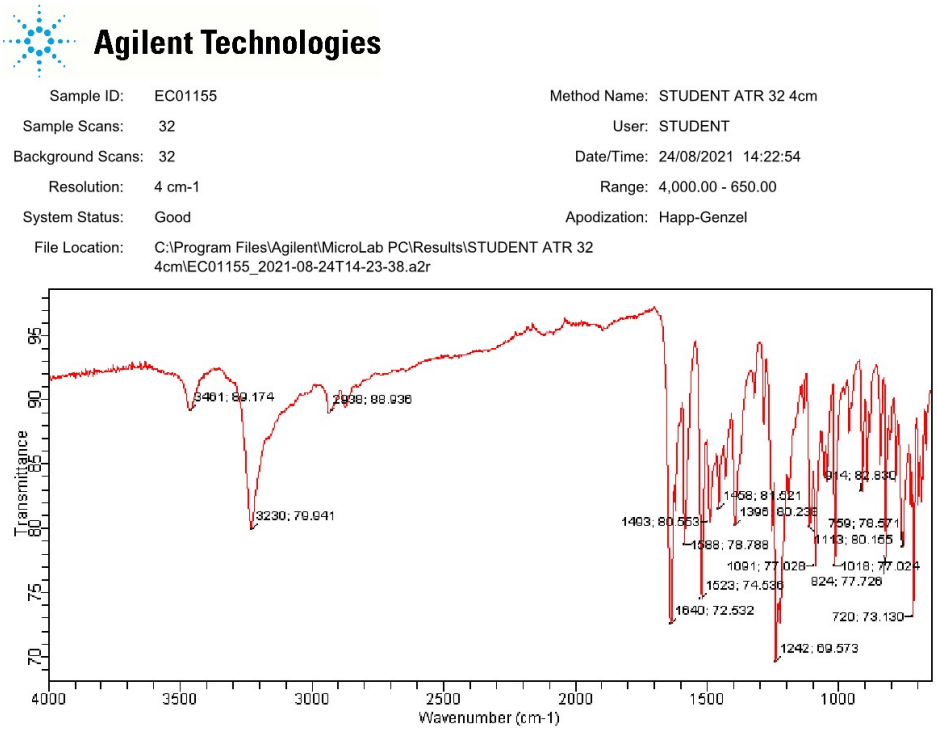


Figure 358. FT-IR spectra of 2-(2-hydroxyethoxy)-5H-benzo[b]carbazole-6,11-dione (**4.75**).

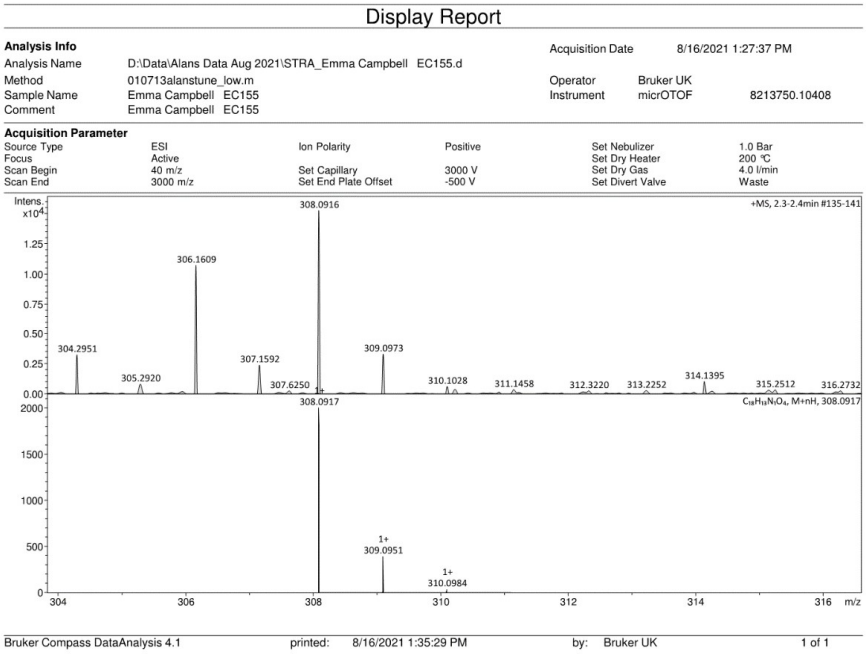


Figure 359. HRMS spectra of 2-(2-hydroxyethoxy)-5H-benzo[b]carbazole-6,11-dione (**4.75**).

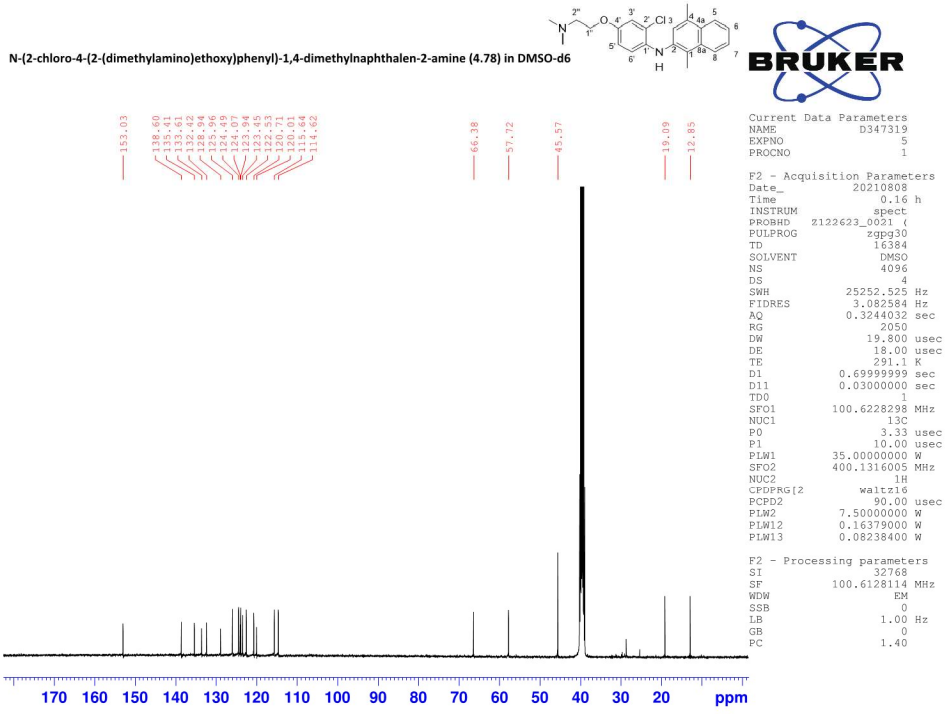


Figure 360. ^{13}C NMR spectra of N-(2-chloro-4-(2-(dimethylamino)ethoxy)phenyl)-1,4-dimethylnaphthalen-2-amine (**4.78**).

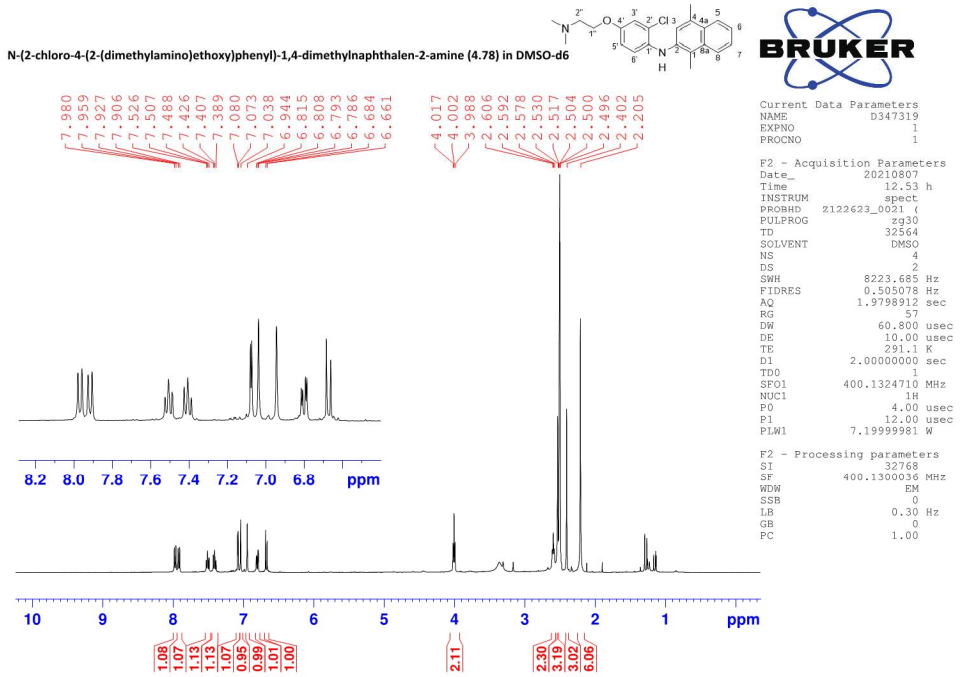


Figure 361. ^{1}H NMR spectra of N-(2-chloro-4-(2-(dimethylamino)ethoxy)phenyl)-1,4-dimethylnaphthalen-2-amine (**4.78**).

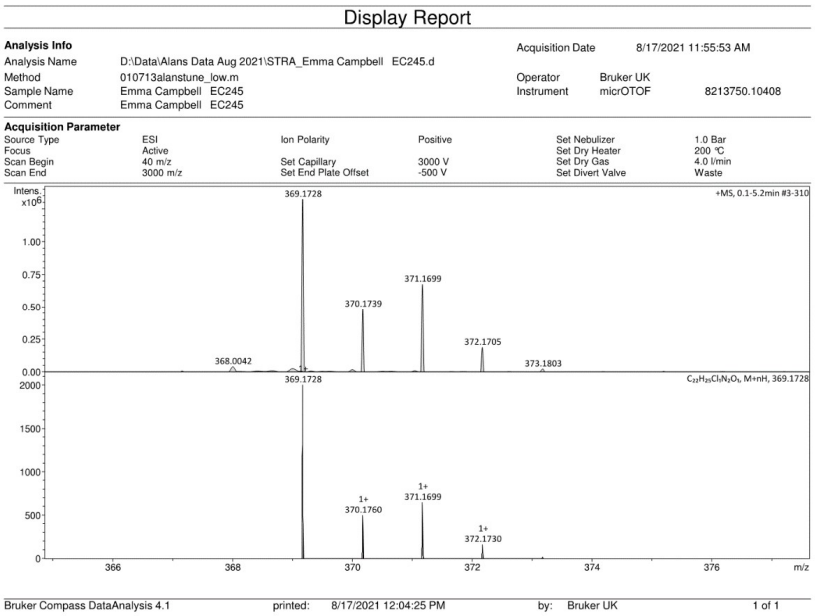


Figure 362. HRMS spectra of N-(2-chloro-4-(2-(dimethylamino)ethoxy)phenyl)-1,4-dimethylnaphthalen-2-amine (**4.78**).

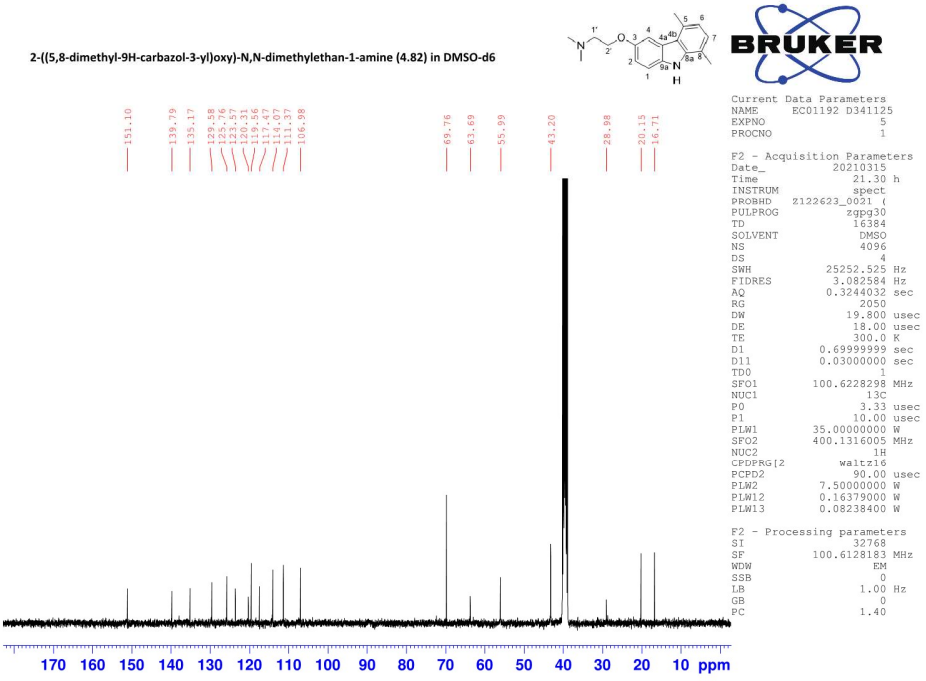


Figure 363. ^{13}C NMR spectra of 2-((5,8-dimethyl-9H-carbazol-3-yl)oxy)-N,N-dimethylethan-1-amine (**4.82**).

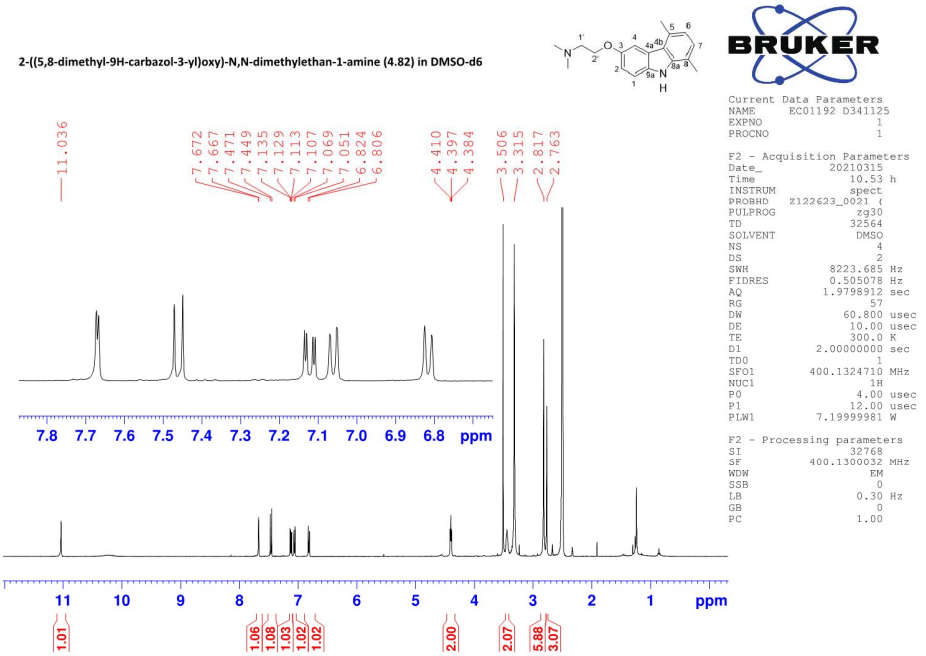


Figure 364. ^{1}H NMR spectra of 2-((5,8-dimethyl-9H-carbazol-3-yl)oxy)-N,N-dimethylethan-1-amine (**4.82**).

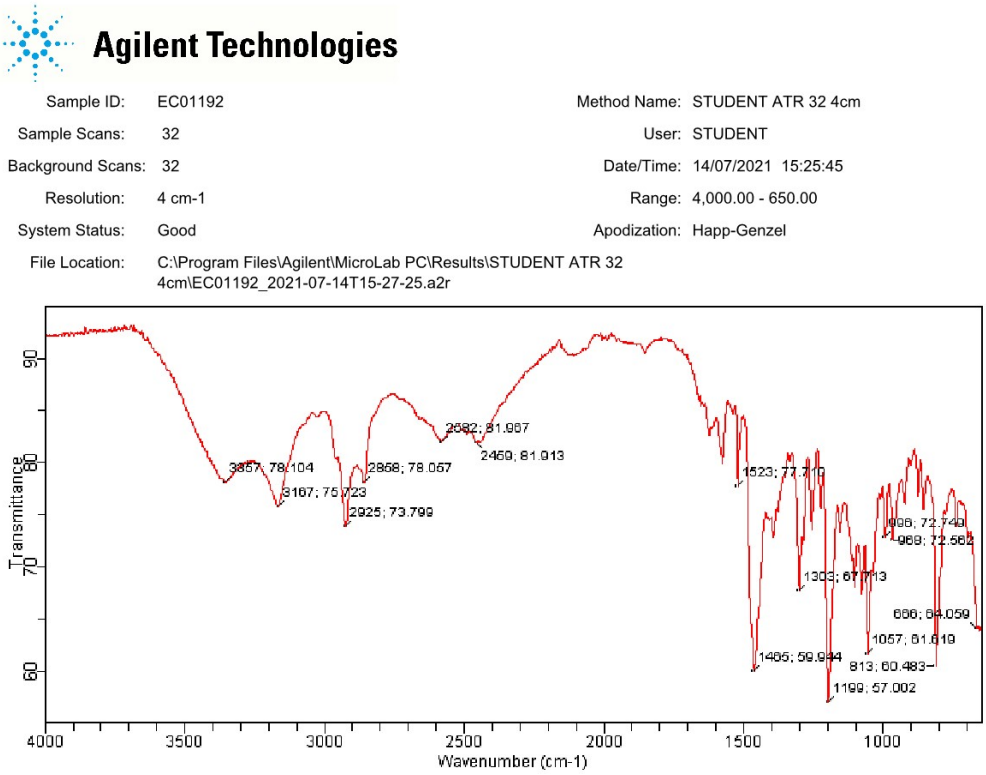


Figure 365. FT-IR spectra of 2-((5,8-dimethyl-9H-carbazol-3-yl)oxy)-N,N-dimethylethan-1-amine (**4.82**).

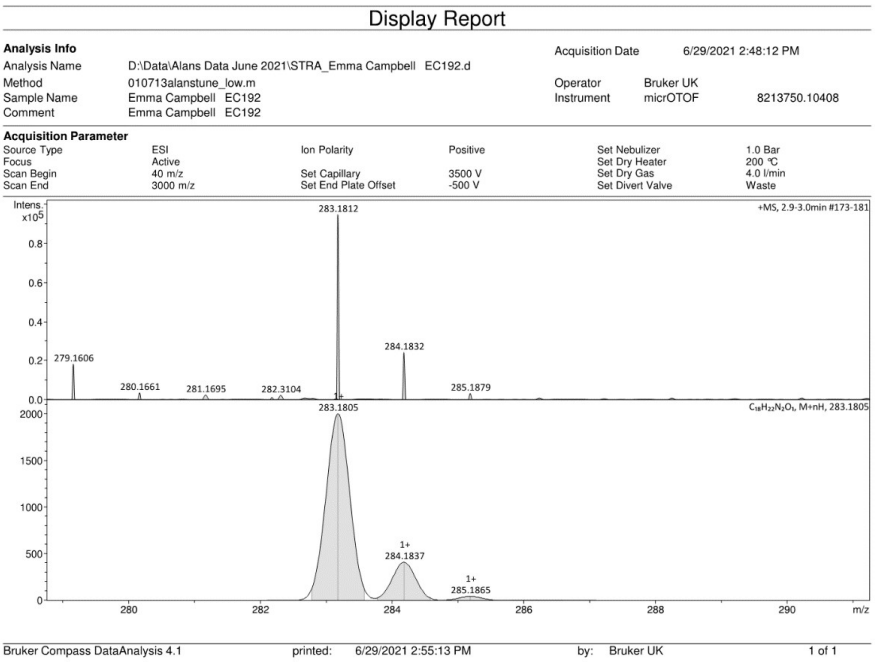


Figure 366. HRMS spectra of 2-((5,8-dimethyl-9H-carbazol-3-yl)oxy)-N,N-dimethylethan-1-amine (**4.82**).